ЖУРНАЛ
ЭКСПЕРИМЕНТАЛЬНОЙ И ТЕОРЕТИЧЕСКОЙ
ФИЗИКИ
АКАДЕМИЯ НАУК СССР

SOVIET PHYSICS

JETP

Volume 36 (9) NUMBER 3

A Translation

of the

Journal of Experimental and Theoretical Physics

of the

Academy of Sciences of the USSR

Volume 36

SEPTEMBER, 1959

Published by the

AMERICAN INSTITUTE OF PHYSICS
INCORPORATED

SOVIET PHYSICS
JETP

A translation of the Journal of Experimental and Theoretical Physics of the USSR.

A publication of the

AMERICAN INSTITUTE OF PHYSICS

Governing Board

RALPH A. SAWYER, *Chairman*
Members:
WALTER S. BAIRD
JESSE W. BEAMS
RAYMOND T. BIRGE
R. H. BOLT
HARVEY BROOKS
J. W. BUCHTA
J. H. DILLON
VERNET E. EATON
HERBERT A. ERF
IRVINE C. GARDNER
S. A. GOUDSMIT
WINSTON E. KOCK
R. BRUCE LINDSAY
WALTER C. MICHELS
G. E. PAKE
R. RONALD PALMER
JOSEPH B. PLATT
RALPH A. SAWYER
H. D. SMYTH
JOHN STRONG
GEORGE E. UHLENBECK

Administrative Staff

ELMER HUTCHISSON
Director
HENRY A. BARTON
Associate Director
WALLACE WATERFALL
Secretary and Treasurer
THEODORE VORBURGER
Advertising Manager
RUTH F. BRYANS
Publication Manager
ALICE MASTRO
Circulation Manager
KATHRYN SETZE
Assistant Treasurer
EUGENE H. KONE
Director of Public Relations
EDWARD P. TOBER
Manager, Production and Distribution
W. C. KELLY
Director of Education Projects
EMILY WOLF
Office Manager

American Institute of Physics Advisory Board on Russian Translations

ROBERT T. BEYER, *Chairman*
J. GEORGE ADASHKO, FREEMAN DYSON, DWIGHT GRAY,
MORTON HAMERMESH, HAROLD F. WEAVER

Editor of SOVIET PHYSICS—JETP

J. GEORGE ADASHKO, 25 WEST 81ST ST., NEW YORK 24, NEW YORK

SOVIET PHYSICS—JETP is a monthly journal published by the American Institute of Physics and contains a complete translation of the JOURNAL OF EXPERIMENTAL AND THEORETICAL PHYSICS of the U.S.S.R. Academy of Sciences.

This translating and publishing project was undertaken by the institute in the conviction that dissemination of the results of researches everywhere in the world is invaluable to the advancement of science. The NATIONAL SCIENCE FOUNDATION of the United States has encouraged the project initially and is supporting it in large part by a grant.

The American Institute of Physics and its translators propose to translate faithfully all the material appearing in the original articles. The views expressed in the translations are therefore those of the original authors, and not those of the translators nor of the American Institute of Physics.

Volume 1 of SOVIET PHYSICS—JETP corresponds to Russian Volume 28 (1955). Two volumes are published annually, each of six issues. Each volume contains the translation of one volume of the JOURNAL OF EXPERIMENTAL AND THEORETICAL PHYSICS.

Beginning with Vol. 9(36), the transliteration of the names of Russian authors follows British Standard 2979, which is being adopted in 1959 by a large number of scientific journals in the United States. The Library of Congress transliteration is followed in the earlier volumes.

Subscription Prices

Per Year (12 issues)

General:

United States and Canada	$75.00
Elsewhere	79.00

Libraries and non-profit degree-granting Institutions:

United States and Canada	$35.00
Elsewhere	39.00
Back Numbers	$ 8.00

Subscriptions should be addressed to the American Institute of Physics, 335 East 45th Street, New York 17, New York.

SOVIET PHYSICS, JETP is published monthly by the American Institute of Physics, Inc. Second Class postage paid at Ann Arbor, Michigan.

Copyright by American Institute of Physics 1959

SOVIET PHYSICS

JETP

A translation of the Journal of Experimental and Theoretical Physics of the USSR.

SOVIET PHYSICS JETP VOL. 36 (9), NO. 3, pp. 453-682 SEPTEMBER, 1959

ACADEMICIAN LEV ANDREYEVICH ARTSIMOVICH

(on his fiftieth birthday)

J. Exptl. Theoret. Phys. (U.S.S.R.) **36**, 649-651 (March, 1959)

ON February 25, 1959 Academician Lev Andreyevich Artsimovich, the outstanding Soviet physicist, celebrated his fiftieth birthday.

Artsimovich, the son of a professor of statistics, was born in Moscow. After completing his secondary schooling he entered the Belorussian State University in Minsk. His brilliant capabilities enabled him to graduate early, and in 1930 he joined the Leningrad Physico-technical Institute.

The Physico-technical Institute, then directed by Academician A. F. Ioffe, occupied in those days undisputed first place among the physics institutes of the country. The atmosphere of devotion to science and scientific enthusiasm, which then characterized the staff of scientists of the Leningrad Physico-technical Institute, has played an exceedingly productive role in the formation of Artsimovich's outlook. During the first years at the Institute, until 1933, Artsimovich did some research, in the laboratory of P. I. Lukirskiĭ, on the optics of x-rays; one particular project, undertaken with A. I. Alikhanov, concerned the difficult problem of the total internal reflection in the x-ray region of the spectrum.[1]

The year 1932 saw the discovery of the neutron, and an intense investigation of its properties began in many laboratories. Much work was also done at the Leningrad Physico-technical Institute on neutron physics. In 1935 Artsimovich, together with I. V. Kurchatov, G. D. Latyshev, and V. A. Khramov investigated, in an interesting research project, one of the simplest nuclear reactions, that of the capture of a neutron by a proton,[2] and demonstrated for the first time that the probability of capture of slow neutrons by protons is relatively large.

However, the main field of Artsimovich's research in the Leningrad Physico-technical Institute, a field in which his outstanding abilities as an experimental physicist — clarity of analysis and high reliability of the results obtained — manifested themselves to the fullest extent, was the investigation of the interaction between fast electrons and matter.[3-5] Artsimovich occupied himself with this problem for approximately four years. It must be recalled that in those days our information on this subject was quite incomplete. It is enough to state that the experimental data on brems-

strahlung and angular distribution of the scattered electrons were at that time different from the theoretical values by two orders of magnitude. Artsimovich's research resulted in extensive experimental material on the dependence of the bremsstrahlung intensity and of the total energy losses on the energy of the fast electrons; he also investigated in detail the spatial characteristics of the scattering process. The final conclusion drawn from these investigations was exceedingly simple: the modern quantum-mechanical theory of the passage of fast electrons through matter agrees with the experimental data, within the limits of experimental accuracy. This important result, which eliminated any existing doubts concerning the correctness of the principal outlines of the theory, pointed at the same time ways towards a precise verification of individual special problems, as the experimental techniques became more perfected.

During the war Artsimovich occupied himself with problems of electron-optics and, in particular, developed a theory of chromatic aberration of electron-optical systems.[6]

In 1945, together with I. Ya. Pomeranchuk, Artsimovich cleared up the important problem of the role of betatron radiation losses.[7] His theoretical analysis made it possible to establish the maximum energy attainable with this new method of electron acceleration.

In the postwar years, the tremendous scope of modern technology has necessitated a new approach to the investigation of natural phenomena. It became Artsimovich's task to guide the development of a new trend in technical physics, namely the development of a technology for electromagnetic isotope separation.

It became necessary to increase by a factor of millions the productivity of the laboratory mass spectrometer, and to convert a feeble and fragile physical instrument into reliably operating technical apparatus. A staff of physicists headed by Artsimovich has solved this problem successfully, and at the present time stable isotopes are used more and more in experimental physics.

In addition to solving numerous specific problems arising in the course of the development of the method, it remained for Artsimovich to make a detailed analysis of the problems involved in aberration-free focusing of wide-angle ion beams in axially-symmetrical magnetic fields. In these investigations he obtained a useful formula to relate the dispersion with the angle of aberration-free focusing. Artsimovich has proposed the construction of the ion-optical system of the source, a system used in all modern equipment.[8]

In the early 50's, the scientific interests of Artsimovich turned towards one of the most interesting and difficult physical problems of our time, the production of a controllable thermonuclear reaction. This type of research calls for a deep insight into the old but far from complete field of plasma physics. Yet, to make progress in this field it is necessary to analyze a large number of theoretical problems and to develop quite new experimental methods. The situation is made even more difficult by the fact that there is no general line of attack on the problem, and that to the present time there have existed and still exist different ways of approaching a possible solution of the problem.

As is known, the group of physicists led by Artsimovich has concentrated its effort during the early stages of the research on a study of high intensity pulsed discharges in rarefied deuterium. During the course of these investigations it became possible not only to obtain (although for only brief instance) a gas-discharge plasma with a temperature of several millions of degrees,[9] but also to discover many new phenomena in the physics of gas discharge. Thus, in 1952 Artsimovich together with A. M. Andrianov, E. I. Dobrokhotov, S. Yu. Luk'yanov, I. M. Pondgornyĭ, V. I. Sinitsyn, and N. V. Filippov has discovered that a high-intensity pulsed discharge in deuterium at low pressure becomes a source of neutron radiation.[10] Sometime later Artsimovich has investigated the important problem of the behavior of a self-constricting plasma in the presence of a longitudinal magnetic field.[11-13] An investigation of this problem is particularly important for the interpretation of experimental data pertaining to so-called plasma paramagnetism.

Further investigations on controllable thermonuclear reactions are being carried out over an extensive front, and the paper by Artsimovich at the Second Geneva Conference on the Peaceful Uses of Atomic Energy[14] contains a brilliant survey of the efforts of Soviet physicists in this direction.

Artsimovich began his pedagogical activity very early. Already in 1930 he lectured at the Leningrad Polytechnic Institute, and then began lecturing at the Leningrad State University. In Moscow he continued to offer courses on atomic and nuclear physics at the Moscow Engineering-Physics Institute, and in recent years at the Moscow State University. Artsimovich's lectures are invariably distinguished for the rigor in which the problem is stated, for clarity, and cleverness of the exposition.

The list of Artsimovich's scientific papers is relatively short, but in the flow of scientific literature that fills the pages of our journals one cannot

skip past any articles signed with the name of L. A. Artsimovich. They are always devoted to urgent and acute problems of modern physics and are characterized by deep critical analysis and lucid exposition.

Artsimovich's scientific merits have been highly valued by the scientific society of our country. In 1946 he was elected a corresponding member of the U.S.S.R. Academy of Sciences and in 1954 he became a full member. Artsimovich was awarded many orders of the Soviet Union: in 1953 he became a Stalin Prize laureate, in 1958 a Lenin Prize laureate.

The editors of the Journal of Experimental and Theoretical Physics wholeheartedly congratulate Lev Andreyevich Artsimovich, and offer sincere wishes of health, happiness, and new creative successes for the benefit of Soviet science and our great Fatherland.

[1] Total Internal Reflection of X-rays from Thin Layers (with A. I. Alikhanov) J. Exptl. Theoret. Phys. (U.S.S.R.) **3**, 115 (1933).

[2] Absorption of Neutrons in Soda, Paraffin, and Carbon (with G. D. Latyshev, I. V. Kurchatov, and V. A. Khramov), Physik. Z. Sowjetunion **8**, 4 (1935).

[3] Bremsstrahlung for High-Energy Electrons (with V. A. Khramov), J. Exptl. Theoret. Phys. (U.S.S.R.) **8**, 913 (1938).

[4] Energy Losses for Fast Neutrons (with V. A. Khramov), Izv. Akad. Nauk SSSR, Ser. Fiz. **2**, 757 (1938).

[5] Angular Distribution of Fast Neutrons Scattered by Aluminum Nuclei (with I. I. Perrimond) Dokl. Akad. Nauk SSSR **52**, 303 (1946).

[6] Electron-Optical Properties of Emission Systems. Izv. Akad. Nauk SSSR, Ser. Fiz. **8**, 313 (1944).

[7] Radiation of Fast Electrons in a Magnetic Field (with I. Ya. Pomeranchuk) J. Exptl. Theoret. Phys. (U.S.S.R.) **16**, 379 (1946).

[8] Electromagnetic Apparatus of High Resolving Power for Separation of Heavy-Element Isotopes (with G. Ya. Shchepkin, V. V. Zhukov, B. N. Makov, S. P. Maksimov, A. F. Malov, A. A. Nikulichev, B. V. Panin, and B. G. Breshnev) Атомная энергия (Atomic Energy) **3**, 483 (1957).

[9] Investigation of Pulsed Discharges with High Current Strengths (with A. M. Andrianov, O. A. Bazilevskaya, Yu. G. Prokhorov, and N. V. Filippov) Атомная энергия (Atomic Energy) **1**, No. 3, 76 (1956).

[10] Hard Radiation of Pulsed Discharges (with A. M. Andrianov, E. I. Dobrokhotov, S. Yu. Luk'yanov, I. M. Podgornyĭ, V. I. Sinitsyn, and N. V. Filippov) Атомная энергия (Atomic Energy) **1**, No. 3, 84 (1956).

[11] Flow of Large Currents through a Plasma in the Presence of a Longitudinal Magnetic Field, Сб. Физика плазмы и проблема управляемых термоядерных реакций (Collection "Physics of Plasma and Problems of Controllable Thermonuclear Reactions") Vol 2, 1958, p 81.

[12] Magnetic Flux in a Self-Constricting Cylinder, ibid. p 87.

[13] Analysis of Pinch Control in the Presence of an External Magnetic Field, ibid. p 101.

[14] Research on Controllable Thermonuclear Reactions in the U.S.S.R., Second International Conference of the United Nations on the Peaceful Use of Atomic Energy, 15/P/2298.

Translated by J. G. Adashko
124

Bi *FISSION AT VERY HIGH EXCITATION ENERGIES*

V. F. DAROVSKIKH and N. A. PERFILOV

Radium Institute, Academy of Sciences, U.S.S.R.

Submitted to JETP editor June 28, 1958

J. Exptl. Theoret. Phys. (U.S.S.R.) **36**, 652-657 (March, 1959)

Nuclear emulsions were used to study relative yields in Bi fission induced by 660-Mev protons as a function of the range ratio of light and heavy fission fragments, l_L/l_H, for groups of nuclei with different mean excitation energies. The dependence of fission yields on the range ratio was found to vary nonmonotonically for some nuclei. The dependence of the mean combined fragment range on l_L/l_H has been obtained. The experimental findings are accounted for on the basis of the shell structure of the product nuclei.

ALTHOUGH the mass and energy distributions of nuclear fission products have been studied extensively both experimentally and theoretically, much work remains to be done. The mass distribution differs between elements and varies with the bombarding energy. For atomic number 90 and higher at low bombarding energies fission is characteristically asymmetric, but the asymmetry diminishes with increasing mass of the fissioning nucleus,[1] and increasing excitation energy.[2] Very high-energy particles induce predominantly symmetric fission.[3] For atomic number 83 and lower symmetric fission is predominant at both high[4] and low[5] excitation energies. Evidence has recently been obtained[6] that fission of elements with Z between 83 and 90 may be even more complex in character. It is difficult to obtain a consistent picture from the large number of separate experimental facts. Various authors have attempted in different ways[7] to account for individual fission modes, but there is no single explanation for all of the observed effects. Further investigations in this field will therefore be extremely important.

1. EXPERIMENTAL PROCEDURE AND RESULTS

The present work is a detailed study of Bi fission induced by high-energy particles. P-9 emulsions impregnated with a Bi salt were irradiated in the synchrocyclotron of the Joint Institute for Nuclear Studies by 660-Mev protons. After processing the emulsions were examined microscopically to detect Bi fission events; the horizontal and vertical projections of fragment tracks were then carefully measured and the true range of each fragment was calculated with allowance for shrinkage. The ratio of true fragment ranges was taken as a measure of fission asymmetry. Special fine-grained emulsions permitted visual determination of the separation point of fission fragments even when unaccompanied by charged particle emission.[8] The number of prongs associated with each fragment separation point was determined and the prongs were identified as belonging to either to singly- or doubly-charged particles. The sensitivity of the emulsions used is about 100 Mev for protons, thus permitting registration of the entire evaporation spectrum of charged particles and a considerable fraction of the knock-on protons. Most unobservable knock-on protons are associated with low excitation energy. On the other hand, at high excitation energies the nuclear cascade branches so strongly that the knock-on proton spectrum contains almost no particles of energy higher than 100 Mev.

It has been shown by Shamov[9] that fission accompanied by the emission of a definite number of charged particles can be associated with a definite mean excitation energy. Thus for each group of fissions with emission of a definite number of charged particles we can determine the average fissioning nucleus on the assumption that all particles escape from the nucleus before fission occurs. The charge of the fissioning nucleus is obtained directly from the number of visible tracks with a correction for the invisible tracks. The number of neutrons in the fissioning nucleus can be calculated very accurately by means of the evaporation theory from a knowledge of the excitation energy expended for neutron evaporation alone.

In order to clarify the different fission modes of different nuclei we for each group plotted the distribution of fissions with respect to the range

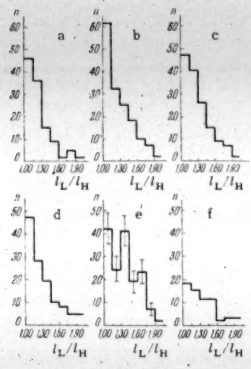

FIG. 1. Distribution of Bi fissions n with respect to the range ratio l_L/l_H of light and heavy fragments from fissions emitting: a – 0, b – 1, c – 2, d – 3, e – 4 or 5, f – 6 or more charged particles. The mean error of measurement of the range ratio is $\Delta(l_L/l_H) = 0.1\ l_L/l_T$.

ratio l_L/l_H of light and heavy fragments; the histograms are given in Fig. 1. In the cases of 0, 1, 2, 3 charged particles the highest yield is consistently observed near the ratio $l_L/l_H = 1$, i.e., for symmetric fission. With increasing asymmetry the yields decrease monotonically in all four cases. An entirely different picture results in the case of 4 and 5 emitted charged particles (Fig. 1e): the yield does not decrease monotonically as the asymmetry increases. Unlike the previous relations histogram e shows three maxima, two of which lie far outside the limits of statistical error. A χ^2 test[10] was performed to determine whether statistical fluctuations could account for these departures from the smooth curves for groups a, b, c and d. The area under a smooth curve was set equal to the area of the experimental histogram; then $\chi^2 = 14.4$ for the best fit of the experimental values. For the number of degrees of freedom involved here, $F = 6 - 1 = 5$, the probability of obtaining such statistical fluctuation is $P < 0.02$, which is so small that statistical errors cannot account for the observed curve. We are also not aware of anything that could cause any systematic errors. When 4 or 5 charged particles are emitted there is apparently about the same probability of asymmetric fission into fragments with the given masses as for the familiar symmetric fission.

It is difficult to make any definite statement regarding the mode of fission of nuclei associated with 6 or more emitted charged particles. In the first place, the data are very meager. Secondly, as was shown in references 11 and 12, Ag and Br stars with 6 or 7 prongs show a very high probability of heavy fragments (including those with range of about 10 μ) together with recoiling nuclei, or pairs of heavy fragments, which can be distinguished from Bi fission only with great difficulty. Because of the large AgBr content of emulsions such spurious "fissions" may comprise a considerable fraction. One must therefore exercise great caution before asserting that the fission of a given group is symmetric as shown in Fig. 1f.

The use of nuclear emulsions enables us to include the important combined range of fission fragments in our analysis in addition to the range ratio. While single ranges, because of the extremely great diversity of nuclear products, cannot serve to determine the kinetic energy release involved in fission, the combined range is very closely related to the total kinetic energy of fission fragments. Photographs of fissions provide a measurement of the range ratio of light and heavy nuclei together with the combined range of these fragments. By averaging the combined ranges over a large number of fissions with given asymmetry we can obtain the dependence of the mean combined range $\bar{l} = \overline{l_L + l_H}$ on the ratio l_L/l_H; this gives approximately the dependence of the total kinetic energy of fragments on the degree of asymmetry. Figure 2 gives $\bar{l} = f(l_L/l_H)$ for two groups of Bi fissions and, for comparison, the same relationship for U fission by thermal neutrons. Unlike the gradually falling curve for U (Fig. 2c), both groups of Bi fissions (Fig. 2a and b) show the same irregular character. For Bi fissions

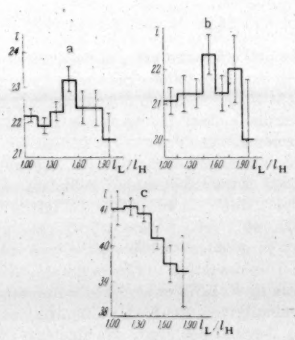

FIG. 2. Mean combined range of fission fragments, $\bar{l} = \overline{l_L + l_H}$, as a function of the range ratio l_L/l_H of light and heavy fragments, for Bi fission accompanied by: a – 0, 1, 2, 3; b – 4 or 5 charged particles ($\bar{l}$ in μ). c – U fissions by thermal neutrons ($\bar{l}$ in relative units).

accompanied by 0, 1, 2, 3 charged particles the highest value of $\bar{l}$ is reached with range asymmetry 1.52. The mean combined range raches just as steep a maximum for the same asymmetry in Fig. 2b (for Bi fission with 4 or 5 emitted charged particles). The second maximum in the vicinity of range ratio $l_L/l_H = 1.82$ is not so reliable. The data indicate that the highest value of the total kinetic energy release in Bi fission induced by 660-Mev protons is observed in asymmetric fission.

2. ANALYSIS AND DISCUSSION OF EXPERIMENTAL RESULTS

We used Bohr's relationships in reference 13 in order to relate the range ratio of light and heavy fission fragments to the corresponding charge values. The energy losses of slowed-down heavy fragments are divided into those at velocities higher than v_0 (the electron velocity in the hydrogen atom) and those at velocities lower than v_0. In the first case ionization loss is dominant, while in the second case nuclear collisions produce most of the energy loss. For the sake of simplicity, Bohr neglects energy losses due to nuclear collisions and extrapolates the expression for ionization loss as far as $v = 0$. For a heavy stopping medium he thus obtains $dv/dl = \text{const}$. The variation of the effective charge as a function of velocity can be represented very well by $Z_1^* = Z_1^{1/3} v/v_0$, whence we easily obtain

$$l_L/l_H = (Z_H/Z_L)^{5/3} f(Z_H, Z_L), \qquad (1)$$

where

$$f(Z_H, Z_L) = [3(2Z_H^{1/3})^{-1/3} + (2Z_H^{1/3})^{-1}]/[3(2Z_L^{1/3})^{-1/3} + (2Z_L^{1/3})^{-1}].$$

Since we are using the ratio of the ranges rather than their absolute values constants that are characteristic of the emulsion disappear; this expression contains neither the mass nor the velocity of the fragments. The ratio l_L/l_H depends only on the nuclear charges of the fission fragments. Extrapolation of the expression for ionization loss to small velocities as a substitute for taking nuclear collisions into account when $v < v_0$ does not result in a very large departure from the true value of l_L/l_H. This deviation can be estimated from the data given by Boggild et al,[14] who determined the range-velocity relation for uranium fission induced by thermal neutrons. We find that the value of l_L/l_H obtained from (1) must be increased by about 10%. Thus a practical formula for the charges would be

$$l_L/l_H = 1.1 (Z_H/Z_L)^{5/3} f(Z_H, Z_L) \qquad (2)$$

The correcting factor is, of course, unnecessary for symmetric fission, i.e., Eq. (1) remains valid near $l_L/l_H = 1$.

Assuming $l_L/l_H = 1.32$ (the experimental value for uranium fission by thermal neutrons), from $Z_H + Z_L = 92$ and (2) we obtain $Z_H = 54$, $Z_L = 38$ in agreement with experiment. Thus (2) is entirely acceptable for the purpose of determining charge asymmetry from the range ratio.

In calculating the charge and mass number of a fissioning nucleus we assume an emission mechanism for Bi fission.[4] This hypothesis has been supported very convincingly in a number of papers[15] and there are hardly any grounds for doubting the emissive character of Bi fission. The calculation was performed in two steps. (1) Observed charged-particle tracks were used to determine the charge carried from the nucleus by charged knock-on and evaporated particles. The number of fast protons not recorded by the emulsion was estimated from a nuclear cascade calculation.[16] The energy carried away by evaporated charged particles was subtracted from the average excitation energy, which has a definite value for each nuclear group.[9] The remaining energy is expended only for the evaporation of neutrons. (2) The number of evaporated neutrons was determined by trial and error, with the calculation continuing until the remainder of excitation energy became smaller than the neutron binding energy.* It was thus possible to determine the mean charge and mean mass number of the fissioning nucleus for each group of fissions.

The calculation shows that for groups of fissions accompanied by the emission of 4 or 5 charged particles the average species of fissioning nucleus is Pt_{78}^{174}. The great majority of fissioning nuclei in this group contain less than 100 neutrons. Fissions with the emission of 3 charged particles have an initial excitation energy which is 100 Mev lower and most of the fissioning nuclei contain more than 100 neutrons. The other groups (Fig. 1a, b, c) give fissioning nuclei which are even richer in neutrons.

Applying (2) to the range ratios 1.52 and 1.82, for which in Fig. 2b we observe the maximum kinetic energy release, we obtain 50 and 28, 56 and 22, respectively as the charges of heavy and light fission fragments. For the group with a smaller number of charged particles (Fig. 2a) exactly the same position of the maximum (at $l_L/l_H = 1.52$)

*In the case of nuclei with sufficiently large Z^2/A fission can occur when the excitation energy slightly exceeds the neutron binding energy. There will then be one or two more neutron in the fissioning nucleus than the calculated number, but this does not essentially change the final result.

corresponds to charges 53 and 29 approximately. The charges calculated in this way which are associated with the maximum yields of asymmetric fission (Fig. 1e) are 47 and 31, 53 and 25, for heavy and light fragments, respectively.

We shall now attempt to account for the observed effects. We assume that the shell structure of the product nuclei is the decisive factor that determines the charge and mass distributions of fission fragments. This hypothesis has frequently been advanced by different investigators to account for asymmetric fission.[7] The symmetric fission which is observed for groups emitting 0, 1, 2, 3 charged particles is then attributed to the influence of the neutron shells of product nuclei. All of the fissioning nuclei of these groups contain more than 100 neutrons and each fragment involved in symmetric fission must contain a little more than 50 neutrons. Thus stable 50-neutron groups induce symmetric deformations of the nucleus resulting in splitting into two identical parts. When a fissioning nucleus is left with less than 100 neutrons (in 4- and 5-pronged fissions) the neutron shells cease to exert their influence while the influence of proton shells containing 50 and 28, or 50 and 20, protons are most influential. Indeed, the mean charge of a fissioning nucleus is $Z = 78$ in this group. Thus when the original nucleus fissions there is a very strong possibility of obtaining product nuclei with 50- and 28-proton shells and a somewhat slighter possibility of obtaining charges somewhat exceeding 50 and 20. The fact that according to the calculation above the maximum-yield fragments (Fig. 1e) have charges 47 and 31 may be attributed either to the estimative character of (2). (Charges 50 and 28, 56 and 22, can possibly correspond to range ratios 1.37 and 1.67.) or to the nature of the actual fission mechanism. In the latter case it can be assumed that asymmetric nuclear deformations are caused by shells of 50 and 28, or 50 and 20 protons. When the critical point has been passed the light fragment in process of formation captures most of the neck between the two portions of the nucleus and receives a greater charge: 31 instead of 28, 25 instead of $20 + n$, $n \leq 4$. The symmetric fission peak seen in Fig. 1e evidently results from the most highly excited fissioning nuclei, just as the symmetric uranium fission yield grows as we pass from thermal to faster neutrons.

The dependence of the total kinetic energy of fission fragments on the degree of asymmetry can also be understood to some extent from the given point of view. Although for fission groups with 0, 1, 2, 3 prongs symmetric fission occurs, because of predominantly symmetric deformations, the highest energy release is observed for fissions into fragments containing about 53 and 29 protons, which are close to the magic numbers 50 and 28. This indicates that with the less frequently encountered types of asymmetric deformations the fragments separate from each other at smaller distances than in the case of symmetric fission.* There is a corresponding increase in the total kinetic energy of the fragments and their excitation energy will be smaller.

For the groups of 4- and 5-pronged fissions the maximum of kinetic energy release is also observed in asymmetric fission. When a nucleus of charge 78 splits into fragments with charges 50 and 28, or 56 and 22, the stable compact product nuclei at the instant of fission are a very short distance apart; this facilitates the greatest release of Coulomb energy.

The foregoing interpretation of our experimental findings is only qualitative and lays claim to neither completeness nor finality. Further investigations are required to improve and supplement the data. We believe that data on fission modes resulting from the bombardment of heavy elements by high-energy particles can be used to answer a number of questions about the fission of weakly-excited nuclei.

[1] W. J. Swiatecki, Phys. Rev. **100**, 936 (1955).

[2] R. W. Spence and G. P. Ford, Ann. Rev. Nuclear Sci. **2**, 399 (1953).

[3] P. R. O'Connor and G. T. Seaborg, Phys. Rev. **74**, 1189 (1948).

[4] R. H. Goeckermann and I. Perlman, Phys. Rev. **76**, 628 (1949).

[5] A. W. Fairhall, Phys. Rev. **102**, 1335 (1956).

[6] R. C. Jensen and A. W. Fairhall, Bull. Am. Phys. Soc., Ser II, **2**, 378 (1957).

[7] J. Frenkel, J. Phys. (U.S.S.R.) **10**, 533 (1946); W. J. Swiatecki, Phys. Rev. **83**, 178 (1951); V. G. Nosov, Reports of the Soviet Delegation to the Geneva Conference on the Peaceful Uses of Atomic Energy (in Russian), Acad. Sci. Press, 1955, p. 303; P. Fong, Phys. Rev. **102**, 434 (1956); D. L. Hill and J. A. Wheeler, Phys. Rev. **89**, 1102 (1953); V. V. Vladimirskii, J. Exptl. Theoret. Phys. (U.S.S.R.) **32**, 822 (1957), Soviet Phys. JETP **5**, 673 (1957); M. G. Mayer, Phys. Rev. **74**, 235 (1948); L. Meitner, Nature **165**, 561 (1950); R. D. Hill, Phys. Rev. **98**, 1272 (1955).

*We here assume that the excitation energy of the nucleus is not converted into kinetic energy of fragments. There is still no experimental evidence that the latter is possible.

[8] Perfilov, Novikova, and Prokof'eva, Атомная энергия (Atomic Energy) **4**, 45 (1958).

[9] V. P. Shamov, Dokl. Akad. Nauk SSSR **103**, 593 (1955).

[10] Evans, R. D., The Atomic Nucleus, McGraw-Hill, New York, 1955.

[11] O. V. Lozhkin and N. A. Perfilov, J. Exptl. Theoret. Phys. (U.S.S.R.) **31**, 913 (1956), Soviet Phys. JETP **4**, 790 (1957).

[12] V. P. Shamov, J. Exptl. Theoret. Phys. (U.S.S.R.) **35**, 316 (1958), Soviet Phys. JETP **8**, 219 (1959).

[13] N. Bohr, Kgl. Danske Videnskab. Selskab, Mat.-fys. Medd., **18**, 8 (1948).

[14] Boggild, Broştrom and Lauritsen, Kgl. Danske Videnskab. Selskab, Mat.-fys. Medd., **18**, 4 (1940).

[15] V. P. Shamov, Атомная энергия (Atomic Energy) Suppl. No. 1, 1957, p. 129 (Supplement No. 1, Physics of Fission, Consultants Bureau, Inc., p. 85); V. P. Shamov, J. Exptl. Theoret. Phys. (U.S.S.R.) **33**, 346 (1957), Soviet Phys. JETP **6**, 268 (1958); G. Harding and F. Farley, Proc. Phys. Soc. (London) **A69**, 853 (1956); Gol'danskiĭ, Tarumov, and Pen'kina, J. Exptl. Theoret. Phys. (U.S.S.R.) **29**, 778 (1955), Soviet Phys. JETP **4**, 677 (1956).

[16] N. S. Ivanova and I. I. P'yanov, J. Exptl. Theoret. Phys. (U.S.S.R.) **31**, 416 (1956), Soviet Phys. JETP **4**, 367 (1956).

Translated by I. Emin
125

RANGE-ENERGY RELATION FOR 660-Mev PROTONS

V. P. ZRELOV and G. D. STOLETOV

Joint Institute for Nuclear Research

Submitted to JETP editor July 15, 1958

J. Exptl. Theoret. Phys. (U.S.S.R.) **36**, 658-668 (March, 1959)

The mean range of protons in copper was determined. The proton energy was computed from the measured angle of Vavilov-Cerenkov radiation emitted by protons in Plexiglas. The corrected range of (658 ± 2)-Mev protons in copper was found to be 257.6 ± 1.2 g/cm^2. Assuming the ionization potential to be independent of the velocity, the calculated value of I_{Cu} is 305 ± 10 ev. The stopping power relative to copper was also measured for H, Be, C, Fe, Cd and W.

INTRODUCTION

BETHE and Livingston's expression[1] for the average ionization losses of charged particles contains the average ionization potential I of the substance traversed by the particles. In the theory of ionization losses it is assumed that the average ionization potential I depends only on the atomic properties of the medium and is in principle independent of the incident particle's velocity. However, considerable experimental evidence (Table I)[2] indicates that the average ionization potential tends to decrease with increasing particle velocity, at least for heavy elements ($Z > 13$).

Lindhard and Scharff[7] used the Thomas-Fermi statistical model to show that for different energies the energy losses of charged particles in substances with large Z is a function of only the parameter x and is given by

$$-\frac{dE}{dx} = \frac{4\pi N (ze^2)^2}{mv^2} L(x), \quad x = \frac{v^2}{Zv_0^2}, \quad v_0 = \frac{e^2}{\hbar}. \qquad (1)$$

As in the Bethe-Bloch theory, L(x) is a logarithmic relation for $x > 100$, in which region the specific form of L(x) proposed by Lindhard and Scharff provided a sufficiently good description of the experimental data available at the time and to some extent confirmed Sachs and Richardson's idea[8] that I might be dependent on energy.

Caldwell[3] subsequently analyzed all available experimental data on the determination of ionization potentials of different elements for different

TABLE I. Summary of ionization potentials in ev

Element	Z	From Caldwell[3] for 18 Mev*	From Bloembergen and van Heerden[4] for 60 Mev	From Thomson for 270 Mev	From Mather and Segrè[5] for 340 Mev	From Bakker and Segrè[3] for 340 Mev
H	1			18.0	15.6	
Li	3				34.0	
Be	4				60.4	59.0
C	6			69.7	76.4	74.4
N	7			75.9		
O	8			87.6		
Al	13	163±3	162±5		150	147.9±3
Cl	17			151.9		
Fe	26				243	
Ni	28	363±19				
Cu	29	377±8	370		279	309.9±3
Rh	45	656±45				
Ag	47	659±50			428	
Cd	48	654±41				
Sn	50	708±59			479	
Ta	73	962±54				
W	74				697	
Au	79	1136±100				
Pb	82		970		758	810.7±12
U	92				881	

*Based on the experimental work of Sachs and Richardson.[8]

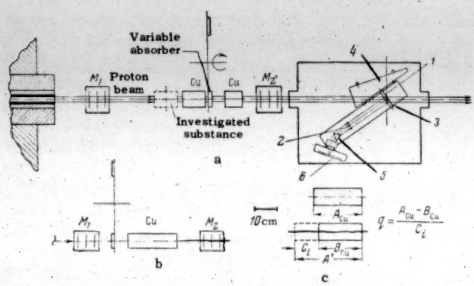

FIG. 1. a – Plan of experiment: 1 – radiator, 2 – radiation, 3 – mirror surface, 4 – angle template, 5 – achromatic prism, 6 – camera; b – arrangement of ionization chambers M_1 and M_2 and copper absorber for total range measurement; c – arrangement for measurements of relative stopping powers.

incident energies, making all essential corrections The result was strong modification of the experimental curve for $x < 100$. Caldwell concluded that there is no basis at present for assuming that I depends on velocity; he was of the opinion that for high energies we must use higher ionization potentials than those given by Bakker and Segrè[5] and Mather and Segrè,[6] which are approximately 13Z ev.

In the present paper we shall present measurements of the range-energy relation for 660-Mev protons in copper.

EXPERIMENT

The mean energy of our external synchrocyclotron beam was 660 Mev, with a spread of ±4 Mev. The beam was formed by a collimator of 20 mm diameter. The instruments for precise measurement of proton energy and range were placed in line on a special truss behind a four-meter reinforced concrete shield 17 m from the exit window of the accelerator vacuum chamber. The experimental arrangement is shown in Fig. 1.

MEASUREMENT OF MEAN PROTON ENERGY

The mean proton energy was determined by Mather's method which was described in reference 9. In the present paper we shall give the experimental results with only a brief description of the procedure. The method is based on the sharply defined directivity of Vavilov-Cerenkov radiation,[10] with the semiangle of the radiation cone given by $\cos\theta(\lambda) = 1/n(\lambda)\beta$, where $n(\lambda)$ is the refractive index of the medium for a given wavelength λ and $\beta = v/c$ is the particle velocity.

Because of the continuous spectrum of Vavilov-Cerenkov radiation the form of the function $n(\lambda)$ must be taken into account in determining velocities from $\cos\theta(\lambda) = 1/n(\lambda)\beta$. Mather[9] developed an ingenious scheme for measuring the emission angle of a given wavelength. In virtue of $n(\lambda)$ the blue portion of the radiation spectrum is located on the outside of the radiation cone while the red portion is located inside. When a portion of the cone of divergent light from the radiator passes through an achromatic prism we obtain an almost parallel light beam which can be focused by a lens into a narrow band of white light with its center of gravity around the position of a given wavelength. The vertex angle α of the achromatic prism is determined from the extinction equation of first order dispersion $d\psi/d\lambda = 0$ written for the case of perpendicular emission from the radiator and minimum prism angle of deviation, where $\psi(\lambda)$ is the direction in which the radiation is viewed after emerging from the prism. We now give this equation, which appears with a misprint in Mather's paper:

$$\frac{d\psi}{d\lambda} = \frac{d\psi}{dn}\frac{dn}{d\lambda}$$

$$= \left\{\frac{1}{(n^2\beta^2-1)^{1/2}} - \frac{2\sin(\alpha/2)}{(1-n^2\sin^2(\alpha/2))^{1/2}}\right\}\frac{dn}{d\lambda} = 0. \qquad (2)$$

Hence

$$\sin\frac{\alpha}{2} = \{n_0^2 + 4(n_0^2\beta_0^2 - 1)\}^{-1/2}, \qquad (3)$$

where α is the vertex angle of the prism, n_0 is the refractive index for the wavelength λ_0 satisfying the condition $d\psi/d\lambda = 0$, and β_0 is the approximate mean velocity. Equation (3) can be used when the radiator and prism are made of the same material.

Proton velocities were determined by precise measurement of the emission angle of Vavilov-Cerenkov radiation from protons passing through Plexiglas. The choice of radiator material and thickness was dictated by the experimental conditions. Plexiglas was chosen as a substance with low atomic number, low density and relatively low dispersion, thus reducing multiple scattering and slowing down.

Preliminary energy measurements[11] were per-

formed with a proton beam of low density (10^6 protons · cm^{-2} sec^{-1}) and, consequently, a relatively thick radiator. Radiation was registered by a camera with a 1:1.5 Yupiter-3 objective on "Negative-A" cine film of 50-unit GOST (All-Union State Standard) sensitivity. With a radiator thickness of 2.9 g/cm^2 in the beam direction exposures lasted 3 minutes.

The present measurements were obtained after the system of proton beam extraction was changed,[12] increasing the intensity more than 100 times. The exposures used with a beam of 4×10^7 protons · cm^2 sec^{-1} ranges from 3 to 5 seconds.

MEASUREMENT OF REFRACTIVE INDEX

An IRF-3 refractometer was used to measure the refractive index of a few samples taken from the same piece of material as the radiator. The absolute refractive index for $\lambda = 5461$ A was $1.4926 \pm 5 \times 10^{-4}$. This value of n was confirmed after the experiment by measurements performed on samples cut from the radiator in the region traversed by the proton beam.

EXPERIMENTAL RESULTS

The emission angle of Vavilov-Cerenkov radiation in Plexiglas was found to be $\theta = (34° 0.5') \pm 3'$ for $\lambda = 5461$ A. The proton energy was calculated from

$$E = E_0 \left\{ \frac{n \cos\theta}{(n^2 \cos^2\theta - 1)^{1/2}} - 1 \right\}, \qquad (4)$$

where E_0 is the proton rest mass, 938.2 Mev,[13] and n is the refractive index of Plexiglas for $\lambda = 5461$ A.

According to the measured values of θ and n the proton energy at the center of the radiator was 654.9 Mev. When account is taken of slowing down up to the middle of the radiator the mean proton energy becomes 658.4 Mev ($\Delta E = 3.5$ Mev for t = 1.45 g/cm^2 and $-dE/dx = 2.40$ Mev/g · cm^{-2}). This was the average of three energy measurements: $E_1 = 658.0$ Mev, $E_2 = 657.6$ Mev, and $E_3 = 659.6$ Mev.

The error in the energy values includes errors in measuring θ and n. $\Delta E_1/\Delta\theta$ and $\Delta E_2/\Delta n$ were determined by means of the relations

$$\frac{\Delta E_1}{\Delta\theta} = E_0 \frac{(n^2\beta^2 - 1)^{1/2}}{\beta\,(\beta^{-2} - 1)^{1/2}}, \quad \frac{\Delta E_2}{\Delta n} = E_0 \frac{\beta^2}{n\,(1 - \beta^2)^{1/2}}. \qquad (5)$$

In our case $\Delta E_1 = \Delta\theta \times 0.59$ Mev when $\Delta\theta$ is given in minutes, and $\Delta E_2 = 2 \times 10^3 \Delta n$ Mev. For $\Delta\theta = \pm 3.0$, $\Delta n = \pm 5 \times 10^{-4}$, n = 1.493 and $\beta \approx 0.81$ we obtain $\Delta E_1 = \pm 1.8$ Mev and $\Delta E_2 = \pm 1$ Mev.

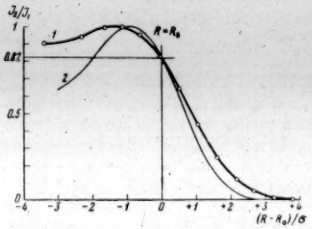

FIG. 2. Ratio of ionization currents in chambers M_1 and M_2 as a function of $(R - R_0)/\sigma$: 1 – experimental curve, 2 – curve computed by Mather and Segrè[6] ($\sigma = 2.68$ g/cm^2).

The total energy error, which is the root mean square of the given errors, is $\Delta E = \pm 2.1$ Mev.

MEASUREMENT OF TOTAL RANGE IN COPPER

While measuring the mean proton energy we also measured the total range in copper (Fig. 1b). A collimated proton beam of 20 mm diameter traversed ionization chambers M_1 and M_2, which were separated by copper blocks. The ionization ratio J_2/J_1 in the chambers was measured as a function of copper thickness.

Ionization chamber M_1 was filled with helium to 0.5 atmos and M_2 was filled with argon to 1 atmos. Measurements at the end of the absorption curve were performed in steps of 1.5 g/cm^2. A portion of a Bragg curve is shown in Fig. 2. Comparison of the experimental curve 1 for J_2/J_1 with the theoretical curve 2 of Mather and Segrè[6] yields the energy spread of the proton beam.

The calculation of the theoretical proton range spread due to energy loss fluctuations took a relativistic factor into account:[7]

$$(\Delta R_1)^2 = 4\pi z^2 e^4 N Z \int_0^E \left(\frac{dE'}{dR'}\right)^{-3} \frac{1 - \beta^2/2}{1 - \beta^2}\, dE', \qquad (6)$$

where $\beta = \beta(E')$ is the particle velocity. For a copper absorber and proton energy E = 658 Mev we have $\Delta R_1 = 2.55$ g/cm^2.

Besides the indicated spread we took into account range fluctuations due to multiple scattering fluctuations:[14]

$$\frac{\overline{s^2} - \bar{s}^2}{t^2} = \frac{E_s^4 E_0^2}{2a_{\text{ef}}^2 (E_0 + \mu)^4} \sum_{n=0}^{\infty} \frac{n+1}{(n+2)^2} \left(\frac{E_0 - \mu}{E_0 + \mu}\right)^{2n}, \qquad (7)$$

where

$$a_{\text{ef}} = \pi m L_i(E_1) / 2Z\alpha L_r, \qquad (8)$$

$L_i(E_1)$ and L_r being given below [see Eq. (9)]. A calculation using (7) and (8) gives

$$\Delta R_2 = \{(\overline{s^2} - \bar{s}^2)/t^2\}^{1/2} = 0.83 \text{ g/cm}^2.$$

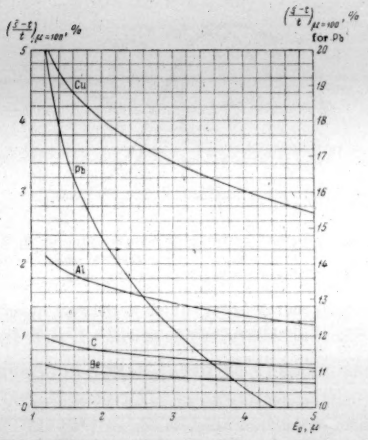

FIG. 3. Multiple-scattering corrections of experimental range as a function of total energy E_0 in units of μ, for different elements and incident particles with rest mass $\mu = 100$.

The total spread $\sigma = \{(\Delta R_1)^2 + (\Delta R_2)\}^{1/2}$ was calculated to be 2.68 g/cm^2 whereas the experimental value was $\Delta R_e = 1.30\,\sigma = 3.48$ g/cm^2. The difference, given by $\{(\Delta R_e)^2 - \sigma^2\}^{1/2} = 2.2$ g/cm^2, yields ± 3.8 Mev as the energy spread of the proton beam. It was shown by Mather and Segrè that the mean range corresponds to the ordinate on the Bragg curve for which $J_2/J_1 = 0.82\,(J_2/J_1)_{max}$. The effective range corresponding to this ordinate is 255.9 g/cm^2. When we take into account the thin copper foils enclosing ionization chambers M_1 and M_2, and the internal electrodes, with a total thickness of 0.50 g/cm^2, the total range becomes 256.4 g/cm^2, which was corrected for multiple scattering of protons in the absorbers. The measured total thickness of an absorber is the effective range, i.e., the range measured in a straight line, whereas the actual range of a particle is somewhat longer because its trajectory is distorted through multiple Coulomb scattering. The total length of the twisted trajectory is the true range which should be used in determining the energy from the range-energy relation.

The difference between the true range $\bar{s}$ and the effective range t was calculated by Pomeranchuk.[14] $(\bar{s}-t)/t$ is given by

$$\frac{\bar{s}-t}{t} \approx \frac{Z\alpha E_0^2 E_0}{\pi m\,(E_0+\mu)^2}\,\frac{L_r}{L_i(E_1)}\,\ln\frac{(E_0+\mu)^2}{4E_0\mu}, \qquad (9)$$

where Z is the charge of absorber atoms, E_0 is the total particle energy, m is the electron rest mass in Mev, $E_S = m\,(4\pi 137)^{1/2} = 21$ Mev, μ is the incident particle rest mass, L_r is the "radiation logarithm" and $L_i(E_1)$ is the "ionization logarithm" for an intermediate energy E_1. E_1 is given by*

$$E_1 = \frac{1}{2}\left[E_0 - \mu - 2\mu\ln\frac{E_0+\mu}{2\mu} + K\mu b^2\right] \times \left[\ln\frac{(E_0+\mu)^2}{4E_0\mu}\right]^{-1}, \qquad (10)$$

where

$$K = \int_0^E (1 - b^2 e^{-2t})^{-1}\,(1 - be^{-t})^{-2} e^{-2t}\,t\,dt, \qquad b = (E_0 - \mu)/(E_0 + \mu). \qquad (11)$$

The values of E_1 (in μ) for E_0 from 1.2 to 5 μ are as follows:

E_0 =	1.2	1.3	1.4	1.5	1.6	1.7	1.8	1.9
E_1 =	1.11	1.16	1.20	1.26	1.31	1.35	1.40	1.44
E_0 =	2	2.2	2.5	3	3.5	4	4.5	5
E_1 =	1.49	1.58	1.70	1.90	2.07	2.27	2.63	2.63

Figure 3 gives the values of $(\bar{s}-t)/t$ for C, Al, Be, Cu and Pb. The ordinates give $(\bar{s}-t)/t$ as a percentage for a particle with the rest mass $\mu = 100$ Mev; for other masses we use the relation $\frac{\bar{s}-t}{t} = \frac{100}{\mu}\left(\frac{\bar{s}-t}{t}\right)_{\mu=100}$ The abscissas give the initial total energy in units of μ. The accuracy of $(s-t)/t$ based on (9), (10), and (11) is $\sim 1\%$.

For 658-Mev protons ($E_0 = 1.7\,\mu$) the correction for multiple scattering of protons in copper is 0.46%; the mean range is then 257.6 g/cm^2.

Accuracy of the range value is determined by the accuracy in measuring the absorber thickness and by the uncertainty resulting from variation of mean proton energy during the course of the experiment. Several checks of the range during the experiment showed that the deviation did not exceed ± 0.2 g/cm^2, while the total error including that involved in measuring absorber thickness amounted to ± 0.3 g/cm^2.

DETERMINATION OF IONIZATION POTENTIAL FOR COPPER

Precise measurements of proton energy and range permit determination of the ionization potential for copper by means of the relation

$$R = \int_0^E \left(\frac{dE}{dx}\right)^{-1} dE, \qquad (12)$$

where R is the total range (in grams per cm^2) of protons with initial energy E_0 (in Mev) in a

*In Pomeranchuk's paper the expressions for E_1 and K contain errors which have been corrected here.

given substance, and dE/dx is the ionization loss in units of Mev/g·cm^{-2}, which is determined from Bethe's formula in the form[15]

$$-\frac{dE}{dx}=\frac{2\pi e^2e^4n}{\rho mc^2\beta^2}\left\{\ln\frac{2mv^2T}{I^2(1-\beta^2)}-2\beta^2-\frac{2}{Z}\sum_{K,L}C_i-\delta\right\}, \quad (13)$$

where e and m are the electron charge and mass, ez is the charge of the incident particle, n is the number of electrons per cm^3 of stopping material with density ρ, $\beta = v/c$ is the particle velocity, I is the mean ionization potential of stopping atoms, ΣC_i represents corrections for particle velocities comparable to electron velocities in K, L, ... shells, δ is the Fermi density correction,[16] for copper $2\pi me^4/\rho mv^2 = 0.0701$ Mev/g·cm^{-2}, and T — the maximum energy transferred by an incident particle to an atomic electron — is given by

$$T=(E^2-\mu^2c^4)/\mu c^2(\mu/2m+m/2\mu+E/\mu c^2), \quad (14)$$

where E is the energy of the incident particle with rest mass μ. For heavy particles with $\mu \gg m$ we have $T \cong 2mv^2/(1-\beta^2)$.

The corrections C_i which take into account electron binding in K and L shells have been calculated by Walske.[17,18] The sum of these corrections reduces the calculated energy loss of particles in matter with Z = 30 by ~4% for 5-Mev protons, by 0.16% for E_p = 250 Mev and by 0.05% for E_p = 660 Mev. In our case the total correction reduces I_{Cu} by 3 ev.

The most accurate calculation of the density effect in different substances is that of Sternheimer.[19] The empirical expression for δ is

$$\begin{aligned}\delta&=4.606X+C+a(X_1-X)^m \quad \text{for } X_0<X<X_1,\\ \delta&=4.606X+C \quad \text{for } X>X_1, \quad (15)\end{aligned}$$

where X = log (pc/μ), and pc and μ are the particle momentum and rest mass, X_1 is the value of X above which δ is linearly dependent on X, X_0 is the value of X below which $\delta = 0$ and is determined from the velocity $\beta_0 = \{1+\sum_i f_i/\nu_i^2\}^{-1/2}$ (where f_i is the oscillator strength of a given transition, which is equal to the number of electrons on the given level divided by the total number of electrons in the atom), and $\nu_i = E_i/\hbar$ is the i-th transition frequency. For copper we have C = −4.13, 10a = 0.99, m = 3.40, X_1 = 3, and X_0 = 0.00.* The value of δ is ~0.12% for 400-Mev protons and ~0.25% for 600-Mev protons. In our case the density effect reduces I_{Cu} by 2 ev.

I_{Cu} was computed as follows. Equation (12) was integrated numerically to determine R_1 and R_2 for two different ionization potentials close to the experimental value, such as I_1 = 375 ev and I_2 = 300 ev. We thus determined $\Delta R/\Delta I = (R_2-R_1)/(I_2-I_1) = 0.126$ g/cm^2 ev, and the ionization potential satisfying initial energy E_0 = 658 Mev and range R_0 = 257.6 g/cm^2 was I_{Cu} = 305 ev. It should be noted that the range was calculated assuming velocity independnce of the ionization potential I_{Cu}. The computed proton range for I_{Cu} = 377 ev is 8.84 g/cm^2 greater than the experimental range.

The error in determining the ionization potential by the foregoing method is a combination of the errors in determining the initial proton energy and the range. The rms error in the range is ±1.2 g/cm^2, which leads to the uncertainty $\Delta I_{Cu} = \pm 10$ ev in the ionization potential. The value I_{Cu} = 305 ± 10 ev obtained in the present experiment agrees well within the limits of error with Mather and Segrè's value of 310 ev for 340-Mev protons.

RELATIVE STOPPING POWERS OF DIFFERENT SUBSTANCES FOR 635-Mev PROTONS

The experimental arrangement is shown in Fig. 1. The thicknesses of the specimens were such that the ionization losses of protons were ~50 Mev, so that the measured relative stopping powers refer to protons with the energy 635 Mev at the center of a specimen. The experiment determined the amount of copper which would slow down protons of 635 Mev mean energy to the same extent as 1 g/cm^2 of a given substance. For this purpose we measured $q = (A_{Cu}-B_{Cu})/C_i$, where A_{Cu} is the total proton range in the copper absorber, B_{Cu} is the thickness of copper absorbers remaining after a fraction of the copper had been replaced by the test substance, and C_i is the thickness of the test specimen. Range values were obtained from the mean range; the results are given in Table II.

TABLE II

Element	q	I, ev	Bloch constant $I_0 = I/Z$, ev
H	3.016	15	15
Be	1.167	61±6	15.3
C	1.268	85±8	14.2
Fe	1.034	273±22	10.5
Cu	1.000	305±10	10.5
Cd	0.887	468±35	9.8
W	0.794	680±50	9.2

*C, a, m, X_1 and X_2 were calculated by Sternheimer in connection with a formula containing the value of the copper ionization potential I_{Cu} = 279 ev which was obtained by Bakker and Segrè.[5] The δ correction to I_{Cu} is so small that the difference between I_{Cu} = 279 ev and the value I_{Cu} = 307 ev used in the present paper has been disregarded.

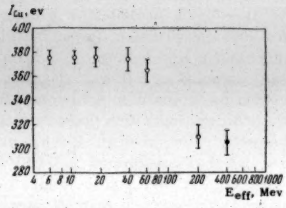

FIG. 4. Ionization potential of copper as a function of proton effective energy. • – present data (E_{eff} – proton effective energy).

Ionization potentials were calculated assuming that $I_{Cu} = 305$ ev for $E_0 = 635$ Mev. Corrections were included for the binding of K and L electrons as well as for the density effect. The final expression for ionization potentials based on measurements of relative stopping powers is

$$\ln I = 13.788 - \frac{A}{Z} 3.670q - \frac{1}{Z}\sum_{K,L} C_i - \frac{\delta}{2}, \quad (16)$$

where A is the atomic weight.

Relative stopping powers were measured with an accuracy of about ±1%; therefore the accuracy of the ionization potentials is ±10%, since $\Delta I/I \approx (\Delta q/q) \ln (2mv^2/I)$. The stopping power of hydrogen* was determined from the $CH_2 - C$ difference.

DISCUSSION OF RESULTS

The paper of Sachs and Richardson[8] contains a graph showing values of the ionization potential for copper that were determined by different methods for different proton energies, as a function of the effective energy, which when I is determined for the entire range equals 0.6 of the initial energy E if we assume $I = I_0 - a \ln E$. The data of the present work for 400 Mev are included in the same graph for comparison (Fig. 4). Up to 60 Mev the ionization potential of copper is ~ 380 ev, while at higher energies it is reduced to ~ 310 ev.

As indicated above, in the present paper I_{Cu} was calculated assuming it to be independent of proton velocity. I_{Cu} was also calculated with the experimental data for low energies taken into account. For proton energies from 0 to 125 Mev we assumed the constant value $I_{Cu} = 377$ ev; from 125 to 660 Mev we assumed 305 ev. The theoretical and experimental ranges could be brought into agreement only by the value 301 ev for I_{Cu} in the 125 – 660 Mev range. No other assumptions were made regarding the energy dependence of I_{Cu}; the assumptions already adopted yield 300 ev as the ionization potential of copper for a mean proton energy of about 400 Mev. The observed drop of 70 – 80 ev in this proton energy range is outside the limits of experimental error and requires an explanation.

If we assume that an ionization potential cannot depend on the velocity of an incident particle the decrease of the former as the particle energy rises can either indicate some additional form of loss at high energies which is not included in Bethe's theory, or that some effect reduces the loss at low energies.

The variation of I with energy may possibly be associated with the effective density at low energies. Indeed, the calculations of ionization potentials from absolute measurements of dE/dx at low energies have usually employed an expression which neglected the Fermi density effect, although this effect does not disappear at low energies. Sternheimer[19] has shown that the reduction of ionization loss $\Delta(dE/dx)$ at low energies due to the density effect is given by

$$\Delta\frac{dE}{dx} = \frac{2\pi n (ze^2)^2}{\rho m v^2}\sum_i f_i \ln\left(\frac{l_i}{\nu_i}\right)^2 = \frac{2\pi n (ze^2)^2}{\rho m v^2}\delta, \quad (17)$$

where $l_i = (\nu_i^2 + f_i)^{1/2}$ with all other notation as in (13). In first approximation, i.e., using transition frequencies ν_i taken from Sommerfeld's tables,[20] we have $\delta(Cu) = 0.26$. $\Delta(dE/dx)$ for protons with ~ 20 Mev in copper may be a few percent.

In calculating the reduction of loss at high proton energies we must use the formula[19]

$$\Delta\frac{dE}{dx} = \frac{2\pi n (ze^2)^2}{\rho m v^2}\left[\sum_i f_i \ln\frac{v_i^2 + l^2}{v_i^2} - l^2(1-\beta^2)\right], \quad (18)$$

where l is defined by

$$\beta^{-2} - 1 = \sum_i f_i/(v_i^2 + l^2).$$

In this case for 600-Mev protons with the same values of the frequencies ν_i, $\Delta(dE/dx)$ for copper is only 0.1% and increases to 3% at 2 Bev.

The reduction of dE/dx by a few percent at low energies is equivalent to reduction of the copper ionization potential by 20 – 30%, i.e., to ~ 300 ev. It should be noted that the value of the sum $\delta = \sum f_i \ln(l_i/\nu_i)$ is uncertain because the transition frequencies ν_i are uncertain. If a more exact calculation eventually shows that the correction factor δ actually has the given value, there will hardly be any reason for regarding I as velocity dependent. I could then be given a constant

*For hydrogen the accuracy of q is ~ 5% and that of I_H is ~ 50%.

value at 10 — 11 Z ev and the density effect would be taken into account in calculations of energy losses over the entire energy range. In the event of the contrary result the reduction of I at higher energies must be accounted for in some other manner.

In conclusion we wish to thank Yu. D. Prokoshkin and I. M. Vasilevskiĭ for discussions and for acquainting us with preliminary data on absolute losses for 650-Mev protons.

[1] S. Livingston and H. A. Bethe, Revs. Modern Phys. **9**, 264 (1937).

[2] S. K. Allison and S. D. Warshaw, Revs. Modern Phys. **25**, 779 (1953).

[3] D. O. Caldwell, Phys. Rev. **100**, 291 (1955).

[4] N. Bloembergen and P. J. van Heerden, Phys. Rev. **83**, 561 (1951).

[5] C. J. Bakker and E. Segrè, Phys. Rev. **81**, 489 (1951).

[6] R. Mather and E. Segrè, Phys. Rev. **84**, 191 (1951).

[7] J. Lindhard and M. Scharff, Kgl. Danske Videnskab. Selskab, Mat.-fys. Medd. **27**, 15 (1953).

[8] D. C. Sachs and J. R. Richardson, Phys. Rev. **89**, 1165 (1953).

[9] R. L. Mather, Phys. Rev. **84**, 181 (1951).

[10] P. A. Cerenkov, Dokl. Akad. Nauk SSSR **2**, 451 (1934).

[11] V. P. Zrelov, Otchet IYaP. Akad. Nauk SSSR (Report, Institute for Nuclear Problems, U.S.S.R. Acad. Sci.) 1954.

[12] Dmitrievskiĭ, Danilov, Denisov, Zaplatin, Katyshev, Kropin, and Chestnoĭ, Приборы и техника эксперимента (Instruments and Measurement Engg.) **1**, 11 (1957).

[13] Cohen, Layton, Du Mond, and Rollett, Revs. Modern Phys. **27**, 363 (1955).

[14] I. Ya. Pomeranchuk, J. Exptl. Theoret. Phys. (U.S.S.R.) **18**, 759 (1948).

[15] R. M. Sternheimer, Phys. Rev. **91**, 256 (1953).

[16] E. Fermi, Phys. Rev. **57**, 485 (1940).

[17] M. C. Walske, Phys. Rev. **88**, 1283 (1952).

[18] M. C. Walske, Phys. Rev. **101**, 940 (1956).

[19] R. M. Sternheimer, Phys. Rev. **88**, 851 (1952).

[20] A. Sommerfeld, Atombau und Spektrallinien I (Russ. Transl.) GITTL, Moscow, 1956, p. 212. [Vieweg, Brunswick, 1955].

Translated by I. Emin
126

INVESTIGATION OF THE CORE OF EXTENSIVE AIR SHOWERS

S. N. VERNOV, N. N. GORYUNOV, G. T. ZATSEPIN, G. V. KULINKOV, Yu. A. NECHIN, Z. S. STRUGALSKIĬ, and G. B. KHRISTIANSEN

Moscow State University

P. N. Lebedev Physics Institute, Academy of Sciences, U.S.S.R.

Submitted to JETP editor July 21, 1958

J. Exptl. Theoret. Phys. (U.S.S.R.) **36**, 669-681 (March, 1959)

A new method of investigation of individual air showers is described. The method is applied to the study of the core of extensive air showers. Some preliminary experimental data, indicating the existence of large fluctuations of the energy flux of the electron-photon and of the nuclear-active components in the core of extensive air showers are presented.

THE necessity of studying individual extensive air showers (EAS) simultaneously at different depths was recently pointed out by D. V. Skobel'tsyn. The present work is an attempt to carry out this idea in connection with the study of the core of EAS.

A detailed study of EAS, carried out in recent years in a series of experiments,[1-4] showed that the lateral distribution of particles in EAS does not vary at different altitudes of the atmosphere and, at any given altitude is, as a whole, described by the electromagnetic cascade theory in the central regions of the shower up to small distances of ~1 m from the shower axis. An analysis of the data pointed to the conclusion that a nuclear cascade is present in the shower, and that the main part of the energy flux of the nuclear cascade should be concentrated at small distances from the axis (~1 m), forming the so-called core of the EAS.[5]

The study of the core region of EAS therefore becomes of special interest, since, in that region, one can observe the specific features of the nuclear-cascade process. In connection with the above, an array for a detailed study of the core of the EAS was constructed. The array for the study of the core of the EAS, which forms a part of the large array set up at Moscow State University for a comprehensive study of EAS, is described below, and preliminary results of measurements, illustrating the method used, are presented. A full report on the experimental results and their analysis will be given in future articles.

DESCRIPTION OF THE ARRAY

The array makes it possible to obtain detailed data on the electron-photon and nuclear-active components in the core of the EAS. A block diagram of the array is presented in Figs. 1a and 1b. The array consists of a diffusion chamber with an area of 0.64 m^2, 124 ionization chambers displayed on a hodoscope and screened by a special absorber, and 672 hodoscope Geiger-Müller counters of various sizes.

A picture of the distribution of the shower-particle flux (mainly electrons) is obtained near the shower axis by means of the diffusion chamber and of the hodoscope counters. This data can be used to determine the number of particles in the shower and also the position of its axis, by means of the well-known method.[2,6] This can be done to an accuracy of ~1 m using the hodoscope-counter data, and to an accuracy of a few centimeters if the axis falls within the diffusion chamber. It is also evident that the diffusion chamber gives a full picture of the directions of single shower particles, and therefore makes it possible to determine the direction of the particle flux near the shower axis.

The distribution of the energy flux carried by the electron-photon component near the shower axis was determined by means of the first row of ionization chambers, consisting of 60 cubic chambers with the dimensions 25×25×25 cm and screened from above by 2.5 cm of lead. In fact, the multiplication coefficient for such a thickness of lead is, with sufficient accuracy, proportional to the mean energy of the particles (electrons and photons) at a given distance from the shower axis, if the energy lies in the range 10^8 to 10^{11} ev. A direct inspection of the distribution of the flux in the first row of ionization chambers makes it possible to determine the position of the shower axis with an accuracy of the same order of magnitude as the dimensions of the chambers.

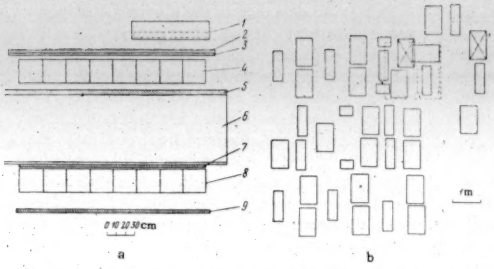

FIG. 1a. Position of the diffusion chamber, ionization chambers and layers of the absorbers. 1 – diffusion chamber (the sensitive region is shown by the dashed line); 2 – Al, 0.3 cm; 3 – Pb, 2.5 cm (28.2 g/cm²); 4 – ionization chambers; 5 – Pb, 5 cm; 6 – graphite, 73 cm (120 g/cm²); 7 – Pb, 2.5 cm; 8 – ionization chambers; 9 – Pb, 2 cm; between the layers 2–3 and 6–7 – wood, 2.5 cm; between 3–4 and 7–8 – plywood, 0.4 cm.

FIG. 1b. Position of ionization chambers, diffusion chambers (shown by dotted line), and Geiger-Müller counters. Large rectangles – effective areas of trays consisting of 12 counters 330 cm² each; middle sized rectangles – 24 counters 100 cm² each; small rectangles – 24 cm² each. The counters in the trays are placed at the distance of half a diameter one from another. The trays denoted by a cross contain a group of counters connected to a six-fold coincidence circuit. The plane of the counters is at a distance of 1.15 m from the first row of ionization chambers 4.

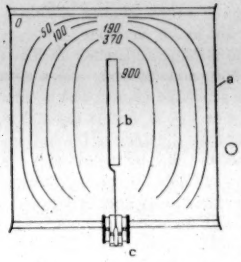

FIG. 2. Cross section of the ionization chamber, a – walls; b – collecting electrode; c – insulator.

The distribution of the energy flux carried by the nuclear-active component in the shower core can be determined by means of the second row, consisting of 64 ionization chambers placed under a composite of 7.5 cm lead, 70 cm of graphite (120 g/cm²), and 2.5 cm of lead. The electron-photon component of the shower coming from the air is almost entirely absorbed, and thus does not reach the lower row of chambers.

Nuclear-active particles incident upon the absorber initiate a nuclear cascade inside it. In each nuclear collision, part of the energy is irreversibly transferred to photons through production and consecutive decay of π^0 mesons. The thickness of the layer of lead placed above the graphite amounts to half of the mean free path of nuclear-active particles, and the thickness of the graphite to 1.7 of the mean free path. Therefore, the energy transfer from nuclear-active particles to photons occurs mainly in graphite, in which the energy is accumulated, since electron-photon cascades develop weakly in graphite. The graphite therefore acts as a singular transformer of the energy of the nuclear-active particles into the energy of the electron-photon component. The development of the electron-photon cascade occurs mainly in the lower layer of lead, and, after it has traversed this layer, the cascade reaches approximately its maximum. The number of electrons falling on the lower chambers is thus proportional to the energy transferred to π^0 mesons in graphite and consequently, on the average, to the energy of the primary nuclear-active particle. The efficiency of such a method for recording of high-energy nuclear-active particles was discussed earlier,[7] and this method was used by Dmitriev, Kulikov, and Khristiansen.[8] The values of energy $E_{n\text{-}a}$ of the nuclear-active component as listed below, are calculated from the relation[9]

$$E_{n\text{-}a} = 5 \cdot 10^8 n \text{ ev},$$

where n is the number of relativistic particles recorded in the lowest row of chambers.

It can be seen from Fig. 1a that the diffusion chamber is screened from below by 3 mm of Al from the electrons and photons scattered by the lead. The ionization chambers of the first and second rows are so to speak in a lead gap, since they are screened by lead also from below. This makes it possible to interpret the experimental data using the cascade theory for heavy elements without any limitations (accounting only for corrections due to the absorption in the walls of the chambers). In calculating the value of the energy flux E of the electron-photon component incident upon the chamber, it was assumed, following Ivanenko,[10] that

$$E = 10^8 n' \text{ ev},$$

where n′ is the number of relativistic particles recorded in the chamber.

The diffusion chamber used in the array measures 800×800×60 mm, where 60 mm is the height of the sensitive layer. The bottom of the chamber is kept at −50°C, and is maintained constant within ±1°, across the area of the bottom and also with respect to time, by means of a special two-stage compression freon refrigerating system. The lid of the chamber is kept at +20°C. The chamber is filled with alcohol vapor. A grid is placed above the sensitive volume and kept at a potential of −40 v with respect to the bottom of the chamber. The use of such an electric field leads to a decrease of the duration of tracks, and considerably lowers the background, which amounts to 50 tracks per grid unit. The sensitive layer is illuminated through a yellow filter by means of pulsed lamps ITS-1500, which are triggered by the master pulse. The sensitive layer is photographed by a stereoscopic camera with 72 mm base through the glass lid of the chamber of 1.5 g/cm^2 thickness.

The block of ionization chambers consists of 124 cubic chambers 25×25×25 cm. Each of the chambers is connected to its own channel of the electronic recording system for the pulse amplitudes. The ionization chambers are filled with a mixture of spectrally pure argon (98%), and chemically pure nitrogen (2%) to the pressure of 830 mm Hg, with preliminary evacuation (and simultaneous heating) to 10^{-4} mm Hg. The cross section of the chamber is shown in Fig. 2.* The walls of the chambers are made of stainless steel 2 mm thick, with the exception of the top wall which is 1 mm thick. The collection electrode is cylindrical in shape, 10 mm in diameter and 100 mm long. A cross section through the equipotential surfaces, for a potential difference between the collecting electrode and the walls equal to 900 v which corresponds to the chosen working voltage† is shown in Fig. 2. The picture of the equipotential surfaces was obtained by the electrolytic-tank method as used by Goryunov and Erlykin.[11] From this picture we can determine the velocity of collection of electrons for local ionization in various places of the chamber. For a uniform volume ionization, the velocity of collection of electrons is such that, within 2×10^{-5} sec, the pulse attains 80% of its amplitude.

*For convenience and speed of filling, the ionization chambers were built as blocks of four chambers with a single outlet for filling.

†The saturation of the electron current in the chamber, for volume ionization equivalent to the passage of 10 000 relativistic particles during the collection time of 20 μsec, produced by a preparate of Co^{60}, occurs at a potential difference of 300 v.

Our basic demands of the electronic circuits are: a possibility of recording pulses with a wide range of amplitudes, and stability of operation. In the experiment, the pulse amplitudes of the ionization chambers are recorded as following: (For a more detailed description see reference 12): A preamplifier with an amplification factor of ~100 is attached to each chamber. The pulse was transmitted by a cathode follower through a cable to a nonlinear amplifier, and then to a switching tube. Whenever this tube receives the master pulse simultaneously, the amplified pulse of the chamber is fed to a storage circuit, and is then collected by means of an electronic switch which serves all 124 chambers. The pulse arrives at the vertical deflection plates of a CRO tube, delayed with respect to the master pulse that triggers the time base by an amount different for each channel. The total picture of the distribution of pulse amplitudes in all ionization chambers is recorded photographically. By means of the setup described, it is possible to record pulses produced by the passage of 5 to 40,000 relativistic particles through the chamber. The lower limit is determined by the amplifier noise and especially that in the pre-amplifier. Evidently, the introduction of a non-linear amplifier, which makes a wider dynamical range possible, leads to a worse accuracy in the determination of the pulse heights. However, for 85% of the range, the accuracy is not worse from 10%, and for 15% of the range it amounts to ~25%.

The chambers were calibrated by photographing pulses from single relativistic particles traversing the volume of the chamber. The pulse on the grid of the first tube of the pre-amplifier, produced by the passage of a single relativistic particle through the chamber, amounts to ~20 μv.

The comparatively low frequency of the observed events, and the ensuing long time needed for measurements makes a systematic check of the operation of the whole electronic system and of the ionization chamber a necessity. All amplifiers and recording channels were calibrated regularly every 24 hours. To this end, pulses of given amplitude from a pulse generator were fed simultaneously through a small capacity to the grids of the first tubes of all pre-amplifiers. From the obtained photographs of calibration pulses of various amplitudes, amplitude characteristics of the separate channels were constructed, and these are used for evaluating the oscillograms. One example of such amplitude characteristics is shown in Fig. 3. Tests showed that the amplitude characteristics did not change substantially during a long period of operation. By means of the above method of calibration, one can check the

amplifying-recording chain as a whole, including the input capacity of the pre-amplifier. The condition of the gas in the chambers which was not checked in the above-described procedure, was tested periodically once very half year. The chambers were irradiated by γ-rays from a Co^{60} source in a fixed geometry, and the value of fluctuations of the electron current in the chamber was measured.

The hodoscope consists of 264 counters with an area 330 cm^2 each, 312 counters with an area of 100 cm^2, and 96 counters with an area of 24 cm^2 each. All counters were connected to HK-7 hodoscope circuits using cold thyratrons of type MTK-90. The average resolving time of the circuit is 15 μsec.

The whole array is triggered by pulses produced whenever an EAS passes through the array, and also when large bursts are produced in the blocks of ionization chambers. The selection of EAS is determined by the requirement of a simultaneous discharge of six groups of counters with an area of 0.132 m^2 each, from those placed 1 m above the first row of ionization chambers. Such a method of selection makes it possible to record showers with a number of particles $N \geq 10^4$, and with axes that are incident, on the average, at a distance of several tens of meters from the array.

The bursts are selected in the following way: The sum of the amplitude of the pulses from all 124 chambers should correspond to the ionization produced in the working volume of the chambers by a vertical flux of 1000 relativistic particles. Such an ionization can be produced by (1) a flux of EAS particles with an axis close to the array, (2) by high-energy nuclear-active particles, (3) by radiation showers from high-energy μ mesons, and (4) by nuclear disintegrations in the gas and in the walls of the chambers. The greater fraction of the bursts selected by the master-system are connected with the passage of EAS and, in their number, showers of comparatively low density whose cores contain high-energy nuclear-active particles. We note that the fourth cause listed above is not significant in view of the following properties of the selection system: The addition of the pulses of the chambers takes place after their nonlinear amplification. For the production of the masterpulse, it is necessary that the amplitude of the total pulse is bigger than a certain value (see Fig. 3, point A). Because of the nonlinearity, it is clear that the required amplitude of the pulse can be reached when several chambers each produce a smaller total burst than that due to a single chamber. When the total ionization is distributed among two or more chambers so that in one of them the observed ionization amounts to not more than half of the total, then the threshold corresponds to 1000 relativistic particles. For ionization in one of the chambers only, the threshold corresponds to 4000 relativistic particles. Nuclear disintegrations thus lead to the production of a master pulse only when the produced ionization is bigger than 4000 relativistic particles.

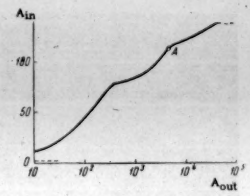

FIG. 3. Amplitude characteristics of one of the channels of nonlinear amplification. The x axis represents the value of ionization in number of relativistic particles, the y axis – the amplitude in mm of the vertical deflection on the CRO tube.

At the same time, bursts produced by nuclear-active particles and μ mesons will cause the appearance of a master pulse with 100% probability if the ionization produced by them is bigger than 1300 relativistic particles since, in that case, at least 10% of the ionization will be produced in adjoining chambers in view of the wide angular distribution of particles of the electron-photon showers in lead. Radiation showers from μ mesons (the third cause) amount to about 20% of all bursts. These bursts are rarely accompanied by shower, and, in the case of μ mesons going close to the horizontal plane, the typical elongation of the burst occurs.

The master pulse from the six-fold coincidence circuit is fed after transformation to switching tubes to the electronic switch and the CRO tube of the block of ionization chambers, to the controls of the flash for the diffusion chamber, and to the master system of the hodoscope HK-7. The flashing of the lamps of the diffusion chamber takes place approximately 0.4 sec after the arrival of the master pulse, which corresponds to the time of growth of the tracks to optimal size. The master pulses are fed to hodoscope circuits with a delay of the order of several μsec, so that they arrive in the middle of the working range of these circuits. The triggering by means of big pulses from the ionization chamber of the two-stage type,[8] which is necessary since the rise time of ionization-chamber pulses is larger than the operation cycle of the hodoscope system. The master pulse is produced every time the total pulse is bigger than the value corresponding to the passage of 300 relativistic particles. However, the hodoscope is photographed

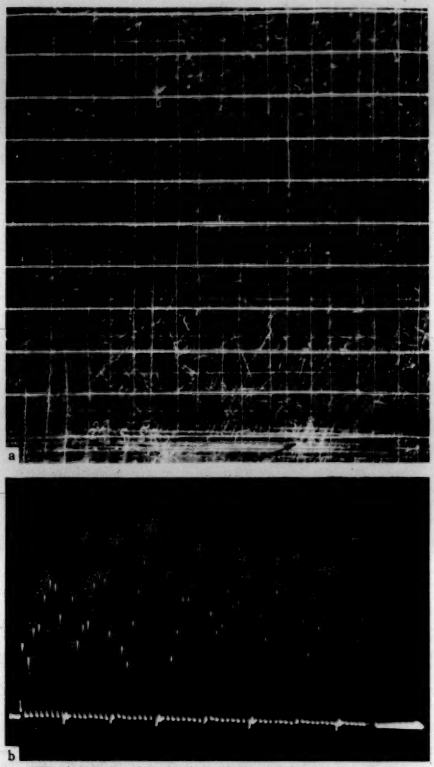

FIG. 4a. A photograph of the diffusion chamber at the moment of passage of an EAS (the arrow indicates the position of the axis.

FIG. 4b. Oscillogram of pulses from 64 ionization chambers during the passage of the core of an EAS through the array.

only when the pulse in the chambers is bigger than 1000 relativistic particles. The dead time of ionization chambers and of hodoscope counters is not greater than 1 sec. The dead time of all elements of the array is not bigger than 10 sec, which makes possible a 90% efficiency of the operation of the array for the chosen frequency of master pulses.

RESULTS AND CERTAIN EXPERIMENTAL PROBLEMS

Up to the present, all elements of the array have been operated for about 1300 hours. During this time, more than 10,000 EAS were recorded. A portion of these events correspond to the incidence of the axes of EAS upon the array. A photograph of the diffusion chamber and an oscillogram of the pulses from ionization chambers corresponding to the arrival of an EAS are shown in Fig. 4.

We shall consider first the densest of the recorded showers. If a shower develops according to the electromagnetic cascade theory, then the axes of high-energy showers may be located within a very small area due to the large density of particle and the presence of high-energy particles which produce a density gradient already at small distances from the axis. For a real shower containing a nuclear cascade, the core of high-energy showers can be studied in greatest detail, since in the development of such showers, a big role is played by nuclear-active particles of energies sufficiently high to concentrate near the axis within a region which is smaller than the dimensions of the array.

When the axis of an EAS passes through the first row of ionization chambers, which records the particles produced as the result of the multiplication of the electrons and photons of the shower in lead, then one can expect an essentially homogeneous distribution of ionization over the whole area occupied by the chambers, together with the presence of a region where the ionization will attain a maximum value.* The axis of the shower can then be determined from the condition that the particle density is maximum at the axis, and is symmetrical about it. We used this method of axis location.

During the 1000 hours of operation of the array, we recorded 28 events interpreted as the passage of EAS with a number of particles $N > 10^5$ through the first row of ionization chambers.†

The number of events observed in which the shower axis fell on the array according to the chosen method of analysis may be compared with

*The difference between a real shower and an electron-photon shower can be observed from the influence, at small distances from axis, of the nuclear scattering of π^0 mesons, producing the electron-photon cascade, as a result of which the axis of the shower may be less sharp than in the case of electron-photon showers. The angular deviation of a photon of energy E from the shower axis amounts to E_0/E. The angle of the π^0 meson in its production is of the order of $\sim \mu_\pi c^2/E_{\pi^0}$. Therefore a photon of given energy, produced directly by a π^0 meson, has a larger angle than a similar photon radiated by an electron.

†The position of the axis can be determined without ambiguity if we consider the incidence of axis into a region surrounded by a single external row of ionization chambers. The area of this region is 2.25 m². Out of the 28 axes, 15 fell into this region. This number corresponds to the one expected, since the area covered by all chambers amounts to 4 m².

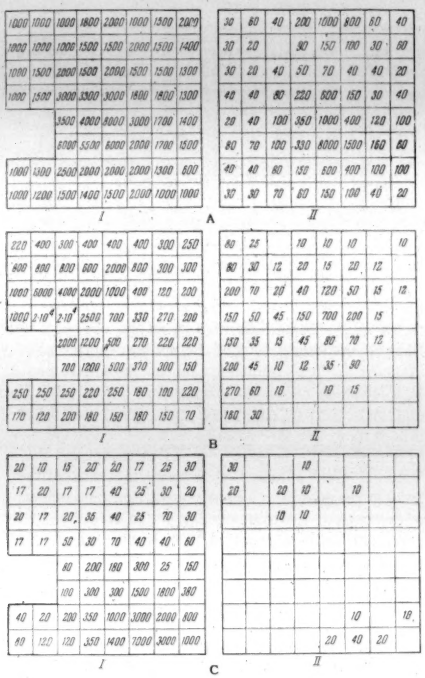

FIG. 5. Distribution of ionization expressed in the number of relativistic particles passing through a chamber, in the first row of ionization chambers (I), and in the second row of ionization chambers (II). A – passage of the shower core with total number of particles $N = 5 \times 10^8$, the lateral distribution of energy flux (first row) $\sim 1/r$; B – $N = 1.3 \times 10^8$, lateral distribution of energy flux $\sim 1/r^2$; C – $N \approx 10^6$, the lateral distribution of energy flux $\sim 1/r^3$.

that which one would expect according to the data on the absolute intensity of showers.[6] According to reference 6, during 1000 hours one would expect 29 axes of showers with a number of particles $N > 10^5$ incident upon the area of 4 m^2, which is in agreement with the data given above.

In all cases, a large gradient of the energy-flux density of the electron-photon component near the axis is observed in the first row of ionization chambers, the degree of which is, however, different for different events. If the gradient is represented by a power law $1/r^k$ for $30\ cm < r < 1\ m$, then the exponent can be within the limits of 1 to 3. The main number of events correspond to values of the exponent $1 < k < 2$. Examples of the observed distribution are shown in Fig. 5.

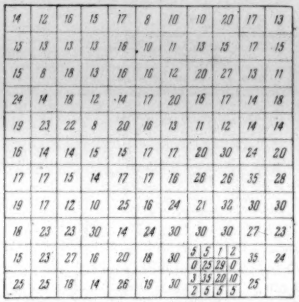

FIG. 6. Distribution of shower particles in the diffusion chamber for an event in which the axis of an EAS with total of particles equal to 2×10^6 passed through the chamber. Total number of shower particles in the chamber – 2308. The number of shower particles is given for cells with an area of 48 cm^2 (12 cm^2 around the axis).

The actual distribution of the energy flux may be steeper since, owing to the large height of the chambers, and the wide angular distribution of particles in lead, the particles from smaller distances may arrive at greater distances from the axis. However, the effect is qualitatively small for the distribution $1/r^k$ for $k < 3$, and for an isotropic distribution of shower particles in lead.

In a number of cases, it was possible to obtain more detailed data on the flux of particles near the core, and on the structure of the shower at still smaller distances from the axis, by means of the diffusion chamber. Out of 28 cases of incidence of the axis of showers on ionization chambers, a marked gradient of particle density is observed in the diffusion chamber for three cases. The distribution of particles in these cases was measured looking at the pictures in a stereoscope. One of these pictures is shown in Fig. 6.

The position of the axis in case of dense showers can be determined from a direct comparison of the particle density in various places in the chamber. The axis of the showers should therefore be found within the limits of such a region where the number of shower particles is larger by an amount greater than the Poisson fluctuation than that in the surrounding adjacent regions of the same dimensions.* The dimensions of this region in the observed three cases were smaller than 5 cm.

The distribution of the particle flux around the shower axis in the diffusion chamber for the observed three cases was found to be $\rho(r) \sim 1/\sqrt{r}$

*Therefore, the accuracy in determining the position of the axis depends essentially on the shower size.

TABLE I

Angle with the axis, ϑ^0	Number of particles in a circle with radius		
	$r = 15$ cm	$r = 30$ cm	$r = 45$ cm
0—2	34(34)	74(54)	74(54)
2—4	62(62)	90(76)	90(76)
4—6	3(3)	25(14)	55(27)
6—8	0(0)	24(12)	46(22)
8—10	0(0)	4(2)	20(10)
10—16	1(1)	8(4)	28(12)

TABLE II

No.	N_s	$E_{e\text{-}p} = N_s 2\beta$ (ev)	$E_{n\text{-}a}$ (ev)	$E_{e\text{-}p}$ in the core (ev)	$\frac{E_{n\text{-}a}}{E_{e\text{-}p}}$	$\frac{E_{e\text{-}p\ core}}{E_{e\text{-}p}}$
1	$5 \cdot 10^5$	$7.2 \cdot 10^{13}$	$9.3 \cdot 10^{12}$	$1.2 \cdot 10^{13}$	0.13	0.17
2	$1.8 \cdot 10^5$	$2.6 \cdot 10^{13}$	$1.3 \cdot 10^{12}$	$1.7 \cdot 10^{12}$	0.049	0.065
3	$2 \cdot 10^5$	$2.9 \cdot 10^{11}$	$4.6 \cdot 10^{11}$	$5.2 \cdot 10^{12}$	0.016	0.18
4	$1.1 \cdot 10^5$	$1.6 \cdot 10^{13}$	$8.5 \cdot 10^{11}$	$8.4 \cdot 10^{11}$	0.053	0.052
5	$2.5 \cdot 10^5$	$3.6 \cdot 10^{13}$	$7 \cdot 10^{11}$	$3.1 \cdot 10^{12}$	0.019	0.14
6	$1.3 \cdot 10^5$	$1.9 \cdot 10^{13}$	$1.7 \cdot 10^{12}$	$7.9 \cdot 10^{12}$	0.092	0.41
7	$1.2 \cdot 10^5$	$1.7 \cdot 10^{13}$	10^{13}	$4 \cdot 10^{12}$	0.59	0.23
8	10^5	$1.4 \cdot 10^{13}$	$1.1 \cdot 10^{12}$	$3.6 \cdot 10^{12}$	0.078	0.26
9	$2.1 \cdot 10^5$	$3 \cdot 10^{13}$	$8.5 \cdot 10^{11}$	$3.6 \cdot 10^{12}$	0.028	0.12

for 5 cm < r < 40 cm, and $\rho(r) \sim 1/r$ for 40 cm < r < 80 cm. The lateral distribution of the energy flux obtained for these cases from the first row of ionization chambers was close to $1/r^2$, which is in agreement with the lateral distribution of particle densities going as $1/r$.

The angular distribution of shower particles and the direction of the particle flux near the shower axis was found for one case by means of the diffusion chamber. The angular distribution with respect to the direction of the axis in this event is shown in Table I. The direction of tracks (ϑ, φ) was determined with an accuracy of 1°. The direction of the axis (ϑ^0, φ^0) was taken as a direction of the particle flux in the region of the axis. The method of the determination of the axis region has been described above. With an accuracy up to 1°, the directions of the trajectories of these particles were identical. The angle with respect to the shower axis θ^* was determined from the usual formula

$$\cos\theta^* = \sin\vartheta^0 \sin\vartheta \cos(\varphi^0 - \varphi) + \cos\vartheta^0 \cos\vartheta.$$

Therefore, the accuracy of the determination of the direction of single trajectories amounted to 2°.

It can be seen that the angular distribution in the shower core is rather broad and the contribution of large angles increases substantially with increasing r (see Table I). A problem arises, therefore, as to the accuracy with which the direction of the particle flux at a certain distance from the shower axis reflects the direction of the axis. In view of the very broad angular distribution of shower particles, we cannot find a vector of a mean direction for the given shower with sufficient accuracy to maintain that it is parallel to the shower axis. Thus, at a distance of about half a meter, the formally determined mean direction forms an angle of ~ 5° with the axis.

We shall mention briefly the data on the nuclear-active component. If the position of the axis is known from the first row of ionization chambers, and its direction from the diffusion chamber with an accuracy to 5°, then we can find the position of the axis from the second row of chambers and study the presence of high-energy nuclear-active particles in the immediate vicinity of the shower axis. Data on the energy flux of the nuclear-active and electron-photon component around the shower axis in a circle of radius 1 m are given in Table II. The energy of the nuclear-active component was determined from the size of the burst in the second row of chambers in the same way as in reference 8. Table II (last column) shows that the ratio of the energy carried by the electron-photon component of the core to the total energy of the electron-photon component in the shower has a large spread.

It can also be seen from Table II, where a part of the mentioned 28 events is discussed, that showers with the same total number of shower particles can have a substantially different amount of high-energy nuclear-active particles in the core and, correspondingly a different total energy of these particles in the core. In a number of events, around the point of intersection of the shower axis or in the prolongation of the axis, one observes one high-energy nuclear-active particle carrying the main fraction of the energy of the selected region near the axis. In a number of cases, the energy is carried by several nuclear-active particles of smaller energies. Therefore, the array makes it possible to study the structure of the core of high-energy showers in sufficient detail. This is not the case for the study of cores of EAS of small energies.

In the case of low energy showers, the density of particle flux near the axis may be insufficient for any accurate location of the axis. It is even more important that, in showers of low density, the nuclear cascade consists of particles of lower energies which suffer a more marked angular spread. It is evident that a marked deviation will also be suffered by π^0 mesons which start the electron-photon cascade, a fact which can cause an ambiguity in the axis location. Therefore, for the core and position of the axis of an individual

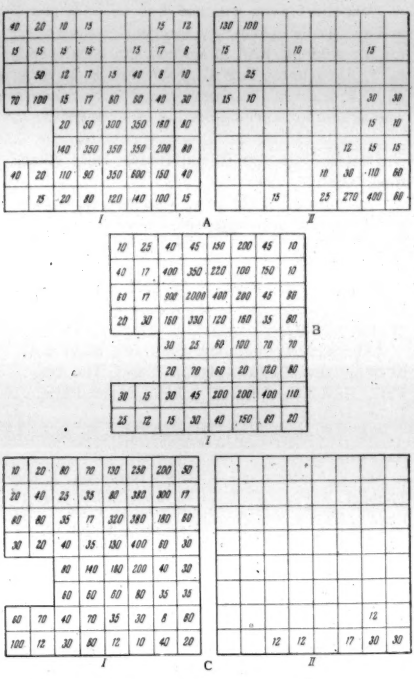

FIG. 7. Distribution of ionization expressed as the number of relativistic particles passing through a chamber in the first row of ionization chamber (I), and in the second row of ionization chambers (II). A – passage of the core of a shower with $N = 10^4$, lateral distribution of energy flow first row $\sim 1/r^2$; B – passage of a core of a shower with the total number of particles $N = 10^4$, lateral distribution of energy flux (first row) $\sim 1/r^2$. No ionization in the second row of ionization chambers (or smaller than the value of the amplifier noise); C – passage of a core of a shower with a total number of particles $N = 2 \times 10^4$, lateral distribution of energy flux (first row) $\sim 1/r$.

shower have no meaning, and the showers can be studied only statistically. In connection with this, we have limited ourselves in the study of low energy showers to EAS of medium size with a number of particles in the range of $2 \times 10^4 - 6 \times 10^4$.

During the operation time of the array (1000 hours), we found 40 events where the axis of such showers fell on the area of the first row of ionization chambers. This number is in good agreement with the one expected according to reference 6. Examples of observed cases are shown in Fig. 7.

All events correspond to the presence of a sufficiently sharp gradient and a region with maximum density of particles. Lateral distribution of energy flux suffers large fluctuations from $1/r$ to $\rho(r)$ close to $1/r^3$ for 30 cm < r < 1 m, and the events with the given $\rho(r)$ are found approximately as frequently as for showers of higher energies discussed above.

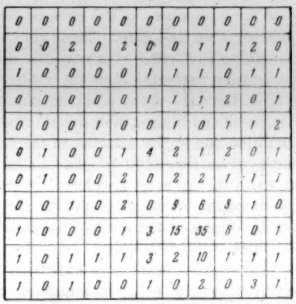

FIG. 8. Distribution of the flux of shower particles in the diffusion chamber accompanying the passage of an axis of an EAS with $N = 3.5 \times 10^4$ through the chamber.

It should be noted that, in a number of cases at a certain distance from the axis, we observed local increases in particle density connected with the fact that high-energy electrons and photons deviate from the shower axis. These increases in density are more noticeable in showers of medium size than in showers of large size, since the axis region in the first group is less rich in energy. However, in the showers discussed above, the energy density of the electron-photon component near the axis is still sufficiently high to localize the axis with an accuracy up to the dimensions of the chamber. This is not the case in a number of events where the axis is located in the diffusion chamber and where the particle density flux, and not the energy flux, is measured. Out of 40 cases of incidence of axis on the first row of ionization chambers, in six events the axis fell on the part of the row which is placed above the diffusion chamber. One of these is shown in Fig. 8. It can be seen that the particle density is so low that it can be distinguished from the background only at distances not greater than 20 – 30 cm from the axis. In a number of events, the axis may be localized satisfactorily even without the data from the first row of ionization chambers. In a number of events, these data are absolutely necessary in view of the small flux of particles. In the first case, there is a sharp increase in density near the axis, from $1/r$ to $1/r^{1.5}$ in the range from 40 to 5 cm while, in the second case, the increase is slower, or even non-existent. The energy fluxes carried by the

nuclear-active component of the core of the observed shower also fluctuate. These fluctuations, however, can be partly due to a possible deviation of nuclear-active particles forming the nuclear cascade from the axis of the electron-photon shower at distances bigger than the size of the array, and also due to fluctuations in the fraction of the energy transferred to π^0 mesons in nuclear interactions in the layer of graphite.

The study of the cores of individual showers at sea-level, by means of the method described above, therefore showed the following phenomena:

1. For EAS with a number of particles $> 10^5$ in the core of the shower ($r < 1$ m) nuclear-active particles are observed, the total energy of which is on the average, of the order of the energy of the electron-photon component at the same distances from the axis. However, in individual showers, the magnitude of the ratio of the energy of the nuclear-active component ot the energy of the electron-photon component can have different values.

2. The density of the energy flux carried by electron-photon component of EAS in showers with $N \geq 10^5$ particles shows a marked increase down to 30 cm from the axis (for the majority of showers). The dependence of the density of the energy flux of the electron-photon component on the distance from the axis of the shower cannot be expressed by a general function for all showers. From the found cores in the distance range of $30 - 100$ cm from the axis, the decrease of the energy flux density with distance varies from $1/r$ to $1/r^3$.

3. The energy of the electron-photon component of showers contained in the core region of the shower ($r < 1$ m), normalized to the number of particles in the shower, has a big spread, and can vary from shower to shower by a factor of up to 10.

4. The energy of the nuclear-active component in showers with $N > 10^5$ also has no non-ambiguous correspondence with the number of particles in the shower, and suffers a large spread.

The authors would like to express their deep gratitude to Academician D. V. Skobel'tsyn for his great help in the work and his constant interest; to V. V. Borisoglebsky for constant help; to Prof. N. A. Dobrotin for his help and discussion of results; and also to the group of co-workers on the array for the study of EAS in Moscow State University: A. T. Abrosimov, S. S. Glagolevskiĭ, B. V. Subotin, A. D. Erlykin, A. B. Kamnev, and E. N. Sosnovets who helped in carrying out the experiments.

[1] Vavilov, Nikol'skiĭ, and Tukish, Dokl. Akad. Nauk SSSR **93**, 233 (1953).

[2] Abrosimov, Bedniakov, Zatsepin, Nechin, Solov'eva, Khristiansen, and Chikin, J. Exptl. Theoret. Phys. (U.S.S.R.) **29**, 693 (1955), Soviet Phys. JETP **2**, 357 (1956).

[3] Dobrotin, Zatsepin, Nikol'skiĭ, Sarycheva, and Khristiansen, J. Exptl. Theoret. Phys. (U.S.S.R.) **19**, 666 (1955).

[4] Abrosimov, Goriunov, Dmitriev, Solov'eva, Khrenov, and Khristiansen, J. Exptl. Theoret. Phys. (U.S.S.R.) **34**, 1077 (1958), Soviet Phys. JETP **7**, 746 (1958).

[5] G. T. Zatsepin, The Oxford Conference on EAS, Harwell, 1956.

[6] G. V. Kulikov and G. B. Khristiansen, J. Exptl. Theoret. Phys. (U.S.S.R.) **35**, 635 (1958), Soviet Phys. JETP **8**, 441 (1959).

[7] Anishenko, Zatsepin, Rosental, and Sarycheva, J. Exptl. Theoret. Phys. (U.S.S.R.) **22**, 143 (1952).

[8] Dmitriev, Kulikov, and Khristiansen, Suppl. Nuovo cimento (in press).

[9] Abrosimov, Dmitriev, Massal'skiĭ, Kulikov, and Khristiansen, J. Exptl. Theoret. Phys. (U.S.R.R.) **36**, 751 (1959); Soviet Phys. JETP, this issue, p. 000.

[10] I. P. Ivanenko, Dokl. Akad. Nauk SSSR **107**, 819 (1956), Soviet Phys. "Doklady" **1**, 231 (1956).
J. Exptl. Theoret. Phys. (U.S.S.R.) **31**, 86 (1956), Soviet Phys. JETP **4**, 115 (1957).

[11] N. N. Goryunov and A. D. Erlykin, Приборы и техника эксперимента (Instruments and Meas. Engg.) No. 1 (1959) (in press).

[12] N. N. Goryunov, Приборы и техника эксперимента (Instr. and Meas. Engg.) No. 3 (1959) (in press).

Translated by H. Kasha
127

SOVIET PHYSICS JETP VOLUME 36 (9), NUMBER 3 SEPTEMBER, 1959

SOME FEATURES OF MULTIPLET FERROMAGNETIC RESONANCE IN FERRITES

V. N. LAZUKIN

Moscow State University

Submitted to JETP editor July 23, 1958

J. Exptl. Theoret. Phys. (U.S.S.R.) **36**, 682-689 (March, 1959)

Preliminary results are presented of the observation of multiplet ferromagnetic resonance in inhomogeneously magnetized single-crystal and polycrystalline ferrite samples. The inhomogeneous magnetizations required for the observation of this effect were produced mainly by the inhomogeneity of the demagnetizing fields of the investigated samples. Some features are noted of the absorption spectra observed under various conditions.

1. INTRODUCTION

USUALLY in the interpretation of experimental results on ferromagnetic resonance in magnetic semiconductors it is assumed that the magnetic fields acting on the sample create within its volume homogeneous magnetizations. This demands the fulfillment of two conditions: (1) the sample must be of such a shape that its demagnetizing field is homogeneous (sphere, ellipsoid, thin plate), and (2) it must be placed in those regions of the resonant cavity where there are no gradients of the high frequency magnetic field. The physical meaning of these conditions is clear: when they are fulfilled all the spins in the sample precess with the same phase. The violation of either of these conditions must lead to the appearance of inhomogeneities either in the constant or in the high frequency magnetizations of the substance under investigation and to a considerable complication of the picture of resonance absorption. These complications manifest themselves in the asymmetry of the observed resonance curve, in its broadening, and in the splitting of the resonance line into several lines of different width and intensity. The last effect which was observed comparatively recently received the not very appropriate name of multiplet ferromagnetic resonance.

The features indicated above do not fall within the framework of the usual theory,[1] and may be understood only on the basis of additional assumptions. In particular, the physical nature of multiplet ferromagnetic resonance is associated with the concept of the existence within the magnetized ferromagnetic medium of a spectrum of spin waves. As is well known,[2] the essence of this concept consists of the following. If the ferromagnet is placed into an external magnetic field, the small but unavoidable inhomogeneities of magnetization can be represented in the form of a superposition of spin waves propagated at a certain angle with respect to the direction of the field. In an infinite medium the spin waves are plane and form a continuous spectrum, while in the case of a sample of finite size the waves are described by more complicated functions (for example, in the case of a spheroid by Legendre functions) and form a discrete spectrum — the totality of the different vibration modes. Each mode corresponds to a certain eigenfrequency and to a certain structure of the magnetic field, and, moreover, cases of degeneracy are possible when the same frequency corresponds to several different types of oscillations which differ in their field structure.

Among all possible types of oscillation of a given sample there exists at least one whose frequency coincides with the frequency of the "normal" resonance given by Kittel's formula.* For large wave numbers (high frequency oscillations) the solutions obtained for an infinite medium may be approximately extended to the case of a sample of finite size. The practically important case of long spin waves is arrived at by the simultaneous solution of the equations of motion and of Maxwell equations without taking into account the exchange interaction and the propagation phenomena. This "magnetostatic" case was discussed by Walker[3] who calculated the low frequency spectrum of the characteristic oscillations of a spheroid.

The action of an external high-frequency field of appropriate structure on a ferromagnetic sample with inhomogeneous magnetization should result in resonance absorption at several frequencies, or, if the frequency is constant, at different values

*Cases are possible when Kittel's resonance does not occur.

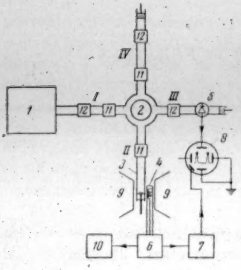

FIG. 1. Diagram of the apparatus: 1 – microwave generator; 2 – separating ring; 3 – segment of wave guide with piston and sample; 4 – fluxmeter coil; 5 – detector; 6 – fluxmeter; 7 – audio-frequency amplifier; 8 – oscillograph; 9 – electromagnet; 10 – fluxmeter wave meter; 11 – matching devices; 12 – ferrite isolators.

of the constant magnetic field. Such phenomena have been observed in specially designed experiments,[4,5] and have been partially studied.

Conditions necessary for such observations are clear from the foregoing: the high-frequency magnetic field of appropriate structure may be produced in the sample by violating either one of the conditions noted above necessary for the observation of "normal" resonance. Moreover, depending on the structure of the oscillating field set up in the sample the resonance absorption spectrum, in general, will be different all other conditions remaining the same.

In the papers quoted above the field of required symmetry was produced by violating the second of the foregoing conditions; the ferrite sphere[4] or disc[5] were placed in regions of the resonance cavity with the largest gradients of the microwave magnetic field. In the experiments described here the greater part of the observations was carried out with the first condition violated: the inhomogeneity of the high-frequency magnetization was produced by the inhomogeneity of the demagnetizing field of the samples.

Undoubtedly the interpretation of the results in the second case is much more difficult than in the first. However, having in mind the importance of the phenomena of multiplet ferromagnetic resonance both from the point of view of the physics of these phenomena in ferrites, and also from the point of view of many technical applications (first of all for the construction of a ferrite microwave amplifier) it appears to us to be useful to study all possible features of this phenomenon under various conditions.

2. EXPERIMENTAL PROCEDURE

The experiments were performed principally at a frequency $\nu_1 = 9200$ Mcs, and partially at $\nu_2 = 14640$ Mcs, by means of usual videospectroscopes[6,7] with a transmitting (at the ν_1 frequency) and a reflecting (at the ν_2 frequency) resonator at room temperature; some observations were taken at liquid-nitrogen temperature.

For sufficiently large samples, whose dimensions unavoidably could not be made smaller, we have tried a method of measurement which does not require continuous tuning associated with the frequency drift of the resonator containing the spheroidal sample. This circuit (Fig. 1) is based on the use of a separating ring which is the analogue of a double-T junction. Power from a stabilized klystron generator is brought through arm I to the separating ring in which it is split in half and enters arms II and IV, and if all the arms leading to the ring are matched it does not reach arm III. Arm II is connected to a section of a waveguide terminated by a shorting piston upon which the sample is mounted. The power reflected from arm II is divided between arms I and III; to the latter is connected a tune detector. Ferrite isolators mounted in arms I, III, IV decouple the generator from the ring and do not allow power reflected from arms III and IV to reach the generator. The system described above is equivalent to a semi-infinite line having the property that half of the power reflected from the load is brought to the detector and does not go back into the line. The system has lower sensitivity than a videospectroscope with a resonator but, as is shown by comparative measurements, the sensitivity is reduced by an amount which is insufficient to prevent the recording of even weak resonance signals from a strongly absorbing sample.

The constant magnetic field of intensity up to

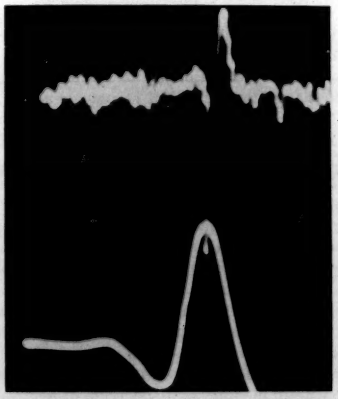

FIG. 2. Measurement of line position and width by means of a double beam oscillograph; lower beam-ferromagnetic resonance signal, upper beam-proton resonance signal in the same magnetic field.

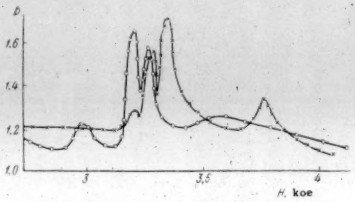

FIG. 3. Absorption by a MnZn polycrystalline ferrite sphere in positions: o – II and x – IV.

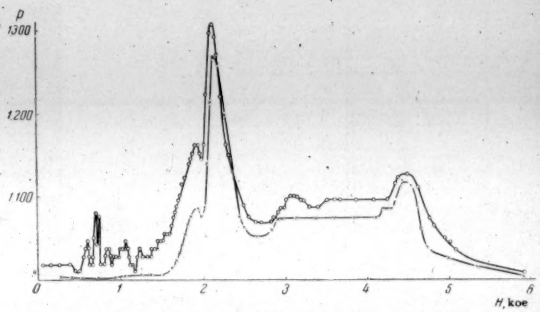

FIG. 4. Absorption by a polycrystalline ferrite ring in positions: x – I and o – III.

9000 oe was produced by an electromagnet with a pole diameter of 160 mm and a variable gap from 20 to 50 mm. The magnetic field was modulated with an amplitude up to 300 oe at 50 cps. The position of resonance absorption signals was determined by means of a proton fluxmeter whose coil was placed in the field of the same intensity as the sample. The proton resonance signal was applied either to the intensity control of a single beam oscillograph, or to the second beam of a double beam oscillograph. In the latter case the method of measurement of the position of resonance signals in the field and of their width is clear from the appended photograph (Fig. 2). The absorption curves were recorded point by point with continuous monitoring of the nature of the signals by means of the oscillograph.

Observations were made on the following samples: (a) single crystals of MnMg-ferrite in the shape of a hemisphere of diameter from 2 to 5 mm; (b) polycrystalline Mn, MnZn, and MnMg-ferrites with different impurities in the shape of rings of external diameter D from 2 to 5 mm, internal diameter d from 1 to 3 mm and of height h from 1 to 3 mm. The different ferrite samples had closely similar properties: a rectangular hysteresis loop, $H_c = 0.1 - 1.5$ oe, B_r from 1900 to 2500 gauss and B_m from 2000 to 2700 gauss.

In order to compare the results with those of other authors, we made several measurements using 2-millimeter spheres of polycrystalline MnZn-ferrite.

The samples were placed in three positions: position I — on the resonator axis at a distance of $\lambda/2$ from the shorting piston, this position corresponds to the condition of observation of "normal" resonance; position II — near the narrow wall at a distance of $\lambda/2$ from the piston; position III — on the shorting piston at its center. Moreover, in the case of spherical ferrites the spectrum was observed in position IV on the resonator axis at a distance of $\lambda/4$ from the piston. In positions I, III and IV the sample could be rotated about the resonator axis through any arbitrary angle which could be measured with an accuracy of the order of 10′.

3. RESULTS OF OBSERVATION

Figure 3 shows sections of microwave absorption curves at frequency ν_1 for a MnZn-ferrite sphere of 1.90 mm diameter in positions II and IV respectively in the range of fields from 2.8 to 4.0 koe. Both curves are very similar to the curves of White and Solt[4] taken at the same positions. The difference consists only in a certain displacement of the maxima towards weaker fields which, undoubtedly, is associated with the difference in the value of B_m, and in the less smooth shape of our curves. In addition to the principal maxima appearing in both curves at fields from 1100 to 7500 oe there are groups of considerably weaker maxima of different intensity and width also in agreement with the results quoted earlier. There does not seem to be any particular ordering in the position of the weak signals. Following Walker,[3] who has examined the results of White and Solt, the maxima in the curves of Fig. 4 may be explained as resonances of the long wavelength modes: (1,2,0) and (2,2,0) in the first case and (1,3,0) and (0,2,0) in the second case.

Both in the case of polycrystalline and of single crystal samples which differ in shape from spheroids the most complicated spectra are obtained in position III. Figure 4 shows absorption curves for a 3-millimeter ring of MnMg-ferrite ($H_c = 0.25$; $B_r = 1900$; $B_m = 2000$) at frequency ν_1 taken in positions I and III. We can see the similarity of the two curves in fields > 1900 oe: the three most

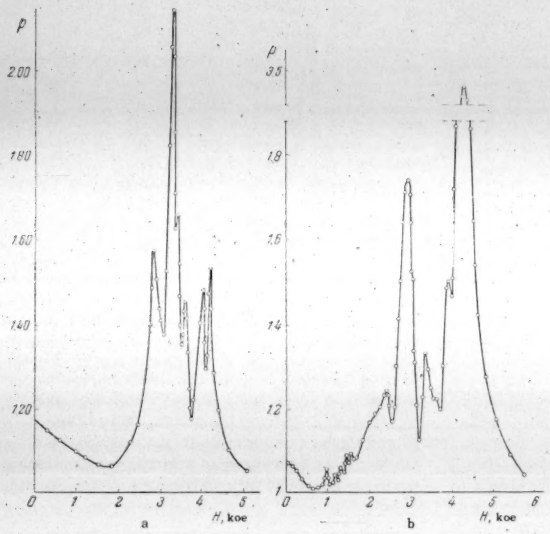

FIG. 5. Absorption by a MnMg-single crystal: a – in position II, b – in position III.

prominent maxima are preserved in going over from position I to position III practically without any change in position, and only with a slight change in intensity and width. However, in fields < 1900 oe the curves are quite different: in position III we observe a large number of less intense and much narrower absorption maxima, which do not appear in position I. Another characteristic feature is the appearance on this curve of a number of short horizontal stretches, which sometimes form a sort of a ladder, along which even with the most careful observations using a sensitive radiospectroseope it is not possible to observe any extremal points.

Figure 5 shows absorption curves for a MnMg-ferrite single crystal (hemisphere of diameter ~4 mm) taken in positions II and III. Here we find large differences both in weak and in strong fields. In fields < 2000 oe these differences are similar to those which occur in the case of a polycrystalline sample: in position III narrower and less intense signals appear which are not observed in position II.

The difference in absorption curves for the same sample placed at different points of the resonator volume are due to the difference in structure of the microwave magnetic field excited in the sample. In position I the characteristic structure of this field is due to the inhomogeneous demagnetizing field of the sample; in position II there is added to this the inhomogeneity of the magnetic component of the microwave field in the given region of the resonator; in position III the screening action of the conducting surface of the piston becomes evident which does not permit the flux of the microwave magnetic field outside the sample to complete its path in the same symmetric manner as in position I, which leads to a redistribution of the microwave magnetization inside the sample and produces a more complicated inhomogeneity in the magnetization, and thereby a structure of the microwave field which is essentially different from the structure in position I. It is natural to assume that in such cases the solution of the magnetostatic problem is considerably more complicated than the one in the cases considered in reference 3, if it is at all possible.

In the curves of Fig. 4 and 5b we can see a small number of additional signals appearing in position III in weak fields; actually, if observations are made with an oscillograph, a considerably greater number of weak signals is observed (in some cases up to 50 or so) and they occur at fields up to the order of 8 koe, however, the most prominent ones among them occur in the range from 400 to 1500 oe. In positions other than III a large number of weak signals is also observed but they occur in fields of not less than 1200 – 1500 oe

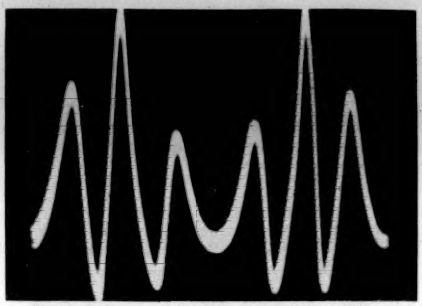

FIG. 6. Ferromagnetic resonance signals in a single crystal in a field of 585 oe (position III).

and, as a rule, are less intense than those observed in position III. An example of an oscillogram recorded in this position is given in Fig. 6. It gives us an idea of the shape, width and relative intensity of some of these signals. The widths of the signals fluctuate from 15 to 100 oe, while the intensity of the signals exceeds noise by a factor of from ~1 to 40. We did not succeed in noting any ordering in the position, width or intensity of these signals, other than the fact that separate groups are formed containing 3 – 8 signals (rarely more) which differ somewhat in their characteristics.

The position and the other characteristics of weak signals are quite different for different samples which are the same with respect to their composition, working, shape, and size. It can be asserted that the details of the "microstructure" of an absorption spectrum (particularly in weak fields < 2000 oe) are of an individual nature, and are not reproduced from sample to sample, although for the same sample placed under the same conditions the spectrum is very reliably reproducible. It appears that this provides a basis for the assertion that a considerable part of the weak signals of an absorption spectrum is due to the small inhomogeneities in the magnetic structure of the ferrites, which apparently unavoidably exist in each sample, and which have an individual character even in the case of exactly the same technique of preparation and working of the sample.

The picture of resonance absorption both in single crystals and in polycrystalline samples is very sensitive to the orientation with respect to the acting fields. All the absorption lines of the MnMg single crystal (with the exception of a small number of very weak ones) exhibit practically the same angular dependence (Fig. 7) which is in agreement

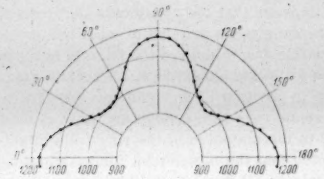

FIG. 7. Angular dependence of weak resonance signals in a single crystal. Rotation in the (100) plane; H in oe is plotted horizontally.

with theory and with previously known data obtained for the "normal" ferromagnetic resonance line.

The absorption lines of polycrystalline samples exhibit different angular dependence: while the fundamental signals like those shown in Fig. 5a do not depend on orientation, weak signals, particularly in fields < 1500 oe, are very sensitive to orientation. As the sample is rotated the signals move in the field, change their shape, width, and intensity, merge and again separate. Figure 8 presents the angular dependence of the position of two absorption signals in a ferrite ring, whose spectrum was given above, which are of interest due to the fact that at certain values of the field and angle they merge into one. The signals have a somewhat different angular dependence which is, however, in general characteristic of a single crystal. This suggests that such signals in a polycrystalline ferrite are due to local inhomogeneities situated at different depths below the surface, which have a different shape and which allow the setting up of vibrational modes of different structure. In the presence of strongly inhomogeneous demagnetizing fields in the sample the resonances of these modes may exhibit an angular dependence.

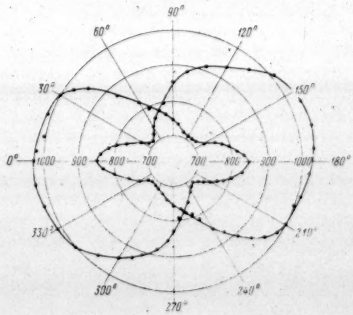

FIG. 8. Angular dependence of two weak resonance signals for a MnMg polycrystalline ferrite ring; H in oe is plotted horizontally.

It appears that the hypothesis that the weak resonance signals are due to local inhomogeneities within the volume of the sample is supported by the following experiment. A ferrite ring was set up in position III and was screened from above by a round very thin conducting plate of diameter equal to the diameter of the ring. We might have expected that the microwave field could penetrate only to a small depth below the external cylindrical surface of the ring, and that only those signals would survive on the absorption curve whose production was due to the inhomogeneity in the thin external layer of the sample. Indeed, only those signals remain on the absorption curve which appear in fields < 1600 oe and which do not change in shape or width. At the same time, signals in high fields (with the exception of a small number of very weak ones) disappear completely.

A few trial experiments at frequency ν_2 at room temperature and at liquid-nitrogen temperature using polycrystalline MnMg (with an admixture of ZnO)-ferrite ring (D = 1.06; d = 1.02; h = 1.00) in position III show that the intensity of weak signals varies but little with frequency. If the temperature is lowered to liquid nitrogen temperature the intensity increases by a factor of approximately 3 – 5.

The results enumerated above show that the phenomenon of multiplet ferromagnetic resonance is quite a complicated one depending on many conditions. Its further study may turn out to be useful both from the point of view of understanding the properties of ferrites, and also for technical applications.

The author expresses his sincere gratitude to A. I. Pil'shchikov for a number of very valuable discussions.

[1] N. Bloembergen, Proc. IRE **44**, 1259 (1956) (cf. also the collection of articles "Ferromagnetic Resonance," in Russian, IIL, Moscow, 1952).

[2] C. Herring and C. Kittel, Phys. Rev. **81**, 869 (1951). T. S. Ament and G. T. Rado, Phys. Rev. **97**, 1558 (1955). H. Suhl, Proc. IRE **44**, 1270 (1956).

[3] L. R. Walker, Phys. Rev. **105**, 390 (1957).

[4] R. L. White and I. H. Solt, Phys. Rev. **104**, 56 (1956).

[5] J. F. Dillon, Bull. Am. Phys. Soc. ser. II, **1**, 125 (1956).

[6] Gordy, Smith, and Trambarulo, Microwave Spectroscopy, Wiley, N. Y. 1953 (Russ. transl. IIL, Moscow, 1955).

[7] A. I. Manenkov, Thesis, Physics Institute, Academy of Sciences, U.S.S.R., 1956.

[8] L. R. Bickford, Phys. Rev. **78**, 449 (1950).

Translated by G. Volkoff
128

GENERATION OF NEUTRAL PIONS IN THE INTERACTION BETWEEN 9 Bev PROTONS AND PHOTOGRAPHIC EMULSION NUCLEI

G. L. BAYATYAN, I. M. GRAMENITSKIĬ, A. A. NOMOFILOV, M. I. PODGORETSKIĬ, and E. S. SKRZYPCZAK

Joint Institute for Nuclear Research

Submitted to JETP editor July 28, 1958

J. Exptl. Theoret. Phys. (U.S.S.R.) **36**, 690-693 (March, 1959)

The mean energy of π^0 mesons produced in collisions between protons of energy ~ 9 Bev and photographic emulsion nuclei was determined to be $\overline{E}_\pi = 750 \pm 180$ Mev. The fraction of the energy carried off by $\pi^{\pm,0}$ mesons in such reactions lies between 0.33 ± 0.08 and 0.27 ± 0.07.

THE question of the fraction of energy k carried off by secondary π mesons is of great importance to the study of the mechanism of interaction of high-energy particles. Investigations of interactions between cosmic-ray particles and light nuclei in the $\sim 10^{10}$ ev energy region have shown that the value of k is ~ 30%.[1] It is of interest to evaluate k for conditions in which the energy and nature of the primary particles are exactly known.

In the present investigation the mean energy was determined for π^0 mesons produced by the interaction of 9-Bev protons with emulsion nuclei.

Electron-positron pairs produced by γ rays from π^0-meson decay were analyzed in a stack of layers, each 450 μ thick, of type "R" NIKFI emulsion, which had been irradiated with protons in an inner beam of the proton synchrotron of the Joint Institute for Nuclear Research. The pairs were found by tracing the separate relativistic tracks selected from a strip perpendicular to the beam and at a distance of 30 mm from the edge of the stack. Tracks with $1° < \varphi \leq 30°$, where φ is the emulsion-plane angle relative to the beam direction and with a projection length $l \geq 1600\,\mu$ in one plate were selected. Tracks that met these conditions were extended back to the generation point of the pair, or to a star, or to a point outside the stack. This line of research had been suggested by King.[2] It suited our purposes because it obviated the necessity of energy discrimination of pairs.

To find the mean energy of γ rays originating directly from π^0 meson decay, one must exclude the background due to bremsstrahlung γ rays. For this reason the area around the generation point of each pair was inspected for an electron track parallel to the pair. Pairs that had such tracks were discarded as secondary. These amounted to ~ 10%, in agreement with the predicted number of secondary pairs for our conditions as based on cascade theory.[3] Moreover, the background due to the γ rays that entered the stack from outside was evaluated and found to be insignificant. The number of pairs found, excluding the secondary ones, was 93. There were 116 relativistic tracks leading to stars.

In both cases distributions were constructed for the emission angles in relation to the primary beam. These distributions are shown in Fig. 1. Also shown is the angular distribution for the tracks of relativistic particles in stars found by tracing along the primary proton tracks. All three distributions coincide within experimental error. Since the distributions for γ rays and π^0 mesons roughly coincide* in the energy region studied, the angular distributions for neutral and charged π mesons can be assumed to be similar to one another.

Evaluation of the ratio $R = n\pi^0/n_s$, taking into account the geometric conditions and γ-ray conversion probability, indicates that $R \sim 0.5$. The exact value of R could be found if there were much more statistical data.

Values of 4.3 ± 0.2 and 7.8 ± 0.7 were found for $\overline{n}_s'$ and $\overline{N}_h$ respectively for the stars located by extending the secondary relativistic tracks. For the present system for locating stars, some increase should be expected in $\overline{n}_s'$ in relation to the value of n_s which corresponds to stars found by extension along the primary proton tracks, or specifically

$$\overline{n}_s' = \overline{n}_s + D/\overline{n}_s,$$

where D is the dispersion of the star distribution

*The analysis given here confirm this supposition (see also King[2]).

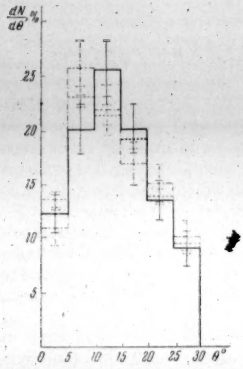

FIG. 1. Distribution of angles of emission for electron-positron pairs (solid line) and for fast charged particles from stars found by extending primary proton tracks (dotted line) and from stars found by tracing secondary fast particles (dash-dot line).

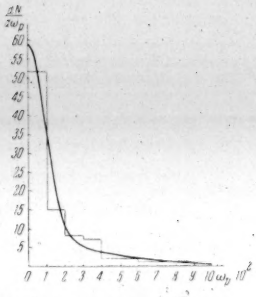

FIG. 2. Distribution of projected divergence angle.

in n_s. According to Gramenitskii et al.,[4] $\bar{n}_s = 3.21 \pm 0.1$ and $D = 3.64 \pm 0.15$, which means that the value of $\bar{n}'_s = 4.3$. This is in good agreement with the experimental value for $\bar{n}'_s$ and indicates that there was no discrimination when the relativistic tracks were selected.

The mean γ ray energy $\bar{E}_\gamma$ can be evaluated from the distribution of the divergence angle ω between the components of a pair, since $\bar{E}_\gamma = \kappa(\overline{1/\omega})$. The coefficient κ was computed by means of the theoretical angular distribution for the given γ-ray energy.[5] The partition of energy between the electron and positron was also taken into account.[6] The numerical value for κ is 4.15, if ω is expressed in radians and the energy in Mev.

For our experimental conditions it was practically impossible to measure the spatial angle ω for narrow pairs. Therefore, the method proposed by Weil et al.,[7] which reduces the influence of multiple scattering, was used to measure the projected divergence angles. The error in the determination of the divergence angle of an individual pair, including the error due to multiple scattering and observation error, amounts to 25%. The distribution of projected divergence angles shown in Fig. 2 was approximated by a linear combination of two Gaussian distributions. Then a transformation was made from this distribution to a distribution for spatial angles ω, and the quantity $(\overline{1/\omega})$ was computed. The value of $(\overline{1/\omega})$ was found equal to 120 ± 10 (the error is purely statistical). Thus, the mean value of the γ-ray energy was $\bar{E}_\gamma = 420 \pm 100$ Mev. The error includes the measuring error, inaccuracy in determining κ, inaccuracy in the approximation, and the statistical error in the determination of $(\overline{1/\omega})$.

To obtain the mean π^0-meson energy $\bar{E}_{\pi^0}$ it is necessary to determine the ratio $f = \bar{E}_{\pi^0}/\bar{E}_\gamma$, where $\bar{E}_\gamma$ is the mean energy of the γ rays entering the examined solid angle. The value of f depends to a rather slight extent on the energy spectrum of the π^0 mesons. The upper limit of f, for a reasonable assumption for the spectrum, would be 1.8. Consequently, the upper limit for the mean energy of the π^0 mesons moving within the examined solid angle is 750 ± 180 Mev.

The mean energy transferred to the π mesons in a single disintegration is determined as follows:

$$\bar{E}_\pi = {}^3/_2(\bar{n}_s - \alpha)\bar{E}_{\pi^0},$$

where α is the average number of fast protons, which is 0.5. If one substitutes the proper value for $\bar{n}_s$ and assumes that the mean π-meson energy does not depend on the emission angle, an upper limit of 3.0 ± 0.7 Bev is obtained for $\bar{E}_\pi$.

A more exact value of $\bar{E}_\pi = 2.5 \pm 0.6$ can be obtained if one assumes that the transverse momentum (i.e., perpendicular to the direction of the primary particles) of the secondary particles* is constant (see, for example, Zhdanov[8]). Since the magnitude of $p_\perp$ does in fact increase somewhat with an increase in the emission angle, the value given here determines the lower limit of the mean energy carried off by the π mesons.

Thus, the fraction of energy carried off by π mesons in interactions between 9-Bev protons and emulsion nuclei lies between 0.33 ± 0.08 and 0.27 ± 0.07.

The authors express their gratitude to M. Ya. Danysh for going over our results and to V. P. Solomakhina for helping with the scanning.

[1] N. L. Grigorov and V. S. Murzin, Izv. Akad. Nauk SSSR, Ser. Fiz. 17, 21 (1953).

*Under our conditions the mean value for the transverse momentum $p_\perp$ is (1 to 2) $\mu_\pi c$.

[2] D. T. King, Phys. Rev. **109**, 1344 (1958).

[3] B. Rossi and K. Greisen, The Interaction of Cosmic Rays with Matter (Russ. Transl.) IIL, 1948. Revs. Modern Phys. **13**, 240 (1941).

[4] Gramenitskiĭ, Danysh, Lyubimov, Podgoretskiĭ, and Tuvdendorzh, J. Exptl. Theoret. Phys. (U.S.S.R.) **35**, 552 (1958), Soviet Phys. JETP **35**, 381 (1958).

[5] A. Borsellino, Phys. Rev. **89**, 1023 (1953).

[6] W. Heitler, The Quantum Theory of Radiation, (Oxford, 1953).

[7] Weill, Gailloud, and Rosselet, Nuovo cimento **6**, 413 (1957).

[8] G. B. Zhdanov, J. Exptl. Theoret. Phys. (U.S.S.R.) **34**, 856 (1958), Soviet Phys. JETP **34**, 592 (1958).

Translated by A. Skumanich
129

EXACT MEASUREMENT OF THE RATIOS OF INTERNAL-CONVERSION COEFFICIENTS OF 411.7-kev GAMMA QUANTA IN Hg^{198}

V. M. KEL' MAN and R. Ya. METSKHVARISHVILI

Leningrad Physico-Technical Institute

Submitted to JETP editor July 29, 1958

J. Exptl. Theoret. Phys. (U.S.S.R.) **36**, 694-696 (March, 1959)

The following internal conversion coefficient ratios have been obtained for 411.8-kev gamma rays in the shells and subshells of Hg^{198}: $K/L = 2.69 \pm 0.02$; $L_I : L_{II} : L_{III} = 1 : (1.05 \pm 0.02) : (0.45 \pm 0.01)$; $L : M : N : O = 1 : (0.252 \pm 0.0045) : (0.077 \pm 0.004) : (0.018 \pm 0.002)$. Within the accuracy of the measurements, the experimental ratios agree with the theoretical ones presented in the tables by Sliv and Band.

IT has been established by various means that the 411.8-kev gamma rays emitted by the excited nuclei Hg^{198} represent E2 electric quadrupole radiation.[1-3] A precision measurement of the conversion coefficients of these rays is therefore of particular interest to the verification of the high-accuracy theoretical calculations of the conversion coefficient now in progress.

The experimental accuracy can be increased substantially by determining not the absolute values of the conversion coefficients, but their ratios. The conversion-coefficient ratios can be measured with any beta spectrometer of sufficient resolution. If the conversion lines are fully separated, the measurement accuracy increases with the closeness of the spacing of the investigated lines, owing to the reduced values of the various necessary corrections. Since we had at our disposal a magnetic-prism beta spectrometer of high resolution (instrument line half-width 0.04% at a source width of 1 mm),[4,5] capable of separating the internal-conversion lines of the foregoing gamma rays on the L sub-shells and on the M, N, and O shells of Hg^{198}, we undertook the measurement of the ratios of the corresponding conversion coefficients. The measurement of the K/L ratio, which does not require high instrument resolution, was made with a double-focusing beta spectrometer, described by Bobykin and Novik,[6] with a resolution of 0.3%. In both cases, the source was a gold film 1.3 × 10 mm, deposited by cathode spattering on an aluminum backing and then activated with neutrons. The thickness of the gold film was 0.34 mg/cm^2. The aluminum backing was 8μ thick. The internal conversion lines on the L subshells and M, N, and O shells, plotted with the high-resolution spectrometer, are shown in Figs. 1 and 2. The same lines and the K line obtained with a double-focusing spectrometer are shown in Fig. 3.

The measurements yielded the following ratio between the conversion coefficients:

$$K/L = 2.69 \pm 0.02;$$

$$L_I : L_{II} : L_{III} = 1 : (1.05 \pm 0.02) : (0.45 \pm 0.01);$$

$$L : M : N : O = 1 : (0.252 \pm 0.004) : (0.077 \pm 0.004) : (0.018 \pm 0.002).$$

The accuracy here represents the probable errors.

The data obtained for the K-shell and the L

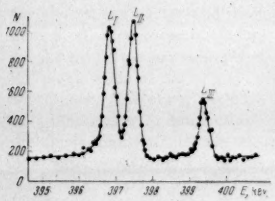

FIG. 1. Internal-conversion lines of 411.8 kev gamma quanta on the L subshells of Hg^{198}.

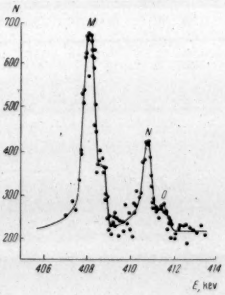

FIG. 2. Internal-conversion lines of 411.8 kev gamma quanta on the M, N, and O shells of Hg^{198}.

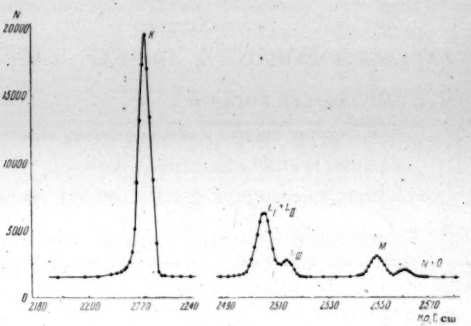

FIG. 3. Internal-conversion lines of the 411.8 kev gamma quanta on the K, L, M, N, and O shells of Hg^{198}, plotted with a double-focusing spectrometer. The only corrections are for decay.

Conversion-coefficient ratios of 4.11.8-kev gamma rays in Hg^{198}

Reference	K/L	$L_I : L_{II} : L_{III}$	L, M, N, O
[1]	2.2±0.8	—	$L/M = 1 : (0.24 \pm 0.17)$
[8]	2.2	—	$L/(M+N) = 1 : 0.25$
[9]	3	—	$L/M = 1:0.3$
[5]	3.1	—	$L/M = 1:0.3$
[3]	2.1±0.5*	$(1.00 \pm 0.16) : (1.16 \pm 0.16) : 0.53$ *	
Present work	2.69±0.02	$1 : (1.05 \pm 0.02) : (0.45 \pm 0.01)$	$L : M : N : O = 1 : (0.252 \pm 0.004) : (0.077 \pm 0.004) : (0.018 \pm 0.002)$
Tables[7]	2.72	1:1.09:0.46	

*In these measurements the accuracy is expressed in terms of the maximum error.

sub-shells were compared with the very detailed conversion-coefficient tables, compiled by Sliv and Band[7] with allowance for screening effects and for the finite dimensions of the atomic nucleus. Sufficiently accurate theoretical calculations of the conversion coefficients at the higher levels are still unavailable at present. An interpolation of the energy data listed in the table for Z = 80 yields K/L = 2.72 and $L_I : L_{II} : L_{III} = 1 : 1.09 : 0.46$. Thus, the theoretical and experimental data agree within the limits of experimental error.

The table has been compiled from the most accurate measurements of the conversion coefficients of 411.8-kev gamma quanta in Hg^{198}, made by various investigators. In addition, it lists the theoretical data obtained from the Sliv and Band table. One general conclusion that can be drawn from an analysis of the table is that as the experimental accuracy is increased, the measured conversion-coefficient ratios approach the theoretical ones. This is evidence of the high accuracy of the latter.

[1] Steffen, Huber, and Humbel, Helv. Physica Acta **22**, 167 (1949).

[2] L. Simons, Phys. Rev. **86**, 570 (1952).

[3] Connors, Miller, and Waldman, Phys. Rev. **102**, 1584 (1956).

[4] Kel'man, Kaminskii, and Romanov, Izv. Akad. Nauk SSSR, Ser. Fiz. **18**, 209 (1954).

[5] Kel'man, Romanov, Metskhvarishvili, and Kolyunov, J. Exptl. Theoret. Phys. (U.S.S.R.) **32**, 39 (1957), Soviet Phys. JETP **5**, 24 (1957).

[6] B. V. Bobykin and K. M. Novik, Izv. Akad. Nauk SSSR, Ser. Fiz. **21**, 1556 (1957), Columbia Tech. Transl. p.1546.

[7] L. A. Sliv and I. M. Band, Таблицы коэффициентов внутренней конверсии гаммаизлучения, ч. 1, *K*-оболочка, ч. 2, *L*-оболочка (Tables of Gamma-Ray Internal Conversion Coefficients: part 1, K-shell, part 2, L-Shell) U.S.S.R. Acad. Sci. Press. 1956-1958.

[8] Dzhelepov, Bashilov, Zolotavin, and Anton'eva, Dokl. Akad. Nauk SSSR **64**, 803 (1949).

[9] K. Siegbahn and A. Hedgran, Phys. Rev. **75**, 523 (1949).

Translated by J. G. Adashko
130

UNDERGROUND MUON SPECTRUM AT ~40 METER WATER EQUIVALENT

M. I. DAĬON and L. I. POTAPOV

P. N. Lebedev Physics Institute, Academy of Sciences, U.S.S.R.

Submitted to JETP editor July 30, 1958

J. Exptl. Theoret. Phys. (U.S.S.R.) **36**, 697-706 (March, 1959)

A magnetic spectrometer was used to measure the momentum spectrum of muons at a depth of ~40 m water equivalent in the $2 \times 10^8 - 5 \times 10^{-10}$ ev/c momentum range.

1. INTRODUCTION

MUON momentum spectra at sea level and on high mountains have been the subject of many experimental investigations. The most complete results, based on the largest statistical material, have been recently obtained by Alikhanyan and Alikhanov,[1,2] Owen and Wilson,[3] Caro et al.,[4] and Kocharyan et al.[5,6] through magnetic analysis of cosmic radiation by the magnetic mass spectrometer method. At sea level the muons comprise the main part of the penetrating component of cosmic radiations. According to Owen and Wilson, not more than 1% of the total intensity is due to protons. Underground, the nucleon component is rapidly absorbed and at depths greater than 8 or 10 meters of earth the penetrating component of cosmic rays consists of muons.

Usually, when necessary, the muon spectrum at a given depth underground is determined from the known muon spectrum at sea level. Approximating the sea-level spectrum at energies $\gtrsim 10^{10}$ ev by

$$N(p)\,dp = p^{-\gamma} N_0\,dp,$$

where p is the particle momentum and $\gamma \approx 2.7 - 3.0$, we obtain for the spectrum at a depth h

$$N(p)\,dp = (p + p_0)^{-\gamma} N_0 dp \qquad (1)$$

(see, for example, references 7 and 8). Here p_0 is the momentum lost by a muon in passing through a layer of earth of thickness h.

Until comparatively recently there were no direct measurement of momentum spectra underground. We note that measurement of the spectra underground is a rather complicated matter: the construction of mass spectrometers is difficult under such conditions for technical reasons, and the use of other methods does not provide the necessary statistical material (see below).

Recently the problem of the underground muon spectrum has assumed great significance in connection with the investigation of the interaction between muons and matter, since usually an extrapolation of spectrum (1) is used to calculate various cross sections — production of δ electrons, stars, cascades, or anomalous scattering. The anomalous scattering of muons is of basic significance, and from this point of view the direct measurement of the muon spectrum at relatively low energies is of great interest. Actually, the observed excess scattering could be explained, were the true number of slow muons at a given depth to exceed that calculated by Eq. (1). We note that when determining the intensity of slow muons at a given depth from data obtained from the number of muons at sea level it is necessary, generally speaking, to consider not only the ionization energy losses that this formula accounts for, but several other factors, such as scattering of slow muons in the ground, etc.

The first reports of attempts at direct measurement of the momentum spectrum of muons underground were not published until 1956. George and Shrikantia[7] give the muon spectrum in the momentum range from 100 to 4,000 Mev/c, obtained experimentally from muon scattering in a photoemulsion exposed at 57 m water equivalent (w.e.). Compared with the spectrum calculated for this depth from the sea-level spectrum, this spectrum exhibits a considerable particle excess in the energy range from 1 to 5 bev and a deficit in the energy range from 5 to 20 bev. George and Shrikantia believe, however, that this discrepancy cannot be seriously considered, since the accuracy of the data is small.

The spectrum in the low-energy region, $E < 10^9$ ev, was analyzed in connection with the problem of the anomalous scattering. Here, however, by virtue of the small statistical accuracy, no conclusion can be reached concerning the type of the spectrum. George and Shrikantia noted that in spite of the long time covered by the investigation

(more than two years), the material gathered was quite meager, merely 317 trajectories included in the spectrum, and the statistical accuracy of the results could hardly be increased with the photoemulsion method.

Nash and Pointon[9] determined the muon spectrum at 40 m w.e. in the energy range of $\sim 2-8\times 10^8$ ev, using experimental data on meson scattering in two lead plates placed inside a cloud chamber. Here, unlike the preceding investigation, where the momentum of each particle was determined, the spectrum was plotted on the basis of a statistical treatment of the experimental scattering data, with allowance for the known distribution function of the scattering angles. The calculation was based first on the assumed muon spectrum at a given depth, and the most probable form of the spectrum was then determined by successive approximation.

In the spectrum obtained by Nash and Pointon, the total number of particles with energies 0.5 – 1.0 Bev agrees with the expected value at the given depth of observation, provided the spectrum measured at sea level is suitably transformed. In the momentum range from 2 to 7.5×10^8 ev/c there is also a qualitative agreement in the general form of the spectra. However, the results of this paper pertain to a rather narrow muon energy range and give only a qualitative idea of the form of the spectrum in this region.

In 1956 the underground laboratory of the Moscow State University initiated research on the muon momentum spectrum at a depth of 40 m w.e. by the most direct method, magnetic analysis of cosmic radiation with the aid of an Alikhanyan-Alikhanov mass spectrometer. We describe below the experimental setup and the results.

2. DESCRIPTION OF APPARATUS

We list here only the salient features of the apparatus, since a detailed description of similar setups can be found in the literature (references 1, 5, 10, etc.).

A diagram of the instrument is shown in Fig. 1. In the electromagnet gap (measuring $20\times 60\times 10$ cm) are located six trays of counters 1, 2, 3, I, II, and III. Three trays of small-diameter counters, i. 2, 3, permit measurement of the radius of the curvature and thus the momentum of the particle. The tray marked O_m is for monitoring purposes. Four other monitoring trays O_{lin}, I, II, and III serve to check the linearity of the trajectory in the plane B. Located under the gap are absorbers IV, V, VI, and VII, and counter trays that determine the ranges of the particles. In the case of

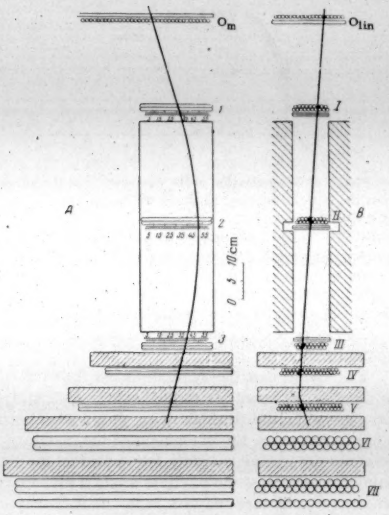

FIG. 1. Diagram of the instrument.

hard particles that pass through all the absorbers, they provide additional control over the linearity of the trajectory in the plane B.

The arrangement of the counters in trays 1 – 3, I – III is shown in the same Fig. 1. Table I lists the counter data. The electronic portion of the apparatus consisted of a coincidence block and a hodoscopic system GK-7,[11] controlled by a 1+2+3 coincidence pulse. Before the start of the investigation, the entire counter system was thoroughly adjusted and the adjustment was checked by a special series of measurements performed without a magnetic field. These control measurements were repeated frequently.

During the actual measurements, the direction of the magnetic field in the gap was reversed twice a day, whenever the films were changed.

TABLE I

Number of trays	Counter diameter, mm	Counter length, mm	Cathode material	Number of counters in tray	Wall thickness, mm
O_m	10	200	Cu	50	0.15
1	4.8	100	Al	59	0.1
2	4.8	100	Al	59	0.1
3	4.8	100	Cu	59	0.1
O_{lin}	10	550	Cu	18	0.15
I	8	200	Al	19	0.15
II	8	200	Al	17	0.15
III	10	200	Cu	15	0.15
IV	10	450	Cu	33	0.15
V	10	550	Cu	37	0.15
VI	20	800	Cu	25	0.15
VII	20	900	Cu	42	0.15

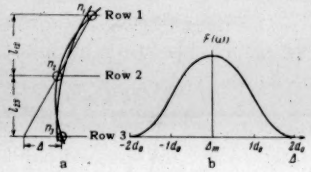

FIG. 2.a) Determination of the deviation Δ of the particle from the initial direction; b) Shape of the distribution function of the values of Δ.

3. PROCESSING OF THE DATA

We shall deal in somewhat greater detail with the processing of the experimental data, since our method differs from that used in most similar investigations.

It is known that the system makes it possible to identify the counters through which a particle has passed by the flashing of corresponding neon lamps. However, the placement of the counters does not determine uniquely the radius of the circular trajectory of the particle since a given combination of counters may lie in the path of trajectories of various curvatures.

We introduce a quantity Δ, uniquely related with the radius of curvature ρ of the particle trajectory (see Fig. 2a). In a narrow long telescope, the following relation between ρ and Δ is satisfied, with good approximation:

$$\rho = (L^2 + \Delta^2)/4\Delta, \qquad (2)$$

where $L = l_{12} + l_{23}$. The distribution function of the quantity Δ within the counter combination characterized by the quantity $\Delta_m = md$ can be represented in the following form[12]

$$F(\omega) = \begin{cases} 2(1/2 - \omega^2), & 0 \leqslant |\omega| \leqslant 1/2, \\ 2(1 - |\omega|)^2, & 1/2 \leqslant |\omega| \leqslant 1, \end{cases} \qquad (3)$$

where $\omega = (\Delta - \Delta_0)/2d$.

In our case $d = d_0/3$, where d_0 is the counter diameter. A plot of this function is shown in Fig. 2b. This yields a statistical error of 0.26 × 2d in the determination of Δ, and a relative error

$$(\delta\Delta/\Delta)_{prob} = 0.26 \cdot 2d/\Delta.$$

For large values of Δ, the error is small and therefore in determining the spectrum in this region (for small ρ) the radius of curvature of each trajectory is determined from the positions of the centers of the corresponding counters,* and the momentum of the particle is calculated from the formula p = 300 Hρ.

*We shall not dwell on the method of calculating the radius.

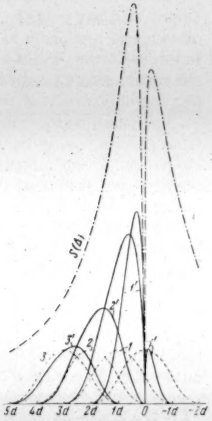

FIG. 3. Arrangement of the primary beam by deviation categories.

The data obtained for small values of $\Delta_m = md$ were processed with allowance for the distribution function (3).* The method used can be most clearly explained with the aid of Fig. 3. Here the abscissas represent the deviations of Δ. The quantities 1d, 2d, 3d, etc. correspond to experimentally-obtained categories of deviations $\Delta_m = md$ (m = 1, 2, 3, ...). The dotted curves show the distribution functions of Δ within each category Δ_m (and are so marked). The same diagram shows the spectrum of the particles incident on the apparatus (dash-dot line).

To determine the probability of entrance of particles with a deviation Δ in category Δ_m, the ordinate of the spectrum for given must be multiplied by the corresponding ordinate of the distribution function (more accurately, taking normalization into account, by a quantity equal to half the ordinate). The curves 1′, 2′, 3′ ... thus obtained give the actual distribution relative to the deviations inside each category of deviations [for a specified primary spectrum s(Δ)].

This raises the question of how the total number of particles N_m, registered in a given category of deviations m (N_m is proportional to the area under curve m′) can be used to determine the primary spectrum in this energy range. In investigations where the distribution function is not taken into account, it is essentially assumed that any deviation category corresponds to a deviation interval

$$\Delta_m - d/2 \leqslant \Delta \leqslant \Delta_m + d/2. \qquad (4)$$

*An analysis of spectra with use of the distribution function is contained in reference 3.

TABLE II

Δ_m	H = 6300 oe				H = 3300 oe			
	$p_m^{(1)}$, Bev/c	σ			$p_m^{(2)}$, Bev/c	σ		
		$\gamma = 2.5$	$\gamma = 2.8$	$\gamma = 3.0$		$\gamma = 2.5$	$\gamma = 2.8$	$\gamma = 3.0$
1	2	3	4	5	6	7	8	9
1/4 d	49.5	1.67	1.92	2.1	26	1.42	1.47	1.7
1 d	12.5	0.7	0.66	0.63	6.5	0.86	0.77	0.72
2 d	6.18	~1	~1	~1	3.25	1.14	1.10	1.08
3 d	4.12	~1	~1	~1	2.17	1.08	1.07	1.06
4 d	3.08	~1	~1	~1	1.62	1.06	1.05	1.05
5 d	2.47	~1	~1	~1	1.31	~1.03	~1.03	~1.03

The average number of particles $\bar{n}_m$ per unit momentum interval is determined, for example, by dividing the total number of particles N_m by the momentum interval corresponding to the deviation interval (4). The resultant value is usually associated, without additional justification, with the momentum p_m corresponding to the center of the category Δ_m (or to the center of the momentum interval). Calculation based on the foregoing scheme of subdividing the primary spectrum into deviation categories shows that the resultant values $\bar{n}_m$ must be subjected to corrections that are different for different deviation categories and depend, furthermore, on the type of the original spectrum.

The corrections were calculated for several initial spectra (see below). In each case curves similar to those shown in Fig. 3 are used to determine the values of $\bar{n}_m$ by calculating the areas under the curves m′ and dividing these areas by the momentum interval corresponding to the deviation interval (4). (This corresponds to the method used to obtain the value of n_m from the experimental data). The resultant values of $\bar{n}_m$ were compared with the true value of the average number of particles per unit momentum interval n_{sp} in the initial spectrum, $S(\Delta)$, at the point Δ_m. The $\sigma_m = \bar{n}_m / n_{sp}$ shows by how much the values of $\bar{n}_m$ obtained with this method of data processing exceed the true values.

4. EXPERIMENTAL RESULTS

Before starting the investigation, a special experiment was set up to measure the intensity of the hard component ($p \gtrsim 3.5 \times 10^8$ ev/c) at sea level (I_0) and at our depth (I_h), using a telescope that subtends the same angle as the telescope of the mass spectrometer. Based on the obtained $I_0/I_h = 11.13 \pm 0.43$ and on the known spectrum of the muons at sea level,[4] the value of p_0 was determined from the condition that the number of particles in the spectrum[4] with momenta greater than p_0 constitutes 1/11.13 of the total number of particles in the spectrum. Such an estimate yields $p_0 \approx 9.8$ Bev/c, which may be somewhat of an underestimate. Other methods of determining these quantities lead approximately to the same value of p_0. Since the absolute intensity of the hard component at sea level is $0.83 \times 10^{-2} \text{cm}^{-2}\text{sec}^{-1}\text{sterad}^{-1}$, the intensity at our depth was assumed to be $0.83/11.13 = 0.745 \text{ cm}^{-2}\text{sec}^{-1}\text{sterad}^{-1}$; the spectrum obtained by us was normalized to this value of absolute intensity (see below).

It is natural to expect that in the momentum range of interest to us the underground muon spectrum would be described, at least approximately, by Eq. (1) with $\gamma \sim 2.5$ to 3.0. Our calculations for σ_m were therefore based on the spectrum (1). Since, for a given p, the deviation Δ depends on the value of the magnetic field H ($p \sim 300 \text{ HL}^2/4\Delta$), the corrections σ_m were calculated for two versions of the experiment: one with a 6300 oe magnetic field (first series of measurements) and one measured at 3300 oe (second series of measurements), and in each case for $\gamma = 2.5$, 2.8, and 3.0.

The values obtained for σ are listed in Table II, from which it is seen that in the first series of measurements the correction plays a noticeable role only for two deviation categories, $\Delta_0 = 0$ and $\Delta_1 = 1\,d$, and that the value of σ depends here on the value assumed for γ.* For the categories $\Delta_m \geq 2\,d$, the coefficient σ is practically independent of γ. Thus, the method for processing the experimental data in this series of measurements, in the region $\Delta_m \geq 2\,d$, is practically independent of the assumed initial muon spectrum. The solid circles in Fig. 4 represent the spectrum we obtained in this range of momenta. The abscissas represent the particle momenta, and the ordinates the absolute intensities within a 1-Mev momentum interval, with allowance for the geometry of the instrument (cf. below).

*In calculating the values of σ_m for the category Δ_0 and Δ_1 we considered that particles of both signs may be included in this category. It was assumed that the spectra of positive and negative mesons are similar and that the positive excess is $n_+/n_- = 1.20$. In the category $\Delta_0 = 0$, the value of σ was calculated at the point d/4.

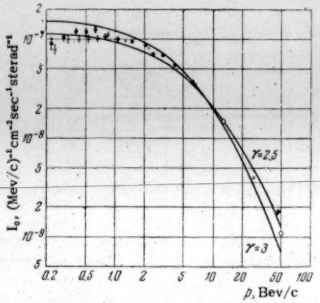

FIG. 4. Comparison of calculated spectra for $\gamma = 2.5$ and $\gamma = 3.0$ with the spectrum obtained for the muons.

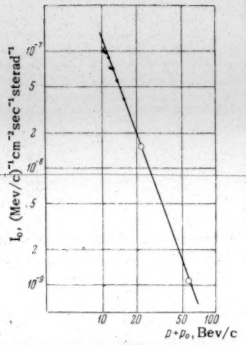

FIG. 5. Spectrum of muons in the momentum range $p > 2 \times 10^9$ ev/c.

Figure 5 shows the same spectrum, for the momentum range $p > 10^9$ ev/c, but at a different scale: the abscissas represent $p+p_0$. It is seen from this that in the momentum range 2×10^9 ev/c $\lesssim p \lesssim 10^{10}$ ev/c the spectrum can be approximated by a straight line, whose slope yields $\gamma \approx 2.7 - 2.8$.

If it is assumed that at large momenta, corresponding to the deviation categories $\Delta_m = 0$ or 1d, the spectrum exponent remains constant, then the corrections listed in column 4 of Table II, and corresponding to $\gamma = 2.8$, should be introduced in the experimental values of $\bar{n}_0$ and $\bar{n}_1$. The intensities obtained with allowance for these corrections are plotted in Figs. 4 and 5 with light dots. It is seen that these two fit well the same straight line. The most probable value of γ, calculated over all points of the spectrum in the region $p \gtrsim 2 \times 10^9$ ev/c, is $\gamma = 2.78 \pm 0.23$. It must be recalled, however, that when $\Delta_m < 2d$ the magnitude of the correction depends on the initial assumptions concerning the shape of the spectrum. Since it is very probable that in this region the true value of the spectrum exponent is greater than the assumed initial value $\gamma = 2.8$, the two last points of the spectrum are only tentative.

In our preceding analysis, the values of $\bar{n}_m$ pertain to the center of the interval Δ_m (only the quantity $\bar{n}_0$ pertained to the deviation $\Delta = d/4$). However, as can be seen from Fig. 3, the maximum number of particles (the maxima of the curves 1′, 2′, 3′, ...) registered within a given category have smaller deviations, $\Delta_{i\,max}$. The quantities $\bar{n}_m$ can be related to the deviations $\Delta_{i\,max}$. It is necessary to use, in this case, when plotting the spectrum, other correction coefficients σ'_m, calculated in the same manner as the coefficients σ_m. The spectrum plotted by this method was not found to differ from the one given here.*

Starting with the results of the first series of measurements, the calculations performed in the examination of the data of the second series were based on a spectrum with $\gamma = 2.8$; the values of the corresponding corrections σ are given in column 8 of Table II. For comparison we give also the values of σ at $\gamma = 2.5$ and 3.0. The spectrum obtained is marked on Fig. 4 by crosses. It is seen that within the limit of statistical errors, the spectra obtained in both series of measurements are the same.

We indicate in the conclusion that the total number of trajectories, selected for the construction of the spectra, is 26,226; of these the spectrum of the first series included 12, 740 trajectories, and the spectrum of the new series included 13,486.

TABLE III

p, Bev/c	$H = 3300$ oe			$H = 6300$ oe		
	Aperture ratio			Aperture ratio		
	$n=1$	$n=2$	$n=3$	$n=1$	$n=2$	$n=3$
1	2	3	4	5	6	7
0.2	0.95	0.92	0.9	0.78	0.74	0.7
0.4	0.98	0.97	0.96	0.94	0.93	0.91
0.6	0.99	0.98	0.98	0.98	0.97	0.96
0.8	0.99	0.98	0.98	0.99	0.98	0.97
1.0	~1	0.99	0.99	0.99	0.98	0.97
2.0	~1	~1	~1	~1	0.99	0.98
5.0	~1	~1	~1	~1	~1	~1

Remarks on Allowance for the Aperture Ratio of the Instrument

When we plotted the spectra for small momenta we took into account the aperture ratio of the instrument, which depends both on the geometry of

*Essentially it is more logical to associate the given deviation category Δ not with the momentum p_m, corresponding to the center of the category Δ_m, or with p_{max}, corresponding to the maximum in the curve showing the Δ distribution, but, say, a momentum p such that the number of particles in the given category, having a momentum less than p, equal the number of particles with momentum greater than p.

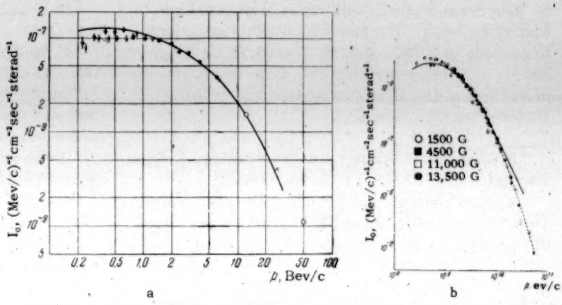

FIG. 6. Comparison of the spectrum obtained with (a) that of Caro et al.,[4] (b) converted to a depth equivalent to ~ 40 m of water.

the telescope and on the angular distribution of the particles in the beam. There are numerous calculations in the literature for the aperture ratios of the mass spectrometers. Our calculation was based on the method described in reference 10. The angular distribution at our depth of observation in the momentum range from 2 to 7×10^8 ev/c, where it influences the magnitude of the aperture ratio, is represented by the law $I_\theta = I_0 \cos^n \theta$, with $n \sim 2.9$.[14] However, allowance for the scattering of mesons in a lead block placed over the apparatus shows that the value of n will be less for the particle beam registered by this instrument. In view of the weak dependence of the aperture ratio on n, an exact calculation of n was not carried out. In Table III we list the values of the aperture ratio, calculated under the assumption that $n = 2$. We show also for comparison the aperture ratios for $n = 1$ and $n = 3$. In plotting the spectra we used the values of the aperture ratio given in columns 3 and 6 of Fig. 3.

5. DISCUSSION OF THE RESULTS

It is interesting to compare the spectrum obtained with the muon spectrum at sea level and with the customary spectrum approximation as represented by Eq. (1) (see Fig. 6). Figure 6b shows the muon spectrum at sea level, obtained by Caro et al.[4] Since the muons lose an energy of 9.8 Bev on the path from the surface of the earth to the specified depth, the spectrum of interest to us will be in the region $E > 9.8$ Bev, where the approximation of reference 4 is shown dotted.

We have recalculated the Caro spectrum to our depth, taking into account the indicated muon energy losses in the earth. We also allowed for the change in the widths of the momentum intervals, to which the same particles belong at sea level (dp) and at the given depth (dp_1). The dp_1/dp ratio was calculated from the expression for dR/dp (R is the particle range) given by Rossi and Greisen.[15] The intensity of the muons having a momentum p at a given depth was determined by dividing the ordinate of the Caro spectrum at the point $p + 9.8$ Bev/c by the quantity dp_1/dp. The results are shown by the solid line in Fig. 6a. If we take into account the statistical errors in the Caro spectrum, we can state that our data agree with the transformed Caro spectrum.

The Owen and Wilson spectrum[3] in the region $p \gtrsim 10^{10}$ ev/c lies somewhat above the Caro spectrum (a comparison of the spectra is cited in reference 3), but the Owen and Wilson data are less trustworthy in this momentum region, since they correspond to the zero category of deviations (see section IV).

The spectrum shown in Fig. 4 was obtained from spectra calculated by formula (1), for $\gamma = 2.5$ and 3.0. In both cases the spectra are normalized to the total number of particles in the experimental spectrum.

6. CONCLUSIONS

1. In the momentum range $p \geq 2 \times 10^9$ ev/c, the muon spectrum can be expressed approximated by the formula

$$N(p)\,dp = N_0 dp/(p + p_0)^\gamma,$$

where $\gamma = 2.78 \pm 0.23$ and $p_0 = 9.8$ Bev/c. The same formula can be used to approximate the spectrum in a wider region, for $p \lesssim 2 \times 10^8$ ev/c.

2. The spectrum obtained leads to the conclusion that the so-called anomalous scattering of muon mesons, observed in many underground investigations, can absolutely not be due to underestimating the number of slow muons.

The authors express their great indebtedness to A. I. Alikhanyan for much help in completing this work, for valuable advice, and for discussion of the results, and also to V. Kh. Volinskikh and

V. Krugovykh for help with the experimental portion of the work. The authors take this opportunity to express gratitude to S. N. Vernov, N. L. Grigorov, and G. B. Khristyansen for affording the opportunity of working at the underground laboratory of the Moscow State University.

[1] Alikhanyan, Alikhanov, and Vaisenberg, J. Exptl. Theoret. Phys. (U.S.S.R.) **18**, 301 (1948).

[2] A. I. Alikhanyan and A. O. Vaisenberg, J. Exptl. Theoret. Phys. (U.S.S.R.) **32**, 413 (1957), Soviet Phys. JETP **5**, 349 (1957).

[3] B. G. Owen and J. G. Wilson, Proc. Phys. Soc. **A68**, 409 (1955).

[4] Caro, Parry, and Rathgeber, Austral. J. Scient. Res. **A4**, 16 (1951).

[5] N. M. Kocharyan, Dissertation, Erevan, 1954, Phys. Inst. Acad. Sci. Arm. S.S.R.

[6] Kocharyan, Aivazyan, Kirokasyan, and Aleksanyan, J. Exptl. Theoret. Phys. (U.S.S.R.) **30**, 243 (1956), Soviet Phys. JETP **3**, 350 (1956).

[7] E. P. George and G. S. Shrikantia, Nucl. Phys. **1**, 54 (1956).

[8] D. Kessler and R. Maze, Nuovo cimento **5**, 1940 (1957).

[9] F. W. Nash and A. J. Pointon, Proc. Phys. Soc. **A69**, 725 (1956).

[10] Daion, Fedorov, Merzon, and Shostakovich, Приборы и техника эксперимента (Instruments and Measurement Engineering) No. 1, 3 (1957).

[11] Новые применения ламп с холодным катодом в импульсной аппаратуре (New Application of Cold Cathode Tubes in Pulse Apparatus), VINITU press, 1956.

[12] Hyams, Mylroi, Owen, and Wilson, Proc. Phys. Soc. **A63**, 1053 (1950).

[13] B. Rossi, Revs. Modern Phys. **20**, No. 3, 1948.

[14] Cousins, Nash, and Pinton, Nuovo cimento **6**, 1113 (1957).

[15] B. Rossi and K. Greisen, Revs. Modern Phys. **13**, 240 (1941).

Translated by J. G. Adashko
131

SOVIET PHYSICS JETP VOLUME 36 (9), NUMBER 3 SEPTEMBER, 1959

IONIZATION ALONG THE TRACKS OF HIGH-ENERGY ELECTRON-POSITRON PAIRS

A. A. VARFOLOMEEV, R. I. GERASIMOVA, L. A. MAKARINA, A. S. ROMANTSEVA, and S. A. CHUEVA

Submitted to JETP editor August 18, 1958

J. Exptl. Theoret. Phys. (U.S.S.R.) **36**, 707-716 (March, 1959)

Experimental data are presented on the track densities of five high-energy electron-positron pairs in nuclear emulsions. The measurements were performed for the first pairs in electron-photon showers. The pair energy was estimated from the energy spectrum of cascade electrons at a distance of 2.5 or 3 radiation lengths from the vertex of the first pair. In three cases the pair energy was close to 10^{12} ev and in two cases was approximately 3×10^{11} ev. The track density was determined from grain density and from the gap length distribution. The track density of a pair near its vertex was found to be smaller than that of a particle for which the specific energy loss is twice as large as the ionization loss of an electron. This decrease of pair track density can be accounted for by the mutual electron-positron screening during the ionization process. The results are compared with the theoretical ionization curves for pairs calculated by Chudakov.

1. INTRODUCTION

WHEN an electron-positron pair is produced with energy greater than 10^{11} or 10^{12} ev a peculiar ionization effect is observed along the initial portion of the track. Before the separation between the electron and positron becomes greater than their range of interaction with electrons of the medium ($\sim 5 \times 10^{-7}$ cm) the specific ionization loss of the pair is less than twice the electron loss. The reduced ionization results from mutual screening of the electron and positron fields and was first calculated by Chudakov[1] as a function of the angle of divergence. Chudakov's result has since been confirmed by other investigators,[2,3] who have shown that reduced ionization can actually be observed for pairs with $\gtrsim 10^{12}$ ev.

Grain density at the vertex of a pair increases with the ionization loss. When the separation of the electron and positron paths becomes $r \sim 5 \times 10^{-7}$ cm the grain density corresponds to that of particles with the double ionization loss $2I_{pl}$ (I_{pl} is the plateau value of the ionization). However, this level will not generally equal twice the track density of an electron with ionization loss I_{pl} because of the nonlinear relation between grain density and ionization.

The practical interest of the screening effect lies in the fact that the length of the track segment along which ionization continues to grow can in principle be used to determine the vertex angle, from which the energy quantum producing the pair can be calculated.[4,5]

Lohrmann[6] has shown that at distances greater than $100 - 1000\,\mu$ from the vertex the separation r of electron and positron tracks is determined mainly by multiple scattering. Therefore measurements to determine the vertex angle must be performed at distances from the vertex which are relatively uninfluenced by multiple scattering. At high energies, however, the tracks coalesce at such distances x from the vertex and it is impossible to determine the angle visually.

At a distance greater than 1 or 2 cm from the vertex of a high-energy pair the tracks of secondary pairs are usually observed and the energy of the pair may be considerably reduced by radiation loss. It thus becomes possible to measure multiple scattering directly along a relatively short track length. Since even the measurement of the relative amount of multiple scattering does not exclude the so called "grain noise" of emulsions ($\sim 0.10\,\mu$) it is clear that pair energies can actually be determined from multiple scattering only at energies $\lesssim 10^{11}$ ev.

The screening effect can thus be used to determine pair energies in the high-energy range where the usual methods are no longer applicable. It is first necessary to determine the energy dependence of the effect, for which purpose both measurements of track densities and independent measurements of pair energies are required.

The present paper gives measurements of grain density and mean gap length along the tracks of five electron-positron pairs with energies $\gtrsim 3 \times 10^{11}$ ev. Pair energies were estimated from the energy spectrum of cascade electrons produced by the pair and track densities were measured

TABLE I

Designation of shower	Range in single emulsion layer, mm	Volume of stack, liters	Layer dimensions, cm	Emulsion type	Exposure altitude, km	Exposure time, hours
E-53	3.5	0.5	10×10	R-NIKFI	20	9.5
O-209	12	3.0	10×20	»	26	9
D-84	9	1.0	10×20	»	20	10
D-44	6.5	1.0	10×20	»	20	10
I-109	3	Part of stack I	13×13	Ilford G5		

TABLE II

Shower	E_γ (after Janossy), ev	E_γ (after Chudakov), ev
E-53	$(8.4^{+7.2}_{-3.4})\cdot 10^{11}$	$2\cdot 10^{12}$
O-209	$(1.0^{+0.62}_{-0.45})\cdot 10^{12}$	$2\cdot 10^{12}$
D-84	$(1.8^{+1.44}_{-0.92})\cdot 10^{12}$	$2\cdot 10^{12}$
D-44	$(3.3^{+2.5}_{-1.3})\cdot 10^{11}$	
I-109	$(2.6^{+1.24}_{-0.98})\cdot 10^{11}$	

over a few millimeters. Three pairs with $\sim 10^{12}$ ev revealed the screening effect. The results are in agreement with Chudakov's theoretical curves.[1]

2. SHOWER CHARACTERISTICS

We studied electron-positron pairs which generated electron-photon showers in emulsions. Table I gives data on the emulsion stacks in which the showers were registered.[7]

The energies E_γ of pair-producing photons were determined from the energy spectrum of the cascade electrons. The method of determining E_γ was similar to that described by Pinkau[8] and by Miesowicz et al.[9]

At distances of 2.5 or 3.0 radiation lengths from the vertex of the first pair the energy spectrum of electrons within $200-300\,\mu$ about the shower axis was measured from multiple scattering. (The total noise in measurements of second differences was $0.13\,\mu$ in a $250\,\mu$ cell.) Cascade curves were used to determine pair energies in first approximation from the number N of electrons with energies $> 3\times 10^8$ ev. After corrections for the spatial distribution of electrons the same cascade curves were used to determine E_γ. We used Janossy's cascade curves;[10] shower energies E_γ are given in Table II.

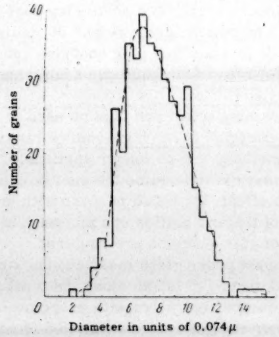

FIG. 1. Size distribution of developed grains in R-NIKFI emulsion. Mean diameter 0.57 μ.

The errors indicated in the table were determined from calculated data on fluctuations of N in a cascade. In accordance with Janossy's results[12] we determined the relative rms deviation σ from the mean value $\overline{N}$ $(> \epsilon)$. The experimental value of N was used to determine the mean value of E_γ, and the upper and lower limits of E_γ were determined from $N+\sigma N$ and $N-\sigma N$, respectively. We are now engaged in obtaining more accurate values of E_γ from curves calculated by the Monte Carlo method, taking into account the influence of the medium on bremsstrahlung;[11,12] the results will be published at a later date.

3. CALIBRATION OF EMULSION

As can be seen from Table I, in the present work we used principally R-NIKFI (Motion Picture and Photography Research Institute) emulsions. Figure 1 gives the size distribution of developed silver grains in one of the emulsion stacks.

Pair track densities were determined in two ways. We first counted grains directly to determine the grain density n. The gap length distribution was also obtained. An exponential description of the integral distribution was determined by least squares, with the exponential index giving the mean gap length $\overline{G}$ (Fowler and Perkins[13]). The procedure for measuring $\overline{G}$ was simplified. Gap lengths were not measured; instead we only determined the number of gaps longer than 1, 2, 3 etc. ocular scale divisions along the track image.

After determining $\overline{G}$ we calculated the coefficient $g = 1/(\overline{G}+\alpha)$, where $\alpha = 0.28\,\mu$ is the average diameter of AgBr crystals. According to O'Ceallaigh[14] g is the density of silver halide crystals which are developable as the result of the passage of a charged particle. We call g the density of developable AgBr grains to distinguish it from n, which is the density of developed Ag grains. In the developing process grain diameter is approximately doubled; one developed grain may appear in place of several closely situated developable AgBr grains. n is thus generally smaller than g.

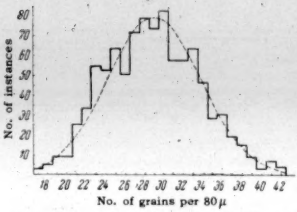

FIG. 2. Distribution of Ag grain density along relativistic electron tracks.

In our R-NIKFI emulsions the average grain density at the ionization plateau was ~32 grains per 100 μ. Figure 2 shows the grain density distribution n per 80 μ along relativistic electron tracks. The χ^2-test probability P compared with the Gaussian distribution is P = 0.5 to 0.6. The root-mean-square deviation from the mean of grain density along electron tracks is $\sigma = 0.89\sqrt{n}$, which is thus smaller than $\sqrt{n}$ (see reference 15).

In order to determine pair-induced ionization from grain density (n, g) we plotted calibration curves of grain density vs ionization. In the region of single ionization on the plateau (I_{pl}) grain density was measured along electron tracks. The track of a relativistic α particle was used to determine grain density for ionization $4I_{pl}$. In the intermediate region ($2-3\,I_{pl}$) we used the tracks of a few pions stopping in the emulsion. Pion-induced ionization for different ranges was determined from the curves of Barkas and Young[16] for specific ionization loss in AgBr crystals of Ilford G5 emulsions. The nuclear composition of the R-NIKFI emulsion[17] is close to that of Ilford G5.

Grain density measurements along the tracks of electrons with $\gtrsim 10^9$ ev and of pions with $\sim 5 \times 10^8 - 10^9$ ev gave the following ratio between the grain density n for plateau ionization and the grain density for minimum ionization:

$$n_{pl}/n(I_{min}) = 1.15 \pm 0.03.$$

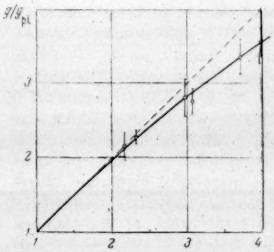

FIG. 4. Developable grain density g as a function of specific ionization loss in AgBr crystals. The dashed line represents g(I) as linear.

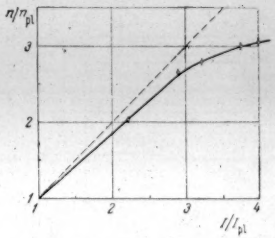

FIG. 3. Grain density n as a function of specific ionization loss in AgBr crystals.

In determining I_{pl} from the known value of I_{min} it was assumed that $I_{pl}/I_{min} \approx n_{pl}/n(I_{min})$. The value used for I_{pl} was 1.01 Mev cm^2/g.

The calibration curve for the density n of developed grains is shown in Fig. 3 with the statistical errors $\sqrt{n}$. It is evident from the curve that the grain density $n(2I_{pl})$ of doubly ionizing particles differs from $2n_{pl}$ (dashed curve) representing twice the density of singly ionizing particles by not more than 8 ± 1%.

Figure 4 shows the calibration curve for the density g of developable grains with the errors $g/\sqrt{N_B}$, where N_B is the total number of counted gaps (equal to the number of blobs along the track). The curves show that g(I) is more nearly linear than n(I). The difference between $g(2I_{pl})$ and $2g_{pl}$ does not exceed 1 or 2%.

4. RESULTS

We measured n and g for each of five electron-positron pairs. Figure 5 gives histograms of the measured grain density n for three pairs with $\sim 10^{12}$ ev along 2-mm track segments at the vertex.

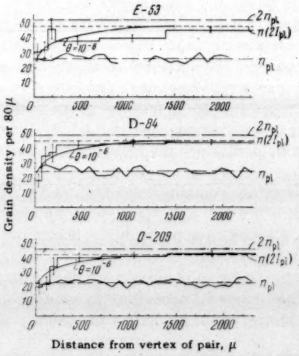

FIG. 5. Grain density n along tracks of pairs with $\sim 10^{12}$ ev (histograms). The irregular line represents the track density for relativistic electrons.

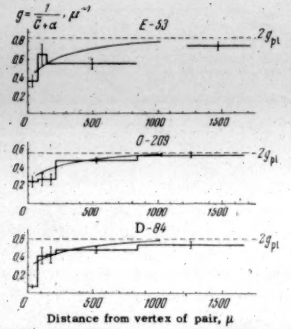

FIG. 6. Density g of developable grains along tracks of pairs with $\sim 10^{12}$ ev.

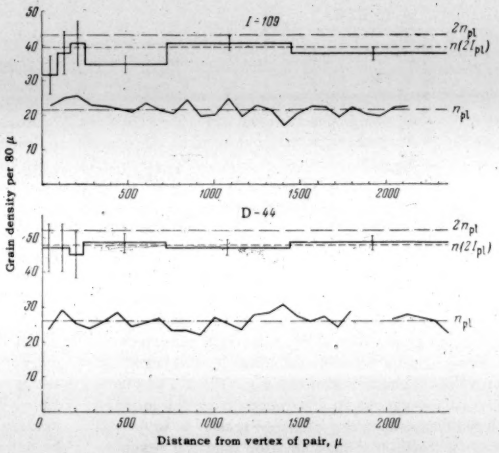

FIG. 7. Grain density n along tracks of pairs with $\sim 3 \times 10^{11}$ ev.

Statistical errors are indicated, as in all succeeding figures.

The irregular curve at the n_{pl} level serves as an index of the uniformity of emulsion properties and processing for the measured segments; it represents measurements of a few electron tracks at the same depth in the emulsion not farther than 100 or 200 μ from a measured segment of a pair track. Results obtained from different emulsion layers in which a single pair was measured were reduced to a single density n_{-1}. The density g was measured similarly along tracks of pairs (Fig. 6), and the results of the two procedures are seen to agree. In a segment $x < 250\,\mu$ at the vertex the observed ionization is clearly less than double ionization. With increase of the distance x from the vertex ionization rises rapidly, but the growth slows down for $x > 250\,\mu$. In 1.5 – 2 mm the grain density along pair tracks approaches the $n(2I_{pl})$ level. Screening evidently occurs here for pairs with $\sim 10^{12}$ ev.

Similar measurements were obtained for two pairs with $\sim 3 \times 10^{11}$ ev (Fig. 7) and, as was to be expected, showed no appreciable reduction of track density at the vertex.

It is interesting to compare our data with Chudakov's calculations,[1] according to which when multiple scattering of electrons is absent pair ionization in an emulsion must obey the law

$$I = 2I_{pl}\frac{23.9 + \ln \theta x}{9.4}, \qquad (1)$$

where θ is the vertex angle of the pair in radians and x is the distance from the vertex in centimeters (4×10^{-11} cm $< \theta \times \lesssim 3 \times 10^{-7}$ cm).

When multiple scattering is taken into account as in reference 1, but with the correct value of the scattering constant $K = 27\sqrt{\pi}$ Mev·deg/$\sqrt{100\,\mu}$ which gives the spatial separation of two electrons departing from the point $x = 0$ in the same direction the formula becomes

$$I = 2I_{pl}\frac{23.9 + \ln(\theta x \sqrt{1 + 70x})}{9.4}, \qquad (2)$$

where θ is the most probable vertex angle.

The best agreement between the experimental results for pairs in D-84, O-209, and E-53 and the theoretical curve (2) was observed for θ close to 10^{-6}. Figures 5 and 6 show the curves of n and g obtained from (2) for $\theta = 10^{-6}$ and the calibration curves. According to Borsellino[4] the angle $\theta = 10^{-6}$ corresponds to the most probable pair energy $E_\gamma = 2 \times 10^{12}$ ev.

Table II shows that the values of E_γ obtained by the different methods are in agreement, thus confirming the possibility of determining pair energies from ionization by using theoretical formulas which take screening into account. The uncertainty in determining E_γ from the screening effect results from statistical errors in determining ionization, from multiple scattering, the probabilistic character of the relation between θ and E_γ and the inexactitude of the theoretical formula. Additional experimental data are obviously needed to determine the errors in the values of E_γ obtained from ionization.

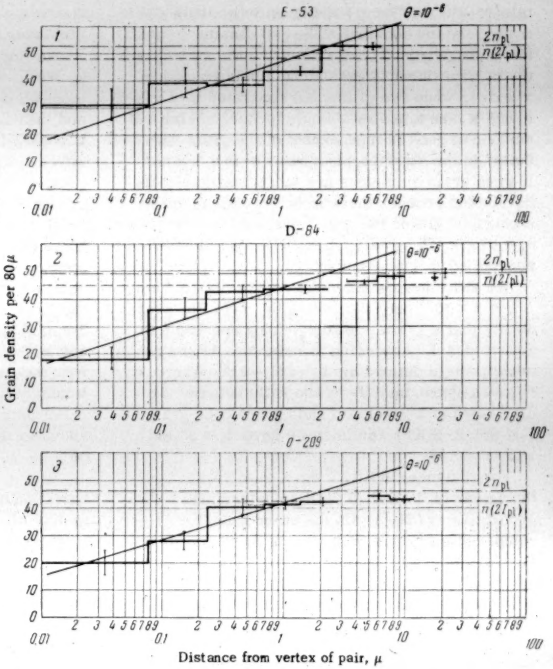

FIG. 8. Grain density n along tracks of pairs with $\sim 10^{12}$ ev.

We have compared our ionization measurements only with formula (2) of Chudakov,[1] which takes multiple scattering into account more correctly than the formula of Yekutieli,[2] for example. The latter ionization formula for a pair separated by the distance r (in cm) is

$$I = 2I_{pl}\,\frac{41.5 + \ln(r^2)}{13}.$$

The average of I is obtained by averaging $\ln(r^2)$. Integration of r multiplied by a function of its distribution is performed over the entire region from 0 to ∞, thus including the region of r where the given formula for I is meaningless ($0 \le I \le 2I_{pl}$).

Grain densities n were also measured at large distances x from the vertex (along almost the entire coalesced track segment). Figure 8, which gives the results for three high-energy pairs, shows a gradual increase of n for $x > 1$ or 2 mm, although the specific ionization loss of a pair remains constant.

A study of the structure of shower E-53 shows that one electron of the first pair possesses much higher energy than the other electron, so that the distance between the paths of the pair members increases more rapidly than in the case of the D-84 and O-209 pairs. This can account for the fact that n approaches the $2n_{pl}$ level more rapidly along the E-53 pair.

It is clear that the growth of grain density from the $n(2I_{pl})$ level to the $2n_{pl}$ level is a purely geometric effect. The $2n_{pl}$ level is reached as the electron separation becomes comparable to the diameter of developed grains ($\sim 5 \times 10^{-5}$ cm), i.e., when the adhesion of grains no longer affects the count. The blob density is even more strongly subject to this geometric effect.

In the present work for a visual count of n the difference $\{2n_{pl} - n(2I_{pl})\}/2n_{pl}$ was 8%, while the corresponding blob difference was about 20%. Weill and his coworkers[18] give 20% as the blob density.

We shall now estimate how much the gap density can be increased by the geometric effect. We first note that in the region where r is greater than or comparable to the diameter of AgBr crys-

tals ($r \gtrsim 2 \times 10^{-5}$ cm) the density g along a pair track remains constant. The gap density b and the average gap G are also constant. Indeed, in the measurement of gaps along a pair track (the x axis), when two grains not separated by a gap along x are taken as a single grain, the size and number of gaps is independent of the grain distribution in the plane perpendicular to the x axis. If when grain diameters are increased during the developing process there is no repulsion between contiguous grains the grain distribution with respect to x along pair tracks will also be independent of r (for constant g).

We shall now consider the region 5×10^{-7} cm $\leq r \leq 2 \times 10^{-5}$ cm. We denote by $\pi(I)$ the probability that a grain is struck during specific ionization loss I. According to reference 19 the gap density b is defined by $b = \pi(1-\pi)^k$, where k is given approximately by the ratio between the diameters of a developed and undeveloped grain. For the R-NIKFI emulsion we have $k \approx 2$ and $\pi(I_{pl}) = 0.08$.

For distances 5×10^{-7} cm $\lesssim r \ll 2 \times 10^{-5}$ cm the values of b and $\bar{G}$ will be determined by the probability $\pi(2I_{pl})$. On the other hand, for r comparable with the diameter of AgBr crystals ($r \sim 2 \times 10^{-5}$ cm) b and $\bar{G}$ will be determined by the probability $2\pi(I_{pl}) - [\pi(I_{pl})]^2$.

With small recombination we have, generally,

$$\pi(2I) \geqslant \{2\pi(I) - [\pi(I)]^2\}$$

and b will not increase with r; there may even be some decrease of b.

The inequality $\pi(2I_{pl}) < \{2\pi(I_{pl}) - [\pi(I_{pl})]^2\}$ can be satisfied if recombination in AgBr grains for double specific losses $2I_{pl}$ is appreciably greater than for I_{pl}.

According to Della Corte et al.[20] $\pi(2I_{pl})$ can be reduced by $\sim 3\%$ as a result of recombination, while $\pi(I_{pl})$ can be reduced by $1-2\%$. Therefore the greatest possible growth of b through the geometric effect is not above $1-2\%$. Thus the geometric effect must be very small for gap density (in the sense of the growth of b), unlike the case for the grain density n and blob density

In principle the geometric effect can also be used to determine the divergence angle of a pair; in this case it is better to use the blob density. The geometric effect will also appear for pairs with lower energies, when screening is absent; but this cannot result in errors when energy is determined from decreased ionization at the vertex since the two effects differ. Screening reduces pair ionization and track density compared with the level for a doubly ionizing particle, while the geometric effect would increase the density above this level.

We find no grounds for the conclusion reached by Weill, Gailloud, and Rosselet[18] that ionization measurements for pairs with energies $\gtrsim 10^{10}$ ev and the use of formulas that take screening into account will increase the result of the geometric effect by a factor of 100. If this were true the geometric effect for 5×10^{-7} cm $\lesssim r \lesssim 2 \times 10^{-5}$ cm could reduce track density compared with the level corresponding to double ionization. Our pairs had a small angle of divergence, so that their components were separated by a small distance for a relatively long time. The investigated region of the geometric effect occupies altogether about 2 cm of pair tracks. This region nowhere showed any appreciable reduction of n or g compared with the double ionization level. This refers particularly to measurements of n and g for the I-109 pair in an Ilford G5 plate. In any event, a reduction below the double ionization level could only be observed at the vertex.

As was stated by Weill et al, in their paper the variation of blob density resulting from the geometric effect is treated as a variation of ionization I; this led to the conclusion regarding the error in determining E_γ from screening. With calibration curves like those in Figs. 3 and 4 it is always possible to distinguish the regions of the geometric effect and screening.

Our results and those obtained by Perkins and by Wolter and Miesowicz[21] thus show the possibility of using the screening to determine pair energies. Any track parameters may be used which are sufficiently sensitive to variation of the ionization near $2I_{pl}$. The geometric effect cannot change the ionization and increase the energy E_γ.

In conclusion the authors wish to thank Professor I. I. Gurevich for his interest and for discussions, A. A. Kondrashina for assistance with the treatment of experimental results and D. M. Samoĭlovich and his group for the developing of the emulsions.

[1] A. E. Chudakov, Izv. Akad. Nauk SSSR, Ser. Fiz., **19**, 651 (1955) (Columbia Tech. Transl. p. 589).

[2] G. Yekutieli, Nuovo cimento **5**, 1381 (1957).

[3] I. Mito and H. Ezawa, Progr. Theoret. Phys. **18**, 437 (1957).

[4] A. Borsellino, Phys. Rev. **89**, 1023 (1953).

[5] M. Stearns, Phys. Rev. 76, 836 (1949).

[6] E. Lohrmann, Nuovo cimento **2**, 1029 (1955).

[7] Varfolomeev, Gerasimova, and Gurevich, Proceedings of the 1958 Annual International Conference on High Energy Physics at CERN, 1958, p. 297.

[8] K. Pinkau, Nuovo cimento **3**, 1285 (1956).
[9] Miesowicz, Stanisz, and Wolter, Bull. Acad. Polon. Sci., Cl. III, **4**, 811 (1956).
[10] L. Janossy and H. Messel, Proc. Roy. Irish Acad. **A54**, 217 (1956).
[11] L. Janossy, Acta Phys. Hung. **2**, 289 (1952).
[12] Varfolomeev, Golenko, and Svetlolobov, Dokl. Akad. Nauk SSSR **122**, 785 (1958), Soviet Phys. "Doklady" **3**, 977 (1958).
[13] P. H. Fowler and D. H. Perkins, Phil. Mag. **46**, 587 (1955).
[14] C. O'Ceallaigh, Compt. rend. Congrès de Bagnères, 1953, p. 73; Supplemento Nuovo cimento **12**, 412 (1954).
[15] P. E. Hodgson, Brit. J. Appl. Phys. **3**, 11 (1952).
[16] W. H. Barkas and D. M. Young, University of California Radiation Laboratory Report UCRL-2579, Berkeley, Cal., 1954.
[17] M. F. Rodicheva, Журн. науч. и прикл. фотограф. и кинематогр. (Journal of Scientific and Applied Photography and Cinematography) No. 3, 286 (1958).
[18] Weill, Gailloud, and Rosselet, Nuovo cimento **6**, 1430 (1957).
[19] Della Corte, Ramat, and Ronchi, Nuovo cimento **10**, 509 (1953).
[20] Della Corte, Ramat, and Ronchi, Nuovo cimento **10**, 958 (1953).
[21] D. H. Perkins, Phil. Mag. **46**, 1146 (1955); W. Wolter and M. Miesowicz, Nuovo cimento **4**, 648 (1956).

Translated by I. Emin
132

INVESTIGATION OF HIGH CURRENT PULSE DISCHARGES IN CONICAL CHAMBERS

N. A. BORZUNOV, D. V. ORLINSKIĬ, and S. M. OSOVETS

Submitted to JETP editor August 26, 1958

J. Exptl. Theoret. Phys. (U.S.S.R.) **36**, 717-726 (March, 1959)

Some general considerations are presented concerning the possibility of formation of a cumulative jet in the course of contraction of a conical plasma envelope. Preliminary results of some experiments performed with so-called single and double conical systems are presented. Photographs of discharges in conical chambers are presented, and also results of some other measurements.

1. INTRODUCTION

THE present work represents an attempt of utilizing the effect of formation of a cumulative jet as a mechanism of communicating additional energy to a certain group of particles in the course of formation of a plasma column in the process of development of a high current pulse discharge in a gas. The principle on which the investigations that we have carried out is based is similar to the principle of jet formation in a cumulative charge.[1]

We shall show that in the process of compression of a gas column of conical shape a jet may also be formed. We consider a conical vessel filled with gas (Fig. 1) through which a rapidly growing current passes. The magnetic forces of the current will compress the gas towards the center of the vessel. In the case of interest to us, when the speed of compression exceeds the speed of sound in the gas, a shock wave is formed moving towards the axis of the vessel. The instant of arrival of the shock wave on the axis (the instant of "singularity") may be determined from the following formula[2]

$$t_s = 1.8 r \left(\frac{1}{c}\frac{dJ}{dt}\right)^{-1/3}\left(\frac{\pi}{3} Mn\right)^{1/4}. \qquad (1)$$

Here Mn is the mass of gas per cm^3, while $r = r_0 + z \tan \alpha_0$. Evidently t_s will be different at different heights within the vessel. If we make the quite rough assumption that dJ/dt is constant, then the speed of displacement of the point z_1 vertically and the total compression time will respectively be equal to

$$\frac{dz}{dt} = 0.56 \cot \alpha_0 \left(\frac{1}{c}\frac{dJ}{dt}\right)^{1/3}\left(\frac{\pi}{3} Mn\right)^{-1/4}, \qquad (2)$$

$$\Delta t = 1.8 l \tan \alpha_0 \left(\frac{1}{c}\frac{dJ}{dt}\right)^{-1/3}\left(\frac{\pi}{3} Mn\right)^{1/4}, \qquad (3)$$

i.e., the compression of plasma will be spread out in time and all the quantities characterizing the process (current, voltage between the electrodes) will vary smoothly.

We consider an intermediate stage of the process of compression (cf. Fig. 1). We assume that at a certain instant of time the front of the shock wave has reached the axis of the chamber at the point z_1, while above this point the wavefront forms a cone whose vertical half angle is equal to α. The gas contained within this cone may be regarded as unperturbed. We shall at first assume that a strong skin effect exists and the magnetic field does not penetrate inside the plasma. Since the pressure in the compressed column is many times greater than the pressure of the unperturbed gas, then at this instant of time large pressure gradients exist in the plasma, with the maximum value being exhibited by the pressure gradient directed along the axis of the cone. As a result a jet of gas will be propagated along the z axis towards the unperturbed gas, which is analogous to a certain extent to the effect of formation of a cumulative jet.

A consistent solution of the problem encounters a number of mathematical difficulties which have not yet been overcome. A rough estimate of the speed of the jet may be obtained if we make use of the results of the solution of the problem on the propagation of a front of a nonstationary rarefaction wave which arises in the case of an instantaneous removal of a barrier which separates a gas from a region of complete vacuum.[3] The speed of the front of the rarefaction wave $v_f = 2u_0/(\gamma - 1)$ or, in the case of a monatomic gas, when $\gamma = c_p/c_v = 5/3$,

$$v_f = 3u_0, \qquad (4)$$

where u_0 is the velocity of sound in the gas prior to the removal of the barrier (since the thermal velocity of the gas atoms $v_{T_0} = (3/\sqrt{5})\, u_0$, then $v_f = 2.2 v_{T_0}$).

If we assume that the gas jet represents a rare-
ction wave, while the angle α determines only
e mass of gas captured into this wave, and
ereby the total momentum of the gas jet, then the
ergy of the particles at the front of jet with re-
pect to a stationary system of coordinates will
e several times greater than the thermal energy
f the particles in the compressed plasma.*

Such is the rough qualitative picture of this phe-
omenon in the case of a strong skin effect. How-
ver, if the skin effect is weak and the magnetic
eld of the current penetrates inside the plasma,
e problem is even more complicated since in
is case the motion of the gas will be determined
ot only by the gradient of the gas pressure, but
lso by the difference of magnetic pressures.

As an example we consider the one dimensional
roblem on the propagation of a rarefaction wave
n the presence of a frozen-in magnetic field. We
ssume that within a certain region of space sep-
rated from the rest of space by the plane $x = 0$
e have a plasma of density ρ_0 with a frozen-in
agnetic field H_0, whose lines of force are per-
endicular to the plane of the diagram (for $x \geq 0$,
$= 0$ and $H = 0$). At a certain instant of time the
lasma together with the field H starts spreading
nto the region of positive values of x. Let us de-
ermine the velocity of the front of the rarefaction
ave.

The intervals of time in which we are inter-
sted are such that the conductivity of the plasma
ay be considered infinite. Then the equations
escribing the process will differ from the equa-
ons of a similar problem in gas dynamics only
y the fact that the pressure of the gas p will be
eplaced by the sum of the pressure p and of the
agnetic pressure $H^2/8\pi$, i.e., by the pressure
$= p + H^2/8\pi$. In virtue of the fact that the mag-
etic field is frozen-in into a perfectly conducting
lasma, we have $H/\rho = H_0/\rho_0$. Taking into account
he equation of an adiabatic $p/p_0 = (\rho/\rho_0)^\gamma$ (which
ay also be written in the form $\rho/\rho_0 = (u/u_0)^{2/(\gamma-1)}$,
here u is the velocity of sound) we obtain:

$$P = \frac{p_0}{\rho_0^\gamma}\rho^\gamma + \frac{H_0^2}{8\pi\rho_0^2}\rho^2,$$

$$\frac{\partial P}{\partial x} = \frac{\partial p}{\partial x} + \frac{\partial (H^2/8\pi)}{\partial x} = [u^2 + w^2 (u/u_0)^{2/(\gamma-1)}] \frac{\partial \rho}{\partial x},$$

here $w = H_0/\sqrt{4\pi\rho_0}$ is the magnetohydrodynamic
elocity in the field H_0. This equation differs from
he corresponding equation for $H_0 = 0$ by the fact
hat in place of u^2 it contains $[u^2 + w^2 (u/u_0)^{2/(\gamma-1)}]$.
Therefore the one dimensional self-similar solu-
ion[3] obtained in the usual gas dynamics $(v - \eta)^2 =$

*Cf. the experimental determination of the optimum value of
he angle α in reference 4.

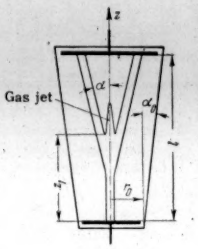

FIG. 1

u^2 (where $\eta = x/t$) must be replaced by the expression

$$(v - \eta)^2 = u^2 + w^2 (u/u_0)^{2/(\gamma-1)}. \quad (5)$$

Further, on utilizing the equation of continuity

$$\frac{\partial \rho}{\partial t} + \frac{\partial (\rho v)}{\partial x} = \frac{1}{t}\left(-\eta \frac{d\rho}{d\eta} + \frac{d(\rho v)}{d\eta}\right) = 0,$$

we obtain

$$\frac{2}{\gamma - 1}\frac{v - \eta}{u}\frac{du}{d\eta} + \frac{dv}{d\eta} = 0. \quad (6)$$

We determine the velocity v by eliminating $v - \eta$ from (5) and (6):

$$v = \mp \frac{2}{\gamma - 1}\int \left[1 + \frac{w^2}{c^2}\left(\frac{u}{u_0}\right)^{2/(\gamma-1)}\right]^{1/2} du.$$

On taking into account the fact that in the case of a monatomic gas $\gamma = 5/3$ and $u = (\sqrt{5/3})\, v_T$, we obtain:

$$v = \mp 0.83 \frac{v_{T_e}^2}{w^2}\left(1 + 1.8\frac{w^2}{v_{T_e}^2} v_T\right)^{3/5} + C.$$

Since $v = 0$ when $v_T = v_{T_0}$, we get

$$v = \mp 0.83 \frac{v_{T_e}^2}{w^2}\left[\left(1 + 1.8\frac{w^2}{v_{T_e}^2} v_T\right)^{3/5} - \left(1 + 1.8\frac{w^2}{v_{T_e}^2}\right)^{3/5}\right], \quad (7)$$

and at the front of the shock wave where $\rho = 0$, and consequently, also $v_T = 0$,

$$v_f = \mp 0.83 \frac{v_{T_e}^2}{w^2}\left[\left(1 + 1.8\frac{w^2}{v_{T_e}^2}\right)^{3/5} - 1\right]. \quad (8)$$

When $w \ll v_{T_0}$ we obtain the already known relation $v_f = 2.2 v_{T_0}$. In the other limiting case when $w \gg v_{T_0}$,

$$v_f = 2w. \quad (9)$$

These results cannot, of course, be directly applied to the case of compression of a conical plasma shell since, first of all, in order to do this a two dimensional problem should be solved, and, secondly, the distribution of gas density and magnetic field in space in our case is no longer uni-

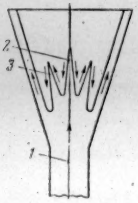

FIG. 2. Probable configuration of currents in the plasma in a discharge in a cone; 1–direction of the main current; 2–gas jet determined by a fall in the gas pressure; 3–gas jet determined by a fall in the magnetic pressure.

form. Nevertheless, we can still draw some qualitative conclusions. On the axis of the vessel where there is no magnetic field the velocity of the front of the jet which will be determined by the fall in gas pressure must be greater, by a factor of 2 or 3, than the thermal velocity of the gas in the compressed column. Nearer to the edge of the column, where the magnetic field increases sharply while the density of particles decreases, a difference of magnetic pressures may prevail and the velocity of the jet at that spot under certain conditions may become greater than the velocity of the jet along the axis (magnetic implosion). Since in this case the moving particles carry the lines of force of the magnetic field along with them the distribution of current over the cross section of the column must change (above the point z_1). As a result of the fact that the total current over the cross section must remain the same local currents may appear in the plasma directed oppositely to the direction of the main current. A possible picture of the distribution of current is shown in Fig. 2.

To increase the energy of interaction of accelerated particles two jets may be created and directed one against the other. Then the distribution of current at a certain instant of time may have the form shown in Fig. 3. Circulating currents flowing within the plasma may lead to the production of very high local electric and magnetic fields which in turn may communicate to a certain group of particles energy tremendous in comparison with thermal energy.

The possibility is not excluded that such a mechanism of acceleration of a group of particles may be used to explain neutron emission observed in a cylindrical gas discharge at a relatively low plasma temperature. As is well known, the constricting cylindrical plasma column is very inhomogeneous along its length.[5] One may suppose that the compression of the plasma towards the axis does not take place strictly simultaneously. At some spots the plasma will reach the axis somewhat earlier and other places somewhat later. Because of this at the instant of compression, conical or more complex surfaces may be formed near the axis of the cylinder. As a result when such surfaces contract a cumulative effect similar to the one described above may take place. The fact that the observed neutron emission is localized along certain segments of the compressed plasma[6] supports this hypothesis. Thus, apparently, it is possible to explain the neutron emission which appears at the instant of the first singularity. A much more intense emission of neutrons at the moment of the next plasma constriction is possibly also due to nonsimultaneous compression. But at this instant along the axis of the tube we no longer have unperturbed gas, as at the instant of the first singularity, but plasma and a magnetic field, and this intensifies the effect of magnetic implosion. It is difficult to indicate the possible configuration of circulating currents at that instant, but it may be supposed that the intensities of the magnetic and the electric fields in such a case may attain very high values.

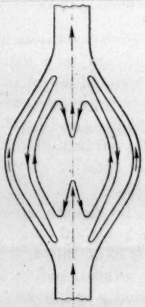

FIG. 3. Probable configuration of currents in the plasma in a discharge in a double cone.

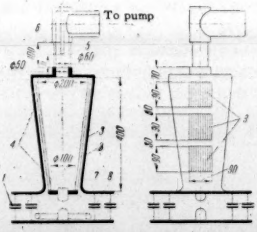

FIG. 4. Diagram of the apparatus. 1–capacitor bank; 2–truncated glass cone; 3–copper coaxial feeder; 4–copper electrodes; in the center of the upper electrode there is an opening of 5 cm diameter; 5–glass cylinder of 6 cm diameter; 6–piezoelectric detector; 7–spark relay; 8–Rogovskiĭ belt; 9–windows in the coaxial line for photographing the discharge.

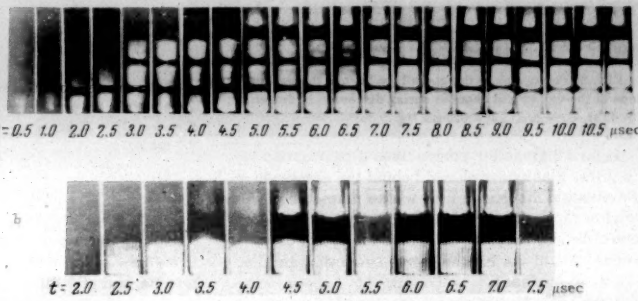

FIG. 5. Photographs of a discharge in deuterium in the conical chamber. C = 43 μf, U_0 = 25 kv, p_0 = 0.2 mm Hg.

2. INVESTIGATION OF THE DISCHARGE IN SIMPLE CONICAL SYSTEMS

1. The object of the first experiments was to study the process of constriction of plasma in a conical vessel and of the determination of the velocity of its propagation along the axis of the system behind the ring electrode. A schematic cross section of the apparatus and its external appearance are shown in Fig. 4.

The discharge current was measured by means of an integrating Rogovskiĭ belt. For the measurement of the velocity of propagation of plasma behind the upper electrode a piezoelectric detector was used. The use of the piezo effect for the determination of plasma pressure encounters at least two serious difficulties. Firstly, the conditions of the flow around the detector of a pressure wave moving with a speed of more than 10^6 cm/sec are still little known. Apparently the magnitude of the recorded pulse must depend both on the density of the particles in the front of the pressure wave, and also on its velocity. Therefore, there can be no certainty that even relative measurements of the pressure pulse under different conditions give a unique result. Secondly, the absolute calibration of the piezo detector must be performed under the same conditions under which these detectors are used, i.e., at a sufficiently high velocity of the pressure wave. Therefore in the present experiments the piezo detector was used only for the determination of the instant of the beginning of the pressure pulse, i.e., of the instant of arrival of the pressure wave at some specified point in the space behind the upper electrode.

For the investigation of the behavior of plasma in the cone in the initial stages of the discharge an ultra high speed photo recorder (u.h.s.p.r.) was used.[5] The speed of rotation of the mirror of the u.h.s.p.r. in all cases amounted to 60000 r.p.m. In accordance with this the time interval between frames in all the photographs shown below is equal to 0.5×10^{-6} sec. In order not to disturb the essentially axial symmetry of the current distribution in the course of photographing the discharge, three openings with conducting covers were made in the coaxial feeder bringing up the current to the discharge gap. Thus in the photograph (cf. Fig. 5a) we can see in each frame four rectangles situated one below the other. The three lower rectangles represent the windows in the coaxial feeder. The upper rectangle is a glass tube placed behind the ring electrode.

The experiments were carried out under the following conditions: the capacitance of the condenser bank which served as the supply for the discharge was $C = 35 - 45\mu f$, the initial voltage on the condensers was $U_0 = 25 - 40$ kv, and the initial deuterium pressure was $p_0 = 0.02 - 1.0$ mm Hg.

2. The photographs of the discharge enable us to obtain some idea about the initial stage of the process. As in the case of a cylindrical chamber breakdown occurs near the walls. Then, as the current increases, the plasma begins to constrict towards the axis of the chamber. From the photograph (Fig. 5) it is seen that constriction of plasma occurs first in the region nearest to the vertex of the cone. With time the region of constriction extends towards the ring electrode. The whole process of compression lasts approximately 1.5 microseconds. However, even when the gas has been compressed only in the central part of the chamber the plasma column near the lower electrode is already beginning to break up. Towards the end of the process of compression when a plasma column can be seen near the ring electrode a compressed column no longer exists in the remainder of the chamber.

Figure 5b shows a photograph of only the upper window in the coaxial cable and the glass tube behind the electrode. The speed of propagation of the luminosity in the tube is approximately equal to 1.1×10^7 cm/sec.

FIG. 6. Photograph of the glass tube beyond the upper electrode of the cylindrical chamber during discharge in deuterium; $C = 43\,\mu f$, $U_0 = 25$ kv, $p_0 = 0.2$ mm Hg.

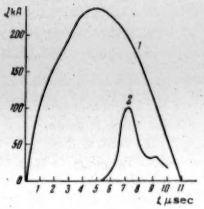

FIG. 7. 1–discharge current, 2–pulse from the piezodetector, $C = 35\,\mu f$, $U_0 = 25$ kv, $p_0 = 0.2$ mm Hg.

Figure 6 gives for comparison a photograph of a similar glass tube placed behind the electrode of a straight discharge tube whose diameter is equal to the diameter of the larger base of the cone (i.e., 20 cm). In this case the speed of propagation of the luminosity is somewhat smaller ($\sim 7 \times 10^6$ cm/sec).

3. As already mentioned, the speed of propagation of the gas jet was determined by a piezoelectric detector.[7] The signal from the detector which was placed on the axis of the cone behind the upper electrode was amplified and applied to the plates of the oscillograph. The signal from the integrating belt was applied to the second pair of plates. Typical curves showing the variation of the discharge current and the pressure are given in Fig. 7. As should have been expected the discharge current varies smoothly. The singularity on the current curve is very much smoothed out. This is in complete accord with the photographs of the discharge which show that the compression of the plasma takes place gradually.

Figure 8 shows the dependence of the instant at which the piezo detector pulse begins on the initial deuterium pressure. The curve was obtained with the distance between the surface of the electrode and the surface of the detector equal to $h = 6.5$ cm. The capacitance of the condenser battery in this case amounted to $C = 36\,\mu f$, while the initial voltage was $U_0 = 35$ kv ($J_m \approx 340$ kiloamp). The dependence of the instant t_p (at which the pressure pulse begins) on the value of h was obtained at $C = 43\,\mu f$, initial deuterium pressure of $p_0 = 0.3$ mm Hg and at 3 different initial voltages ($U_0 = 25$, 30, and 38 kv). A common characteristic of all three curves is the fact that initially (as h changes from 0 up to approximately 5 – 8 cm) t_p varies linearly, but at larger h an appreciable deviation from a straight line occurs. Figure 9 shows this dependence obtained at $U_0 = 30$ kv ($J_m \approx 300$ kiloamp). For convenience, the time is plotted along the horizontal axis. For comparison we have plotted in the same graph the form of $h(t_p)$ obtained when the cone was replaced by a cylinder of 20 cm diameter, but with the same initial voltage and deuterium pressure. Each point on the graph has been obtained by averaging the results of several independent measurements. At h = 15 cm the results of all the individual measurements are shown. By utilizing this graph it is possible to make an estimate of the speed of propagation of the front of the jet behind the electrode. In the case of the cylinder this velocity amounts to approximately 6×10^6 cm/sec. For the cone the velocity of the front of the jet increases as it moves away from the electrode from 6×10^6 cm/sec to $\sim (1.5 - 2.0) \times 10^7$ cm/sec. An increase in velocity begins when h is of the order of the di-

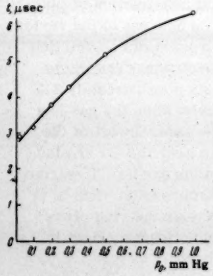

FIG. 8. Dependence of the initial instant of the pulse from the piezodetector on the initial deuterium pressure.

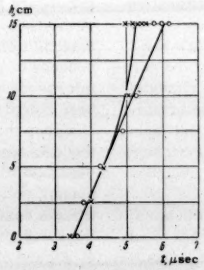

FIG. 9. Position of the front of the gas jet at time t. × – cone, o – cylinder.

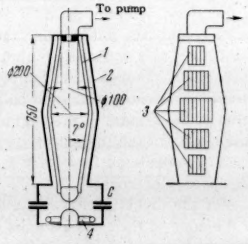

FIG. 10. Diagram of the double conical system. 1–glass chamber; 2–copper coaxial feeder; 3–windows with covers; 4–Rogovskiĭ belt.

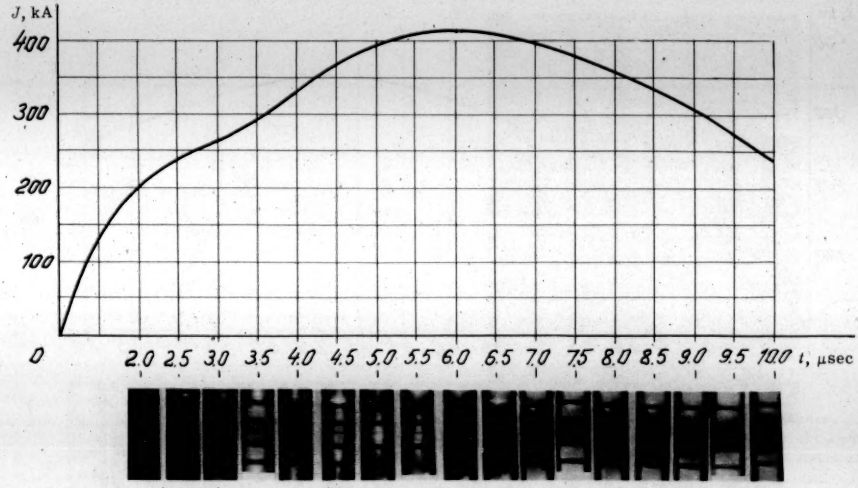

FIG. 11. Photograph and oscillogram of the discharge current in deuterium in a double conical system.

ameter of the opening in the upper electrode. One might conjecture that here apparently some electrode effects are felt as a result of which the jet is no longer formed in the region close to the upper electrode.

3. INVESTIGATION OF THE DISCHARGE IN DOUBLE CONICAL SYSTEMS

1. To use the energy of the particles carried by the gas jet it seems advisable to produce in the same system two jets directed one against the other. A diagram of the simplest apparatus in which such a process may be realized is given in Fig. 10.

A photograph of the discharge in such a system obtained with $C = 43\mu f$, $U_0 = 35$ kv ($J_m \approx 410$ kiloamp) and $p_0 = 0.2$ mm Hg is shown in Fig. 11. The following two features should be noted. First, the compression of the plasma begins at the electrodes and extends towards the center of the chamber. This indicates that in such a system two opposing jets may actually be formed. Secondly, the breaking up of the compressed column also begins near the electrodes. The compressed column of plasma in the central part of the system exists for a relatively long time (~ 2 μsec). This may be explained by the fact that when the plasma column near the electrode begins to break up, the inductive reactance of the discharge decreases, the current rises, and the electrodynamic forces compressing the plasma are also increased. Because of this, just in that part of the discharge where the greatest number of particles is available per unit length (and, correspondingly, the density of particles in the constricted plasma column is greatest) and where the energy of the particles is also a maximum, as a result of the formation of the jet, the constricted column lasts for a longer time, than in the case of a discharge in a straight tube under the same conditions.

Figure 12 shows a photograph and an oscillogram of the discharge current in argon, where all the characteristic phenomena are exhibited more distinctly. The photograph was obtained at an initial voltage of $U_0 = 32$ kv ($J_m \approx 350$ kiloamp) and at an initial pressure of $p_0 = 0.05$ mm Hg. The plasma column in the central part of the system lasts approximately until the end of the first half period of the discharge current.

2. Some measurements were carried out using a double porcelain cone whose dimensions differed somewhat from the dimensions of the glass cone. The diameter of the larger base of the truncated porcelain cone was 250 mm, the diameter of the smaller base was 90 mm, the height of each cone was 275 mm, the distance between the electrodes was 550 mm, the half-angle at the vertex of the cone was 17°.

Figure 13 shows oscillograms of the discharge current and of the voltage between the electrodes

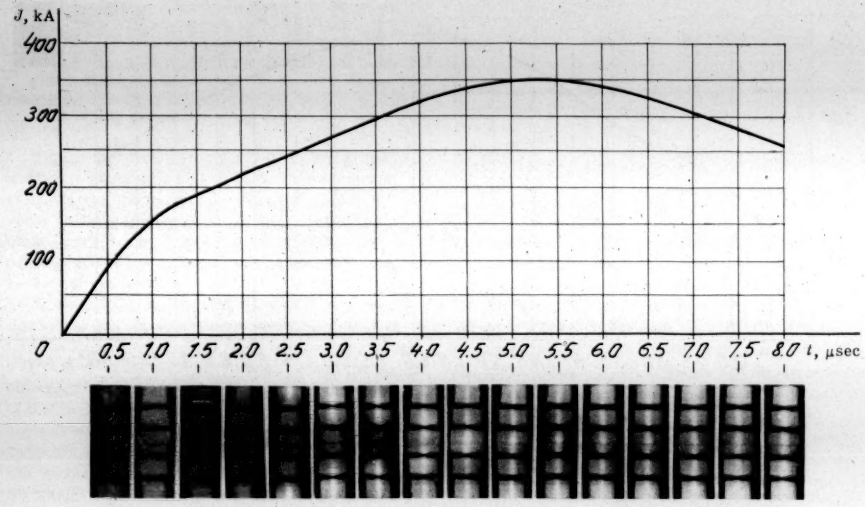

FIG. 12. Photograph and oscillogram of the discharge current in argon in a double conical system.

in the double cone, and for comparison also the same oscillograms obtained for the discharge in a cylinder. While the latter (curves c and d) exhibit three singularities, the oscillogram for the cone (curves a and b) shows only one smooth singularity indicating that the compression of plasma and its decay occur gradually, which is in accord with the photographs of the discharge. This is also confirmed by measurements of the velocity of propagation of the discharge current from the periphery towards the axis of the chamber carried out by means of magnetic probes (cf. Fig. 14).

Two small coils (of cross section 0.4 × 0.6 cm and with a number of turns w = 15) were placed inside the chamber. One of these was placed in the median plane (coil 1) while the other was placed at a distance of 12 cm from the first one in the direction towards the upper electrode (coil 2). Thus the radius of the first cross section was 12.5 cm, while the radius of the second was 9 cm. Both coils could be displaced radially. Since all the oscillograms were obtained consecutively it is not possible to obtain from these measurements the distribution of the current density over the cross section of the chamber, but the data on the propagation of the current front shown in Fig. 14 may be regarded as sufficiently reliable. Moreover, from the oscillograms obtained it is seen that near the axis of the chamber, in its median cross section, at the time of compression a current exists in a direction opposite to the discharge current. This supports to some extent the hypothesis concerning the existence of closed cir-

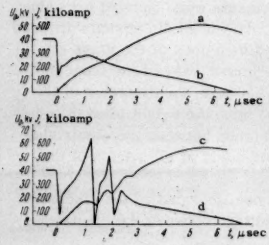

FIG. 13. Oscillograms of the voltage between the electrodes and of the discharge current in the porcelain double cone and in the straight tube. In both cases C= 65 μf, U_0 = 40 kv, p_0 = 0.06 mm Hg. (deuterium).

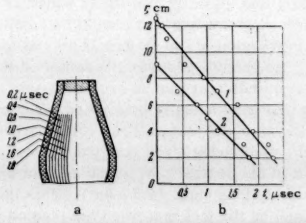

FIG. 14. a–propagation of the current front towards the axis of the system, b–curves showing the compression of the inner boundary of the current towards the axis of the porcelain double cone: 1–magnetic probe No. 1; 2–magnetic probe No. 2.

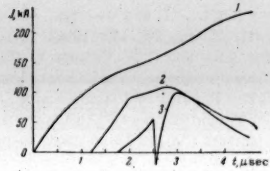

FIG. 15. Current in the region near the axis of the porcelain double cone. 1–total current; 3–current in the middle section of the chamber measured by means of a small coil placed at a distance of 4 cm from the axis; 2–the same current in a section situated 12 cm above the first.

culating currents in the discharges of such a type. The duration of the "reverse" current does not exceed 0.3 μsec. Figure 15 shows curves of the variation of current recorded by both coils at a distance from the chamber axis of $r_1 = r_2 = 4$ cm (it is assumed that the cylindrical symmetry of current distribution in the initial stage of the discharge is not upset).

3. In the course of all the experiments with the porcelain double cone the neutrons and the x rays was recorded. A scintillation counter with a NaI crystal or naphthalene with anthracene* served as a detector. Experiments were carried out with $C = 65\mu f$, $U_0 = 40$ kv ($J_m \approx 500$ kiloamp) and at various deuterium or hydrogen pressures.

The neutron radiation appears after several conditioning discharges, with the pulse of this radiation beginning between the singularity and the current maximum (cf. Fig. 16). No hard x rays (which would be capable of penetrating 2.5 cm of porcelain, 0.1 cm of copper, 0.3 cm of lead and an aluminum screen of thickness 0.5 cm) were observed when the discharge chamber was filled with hydrogen.

CONCLUSION

1. The theoretical investigation of the processes occurring during the constriction of a conical plasma envelope of a high current pulse discharge is a very complicated problem which at present has not yet been solved. Nevertheless, the considerations presented in the first section of this paper allow us to postulate that under certain conditions additional energy may be communicated to a certain small group of particles. In particular, in a double conical chamber the temperature of the plasma in the central portion of the column may be increased by these means.

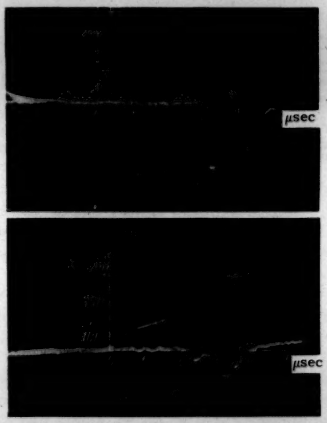

FIG. 16. Oscillogram of the discharge current J, of the voltage between the electrodes U and of the neutron emission n in the case of a discharge in the double conical chamber.

2. Experimental investigations indicate that the cumulative process which occurs in a single conical system leads to a certain increase (by factor of approximately 2 or 3) of the velocity of the plasma along the axis of the column compared to the velocity of the plasma along the axis of a cylindrical system. It should be emphasized that to obtain more accurate and complete information on the motion of plasma in such systems further detailed investigation is required.

3. Investigation of the neutron emission by the plasma produced in a double conical system indicates that this radiation, first, is not related in time to the singularities in the oscillograms of the current and of the voltage and, secondly, is not accompanied by x rays. Unfortunately the experimental data available to us are insufficient to explain either the magnitude of the neutron yield, or the displacement in time between the negative spike of current near the axis (Fig. 15) and the moment of initiation of the neutron pulse.

4. The photographs of Fig. 14 apparently point to a possibility of stabilizing a plasma column by means of prescribing a definite initial configuration of the discharge.

The present work must be regarded only as a

*The threshold of sensitivity of this counter is not lower than 10^4 neutrons per pulse. Since the sensitivity of another method of recording neutrons (by means of the induced β activity in a silver foil), which is approximately equal to 10^6 neutrons per pulse, turned out to be insufficient to detect the neutrons, the observed yield must lie in the range from 10^4 to 10^6 neutrons per pulse.

preliminary attempt to study phenomena occurring in the constriction of a conical plasma envelope with the formation of a cumulative jet. To obtain more complete information further theoretical and experimental investigations are necessary.

[1] Birkhoff, MacDougall, Pugh, and Taylor, J. Appl. Phys. **19**, 563 (1948).

[2] M. A. Leontovich and S. M. Osovets, Атомная энергия (Atomic Energy) **1**, 81 (1956).

[3] L. D. Landau and E. M. Lifshitz, Механика сплошных сред (Mechanics of Continuous Media), GITTL, 1954, p. 439.

[4] V. Josephson, J. Appl. Phys. **29**, 31 (1958).

[5] Borzunov, Orlinskiĭ, and Osovets, Атомная энергия (Atomic Energy) **4**, 149 (1958).

[6] N. A. Borzunov and D. V. Orlinskiĭ, Сб. Физика плазмы и проблема управляемых термоядерных реакций, (Anthology, The Physics of Plasma and the Problem of Controlled Thermonuclear Reactions), M. A. Leontovich, editor, U.S.S.R. Acad. Sci. Press, 1958, vol. 2, p. 150.

[7] N. V. Filippov, ibid., vol. 3, p. 231.

Translated by G. Volkoff
133

HIGH-ENERGY NEUTRONS IN COSMIC RAYS

G. N. FLEROV, V. I. KALASHNIKOVA, A. V. PODGURSKAYA, E. D. VOROB'EV, and G. A. STOLYAROV

Submitted to JETP editor September 2, 1958

J. Exptl. Theoret. Phys. (U.S.S.R.) **36**, 727-734 (March, 1959)

Multiple-plate ionization chambers were used to detect the fission of heavy nuclei by cosmic rays. The altitude dependence of fission was investigated as well as the angular distribution of the fission-inducing particles. The energy and momentum of the latter were estimated. It is shown that in the great majority of cases the fission of nuclei is induced by the nucleonic component of cosmic radiation.

A number of remarkable phenomena have been discovered through studies of the interactions between cosmic ray particles and matter. Cosmic rays are far from being homogeneous and their energies can be very high. It is known that the fission of heavy nuclei such as uranium and thorium requires excitation energies of only a few Mev independently of the excitation mechanism. It could naturally be expected that cosmic radiation would be able to induce the dission of heavy nuclei. Conversely, the study of fission induced by cosmic rays furnishes additional information about the composition of cosmic rays.

Flerov and Stolyarov detected in 1945 the fission of uranium and thorium by cosmic rays. Flerov's dissertation in 1950 was based on a number of experimental studies of the cosmic ray component which can induce the fission of heavy nuclei.

The fission of heavy nuclei can be recorded by many means such as thick emulsions containing a heavy element, ionization chambers or counters and chemical techniques. We used multiplate ionization chambers, which had previously been employed in the study of spontaneous fission.[1] Substantial improvements in the design of the chambers and in the methods of amplification increased the efficiency of this technique a factor of 50 to 100 compared with the apparatus of 1939 — 1941 and thus made it possible to observe fission induced by cosmic rays, whereas attempts which have been made by means of photographic plates[2,3] did not yield definite results because of the low efficiency of this latter method.

In 1945 an ionization chamber containing uranium was raised to an altitude of 11 or 12 km above sea level. This first chamber contained only 0.3 g of fissionable uranium. In the course of 30 minutes the chamber, which was entirely surrounded by a thick layer of boron, registered 9 ionization pulses, of which 3 or 4 pulses could be attributed to spontaneous uranium fission occurring with a lifetime of about 10^{16} years.

The ionization pulses could be produced by (1) nuclear disintegrations releasing large amounts of energy, (2) cosmic ray showers of large numbers of particles, or (3) nuclear fission. Since this last cause only applied to a chamber contafning uranium, another ionization chamber containing plates covered with lead was raised to the same altitude. The absence of any effect in the control chamber eliminated the first two causes so that some of the ionization pulses, after subtracting those resulting from spontaneous fission, could be attributed to the fission of uranium by cosmic rays.

The small magnitude of the observed effect even at high altitudes and the large spontaneous fission background made it practically impossible to obtain quantitative results with a uranium-loaded chamber. We therefore prepared multiplate chambers containing thorium as the working material. Special experiments showed that the spontaneous fission lifetime of thorium is at least 10^{20} years.[4] Experiments with these chambers at high altitudes furnished even more convincing evidence that cosmic rays can cause fission.

The first experiments with the fission-inducing component aimed to establish some basic laws such as the variation of intensity with altitude and the angular distribution of fission-inducing particles. Sounding balloons were used in 1945 — 1948 to investigate the altitude dependence. Measurements were obtained at 9 — 22 km, at geomagnetic latitude $\lambda = 52°$. From 9 km to 15 km the chamber counting rate increased by a factor of about 4 and amounted to 10 fissions per gram of thorium per hour. At greater altitudes the count decreased appreciably instead of increasing, leading to the very important conclusion that the particles which induce fission in the chamber do not belong to the primary cosmic ray component.

At lower altitudes the effect becomes very small

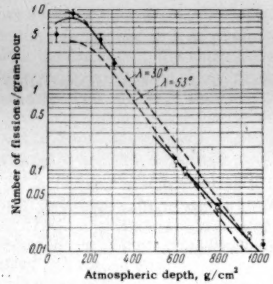

FIG. 1. ○ – λ = 28° (Pamir), ● – λ = 52° (120 m above sea level); solid curves – experimental, dashed curves – calculated.

(1 or 2 fissions per gram of thorium per day) and measurements are extremely difficult. Thorium fission by cosmic rays was measured at 4700, 3860, and 2200 m (Pamir, λ = 28°) as well as 120 m above sea level (λ = 52°).

Figure 1 shows the altitude dependence of the fission-inducing component. The results obtained with apparatus raised by sounding balloons are seen to be somewhat shifted with respect to those obtained at Pamir. This shift can apparently be attributed to the difference of latitude, which is associated with the geomagnetic effect of primary cosmic rays.

At Pamir the angular distribution of the fission-inducing component was measured at 3860 m. Three pits were dug in the sandy soil, which were 2 m deep and had the shapes of cones with angles $2\alpha = 80$, 60, and 44. The counting rate $N(2\alpha)$ at the bottom of a pit was compared with the rate for the same chamber, $N(\pi)$, at the surface. There was relatively little background from radiation passing through the soil.

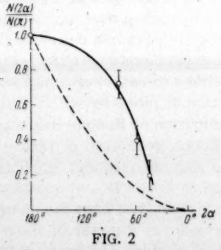

FIG. 2

The results, with a background correction, are shown in Fig. 2, where the dashed curve represents the calculated effect for isotropically directed radiation and the solid curve gives the actual intensity of the fission-inducing component as a function of 2α. A comparison of the two curves shows that the fission-inducing particles are mainly included within a relatively small solid angle around the vertical direction.

Experiments on altitude dependence and angular distribution do not, however, clearly determine the nature of the fission-inducing radiation since, as we know, uranium and thorium can be fissioned at a few Mev regardless of the type of particle which contributes this energy to the nucleus. Accordingly, further experiments were directed toward the study of the fission-inducing particles themselves for the purpose of determining their nature.

The essential properties of a particle are its charge, energy, momentum (mass) and lifetime (if the particle is unstable).

In order to determine whether the fission-inducing component is charged or neutral we ran a series of experiments at 3860 m in which a multiplate chamber registering thorium fission was surrounded on all sides by one or two rows of Geiger counters. Pulses from fission fragments were registered on film, while a special electronic circuit recorded coincidences between fission pulses and counter pulses, thus permitting a rough estimate of the number of ionizing particles as registered by the counter system for all coincidences.

In some runs 690 fissions were recorded in the chamber, of which only 89 were accompanied by counter pulses. These data lead to the conclusion that most of the radiation which induces fission is neutral. The ionizing component apparently does not exceed 15%.

The first experiments on the absorption of the fission-inducing component by lead showed that this component is highly penetrating and completely eliminated the hypothesis that fission might be induced by cosmic gamma rays. We must thus attribute fission to cosmic neutrons.

The energy of the fission-inducing cosmic particles was determined by means of an ionization chamber with bismuth-loaded plates. We know from experiments on heavy-element fission by fast neutrons[5] that for neutron energies of a few tens of megavolts the fission cross section of bismuth is about $10^4 - 10^3$ times smaller than the thorium cross section. The bismuth fission cross section grows quite rapidly with increasing neutron energy and at 100 Mev becomes 3×10^{-2} barns, whereas the thorium fission cross section, which is one barn at a few tens of megavolts, remains practically unchanged in this region. Thus the bismuth-loaded chamber registered essentially only those fission events in which the fission-inducing particle contributes more than 100 Mev to

the nucleus, whereas the thorium-loaded chamber can be regarded as integrating the intensity of the fission-inducing component over its energy spectrum because the threshold for thorium fission by neutrons is very low (~ 1 Mev).

In 1949 bismuth-loaded multiplate ionization chambers were carried by balloons to a height of 13 – 20 km. In two ascents lasting two hours at a high altitude 18 bismuth fissions were recorded, comprising about 1.5 fissions per hour per gram of working material. Experiments with a large chamber containing about 40 g of effective bismuth were performed at 3860 m, at which altitude during 370 hours of observation 123 fissions were registered, comprising 0.33 ± 0.03 fissions per hour. By comparison a similar thorium-loaded chamber registered 4.0 ± 0.2 fissions per hour under the same conditions. The ratio of 12 should be determined by the ratio of the mean thorium and bismuth fission cross sections taking into account the cosmic ray spectrum. Assuming that thorium and bismuth fission is caused by neutrons and considering that the thorium fission cross section is not reduced when the neutron energy increases up to 400 Mev (at 380 Mev, $\sigma_{f\ Th} = 0.9$ barns) while the bismuth fission cross section continues to grow (at 380 Mev, $\sigma_{f\ Bi} = 0.074$ barns), we can infer from our results that the fission-inducing neutrons have an effective energy of about 400 Mev. A chamber containing tungsten, which has a fission cross section for 400-Mev neutrons that is about 20 times smaller than the bismuth cross section, yielded practically no result, which indicates that the fission-inducing component contained no neutrons with energies considerably above 400 Mev.

Particles with energies of a few hundred Mev transfer considerable momentum to fissioning nuclei. The mass of a particle can be determined from its energy and momentum; we therefore ran a series of experiments to determine the recoils of fissioning nuclei which have captured very fast particles. We prepared special multiplate ionization chambers in which the thorium layers were deposited on only one side of each plate. Since the motion of the fission-inducing particles is predominantly in the vertical direction, the momentum of a fissioning nucleus would be revealed by the fact that fission fragments would not have an isotropic spatial distribution but would tend to emerge from the fissioning material in the downward direction of the incident particle. The pulse counting rate would then depend on the ionization chamber arrangement, i.e., on whether the active layers were on the upper or lower surfaces of the plates.

Two identical chambers operating simultaneously, but alternately with respect to the "up" and "down" positions, during 944 hours registered 431 downward fissions and 296 upward fissions, thus establishing an asymmetrical fission fragment distribution. It is easily seen that the difference between the downward and upward effects compared with the total number of fissions is directly proportional to the momentum imparted to the fissioning nucleus. The observed asymmetry is somewhat reduced by the fact that the direction of the fission-inducing particle is not strictly vertical. Allowance for the angular distribution of fission-inducing particles increases the observed effect by about 20%, so that the asymmetry amounts to about 0.23 ± 0.5.

This result was compared with the corresponding data from thorium fission in the same chambers induced by fast 4- or 5-Mev neutrons from a Po + Be source. In this latter case the asymmetry is much smaller, amounting to only 0.034 ± 0.008. Therefore the momentum imparted to a fissioning nucleus by a cosmic particle exceeds that imparted to thorium by neutrons from the given source by a factor of about 7 ± 2. If we assume that the mass of the cosmic particle is of the order of a nucleonic mass we can estimate the mean energy of the fission-inducing particle from the momentum ratio. A rough estimate gives 100 – 400 Mev as the mean energy of the particles that induce thorium fission. In actuality the energy values derived from recoil experiments is considerably reduced through the fact that the momentum imparted to the nucleus by a fission-inducing particle may be partly carried away by a considerable number of fast neutrons escaping from a highly excited nucleus before it fissions.

Thus the rough estimate of neutron energy based on the recoil experiments is not in conflict with the more exact results obtained for bismuth fission; that is, the effective energy of cosmic neutrons which induce the fission of heavy nuclei is about 400 Mev.

We also performed a long series of experiments at 3860 m on the absorption of the fission-inducing component in dense matter (graphite and aluminum) whose atomic weight is close to that of air. These results were compared with data on the altitude dependence of the fission-inducing component intensity. The range of this component in air as determined from the altitude dependence (Fig. 1) is about 140 g/cm^2, which is in good agreement with the 120 g/cm^2 range of the nucleonic component. The ranges of the fission-inducing component in graphite and aluminum considerably exceed the ranges calculated from the mass and

Absorber	Thickness of absorber, g/cm²	Thickness of absorber allowing for its atomic weight, g/cm²	Range of fission-inducing component in g/cm² allowing for atomic weight of absorber	
			Experimental	Calculated
Graphite	119	126	410±120	130
"	136	144	550±100	130
"	177	188	340±90	130
"	195	207	410±80	130
Aluminum	150	120	340±110	170
"	300	240	330±85	170

atomic weight of the absorbers by comparison with the experimental range in air. Thus, the calculated ranges are 130 g/cm² for graphite and 170 g/cm² for aluminum, while the experimental ranges are ~400 g/cm² (see the table).

A similar but somewhat smaller effect has been observed by a number of investigators of the absorption of the nucleonic component in dense matter.[6] However, the complex processes which occur when cosmic particles pass from air into a dense medium make it very difficult to interpret the experimental results. In free air different portions of the nucleonic component are approximately in equilibrium, with a relatively small number of pions present in virtue of their short lifetime. The relative number of pions is strongly enhanced in dense matter, as noted by G. T. Zatsepin in 1949 during a discussion of these results. The observed low absorptivity of graphite and aluminum compared with air could be accounted for by an additional number of fissions under dense matter due to the pion excess. We might then expect that under dense matter the ratio of fissions induced by neutral and charged particles would change strongly in favor of the latter. However, it was found that an ionization chamber surrounded by counters connected for coincidence with fission fragments and placed under an 80-cm graphite absorber registers, as previously, an overwhelming majority of fissions induced by neutral particles. The percentage of registered coincidences compared with the total number of fissions under the absorber is somewhat increased (~20%), but the nature of the effect suggests that a considerable fraction of the coincidences results from the fact that the chamber under the absorber also registers large dense showers (0.5 particle/cm²). This also follows from experiments on enhanced ionization in a tungsten-loaded chamber surrounded by counters. In the open air this counter revealed no practically measureable effect, whereas under an 80-cm graphite absorber a considerable number of pulses was observed, all accompanied by the triggering of all or a large fraction of the counters. We can thus assume that under an absorber thorium fission is induced mainly by neutrons. The extra number of thorium fissions under a dense material could be attributed to some difference in the neutron spectra within the atmosphere and under an absorber such as graphite. Indeed, the interaction of neutrons with atmospheric nitrogen involves a (n, α) reaction which can considerably attenuate the flux of neutrons possessing energies of a few tens of megavolts. It is difficult to calculate this effect exactly; an experimental estimate was obtained by measuring the number of fissions in a thorium-loaded chamber surrounded by 20-cm thick paraffin under a graphite absorber and in air. However, these experiments showed that the relative number of neutrons with 10 — 20 Mev is small in both cases, that there is no essential observable difference and that this effect can therefore not account for the absorption data.

It is therefore most reasonable to associate the unusually long range of the fission-inducing component with the extra number of pions in dense substances. Experiment has shown, however, that fission is not induced directly by pions, but evidently by neutrons which appear as a result of pion-induced nuclear reactions in dense matter. The given measurements as a whole therefore suggest that the enhanced ionization registered by the ionization chambers was produced by fragments from fissions induced mainly (~85%) by the neutron portion of the nucleonic component.

An effective nucleonic energy ~400 Mev was estimated from experiments with bismuth as well as from the recoils of fissioning nuclei after neutron capture.

The angular distribution of particles which induce the fission of heavy nuclei was found to be sharply anisotropic, with most of the particles within a solid angle of about 60 — 80° about the vertical direction.

It follows from the altitude dependence of the fission-inducing component that its intensity rises approximately exponentially with the exponential index 140 g/cm². A peak of the altitude dependence was observed at a depth of the order of 100 g/cm² from the top of the atmosphere, thus indi-

cating the secondary character of these particles.

Finally, our experiments permitted an estimate of neutron flux at a few hundred Mev. Since the thorium fission cross section in this energy region is practically invariant at about one barn, the flux can be estimated from the measured counting rate in a chamber containing a known amount of active thorium. The latter quantity was determined by comparison of the counting rates produced by a Ra + Be neutron source in two chambers of identical dimensions loaded with thorium and uranium, respectively. The ratio of the uranium and thorium fission cross sections was taken to be 4. The amount of active uranium was computed from the number of spontaneous fissions in the uranium-loaded chamber. It was also shown that the pulse-height distribution resulting from cosmic-ray-induced fission does not differ generally from that induced by neutrons from a Ra + Be source (Fig. 3).

At 3860 m above sea level (atmospheric depth 655 g/cm^2) a chamber containing 11 ± 1 g of thorium (2.85×10^{22} atoms) registered 741 fission events in 672 hours. Thus the nucleon flux, assuming $\sigma_{f\ Th} = 1$ bn, was 10^{-2} nucleon/cm^2-sec. The accuracy of this flux measurement is not better than 10% without including the uncertainty introduced by using the given cross section for thorium fission. A comparison can be made with calculations of nucleon flux at different heights recently published by Benioff.[7] Figure 1 gives the calculated total nucleon flux with energies ≥ 40 Mev plotted against elevation for geomagnetic latitudes $\lambda = 30°$ and 53°. With allowance for the accuracy of the experiment (solid curve) and of the calculation the agreement at different elevations is quite satisfactory. There was also good agreement between experiment and calculations with respect to the position of the maximum on the altitude curve, the magnitude of the geomagnetic effect and the neutron-proton ratio in the total nucleon flux.

Experiments on the passage of the fission-inducing component through air and through dense absorbers lead to the conclusion that under dense absorbers an essential role in fission is played by neutrons which apparently result from interactions between pions and absorber nuclei.

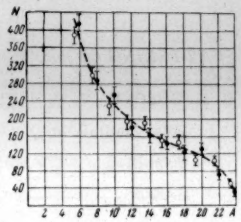

FIG. 3. ○ – Th fission induced by neutrons from a Ra + Be source; ● – Th fission induced by cosmic rays; N – number of pulses; A – pulse height in relative units.

In conclusion the authors wish to acknowledge their great indebtedness to the staff of the P. N. Lebedev Physics Institute of the U.S.S.R. Academy of Sciences, who assisted in a large portion of the experimental work at high altitudes and in Pamir, and to Academician I. V. Kurchatov for his interest.

[1] K. N. Peterzhak and G. N. Flerov, J. Exptl. Theoret. Phys. (U.S.S.R.) **10**, 1013 (1940).

[2] K. Lark-Horovitz and W. A. Miller, Phys. Rev. **59**, 941 (1941).

[3] Froman, Rosen, and Rossi, Phys. Rev. **72**, 525 (1947).

[4] Podgurskaya, Kalashnikova, Stolyarov, Vorob'ev, and Flerov, J. Exptl. Theoret. Phys. (U.S.S.R.) **28**, 503 (1955), Soviet Phys. JETP **1**, 392 (1955).

[5] Gol'danskiĭ, Pen'kina, and Tarumov, J. Exptl. Theoret. Phys. (U.S.S.R.) **29**, 778 (1955), Soviet Phys. JETP **2**, 677 (1956).

[6] B. Rossi, B., High-Energy Particles, Prentice-Hall, Inc., New York, 1952.

[7] P. A. Benioff, Phys. Rev. **104**, 1122 (1956).

Translated by I. Emin
134

SCATTERING OF 590 Mev NEUTRONS BY PROTONS IN THE SMALL ANGLE REGION

B. M. GOLOVIN, V. P. DZHELEPOV, Yu. V. KATYSHEV, A. D. KONIN, and S. V. MEDVED'

Joint Institute for Nuclear Research

Submitted to JETP editor September 3, 1958

J. Exptl. Theoret. Phys. (U.S.S.R.), **36**, 735-738 (March, 1959)

The ring scatterer method was used to determine the differential elastic n-p scattering cross section for 590 Mev neutrons for angles from 5 to 35° in the c.m.s. A strong increase of the cross section was found with decrease of scattering angle. Furthermore, the forward scattering cross section was found to exceed the backward cross sections. A comparison of the results obtained with the prediction of the optical theorem shows that it is incorrect to treat nucleon-nucleon scattering at ~600 Mev on the basis of the opaque-nucleon concept.

INTRODUCTION

ONE of the problems arising in the investigation of nucleon-nucleon interactions is the synthesis of the elastic-scattering amplitude.

$$M = \alpha + \beta(\sigma_1 + \sigma_2)\cdot\mathbf{n} + \gamma(\sigma_1\cdot\mathbf{n})(\sigma_2\cdot\mathbf{n}) + \delta(\sigma_1\cdot\mathbf{l})(\sigma_2\cdot\mathbf{l}) + \varepsilon(\sigma_1\cdot\mathbf{m})(\sigma_2\cdot\mathbf{m}), \quad (1)$$

i.e., the determination of the complex quantities α, β, γ, δ, and ϵ from the experimental data for each scattering angle and for all energies of incident nucleons. The presently available experimental data are quite inadequate for the solution of this problem. It is therefore of interest to obtain from individual experiments numerical values of various independent combinations of amplitude coefficients. In the particular case of forward scattering ($\vartheta = 0°$) the expression (1) simplifies somewhat because the coefficient γ ($\vartheta = 0°$) vanishes. As a result, the scattering cross section at $\vartheta = 0°$ becomes:

$$\sigma(\vartheta = 0°) = |\alpha|^2 + |\beta|^2 + |\delta|^2 + |\varepsilon|^2.$$

On the other hand, the optical theorem makes it possible to find the imaginary part of the spin-free term α of the forward scattering amplitude, from data on the total cross sections σ_t of the nucleon-nucleon interactions at the same energy

$$\mathrm{Im}\,\alpha(\vartheta = 0°) = k\sigma_t/4\pi, \quad (2)$$

where k is the wave number of the incident nucleon. The difference

$$\sigma(\vartheta = 0°) - [\mathrm{Im}\,\alpha(\vartheta = 0°)]^2 = |\mathrm{Re}\,\alpha|^2 + |\beta|^2 + |\delta|^2 + |\varepsilon^2| \quad (3)$$

determines the contribution of the real part of the spin-free and spin-dependent terms of the amplitude in the forward scattering of the nucleus. Thus, knowledge of the total interaction cross sections and of the differential scattering cross section at $\vartheta = 0°$ makes it possible to find the numerical values of the two independent functions (2) and (3) from the scattering amplitude coefficients for this angle.

EXPERIMENTAL PROCEDURE AND DATA

We determined the differential n-p scattering cross sections at a mean neutron energy $E_n = 590$ Mev in the interval from 5 to 35° in the c.m.s. We used for the measurement a specially constructed setup with ring scatterers (described in detail in reference 1), shown schematically in Fig. 1. A collimated neutron beam with a spread $\varphi = 0.5°$ and an annular cross section was incident on the scatterer; the beam and scatterer had a common axis. The scatterer was a ring, or more accurately a polygon built up of cylindrical blocks 62 mm in diameter, arranged in a circle of mean radius R = 32 cm. The neutrons were scattered by an angle

$$\Phi_{l.s.} = \tan^{-1}(R/x) + \varphi, \quad (4)$$

and registered with a neutron telescope, mounted at a distance x from the ring scatterer. By moving the telescope along the axis of the neutron beam (by varying the distance x) it was possible to investigate neutron scattering at various angles. The effect due to the scattering of neutrons by protons was determined by taking the difference of the counts produced by polyethylene and graphite scatterers.

Only the realtive values of the cross sections were determined directly in this experiment, so that it was possible to dispense with the determination of the absolute value of the neutron cur-

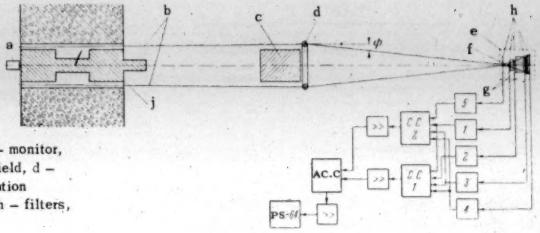

FIG. 1. Overall diagram of the experiment. a – monitor, b – annular neutron beam, c – additional lead shield, d – ring scatterer, ϕ – scattering angle, e – scintillation counters, f – neutron telescope, g – converters, h – filters, j – brass core of the collimator.

rent and of many characteristics of the neutron telescope. The relative cross sections were normalized to the n-p scattering cross section for $\vartheta = 35°$, which is known for this energy.[2] The results of the measurements are given in Table I. The deviations indicated include statistical measurement errors and deviations in the cross section used for normalization.

The 11° and 23° n-p scattering cross sections for neutrons having the same energy were measured earlier in our laboratory by a different procedure.[3] The values of the cross sections obtained for these angles are in good agreement with the corresponding quantities determined in this investigations

GENERAL REMARKS ON THE CHARACTER OF n-p SCATTERING AT ~600 Mev

The data of Table I show a strong increase in cross section with diminishing scattering angle. Furthermore, a comparison of the cross sections for angles close to 180°,[2] shows that the "forward" scattering ($\vartheta = 0°$) at 590 Mev becomes even more probable than the "backward" scattering ($\vartheta = 180°$), in contrast with what was observed at lower neutron energies. One of the causes of this change in the energy dependence of the elastic n-p scattering is the sharp increase in the contribution of inelastic processes to the n-p interaction cross section at energies exceeding 400 Mev, imparting a diffraction character to the scattering.

The great scattering anisotropy, characterized by the fact that at 590 Mev the cross section

TABLE I

Scattering angle ϑ° c.m.s.	Relative n-p scattering cross section	n-p scattering cross section, 10^{27} cm^2/sterad
5	2.7±0.4	10±1.5
8	2.2±0.3	8.2±1.4
11.5	1.7±0.2	6.4±0.9
23	1.2±0.1	4.3±0.5
35 (normalization)	1	3.7±0.2 [2]

$\sigma_{np}(5°)$ is eleven times greater than the cross section $\sigma_{np}(90°)$ (which, according to reference 2, equals $(0.91 \pm 0.06) \times 10^{-27}$ cm^2/sterad) and the sharp increase in the cross sections in the region of small angles ($\vartheta = 10° - 5°$) are additional arguments in favor of the necessity, demonstrated in reference 3, of accounting for states with orbital moments on the order of six and higher in the analysis of data on elastic n-p scattering at this energy.

NUMERICAL VALUES OF EQUATIONS (2) AND (3); CONCLUSIONS

The experimental data in the current literature permit a determination of the imaginary part of the coefficient α in Eq. (1) for $\vartheta = 0°$ over a wide range of energies. The corresponding values for the interaction of nucleons in states with isotopic spins T = 0 and T = 1, calculated from the following formulas

$$\operatorname{Im} \alpha_{T=1}(\vartheta = 0°) = kz_t(pp)/4\pi,$$
$$\operatorname{Im} \alpha_{T=0}(\vartheta = 0°) = [2kz_t(np) - kz_t(pp)]/4\pi, \qquad (5)$$

are shown in Fig. 2. We used here total cross sections obtained both in our laboratory and abroad, as listed in the surveys.[4] It is seen that, at neutron energies less than 200 Mev, the value of Im α ($\vartheta = 0°$) is determined essentially by the contribution from states with T = 0, while at energies ~ 600 Mev the contributions from both types of states become equal.

To find the second of the foregoing combinations of amplitude coefficients [Eq. (3)] it is necessary to know the differential n-p scattering cross section

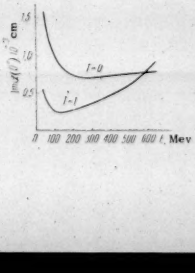

FIG. 2. Measurement dependence of Im α ($\vartheta = 0°$) for the interaction of nucleons in states with T = 0 and T = 1(accuracy ~ 10%).

TABLE II

E_n, Mev	$\sigma_{extr.}(0°)$,	$\sigma_{extr.}(0°) - [\mathrm{Im}\,\alpha_{np}(0°)]^2$,
	10^{-27} cm²/sterad	
90 [5]	14	10
137 [6]	11	8.5
400 [7]	4.0	0.5
590, present work	12	6

for $\vartheta = 0°$. Since such data cannot be found in any of the known investigations, we chose those investigations, in which the angular dependences of the cross sections were investigated for angles closest to 0°, and extrapolated these to $\vartheta = 0°$. The extrapolation of the cross section for four energies, and the resultant contributions to the real part of the spin-free and spin-dependent terms of the amplitude in the n-p forward scattering amplitude, are listed in Table II (accuracy $10 - 20\%$).

The optical theorem, inasmuch as it permits calculation of the imaginary part of the spin-free term of the scattering amplitude, determines thereby the minimum possible forward scattering cross section, which for 590 Mev neutrons is

$$\sigma_{min}(\vartheta = 0°) = [\mathrm{Im}\,\alpha_{np}(\vartheta = 0°)]^2 = 5.8 \cdot 10^{-27}\,\mathrm{cm}^2/\mathrm{sterad}.$$

A comparison of our results with the predictions of the optical theorem shows that the n-p scattering cross section for $E_n = 590$ Mev reaches a value $\sigma_{min}(0°)$ even at $\vartheta = 11°$ and continues to increase with diminishing angle. The value found for the difference $\sigma_{extr}(0°) - [\mathrm{Im}\,\alpha_{np}(0°)]^2$ (see Table II) is evidence that at this energy the real part of the spin-free amplitude and the spin-dependent terms of the amplitude make a considerable contribution to the n-p forward scattering. This fact, together with the data obtained by us on the considerable polarization of nucleons in n-p scattering,[8] leads to the conclusion that there is no justification for attempting to consider the scattering of neutrons by protons at approximately 600 Mev by using the concept of the nucleon as a black sphere, since the forward scattering amplitude for such a model reduces to the imaginary part of the spin-free term, and there is no polarization.[9] This conclusion can be extended to include p-p scattering at the same energies, since in this case, too, the polarization is considerable,[10] and the differential cross sections, increasing rapidly with diminishing angle, reach the minimum value predicted by the optical theorem even at $\vartheta = 15°$.[11]

[1] Golovin, Dzhelepov, Katyshev, Konin, and Medved', Приборы и техника эксперимента (Instruments and Measurement Engineering), in press.

[2] Yu. M. Kazarinov and Yu. N. Simonov, J. Exptl. Theoret. Phys. (U.S.S.R.) **31**, 169 (1956), Soviet Phys. JETP **4**, 161 (1957).

[3] N. S. Amaglobeli and Yu. M. Kazarinov, J. Exptl. Theoret. Phys. (U.S.S.R.) **34**, 53 (1958), Soviet Phys. JETP **7**, 37 (1958).

[4] Beretta, Villi, and Ferrari, Nuovo cimento Suppl. **3**, 499 (1954). V. P. Dzhelepov and B. M. Pontecorvo, Usp. Fiz. Nauk **64**, 15 (1958).

[5] O. Chamberlain and J. W. Easley, Phys. Rev. **94**, 208 (1954).

[6] Thresher, Voss, and Wilson, Proc. Roy. Soc. **A229**, 492 (1955).

[7] Hartzler, Siegel, and Opitz, Phys. Rev. **95**, 591 (1954).

[8] Golovin, Dzhelepov, Dadezhdin, and Satarov, J. Exptl. Theoret. Phys. (U.S.S.R.) **36**, 433 (1959), Soviet Phys. JETP **9**, 302 (1959).

[9] L. I. Lapidus, J. Exptl. Theoret. Phys. (U.S.S.R.) **34**, 1148 (1958), Soviet Phys. JETP **7**, 794 (1958).

[10] Meshcheryakov, Nurushev, and Stoletov, J. Exptl. Theoret. Phys. (U.S.S.R.) **33**, 37 (1957), Soviet Phys. JETP **6**, 28 (1958).

[11] N. P. Bogachev, Dokl. Akad. Nauk SSSR **108**, 806 (1956), Soviet Phys. "Doklady" **1**, 361 (1956). Bogomolov, Zombkovskiĭ, Nikitin, and Selektor, CERN Symposium **2**, 129 (1956).

Translated by J. G. Adashko
135

SOVIET PHYSICS JETP VOLUME 36 (9), NUMBER 3 SEPTEMBER, 1959

RATIO OF THE DEUTERON AND PROTON YIELDS IN THE PHOTODISINTEGRATION OF Au^{197}

E. D. MAKHNOVSKIĬ

Leningrad Physico-Technical Institute, Academy of Sciences, U.S.S.R.

Submitted to JETP editor September 5, 1958

J. Exptl. Theoret. Phys. (U.S.S.R.) **36**, 739-743 (March, 1959)

The ratio of the yields of photodeuterons and photoprotons has been measured for gold irradiated with bremsstrahlung of maximum energy 70 Mev. This ratio equals 0.14 ± 0.07. The protons and deuterons were identified by grain counting in emulsions over the last 90μ of their range.

In a series of papers on the photodisintegration of nuclei a rather high deuteron yield has been reported.[1-7] In these investigations it was also found that for low and medium photon energies the deuteron yields fluctuate strongly from element to element. A theoretical interpretation of these results is however frustrated by the lack of a sufficient amount of data.

The aim of the present work is the determination of the ratio of the deuterium yield to the proton yield from gold under irradiation with bremsstrahlung of maximum energy of 70 Mev. As the detector nuclear emulsions of type NIKFI Ya-2 were utilized. The particle masses were determined by the well known method of grain counting.[7]

EXPERIMENTAL METHOD

The gold target was irradiated inside a multiplate chamber. The experimental arrangement is shown schematically in Fig. 1. The chamber consisted of a cylindrical brass vessel with a cover plate and with two nipples. The entrance nipple was placed in a constant magnetic field to clear the beam of electron and positron contamination. The chamber was evacuated to 2.5×10^{-2} mm Hg pressure. The target was a gold foil 99.1 mg/cm^2 thick. It was placed at an angle of 40° with respect to the photon beam. An area of 1.7×2.2 cm^2 was irradiated. Bremsstrahlung with a maximum energy of 70 Mev was utilized. The relative dose of the irradiation was measured with an ionization chamber placed in the photon beam. The reaction products were registered in nuclear emulsions type NIKFI Ya-2 of thickness 200μ placed at 90° with respect to the beam. The particles entered the emulsions with a mean angle of 15°. The camera was surrounded by heavy lead shield. The exposed plates were developed with a metol hydroquinon developer. The developing was controlled by the temperature of the developer. The scanning was performed with an MBI-2 microscope with a 90× objective and a 10× ocular. The horizontal projection of the tracks was measured with an ocular scale graduated 1.23μ per division. The micrometer with which the vertical track projections were determined had a graduation of 1μ per division. The tracks between 90 and 500μ long which entered the emulsions were selected for measurement if their direction indicated that they came from the illuminated region of the target. Furthermore, 89 tracks of recoil protons were found and the characteristic grain distributions were obtained from these. They were selected such that they began and terminated within the emulsion and had a track length of at least 90μ. The grains in the last 90μ of these tracks were counted twice each. The average of these two counts was taken to be the true number. Additionally the grains on the last 45μ of each recoil proton track were counted.

The ends of the tracks of the photoparticles and of the recoil protons were inclined 0° to 40° to the surface of the emulsion. If the grain numbers were determined similarly in all tracks, one would obtain a smaller count in the steeper tracks compared with the more horizontal ones, because the number of optically nonresolvable grain pairs

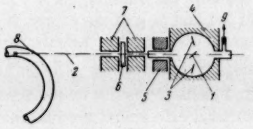

FIG. 1. Experimental arrangement. 1 – target, 2 – γ-ray beam, 3 – nuclear emulsions, 4 – lead shielding, 5 – sweeping magnet pole pieces, 6 – monitor, 7 – lead collimators, 8 – synchrotron, 9 – to the pump.

increased with increasing track steepness. In order not to distort the results, all measurements were reduced to an inclination of 15°. The correction curves were obtained from the recoil-proton tracks since they were uniformly distributed in inclination.

The surface of an emulsion is usually more fully developed than the interior. Therefore the grain density of tracks near the surface was greater than of those near the backing. To correct for this effect all grain counts were reduced to the middle of the emulsion. The necessary corrections were also obtained from the proton recoil tracks, which were distributed uniformly in depth. The grain count obtained by the same observer may differ at different times (drift).[7] To establish this subjective factor in the course of determining the stabilized grain count, the number of grains was counted for 64 recoil proton tracks. The grain count was repeated a short time afterwards. A possible drift was eliminated by alternating grain counts on photoparticle tracks with counts on proton recoil tracks, thus establishing checkpoints.

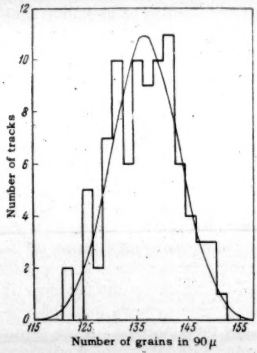

FIG. 2. Distribution of recoil protons as a function of the number of grains in the last 90 μ of the track. The smooth curve is the normal distribution.

Figure 2 shows the distribution of the number of grains of the last 90 μ of the proton recoil tracks. The mean grain count of this distribution is $N^p_{90\mu}$ 136.8; its standard deviation is $\sigma^p = 0.56\sqrt{N^p_{90\mu}}$.

The indicated deviation is not in disagreement with the value $\sigma \approx 0.7\sqrt{N}$ which has been proposed by Hodgson.[8] It is known that for singly charged particles[9]

$$N_R = mF(R/m)$$

and thus

$$N^d_{90\,\mu} = 2N^p_{45\,\mu}, \qquad (1)$$

where R is the residual range, m the particle mass, N_R the grain number in the residual range R, and p and d denote the respective particles. One can thus obtain the mean number of grains in the last 90 μ of deuteron track from the number of grains of the last 45 μ of the proton track, by means of (1). Such a distribution is shown in Fig. 3. From the mean proton grain count $N^p_{45\mu} = 72.7$ we thus obtain for the deuterons $N^d_{90\mu} = 145.4$.

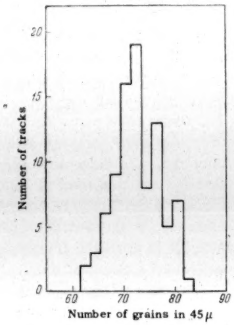

FIG. 3. Distribution of the tracks of recoil protons as a function of the number of grains in the last 45 μ of the track.

Like in reference 7, it was assumed that the number of grains on the last 90 μ of the proton tracks forms a normal distribution with a mean value $N^p_{90\mu}$ and a standard deviation $\sigma^p = 0.56 \times \sqrt{N^p_{90\mu}}$. The observed distribution was checked by means of the well known χ^2 test and was found to fully agree with this hypothesis. The smooth curve in Fig. 2 shows the calculated normal distribution. It was further assumed that the grain number of the deuteron tracks also forms a normal distribution with mean value $N^d_{90\mu}$ and standard deviation $\sigma^d = 0.56\sqrt{N^d_{90\mu}}$.

The ratio $(N^d/N^p) = 1.06$ thus obtained for plates developed in a metol-hydroquinon developer is rather low. Under these circumstances it was not possible to resolve single protons from deuterons. It was therefore necessary to represent the experimentally observed distribution in the best possible manner by a sum of two normal distributions. This was done by the method of least squares.[11] The analysis was performed in the following manner. The experimental distribution obtained from 180 photoparticles was plotted as a histogram (Fig. 4). The ratio of the number of photoprotons to the total number of photoparticles was then assigned several values θ, and the corresponding number of photoprotons and photoneutrons was determined. Then the corresponding normal distributions were computed[10] with account

of the known characteristic distributions, and both distributions were added. Finally the sum of the squares of the differences between the distribution so determined and the points of the histogram was computed. The most probable value was found to be $\theta = 0.878$. The corresponding individual distributions are shown as the dashed curves in Fig. 4 while their sum is plotted as the full curve. The uncertainty of θ was obtained from the magnitude of the sum of the squared deviations of the calculated from the observed distribution. It was found that for $\theta = 0.878$, $\Delta\theta = \pm 0.057$. It is possible for systematic errors to occur when the corrections for track stopping depth and inclination are applied to the grain count. Such errors can occur if there exist small differences between the angular and stopping depth distributions of the photoprotons and the recoil protons. This error will not exceed 0.5% for the photoprotons and will be $\leq 0.4\%$ for the photodeuterons.

RESULTS AND DISCUSSION

The ratio of the yield of deuterons of energy 7 – 14 Mev to that of protons of energy 5 – 11 Mev was found in the present experiment to be

$$Y(\gamma, d)/Y(\gamma, p) = 0.14 \pm 0.07.$$

The indicated error was calculated from the above given value $\Delta\theta$. The small systematic errors in the determination of the grain number of the photoproton and photodeuteron tracks and the background of approximately 5% were not taken into account. In addition to the 180 tracks making up the histogram of Fig. 4 there had been found three further tracks of lengths between 90 μ and 100 μ. They had grain counts of 117, 108, and 114. They were considered to be photoproton tracks and were included in obtaining the final result. It was assumed that the possible contribution of triton tracks was negligible.

Evidently, a rather high yield ratio was obtained. It is interesting to note that also in the case of sulfur and copper the obtained deuteron yields are rather high for irradiation with bremsstrahlung of $E_{\gamma\,max}$ around 70 Mev.[2,4] They are several times greater than those obtained with bremsstrahlung of $E_{\gamma\,max} \approx 30$ Mev.[3,7]

The energy distribution of photoprotons from gold[12] has a sharp rise between 8 and 10 Mev with the maximum at 10.5 Mev. The computations performed in reference 12 according to the statistical theory and to the direct photoemission were not able to explain these facts. From the evaluation of the photodeuteron yield of this work we can conclude that these facts are not related to deuterons, since otherwise there would have had to be observed a significantly higher photodeuteron yield.

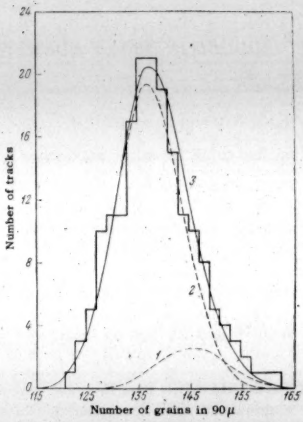

FIG. 4. Distribution of the tracks of photoparticles as a function of the number of grains in the last 90 μ of the track. 1 – normal distribution of photodeuterons, 2 – normal distribution of photoprotons, 3 – sum of both.

The author is grateful to A. P. Koman for valuable comments and for his collaboration in the work and to E. G. Stepanov for his help in performing the computations.

[1] P. R. Byerly, Jr. and W. Stephens, Phys. Rev. **81**, 473 (1951); **83**, 54 (1951).

[2] W. H. Smith and L. J. Laslett, Phys. Rev. **86**, 523 (1952).

[3] L. Katz and A. S. Penfold, Phys. Rev. **81**, 815 (1951); **83**, 169 (1951).

[4] L. S. Ring Jr., Phys. Rev. **99**, 137 (1955).

[5] M. E. Toms and W. E. Stephens, Phys. Rev. **92**, 362 (1953).

[6] M. E. Toms and W. E. Stephens, Phys. Rev. **95**, 1209 (1954).

[7] B. Forkman, Ark. Fys. **11**, 265 (1956).

[8] P. E. Hodgson, Brit. J. Appl. Phys. **3**, 11 (1952).

[9] Lattes, Occialini, and Powell, Proc. Phys. Soc. **61**, 173 (1948).

[10] A. G. Worthing and J. Geffner, Treatment of Experimental Data (Russ. transl.), GITTL, Moscow, 1953; pp 192, 326, 328 (Wiley & Sons, New York, 1943).

[11] K. P. Yakovlev, Математическая обработка результатов измерений (Mathematical Treatment of Results of Measurements) GITTL, Moscow, 1950, p 365.

[12] W. K. Dawson, Can. J. Phys. **34**, 1480 (1956).

Translated by M. Danos
136

FISSION INDUCED IN HEAVY ELEMENTS BY CARBON, NITROGEN, AND OXYGEN NUCLEI

S. M. POLIKANOV and V. A. DRUIN

Submitted to JETP editor September 13, 1958

J. Exptl. Theoret. Phys. (U.S.S.R.) **36**, 744-747 (March, 1959)

The energy dependences of the cross sections for bismuth and uranium fission induced by accelerated C^{12}, N^{14}, and O^{16} nuclei are presented along with the dependences of the gold, rhenium, and ytterbium fission cross sections on the N^{14} ion energy. The measurements were performed with an ionization chamber and a monochromatic beam from a 150-cm cyclotron. Experimental results of the measurement of the ranges and angular anisotropies of the U^{238} and Au fission fragments produced by accelerated C^{12} ions are also presented.

MULTIPLY-CHARGED ions interact with nuclei of heavy elements to form compound nuclei excited to an energy equal to several tens of Mev. The decay of these nuclei proceeds either via fission or via neutron evaporation. The relation between these two processes depends on the charge and mass of the compound nucleus and on the excitation energy. We have carried out several experiments on the determination of the fission cross section of several elements irradiated by multiply-charged ions. In addition, we began experiments on the more detailed investigation of the fission process; in particular on the study of the angular distribution and the ranges of the fragments.

We report below the result of these experiments.

1. EXPERIMENTS ON THE DETERMINATION OF THE FISSION CROSS SECTION OF NUCLEI INTERACTING WITH MULTIPLY-CHARGED IONS

Experiments on the determination of the fission cross section were performed both inside the cyclotron chamber as well as with the external ion beam at a distance of 12 meters from the cyclotron. We investigated the energy dependences of the fission cross sections σ_f of various elements acted upon by C^{12}, N^{14}, and O^{16} nuclei.

In the experiment with the external beam, the fission fragments were registered with an ionization chamber. In this case we determined both the relative course of the curve $\sigma_f = f(E)$ and the absolute magnitude of the fission cross section. In experiments with the internal beam we determined only the relative variation of σ_f with energy of bombarding particle. The fragments were identified by their beta activity.

The energy of carbon, nitrogen, and oxygen ions, as determined from their absorption in aluminum and from the energy dependence of the ion range in aluminum as determined experimentally in our laboratory.[1] The particle energy was varied by placing aluminum absorbers in front of the target.

In the first experiments on the fission of uranium, bismuth, gold, and rhenium by nitrogen nuclei,[2] the energy of the N^{14} was measured and varied with the aid of a focusing magnet, placed between the ionization chamber and the cyclotron. The magnet was calibrated here with deuterons of known energy. However, owing to a certain difference between the trajectories of the multiply-charged ion and the deuteron, and also owing to the presence of ions entering the gap of the focusing magnet at different angles, the energy of the multiply-charged ion corresponding to a specified value of the magnetic field was not determined sufficiently accurately. Experiments with aluminum absorbers permitted to dispense with the calibration of the focusing magnet and made it possible to obtain a more exact energy dependence of the cross section. The results of the experiments are shown in Figs. 1, 2, and 3.

It is seen from Figs. 1 and 2 that the cross section of fission of Bi and U^{238} by C^{12}, N^{14}, and O^{16} nuclei are adequately described by the following formula

$$\sigma = \pi r_0^2 (A_{\text{targ. nuc.}}^{1/3} + A_{\text{part.}}^{1/3})^2 (1 - B/E)$$

with $r_0 = (1.4 - 1.5) \times 10^{-13}$ cm for bombarding-particle E energies exceeding the coulomb barrier B. Figure 3 shows the great dependence of the fission cross section on the Z^2/A of the compound nucleus for a specified excitation energy.

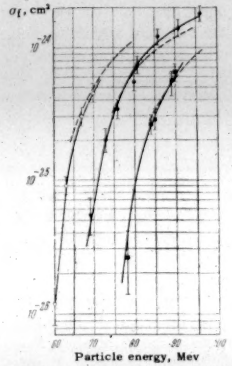

FIG. 1. Dependence of the fission cross section of bismuth on the ion energy: ○ – C, ● – N, ■ – O (solid lines – experimental curves, dotted lines – calculated from the formula $\sigma = \sigma_0(1 - B/E)$ for values of $r_0 = 1.5f$ (light circles) and $1.55f$ (solid circles).

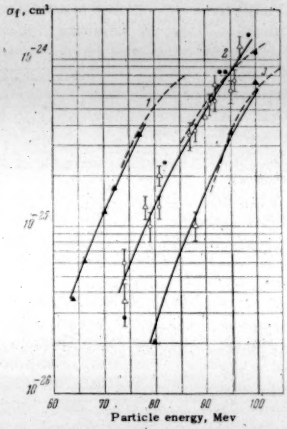

FIG. 2. Dependence of the uranium fission cross section on the ion energy: 1) C, 2) N, 3) O. Solid curves – experimental, dotted – theoretical for r_0 values of $1.4f$ (1), $1.45f$ (2), and $1.52f$ (3). Δ – chamber data for U^{238}, ○ – chamber data for U^{235}, ●▲ – activation data for U^{238}.

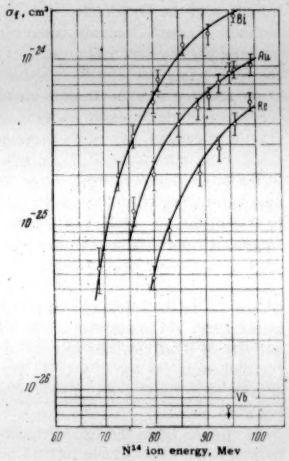

FIG. 3. Dependence of the fission cross section of bismuth, gold, uranium, and ytterbium on the energy of the N^{14} ions.

2. ANGULAR DISTRIBUTION AND RANGES OF FRAGMENTS OF THE FISSION OF URANIUM AND GOLD BY CARBON

One of the features of the reactions that occur in the interactions with multiply-charged ions is that the resultant compound nuclei have large angular momenta. Theoretical estimates made by Strutinskiĭ and Pik-Pichak (private communication) show that the large angular momentum of the compound nucleus leads to an anisotropic distribution of the fission fragments. One can expect the fission fragments to be emitted essentially in the forward direction.

We undertook an experimental investigation of the angular anisotropy in the fission of nuclei of uranium and gold by carbon nuclei. In the performance of these experiments we also succeeded in obtaining experimental estimates of the ranges of the fragments.

The experiments were made in the internal cyclotron beam. The fission fragments emitted at angles of 90 and 135° to the beam of incident particles were registered. The targets employed were thick foil (several microns) of uranium and gold, located at 45° to the carbon-ion beam. The fission fragments, emitted at angles of 90° and 135°, were stopped in 35-micron aluminum foils placed at these angles. After irradiation for an hour, the number of beta particles emitted from these foils was measured. No chemical separation of the fragments was made. This involves the danger of appearance of a background due to the activation of the aluminum and of its various impurities by neutrons and scattered carbon nuclei. However, control experiments carried out by irradiating a copper foil instead of an uranium or gold foil have shown that the background can be neglected in practice. The experiments have shown that the ratio of the activity of a foil at 135° to that of a foil at 90° is 1.18 ± 0.06 for uranium and 1.48 ± 0.06 for gold. Here the fragments registered are those leaving a layer of thickness equal to the range of the fragment. The fragment-registration efficiency for 135° is therefore higher than that for 90°. Knowledge of the dependence of the fission cross section on the energy makes it possible to determine this difference. After taking this difference into account, we obtain for $J(135°)/J(90°)$ values of 1.05 ± 0.10 for uranium and 1.21 ± 0.10 for gold. A recalculation to the center-of-mass system yields $J(141°)/J(99°) = 1.15 \pm 0.10$ for uranium and $J(142°)/J(101°) = 1.36 \pm 0.13$ for gold. The effect obtained is averaged in the carbon energy range of 73 – 78 Mev.

The measurements began immediately after ter-

mination of the irradiation and continued until the number of counts became comparable with the counter background. The ratio of the activities of the foils remained almost constant in this case.

In addition to experiments on the angular anisotropy, we made an experimental estimate of the fragment ranges. For this purpose we placed other aluminum foils, 5, 7, or 10 μ thick in front of the 35-μ aluminum foil. After irradiation we measured the ratio of the activity of the first foil to that of the 35-μ foil. This ratio is related to the fragment range R as follows

$$R = \Delta [1 + (N_{35} / N_x) \alpha],$$

where Δ is the thickness of the first foil, N_{35}/N_X is the ratio of the activity of the 35-μ foil to the activity of the first foil, and α is a coefficient that accounts for the change in the fission cross section with the depth of the layer of the fissioning substance.

It is seen from the experiments that in changing from a 5-μ foil to a 10-μ foil the ratio N_{35}/N_X diminishes, in the case of uranium, by a factor 7.5 for 90° and 8.2 for 135°, while in gold the decrease is 10 and 27 fold for 90° and 135° respectively.

After processing the experimental data we obtain the following values for the range of aluminum fragments (in microns):

Angle	Element	
	Uranium	Gold
90°	11.2±0.8	10.8±1.0
135°	11.1±0.8	10.1±1.0

The authors are indebted to Prof. G. N. Flerov for continuous attention to the work. We thank Yu. V. Lobanov for help in the measurements and in the processing of the results.

[1] Yu. Ts. Oganesyan, J. Exptl. Theoret. Phys. (U.S.S.R.) **36**, 936 (1959), Soviet Phys. JETP this issue, p. 660.

[2] Druin, Polikanov, and Flerov, J. Exptl. Theoret. Phys. (U.S.S.R.) **32**, 1298 (1957), Soviet Phys. JETP **5**, 1059 (1957).

Translated by J. G. Adashko
137

SOVIET PHYSICS JETP VOLUME 36 (9), NUMBER 3 SEPTEMBER, 1959

TWO-NEUTRON CAPTURE REACTION IN THE INTERACTION BETWEEN N^{14} AND NUCLEI OF SOME ELEMENTS*

V. A. KARNAUKHOV, G. M. TER-AKOP' YAN, and V. I. KHALIZEV

Submitted to JETP editor September 13, 1958

J. Exptl. Theoret. Phys. (U.S.S.R.) **36**, 748-750 (March, 1959)

Targets made of LiF, Al, and Cu were irradiated with ~92-Mev N^{14} ions. The radioactive isotope N^{16} was identified among the reaction products by its decay period and by the beta-particle energy. It is concluded that N^{16} is formed through "capture" of two neutrons from the target by the bombarding particle.

In many investigations of the interaction between heavy particles (C, N, O) with nuclei[1-6] there were observed the so called "capture" and "stripping" reactions, in which the bombarding particle captures a neutron, proton, or α particle from the target nucleus, or else adds such a particle to it. A detailed investigation of the "stripping" of a neutron in the bombardment of various targets by N^{14} ions $[Z^A(N^{14}, N^{13})Z^{A+1}]$[3,6] indicates that reactions of this type occur, in all probability, in the case of glancing collision between the interacting nuclei, without formation of a compound nucleus. The energy transferred in this case is small. This causes, in particular, the kinetic energy (and consequently the range) of the N^{13} nuclei not to differ much from the kinetic energy and range of the N^{14} ions. The large range of the reaction products of "stripping" and "capture" makes it possible to separate them from the reaction products of the decay of the compound nucleus, without having to resort to radiochemical methods.[6]

It appears to us that to investigate the mechanism of interaction between heavy particles and nuclei in the case of glancing collisions it is advisable to study not only the foregoing reactions, but also the "stripping" and "capture" of two neutrons. A detailed investigation of this process may yield useful information on the structure of the periphery of the nucleus, particularly on the character of the interaction of the outer neutrons. The possibility of "capture" of two neutrons follows from the work of Alkhazov et al.,[7] who observed the formation of N^{16} in the irradiation of LiCl by 15.6-Mev N^{14} ions. However, the results obtained do not lead to definite conclusions concerning the mechanism by which this isotope is produced.

*The results of this work were reported in the survey paper by G. N. Flerov at the All-Union Conference on Nuclear Reactions at Low and Medium Energies (1957).

It was the purpose of this investigation to observe the "capture" of two neutrons in the interaction between accelerated N^{14} ions and nuclei of several elements.

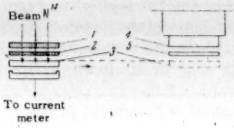

The experiments were performed with the internal beam of the 150-cm cyclotron of the U.S.S.R. Academy of Sciences. Five-charge N^{14} ions with energy ~ 92 Mev were used to bombard targets of LiF, Al, and Cu. The figure shows the arrangement of the experiment. The thickness of the targets 1 was chosen such that the nitrogen ions were emitted by the target at an energy of ~ 55 Mev. Placed behind the layer of the investigated substance was a 9-μ gold foil, 2, in which the short-range reaction products were absorbed. No nuclear reactions were produced in the gold itself, since the energy of the N^{14} ions (55 Mev) was not enough for this. Placed beyond that was a tantalum plate, 3, which collected both the beam and the reaction products that passed through the gold foil. The collector was moved periodically to a luminescent beta-particle counter 4, with a thick stilbene crystal (30 mm in diameter and 30 mm high), so that the counting could start 5 seconds after the end of the irradiation. The counter, placed in a magnetic shield, was 2 meters away from the target. To reduce the background due to beta particles with energies less than 1.0 Mev, a 1.5-mm aluminum absorber, 5, was placed in front of the crystal. The electronic circuitry employed comprised a single-channel amplitude analyzer, which determined the beta-particle energy and simultaneously measured the drop in

activity with time. The beam intensity was measured when the collector was near the counter. The ion current amounted to $0.1 - 0.3\,\mu a$. The intensity of the beam was stable enough throughout the experiments for quantitative estimates of the cross sections.

The irradiation of each target (LiF, Al, Cu) resulted in a beta activity with a half-life $T = 7.5 \pm 1$ sec and a maximum beta-particle energy $E_{max} > 7$ Mev.

In the experimental setup used, the only nuclei that could proceed from the target to the tantalum collector were those formed by "stripping" or "capture." The registration of isotopes — decay products of the compound nucleus — was excluded, since they were absorbed in the gold-foil shield. The fact that irradiation of targets having so wide a range of atomic numbers produced the same activity also indicates that this activity is obviously connected with the decay of the isotope that is produced by the "stripping" or "capture" reactions. An analysis of the possible products of such reactions leads to the conclusion that the observed beta activity must be attributed to the decay of the N^{16} nucleus ($T = 7.35$ sec., $E_{max} = 10.4$ Mev) which is formed by "capture" of two neutrons by the N^{14} nitrogen from the target nucleus.

Target	LiF		Cu		Al
	Li	F	Cu^{63}	Cu^{65}	
Q, Mev	+0.55	−6.65	−5.86	−4.37	−11.06
Relative yield of β activity with $T \approx 7.5$ sec.	100		30		3

A characteristic feature of the reaction that occur during glancing collisions, as already mentioned, is the large range of the nuclei formed from the bombarding particle. To disclose more clearly this feature of the mechanism of N^{16} production, an experiment was performed, in which we used a thinner target made of copper, covered on the collector side with a gold foil $15\,\mu$ thick. The yield of N^{16} per single copper atom was reduced here by 20 − 40%. For comparison we indicate that 2 or $3\,\mu$ of gold are sufficient to absorb completely the decay products of the compound nucleus formed upon fusion of the gold and copper nuclei.[8] No beta activity with a half-life of approximately 7.5 sec. was observed in a control experiment in which a gold target of equivalent thickness was irradiated.

The table lists a relative yield of the observed beta activity for various targets, referred to one atom of the investigated matter. The table also lists the values of Q, the difference in the binding energy of two neutrons in N^{16} and in the target nucleus:

$$Q = E_{2n}(N^{16}) - E_{2n}(Z^A).$$

(In the calculation of this quantity we used the data of reference 9 on the binding energy of the nuclei). It is seen that as Q decreases the activity yield decreases. This variation serves as further confirmation of the conclusions concerning the production of N^{16}. It must be noted that in the case of LiF target, the N^{16} nucleus appears obviously mostly as the result of the interaction of the nitrogen N^{14} with lithium.

What attracts attention is the absence of this effect in the bombardment of a gold target, although in this case the reaction of "capture" of two neutrons is energetically quite feasible. This is obviously connected with the fact that the produced N^{16} nuclei are so strongly deflected in the field of a target nucleus away from the direction of the bombarding-particle beam, that they do not fall on the collector.

The cross section of the reaction that leads to the appearance of the radioactive N^{16} upon interaction of N^{14} with lithium, averaged over the ion energy in the interval from ~ 92 to ~ 55 Mev, amounts to $\sim 5 \times 10^{-28}$ cm^2. This quantity must be considered as the lower limit of the cross section for the "capture" of two neutrons by a N^{14} nucleus, since the production of N^{16} in the excited state at sufficiently high excitation leads to the evaporation of a neutron: $N^{14} + 2n \rightarrow N^{16*} \rightarrow N^{15} + n$. This circumstance may also cause the yield of N^{16} to decrease with increasing energy of bombarding particles, owing to the increase in the average excitation energy of the nitrogen nucleus in the "capture" of the two neutrons.

The authors are grateful to Prof. G. N. Flerov for continuous attention in the work, and also to the cyclotron crew members, headed by Yu. M. Pustovoĭt, for ensuring correct operation of the apparatus.

[1] K. F. Chackett and I. H. Fremlin, Phil. Mag. **45**, 735 (1954).

[2] Chackett, Chackett, and Fremlin, Phil. Mag. **46**, 1 (1955).

[3] H. L. Reynolds and A. Zucker, Phys. Rev. **101**, 166 (1956).

[4] Reynolds, Scott, and Zucker, Phys. Rev. **102**, 237 (1956).

[5] H. L. Reynolds and A. Zucker, Phys. Rev. **106**, 251 (1957).

[6] Volkov, Pasyuk, and Flerov, J. Exptl. Theoret. Phys. (U.S.S.R.) **33**, 595 (1957), Soviet Phys. JETP **6**, 459 (1958).

[7] Alkhazov, Gangarskii, and Lemberg, J. Exptl. Theoret. Phys. (U.S.S.R.) **33**, 1160 (1957), Soviet Phys. JETP **6**, 892 (1958).

[8] Parfanovich, Rabin, and Semchinova, J. Exptl. Theoret. Phys. (U.S.S.R.) **31**, 188 (1956), Soviet Phys. JETP **4**, 99 (1956).

[9] A. H. Wapstra, Physica **21**, 367 (1955).

Translated by J. G. Adashko
138

HIGH-ENERGY NUCLEAR-ACTIVE COMPONENT OF EXTENSIVE AIR SHOWERS AT SEA LEVEL

A. T. ABROSIMOV, V. A. DMITRIEV, G. V. KULIKOV, E. I. MASSAL' SKIĬ, K. I. SOLOV' EV, and G. B. KHRISTIANSEN

Nuclear Physics Institute, Moscow State University

Submitted to JETP editor September 15, 1958

J. Exptl. Theoret. Phys. (U.S.S.R.) **36**, 751-761 (March, 1959)

Data are presented on the number of high-energy nuclear-active particles in showers containing a total number of particles between 1×10^4 and 2×10^6, and also on the lateral distribution of the energy flux of the nuclear-active component. It has been found that the energy of the nuclear-active component in individual showers with an equal number of particles may differ widely. Some conclusions are drawn from the shape of the spectrum of the nuclear-active particles and from the lateral distribution of the energy flux of the nuclear-active component regarding the nature of the elementary interaction of the nuclear-cascade process.

INTRODUCTION

EXPERIMENTS on extensive air showers (EAS)[1,2] prove the presence of high-energy nuclear-active particles at sea level. The cascade of nuclear-active particles contained in EAS has, in the majority of past experiments, been studied indirectly by measuring the electron-photon and μ-meson components accompanying the shower, or by methods which did not permit one to measure the energy of the nuclear-active particles directly.[3] The study of these cascades is of great interest in explaining the interaction process.

We carried out a statistical study of nuclear cascade in EAS at sea level, using a detector having a high efficiency for the detection of high-energy nuclear particles. The measurements were carried out in 1957, using the array for the comprehensive study of EAS operating at present at the Moscow State University.

DESCRIPTION OF THE ARRAY*

For the detection of nuclear-active particles and the determination of their energy, we used four cylindrical pulse ionization chambers placed under a composite absorber made of lead and graphite. The charged particles in EAS were recorded by 720 Geiger-Müller counters with different areas. The counters were connected to a hodoscope. The masterpulse for the chambers and the hodoscope was given by a six-fold coincidence of pulses from counter groups connected to a coincidence circuit. The area of each group amounted to $330 \times 4 = 1320$ cm^2. The position of the chambers, the master counters, and a cross section of the detector are given in Fig. 1.

As has been mentioned,[5] the use of a composite absorber containing low-Z material (graphite) together with high-Z material (lead) makes it possible to separate, to a maximum extent, the nuclear and electron-photon cascades along the depth of the absorber. The development of the nuclear cascade takes place mainly in the graphite, while that of the electron-photon cascade takes place mainly in lead. In this way, an approximate proportionality of the number of particles in the electron-photon cascade to the energy carried away by π^0 mesons is assured for any place of initiation of the nuclear cascade. In the study of showers of large size (with total number of particles $N \geq 1 \times 10^5$) the thickness of the top layer of lead was increased to 8 cm since, in such showers, the frequency of incidence of electrons or photons with energies of about 10^{11} ev on the array is high and the cascades produced by these particles are not fully absorbed by 4 — 5 cm lead.[2]

RESULTS OF MEASUREMENTS

The selection system efficiently detected showers with $N \geq 10^4$. The spectrum of EAS selected by the array is the usual one for arrays of a similar type, with a maximum for $N = 2.5 \times 10^4$. The density of the distribution of the axes of registered showers was practically constant in a circle with radius 2.5 m for showers with $N \geq 1 \times 10^4$, and

*A detailed description of the apparatus and of the setup is given in references 2 and 4.

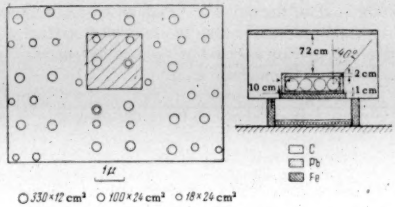

FIG. 1. Plan of the array and cross section through the detector.

the density of the axes of low-density showers fell off for large distances. For showers with $N \geq 1 \times 10^5$, the axes are distributed uniformly in a circle with radius R = 5 m.

Reduction of the hodoscope data by the usual method[6] made it possible to determine, for each individual shower, the total number of particles N and the position of the axis. A part of the hodoscope data was reduced using an electronic computer, and in these cases, the method used was that of directly finding the probability maximum for a given distribution of discharged counters in all hodoscope points as a function of N and the position of the shower axis.[7] Thus, it was unnecessary to calculate the density of each hodoscopic point. A comparison of the characteristics of showers reduced by the usual method and by means of the computer shows, that the error in finding the shower axis in the first method was not greater than 1 m, while the error in the determination of the total number of particles was not greater than 20% (when the shower axis fell into the hodoscope area).

The chamber section records the amplitude of ionization bursts produced in the chambers when an EAS passes through the array. The size of the bursts is expressed in the number of N relativistic particles passing through the chamber along the mean chord. In order to obtain the energy of the nuclear-active particle from the burst size, we used the same coefficient for all energies of nuclear-active particles. The value of the coefficient is given in the appendix. The contribution of bursts from nuclear disintegrations and radiation bursts from μ-mesons have been discussed earlier,[5] and were found to be insignificant.

All recorded and reduced showers were divided into four groups, according to the number of particles in the shower:

$$1 \cdot 10^4 \leqslant N_1 < 3 \cdot 10^4; \quad 3 \cdot 10^4 \leqslant N_2 < 1 \cdot 10^5;$$
$$1 \cdot 10^5 \leqslant N_3 < 3 \cdot 10^5; \quad N_4 \geqslant 3 \cdot 10^5.$$

To obtain more data we considered 218, 270, 186, and 100 showers in each group respectively. Plots of the number of particles with energy greater than a given value were constructed for an average shower of each group. In fact, the number of recorded showers N(E) of each group accompanied by bursts of n particles, i.e., produced by a particle of energy E = kn, is related to the total number of showers $N_S (\leq R)$ in a circle of radius R for a constant probability of shower detection, the axes of which fall within a circle with radius R, according to the formula

$$M(E) = \int_0^R \sigma \varphi(N)\, W(N, r)\, \rho(E, r)\, 2\pi r\, dr$$
$$= \sigma W \varphi(N) \int_0^R \rho(E, r)\, 2\pi r\, dr = \sigma N_s (\leqslant R)\, n(E) / S,$$

i.e.,

$$n(E) = M(E)\, S / N_s (\leqslant R)\, \sigma.$$

Here n(E) is the number of particles with energy E in the average shower in a circle with radius R, r is the distance from the shower axis to the center of the detector, W is the probability of shower detection, σ is the detector area, $\rho(E, r)$ is the density of particle energy E in the shower, $\varphi(N)$ is the number of showers in the interval under consideration per unit area, and $S = \pi R^2$. The condition W = constant determines the choice of the radius of the circle for the construction of the spectra of particles (bursts), for different number of particles in the shower. For the groups mentioned above, the radii equal to 3, 4, 5, and 6 m respectively were chosen.* The mean

TABLE I. Number of particles with energy larger than a given value in a circle with radius R in showers of different size, and the maximum energy of nuclear-active particles detected in the shower

E, ev	R = 3 m; $10^4 \leqslant N < 3 \cdot 10^4$	R = 4 m; $3 \cdot 10^4 \leqslant N < 10^5$	R = 5 m; $10^5 \leqslant N < 3 \cdot 10^5$	R = 6 m; $3 \cdot 10^5 \leqslant N \leqslant 2 \cdot 10^6$
10^{11}	2	7	29	55
$3 \cdot 10^{11}$	1.3	3	14	29
10^{12}	0.7	2.5	10	24
$2 \cdot 10^{12}$	0.1	0.7	2.5	9
$5 \cdot 10^{12}$		0.4	1.0	5
$7 \cdot 10^{12}$		0.2	0.8	3
$1.5 \cdot 10^{13}$			0.4	2
$5 \cdot 10^{13}$				1.0
E_{na}^{max}, ev	$4.7 \cdot 10^{12}$	10^{13}	$1.8 \cdot 10^{13}$	$6 \cdot 10^{13}$

*It should be noted that the condition W = constant is satisfied in practice also for low-density showers, since the master counters are separated by a distance of about 2 m; the probability of recording such showers is smaller than unity, but its value does not change greatly. For a shower with $N = 1 \times 10^5$, W changes in the chosen circle by 5%; for $N = 2 \times 10^6$ by 30%. It can be shown easily that the errors introduced into the value of n(E) are smaller than the given change of W.

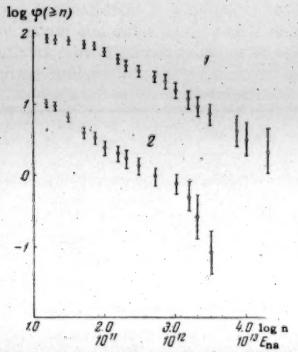

FIG. 2. Spectrum of nuclear-active particles in showers of different density: 1 – in showers with $N = 5.6 \times 10^5$ ($R \leq 6$ m); 2 – in showers with $N = 2 \times 10^4$ ($R \leq 3$ m).

number of particles with energy greater than a given value in the above-mentioned average shower of each group, obtained by means of the formula given above, is given in Table I. In Fig. 2, the integral spectra for the two limiting groups of showers are given. In the region $E \geq 10^{12}$ ev, the spectra are characterized by different values of exponents: for N_1 $\gamma = 1.8 \pm 0.5$, for N_3 $\gamma = 0.9 \pm 0.3$, and for N_4 $\gamma = 0.7 \pm 0.3$. The spectrum of bursts in the same region for all showers with $N \geq 1 \times 10^4$ is given in Fig. 3. In that case, $\gamma = 1 \pm 0.2$.

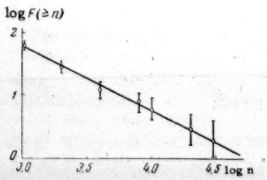

FIG. 3. Spectrum of large bursts ($n \geq 1000$) in showers with $N \geq 1 \times 10^4$.

Data on the number of particles with a given energy $n(E)$ in the average shower make it possible to determine the value of the total energy carried by the nuclear-active component of the shower in the circle of radius R ($E_{na} = \Sigma n(E_i)\,\overline{E}_i$, where the summation is carried out over all energy ranges). In Table II, these data are given for two groups of showers.* When the position of the axis and the size of the burst for each shower are known, it is possible to determine the lateral distribution of the energy flux carried by the nuclear-active component at the shower axis.

The energy flux density $\rho_E(r)$ at the distance r, $r + \Delta r$ was determined from the formula

$$\rho_E(r) = \sum E_i / N_s(r)\,\sigma,$$

where the summation is carried out over all energy values recorded at the distance r, $r + \Delta r$; $N_S(r)$ is the number of recorded showers whose axis fell between r and $r + \Delta r$ from the detector. The distribution of energy density for separate groups of showers and for the average shower are given in Figs. 4 and 5.*

Data were also obtained on the lateral distribution function of particles of various energies in showers. If $m(r, n)$ out of $N_S(r)$ showers whose axis fell between r and $r + \Delta r$ were accompanied by a burst of n particles then, for $\rho\sigma \ll 1$,

$$\rho(r, n) = m(r, n) / \sigma N_s(r),$$

where σ is the area of the detector, and $\rho(r, n)$ is the particle density of a given energy. The experiment shows that $m(r, n) \ll N_S(r)$ and, consequently, the formula is correct.

Figure 6 shows histograms for particles of various energies and also data obtained for particles with $E_{na} \geq 8 \times 10^{11}$ ev in showers evaluated using the electronic computer. It should be noted that the maximum distance of particles with energy $E_{na} \sim 10^{12}$ ev from the shower axis recorded by us corresponds to 5 m and, for showers with $E_{na} \sim 10^{11}$ ev, to 30 m. This cannot be due to several particles of smaller energy, since the corresponding bursts were due to ionization in one chamber only.

DISCUSSION OF RESULTS

Data on the spectra of nuclear-active particles given above show that the shape of the spectrum in various energy ranges is not the same for showers with different number of particles. For showers

*The use, in the energy of estimates, of circles of larger radius for larger showers does not change the energy appreciably. Thus, the value of energy in the circle 4 m in radius for showers of the group N_1 is different only by 4% from that given in Table II, and for showers in the group N_4 by 5%.

*Data on the lateral energy distribution make it possible to determine the energy flux carried by the nuclear-active component in another way: $E'_{na} = \sum_i \rho_E(r_i)\,\Delta S_i$ where ΔS_i is the area of the ring in which $\rho_E(r_i)$ has been determined. Such a determination of E'_{na} is, in principle, less accurate, since the influence of the recorded individual value of the energy vary strongly for different ranges of r in the same shower. This process of axis translation takes place since the accuracy of determination of the axis is of the order of ~ 1 m $\sim \Delta r$. The values of E'_{na} are given in Table II.

TABLE II. Values of the energy carried by the nuclear-active component in a circle with radius R in showers of different size

N	$10^4 \leqslant N < 3\cdot10^4$	$3\cdot10^4 \leqslant N < 10^5$	$1\cdot10^5 \leqslant N < 3\cdot10^5$	$3\cdot10^5 \leqslant N$
E_{na}, ev	$(2.1 \pm 0.5)\cdot10^{12}$	$(7.6 \pm 2.2)\cdot10^{12}$	$(2.9 \pm 0.9)\cdot10^{13}$	$(1.3 \pm 0.67)\cdot10^{14}$
E'_{na}, ev	$2.1\cdot10^{12}$	$8.0\cdot10^{12}$	$3.1\cdot10^{13}$	$6.3\cdot10^{13}$

of the group N_1, the region with an exponent $\gamma > 1$ ($\gamma = 1.8 \pm 0.5$) starts for the energy $E'_{na} > 10^{12}$ ev. (For showers of a smaller size, according to reference 2, for $E_{na} \geq 10^{12}$ ev, $\gamma = 1.5 \pm 0.2$.) In the same energy range of nuclear-active particles (10^{12} ev $\leq E_{na} \leq 10^{13}$ ev) and for showers with larger number of particles (group N_3), $\gamma = 0.9 \pm 0.3$, and for showers of the group N_4, $\gamma = 0.7 \pm 0.3$. The value $\gamma \leq 1$ for showers with small number of particles of the group N_1 corresponds to the energy region 10^{11} ev $\leq E_{na} \leq 10^{12}$ ev. Such a character of the energy spectra follows from the assumption that the nuclear cascade does not depend greatly on the energy. Several authors[8] assume that the character of the elementary interaction for the energies $E \gtrsim 10^{14}$ ev changes abruptly. In order to test the effect of a change of the elementary interaction, as done by Nikol'skiĭ et al.,[8] we calculated the

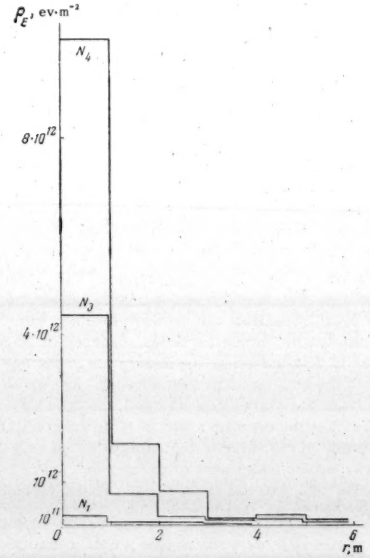

FIG. 4. Energy flux density of nuclear-active particles in showers with different N.

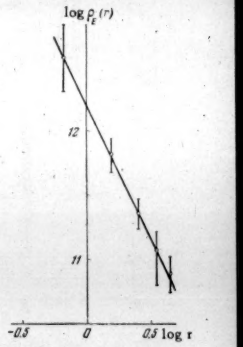

FIG. 5. Distribution of the energy flux in showers for $\bar{N} = 2 \times 10^5$. ρ is the energy flux density in ev/m^2, r in m.

spectra of nuclear-active particles in showers with different initial energy ($E_0 \sim 3 \times 10^{15}$ ev and $E_0 \sim 3 \times 10^{14}$ ev) for constant characteristics of the interaction and for a sharp dispersal of the energy in interactions with $E \geq 10^{14}$ ev. The calculation was done by the method of consecutive generations.[9] It was assumed, after Vernov et al.[10] that two particles with $E = 0.3\,E_0$ are produced in the interaction, and that, for $E \geq 10^{14}$ ev, six particles with $E = 0.1\,E_0$ are produced. The calculations carried out under the assumption that the character of the interaction between particles does not vary with the particle energy, show that the mean exponent of the spectrum for showers of different size in the intervals 10^{11} ev $< E_{na} < 10^{12}$ ev and 10^{12} ev $< E_{na} < 10^{13}$ ev differ greatly (for $E_0 = 3 \times 10^{15}$ ev, $\gamma_1 = 0.9$, $\gamma_2 = 1.1$; for $E_0 \approx 3 \times 10^{14}$ ev, $\gamma_1 = 1.1$, and $\gamma_2 = 1.4$). For the above variation of the character of the interaction, the spectra are very similar in both ranges ($\gamma_1 = 1.1$, $\gamma_2 = 1.4$, and $\gamma_1 = 1.2$, $\gamma_2 = 1.5$ correspondingly). Such a result is natural: for rapid dispersal of the energy, the energy of nuclear-active particles becomes smaller than the "critical" energy ($\leq 10^{14}$ ev) already after a small number of interactions. Further development of showers produced by primary high-energy particles then proceeds in the same way as for shower produced by particles of lower energies. The contribution of high-energy particles produced in the first interaction is small at sea level, in view of

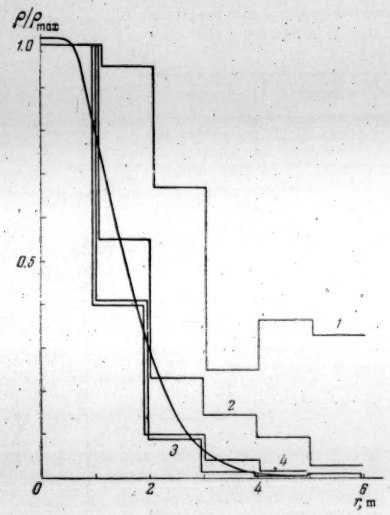

FIG. 6. Lateral distribution of nuclear-active particles in showers for particles with energy: 1 – 1×10^{11} to 3×10^{11} ev; 2 – 3×10^{11} to 1×10^{12} ev; 3 – $\geq 1 \times 10^{12}$ ev; 4 – data for particles with $E \geq 8 \times 10^{11}$ ev calculated with an electronic computer.

the large depth of the observation level. Therefore, the result will be the same for any other assumption concerning the character of the interaction, if only we assume a strong degeneration of energy for energies higher than a certain "critical" value.

The comparison of the experimental data with the calculation shows that the assumption about an abrupt change of the elementary interaction for $E \geq 10^{14}$ ev is unnecessary, and indicates rather a weak dependence of the characteristics of the elementary act of interaction on the energy. For a final solution of this problem, more accurate data in the range of large energies of E_{na} are necessary.

As may be seen from Table II, the value of the energy carried out by the nuclear-active component in the average shower is of the order of the energy carried by the electron-photon (e.p.) component of the shower, and is proportional to shower size, at least in the range of N from 1×10^4 to 1×10^6 (energy of the e.p. component $E_{ep} \approx 3\beta N \approx 2 \times 10^8 N$ ev). The values given in the table represent the lower estimate of the energy carried by the nuclear-active component of the shower. In fact, in the showers with $N \geq 1 \times 10^4$, the spectrum of nuclear-active particles has been studied by us up to the energy range where the spectrum exponent γ is of the order of 1. On the other hand, we took into account the energy of the nuclear-active component in the circle with radius 6 m, where the gradient of the lateral distribution function of the energy flux is of the order of $\sim r^{-2}$ (see below). It is therefore possible in principle, that we did not take into account a part of the energy of the nuclear-active component.

The presence of such energy in the nuclear-active component at the observation level can substantially change the absorption of the shower particles. The variation of the energy of the electron-photon component in a layer with thickness dt is given by the equation

$$dE_{ep} = -\beta N\, dt + (1-\alpha)(t_0/\lambda) E_{na}\, dt,$$

where $(1-\alpha)$ is the energy fraction carried away by π^0 mesons in nuclear interactions, E_{na} – the energy carried by the nuclear-active component, t_0 – the radiation length in g/cm², and λ – the mean free path for nuclear interactions in g/cm². In the electron-photon cascade for $1.5 \geq s \geq 1.2$, the mean energy $\bar{\epsilon}$ per charged particle is practically independent of s,[11] and therefore:

$$\bar{\epsilon}\, dN = -\beta N\, dt + aE_{na}\, dt.$$

The solution of this equation can be obtained easily if the absorption of the energy of the nuclear-active component in the atmosphere is known. Assuming that $E_{na} = E_0 \exp(-\mu_n t)$ where μ_n is the absorption coefficient of the energy of nuclear-active component in the air, and E_0 is the energy of the nuclear-active component at the observation level, we obtain for (for $\mu_0 > \mu_n$)

$$N(t) = \left[N_0 - \frac{aE_0}{\bar{\epsilon}(\mu_0 - \mu_n)}\right] e^{-\mu_0 t} + \frac{aE_0}{\bar{\epsilon}(\mu_0 - \mu_n)} e^{-\mu_n t},$$

where N_0 is the number of particles in the shower at the observation level, and μ_0 is the absorption coefficient of particles in showers for $E_{na} = 0$. The number of shower particles absorbed at large depths is determined by the absorption of the energy of the nuclear-active component. As can be seen from the expression obtained, the development of the shower with a given N is substantially dependent on the value of the energy E_0 of the nuclear-active component of the shower. Near the observation level, the absorption is characterized by the absorption coefficient

$$\mu = \mu_0 - aE_{na}/E_{ep}; \quad \Delta\mu = \mu_0 - \mu = aE_{na}/E_{ep}.$$

The absorption coefficient of shower particles is $\mu = 0.17$.[3] For $(1-\alpha) = 0.3$ and $E_{na}/E_{ep} = 1.0$,

we have $\Delta\mu = 0.05$; for $(1-\alpha) = 0.1$, $\Delta\mu = 0.08$. The measured values of the coefficient $\mu_0 = 0.22 - 0.25$, correspond to $s = 1.3$.[12]

Data on the average number of nuclear-active particles of various energies in showers of different size show that, in certain showers, we recorded nuclear-active particles of such energies that the mean frequency per shower was less than unity. The energy of single particles recorded in the first group of showers is equal to the total energy carried by the electron-photon component of such a shower. The exponent of the energy spectrum in this energy region for showers with $N \geq 3 \times 10^4$ is $\gamma \leq 1$, and, consequently, the total energy of the nuclear-active component in such showers is large ($E_{na} \gg E_{ep}$). This indicates a strong variation of the absorption coefficient μ in the shower.

In showers of small size, $N \leq 1 \times 10^4$, we recorded[2] showers with the measured energy of nuclear-active component larger by a factor of 10 than the energy of the electron-photon component. In such showers, one would expect a further increase in the number of particles rather than their absorption.

The fact that in individual showers, nuclear-active particles are present with an energy much larger than the average energy of particles which are found in each shower indicates strong fluctuations in shower development. This conclusion, drawn in reference 2 for showers with small number of particles, is correct for showers with $N < 3 \times 10^5$. Insufficient statistics does not permit to make an analogous conclusion for showers with $N > 3 \times 10^5$.

The large fluctuations in the energy balance of the showers, the energy carried by the nuclear-active component may be much lower than the average. In the limiting case, (for $E_{na} = 0$), the absorption of particles in showers is determined by μ_0. It should be noted that the detection of such showers is possible from a study of the energy balance of the different components in the shower core, since the difference in the lateral distribution of the particle flux due to different shower age may be insufficient for determining the age in individual showers by means of the method of correlated hodoscopes.

At the same time, it should be noted that, the observed value of the energy of the nuclear-active particles in the average shower confirms the limiting assumption about the relation between the nuclear-active and the electron-photon shower components (i.e., that on the average, an equilibrium exists between the nuclear-active and electron-photon components). In reference 1, the energy of the nuclear-active components was estimated for such a case. The relation which was obtained, namely $E_{na} \gtrsim 10^8 N$ ev, is satisfor all N, as can be seen from Table II. Data on the energy composition of showers obtained at mountain altitudes[13] indicate also that the nuclear component plays a large role. The conservation of the relative contribution of the energy carried in the shower by the different components at two altitudes also confirms the assumption that, on the average, the two components are in equilibrium.

The obtained lateral distribution of the energy flux of nuclear-active component in showers with given N (Fig. 5) can be well approximated by a power law with an exponent $n = 2 \pm 0.4$, apart from the dependence on the shower size.*

Recently various authors[14] have obtained data showing that the transverse momentum of particles produced in nuclear interactions is independent of the energy carried away by the particle. This fact can be used to obtain the lateral distribution of the energy flux of nuclear-active particles. We carried out such a calculation in which we used the method of consecutive generations, in order to obtain the energy spectrum of particles produced in interactions. We used very simple models of the interactions, following reference 10. From the same work we took also the values of the mean free path for the interactions for various models, obtained from the normalization to the observed number of particles with energy greater than a given value in a shower at sea level. The mean production level for particles of each generation was introduced. It was assumed that the particles of given energy are distributed uniformly in a circle, the mean radius of which is determined from the value of the particle energy and the level of production. The transverse momentum, according to our estimates (see below) and estimates of reference 14, is assumed to be equal to 10^9 ev/c. The atmosphere was assumed to be homogeneous, since the production level of particles which are essential to the discussion was not greater than one third of the atmosphere.

The obtained lateral distribution of the energy flux, was, for the same transverse momenta, found to be sensitive to the type of interaction. For distances of $0.5 - 8$ m, the lateral distribution can be

*Lateral distribution of the energy flux of the nuclear-active component averaged over showers with $N = 1 \times 10^4 - 2 \times 10^6$ is characterized by an exponent $n = 2 \pm 0.25$.

described by a power law with exponent n, where n depends on the model of interaction:

If 7 particles with energy 0.1 E_0 are produced, then n = 1.8
" 2 " " " 0.3 E_0 " " " n = 2.1
" 1 " " " 0.7 E_0 " " " n = 2.4
" 1 " " " 0.1 E_0 " " "

An even sharper difference is observed for r > 10 m. These distances, however, were not investigated in our work. A comparison of the experimental data with the calculations shows that, for the accuracy attained, a final unambiguous conclusion on the shape of the function of the lateral energy distribution cannot be drawn.

The data of Fig. 6 show a sharp concentration of particles of high energies ($E \gtrsim 10^{12}$ ev) near the shower axis. For the estimate of the width of the distribution of high-energy particles, a calculation of the lateral distribution of shower axes in the plane of hodoscope counters was carried out, based on the following assumptions: (1) the accuracy of axis location by means of hodoscope counters is ±1 m, and the fluctuations are subject to the Gauss distribution law, (2) the zenith-angle distribution of shower axes is given by the relation $I(\theta) = I_0 \cos^8 \theta$, (3) nuclear-active particles of high energies are concentrated near the shower axis.

The area of the chamber amounts to $\sigma = 1$ m^2, and the height of the counter plane above the chamber $h = 2$ m. The curve obtained as a result of the calculation, which reduces to a numerical integration of the Bessel function $I_0(x)$, is shown in Fig. 6 (solid line).

It can be seen from a comparison of the calculated results with the experimental data that the high-energy particles ($E_{na} \geq 10^{12}$ ev) are concentrated in a narrow region around the shower axis, of the order of the size of the chamber ($r \lesssim 1.0$ m). Particles with energy $1 \times 10^{11} - 3 \times 10^{11}$ ev are distributed much more widely: their density at the distance of 6 m falls off only by a factor of three as compared with the central region.

The lateral distribution of particles with $E \geq 10^{12}$ ev makes it possible to estimate the value of the transverse momentum obtained by such particles during their production. Assuming a height of production of $\sim 2\lambda_{inter} \sim 10^3$ m, we obtain $p_\perp c \leq 10^{12} \times 10^{-3} = 10^9$ ev.

In conclusion, the authors would like to express their gratitude to S. N. Vernov, and G. T. Zatsepin for their great help in the carrying out of the work and for helpful advice in discussing the results, and to G. V. Bogoslovskiĭ, V. I. Artemkin, and V. N. Sokolov, who took part in the measurements.

APPENDIX

CONNECTION BETWEEN THE SIZE OF THE BURST AND THE MEAN VALUE OF THE PRIMARY-PARTICLE ENERGY

In references 2 and 5, we obtained the value of the coefficient relating the number of particles in the burst to the energy of the particle producing the burst, by means of an actual analysis of the interaction of the first four generations of a nuclear cascade in the absorber. The connection between the average energy carried away by mesons and the energy of the primary particle can also be found from energy considerations. In fact, the variation of the energy flux $E_{\pi^0}(x)$ carried by the π^0 mesons at the depth of the absorber x (in nuclear units) is described, if we neglect the $\pi \to \mu$ decay, by the equation

$$dE_{\pi^0}(x)/dx = \beta(1-\alpha)E_N(x) + \beta E_{\pi^\pm}(x),$$

where $E_N(x)$ is the energy carried by nucleons at the depth x, $E_{\pi^\pm}(x)$ is the same for $\pi^\pm$ mesons, α is the energy fraction conserved by nucleons in interaction, and β is the energy of π^0 mesons compared with the energy transferred to π mesons in the interaction.

Analogous equations determine the absorption of the energy carried by the nucleons and $\pi^\pm$ mesons. The solution for the equation for $E_{\pi^0}(x)$ is

$$E_{\pi^0}(x) = \left[1 - \frac{\alpha\beta}{\alpha+\beta-1} e^{-(1-\alpha)x} + \frac{(1-\alpha)(1-\beta)}{\alpha+\beta-1} e^{-\beta x}\right] E_N^0,$$

where E_N^0 is the energy of the nucleon incident on the absorber. Assuming, after reference 15, $\alpha = 0.7$ and $\beta = 1/3$, we obtain for $x = 1.5$, $E_{\pi^0}(1.5) = 0.18 \times E_N^0$, and for $x = 2$, $E_{\pi^0}(2) = 0.25 \times E_N^0$. The value $x = 2$ corresponds to an absorber with 8 cm of lead over the graphite. In collision with the lead nucleus, a larger fraction of the energy is carried away by the mesons ($\alpha < 0.7$),[17] but, in that case, a strong development of the electron-photon cascade from π^0 occurs in the lead, and only a small part of the cascade energy reaches the lower layer of lead. We can therefore assume, to a first approximation, that the relations between the burst size and the energy of the primary particles, taking account of these interactions, will not change greatly. The development of a cascade in the lower layer of lead was considered on the basis of the data of Ivanenko.[16] Since the spectra of secondary π^0 mesons are not known, average values were taken from the number of particles under lead, obtained

under the assumption that the cascade is due to one π^0 meson with energy E_{π^0}, or to 10 mesons with energies $0.1\,E_{\pi^0}$ (the difference between these numbers amounts to about 20% for an energy $E_{\pi^0} \sim 10^{10}$ ev). The value obtained for the coefficient is $k = 7 \times 10^8$ ev for $E_N^0 \sim 5 \times 10^{11}$ ev, and it increases slowly with the energy. If we assume that the energy is carried by a small number of high-energy π^0 mesons, then for $E_N^0 \sim 4 \times 10^{12}$ ev we have $k = 2 \times 10^9$. However, π^0 mesons produced in the secondary interactions of $\pi^\pm$ mesons have, on the average, an energy smaller by an order of magnitude than that of the π mesons produced in the interactions of the primary nucleon, and the energy fraction carried by them is insignificant. Taking this fact into account leads to a slower change of k with energy.* For $E_N^0 \sim 4 \times 10^{12}$ ev, we obtained the value $k = 1.3 \times 10^9$ ev. In the following discussion we used the mean value of the coefficient $k = 1 \times 10^9$ ev.

*For this purpose we solved the equations for the energy directly transferred to π^0 mesons in interactions of the nucleon, and also in interactions of secondary $\pi^\pm$ mesons.

[1] Abrosimov, Goryunov, Dmitriev, Solov'eva, Khrenov, and Khristiansen, J. Exptl. Theoret. Phys. (U.S.S.R.) **34**, 1077 (1958), Soviet Phys. JETP **7**, 746 (1958).

[2] Dmitriev, Kulikov, and Khristiansen, J. Exptl. Theoret. Phys. (U.S.S.R.) (in press), Soviet Phys. JETP (in press).

[3] K. Greisen, Progress in Cosmic Ray Physics, Vol. III, Amsterdam (1956).

[4] Bekkermann, Dmitriev, Molchanov, Khristiansen, and Yarygin, Приборы и техника эксперимента (Instruments and Meas. Eng.) No. 4, (1958).

[5] Dmitriev, Kulikov, and Khristiansen, Suppl. Nuovo cimento **2**, 587 (1958).

[6] G. B. Khristiansen, Dissertation, Phys. Inst. Acad. Sci. 1953.

[7] G. V. Kulikov and G. B. Khristiansen, J. Exptl. Theoret. Phys. (U.S.S.R.) **35**, 625 (1958), Soviet Phys. JETP **8**, 44 (1959).

[8] Nikol'skiĭ, Vavilov, and Batov, Dokl. Akad. Nauk SSSR **111**, 71 (1956), Soviet Phys. "Doklady" **1**, 625 (1956).

[9] G. T. Zatsepin and I. L. Rosental, Dokl. Akad. Nauk SSSR **99**, 369 (1954).

[10] Vernov, Gorchakov, Ivanenko, and Khristiansen, J. Exptl. Theoret. Phys. (U.S.S.R.) (in press), Soviet Phys. JETP (in press).

[11] I. P. Ivanenko, J. Exptl. Theoret. Phys. (U.S.S.R.) **35**, 132 (1958), Soviet Phys. JETP **8**, 94 (1959).

[12] S. E. Belen'kiĭ, Лавинные процессы в космических лучах (Cascade Processes in Cosmic Rays), M-L 1948.

[13] Dovzhenko, Zatsepin, Murzina, Nikol'skiĭ, and Rakobol'skaya, Dokl. Akad. Nauk SSSR **118**, 899 (1958), Soviet Phys. "Doklady" **3**, 122 (1958).

[14] G. L. Milekhin and I. L. Rozental', J. Exptl. Theoret. Phys. (U.S.S.R.) **33**, 197 (1957), Soviet Phys. JETP **6**, 154 (1958). Birger, Grigorov, Guseva, Zhdanov, Slavatinskiĭ, and Stashkov, J. Exptl. Theoret. Phys. (U.S.S.R.) **31**, 971 (1956), Soviet Phys. JETP **4**, 872 (1957); G. B. Zhdanov, J. Exptl. Theoret. Phys. (U.S.S.R.) **34**, 856 (1958), Soviet Phys. JETP **7**, 592 (1958).

[15] I. L. Grigorov, Usp. Fiz. Nauk **58**, 599 (1956).

[16] I. L. Ivanenko, Dokl. Akad. Nauk SSSR **107**, 819 (1956), Soviet Phys. "Doklady" **1**, 231 (1956).

[17] Grigorov, Podgurskaya, Savel'eva, and L. M. Poperekova, J. Exptl. Theoret. Phys. (U.S.S.R.) **35**, 3 (1958), Soviet Phys. JETP **8**, 1 (1959).

Translated by H. Kasha
139

SOVIET PHYSICS JETP VOLUME 36 (9), NUMBER 3 SEPTEMBER, 1959

CROSS-SECTIONS FOR THE PRODUCTION OF CALIFORNIUM ISOTOPES BY THE BOMBARDMENT OF U^{238} BY ACCELERATED CARBON IONS

V. V. VOLKOV, L. I. GUSEVA, A. S. PASYUK, N. I. TARANTIN, and K. V. FILIPPOVA

Submitted to JETP editor September 16, 1958

J. Exptl. Theoret. Phys. (U.S.S.R.) **36**, 762-765 (March, 1959)

The energy dependence of the reactions $U^{238}(C^{12}, 4n\text{-}5n)Cf^{246-245}$ and $U^{238}(C^{13}, 5n\text{-}6n)Cf^{246-245}$ was investigated. The method of irradiating a stack of foils combined with the use of radiochemical analysis of the fission products was used for this work. The results obtained show that the reactions investigated take place by means of the formation of a compound nucleus with subsequent neutron evaporation. The reaction cross-sections are used to estimate the competition between the process of neutron evaporation from the compound nucleus and fission.

In the bombardment of heavy elements by multiply charged ions compound nuclei are formed with a high excitation energy. The subsequent fate of such nuclei is determined primarily by the competition between the process of neutron evaporation and fission. A study of the ratio of these processes as a function of excitation energy and of the parameters of the compound nucleus is of considerable interest for the synthesis of new transuranic elements.

In the present work we have investigated the energy dependence of the reactions $U^{238}(C^{12}, 4n\text{-}5n)$ and $U^{238}(C^{13}, 5n\text{-}6n)$. The cross-sections for these reactions were determined by the yield of the α-active isotopes Cf^{246} and Cf^{245} which have half-lives convenient for recording.

The production of californium in the bombardment of U^{238} by carbon ions has been studied earlier in references 1 – 3.* However, these references contain data only for the integrated yield of californium in a thick target.

DESCRIPTION OF THE EXPERIMENT

The method of bombarding a stack of foils with the use of radiochemical analysis of the reaction products was employed for the study of the energy dependence of the reactions given above.

The $^{+4}C^{12}$ and $^{+4}C^{13}$ ions produced directly in an ion source[4] were accelerated by means of the one-and-a-half meter cyclotron of the U.S.S.R. Academy of Sciences. The energy of the bombarding particles measured by their absorption in aluminum amounted to 78 Mev for the $^{+4}C^{12}$ ions and to 84 Mev for the $^{+4}C^{13}$ ions. The energy spread of the particles did not exceed 3%. The ion current to the target was measured by means of a current integrator. To avoid overheating of the target the beam intensity was maintained at a level of 0.2 – 0.3 μa.

The uranium was deposited on a nickel foil by means of evaporation in vacuo. The amount of U^{238} on each foil of the stack was determined by means of an ionization chamber by the number of α-particles emitted per unit time. The thickness of the uranium layers amounted to 0.3 – 0.5 mg/cm^2. The nickel foils prepared by electrolytic deposition were of thickness 1.3 – 2.0μ. The stack of foils was assembled in such a way that the uranium layers faced in the direction of the beam. In this case those californium nuclei which were ejected from the uranium layer were completely stopped by the nickel foil on which this layer was deposited.

Irradiation of the stack of foils was carried out in the internal beam of the cyclotron during 3 – 5 hours. In order to take into account the variations in intensity of the beam the values of the current were recorded every 5 min.

After irradiation each foil was dissolved in concentrated nitric acid to which 400 μg of lanthanum had previously been added as carrier. For the separation of the actinides a precipitation of lanthanum fluoride was carried out. The precipitate was then dissolved in several drops of concentrated nitric acid and deposited on a platinum plate. The Cf^{246} and Cf^{245} isotopes were identified by the energy of the α-particles and by their half-lives. For this purpose the platinum plate was placed in an ionization chamber with a spherical electrode; the pulses from the chamber were fed into a multichannel analyzer.

*As has been shown by additional measurements the value of the energy of the C^{12} ions given in reference 3 was somewhat high.

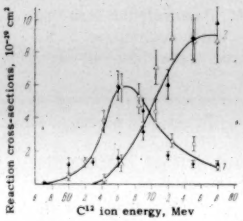

FIG. 1

FIG. 1. The cross-sections for the reactions U^{238} (C^{12}, 4n) Cf^{246} (1) and U^{238} (C^{12}, 5n) Cf^{245} (2) as a function of the energy of the bombarding particle. △ and ○ – first experiment, ▲ and ● – second experiment.

FIG. 2. Cross-sections for the reactions U^{238} (C^{13}, 5n) Cf^{246} (open circles) and U^{238} (C^{13}, 6n) Cf^{245} (black points) as a function of the bombarding particle energy.

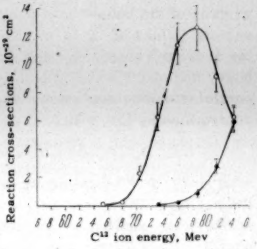

FIG. 2

In some cases the actinide fraction was fed through an ion exchange column filled with cationite Dowex-50 X-12. The washing was with 0.4 M lactic acid at a pH = 4.5 and t = 87°C. It was found that all the α activity, of energies 6.75 and 7.1 Mev and of half-lives 36 hours and 44 min respectively, belongs to the californium fraction.

The chemical yield of the californium isotopes was determined by the yield of Am^{241} which was added as a tracer when each foil was dissolved.

RESULTS AND DISCUSSION

The results of the measurements of the energy dependence of the cross-sections for the reactions

$$U^{238}(C^{12},\ 4n-5n)Cf^{246-245},$$
$$U^{238}(C^{13},\ 5n-6n)Cf^{246-245}$$

are shown in Figs. 1, 2.

The energy of the carbon ions incident on each foil was calculated from the range-energy curve for nickel.[7] The energy losses in the uranium oxide layer were determined from the data on the stopping power of the appropriate substances for α particles. For the calculation of the yield of Cf^{245} it was taken into account that the fraction of the nuclei decaying with the emission of α particles is 34%. The total experimental error is shown in the figures.

Additional experiments were also carried out on the irradiation of a thick uranium target. A comparison of the yield of californium obtained in these experiments with the yield calculated from the cross-section curves for the reactions showed that the discrepancy in the results does not exceed 20%.

As may be seen from Figs. 1 and 2 the cross-section curves for the reactions have characteristic maxima whose shape and relative position indicate that the californium isotopes are produced as a result of the evaporation of neutrons from the excited compound nucleus. A comparison of the curves for the reactions (C^{12}, 5n) and (C^{13}, 5n) shows that the addition to the compound nucleus of one neutron does not change the magnitude of the cross-section significantly.

A comparison of the data obtained on the cross-section for the production of californium isotopes with the uranium fission cross-section under the action of carbon ions[9] shows that only a small fraction of the californium nuclei formed does not undergo fission.

Figure 3 gives the cross-section curves for these reactions as a function of excitation energy referred to the total cross section for the production of the compound nucleus. The data on the fission cross-section of U^{238} by carbon ions required for our calculations were taken from reference 9. The displacement of the maxima of the reactions (C^{12}, 5n) and (C^{13}, 5n) with respect to one another may be associated with a certain inaccuracy in the determination of the initial energy of the C^{12} and C^{13} ions.

It may be seen from the diagram that as the number of neutrons emitted increases the fraction of compound nuclei which do not undergo fission decreases. This fact indicates that fission occurs at all stages of neutron evaporation from the compound nucleus.

Although the probability of neutron emission W_n and the probability of fission W_f may vary somewhat as the neutrons are evaporated from the compound nucleus, nevertheless for the com-

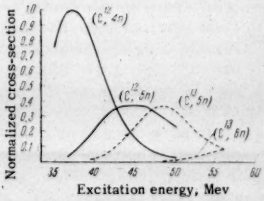

FIG. 3. Cross-sections for the reactions (C^{12}, 4n–5n) and (C^{13}, 5n–6n) referred to the total cross-section for the production of the compound nucleus as a function of excitation energy.

parison of the behavior of compound nuclei with various values of Z it may be useful to introduce the average values $\overline{W}_n$ and $\overline{W}_f$. In the case of heavy nuclei for which the emission of charged particles can be neglected, $\overline{W}_n$ and $\overline{W}_f$ will be determined by the relation

$$\sigma_n = \sigma_t (\overline{W}_n / (\overline{W}_n + \overline{W}_f))^n,$$

where σ_n is the total cross-section of the reactions with neutron emission at a given energy, σ_t is the cross-section for the formation of the compound nucleus at the same energy, n is the average number of neutrons emitted. The ratio $\overline{W}_n/\overline{W}_f$ calculated by means of this formula in the case of californium amounts to $\sim 1/4$ and does not vary appreciably in the excitation energy range from 35 to 55 Mev. The values of W_n/W_f calculated for the Cf^{246} nucleus from the ratio of the maxima of the normalized cross-sections for the reactions (4n-5n) and (5n-6n) (Fig. 3) amount respectively to $\sim 1/2$ and $1/3$. Although it is not possible to exclude a difference in the value of W_n/W_f for the states of the Cf^{246} nucleus obtained in the different reactions (4n or 5n), it seems to us more probable that the first value ($1/2$) is too high due to the inaccuracy in the determination of σ_t at low energies.

In conclusion we regard it as our pleasant duty to express our gratitude to Prof. G. N. Flerov for directing this work. The authors also express their gratitude to the members of the cyclotron crew directed by Yu. M. Pustovoĭt for ensuring the smooth operation of the machine, and L. K. Tarasov who participated in the chemical part of the work.

[1] Ghiorso, Thompson, Street, and Seaborg, Phys. Rev. **81**, 154 (1951).

[2] Fremlin, Glover, and Milsted, J. Inorg. Nucl. Chem. **2**, 263 (1956).

[3] Gerlit, Guseva, Myasoedov, Tarantin, Filippova, and Flerov, J. Exptl. Theoret. Phys. (U.S.S.R.) **33**, 339 (1957), Soviet Phys. JETP **6**, 263 (1958).

[4] Morozov, Makov, and Ioffe, Атомная энергия (Atomic Energy) **3**, 272 (1957).

[5] Hulet, Thompson, Ghiorso, and Street, Phys. Rev. **84**, 366 (1951).

[6] Chetham-Strode, Choppin, and Harvey, Phys. Rev. **102**, 747 (1956).

[7] Yu. Ts. Oganesyan, J. Exptl. Theoret. Phys. (U.S.S.R.) **9**, 936 (1959), Soviet Phys. JETP, this issue, p. 660.

[8] E. Segre, Experimental Nuclear Physics, (Russ. transl.) vol. 1, IIL, Moscow, 1955 [Wiley, N. Y., 1953].

[9] S. M. Polikanov and V. A. Druin, J. Exptl. Theoret. Phys. (U.S.S.R.) **9**, 744 (1959), Soviet Phys. JETP, this issue, p. 522.

Translated by G. Volkoff
140

SOVIET PHYSICS JETP VOLUME 36 (9), NUMBER 3 SEPTEMBER, 1959

INVESTIGATION OF WEAK FERROMAGNETISM IN THE $MnCO_3$ *SINGLE CRYSTAL*

A. S. BOROVIK-ROMANOV

Institute of Physics Problems, Academy of Sciences, U.S.S.R.

Submitted to JETP editor October 3, 1958

J. Exptl. Theoret. Phys. (U.S.S.R.) **36**, 766-781 (March, 1959)

The magnetic properties of a very pure natural $MnCO_3$ single crystal have been studied in the temperature range from 1.3 to 300°K. In accord with the predictions of the theory,[7] it has been found that the ferromagnetic moment σ is observed only in the basal plane. Along the triple axis, the crystal is paramagnetic. The temperature dependence of σ, $\chi_\perp$, and $\chi_\parallel$ has been investigated in detail through the entire region of existence of antiferromagnetic ordering. It is shown that, in agreement with the theory of second-order phase transitions, $\sigma/\chi_\perp \sim \sqrt{T_N - T}$ near the transition point.

At low temperatures, σ is proportional to T_2 in a broad range from 1.5 to 23°K ($0.7\,T_N$). The dispersion law and the temperature dependences of the thermodynamic quantities for antiferromagnets with magnetic structure of the $MnCO_3$ type have been obtained by the spin-wave theory method. In this case the spontaneous magnetization vector is perpendicular to the crystal axis. As a result, the gap associated with the anisotropy field is missing from the energy spectrum. The theoretical formulas obtained are in qualitative agreement with the experimental results. The possible causes of the large quantitative discrepancy between the values of the coefficients that determine the temperature dependence of σ and $\chi_\perp$ are discussed.

1. INTRODUCTION

THE problem of weak ferromagnetism in antiferromagnets has been attracting considerable attention recently. This phenomenon was observed first experimentally in hematite (α-Fe_2O_3) by Smith[1] as early as in 1916, long before the discovery of antiferromagnetism. The magnetic properties of hematite single crystals have been investigated later in detail by Neel and Pauthenet,[2] while Shull, Strauser, and Wollan[3] proved via neutron diffraction that this compound is antiferromagnetic. The strong dependence of the ferromagnetic properties hematite on the method of preparation of the specimen[4] has led most investigators[2,3,5] to believe that this phenomenon is due to impurities and to lattice defects. Carbonate salts of the elements of the iron group have the same crystallographic structure as hematite. The presence of weak ferromagnetism in $MnCO_3$ and $CoCO_3$ was observed by the author and Orlova.[6] It was shown that the observed weak ferromagnetism was independent of the chemical production of the compounds, and the hypothesis was advanced that it was due to the spins not being completely parallel during the antiferromagnetic ordering. Dzyaloshinskiĭ[7] has shown that antiferromagnetic ordering with incompletely parallel spins is a necessary consequence of the symmetry of the magnetic structure, both in the case of $MnCO_3$ or $CoCO_3$ and in the case of hematite. His detailed thermodynamic investigation of the magnetic properties of such substances led to many interesting conclusions regarding the anisotropy and temperature dependence of the ferromagnetic moment and the paramagnetic susceptibility. To test experimentally the theoretical conclusions, we undertook the investigation of the magnetic properties of single-crystal $MnCO_3$, the results of which are reported in this paper.

Another feature of antiferromagnets with magnetic structure of the $MnCO_3$ type is that the vector of spontaneous magnetization in them does not have one fixed direction, but may rotate almost freely in the basal plane of the crystal. Calculations, given in the first part of this paper, show that one of the branches of the energy spectrum of the spin waves has practically no gaps. As a result, starting already with temperatures less than 1°K, the spontaneous magnetization, the susceptibility, and the specific heat should obey simple power laws. An important advantage of such objects for experimental verification of the theory of spin waves has caused us to make a detailed study of the temperature dependence of the spontaneous magnetization and susceptibility of $MnCO_3$ at low temperatures. The results of these meas-

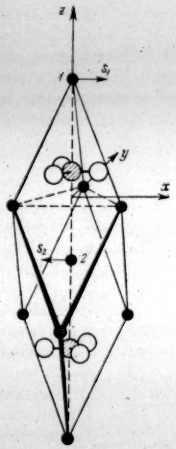

FIG. 1. Structure of $MnCo_3$. Black circles – Mn, white ones – O, crosshatched – C.

urements are reported and compared with the conclusions of the spin-wave theory in the second part of this paper.

2. THEORY

1. $MnCO_3$ has a rhombohedral structure.[8] Its elementary cell (see Fig. 1) contains two metallic ions, 1 and 2. We denote their mean spins as s_1 and s_2. We introduce the molar quantities $\mathbf{M}_1 = N\mathbf{s}_1/2$ and $\mathbf{M}_2 = N\mathbf{s}_2/2$, and their linear combinations $\mathbf{l} = \mathbf{M}_1 - \mathbf{M}_2$ and $\mathbf{m} = \mathbf{M}_1 + \mathbf{M}_2$. In the future we shall use a coordinate system in which the z axis is aligned with the trigonal axis, the x axis with one of the binary axes, and the y axis lies in the symmetry plane.

It was shown by Dzyaloshinskiĭ[7] that if the elementary cell does not change in such a structure during antiferromagnetic transition, three types of ordering are possible in the absence of a magnetic field:

I. The antiferromagnetic vector $\mathbf{l}$ coincides with the z axis and there is no ferromagnetic moment $\mathbf{m}$.

II. The antiferromagnetic vector $\mathbf{l}$ is directed, in the first approximation, along the y axis; there is a weak ferromagnetic moment $\mathbf{m}$ directed along the x axis. In the second approximation the vector $\mathbf{l}$ has a small component along the z axis.

III. The antiferromagnetic vector $\mathbf{l}$ is directed along the x axis; there exists a weak ferromagnetic moment $\mathbf{m}$, direct in first approximation along the y axis, with a small component along the z axis in the second approximation.

As follows from our earlier paper[6] and also from the results of this investigation, the order-disorder transformation realized in the case of $MnCO_3$ is of type II or III. In what follows we refer indeed to these two types of order-disorder. Dzyaloshinskiĭ has shown that if a sufficiently strong magnetic field $\mathbf{H}$ is applied* the following situation occurs. If the field is applied in the basal plane, the vectors $\mathbf{l}$ and $\mathbf{m}$ rotate so that $\mathbf{m}$ is always parallel to $\mathbf{H}$ and $\mathbf{l}$ is perpendicular to $\mathbf{H}$. If $\mathbf{H}$ is directed along the z axis, then in the first approximation the antiferromagnetic vector $\mathbf{l}$ and the ferromagnetic moment always remain in the basal plane. A more detailed analysis of this case, as will be shown below, disclosed that the application of a field along the z axis may lead to rotation of the vector $\mathbf{l}$ in the basal plane.

2. To derive the temperature dependence of the magnetic properties near the transition point, we write down the thermodynamic potential† proposed by Dzyaloshinskiĭ, with allowance for terms up to fourth order in $\mathbf{l}$ and $\mathbf{m}$. Without loss of generality we can confine ourselves to an examination of the case when the magnetic field is perpendicular to the y axis.

$$\tilde{\Phi} = \frac{A}{2} l^2 + \frac{B}{2} m^2 + \frac{b}{2} m_z^2 - \beta m_x l + \frac{C}{4} l^4 + \frac{D}{2} l^2 m^2 + \frac{d}{2} l^2 m_z^2 - \mathbf{m}\cdot\mathbf{H}. \quad (1)$$

Minimizing this potential and putting, as usual, $A = \lambda'(T - T_N)$, we obtain

$$l \approx \sqrt{\lambda (T_N - T)}, \quad \lambda = \lambda'/C, \quad (2)$$

and for the magnetic moment in the basal plane

$$m_x = \frac{\beta \sqrt{\lambda (T_N - T)}}{B + D\lambda (T_N - T)} + \frac{H_x}{B + D\lambda (T_N - T)}$$

$$= \sigma + \chi_\perp H_\perp \text{ for } T < T_N. \quad (3a)$$

In virtue of the isotropy of the magnetic properties in the basal plane, established in reference 7, this formula holds for any direction of the magnetic field in this plane. We have for the magnetic susceptibility along the trigonal axis

$$m_z = H_z / [B + b + (D + d)\lambda (T_N - T)]$$

$$= \chi_\parallel H_\parallel \text{ for } T < T_N. \quad (3b)$$

*A sufficiently strong field is considered here one in which the magnetic energy $\mathbf{m}\cdot\mathbf{H}$ is much greater than the anisotropy energy in the basal plane. As will be seen from our experimental results, this condition is satisfied when H exceeds 2000 oersteds.

†The symbols we use here for several coefficients differ from those in reference 7. Attention should be called to the fact that similar letters are used for different coefficients in expansions (2) and (3) of reference 7: In Eq. (2) these are constants, and in (3) these are temperature-dependent quantities.

Above the transition point $l = 0$, and therefore

$$m_\perp = H_\perp / B = \chi_\perp H_\perp \text{ and } m_z = H_z/(B+b) = \chi_\parallel H_\parallel \text{ for } T > T_N. \quad (4)$$

Equations (3) and (4) describe the temperature dependence of the quantities measured in this investigation near the transition temperature.

3. The results of our measurement of the magnetic properties of $MnCO_3$ along the z axis (cf. below) display an anomaly, and a more detailed analysis of the behavior of m_z in fields commensurate with the anisotropy field was deemed advisable to explain this anomaly. For this purpose, we must consider the thermodynamic potential with inclusion of the terms that describe the anisotropy in the basal plane [Eq. (6) of reference 7]. To simplify the derivation we neglect in all further calculations the anisotropy of the susceptibility ($b = 0$) and the deviation of the antiferromagnetic vector from the basal plane ($\theta = \pi/2$). Then

$$\tilde{\Phi} = \frac{B}{2} m^2 - q(m_y \cos\varphi - m_x \sin\varphi) + \frac{D}{2}(m_x \cos\varphi + m_y \sin\varphi)^2 + e\cos 6\varphi - f m_z \cos 3\varphi - m_z H_z, \quad (5)$$

where φ is the angle between the direction of the antiferromagnetic vector and the x axis, and the previous remarks apply to the expansion coefficients. Minimizing (5) relative to m for a specified value of φ, we get

$$m_x = (q/B)\sin\varphi; \quad m_y = -(q/B)\cos\varphi; \quad m_z = H_z/B - (f/B)\cos 3\varphi. \quad (6)$$

Inserting (6) into (5) we find the dependence of $\tilde{\Phi}$ on φ and H_z:

$$\tilde{\Phi} = -q^2/2B - H_z^2/2B - e - 2(e - f^2/4B)\cos^2 3\varphi - (fH_z/B)\cos 3\varphi. \quad (7)$$

Differentiating this expression with respect to φ, we obtain two equations for the equilibrium value of the angle φ:

$$\sin 3\varphi = 0, \quad (e - f^2/4B)\cos 3\varphi = fH_z/4B. \quad (8)$$

Which of these conditions corresponds to the minimum of (7) depends on the sign of the coefficient* $e' = (e - f^2/4B)$.

If $e' < 0$, Φ has a minimum for all field intensities when $\sin 3\varphi = 0$. Thus, if a type III (see above) order-disorder is established in the absence of a field, it is retained at all values of H_z and

$$f\cos 3\varphi \leq 0. \quad (8a)$$

$$m_z = H_z/B + |f|/B. \quad (9a)$$

If $e' > 0$, the minimum of $\tilde{\Phi}$ at $H = 0$ occurs when $\cos 3\varphi = 0$. A type II order-disorder is established here. When the field H_z is applied, the angle φ begins to change such as to retain Eq. (8) in force. The rotation of the antiferromagnetic vector in the basal plane will continue until the field reaches a value $H_{cr} = 4e'B/|f|$. Here $\tilde{\Phi}_{II} = \tilde{\Phi}_{III}$ and the crystal will be in state III as the field is further increased. Thus, the magnetic moment in this case will change in the field in accordance with the following law

$$m_z = (1 + f^2/4Be')H_z/B \text{ for } H \leq 4e'B/|f|,$$
$$m_z = H_z/B + |f|/B \text{ for } H \geq 4e'B/|f|. \quad (9b)$$

It must be noted that the ferromagnetic moment $\sigma_z = |f|/B$ should be much less than the moment σ in the basal plane, considered above.

4. To obtain the theoretical temperature dependence of $m_\perp$ and $m_\parallel$ at temperatures close to absolute zero, we must resort to the theory of spin waves. The spin-wave theory for antiferromagnets was developed by several authors.[9-12] A very simple mathematical formalism for the theory of spin waves was developed by Kaganov and Tsukernik *[13] on the basis of a phenomenological examination of an antiferromagnet with two sublattices, characterized by magnetic moments specified as functions of the coordinates and of the time.†

All the theoretical investigations performed to date have considered uniaxial antiferromagnets, in which the direction of the spontaneous magnetization of the sublattices coincides with the principal axis of the crystal. In the case of $MnCO_3$ the spontaneous magnetization is perpendicular to the axis and this, as will be shown below, leads to a substantial modification of the spectrum of the spin waves.

We have used the calculation procedure proposed by Kaganov and Tsukernik to find the spectrum of antiferromagnets with magnetic structure of the $MnCO_3$ type. In accordance with the type of the thermodynamic potential (1) the Hamiltonian must be written in this case as follows:

*In the equilibrium state, the last term in (7) is always negative, since, regardless of the sign of f,

*An analogous investigation was carried out independently by Turov and Irkhin.[14]

†Dzyaloshinskii (private communication) points out that in the case of antiferromagnets such an approach is strictly phenomenological and involves a model in which the absolute value of the sublattice spontaneous-magnetization vector is independent of the applied field at absolute zero. This model is used in the determination of the ground state of the antiferromagnet.

$$\mathcal{H} = \int dv \Big\{ \varkappa \mathbf{M}_1 \cdot \mathbf{M}_2 + \frac{a+b}{2} (M_{1z}^2 + M_{2z}^2) + (b-a) M_{1z} M_{2z} + 2\beta (M_{1x} M_{2y} - M_{2x} M_{1y}) - (\mathbf{M}_1 + \mathbf{M}_2) \mathbf{H} + \frac{\rho}{2} \left(\frac{\partial \mathbf{M}_1}{\partial x_k} \right)^2 + \rho_{12} \frac{\partial \mathbf{M}_1}{\partial x_k} \frac{\partial \mathbf{M}_2}{\partial x_k} + \frac{\rho}{2} \left(\frac{\partial \mathbf{M}_2}{\partial x_k} \right)^2 \Big\}, \quad (10)$$

where $\mathbf{M_1(r, t)}$ and $\mathbf{M_2(r, t)}$ are the magnetic moments of each of the sublattices. We disregard here terms connected with the anisotropy in the basal plane, since (as follows from the results cited later) this anisotropy is very small and is overcome when a field of several hundreds oersteds is applied.

If the external field $\mathbf{H_0}$ is applied in the basal plane (to be specific, we assume it to be directed along x axis) then in the ground state (T = 0°K)

$$M_{1x}^0 = M_{2x}^0 = \beta M_0 / \alpha + H_0 / 2\alpha; \quad M_{1y}^0 = -M_{2y}^0 \approx M_0; \quad M_{1z} = M_{2z} = 0, \quad (11)$$

where M_0 is the absolute spontaneous magnetization of each of the sublattices at T = 0°K. The excited states are characterized by the vectors

$$\mathbf{M}_1 = \mathbf{M}_1^0 + \boldsymbol{\mu}_1, \quad \mathbf{M}_2 = \mathbf{M}_2^0 + \boldsymbol{\mu}_2, \quad (12)$$

where $\boldsymbol{\mu}_1$ and $\boldsymbol{\mu}_2$ are considered proportional to $\exp\{-i(\omega t + \boldsymbol{\kappa} \cdot \mathbf{r})\}$. Using the equation of motion of magnetic moments and the equations of magnetostatics, we obtain, after suitable simplification, the following system of equations for $\boldsymbol{\mu}_1$ and $\boldsymbol{\mu}_2$:

$$\begin{aligned}
&i\omega (\mu_{1x} + \mu_{2x}) - \gamma M_0 (a + (\rho - \rho_{12}) \varkappa^2) (\mu_{1z} - \mu_{2z}) = 0, \\
&i\omega (\mu_{1y} + \mu_{2y}) + (\gamma H_x + 2\beta\gamma M_0) (\mu_{1z} + \mu_{2z}) = 0, \\
&\gamma M_0 (\rho - \rho_{12}) \varkappa^2 (\mu_{1x} - \mu_{2x}) - \gamma H_x (\mu_{1y} + \mu_{2y}) + i\omega (\mu_{1z} + \mu_{2z}) = 0, \\
&i\omega (\mu_{1x} - \mu_{2x}) - 2\alpha\gamma M_0 (\mu_{1z} + \mu_{2z}) = 0, \quad \mu_{1y} - \mu_{2y} = 0, \\
&2\alpha\gamma M_0 (\mu_{1z} + \mu_{2x}) - 2\beta\gamma M_0 (\mu_{1y} - \mu_{2y}) + i\omega (\mu_{1z} - \mu_{2z}) = 0,
\end{aligned} \quad (13)$$

where γ is the gyromagnetic ratio.

From this we obtain directly the energy spectrum

$$\begin{aligned}
&\varepsilon_1 = [(\mu H_A)^2 + (\mu H_E)^2 (\varkappa d)^2]^{1/2}, \\
&\varepsilon_2 = [(\mu H_E)^2 (\varkappa d)^2 + (\mu H_x) 2\beta H_x 2\beta M_0]^{1/2}; \\
&H_A = M_0 \sqrt{2\alpha}; \\
&H_E = M_0 \sqrt{2\alpha (\rho - \rho_{12})} / d; \quad \mu = \gamma\hbar,
\end{aligned} \quad (14)$$

where d is the lattice constant.

A substantial difference between this spectrum and the spectra of uniaxial antiferromagnets with spontaneous magnetization, previously considered, with spontaneous magnetization directed along the axis, is the presence of two branches. In one branch, as in the ordinary case, there is an energy gap caused by the anisotropic field, while the other branch has no such gap and is purely phonon in the absence of a magnetic field.*

If the magnetic field is directed along the z axis, the ground state is characterized by the following values of the moments:

$$M_{1x}^0 = M_{2x}^0 = \beta M_0 / \alpha; \quad M_{1y}^0 = -M_{2y}^0 \approx M_0; \quad M_{1z}^0 = M_{2z}^0 = H_z / 2(\alpha + b). \quad (15)$$

The spin-wave spectrum again has two branches:

$$\varepsilon_1 = [(\mu H_A)^2 + (\mu H_E)^2 (\varkappa d)^2 + (\mu H_z)^2]^{1/2}; \quad \varepsilon_2 = \mu H_E \varkappa d. \quad (16)$$

Knowing the laws of dispersion (14) and (16) we can determine the thermodynamic potential Ω of the spin-wave gaps and use the latter to determine the thermodynamic quantities that characterize the magnetic properties and the specific heat of the spin waves.

If the magnetic field is in the basal plane of the crystal, we obtain from (14)

$$m_{\mathbf{sp.w}} = -(\mu / 12 d^3 H_E) (kT / \mu H_E)^2 (\beta M_0 + H). \quad (17)$$

Allowing for the magnetic moment of the ground state, (11), we get

$$\begin{aligned}
&\sigma = \sigma_0 \{1 - \gamma_1 (T / T_N)^2\}, \\
&\chi_\perp = \chi_{\perp 0} \{1 - 2\gamma_1 (T / T_N)^2\},
\end{aligned} \quad (18)$$

where

$$\begin{aligned}
&\sigma_0 = 2\beta M_0 / \alpha; \quad \chi_{\perp 0} = 1 / \alpha; \\
&\gamma_1 = (\mu / 12 d^3 \chi_{\perp 0} H_E) (kT_N / \mu H_E)^2.
\end{aligned}$$

If the magnetic field is directed along the diagonal axis, the expression for this branch of the spectrum, which depends on the external field, coincides with the corresponding expression for the perpendicular field, cited by Kaganov and Tsukernik.[13] The formulas for $\chi_\parallel$ in our case will therefore coincide with the formulas for $\chi_\perp$ in reference 13, i.e., at very low temperatures ($kT \ll \mu H_A$) we have

$$\chi_\perp = 1 / (\alpha + b) - Qe^{-\mu H_A / kT},$$

and for higher temperatures ($\mu H_A \ll kT \ll \mu H_E$) the expression for $\chi_\parallel$ coincides with equation (18) for $\chi_\perp$.

The two branches of the energy spectrum will correspond to two terms in the magnetic specific heat

$$c_{\mathbf{magn}} = c_1 + c_2, \quad (19)$$

and the second term is

$$\begin{aligned}
c_2 &= (2\pi^2 k / 15 d^3) (kT / \mu H_E)^3 \\
&= (8\pi^2 k^2 \chi_{\perp 0} \gamma_1 T_N / 5\mu^2) (T / T_N)^3,
\end{aligned} \quad (20)$$

*Allowance for the anisotropy in the basal plane would obviously lead to a gap in this branch, too, although its value, in accordance with the foregoing estimates, does not exceed 0.01°K.

while the first term c_1, as in the ordinary case, has an exponential temperature dependence at low temperatures ($kT \ll \mu H_A$) and is equal to c_2 at higher temperatures.

To conclude this analysis of the application of spin-wave theory to antiferromagnets with $MnCO_3$-like magnetic structure we wish to emphasize that this case is the most convenient from the point of view of comparing theory with experiment, since the power laws obtained above are much easier to verify experimentally than the exponential laws obtained for the case when the spontaneous magnetization is parallel to the anisotropy axis. On the other hand, the condition $\mu H_A \ll kT \ll \mu H_E$ necessary for power laws to be obtained in the latter case, may be impossible to satisfy in general for many substances.

3. EXPERIMENT AND RESULTS

To investigate the anisotropy of magnetic properties of $MnCO_3$ we used a natural crystal of rhodochrosite (from a deposit in the valley of the Aura river in the Pyrenees). We obtained the rhodochrosite from the minerological museum of the U.S.S.R. Academy of Sciences.* From the crystals obtained we chose some of the better ones, fully transparent and having no irregularities that could be seen with the microscope, and with good formation. One of the crystals, 3.8 mg in weight, was used for the magnetic investigations, and two others were used for spectral impurity analysis.† It was established that both crystals alike contain approximately 0.1 – 1% calcium and magnesium and approximately 0.01% silicon.

Magnetic measurements were carried out with apparatus analogous to that previously described.[15] To increase the accuracy of the measurement, the magnetic balance was improved considerably – an automatic photocompensation scheme was produced to increase considerably the stability of the readings, the voltage of the motor-generator supply to the magnet was stabilized, and automatic temperature control was introduced. As a result, the accuracy of the relative measurements of the magnetic moment was ±0.5%. Temperatures were measured by helium vapor pressure from 1.3 to 4°K, with a carbon resistance thermometer from 4 to 20°K, and with a copper resistance thermometer,[17] calibrated against a standard platinum thermometer,[18] from 20 to 300°K.

The accuracy of the temperature measurement in the vicinity of T_N (approximately 30°K) was ±0.02°. In the region most difficult to measure (near 10°K) the accuracy was approximately ±0.1°.

Owing to the good formation, it was not difficult to orient the crystal suitably on the goniometer, after which BF glue was used to secure to it the suspension rod. The accuracy of the crystal orientation was 2 or 3 degrees.

The main investigations were carried out with the specimen so suspended that the suspension vertical line coincided with one of the binary axes of the crystal (the x axis in our notation), while the y and z axes were in a horizontal plane. The magnetic field was rotated in this plane.

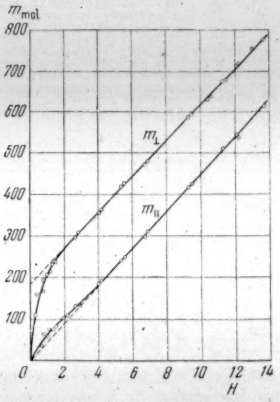

FIG. 2. Dependence of the molar magnetic moment m on the field intensity H at T = 4.2°K. $m_\parallel$ – field along the z axis, $m_\perp$ – field along the y axis (m is in CGS magnetic units and H is in kilo-oersteds).

Figure 2 shows the results of the measurement of the magnetic moment (all the quantities in this paper are per mole), as a function of the applied field, at T = 4.2°K. The upper curve is obtained when the field is applied along the y axis. As is seen from the diagram, the dependence of the magnetic moment on this field, for H > 2000 oe, can be represented by the following formula

$$m_\perp(H, T) = \sigma(T) + \chi_\perp(T) H_\perp. \qquad (21)$$

Along the trigonal axis (lower curve) in strong fields (H > 4000 oe) the magnetic moment changes linearly with field, like in ordinary paramagnets:

*The author takes this opportunity to thank Prof. G. P. Barsanov and N. A. Kruglov, who graciously helped select very pure rhodochrosite crystals.

†The spectral analysis of the specimens was performed at the Institute of Geochemistry and Analytical Chemistry of the Academy of Sciences of the U. S. S. R. by M. M. Farafonov, to whom the author expresses deep gratitude.

$$m_{\parallel} = \chi_{\parallel} H_{\parallel} \qquad (22)$$

In weak fields one observes an anomalous variation of the magnetic moment with the field. This anomaly is seen at all temperatures below the Neel temperature ($T_N = 32.4°K$), as shown in Fig. 3

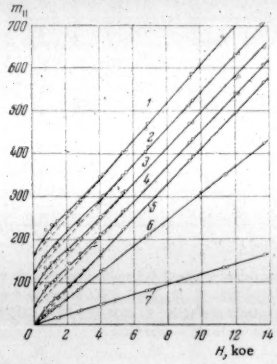

FIG. 3. Dependence of the molar magnetic moment $m_{\parallel}$ on the field intensity at the following temperatures: 1) 4.2°K, 2) 20.3; 3) 29.7 4) 30.8; 5) 31.2; 6) 78.4; 7) 295°K. Curve 4 is shifted along the ordinate axis by $\Delta m = 40$ CGS magnetic units. Curve 3 is shifted by 80 units, curve 2 by 120 units, and curve 1 by 160 units.

where the results of an investigation of this anomaly are given for five temperatures. It must be noted that the readings of the balance, in measurement along the z axis at weak fields, are quite unstable and the reproducibility of the results is several times worse than in other measurements. We can therefore describe the observed anomaly only qualitatively.

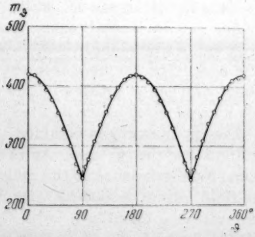

FIG. 4. Angular dependence of the moment in the yz plane at H = 5.37 kilo-oersteds (ϑ is the angle between the direction of the magnetic field and the y axis).

Figure 4 shows the dependence of the magnetic moment m on the angle ϑ between the direction of the magnetic field and the y axis at T = 4.2°K and at a constant value of the field. The experimental results are represented by the dots. The solid curve is the function $m_{min} + a|\cos\vartheta|$, where

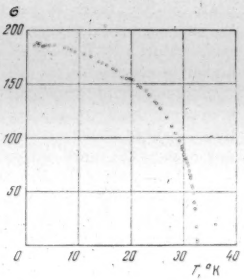

FIG. 5. Temperature dependence of the spontaneous ferromagnetic moment σ (σ is given in CGS magnetic units per mole).

the coefficient $a = m_{max} - m_{min}$ is selected to fit the experimental data.

Our measurements for the case when the trigonal axis coincides with the direction of the suspension have shown that, within the limit of experimental error, the values of m are the same in all directions lying in the basal plane, for all values of the magnetic field.

Curves analogous to those given in Fig. 2 were obtained by us for 50 temperatures, ranging from 1.3 to 32.3°K. These curves were used to obtain graphically the values of $\sigma(T)$, $\chi_{\perp}(T)$, and $\chi_{\parallel}(T)$. In determining σ by extrapolation to H = 0, the accuracy of the results obtained is naturally lower. We estimate the error in the values of σ to be ± 2 CGS magnetic units, amounting to approximately 1% of σ_0. The error in the values of $\chi_{\perp}$ and $\chi_{\parallel}$ amounts to approximately $\pm 0.3\%$. The temperature dependence $\sigma(T)$ is shown in Fig. 5. We see that when $T \to 0$ we get $\sigma(T) \to 188$ CGS magnetic units. The spontaneous moment σ vanishes at $T_N = 32.43°K$. Figure 6 shows the values of $\chi_{\perp}(T)$ and $\chi_{\parallel}(T)$, while above 32.43°K $MnCO_3$ becomes paramagnetic, and consequently χ is the ordinary paramagnetic susceptibility for these temperatures.

As can be seen from Fig. 6, the susceptibility of $MnCO_3$ is isotropic above 34°K, within the limits of accuracy of our measurements. Our measurements have shown that in the temperature range from 70 to 300°K the paramagnetic susceptibility obeys the Curie-Weiss law

$$\chi = C/(T - \Theta), \qquad (23)$$

with C = 4.46 and $\Theta = -64.5°K$. The dotted Curve 1 of Fig. 6 corresponds to an extrapolation of the Curie-Weiss law (23) to the transition-temperature region. Within the very narrow vicinity of T_N, the susceptibility $\chi_{\perp}$ has small sharp maximum, and at lower temperatures $\chi_{\parallel}$ and $\chi_{\perp}$ are almost parallel to each other, with $\chi_{\perp}$ being 3% less than $\chi_{\parallel}$.

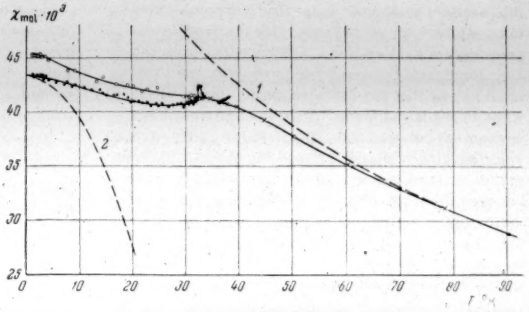

FIG. 6. Temperature dependence of the magnetic susceptibility of $MnCO_3$ in the paramagnetic and antiparamagnetic states. ○ – $\chi_{\parallel}$; ● – $\chi_{\perp}$, × – coinciding values $\chi_{\parallel} = \chi_{\perp}$; Curve 1 – extrapolation of the Curie-Weiss law. Curve 2 – is based on the spin-wave theoretical formula (18) (χ is in CGS magnetic units).

Only two papers devoted to a study of magnetic properties of $MnCO_3$ at low temperatures are known at present. Bizette and Tsai[19] also investigated a natural single crystal $MnCO_3$. They give no analysis of the m(H) curves, and restrict themselves to indicating that at low temperatures $\chi_{\perp}$ depends on the field intensity. We have calculated, using our data for σ and $\chi_{\perp}$, the values of $\chi'_{\perp} = \chi_{\perp} + \sigma/H$ for those values of the field intensity H, given in reference 19. Figure 7 shows

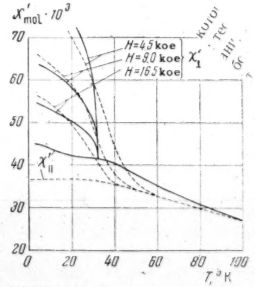

FIG. 7. Comparison of our data of the molar susceptibility of various values of the field (solid curves) with the data of Bizette and Tsai[19] (dotted curves).

the comparison of our values of χ' with those of Bizette and Tsai. We see that the data for the paramagnetic region agreed satisfactorily, but below that the discrepancy becomes noticeable — our values of $\chi_{\parallel}$ are approximately 15% higher than the values of $\chi_{\parallel}$ given in reference 19. Only very rough qualitative agreement is observed for $\chi'_{\perp}$. The quantitative discrepancies in $\chi'_{\perp}$ reach 20 or 30%. Our data characterize a very sharp transition temperature, $T_N = 32.4°K$, below which $\chi'_{\perp}$ begins to depend on the field. In reference 19 this temperature is rather smeared in the region between 40 and 60°K. At low temperatures the discrepancy in the data on $\chi'_{\perp}$ decreases. We believe that these discrepancies are due to the fact that the crystal used by Bizette and Tsai was not sufficiently pure, leading to a considerable smearing of the transition point. This assumption is also confirmed by the fact that Bizette and Tsai investigated large crystals (weighing up to 0.5 grams). Naturally, it was quite difficult to select sufficiently pure crystals of this size.

As already indicated, the author and Orlova[6] were the first to observe a dependence of type (21) for $MnCO_3$. The measurements reported in that reference pertain to polycrystalline chemically-pure specimens. The values we obtained for the moments at different values of H and T agree, within the limit of experimental error, with the data of the present paper. The small discrepancy in the transition temperature (approximately 1°K) is obviously due to the insufficient accuracy of calibration of the thermocouple in the earlier work. The fields employed in reference 6 were not strong enough (reaching 2500 oe) to produce sufficient saturation of the magnetic moment. Consequently, there is a considerable error (approximately 40 – 50%) in the resultant extrapolated values of the ferromagnetic moment σ. In the present work we carried out the measurements at fields five or six times the saturation value. This guarantees sufficiently accurate extrapolation in the determination of the ferromagnetic moment.

4. DISCUSSION OF THE RESULTS

1. From the result of our measurements of the magnetic properties of $MnCO_3$ in the high-temperature region we can determine the value of the g-factor. The value g = 2.04 obtained and its isotropy are in good agreement with the theory that the Mn^{++} ion is in the S state. The large negative value of Θ in (23) indicates the presence of an antiferromagnetic interaction.

2. Below $T_N = 32.43°K$ the substance goes

into antiferromagnetic state that has weak ferromagnetism.* In accordance with the model proposed by us earlier,[6] and in accordance with the Dzyaloshinskiĭ thermodynamic theory, our experiments show that the ferromagnetic vector is always in the basal plane. This is confirmed by agreement between the experimentally established relationships (21) and (22) and the theoretical formulas (3), and is seen particularly clearly on the rotation diagram (figure 4). Were the ferromagnetic vector inclined to the basal plane, we would obtain a curve represented not by $|\cos\vartheta|$, but by a curve with a gentler maximum at $\vartheta = n\pi$ and with a steeper descent at $\vartheta = \pi/2 + n\pi$.

3. The results of our measurements on $m_\perp$ at weak fields ($H < 2000$ oe) shows that, in the case of weak ferromagnetism, domains that become remagnetized at fields of 2 – 2.5 kilo-oersteds are formed in antiferromagnets. The hysteresis of this process is very small. On the other hand, comparison of our results on the anisotropy in the basal plane (which at all fields is less than the accuracy of our measurements) with the theoretical curves (Fig. 5 of reference 7) shows that the effective anisotropy field in the basal plane is at any rate less than 100 oe. Anderson et al.[20] investigated the ferromagnetic resonance in hematite. In this case the value of the anisotropy field in the basal plane was found to be 60 oe.

The foregoing anomalous behavior of $m_\parallel$ in a weak field may be due to the rotation of the direction of spontaneous magnetization of the sublattices in the basal plane, considered in the first part of this paper. True, the experimental data (see Figs. 2 and 3) do not agree with (9a) and (9b). It must be borne in mind, however, that in these experiments the angle φ can assume, in the process of rotation, values corresponding to non-equilibrium states. This violates condition (8) which was assumed in the derivation of (9). The instability in the readings of the balance, noted previously, may also be due to this departure from equilibrium. In any case, the observed anomaly is evidence in favor of assuming that the crystal $MnCO_3$ is in state II when $H = 0$, as does occur in the case of hematite.[3]

4. It is interesting to compare the temperature dependences of σ, $\chi_\perp$, and $\chi_\parallel$, obtained by us, with the theory. We first consider the temperature region close to the transition point. A comparison of the experimental results on the isotropy of below T_N with Eq. (4) leads to $b = 0$. To reconcile (3) with the experimental curves for $\chi_\parallel$ and $\chi_\perp$ (Fig. 6), we must put $D = -d$ and $D > 0$, so that

$$\chi_\parallel = 1/B, \qquad \chi_\perp = 1/(B + Dl^2). \tag{3'}$$

The experimentally-observed anisotropy below T_N is due to the term $Dl^2(m_x^2 + m_y^2)/2$ in the expression for the thermodynamic potential (1).

Of greatest interest is the temperature dependence of the spontaneous magnetization of the antiferromagnet near the transition point. Using the previously-adopted symbols, the spontaneous magnetization of each of the sublattices is $M \approx l/2$, and, according to (3a) and (2)

$$2M = l = \sigma/\beta\chi_\perp. \tag{24}$$

It is thus possible to determine, from the temperature dependences of σ and $\chi_\perp$ measured by us, the temperature dependence of the magnetization of the sublattices. If it is assumed that the coefficients β in the expression for the thermodynamic potential (1) and the Hamiltonian (10) are of the same magnitude,* and in accordance with Eq. (11) we get

$$M/M_0 = (\sigma/\sigma_0)\chi_\perp^0/\chi_\perp. \tag{25}$$

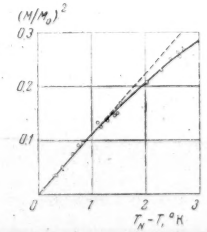

FIG. 8. Temperature dependence of the square of the relative spontaneous magnetization of the sublattices near the transition temperature.

Figure 8 shows the dependence of the quantity $(M/M_0)^2$, calculated from the experimental values of σ and $\chi_\perp$, on the temperature difference $T_N - T$. We see that near 1.5° ($\Delta T/T_N \sim 5\%$) the experimental points fit the straight line

$$(M/M_0)^2 = \xi(1 - T/T_N), \tag{26}$$

where $\xi = 3.6$. Deviations from this law begin when M/M_0 reaches 40%. It is known that molecular-field theory leads to an equation similar to (26) with $c = 3$.[21] Experiments made on ferromagnetic metals have led to values greater than 3,

*Magnetic measurements alone can only permit us to assume, with high probability, the establishment of antiferromagnetic order-disorder transitions. To obtain a rigorous experimental proof of this fact neutron-diffraction investigations must also be performed.

*Such an assumption is tantamount to adopting the molecular-field model.

namely c = 5 to 7 for nickel (references 22 and 23 respectively) and c = 7 for iron.[24] Measurements made on ferrites yield values of ξ from 0.1 to 0.7. Thus the simple model of the molecular field describes the behavior of the spontaneous magnetization of antiferromagnets more accurately than that of metallic ferromagnets and ferrites. This conclusion is in agreement with the theoretical work of Vonsovskiĭ and Vlasov[26] for ferromagnets and of Neel[27] for ferrites. Prior to this investigation, only one paper was published on a study of the temperature dependence of M near T_N (for $CuCl_2 \cdot 2H_2O$).[28] The curve obtained there is much steeper than ours, and shows no quadratic region. It is possible that this is due to the chain structure of the antiferromagnetic order-disorder in $CuCl_2 \cdot 2H_2O$.[29]

If we assume further that the sublattice magnetization at T = 0°K has the nominal value, i.e., $M_0 = (1/2)\, N\mu_B gS = 14.1 \times 10^3$ CGS magnetic units per mole, then $\sigma_0/2M_0 = 0.0067$, i.e., the ferromagnetic moment amounts to 0.67% of the nominal magnetization. We then obtain, from (11), $\beta = 0.15$. According to the data of Neel and Pauthenet,[2] $\beta = 0.7$ for α-Fe_2O_3. Using Eqs. (2) and (26) and the value of M_0, we get $\lambda = 89 \times 10^6$. The value of $\chi_\parallel$ obtained from (3b) yields B = 24.2. The temperature variation of $\chi_\perp$ makes it possible to estimate, using Eq. (3a), the coefficient $D = 2 \times 10^{-9}$. The foregoing representation of the molecular-field theory model were used by us only to estimate the coefficients of the thermodynamic potential (1). A qualitative thermodynamic derivation of the validity of Eq. (2) near T_N is confirmed by our experiments independently of these assumed models.

5. Let us turn now to compare our results with Eqs. (18) of the spin-wave theory, derived in the first section of this paper. As follows from these formulas, σ and $\chi_\perp$ should diminish with temperature, following a quadratic law. Figure 9 shows the temperature dependence we have obtained for σ/σ_0. Of the three curves shown in the diagram, the first corresponds to linear temperature scale along the abscissa, the second to a quadratic scale, and the third to a cubic. It is seen from the diagram that the experimental points fit the straight line well only in the case of a quadratic temperature scale. This proves at the same time that Eq. (18) fits correctly the temperature dependence of the spontaneous ferromagnetic moment in $MnCO_3$, in the temperature region down to $0.7\, T_N$. This corresponds to a 25% reduction in the spontaneous moment. We find from these experimental data that the coefficient η in Eq. (18) has a value of 0.48. An important factor for the verification of the spin-wave theory is that in our derived equations the same coefficient η determines both the temperature dependence of the spontaneous magnetization and the susceptibility $\chi_\perp$. However, as can be seen from Fig. 6, the experimental points for $\chi_\perp$ exhibit a much lesser temperature dependence than predicted by (18) with the aforementioned value $\eta = 0.48$ (curve 2). An equally weak dependence is displayed also by the parallel susceptibility $\chi_\parallel$. The accuracy of our experiments is insufficient to derive an expression for this weak decrease in $\chi_\parallel$ and $\chi_\perp$.

The discrepancy we observed in the coefficients of the thermal dependence of σ and $\chi_\perp$ is obviously proof of the shortcomings of the spin-wave theory used to derive (18). We have already noted that the principal shortcoming of the theory is that in the assumed model application of an external field at T = 0°K does not change the magnitude of the lattice-magnetization vectors, but merely rotates them. If we forego this model, the Hamiltonian of (10) must be written in the form of an expansion in the terms of the small quantities μ_i.

As already indicated above, antiferromagnets with a magnetic structure of $MnCO_3$ are the most suitable objects for verifying the spin-wave theory. In other crystals, owing to the presence of the large gap in the spin-wave spectrum ($> 0.1\, T_N$), all the thermodynamic quantities should have an exponential temperature dependence at low temperatures, a dependence difficult to verify experimentally. Measurements of the temperature dependence of the magnetic susceptibility of MnF_2,[30] $NiSO_4$,[31] and $CuSO_4$[32] in the region above $(0.2 - 0.4)\, T_N$, confirm that the T^2 law holds, as called for by the spin-wave theory. However, what fails to make this deduction convincing is that the temperature range in which the T^2 law

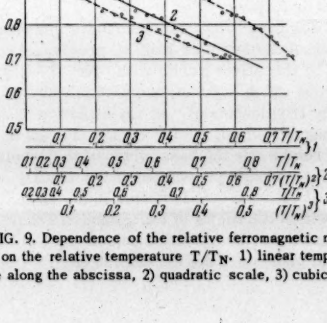

FIG. 9. Dependence of the relative ferromagnetic moment σ/σ_0 on the relative temperature T/T_N. 1) linear temperature scale along the abscissa, 2) quadratic scale, 3) cubic scale.

holds may, generally speaking, lie above the limits of applicability of the theory. On the other hand, more accurate measurements of the temperature dependence of the sublattice magnetization, performed by the nuclear-resonance method, give contradictory results. Poulis and Hardeman[28] have found in the case of $CuCl_2 \cdot 2H_2O$ that $M - M_0 \sim T^4$ in the range $(0.3 - 0.7)\,T_N$. Jaccarino and Shulman have found that $M - M_0 \sim T^{3.5}$ for MnF_2[33] in the region $(0.02 - 0.3)\,T_N$, and $M - M_0 \sim T^5$ for CoF_2[34] in the region $(0.03 - 0.5)\,T_N$. We believe that these results apply to temperatures in the transition region between the exponential and power laws.

For a more complete experimental verification of the spin-wave theory it would be important to obtain data on the specific heat of $MnCO_3$. We used Eq. (20) to estimate the value of the magnetic specific heat $MnCO_3$, using the previously mentioned value $\eta = 0.48$, and found for the magnetic specific heat

$$c_2 = 460\,(T/67)^3 \text{ cal/deg-mole}$$
$$= 1.9 \cdot 10^{10}\,(T/67)^3 \text{ erg/deg-mole.}$$

For convenience in comparing the magnetic specific heat with the lattice specific heat we write here the formulas with the same numerical coefficients as in the Debye law, choosing suitable values of Θ_D. These formulas show that the magnetic specific heat will be the same as that of a lattice with $\Theta_D = 67°$K. According to Anderson[35] who measured the specific heat of $MnCO_3$ from 50 to 300°K, $\Theta_D = 220°$. This value, obtained from experimental data at relatively high temperatures, may be grossly in error. In any case, one might think that at helium temperatures the magnetic specific heat should exceed the lattice specific heat by 5 or 10 times.

CONCLUSION

The principal results of this paper can be formulated as follows:

1. It has been shown experimentally that the weak ferromagnetism of $MnCO_3$, previously observed by the author jointly with Orlova[6] has an anisotropy which is predicted by the theory proposed by Dzyaloshinskiĭ. At any direction of applied magnetic field, the ferromagnetic vector σ always remains in the basal plane of the crystal.

2. The magnetic properties of the $MnCO_3$ crystal at $T < T_N$ are isotropic in the basal plane, within the limits of experimental accuracy. This means that the effective anisotropy field in the basal plane does not exceed 100 oe.

3. An anomaly has been observed in the dependence of the magnetic moment on the field ($H < 2500$ oe), when the field is directed along the trigonal axis. This anomaly may be due to rotation of the antiferromagnetic vector $\boldsymbol{l}$ in the basal plane, due to the field applied along the trigonal axis. Such a rotation was justified theoretically as a consequency of reference 7.

4. It has been shown that near T_N the spontaneous magnetization of the sublattices, M, in $MnCO_3$ in accordance with the thermodynamic theory, obeys the following law

$$(M/M_0)^2 = \xi\,(1 - T/T_N).$$

The value $\xi = 3.6$ agrees satisfactorily with $\xi = 3$, predicted by the molecular-field theory.

5. From an analysis of the experimental curves of the temperature dependence of σ, $\chi_\parallel$, and $\chi_\perp$, we estimated the coefficients in the expansion for the thermodynamic potential.

6. It has been established that in the $1.3 - 23°$K range the spontaneous ferromagnetic moment decreases and follows a quadratic law.

7. The spin-wave theory was used to calculate the dispersion of an antiferromagnetic with a magnetic structure of $MnCO_3$ and to show that in this case two branches of the structure were obtained, one of which has practically no gap.

8. With the aid of the dispersion law obtained, formulas were derived for the temperature dependence of σ, $\chi_\perp$, $\chi_\parallel$, and c_{magn}. These formulas show that σ and $\chi_\perp$ should diminish as the second power, with $\chi_\perp$ decreasing twice as fast as σ. The experimental results, to the contrary, show very small decrease in $\chi_\perp$ as compared with σ. This is evidence of the incompleteness of the existing spin-wave theory.

In conclusion the author expresses deep gratitude to Academician P. L. Kapitza for continuous interest in this work. The author is very grateful to I. E. Dzyaloshinskiĭ for useful discussions and to V. I. Kolokol'nikov for help with the performance of the experiment.

[1] T. Smith, Phys. Rev. **8**, 721 (1916).

[2] L. Neel and R. Pauthenet, Compt. rend. **234**, 2172 (1952). L. Neel, Revs. Modern Phys. **25**, 58 (1953).

[3] Shull, Strauser, and Wollan, Phys. Rev. **83**, 333, (1951).

[4] R. Chevallier, J. Phys. et radium **12**, 172 (1951).

[5] G. Haigh, Phil. Mag. **2**, 877 (1957).

[6] A. S. Borovik-Romanov and M. P. Orlova, J. Exptl. Theoret. Phys. (U.S.S.R.) **31**, 579 (1956), Soviet Phys. JETP **4**, 531 (1957).

[7] I. E. Dzyaloshinskiĭ, J. Exptl. Theoret. Phys. (U.S.S.R.) **32**, 1547 (1957), Soviet Phys. JETP **5**, 1259 (1957).

[8] B. F. Ormont, Структуры неорганическех веществ (Structures of Inorganic Substances), M-L, 1950.

[9] J. M. Ziman, Proc. Fiz. Soc. **65**, 540 (1952).

[10] R. Kubo, Revs. Modern Phys. **25**, 344 (1953).

[11] W. Marshall, Proc. Roy. Soc. **A232**, 69 (1955).

[12] P. W. Anderson, Phys. Rev. **86**, 694 (1952).

[13] M. I. Kaganov and V. M. Tsukernik, J. Exptl. Theoret. Phys. (U.S.S.R.) **34**, 106 (1958), Soviet Phys. JETP **7**, 73 (1958).

[14] E. A. Turov and Yu. P. Irkhin, Izv. Akad. Nauk SSSR, Ser. Fiz. **22**, 1168 (1958), Columbia Tech. Transl., in press.

[15] A. S. Borovik-Romanov and N. M. Kreines, J. Exptl. Theoret. Phys. (U.S.S.R.) **29**, 790 (1955), Soviet Phys. JETP **2**, 657 (1956).

[16] J. R. Clement and E. H. Quinnell, Rev. Sci. Instr. **23**, 213 (1952).

[17] T. M. Douphinee and H. Preston-Thomas, Rev. Sci. Instr. **25**, 884 (1954).

[18] Borovik-Romanov, Orlova, and Strelkov, Установление шкалы низких температур между 90, 19° K и 10° K (Establishment of a Low-Temperature Scale between 90.19° K and 10° K) M, 1954.

[19] H. Bizette and B. Tsai, Compt. rend. **241**, 369 (1955).

[20] Anderson, Merritt, Remeika, and Yager, Phys. Rev. **93**, 717 (1954).

[21] S. V. Vonsovskiĭ and Ya. S. Shur, Ферромагнетизм (Ferromagnetism), M-L, 1948.

[22] P. Weiss and R. Forrer, Ann. de Phys. **5**, 153 (1926).

[23] K. P. Belov and A. N. Goryaga, Физика металлов и металловедение (Physics of Metals and Metal Research), **2**, 3 (1956).

[24] H. H. Potter, Proc. Roy. Soc. **146**, 362 (1934).

[25] Belov, Bol'shova, and Elkina, Izv. Akad. Nauk SSSR, Ser. Fiz. **21**, 1047 (1957), Columbia Techn. Transl. p. 1051.

[26] S. V. Vonsovskiĭ and K. B. Vlasov, J. Exptl. Theoret. Phys. (U.S.S.R.) **25**, 327 (1957).

[27] L. Neel, Ann. de Phys. **3**, 137 (1953).

[28] N. J. Poulis and G. E. G. Hardeman, Physica **19**, 391 (1953).

[29] W. Marshall, J. Phys. Chem. Solids **6**, (1958), in press.

[30] M. Griffel and J. W. Stout, J. Chem. Phys. **18**, 1455 (1950).

[31] Borovik-Romanov, Karasik, and Kreines, J. Exptl. Theoret. Phys. (U.S.S.R.) **31**, 18 (1956), Soviet Phys. JETP **4**, 109 (1957).

[32] N. M. Kreines, J. Exptl. Theoret. Phys. (U.S.S.R.) **35**, 1391 (1958), Soviet Phys. JETP **8**, 972 (1959).

[33] V. Jaccarino and R. G. Shulman, Phys. Rev. **107**, 1196 (1957).

[34] Jaccarino, Shulman, Davis, and Stout, Bull. Am. Phys. Soc. **3**, 41 (1958).

[35] C. T. Anderson, J. Am. Chem. Soc. **56**, 849 (1934).

Translated by J. G. Adashko
141

SOVIET PHYSICS JETP VOLUME 36 (9), NUMBER 3 SEPTEMBER, 1959

CONVERGING CYLINDRICAL DETONATION WAVE

Ya. B. ZEL' DOVICH

Submitted to JETP editor September 13, 1958

J. Exptl. Theoret. Phys. (U.S.S.R.) **36**, 782-792 (March, 1959)

The properties of detonation waves close to the normal detonation wave are considered. A theory is set up for the amplification of cylindrical converging detonation waves, which describes exactly the amplification in the initial stages of the process. By comparison with numerical calculations, it is shown that the theory remains satisfactory even for small radii and appreciable amplification of the wave.

1. INTRODUCTION

A converging detonation wave was first considered by L. D. Landau and K. P. Stanyukovich in 1944 (this research was reported in the well-known monograph of Stanyukovich,[1] pp. 567-574). The authors found the asymptotic law of the increase in pressure for the approximation of a spherical wave at the center or for a cylindrical wave on the axis. If the adiabatic exponent is $n = 3$, the pressure in this case increases as $r^{-1.13}$ in the spherical case and as $r^{-0.47}$ in the cylindrical case.

This research was noteworthy not only in its physical results but also in its methodology as an example of a power solution in which the exponent of the power was determined by the singular points of an ordinary differential equation and not by considerations of dimensionality. In the case of an unrestricted increase in the pressure, it is possible to neglect the chemical energy of the explosive material in comparison with the action of the pressure. Therefore, the theory developed by the authors is the same for converging detonation waves and for converging shock waves in a chemically inert substance.*

Neglect of the chemical energy is not only a consequence but also a premise of the theory: from dimensionality it follows that only in this approximation does the power solution satisfy the equations and we can go from the equation in partial derivatives to ordinary differential equations. Neglect of the chemical energy, which is valid in the last stage of convergence, is quite unsuitable at the beginning of the detonation of the charge of explosive material: at the beginning of the process, the pressure is entirely determined precisely by the chemical energy which is released upon the explosion.

The purpose of the present research was the approximate (asymptotic) treatment of just this initial stage of the process of convergence of the detonation wave. At the starting moment, in the excitation of the explosion on the external surface of the sphere or cylinder, a normal detonation wave appears which does not differ from a plane detonation wave. The normal detonation wave is essentially different from a shock wave primarily because the amplitude of the detonation wave is determined by the properties of the explosive substance and does not depend upon the method of generation, while the amplitude of the shock wave is entirely determined by the external action which the phenomenon of the shock wave brings about.

This independence of the normal shock wave of the external reaction is associated with the fundamental properties of the state achieved in a detonation wave; these properties are considered in Sec. 2.

Along with the convergence there begins an increase in the pressure at the front of the wave and the normal detonation wave is replaced by the so-called compressional detonation wave, in which the pressure is higher than the normal; the state in the compressional wave depends not only on the chemical energy but also on the state of the products of the explosion which are found at the front of the detonation. Experimentally, the existence of the compressional wave in gaseous detonation was first shown by B. V. Al'vazov and the author.[3]

The reasons for the increase in pressure is the center- (or axially) directed motion of the products of the explosion behind the detonation wave front: the products of the explosion move

*The work of Stanyukovich and Landau was completed independently of similar work by Guderley[2] on the theory of converging shock waves in air.

in the direction of decreasing radius as though they were compressed and their compression is transferred to the wave front. In the limit of high pressure, the compressional detonation wave does not differ from a shock wave. However, we shall use the opposite limiting case, that is, we shall make use of the circumstance that at the beginning of the process the compressional wave differs slightly from the normal detonation wave. This circumstance, together with the fundamental properties of the normal detonation wave, allow us to develop a very effective approximate method of calculation of the pressure on the wave front, which is given in Sec. 3. This method is applicable, inasmuch as the amplitude is not too large; since the pressure in a cylindrical wave grows more slowly than in a spherical wave, the calculations are given for the cylindrical case where the range of applicability of the method is the greater. In Sec. 4 we give the numerical results of a calculation according to this method.

Finally, in Sec. 5, we compare our approximate method with the results of the numerical solution of the partial differential equation. The region of applicability is shown to be greater and the accuracy better than could be expected a priori; differences in the pressure, velocity, density do not exceed 10 per cent for convergence of the wave up to a radius equal to $1/25$ of the original, when the pressure itself increases three times in comparison with the original. All the calculations are carried out for the simplest case of an equation of state with $n = 3$; however, in reality, the assumed approximate method is applicable for any equation of state for the products of the explosion, since it is based upon very general properties of the detonation wave.

2. PROPERTIES OF A NORMAL DETONATION WAVE

It is well-known that for a detonation wave of explosive materials, the equations for the conservation of mass, momentum and energy can be satisfied for any pressure exceeding the pressure which is developed in the chemical reaction in the material at rest. To each value of the pressure there corresponds the definite density (the corresponding line in the plane p, $v = 1/\rho$ is known as the Hugoniot adiabatic), a definite velocity of motion of the products of the explosion, etc.

Of this series of states in the normal detonation there exists only one completely determined state (the corresponding point on the Hugoniot adiabat is known as the Jouguets point[4]). The fundamental property of this state is the condition

$$D_0 = u_0 + c_0, \tag{1}$$

where D is the propagation velocity of the detonation wave, u is the velocity of motion of the material, c is the velocity of sound. The 0 indicates the quantities are evaluated at the Jouguets point.

With the aid of thermodynamical relations, we can obtain the following properties of the Jouguets point and the properties of the Hugoniot adiabatic near the Jouguets point from Eq. (1):

$$(dD/dp)_{H,0} = 0. \tag{2}$$

The symbol H indicates that the derivative is taken along the Hugoniot adiabatic, the 0 indicates the Jouguets point; at this point D has a minimum. Further,

$$(dS/dp)_{H,0} = 0. \tag{3}$$

In Eq. (3), S is the entropy of the products of the explosion; the entropy also has a minimum at the Jouguets point on the Hugoniot adiabatic. Finally,

$$(du/dp)_{H,0} = 1/\rho c. \tag{4}$$

This latter property will be resolved in Sec. 3.

In the propagation of a plane detonation wave from the free boundary of explosive material there enters into the products of the explosion the so-called central rarefaction wave, in which the pressure and all other quantities depend upon the ratio x/t, where x is the coordinate measured from the original position of the boundary of the explosive material, t is the time from the beginning of the detonation (A. A. Grib[9], see also refs. 4, 5, and 13).

At the coordinates x, t for which the characteristics are determined, i.e., the lines on which

$$\alpha)\ dx/dt = u + c, \quad \beta)\ dx/dt = u - c, \tag{5}$$

the plane detonation wave corresponds to the picture of Fig. 1: the α lines (solid) represent the set of straight lines diverging from the coordinate origin; the β lines (dash) are, in the general case the set of similar curves with the center of similarity at the origin of coordinates. In the special case where the adiabatic exponent is $n = 3$,

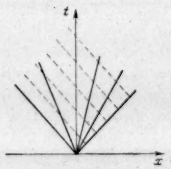

FIG. 1

the β lines form a family of parallel straight

lines. This picture of the hydrodynamic dispersal of the explosive products behind the front of the detonation wave leads to the condition

$$D \geqslant u + c \tag{6}$$

for the detonation wave itself.

On the other hand, consideration of the chemical reaction of the conversion of the explosive material to products of the explosion leads to the condition

$$D \leqslant u + c \tag{7}$$

(this condition was first obtained in this manner by the authors[6] and later (independently) by Döring[7] and von Neumann[8]; see also the researches of Grib[9] and Abramovich and Vulis[10]). In the aggregate, (6) and (7) lead to the condition (1).

In what follows we shall consider the width of the zone of the chemical reaction to be very small and shall use only condition (7), which does not depend upon the absolute value of the reaction rate and the width of the zone. The impulse of pressure which produces (initiating) the detonation on the surface both above in the consideration of the non-trivial rarefaction wave and also below in Sec. 3, we shall consider small and shall not take into account.

3. CONVERGING CYLINDRICAL WAVE, EQUATIONS, AND PRINCIPLES OF ITS APPROXIMATE SOLUTION

We consider the detonation and the movement of products of the explosion soon after the time when the detonation was initiated at the moment $t = 0$, simultaneously on both lateral surfaces of a long cylindrical charge, $r = r_0$. Initially, although, for the path described by the wave, $Dt \ll r_0$, the process is evidently not different from the propagation of a plane wave and we shall deal with the normal detonation wave and a central rarefaction wave adjoining it (for further details see Fig. 2). In comparison with Fig.1, the only purely formal difference lies in the fact that instead of $x = 0$ we must set $r = r_0$ and reverse the direction: the detonation is propagated inside, in the direction of the decreasing r.

Along with the propagation of the detonation wave, a compressional wave develops; however, we limit ourselves to that region in which we can consider the wave as differing but slightly from the normal. Then, from the properties of (2), we conclude that we can regard

$$D = D_0 = \text{const}. \tag{8}$$

It follows from the property (3) that

$$S = S_0 = \text{const}. \tag{9}$$

Finally, we get from the property (4) that (on the wave front)

$$-u = -u_0 + \int_{p_0}^{p} \frac{dp}{\rho c}; \quad u + \int_{p}^{p_0} \frac{dp}{\rho c} = u_0 + \int_{p_0}^{p_0} \frac{dp}{\rho c} \tag{10}$$

(with account of the fact that the wave now moves from right to left; we change the side of the velocity on the front $u < 0$).

We now consider the motion of explosion products behind the front and shall make clear in what manner the approximations (8) — (10) simplify the calculation of the process.

The equations of motion, for cylindrical symmetry, take the form

$$\frac{du}{dt} = \frac{\partial u}{\partial t} + u\frac{\partial u}{\partial r} = -\frac{1}{\rho}\frac{\partial p}{\partial r}; \quad \frac{dS}{dt} = \frac{\partial S}{\partial t} + u\frac{\partial S}{\partial r} = 0;$$

$$\frac{d\rho}{dt} = \rho\frac{\partial u}{\partial t} + u\frac{\partial \rho}{\partial t} = -\frac{\rho}{r}\frac{\partial}{\partial r}ru. \tag{11}$$

We must add to these the thermodynamical equation of state $p = p(\rho, s)$.

Since the entropy is conserved in each particle in the course of time, the entropy at the moment of completion of the chemical reaction in the approximation considered is also the same, according to (3) and (9), consequently the entire motion as a whole is isentropic, $S = S_0$ everywhere, and the pressure can be regarded as a function of the density alone.

It is known that Eqs. (11) can be written in terms of characteristics

$$\frac{d\alpha}{dt}\Big|_{dx=(u+c)\,dt} = -\frac{uc}{r}; \quad \frac{d\beta}{dt}\Big|_{dx=(u-c)\,dt} = \frac{uc}{r}, \tag{11'}$$

where

$$d\alpha = du + \frac{1}{\rho c}dp; \quad d\beta = du - \frac{1}{\rho c}dp. \tag{12}$$

Since the entropy is constant, we can then regard ρ and c as functions of a single pressure, and introduce

$$\varphi = \varphi(p) = \int \frac{dp}{\rho c}; \quad \alpha = u + \varphi; \quad \beta = u - \varphi. \tag{13}$$

it is appropriate to express all quantities in terms of α and β. For this purpose we must transform the dependence of $\varphi(p)$. We obtain

$$u = \frac{\alpha + \beta}{2}; \quad \varphi = \frac{\alpha - \beta}{2};$$

$$p = p(\varphi); \quad c = c(\rho) = c\left(\frac{\alpha - \beta}{2}\right). \tag{14}$$

For the known dependence of $p(\rho)$, the function $c(\alpha - \beta)/2$ is found to be elementary. As was noted by Stanyukovich,[11] an especially simple

dependence is obtained for $p = \text{const}\ \rho^3$: in this case,

$$\gamma = c; \quad c = (\alpha - \beta)/2; \quad u + c = \alpha; \quad u - c = \beta. \tag{15}$$

This case will be considered below in concrete calculations; however, we can also make some steps toward a general form for arbitrary dependence of $c(\varphi)$.

The picture of the motion under consideration in the plane r, t is shown in Fig. 2. The broad line represents the front of the detonation wave; its equation is $r = r_0 - Dt = r_0 - D_0 t$ in our approximation (D is the absolute value of the speed of the detonation). In comparison with Fig. 1, the roles of α- and β-characteristics are reversed.

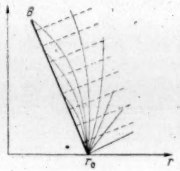

FIG. 2

The thin solid lines in Fig. 2 are the β-characteristics ($dr/dt = u - c$), while the dashed lines are the α-characteristics ($dr/dt = u + c$); in the region around the point $t = 0$, $r = r_0$, the motion is not different from a plane wave; we have a central wave and from this point there go out the rays of the β-characteristics. The α-characteristics go out from the wave front.

Equations (4) and (10) show that, close to the Jouguets point, when the wave has become compressed, in our approximation,

$$\alpha = u + \int dp/\rho c = \text{const} = \alpha_0; \tag{16}$$

the invariant α remains constant on the wave front.

As a consequence of the fact that the motion is not plane but axially symmetric, there is a right hand part to Eq. (11′), and along the α-lines, the value of α does not remain constant; also the value of β is not a constant along the β-characteristic. Close to the front, $|\beta|$ increases with time, in accord with (11′) ($u < 0$, $\beta = u - \varphi < 0$, $d\beta/dt < 0$); therefore the velocity of propagation of the β-characteristic increases, and the β-lines, which were initially close to r_0 are propagated somewhat more slowly than the detonation wave; they then overtake it as is shown in Fig. 2. The growth law of the amplitude of the detonation wave depends on the β-characteristics intersecting it. We note that the fact of intersection is itself connected with the fact that for the compressed wave, $D < |u| + c$, which is quite permissible from the chemical point of view. Equation (1) which applies to the normal (non-compressional) wave cannot be differentiated along the Hugoniot adiabatic.

The value of β on the characteristic at the point of intersection of the β line with the front is determined by the previous motion of the product of the explosion. The value of β, together with the equations of conservation (the Hugoniot adiabatic), completely determines the parameters of the detonation wave. In this case, for $|\beta| > |\beta_0|$, we obtain a compressed detonation wave (the value of β_0 corresponds to the Jouguets point).

On the other hand the β line on which $|\beta| < |\beta_0|$ does not overtake, and does not intersect, the line on the detonation wave so that the states below the Jouguets point do not exist (for more details on this subject see reference 12).

As is seen from Fig. 2, the pressure on the wave front of interest to us is entirely determined in the r, t plane by the motion in a narrow segment bounded on the left by a detonation wave emanating from the point $t = 0$, r_0 at the point B, and the right, by the β-characteristic which joins these two points. The assumed approximation is that in this segment we have

$$\alpha = \alpha_0. \tag{17}$$

As has already been pointed out, inside this segment, $d\alpha/dt \neq 0$ along the α-characteristic. However, $\alpha = \alpha_0$, $d\alpha/dt = 0$ along the detonation wave.

Since the segment is narrow, then the value of α for a finite derivative changes only slightly inside the segment.

For a given curvature of the β line, the width of the segment is proportional to $(r_0 - r)^2$, so that for small $r_0 - r$, for investigation of the initial period of convergence of a cylindrical wave, the assumption (17) appears asymptotically accurate, the terms thrown away in this case being of much higher order in smallness of $(r_0 - r)$ in comparison with those retained. Actually, thanks to a favorable numerical factor, the approximation (17) is applicable in practice for any r.

Because of (17), Eq. (11′) for the β-characteristics becomes an ordinary differential equation and is solved in elementary fashion. Actually, we can write it in the form

$$\left.\frac{d\beta}{dt}\right|_{dr=(u-c)dt} = (u-c)\left.\frac{d\beta}{dr}\right|_{dt=dr/(u-c)} = \frac{uc}{r}. \tag{18}$$

In this equation u and c can always be expressed

in terms of β and α. Moreover if, in accord with (17), α is constant, then we get

$$d\beta / dr = F(\beta, \alpha_0) / r; \tag{19}$$

The variables are separable and the equation can be integrated in elementary fashion.

In integrating the equations, we must put in the initial conditions; a whole pencil of β-characteristics emanate from the point $r = r_0$. We select one of these, giving the definite initial value $\beta = \beta_1$, at the point $r = r_0$, $t = 0$. We shall take α_0 to be constant in what follows.

Let us find $r(\beta, \beta_1)$ and then the equation of the β-characteristic in the plane $r - t$. Knowing the expressions u and c in terms of β (for a constant $\alpha = \alpha_0$), we write $1/(u - c) = \psi(\beta)$. Then

$$\frac{dt}{dr} = \frac{1}{u - c} = \psi(\beta);$$

$$dt = \psi(\beta)\, dr = \psi(\beta) \frac{dr(\beta, \beta_1)}{d\beta} d\beta. \tag{20}$$

Integrating the latter expression, we find $t = t(\beta, \beta_1)$. Thus the family of β characteristics is given by two parameters:

$$r = r(\beta, \beta_1); \quad t = t(\beta, \beta_1). \tag{21}$$

Varying β_1, we change from one characteristic to another; varying β for constant β_1, we move along the characteristic.

Now the amplitude of the detonation wave at a given radius r is found in simple manner: we substitute in (21) the value of r and the instant of time corresponding to it on the detonation wave, $t = (r_0 - r)/D_0$. Solving the two equations (21) for β_1 and β, we find the value of β on the wave front at the given radius. The value of β, together with the Hugoniot equations, determine the amplitude of the wave. The numerical side of the work is given in the following section.

On the theoretical side the treatment is connected with the singular acoustical properties of the normal detonation wave: the characteristic bearing the corresponding value of β is such that ($|\beta| < |\beta_0|$) does not reach the detonation wave and then the wave "yields" the value $\alpha = \alpha_0$ and the entropy $S = S_0$, which depend only on the properties of the explosion material. The characteristic possessing such a β that $|\beta| > |\beta_0|$, reaches the detonation wave, transforms the normal wave into a compressional wave. In principle now, α and S, created by the wave, depend on the incoming β, but in first approximation (in the value of $p - p_0$ or $\beta - \beta_0$), the excitation carried by the β characteristic is not reflected from it as though completely absorbed by the detonation wave. This leads to the fact that in first approximation the values of S and α going out from the surface of the detonation wave do not change with β. In the following approximation it can be shown that $S - S_0$ and $\alpha - \alpha_0$ are proportional to $(\beta - \beta_0)^2$, i.e., are of a higher order of smallness.

4. NUMERICAL RESULTS OF THE APPROXIMATE METHOD

Let us consider the case of the equation of state $p = A\rho^3$, $c = \sqrt{\partial p / \partial \rho} = \rho \sqrt{3A}$, $\alpha = u + c$, $\beta = u - c$. In this case, as is well-known,[11]

$$\rho_0 = {}^4/_3 \rho_{00}, \quad D_0 = {}^4/_3 c_0 = {}^4/_3 \sqrt{3A}\, \rho_0,$$

$$c_0 = {}^3/_4 D_0, \quad u_0 = {}^1/_4 D_0, \quad \alpha_0 = {}^1/_2 D_0, \quad \beta_0 = -D_0. \tag{22}$$

Here the initial density of the exploded material before the detonation is designated by ρ_{00}, in contrast to ρ_0 — the density of the products of the explosion at the Jouguets point. The equation in characteristics (11′) has the form

$$\frac{d\beta}{dt}\Big|_{dr/dt=\beta} = \beta \frac{d\beta}{dr}\Big|_{dt/dr=1/\beta} = \frac{\alpha^2 - \beta^2}{4r}. \tag{23}$$

Substituting $\alpha = \alpha_0 =$ constant and the initial conditions $\beta = \beta_1$, $r = r_0$, we find

$$r = r_0 (\beta_1^2 - \alpha_0^2) / (\beta^2 - \alpha_0^2), \tag{24}$$

$$t = -\frac{r_0 (\beta_1^2 - \alpha_0^2)}{4\alpha_0^3} |\chi(\beta) - \chi(\beta_1)|,$$

$$\chi = \frac{4\alpha_0^3 \beta}{(\beta^2 - \alpha_0^2)^2} - \frac{6\alpha_0 \beta}{\beta^2 - \alpha_0^2} + 3 \ln \frac{\alpha_0 + \beta}{\alpha_0 - \beta}. \tag{25}$$

After $\beta'(r)$ on the front is found from (24), (25), and $t = (r_0 - r)/D$, we find, within the framework of our approximation,

$$u = (\alpha_0 + \beta')/2, \quad c = (\alpha_0 - \beta')/2,$$

$$\rho = \text{const} \cdot c, \quad p = \text{const} \cdot c^3 \tag{26}$$

(the numerical values of β'/D_0 and p'/p_0 as functions of r/r_0 are given in Table I)

TABLE I

$\frac{r}{r_0}$	$-\frac{\beta'}{D_0}$	$\frac{p'}{p_0}$	$\frac{r}{r_0}$	$-\frac{\beta'}{D_0}$
1	1.000	1.000	0.02	1.908
0.8	1.023	1.047	0.01	2.238
0.6	1.055	1.115		
0.4	1.108	1.230		
0.2	1.224	1.544		
0.15	1.283			
0.10	1.376			
0.08	1.435			
0.06	1.516			
0.04	1.646			

However, the condition $\alpha = \alpha_0$ on the front of the compressed wave is only approximate; there-

fore such p, ρ satisfy the conservation equations only with accuracy up to terms $(\beta' - \beta_0)^2$. To obtain internal consistency of the value u, ρ, p on the front, we must take the exact Hugoniot adiabatic, find $u(p)$, $\rho(p)$, $c(p)$, on it, construct $\beta(p) = u(p) - c(p)$ (we remember that $u < 0$, $\beta < 0$ for the case of motion toward the center) and for a given β' find p, ρ, u which satisfy the conservation equations exactly.

At the radius 0.2, even if the calculation of β' does not contain a large error, in each case it is no longer possible to make use of Eqs. (26) for the determination of u, c, ρ, p for a given β' (see Sec. 5).

For r/r_0 close to unity at the beginning of the process, it is not difficult to obtain expansion of the solution in a series. We find

$$-\frac{\beta'(r)}{D_0} = 1 + \frac{3}{32}\left(1 - \frac{r}{r_0}\right);$$

$$\frac{p'(r)}{p_0} = 1 + \frac{3}{16}\left(1 - \frac{r}{r_0}\right) = \left(\frac{r}{r_0}\right)^{-1/\varepsilon}.$$

Thus, the rate of growth of the pressure at the beginning of the process close to the free surface of the charge is approximately twice as slow as the asymptotic rate, close to the axis, found by Landau and Stanyukovich ($r^{-0.188}$ instead of $r^{-0.47}$).

In the solution of Landau and Stanyukovich, the pressure at each moment has a maximum at a certain distance from the surface of the detonation wave (Fig. 3a); it can be thought that this maximum passes on its excess pressure to the wave front and is the reason and the necessary condition for the growth of pressure on the wave front in connection with the propagation.

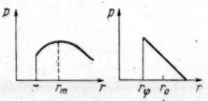

FIG. 3

In our solution, the pressure distribution at the beginning of propagation (Fig. 3b) differs but little from a plane wave; the pressure is maximum on the front and has a finite negative partial derivative with respect to the coordinates in the vicinity of the wave front. Nevertheless, as is seen from the result obtained above, the pressure on the front begins to increase rapidly along with the convergence of the wave, beginning with $r = r_0$, the increase is determined by the arrival at the front of the β-characteristics, which yield a value of β which increases in absolute magnitude; the quantity β depends not only on the pressure but also on the velocity of the material. Any estimate of the variation of the wave derived from a single distribution of pressure is invalid.

5. EXTRAPOLATION OF THE SOLUTION AND THE EQUATION OF STATE

It must be expected that the solution remains numerically satisfactory even there where it is impossible to consider the change of pressure on the front of the detonation wave ("compression") as small, and therefore the value of the entropy and the invariant α wil differ significantly from S_0 and α_0 at the Jouguets point.

The basis for such optimism lies in the fact that the approximation is contained in the replacement of α by α_0 in the expression $(\beta^2 - \alpha^2)/ur$. In this case, β^2 is initially four times α^2 and then even greater; in such a case, a significant relative change of α changes $\beta^2 - \alpha^2$ but slightly.

However, in the final stage of the calculation, in computing the pressure and other quantities corresponding to a given β, it is no longer possible on the wave front to make use of the simple relations (26), which refer only to the vicinity of the Jouguets point. One must construct an exact adiabat. Here there arises a question on the equation of state of the products of the explosion. Following Landau and Stanyukovich, we have assumed $p = A\rho^3$, where the quantity A is easily found from the velocity of a normal detonation.

Up to the present time, although isentropic processes of the expansion of the products of the explosion (slight supercompression) have been considered, nothing more has been required for the calculation of the hydrodynamic side of the problem, inasmuch as we are not especially interested in the temperature of the explosion products. However, for strong supercompressions that reach (in the approximation of the wave) to the axis of symmetry, is necessary for the hydrodynamical calculation to know not only the pressure but also the energy of the explosion products, in their dependence on density and entropy.

We can write the equation of state in the form

$$E = {}^1/_2 A_0 \rho^2 + E_{\text{therm}}; \quad p = A_0\rho^3 + \omega E_{\text{therm}} \rho, \qquad (27)$$

where $A_0\rho^3$ is the elastic pressure, $A_0\rho^2/2$ is the corresponding elastic energy; we can calculate these as well as the pressure and energy at absolute zero. (Actually at absolute zero the pressure vanishes for a density ρ_c of the condensed products of the explosion (solid hydrocarbons, ice, etc.) which is close to 1 gm/gm^3, and it would be more accurate to write $\rho^3 - \rho_c^3$ in place of ρ^3. Inasmuch as we are interested in densities of 2 – 3

gm/cm^3 and higher, we do not need to consider this correction). The second term E_{therm} represents the thermal energy, ω is a dimensionless constant.

It follows from thermodynamics that

$$p_{therm} = -\frac{\partial E_{therm}(\rho, S)}{\partial (1/\rho)} = \rho E_{therm} \frac{\partial \ln E_{therm}(\rho, S)}{\partial \ln \rho}, \quad (28)$$

in which the meaning of the dimensionless constant ω of (27) is determined. For a power-law dependence of E_{therm} on ρ, ω is constant.

For ideal gasses and constant heat capacity, $\omega = \kappa - 1$ where $\kappa = c_p/c_v$ is the adiabatic exponent. In our case, ω cannot be constant. Here we shall not enter into the physical theory of ω. In the consideration of the detonation, two limiting assumptions are possible, each of which simplifies the calculation considerably.

The first assumption $\omega = 0$:

$$E = A_0\rho^2/2 + F(S); \quad p = A_0\rho^3 \quad (29)$$

corresponds to a representation of a purely elastic pressure. The elastic term in the energy $A_0\rho^2/2$ corresponds to the elastic pressure; moreover, there is also a thermal term $F(S)$ in the energy; however the thermal pressure is equal to zero, since $\partial F/\partial\rho = 0$.

The second assumption, $\omega = 2$, leads to the equations

$$E = A(S)\rho^2/2; \quad p = A(S)\rho^3 = 2E\rho. \quad (30)$$

In this case there are elastic and thermal pressures, but the value of ω is specially chosen so that the adiabatics of the heated explosion products ($S \neq 0$) have the same form functionally, $A \sim \rho^3$, as does the elastic pressure, $p = A(0)\rho^3$. In this case,

$$E_{therm} = {}^1/_2 [A(S) - A(0)]\rho^2;$$

$$p_{therm} = [A(S) - A(0)]\rho^3. \quad (31)$$

Estimates based on statistical mechanics show that the probable value of ω lies between zero and 2, so that the actual results lie somewhere in the region between the two assumptions (29) and (30).

It is easy for each case to construct the Hugoniot adiabatic of the detonation process. It is convenient to be given the magnitude of ρ; then, in the first case (29),

$$p = A_0\rho^3; \quad c = \rho\sqrt{3A_0}; \quad u = -\rho\,(A_0(\rho - \rho_{00})/\rho_{00})^{1/2},$$
$$D = \rho^2 (A_0/\rho_{00}(\rho - \rho_{00}))^{1/2}. \quad (32)$$

the sign of the velocity u corresponds to the motion of the detonation toward the center.

From the energy equation we obtain

$$F(S) = Q - A_0\rho^2 + A_0\rho^3/2\rho_{00}, \quad (33)$$

where Q is the chemical energy of the exploded material.

The Jouguets point corresponds to $\rho_0 = {}^4/_3\rho_{00}$, all its properties are easily verified directly from Eqs. (32) — (33). Precisely in this case, the velocity of the normal detonation is directly proportional to the initial density

$$D_0 = \frac{16}{9}\rho_{00}\sqrt{3A_0}. \quad (34)$$

D and D_0 do not depend on the chemical energy, only the entropy S depends upon Q. The regime is possible only for $Q > {}^{16}/_{27}\,A_0\rho_{00}^2$. In the compression wave, the density can increase without limit. With the aid of (32) we find $\beta = u - c = \beta(\rho)$. In the previous section, $\beta(r)$ was found (Table I). From this it is easy to find $\rho(r)$ and $p(r)$, i.e., to bring to conclusion the approximate solution of the problem of the pressure of a converging cylindrical detonation wave without assumptions on the smallness of the compression. The results are tabulated in Table II. The pressure is given in column 2 and is found from our approximate theory. The pressure plotted in column 3 was found under the same assumptions on the equation of state by numerical integration in differences of the partial differential equations; integration was carried out with an electronic computer.

TABLE II

$\frac{r}{r_*}$	$\frac{p}{p_*}$	$\left(\frac{p}{p_*}\right)_{exact}$
1	2	3
1	1	1
0.8	1.05	1.05
0.6	1.11	1.11
0.4	1.23	1.24
0.2	1.51	1.54
0.15	1.67	1.71
0.1	1.94	2.01
0.08	2.12	2.20
0.06	2.40	2.49
0.04	2.86	3.00
0.02	3.96	4.18

The limiting law for $r \to 0$ was obtained in the following fashion: in accord with (24), for large β,

$$r \sim (\beta^2 - \alpha_0^2)^{-2} \sim \beta^{-4}; \quad \beta \sim r^{-1/4}.$$

On the other hand from (32) for large ρ and p,

$$u \sim \rho^{3/2} \sim \sqrt{p}; \quad c \sim \rho \sim p^{1/3}; \quad u \gg c; \quad \beta \approx u \sim \sqrt{p}.$$

Hence

$$r^{-1/4} \sim \sqrt{p}; \quad p \sim r^{-1/2}. \quad (35)$$

We now carry out a similar analysis of the second assumption with regard to the equations of

state (30). In this case we must make direct use of all the conservation equations, eliminating the energy equation. We obtain

$$p = 2\rho_{00}\rho Q/(2\rho_{00}-\rho);$$

$$c = \sqrt{3p/\rho};\quad u = -[p(\rho-\rho_{00})/\rho_{00}\rho]^{1/2};$$

$$D = [p\rho/\rho_{00}(\rho-\rho_{00})]^{1/2},\quad A(S) = 2\rho_{00}Q/\rho^2(2\rho_{00}-\rho). \quad (36)$$

Again the Jouguets point corresponds to $\rho_0 = 4\rho_{00}/3$. The velocity of the normal detonation

$$D_0 = 4Q \quad (37)$$

does not depend upon the density as is the case for ideal gasses. Actually, the velocity of the detonation of given explosive material with given Q increases appreciably, although somewhat more slowly than ρ_{00}, with increase in the initial density; it is therefore evident that the second variant, Eq. (30) certainly does not exist in pure form, $\omega < 2$. On the other hand, $\omega = 0$ would denote the complete absence of thermal expansion, absence of the effect of temperature on pressure. In the same way, it is shown that (29) and (30) are actually limiting assumptions; the truth actually lies in between.

Returning to the second variant [equation of state (30)], we note that, in accord with (36), the density in the compression wave never exceeds $2\rho_{00}$. Landau and Stanyukovich in the theory of a converging cylindrical detonation wave considered just this case.

In the second variant, when the entropy is a variable, strictly speaking, the fundamental equation (11′) also changes, and the very definition $\beta = u - c$ becomes inaccurate, since the density ρ now depends not only on p but also on S. Neglecting these corrections, we find the value of $u - c$ from (36) in its dependence on ρ and with the help of the known $\beta'(r)$ we finally obtain $p(r)$ as in the first variant. We have positive results in Table III. In column 2 are given the results of the approximate calculation described above. In column 3 are given the results obtained on an electronic computer.

TABLE III

$\frac{r}{r_s}$	$\frac{p}{p_s}$	$\left(\frac{p}{p_s}\right)_{\text{exact}}$
1	2	3
1	1	1
0.8	1.05	1.05
0.6	1.11	1.12
0.4	1.23	1.25
0.2	1.51	1.57
0.15	1.67	1.76
0.1	1.93	2.08
0.08	2.10	2.30
0.06	2.36	2.63
0.04	2.93	3.21
0.02	3.80	

The asymptote of the second variant does not differ from the asymptote of the first: $p = r^{-1/2}$. It is significantly close to the result of Landau and Stanyukovich: $p \sim r^{-0.47}$ for this case. We note that the opposite limiting case of a cylindric acoustical (weak) case also yields $p \sim p_0 \sim r^{-1/2}$.

As a whole, as is seen from a comparison with numerical calculations and the asymptote, the region of applicability of the approximate theory is much broader than could be presumed previously.

We note that it follows from the very nature of the derivations that the approximate theory gives only a description of the conditions on the wave front, but is neither intended nor suitable for a description of the motion of the entire mass of the explosion products.

I take this opportunity to express my thanks for discussion of the work and help in the calculations to S. B. Aratskin, E. I. Zababakhin, Ya. M. Kazhdan, A. S. Kompaneets, K. A. Semendyaev, and K. P. Stanyukovich.

[1] K. P. Stanyukovich, Неустановившееся движение сплошной среды (Unsteady Motion of a Continuous Medium) Gostekhizdat, 1955.

[2] Guderley, Luftfahrtforschung **19**, No. 9 (1943).

[3] B. V. Al'vasov and Ya. B. Zel'dovich, J. Exptl. Theoret. Phys. (U.S.S.R.) **17**, 889 (1947).

[4] E. Jouguets, Mécanique des Explosifs (Paris, 1917).

[5] R. Courant and K. Friedrichs, Supersonic Flow and Shock Waves (Interscience, N. Y., 1948).

[6] Ya. B. Zel'dovich, J. Exptl. Theoret. Phys. (U.S.S.R.) **10**, 542 (1940).

[7] W. Döring, Ann. Physik **43**, 421 (1943).

[8] J. von Neumann, OSRD Report 549 (1942).

[9] A. A. Grib, Прикл. матем. мех. (Appl. Math. and Mech.) **8**, 169 (1944).

[10] G. N. Abramovich and L. A. Vulis, Dokl. Akad, Nauk SSSR **80**, [sic] 525 (1946).

[11] K. P. Stanyukovich, Dokl. Akad, Nauk SSSR **60**, [sic] 628 (1947).

[12] Ya. B. Zel'dovich and A. S. Kompaneets, Теория детонации (Theory of Detonations) Moscow, GTTI, 1955.

[13] Ya. B. Zel'dovich, J. Exptl. Theoret. Phys. (U.S.S.R.) **12**, 389 (1942).

Translated by R. T. Beyer
142

FISSION OF NONSPHERICAL NUCLEI

A. G. SITENKO

Khar'kov State University

Submitted to JETP editor June 12, 1958

J. Exptl. Theoret. Phys. (U.S.S.R.) **36**, 793-797 (March, 1959)

The direct fission of a nonspherical nucleus, which occurs when the absorbed particle transfers a large amount of angular momentum to the nucleus, is considered.

1. It is well known that the fission of stable nuclei under the action of fast particles is possible if the excitation energy of the compound nucleus formed in the process turns out to be larger than the critical energy for fission. The critical energy for fission can be found from the conditions of unstable equilibrium of a nucleus under the action of forces of surface tension and forces of Coulomb repulsion.[1,2] However, in the case of nonspherical nuclei which have a rotational degree of freedom such a discussion turns out to be incomplete.

Indeed, since the moment of inertia of a nonspherical nucleus differs from zero a collective rotation of the nucleus is possible.[3,4] This rotation leads to the appearance of centrifugal forces which in the case of sufficiently large angular momentum may lead to nuclear fission. The condition for fission of a rotating nonspherical nucleus may be obtained by investigating its stability under rotation with respect to small deformations. The angular momentum of rotation which may lead to fission can be communicated to the nucleus by some fast particle absorbed by it if the impact parameter of this particle with respect to the center of the nucleus exceeds a certain critical value. Indeed, as a result of the law of conservation of angular momentum the mechanical angular momentum of the absorbed particle is transferred to the nucleus, and such a transfer will be accompanied by fission as a result of the instability of the rotating nucleus with respect to small deformations.

The fission of nonspherical nuclei arising as a result of the absorption of particles with large amounts of mechanical angular momentum will evidently occur without the intermediate stage of a compound nucleus. Therefore the indicated fission mechanism for nonspherical nuclei may be regarded as a mechanism of direct fission.* The angular distribution of fission products in the case of such a direct mechanism will have properties characteristic of distributions pertaining to direct processes.

2. First let us obtain the condition for the fission of a rotating nonspherical nucleus. For the sake of simplicity we shall assume that the nonspherical nucleus has the shape of an elongated ellipsoid of revolution. We denote the length of the semi-axes of the ellipsoid by a (axis of symmetry) and b ($a \geq b$). We denote the eccentricity of the ellipsoid by ϵ:

$$\varepsilon^2 = 1 - b^2/a^2.$$

The total energy of the rotating nonspherical nucleus $\mathcal{E}$ may be written in the form of a sum of the surface energy $\mathcal{E}_s$, the Coulomb energy $\mathcal{E}_q$ and the rotational energy $\mathcal{E}_{rot}$.

The surface energy of the nucleus is equal to

$$\mathcal{E}_s = 2\pi O a b \left\{ \sqrt{1-\varepsilon^2} + \frac{1}{\varepsilon} \arcsin\varepsilon \right\}, \qquad (1)$$

where O is the phenomenological surface tension coefficient.

On the assumption that the electric charge is distributed in the nucleus with the constant density $\rho = Ze/V$ the Coulomb energy of the nucleus may be written in the form

$$\mathcal{E}_q = \frac{1}{2} \rho \int \varphi(\mathbf{r})\, dV,$$

where $\varphi(\mathbf{r})$ is the electrostatic potential inside the nucleus and the integration is taken over the volume of the nucleus. By utilizing for the electrostatic potential of a uniformly charged ellipsoid the expression[5]

$$\varphi(\mathbf{r}) = \pi\rho ab^2 \int_0^\infty \left\{ 1 - \frac{x^2}{a^2+s} - \frac{y^2+z^2}{b^2+s} \right\} \frac{ds}{\sqrt{(a^2+s)(b^2+s)}},$$

we will obtain the Coulomb energy of the nucleus in the form

$$\mathcal{E}_q = \frac{3}{10} \frac{(Ze)^2}{a\varepsilon} \ln \frac{1+\varepsilon}{1-\varepsilon}. \qquad (2)$$

*Pik-Pichak[3] has investigated fission with formation of a rotating compound nucleus.

The rotational energy of the nucleus is equal to

$$\mathscr{E}_{rot} = L^2/2I, \tag{3}$$

where L is the angular momentum of rotation of the nucleus, I is the moment of inertia of the nucleus which depends on the eccentricity ϵ. For a spherical nucleus the moment of inertia I must reduce to zero. Therefore the nucleus cannot be regarded as a solid. In order to determine the moment of inertia of the nucleus we can make use of the model of potential flow of an ideal fluid inside a rotating nonspherical shell.[4,7] In this case the moment of inertia will be determined by the following expression

$$I = \frac{Ma^2}{5}\frac{\varepsilon^4}{2-\varepsilon^2}\gamma, \tag{4}$$

where M is the mass of the nucleus and γ is a numerical coefficient ($\gamma \sim 4$), which must be introduced in order that for a given nuclear deformation ϵ a value for the moment of inertia will be obtained which corresponds to experimental data.

Let us consider infinitesimal deformations of the nucleus of the form $a \to a + \delta a$, where $\delta a > 0$. By assuming that nuclear matter is incompressible we obtain from the condition of constancy of nuclear volume during deformations (V = const)

$$\delta b = -\frac{b}{2a}\delta a, \quad \delta\varepsilon = \frac{3}{2}\frac{1-\varepsilon^2}{a\varepsilon}\delta a.$$

The total change in energy in the case of such a nuclear deformation is equal to

$$\delta\mathscr{E} = \delta\mathscr{E}_s + \delta\mathscr{E}_q + \delta\mathscr{E}_{rot}, \tag{5}$$

where $\delta\mathscr{E}_s$ and $\delta\mathscr{E}_q$ are the changes in the surface and in the Coulomb nuclear energies and $\delta\mathscr{E}_{rot}$ is the change in rotational energy due to a change in the moment of inertia of the nucleus as a result of deformation at a given angular momentum.

$$\delta\mathscr{E}_s = \pi Ob\left\{\sqrt{1-\varepsilon^2} + \frac{1}{\varepsilon}\arcsin\varepsilon + 3\frac{1-\varepsilon^2}{\varepsilon^2}\left[\sqrt{1-\varepsilon^2} - \frac{1}{\varepsilon}\arcsin\varepsilon\right]\right\}\delta a,$$

$$\delta\mathscr{E}_q = \frac{9}{10}\frac{(Ze)^2}{a^2\varepsilon^2}\left\{1 - \frac{3-\varepsilon^2}{6\varepsilon}\ln\frac{1+\varepsilon}{1-\varepsilon}\right\}\delta a,$$

$$\delta\mathscr{E}_{rot} = -\frac{L^2}{Ia}\left\{1 + 3\frac{1-\varepsilon^2}{\varepsilon^2} + \frac{3}{2}\frac{1-\varepsilon^2}{2-\varepsilon^2}\right\}\delta a. \tag{6}$$

Evidently the nucleus will be stable with respect to deformations of the form indicated above provided $\delta\mathscr{E} > 0$. However, if $\delta\mathscr{E} \le 0$ then the nucleus will be absolutely unstable, i.e., an arbitrarily small deformation will lead to nuclear fission. On substituting into the inequality $\delta\mathscr{E} \le 0$ the expressions (6), and on solving this inequality with respect to the square of the angular momentum L^2, the condition for the fission of a rotating nucleus may be written in the form

$$L^2 \geqslant L_m^2, \tag{7}$$

where the critical value of the square of the angular momentum is determined by the following expression

$$L_m^2 = Ia\left\{\pi Ob\left[\sqrt{1-\varepsilon^2} + \frac{1}{\varepsilon}\arcsin\varepsilon + 3\frac{1-\varepsilon^2}{\varepsilon^2}\left(\sqrt{1-\varepsilon^2} - \frac{1}{\varepsilon}\arcsin\varepsilon\right)\right] + \frac{9}{10}\frac{(Ze)^2}{a^2\varepsilon^2}\left[1 - \frac{3-\varepsilon^2}{6\varepsilon}\ln\frac{1+\varepsilon}{1-\varepsilon}\right]\right\}\{1 + 3(1-\varepsilon^2)/\varepsilon^2 + 3(1-\varepsilon^2)/2(2+\varepsilon^2)\}^{-1}. \tag{8}$$

From condition (7) it follows that a nonspherical nucleus cannot have an angular momentum greater than the critical value L_m. If a nonspherical nucleus is given an angular momentum exceeding the critical value L_m, then this will immediately lead to the fission of the nucleus.

3. A nonspherical nucleus can acquire an amount of angular momentum which leads to fission by absorbing a fast nucleon with sufficiently large impact parameter with respect to the center of the nucleus. Evidently the maximum value of the impact parameter of the absorbed nucleus is equal to a; in this case the angular momentum communicated to the nucleus is equal to $L = a\sqrt{2mE}$, where m is the mass and E is the kinetic energy of the nucleon. By utilizing (8) one can find the critical value for the energy of the incident nucleon

$$E_m = \frac{1}{8}\frac{I}{mr_0^2}\sqrt{1-\varepsilon^2}\,U_s\left\{\sqrt{1-\varepsilon^2} + \frac{1}{\varepsilon}\arcsin\varepsilon + 3\frac{1-\varepsilon^2}{\varepsilon^2}\times\left(\sqrt{1-\varepsilon^2} - \frac{1}{\varepsilon}\arcsin\varepsilon\right) + 12\frac{\sqrt{1-\varepsilon^2}}{\varepsilon^2}\left(1 - \frac{3-\varepsilon^2}{6\varepsilon}\ln\frac{1+\varepsilon}{1-\varepsilon}\right)x\right\} \times \{1 + 3(1-\varepsilon^2)/\varepsilon^2 + 3(1-\varepsilon^2)/2(2-\varepsilon^2)\}^{-1}. \tag{9}$$

Here

$$ab^2 = Ar_0^3, \quad U_s = 4\pi r_0^2 O, \quad (Z^2/A)_0 = (40\pi/3)(r_0^3 O/e^2),$$

$$x = (Z^2/A)/(Z^2/A)_0,$$

A is the mass number.

If the energy of the incident nucleon exceeds the critical value $E \ge E_m$, then the absorption of the nucleon may be accompanied by direct fission of the nonspherical nucleus. However, if $E < E_m$, then fission is possible only with the formation of a compound nucleus.

By setting $r_0 = 1.4 \times 1.0^{-13}$ cm, $U_s = 15$ Mev, $I = 2 \times 10^{-47}$ g-cm^2, a/b = 1.5 and x = 0.7 (the

nonspherical nucleus Hf^{180}) we obtain for the critical energy in the case of neutrons the value E_m = 20 Mev. (The value for E_m obtained above is correct only in order of magnitude, since in the course of finding E_m the expression (4) for the moment of inertia of the nucleus has been utilized. If the nucleus is regarded as a solid then we shall obtain for E_m a value which is several times larger.)

We note that the criterion $E \geq E_m$ for the possibility of fission of a nonspherical nucleus under the action of particles of energy E holds only in the case when $E_m > \hbar^2/I$. Indeed, if $E_m < \hbar^2/I$, then even though the inequality $E > E_m$ is fulfilled, the condition $E > \hbar^2/I$ may not be fulfilled, which means that there is a possibility of the incident nucleon transferring energy to the rotational degree of freedom of the nucleus. Therefore the whole discussion is valid only for sufficiently large values of moments of inertia of nuclei.

4. Let us find the cross section for the direct fission of nonspherical nuclei under the action of fast nucleons. For the sake of simplicity we shall consider the nucleus to be perfectly absorbing.

We choose a system of coordinates in such a manner that the momentum of the incident nucleon **p** will be directed along the Y axis, while the axis of symmetry of the nucleus lies in the XY plane. Then the extent of the shadow of the nucleus on the plane perpendicular to the momentum will be defined by the ellipsoid with the semi-axes $\xi(\theta) = a\sqrt{1-\epsilon^2\cos^2\theta}$ and b, where θ is the angle between the momentum of the incident nucleon and the axis of symmetry of the nucleus.

The angular momentum of the nucleon with respect to the axis perpendicular to the momentum of the nucleon and to the axis of symmetry will be given in the chosen system of coordinates by L = xp. When the nucleon is absorbed by the nucleus this angular momentum will be transferred to the nucleus. If $L \geq L_m$, i.e., $x \geq L_m/p$, then the absorption of the nucleon will be accompanied by direct fission of the nucleus. The cross section for such a process will evidently be equal to the area of the segments cut off from the shadow by the straight line $x = +L_m/p$:

$$\sigma(E, \theta) = 2b\xi\left(\arccos\frac{x_m}{\xi} - \frac{x_m}{\xi}\sqrt{1-\frac{x_m^2}{\xi^2}}\right),$$

$$x_m = \frac{L_m}{p}. \qquad (10)$$

The cross section (10) corresponds to a definite orientation of the axis of symmetry of the nonspherical nucleus. In the case of nonoriented nonspherical nuclei the expression (10) should be averaged over all the possible orientations of the nuclear axis of symmetry. As a result of such averaging we obtain

$$\sigma(E) = \frac{2ab}{\varepsilon}\int_0^{\eta}\sqrt{1-y^2}\left\{\arccos\frac{\Lambda}{\sqrt{1-y^2}} - \Lambda\frac{\sqrt{1-y^2-\Lambda^2}}{1-y^2}\right\}dy, \qquad (11)$$

where $\Lambda = L_m/ap = \sqrt{E_m/E}$, while the upper limit for the integration η should be taken equal to

$$\eta_1 = \begin{cases} \varepsilon, & \varepsilon < \sqrt{1-\Lambda^2}, \\ \sqrt{1-\Lambda^2}, & \varepsilon > \sqrt{1-\Lambda^2}. \end{cases} \qquad (11a)$$

Expression (11) may be integrated in two limiting cases. Near the threshold the cross section for direct fission is equal to

$$\sigma(E) = (ab/4\varepsilon)(1-E_m/E)^2, \quad E - E_m \ll E. \qquad (12)$$

In the case of high energies of incident nucleons ($E \gg E_m$) the cross section of direct fission coincides with the total cross section for the absorption of nucleons by a nonspherical nucleus

$$\sigma = \frac{\pi}{2}ab\left(\sqrt{1-\varepsilon^2} + \frac{1}{\varepsilon}\arcsin\varepsilon\right), E \gg E_m \qquad (13)$$

Formula (11) determines the maximum possible value of the cross section. Actually the cross section for direct fission will be less than (11) as a result of competition of other processes both direct ones and also those with the formation of a compound nucleus. Qualitatively this may be taken into account by introducing into formula (11) a factor smaller than unity which describes the probability of direct interaction between the incident particle and the nucleus accompanied by transfer of a large amount of angular momentum to the whole nucleus.

5. The study of direct fission of nonspherical nuclei in the case of deuteron stripping may be of particular interest. As a result of the law of conservation of angular momentum the fission products of a nonspherical nucleus will fly apart in the case of a direct fission process in the plane containing the direction of motion of the absorbed nucleon and the axis of symmetry of the nucleus. The other nucleon from the deuteron liberated as a result of stripping will also come out in the same plane. Thus, the direction of emission of the nucleon liberated during stripping and the direction of separation of the fission products of a nonspherical nucleus will be correlated. The establishing of such a correlation may be utilized for the separation of the direct process from fission processes with the formation of a compound nucleus.

Let us determine the cross section for the

stripping reaction accompanied by direct fission of a nonspherical nucleus on the assumption that the deuteron radius is considerably smaller than the nuclear dimensions ($R_d \ll a$ and b). Under this assumption the total cross section for the stripping reaction is equal to the perimeter of the area of the nuclear shadow multiplied by one-quarter of the deuteron radius R_d. The cross section for the stripping reaction accompanied by direct fission will be proportional to the length of the arcs cut off by the straight lines $x = + L_m/p$ from the ellipsoid which forms the boundary of the region of the nuclear shadow on the plane perpendicular to the momentum of the incident deuteron. By noting that the length of these arcs is equal to

$$l = 4\zeta \left\{ E\left(\frac{\pi}{2}, \sqrt{1-\frac{b^2}{\zeta^2}}\right) - E\left(\tan^{-1}\frac{x_m}{b\sqrt{1-x_m^2/\zeta^2}}, \sqrt{1-\frac{b^2}{\zeta^2}}\right)\right\}$$

(where $E(\varphi, k)$ is the elliptic integral of the second kind), and on averaging over different orientations of the nuclear axis of symmetry we shall obtain the following expression for the cross section for the stripping reaction accompanied by direct fission of a nonspherical nucleus

$$\sigma(E) = \frac{aR_d}{\varepsilon}\int_0^{\eta} \sqrt{1-y^2}\left\{E\left(\frac{\pi}{2}, \sqrt{1-\frac{1-\varepsilon^2}{1-y^2}}\right) - E\left(\tan^{-1}\frac{\Lambda}{[(1-\varepsilon^2)(1-y^2-\Lambda^2)/(1-y^2)]^{1/2}}, \sqrt{1-\frac{1-\varepsilon^2}{1-y^2}}\right)\right\} dy, \quad (14)$$

where E is half the energy of the incident deuteron, while η is determined by (11a).

Near the threshold of the stripping reaction accompanied by fission the cross section is equal to

$$\sigma(E) = \frac{\pi}{4} aR_d \frac{1-\varepsilon^2}{\varepsilon}\left(1-\frac{E_m}{E}\right), \quad E - E_m \ll E. \quad (15)$$

In the limiting case of high energies $E \gg E_m$ the cross section of the process under consideration coincides with the total cross section of the stripping reaction in the case of a nonspherical nucleus

$$\sigma = \frac{\pi}{4} aR_d\left\{1 + \frac{1-\varepsilon^2}{2\varepsilon}\ln\frac{1+\varepsilon}{1-\varepsilon}\right\}, \quad E \gg E_m. \quad (16)$$

Both in formulas (11) and (14) one should introduce a factor describing the probability of direct excitation of the fission degree of freedom of the nucleus.

I express my gratitude to A. I. Akhiezer and K. A. Ter-Martirosyan for the discussion of the work, and to N. A. Khizhnyak for a useful remark.

[1] N. Bohr and J. A. Wheeler, Phys. Rev. **56**, 426 (1939).

[2] A. I. Akhiezer and I. Ya. Pomeranchuk, Некоторые вопросы теории ядра (Certain Problems of the Theory of the Nucleus). Moscow-Leningrad, GITTL, 1950.

[3] A. Bohr, Rotational States of Atomic Nuclei, København, 1954.

[4] A. Bohr and B. Mottelson, Kong. Danske Vidensk. Selks., Mat.-fys. Medd. **30**, 1 (1955).

[5] G. A. Pik-Pichak, J. Exptl. Theoret. Phys. (U.S.S.R.) **34**, 341 (1958), Soviet Phys. JETP **7**, 238 (1958).

[6] L. N. Sretenskiĭ, Теория ньютоновского потенциала (Theory of the Newtonian Potential) Moscow-Leningrad, GITTL, 1946.

[7] L. D. Landau and Ya. A. Smorodinskiĭ, Лекции по теории атомного ядра (Lectures on the Theory of the Atomic Nucleus), Moscow, GITTL, 1955.

Translated by G. Volkoff
143

SOVIET PHYSICS JETP VOLUME 36(9), NUMBER 3 SEPTEMBER, 1959

ON THE THEORY OF THE COHERENT SPONTANEOUS EMISSION

V. M. FAĬN

Radio Physics Institute, Gorkiĭ State University

Submitted to JETP editor June 30, 1958

J. Exptl. Theoret. Phys. (U.S.S.R.) **36**, 798-802 (March, 1959)

Some problems of the theory of coherent spontaneous radiation are considered. It is shown that the interaction of the particles through the common radiation field leads to a shift of the natural frequencies of the system.

1. INTRODUCTION

WHEN considering the spontaneous emission by a system of particles which has dimensions smaller than the wavelength of the emitted radiation one has to take into account the coherence of the radiation emitted by the different particles.* The quantum mechanical account of this coherence in the spontaneous emission has been given in a number of papers.[2-5]

However, these papers did not take into account that each particle is located in the quasi-stationary induction zone of the field of all other particles. This will lead to a change in the state of the particles as compared to the state which they would be in in the absence of the interaction. Taking into account this interaction could lead for example to a change in the eigenfrequencies of the system. In references 3 and 5 only that part of the interaction was considered which leads to line broadening. A possible shift of the eigenfrequencies was not considered.

In view of the promises offered by apparatus which utilize the coherent spontaneous radiation in the radio-frequency range,[6,4,7,8] it seems advisable to investigate this question. The classical interaction energy of a system of charges is given up to terms of order v^2/c^2 by[9]

$$\mathcal{H}' = \sum_{A>B} \frac{e_A e_B}{R_{AB}} - \sum_{A>B} \frac{e_A e_B}{2c^2 m_A m_B R_{AB}} \times [(\mathbf{p}_A \cdot \mathbf{p}_B) + (\mathbf{p}_A \cdot \mathbf{n})(\mathbf{p}_B \cdot \mathbf{n})]; \quad (1)$$

here e_A is the charge, m_A the mass and $\mathbf{p}_A$ the momentum of a particle, R_{AB} the distance between particles, and $\mathbf{n} = \mathbf{R}_{AB}/R_{AB}$ the unit vector pointing from e_A to e_B. The first term of (1) gives the energy of the Coulomb interaction and will lead to the dipole interaction between the molecules. One can show that this term averages to zero for a large number of molecules. In the paramagnetic or ferromagnetic case this term vanishes for spherical specimens. One can easily see that the second term is important if the distances between the particles are shorter than the wavelength of the emitted radiation. If one considers the charge to be smeared out over the extent of the system then the second term of (1) can be approximately written as $(e^2/Mc^2R)\mathbf{P}^2$, where $\mathbf{P}$ is the momentum of the whole system, M its mass, R its radius, and e its charge. This term is of the same type as the kinetic energy of the system. One sees from this that connected with this term is a shift in the natural frequencies of the system. The next term in the expansion in powers of v/c (which has not been given here) will lead to radiative damping and has been treated in references 2 – 5.

In the present paper the interaction of the particles due to the common radiation field will be investigated.

2. CLASSICAL CONSIDERATIONS

We consider a system of particles, with spins and magnetic moments, located in a constant external magnetic field. In the following we shall speak, to be specific, of a system of electrons.

An electron in an external magnetic field H_0 has two energy levels associated with the two possible orientations of its magnetic moment — parallel and antiparallel to the magnetic field. We shall see later that the results obtained for the system of electrons in a magnetic field can almost completely be applied to an arbitrary system of quantum-mechanical objects with two energy levels.

For a sufficiently large number of electrons, one can assume that the magnetic moment of the system has a continuous distribution.

Now, according to Ginzburg[10] we can write the

*The necessity of considering this in classical theory was indicated in essence in the paper of Mandel'shtam.[1]

following system of equations determining the motion of the magnetic moment μ:

$$d\mu/dt = \gamma[\mu \times \mathbf{H}_e] + \gamma \int [\mu \times \mathbf{H}(\mathbf{x})] D(\mathbf{x})\, dv, \qquad (2)$$

$$\mathbf{H} = \operatorname{curl} \mathbf{A}; \quad \Box \mathbf{A} = -4\pi \operatorname{curl} \mathbf{M} = 4\pi [\mu \times \operatorname{grad} D],$$

$$\mathbf{M} = \mu D(\mathbf{x}); \quad \int D(\mathbf{x})\, dv = 1. \qquad (3)$$

Here $\mathbf{H}_e$ is the external magnetic field, $\mathbf{H}(\mathbf{x})$ the local magnetic field, $\gamma = -g\mu_B/\hbar$ the gyromagnetic ratio (μ_B is the Bohr magneton, $g = 2$ for a free electron), $\mathbf{x}$ the radius vector of a point in the electron system, $\mathbf{M}$ the magnetization vector, and $D(\mathbf{x})$ the distribution function of the magnetic moment. Elimination of the magnetic field leads to the following expression:[10]

$$\dot{\mu} = \gamma[\mu \times \mathbf{H}_e] - (4\omega_m \gamma/3\pi c^3)[\mu \times \ddot{\mu}] + (2\gamma/3c^3)[\ddot{\mu} \times \dot{\mu}], \qquad (4)$$

where $\omega_m = c/R$, R — a magnitude of the order of the radius of the system (or of another characteristic linear dimension).

We now consider the case where the external field $\mathbf{H}_e$ is sufficiently large. Then one can insert into the second and third terms of (4) for $\dot{\mu}$ the value following from $\dot{\mu} = \gamma \mu \times \mathbf{H}_e$. If $\mathbf{H}_e$ is a constant field directed parallel to the z-axis then μ_x and μ_y are harmonic functions of time with a frequency $\omega_0 = |\gamma \mathbf{H}_e|$ and $\mu_z = \text{const}$.

In the dipole approximation (when the dimensions of the system are much smaller than the wavelength of the emitted radiation) the radiation of the system will be fully determined by the variation of μ. It is easy to see that the second term leads to a shift of the emitted radiation with respect to ω_0 by the amount

$$\Delta_1 \omega = (4\omega_m \omega_0^2/3\pi c^3)\gamma |\mu_z|; \qquad (5)$$

while the third term produces a line broadening

$$\Delta_2 \omega = \omega_0^3 \gamma |\mu_z|/3c^3. \qquad (6)$$

In deriving (6) it was assumed that $\mu_x, \mu_y \ll \mu_z$ and $\mu_z \approx \mu$. The line broadening associated with the coherent spontaneous emission has been treated earlier in detail within the framework of quantum mechanics by the author.[4] Introducing the spin $\mathbf{s}$ measured in units of $\hbar$ corresponding to the magnetic moment $\mu = \gamma\hbar\mathbf{s}$, (4) describes the process of emission of quanta with energy $\hbar\omega_0$ associated with a varying quantum number m (projection of the spin on the z axis) and a constant spin s ($\sqrt{s(s+1)}$ is the absolute value of the magnitude of the spin vector).

For an arbitrary system of quantum-mechanical objects with two energy levels one can introduce the operator $\mathbf{R}$,[2,4,11] which is the analog of the total spin of the system. The emission will proceed without change of r (quantum-mechanical "cooperation number," the analogue of s) but by changing m, a quantity analogous to the projection of the spin on the z axis.

One can easily verify that Eq. (4) (without the second term) describes also the radiation process of any arbitrary system of quantum-mechanical objects which have two energy levels (even if an external magnetic field is absent). One just has to change $\gamma\mathbf{H}_e$ to $\omega_0 = (E_2 - E_1)/\hbar$, $\mathbf{s}$ to $\mathbf{R}$ and $(g\mu_B)^2$ to $2|\mu_{12}|^2$ where μ_{12} is the matrix element of the (magnetic or electric) dipole moment of the particle. After this exchange we can compare (4) with the corresponding equation describing the change of m (see reference 4). Here it has been assumed that the condition $\omega_0 \gg \Delta_2\omega$ is fulfilled (the equations in reference 4 are given in the same approximation).

Thus the line width calculated by means of (4) has to coincide after the above indicated exchange with the line width of any arbitrary system of quantum-mechanical objects with two energy levels[4] (naturally for the case of large m and r where the classical and quantum-mechanical calculations have to coincide). Concerning the shift we shall show in the next section that the quantum-mechanical calculation also leads to $\Delta_1\omega$ of (5).

3. QUANTUM-MECHANICAL CALCULATION OF THE FREQUENCY SHIFT

The states of a system of weakly interacting quantum-mechanical objects with two energy levels can be described by two quantum numbers, r and m. Here $m = (n_+ - n_-)/2$ (with n_+ objects in the excited state and n_- in the ground state). If the interaction through the common field is not taken into account, the energy levels of the system are uniquely given by the quantum numbers m and ordered by the quantum number r. The energy of the system has a spectrum of the form $E_{rm} = m\hbar\omega$. We now calculate the level shifts due to the interaction of the system with the radiation field. The second-order term corresponding to emission and reabsorption of a photon of energy $k = \hbar\omega$ by the system gives a nonvanishing contribution:

$$W_{rm} = -\frac{2}{3\pi\hbar c^3} \int_0^K k\,dk \sum_{r'm'}^{1} |\hat{\mu}_{rm;\, r'm'}|^2 / (E_{r'm'} - E_{rm} + \hbar k). \qquad (7)$$

Here $\hat{\mu}$ is the operator of the (electric or magnetic) dipole moment of the system, and $K = \hbar\omega_m$ the energy of the quantum with maximum possible frequency ω_m [this frequency coincides with the frequency $\omega_m = c/R$ introduced in (4)].

The matrix elements of the dipole moment of the system have the form[2,4]

$$|\mu_{rm;\,r\mp1}|^2 = |\mu_{12}|^2 (r \pm m)(r \mp m + 1), \qquad (8)$$

where μ_{12} is the matrix element of the transition $+ \rightarrow -$ for the particular quantum-mechanical object.

From (7) and (8) we find

$$W_{rm} = -\frac{2\omega_0^2}{3\pi\hbar c^3}|\mu_{12}|^2 \left\{(r^2 - m^2 + r)\left(2K + \hbar\omega_0 \ln\left|\frac{K-\hbar\omega_0}{K+\hbar\omega_0}\right|\right) + m\hbar\omega_0\left(\ln\frac{|K-\hbar\omega_0|(K+\hbar\omega_0)}{(\hbar\omega_0)^2}\right)\right\}. \qquad (9)$$

For $K \gg \hbar\omega_0$ (i.e., for a system with dimensions much smaller than the wavelength) we can write (9) in the form

$$W_{rm} = -(4\omega_0^2/3\pi\hbar c^3)|\mu_{12}|^2 (r^2 - m^2 + r) K. \qquad (10)$$

The energy of the level rm now equals $E_{rm} + W_{rm}$. The frequency shift corresponding the transition $m \rightarrow m-1$ is then given (for $m \gg 1$) by

$$\Delta_1\omega = (W_{rm} - W_{r,m-1})/\hbar = (4\omega_m\omega_0^2/3\pi c^3\hbar)|\mu_{12}|^2 2m. \qquad (11)$$

This expression coincides with (5) which can be obtained in a classical way from (4) by replacing $(g\mu_B)^2$ with $2|\mu_{12}|^2$.*

4. CONCLUSION

The introduction of the quantum numbers r and m allows us to establish a certain correspondence principle, which states that to calculate the emission from a system† consisting of a sufficiently large number of quantum-mechanical objects having two energy levels, it is enough to calculate the classical equation, (4), describing the motion of a magnetic top in a magnetic field and then perform an appropriate substitution.

To illustrate this principle we juxtapose the classical [from Eq. (4)] and quantum mechanical formulae on the line shift and broadening‡ for a system of objects with two energy levels:

$$(\Delta_1\omega)_{cl} = \frac{4\omega_m\omega_0^2}{3\pi c^3}\gamma\mu_z, \qquad (\Delta_1\omega)_q = \frac{4\omega_m\omega_0^2}{3\pi c^3}\frac{2|\mu_{12}|^2}{\hbar}m,$$

$$(\Delta_2\omega)_{cl} = \frac{\omega_0^3\gamma}{3c^3}\mu, \qquad (\Delta_2\omega)_q = \frac{\omega_0^3}{3c^3}\frac{2|\mu_{12}|^2}{\hbar}r.$$

We see readily that the line shift (5) due to the interaction with the common radiation field is $\omega_m/\omega_0 \sim \lambda/R$ times greater than the corresponding line width of the radiation. This shift evidently can be experimentally observed in the radiation from ferromagnetic or paramagnetic materials or from a gas of molecules which have suitable levels in the radio-frequency range (where the condition $R \ll \lambda$ can be easily fulfilled).

We emphasize that we talk here about spontaneous radiation in free space. The radiation within resonators has an essentially different character (see, e.g., reference 11).

The radiation reaction and the interaction through the radiation field can achieve appreciable values in ferromagnetic materials (for example, ferrites),* which have a large concentration of electron spins.† Thus, for a ferrite with a volume of 10^{-3} cm^3 at $\lambda = 3$ cm we have $\Delta_2\omega \approx 10^8$ cps (the saturation magnetization is of the order 10^3 gauss).

Considering the radiation damping, we thus find that the relaxation time connected with the radiation is of the order 10^{-8} sec. It should be mentioned that for the case $\Delta_2\omega \ll \omega_0$ we can obtain from (4) the following equation‡ for the magnetization M [dropping the second term of (4)]:

$$d\mathbf{M}/dt = \gamma[\mathbf{M}\times\mathbf{H}] - (2\gamma^2\omega^2/3c^3)V[\mathbf{M}\times\mathbf{M}\times\mathbf{H}], \qquad (12)$$

where V is volume of the ferromagnetic sample. The dissipative term in this expression coincides with that of Landau and Lifshitz.[13]

In the considered example the frequency shift is of the order 10^9 cps. which is large enough to be observed experimentally.

However, the experiment has to be conducted in free space. The possibility of generation of radiation in free space is discussed in another paper by the author.[8]

The author is grateful to Professor V. L. Ginzburg for his consideration of the results of this paper, and to A. V. Gaponov and M. A. Miller for stimulating discussions.

*This replacement is connected with the fact that in the classical case the oscillator is circularly polarized while in the present quantum-mechanical case it is linearly polarized. If the quantum-mechanical calculation is done for the case of circular polarization, we must replace $(g\mu_B)^2$ with $|\mu_{12}|^2$.

†We have here in mind a system of the type of an ideal gas (where the only interaction is through the radiation field).

‡The line width is calculated with the assumption μ_x, $\mu_y \ll \mu \approx \mu_z$. For the quantum-mechanical treatment the corresponding assumption is $r \approx |m|$. For the general case see ref. 4.

*An important characteristic of the ferrites is their small conductivity.

†A ferromagnetic material does not act like an ideal gas because of the strong exchange interaction. However, in a homogeneous ferromagnet the exchange forces do not have an effect on the equations of motion (4). This follows from the fact that the operator of the magnetic moment $\hat{\mu} = \sum_j \hat{\mu}_j$ commutes with the operator of the exchange energy $\sum_{ik} A_{ik}\hat{\mu}_i\hat{\mu}_k$ or, in the classical language, that the effective molecular field $H_M = qM$ is always parallel to the magnetization M. Therefore the torque M × qM vanishes (see ref. 12 on this).

‡In the case of ferromagnets we must consider H to be effective field.

[1] L. I. Mandel'shtam, Works, I, U.S.S.R., Acad. of Sci. Press, p. 125 (1948), Physik Z. **8**, 608 (1907).

[2] R.H. Dicke, Phys. Rev. **93**, 99 (1954).

[3] V. M. Faĭn, J. Exptl. Theoret. Phys. (U.S.S.R.) **32**, 607 (1957); Soviet Phys. JETP **5**, 501 (1957).

[4] V. M. Faĭn, Usp. Fiz. Nauk **64**, 273 (1958).

[5] M. A. Itkina and V. M. Faĭn, Радиофизика (Radio Physics) **1**, 30 (1958).

[6] R. H. Dicke and R. H. Romer, Rev. Sci. Instr. **26**, 915 (1955).

[7] V. M. Faĭn, J. Exptl. Theoret. Phys. (U.S.S.R.) **34**, 1032 (1958), Soviet Phys. JETP **7**, 714 (1958).

[8] V. M. Faĭn, Радиофизика (Radio Physics) **1**, No. 5, (1958).

[9] L. D. Landau and E. M. Lifshitz, Теория поля (Theory of Fields) 2d. ed., Moscow (1948) [The Classical Theory of Fields, Addison Wesley, Cambridge, 1951.

[10] V. L. Ginzburg, Тр. ФИАН (Trans. Phys. Inst. Acad. Sci. U.S.S.R.) Vol. 3 (1946), J. Exptl. Theoret. Phys. (U.S.S.R.) **13**, 13 (1943); J. Phys. (U.S.S.R.) **8**, 33 (1944).

[11] V. M. Faĭn, Радиофизика (Radio Physics) **2**, No. 1 (1959).

[12] C. Kittel and C. Herring, Phys. Rev. **77**, 725 (1950); J. H. Van Vleck, Phys. Rev. **78**, 266 (1950).

[13] L. D. Landau and E. M. Lifshitz, Z. Physik Sow. Union **8**, 153 (1935).

Translated by M. Danos
144

QUADRUPOLE OSCILLATIONS OF DEFORMED NUCLEI

B. L. BIRBRAIR, L. K. PEKER, and L. A. SLIV

Leningrad Physico-Technical Institute, Academy of Sciences, U.S.S.R.

Submitted to JETP editor July 9, 1958

J. Exptl. Theoret. Phys. (U.S.S.R.) **36**, 803-809 (March, 1959)

Formulas are derived for quadrupole oscillations of deformed nuclei. The interaction between the rotation and the oscillations is considered, and a general formula is given for the corrections to the level energy of the ground rotational band. Presently-available experimental data for nuclei in the rare earth group are discussed and the difficulties encountered in the analysis are mentioned.

EQUATIONS FOR BETA AND GAMMA-OSCILLATIONS

A study of the oscillational levels yields new information on the properties of deformed nuclei. Two types of quadrupole oscillations are considered: (1) Beta oscillations about the equilibrium value β_0 along the deformation axis for an axially-symmetrical nucleus ($\gamma = 0$). (2) Gamma oscillations perpendicular to the deformation axis at equilibrium value β_0.

We start with the Bohr Hamiltonian[1] for a nucleus consisting of a core and n external nucleons.

$$\hat{H} = -\frac{\hbar^2}{2B}\left[\frac{1}{\beta^4}\frac{\partial}{\partial\beta}\left(\beta^4\frac{\partial}{\partial\beta}\right)+\frac{1}{\beta^2\sin 3\gamma}\frac{\partial}{\partial\gamma}\left(\sin 3\gamma\frac{\partial}{\partial\gamma}\right)\right] + \frac{\hbar^2}{8B\beta^2}\sum_{\kappa=1}^{3}\left(\hat{I}_\kappa-\sum_{i=1}^{n}\hat{j}_\kappa^{(i)}\right)^2\Big/\sin^2\left(\gamma-\frac{2\pi}{3}\kappa\right)+\frac{1}{2}C_{\text{core}}\beta^2 + \sum_{i=1}^{n}\hat{H}_p(x_i;\beta,\gamma)+\frac{1}{2}\sum_{i,k}\hat{W}_{ik}. \quad (1)$$

In the hydrodynamic approximation, in which the Hamiltonian (1) is written, there is a single inertia parameter B. However, such an approximation was found to be poor for real nuclei, and it became necessary to introduce three parameters: the inertia parameters of the β and γ oscillations, B_β and B_γ, and the moment of inertia J.* We assume the adiabatic approximation to hold, at least for the first oscillation levels of even-even nuclei, and average (1) over the internal states of the nucleons. Confining ourselves to small oscillations about to the equilibrium values $\beta = \beta_0$ and $\gamma = 0$, we can write the Hamiltonian (1) as

$$\hat{H} = E(\beta_0) + \hat{H}_\beta + \hat{H}_\gamma + \hat{H}_r + \hat{U}, \quad (2)$$

where

$$\hat{H}_\beta = -\frac{\hbar^2}{2B_\beta}\left(\frac{\partial^2}{\partial\beta_1^2}+\frac{4}{\beta_0+\beta_1}\frac{\partial}{\partial\beta_1}\right)+\frac{1}{2}C_\beta\beta_1^2, \quad (2a)$$

$$\hat{H}_\gamma = -\frac{\hbar^2}{2B_\gamma}\left[\frac{1}{\gamma}\frac{\partial}{\partial\gamma}\left(\gamma\frac{\partial}{\partial\gamma}\right)-\frac{\hat{I}_3^2}{4\gamma^2}\right]+\frac{1}{2}C_\gamma\gamma^2, \quad (2b)$$

$$\hat{H}_r = (\hbar^2/2J)(\hat{I}^2-\hat{I}_3^2); \quad (2c)$$

$$\hat{U} = (\gamma\hbar^2/\sqrt{3}J)(\hat{I}_1^2-\hat{I}_2^2). \quad (2d)$$

Here $\beta_1 = \beta - \beta_0$, $\beta_1 \ll \beta_0$; C_β and C_γ are parameters of the stability of the nucleus relative to β and γ oscillations, which will be considered below. H_β is the Hamiltonian of the β oscillations, H_γ that of the γ oscillations, and H_r that of the rotation of the nucleus; finally, $\hat{U}$ takes into account the interaction between the rotation and the γ oscillations.* In the derivation of the Hamiltonian (2) we assumed that in even-even nuclei $\Omega = \Sigma\Omega_i = 0$. Considering the rotation and oscillations to be independent in the zero approximation, we obtain a nuclear wave function in the form

$$\Psi_{IKMn_\beta n_\gamma} = \sqrt{N^2/2(1+\delta_{K0})}\,\psi_{n_\beta}(\beta_1)\,\varphi_{n_\gamma}(\gamma)\,X(x_1\ldots x_n)\times[D^I_{MK}+(-1)^I D^I_{M-K}], \quad (3)$$

where N is the normalizing factor.

The function ψ_{n_β} satisfies the following equation

$$\hat{H}_\beta\psi_{n_\beta} = \varepsilon_\beta\psi_{n_\beta}; \quad (4)$$

Putting $\psi = \exp(-2\beta_1/\beta_0)$, we bet

$$-\frac{\hbar^2}{2B_\beta}\frac{d^2f}{d\beta_1^2}+\frac{1}{2}C_\beta\beta_1^2 f = \varepsilon_\beta f, \quad (4a)$$

*In the Bohr Hamiltonian, $B_\beta = B$, $B_\gamma = B\beta^2$, and $J = 3B\beta^2$.

*It must be noted that $\hat{U}$ does not take the interaction into account too accurately. In fact, the formula $\hat{U} = \frac{\gamma}{\sqrt{3}}\frac{\hbar^2}{J}(\hat{I}_1^2-\hat{I}_2^2)$ contains still another factor on the order of unity, depending on the model. In the hydrodynamic approximation this factor equals unity exactly.

from which we get

$$\varepsilon_\beta = \hbar\omega_\beta(n_\beta + {}^1/_2),\quad \omega_\beta = \sqrt{C_\beta / B_\beta},\quad n_\beta = 0,\ 1,\ 2,\ \ldots, \tag{5a}$$

$$f_{n_\beta} = \exp\left(-B_\beta\omega_\beta\beta_1^2/2\hbar\right) H_{n_\beta}\left(\beta_1\sqrt{B_\beta\omega_\beta/\hbar}\right); \tag{5b}$$

$H_{n\beta}$ is the Hermite polynomial.

The equation for the γ oscillations is

$$-\frac{\hbar^2}{2B_\gamma}\frac{1}{\gamma}\frac{d}{d\gamma}\left(\gamma\frac{d\varphi}{d\gamma}\right) + \frac{\hbar^2}{8B_\gamma}\frac{K^2}{\gamma^2}\varphi + \frac{1}{2}C_\gamma\gamma^2\varphi = \varepsilon_\gamma\varphi, \tag{6}$$

where K is the eigenvalue of the operator $\hat{I}_3$. Solution of (6) is

$$\varepsilon_\gamma = \hbar\omega_\gamma(n_\gamma + 1),\quad \omega_\gamma = \sqrt{C_\gamma / B_\gamma}, \tag{6a}$$

$$n_\gamma = K/2,\ K/2+2,\ K/2+4\ldots$$

$$= \begin{cases} 0,\ 2,\ 4,\ldots & \text{for } K = 0, \\ 1,\ 3,\ 5,\ldots & \text{for } K = 2, \end{cases} \tag{6b}$$

$$\varphi_{n_\gamma} = \exp\left(-\frac{B_\gamma\omega_\gamma}{2\hbar}\gamma^2\right)$$

$$\times\gamma^{K/2}F\left(-\frac{2n_\gamma - K}{4};\ \frac{K}{2}+1;\ \frac{B_\gamma\omega_\gamma}{\hbar}\gamma^2\right), \tag{6c}$$

F is the hypergeometrical polynomial.

The rotational energy ϵ_r, according to (2c), is

$$\varepsilon_r = (\hbar/2J)[I(I+1) - K^2]. \tag{7}$$

For the total energy of the nucleus we obtain

$$E_{IKn_\beta n_\gamma} = E(\beta_0) + \hbar\omega_\beta(n_\beta + {}^1/_2)$$

$$+ \hbar\omega_\gamma(n_\gamma + 1) + (\hbar^2/2J)[I(I+1) - K^2]. \tag{8}$$

In the ground state

$$E_0 = E(\beta_0) + {}^1/_2\,\hbar\omega_\beta + \hbar\omega_\gamma. \tag{8a}$$

the energy of the first β-oscillation level is

$$\varepsilon(I = K = 0,\quad n_\beta = 1,$$

$$n_\gamma = 0) = E_{00\,10} - E_0 = \hbar\omega_\beta, \tag{8b}$$

and the energy of the first γ-oscillation level is

$$\varepsilon(I = K = 2,\quad n_\beta = 0,\quad n_\gamma = 1) = \hbar\omega_\gamma + \hbar^2/J. \tag{8c}$$

The operator of the E2 transition is

$$\mathfrak{M}_\mu(E2) = \frac{3}{4\pi}ZeR_0^2\alpha_\mu^*$$

$$= \frac{3}{4\pi}ZeR_0^2\left[\beta\cos\gamma D_{\mu 0}^2 + \frac{\beta}{\sqrt{2}}\sin\gamma\,(D_{\mu 2}^2 + D_{\mu,-2}^2)\right]. \tag{9}$$

The reduced probability of transition to the β-oscillation level with spin I = 2 (we are speaking, naturally, of a suitable level of the rotational band) is

$$B_{0\to 2}^{(\beta)}(E2) = \left(\frac{3}{4\pi}ZeR_0^2\right)^2\sum_\mu|\langle 20\mu\,10\,|\,\beta_1 D_{\mu 0}^2\,|\,00000\rangle|^2$$

$$= \left(\frac{3}{4\pi}ZeR_0^2\right)^2\frac{\hbar}{2\sqrt{B_\beta C_\beta}}. \tag{10}$$

In (10) we used the following matrix element

$$\langle 1\,|\,\beta_1|0\rangle = \sqrt{\hbar/2B_\beta\omega_\beta} = (\hbar^2/4B_\beta C_\beta)^{1/4}.$$

The reduced probability of a transition from the ground state to the γ-oscillation level is

$$B_{0\to 2}^{(\gamma)}(E2)$$

$$= \left(\frac{3ZeR_0^2}{4\pi}\right)^2\beta_0^2\sum_\mu|\langle 22\mu 01\,|\,\frac{\gamma}{\sqrt{2}}(D_{\mu 2}^2 + D_{\mu,-2}^2)\,|\,00000\rangle|^2$$

$$= \left(\frac{3}{4\pi}ZeR_0^2\right)^2\beta_0^2\frac{\hbar}{\sqrt{B_\gamma C_\gamma}}. \tag{11}$$

Here we use the matrix element

$$\langle 1\,|\,\gamma\,|\,0\rangle = \sqrt{\hbar/B_\gamma\omega_\gamma} = (\hbar^2/B_\gamma C_\gamma)^{1/4}.$$

It is interesting to compare (11) with the reduced probability of transition to the first rotational level of the ground band

$$B_{0\to 2}^{(\gamma)}(E2) = B_{0\to 2}^{\text{rot}}(E2)\,\hbar\omega_\gamma/C_\gamma. \tag{12}$$

For γ-oscillation levels at the borders of the rare-earth group (isotopes of Sm, W, Os), $\hbar\omega_\gamma$ is on the order of 1 Mev, and C_γ on the order of 20 Mev, hence

$$B^{(\gamma)}(E2)/B^{\text{rot}}(E2) \approx {}^1/_{20}. \tag{12a}$$

2. CONNECTION BETWEEN C_β AND C_γ

Let us consider in greater detail the problem of the averaging of the Hamiltonian (1) over the entire states of the nucleons. The Hamiltonian of the nucleon in a deformed nucleus is of the form

$$\hat{H}_p = -\frac{\hbar^2}{2m}\Delta + V(r) + \frac{\alpha}{r}\frac{dV}{dr}\mathbf{l}\cdot\mathbf{s}$$

$$+ \frac{\beta^2}{8\pi}\left(r^2\frac{d^2V}{dr^2} + 4r\frac{dV}{dr}\right) - \beta\cos\gamma r\frac{dV}{dr}Y_{20}$$

$$- \frac{\beta}{\sqrt{2}}\sin\gamma r\frac{dV}{dr}(Y_{22} + Y_{2,-2}). \tag{13}$$

The Hamiltonian of n nucleons contains, in addition to h_p, also the energy of the residual interaction and therefore

$$\hat{H}_{\text{nucl}} = \sum_{i=1}^{n}\hat{H}_p(i) + \sum_{i<k}\hat{W}_{ik}. \tag{14}$$

It can be shown (see, for example, reference 3) that in the observed nuclear deformations the energy of the residual interaction W is no longer dependent on β and is constant. Let us average (13), choosing the solution for $\gamma = 0$ as the zeroth approximation. The β-dependent portion of the nuclear energy will then be

$$E(\beta) = W + \frac{\beta^2}{2}\left[C_c + \frac{1}{4\pi}\sum_{i=1}^{n}\left\langle \Omega_i \left| r^2\frac{d^2V}{dr^2} + 4r\frac{dV}{dr} \right| \Omega_i \right\rangle\right]$$

$$-\beta\sum_{i=1}^{n}\left\langle \Omega_i \left| r\frac{dV}{dr}Y_{20} \right| \Omega_i \right\rangle$$

$$= W + \frac{1}{2}C_\beta\beta^2 - \beta\sum_{i=1}^{n}\left\langle \Omega_i \left| r\frac{dV}{dr}Y_{20} \right| \Omega_i \right\rangle. \quad (15)$$

The equilibrium deformation β_0 is determined, as usual, from the condition

$$\frac{dE}{d\beta} = C_\beta\beta_0 - \sum_{i=1}^{n}\left\langle \Omega_i \left| r\frac{dV}{dr}Y_{20} \right| \Omega_i \right\rangle = 0 \quad (16)$$

and, through the use of (16), $E(\beta)$ is represented by

$$E(\beta) = E(\beta_0) + {}^1/_2 C_\beta(\beta - \beta_0)^2. \quad (15a)$$

The portion of the energy that depends on γ (for fixed $\beta = \beta_0$), is, within accuracy to second-order perturbation-theory terms,

$$E(\gamma) \equiv -\beta_0\cos\gamma\sum_{i=1}^{n}\left\langle \Omega_i \left| r\frac{dV}{dr}Y_{20} \right| \Omega_i \right\rangle - \frac{1}{2}\beta_0^2\sin^2\gamma$$

$$\times\sum_{i=1}^{n}\sum_{k}\left| \left\langle \Omega_k \left| r\frac{dV}{dr}(Y_{22} + Y_{2,-2}) \right| \Omega_i \right\rangle \right|^2 / (E_{\Omega_k} - E_{\Omega_i}). \quad (17)$$

The summation over k is carried out over the unfilled states. It is seen from (17) that the equilibrium value of γ, determined from the condition $dE/d\gamma = 0$, is zero, i.e., deformed even-even nuclei have an axially-symmetrical equilibrium form.

The parameter of the stability of the nucleus relative to γ oscillations is

$$C_\gamma = \left(\frac{d^2E}{d\gamma^2}\right)_{\gamma=0} = \beta_0\sum_{i=1}^{n}\left\langle \Omega_i \left| r\frac{dV}{dr}Y_{20} \right| \Omega_i \right\rangle$$

$$-\beta_0^2\sum_{i=1}^{n}\sum_{k}\left| \left\langle \Omega_k \left| r\frac{dV}{dr}(Y_{22}\right.\right.\right.$$

$$\left.\left.\left. + Y_{2,-2}) \right| \Omega_i \right\rangle \right|^2 / (E_{\Omega_k} - E_{\Omega_i}), \quad (18)$$

and, considering (16), we get

$$C_\gamma = \beta_0^2\left[C_\beta - \sum_{i=1}^{n}\sum_{k}\right.$$

$$\left.\times\left| \left\langle \Omega_k \left| r\frac{dV}{dr}(Y_{22} + Y_{2,-2}) \right| \Omega_i \right\rangle \right|^2 / (E_{\Omega_k} - E_{\Omega_i})\right] \leqslant C_\beta\beta_0^2. \quad (19)$$

Since the denominator in the sum contains the difference of energy levels for which we have no accurate values, it is impossible in general to calculate C_γ and C_β. However, if it is known that for a given nucleus there are no nearby levels, it is possible to use the calculations of Nilsson[2] to obtain a rough estimate of C_γ. We thus obtain C_γ = 24 Mev for W^{182} and C_γ = 27 Mev for W^{186}.

3. INTERACTION BETWEEN THE ROTATION AND THE OSCILLATIONS

The correction to the energy of the rotational levels in the ground band, proportional to $I^2(I+1)^2$, is due to two causes: (1) γ oscillations cause the shape of the nucleus to deviate from that of an axially-symmetrical top. (2) The moment of inertia changes during β oscillations.

The interaction between the rotation and the γ oscillations is taken into account by operator $\hat{U}$ [Eq. (2d)], which is not diagonal in the I, j_3 representation. We then obtain in the second perturbation-theory approximation

$$\Delta E_\gamma = -\frac{|\langle 1201|\hat{U}|1000\rangle|^2}{\hbar\omega_\gamma}$$

$$= -\frac{\hbar^2}{6B_\gamma}\left(\frac{\hbar^2}{J}\right)^2\frac{I^2(I+1)^2 - 2I(I+1)}{(\hbar\omega_\gamma)^2}. \quad (20)$$

The portion of ΔE_γ that is proportional to $I(I+1)$ can be included in the expression for the rotational energy in the zeroth zpproximation, since it leads to an insignificant change in the moment of inertia. The remaining portion will yield deviations from the $E \sim I(I+1)$ law, namely

$$\Delta E_\gamma = -\frac{\hbar^2}{6B_\gamma(\hbar\omega_\gamma)^2}\left(\frac{\hbar^2}{J}\right)^2 I^2(I+1)^2$$

$$= -\frac{1}{6C_\gamma}\left(\frac{\hbar^2}{J}\right)^2 I^2(I+1)^2. \quad (21)$$

In the model of a rotating liquid drop, $J = 3B_\gamma$, and this leads to Bohr and Mottelson's Eq. (6.35) of reference 4.

$$\Delta E_\gamma = -\frac{1}{2(\hbar\omega_\gamma)^2}\left(\frac{\hbar^2}{J}\right)^3 I^2(I+1)^2. \quad (21a)$$

The correction due to the interaction with the β oscillations can be determined by taking it into account that the moment of inertia is a function of β. Expanding $\hbar^2/2J$ in powers of β_1, we obtain in the second approximation

$$\Delta E_\beta = -\frac{1}{2C_\beta}\left(\frac{\partial}{\partial\beta}\frac{\hbar^2}{2J}\right)^2 I^2(I+1)^2. \quad (22)$$

The total correction to the energy of the levels of the principal rotational band will be

$$\Delta E = \Delta E_\gamma + \Delta E_\beta = -\left[\frac{1}{6C_\gamma}\left(\frac{\hbar^2}{J}\right)^2 + \frac{1}{2C_\beta}\left(\frac{\partial}{\partial\beta}\frac{\hbar^2}{2J}\right)^2\right] I^2(I+1)^2$$

$$= -FI^2(I+1)^2. \quad (23)$$

F depends on the three parameters J, C_β, and C_γ as well as on the derivative $(\partial/\partial\beta)\hbar^2/2J$. These parameters can be determined from Eqs. (7), (10), and (11). The derivative can then be determined from (23).

4. ANALYSIS OF AVAILABLE EXPERIMENTAL DATA

Tables I and II list the experimental data on the oscillational and rotational levels of nuclei near the rare-earth group. What is most striking in an examination of the β-oscillation levels is the strong dependence of the energies ϵ_γ of the γ levels on the parameter β_0 of the equilibrium deformation. At the borders deformed-nuclei regions $\epsilon_\gamma \approx$ 600 kev (Os^{190}); when the deformation increases, ϵ_γ rises rapidly, reaching 1220 kev for W^{182} and on the order of 2 Mev and above for Dy, Er, and Yd. It is quite possible that the ϵ_γ vs. β_0 curve has a fine structure, so that all the isotopes of the given element fit a separate curve (see diagram).

Let us consider now the behavior of the derivative $(\partial/\partial\beta)(\hbar^2/2J)$, making use of the data of Tables I and II.

We begin with the isotopes of tungsten, for

TABLE I. Oscillational levels in deformed even-even nuclei

γ-oscillation levels, I = K = 2+		γ-oscillation levels, I = K = 2+		β-oscillation levels, I = K = 0+	
Isotope,	Energy, kev	Isotope	Energy, kev	Isotope	Energy, kev
Sm^{152}	1086	Os^{188}	633	Sm^{152}	685
Gd^{154}	996.6	Os^{190}	586	Gd^{154}	679
Gd^{156}	1160	Th^{228}	964	Er^{166}	1460?
Dy^{160}	996	Th^{230}	1060?	Th^{232}	720
Er^{166}	786	U^{232}	868	U^{234}	805
Er^{168}	822	Pu^{238}	1030	Pu^{238}	935
W^{182}	1222	Pu^{240}	1020	Pu^{240}	940
W^{184}	890	Cm^{246}	1300		
W^{186}	730	Cf^{250}	1200		
Os^{186}	764	Fm^{254}	700		

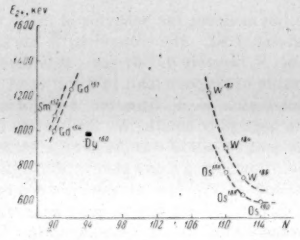

which C_γ have been measured by the Coulomb-excitation method. Inserting in

$$\Delta_\beta^2 \equiv \frac{1}{C_\beta}\left(\frac{\partial}{\partial\beta}\frac{\hbar^2}{2J}\right)^2 = 2F - \frac{1}{3C_\gamma}\left(\frac{\hbar^2}{J}\right)^2 \qquad (24)$$

the values C_γ = 21 Mev, $\hbar^2/J$ = 33.6 kev, and F = 0.015 kev for W^{182}, we obtain $\Delta_\beta = 0.110$ (we shall call the quantity Δ_β the "β-deformability" of the nucleus). If we now assume $C_\gamma \approx C_\beta\beta_0^2$ for W^{182}, we get $|(\partial/\partial\beta)\hbar^2/2J| = 65$ kev. A similar value is obtained for the derivative if the moment of inertia depends linearly on β.

We now perform analogous calculations for W^{184}, using the values C_γ = 18 Mev, $\hbar^2/J$ = 30 kev, and F = 0.073 kev. It then follows from (24) that $\Delta_\beta = 0.31$. The three-fold increase over the value for W^{182} can naturally not be attributed to a corresponding decrease in $\sqrt{C_\beta}$, for this would necessitate a ten-fold decrease in C_β. On the other hand, the moments of inertia and the value of the parameter β_0 for these two isotopes are the same, within the accuracy of measurement. To verify whether we deal, in the case of W^{184}, with fluctu-

TABLE II. Parameters β_0, A, and F in the rare earth region. The parameters of equilibrium deformation have been experimentally determined from the Coulomb excitation. The parameters A and F determine the energy of the rotation-band levels of the ground state: $E = AI(I+1) - FI^2(I+1)^2$

Nucleus	β_0	A, kev	F, kev
Sm^{152}	0.28	21.18	0.141
Gd^{154}	0.30	21.34 (20.20±0.60)	0.139 (0.072 ±0.015)
Gd^{156}	0.41	15.02 (14.81±0.12)	0.0324 (0.022 ±0.003)
Gd^{158}	0.46	13.25	0.0102
Dy^{160}	0.35	14.53	0.019
Dy^{162}	0.36	13.55 (13.54±0.23)	0.0133 (0.010 ±0.006)
Er^{166}	0.33	13.63	0.0194
Er^{168}	0.33	13.37 (13.48±0.05)	0.0060 (0.0119±0.0012)
Yb^{170}	0.30	14.11	0.0110
Yb^{172}	0.31	13.16	0.0076
Hf^{176}	0.29	14.93 (14.94±0.05)	0.0166 (0.0166±0.012)
Hf^{178}	0.31	15.61 (15.64±0.14)	0.0132 (0.0132±0.0021)
Hf^{180}	0.27	15.60 (15.54±0.08)	0.0079 (0.0067±0.0013)
W^{182}	0.26	16.78	0.0156
W^{184}	0.24	16.78	0.0729
Os^{190}	0.15	32.59 (30.1±1.1)	0.264 (0.12±0.03)

ations, we consider the behavior of the derivative in isotopes of Hf. The isotope Hf^{180} has the least value of F, namely 0.0067 kev. It is therefore reasonable to propose that, in the case of Hf^{180}, the contribution to F from the β-deformability term is negligibly small. We then obtain from (24), by putting $\hbar^2/2J = 15.54$ kev, a value $C_\gamma = 24$ Mev. Comparing this value with $C_\gamma(W^{184}) = 18$ Mev and $C_\gamma(W^{182}) = 21$ Mev, we see that a value $C_\gamma(Hf^{180}) = 24$ Mev is quite reasonable.* Quite reasonable, too, is the assumption that C_γ cannot be less than 24 Mev in the case of Hf^{178} and Hf^{176}. Then, according to (24), using the data of Tables I and II, we get

$$\Delta_\beta \geqslant \begin{cases} 0.11 \text{ for } Hf^{178}, \\ 0.14 \text{ for } Hf^{176}. \end{cases}$$

If we take for Hf^{180} the same value for the β-deformability parameter as for Hf^{178}, C_γ will be several times greater than that obtained. On the other hand, it is difficult to assume that C_γ or $(\partial/\partial\beta)\hbar^2/2J$ changes abruptly in going from one isotope to another. One can propose that such an abrupt change in F is due to violation of adiabaticity for rotational levels. To check such an assumption, we calculated F first using data on two levels, and then from data on four levels (the values of F in parentheses in Table II). The good agreement between the results argues against the assumed violation of adiabaticity. One is left with the assumption that the rotational band is perturbed by single-particle levels that lie close to the oscillational levels. Such a perturbation can be proportional to $I^2(I+1)^2$ and lead to differing increases in F for different isotopes, if the single-particle levels are different. So far there are no detailed information on the levels in the 1 to 2 Mev region, and therefore the latter assumption cannot be verified.

It must be noted in conclusion that an experimental investigation of the high levels of the Hf isotopes would yield new information on the character of the oscillations and rotation of nuclei.

*The reasonable value of C_γ obtained for Hf^{180} indicates that the parameter referred to in the preceding footnote should be close to unity.

[1] A. Bohr, Kong. Danske Vidensk. Selsk. Mat.-fys. Medd. **26**, No. 14 (1952).

[2] S. G. Nilsson, Kong. Danske Vidensk. Selsk. Mat.-fys. Medd. **29**, No. 16, 1955.

[3] B. L. Birbriar, J. Exptl. Theoret. Phys. (U.S.S.R.) **33**, 1235 (1957), Soviet Phys. JETP **6**, 951 (1958).

[4] A. Bohr and B. Mottelson, Kong. Danske Vidensk. Selsk., Mat.-fys. Medd. **27**, No. 16 (1953).

Translated by J. G. Adashko
145

CONTRIBUTION TO THE THEORY OF LIGHT SCATTERING NEAR THE SECOND-ORDER PHASE-TRANSITION POINTS

A. P. LEVANYUK

P. N. Lebedev Physical Institute, Academy of Sciences U.S.S.R.

Submitted to JETP editor July 8, 1958

J. Exptl. Theoret. Phys. (U.S.S.R.) **36**, 810-818 (March, 1959)

Formulas for the intensity of scattered light near transition points have been derived on the basis of the exact Gibbs expression for fluctuations of the parameter characterizing second-order phase transition. These formulas are employed to estimate the minimum width of the temperature region near the transition point at which the usual macroscopic theory of phase transitions of second order becomes meaningless. The formulas are also used to substantiate the validity of calculations of the scattered light intensity which are presented in reference 1.

IN the work of Ginzburg and the author[1] on the calculation of the intensity of fluctuation light scattering in the case of second-order phase transitions, use was made of Boltzmann's principle. In this case the scattering intensity was divided into two parts. One of these, which is connected with fluctuations of second order, gives the principal part of the observed scattering effect. Calculation of this part for the accepted thermodynamic potential leaves no question, since the expression for the fluctuation obtained with the help of Boltzmann's principle coincides with the exact Gibbs expressions (see reference 2). The second part of the scattering in connected with fluctuations of fourth order, and calculation of its intensity requires a foundation which we shall delineate below.

As is well known,[3,4] the intensity of light scattering from fluctuations of the dielectric constant ϵ is given by the formula

$$I = \frac{V^2}{(4\pi)^2}\left(\frac{2\pi}{\lambda_0}\right)^4 \overline{|\Delta\varepsilon_q|^2}\sin^2\varphi, \quad q = \frac{4\pi n}{\lambda_0}\sin\frac{\varphi}{2}. \qquad (1)$$

here V is the volume in which the scattering takes place, λ_0 is the wavelength in a vacuum, φ is the angle between the electric vector of the incident wave and the direction of observation, θ is the scattering angle, and

$$\Delta\varepsilon_q = \frac{1}{V}\int_V \Delta\varepsilon e^{-i\mathbf{q}\cdot\mathbf{r}}\,d\mathbf{r}. \qquad (2)$$

Close to second order phase transition points, the fluctuations of ϵ are produced by fluctuations of the characteristic parameter η (see references 5 and 1), while, neglecting optical anisotropy,

$$\Delta\varepsilon = a\Delta\eta^2 = 2a\eta_0\Delta\eta_i + a(\Delta\eta_i)^2. \qquad (3)$$

The dependence (3) is obtained from the same considerations as the dependence on η of the thermodynamic potential F (see reference 6). We note that in the complete expression for the quadratic fluctuations of ϵ terms appear that are connected with fluctuations of other thermodynamic variables, and also with mixed fluctuations of η and other variables. However, close to the transition point, where the fluctuations of η are anomalously large, one can neglect all other fluctuations and mixing terms in comparison with the fluctuations of η. This is the more valid in that the smallness of the mixing terms has been shown in reference 1 by direct estimation.

Expanding $\Delta\eta$ in a Fourier series:

$$\Delta\eta_i = \sum_{\mathbf{k}} A_{\mathbf{k}} e^{i\mathbf{k}\cdot\mathbf{r}}\,\mathbf{k} = \mathbf{i}\,\frac{2\pi}{L}n_x + \mathbf{j}\,\frac{2\pi}{L}n_y + \mathbf{k}\,\frac{2\pi}{L}n_z \qquad (4)$$

(n_x, n_y, n_z, are integers) and making use of (3), we obtain

$$\overline{|\Delta\varepsilon_q|^2} = \overline{\Delta\varepsilon_q\Delta\varepsilon_{-q}} = 4a^2\eta_{i0}^2\overline{A_q A_{-q}} + 2a^2\eta_{i0}\sum_{\mathbf{k}}\overline{A_{-q}A_{q-k}A_k} + 2a^2\eta_{i0}\sum_{\mathbf{k}}\overline{A_q A_{-q-k}A_k} + a^2\sum_{\mathbf{kk'}}\overline{A_{q-k}A_k A_{k'}A_{-q-k'}}. \qquad (5)$$

Expressions for the mean square of $\Delta\epsilon_q$ were obtained in reference 1 with the help of Boltzmann's principle. However, as is well known (see reference 2), the Boltzmann principle is not always valid; in particular, at the transition point, the possibility of its application is in considerable doubt. Nonetheless, the expression for the mean square fluctuation is an exact Gibbs expression for which it is impossible to speak of fluctuations of the higher orders. Therefore, additional justification is required for the calculation carried out in reference 1 where, in the calculation of the intensity of

the scattering, use was made of Eqs. (1) and (5), and averaging was carried out on the basis of the Boltzmann principle. This justification will consist in the obtaining of an exact expression for the intensity of scattered light and a comparison of it with the expressions of reference 1 obtained with the help of the Boltzmann principle.

1. The method of obtaining the exact Gibbs expression for the fluctuations of any order is given in reference 7. However, the concept of the thermodynamic potential of nonequilibrium states, which is essential in our consideration, was not employed there. Therefore, we shall given a brief derivation of these formulas by the method employed in reference 2, to prove that the Boltzmann expression for the mean-square fluctuation is the exact Gibbs expression. For the derivation it is necessary to introduce the concept of the thermodynamic potential of nonequilibrium states. Let there be a certain parameter characterizing the lack of equilibrium, $\eta = \hat{\eta}(X)$, where X is the aggregate of mechanical variables of the system under consideration. The state with $\eta \neq \eta_0$ is brought into equilibrium with the inclusion of the external field with potential energy U, so that this state becomes an equilibrium one. Then

$$\eta_l = \int \hat{\eta}_l(X) \exp\left\{\frac{\Psi - H(X) - U}{kT}\right\} dX. \qquad (6)$$

here $H(X)$ is the Hamiltonian of the system, Ψ is the thermodynamic potential of the system located in the field. The single-valuedness of the thermodynamic potential of the nonequilibrium state is achieved by laying an additional condition on U (for details see reference 2) which is satisfied for $U = a\hat{\eta}(X)$, a is some constant.

$\Psi(a)$ is the thermodynamic potential of a system located in the external field $U = a\hat{\eta}(X)$, and is determined by the relation

$$\Psi(a) = -kT \ln \int \exp\left\{-\frac{H(X) - a\hat{\eta}_l(X)}{kT}\right\} dX. \qquad (7)$$

It follows from (7) that

$$\eta = \partial\Psi / \partial a. \qquad (8)$$

The thermodynamic potential of a nonequilibrium state corresponding to the value η is determined by the relation

$$F(\eta_l) = \Psi(a) - \bar{U} = \Psi(a) - a\partial\Psi / \partial a. \qquad (9)$$

Differentiating (6) after first setting $U = a\hat{\eta}(X)$, taking (8) into account and then setting $a = 0$, we obtain

$$\overline{(\Delta\eta_l)^2} = -kT\Psi_0' = kT / F_0'; \qquad (10)$$

$$\overline{(\Delta\eta_l)^3} = (kT)^2 \Psi_0''' = -(kT)^2 F_0''' / (F_0')^3; \qquad (11)$$

$$\overline{(\Delta\eta_l)^4} = 3(kT)^2 (\Psi_0')^2 - (kT)^3 \Psi_0^{IV}$$
$$= 3(kT)^2 / (F_0')^2 + 3(kT)^3 (F_0''')^2 / (F_0')^5$$
$$- (kT)^3 F_0^{IV} / (F_0')^2. \qquad (12)$$

Here the primes denote differentiation of Ψ and F by a and η, respectively, the index 0 signifies that the derivatives are taken at $a = 0$ and $\eta = \eta_0$. The derivatives of Ψ with respect to a are expressed by the derivatives of F with respect to η by means of (8) and (9).

In a similar way, equations are obtained for the fluctuations of many variables. We now introduce the following necessary expressions:

$$\overline{\Delta\eta_{i_k}\Delta\eta_{i_k}} = kT\langle F_{ik}^{-1}\rangle; \qquad (13)$$

$$\overline{\Delta\eta_{i_l}\Delta\eta_{i_k}\Delta\eta_{i_l}} = (kT)^2 \langle \partial F_{ik}^{-1} / \partial\eta_{i_p}\rangle\langle F_{pl}^{-1}\rangle; \qquad (14)$$

$$\overline{\Delta\eta_{i_l}\Delta\eta_{i_k}\Delta\eta_{i_l}\Delta\eta_{i_m}} = (kT)^3 \langle F_{qm}^{-1}\rangle\langle \partial F_{pl}^{-1} / \partial\eta_{i_q}\rangle\langle \partial F_{ik}^{-1} / \partial\eta_{i_p}\rangle$$
$$+ (kT)^3 \langle F_{qm}^{-1}\rangle\langle F_{pl}^{-1}\rangle\langle \partial^2 F_{ik}^{-1} / \partial\eta_{i_p}\partial\eta_{i_q}\rangle + (kT)^2 \langle F_{kl}^{-1}\rangle\langle F_{lm}^{-1}\rangle$$
$$+ (kT)^2 \langle F_{km}^{-1}\rangle\langle F_{il}^{-1}\rangle + (kT)^2 \langle F_{lm}^{-1}\rangle\langle F_{ik}^{-1}\rangle. \qquad (15)$$

Here F_{ik}^{-1} is an element of the matrix inverse to the matrix with elements $F_{ik} = \partial^2 F / \partial\eta_i \partial\eta_k$; the brackets $\langle \ldots \rangle$ denote that the derivatives are taken at the equilibrium values of all parameters.

2. In the calculation of the intensity of light scattering in reference 1, the expansion

$$F(P, T, \eta_l) = F_0(P, T) + \alpha(P, T)\eta_l^2$$
$$+ \frac{\beta(P, T)}{2}\eta_l^4 + \frac{\gamma(P, T)}{6}\eta_l^6 + \delta(\mathrm{grad}\,\eta_l)^2, \qquad (16)$$

was employed as the thermodynamic potential of the nonequilibrium states. This expression is fundamental to the macroscopic theory of second-order phase transitions.[6] In this case, it is assumed that $\alpha = 0$ at the transition point, $\beta = \text{const}$ and $\gamma = \text{const}$, far from the critical Curie point, and $\gamma = \text{const}$ close to this point. We shall now exhibit the region close to the transition point in which the expansion (16) becomes invalid if the coefficients α, β, γ behave in the manner shown.

It was shown by M. A. Leontovich[2] that the thermodynamic potential of nonequilibrium states [introduced with the aid of (8) and (9)] is a minimum at equilibrium. However, this is not the only property of $F(\eta)$, inasmuch as the fluctuations of η of different order are expressed by the derivatives of $F(\eta)$. The requirement of the positiveness of fluctuations of even orders represents certain conditions on the derivatives of $F(\eta)$. Moreover, it is natural to require that the relation (8), for an arbitrary η in the region of values of interest to us, be satisfied for but a single a. In the case in which we are interested, this latter requirement gives nothing new and we make no use of it.

We now write down the necessary equations for the derivatives:

$$F_0' = 2\alpha + 3\beta\eta_0^2 + 5\gamma\eta_0^4; \tag{17}$$

$$F_0''' = 12\beta\eta_0 + 20\gamma\eta_0^3; \tag{18}$$

$$F_0'''' = 12\beta + 60\gamma\eta_0^2. \tag{19}$$

We now consider the region of temperatures $T > \Theta$, where Θ is the transition temperature. Here $\eta_0 = 0$, $F_0''' = 0$, $F_0'' = 2\alpha$. The condition of the positiveness of the fluctuations of even order yields

$$\alpha^2 V / kT > \beta. \tag{20}$$

The volume appears in this relation, since it has been taken into consideration that $F(P, T, \eta)$ is the thermodynamic potential per unit volume. Similarly, making use of the equation for the fluctuations of sixth order, we can obtain a condition for γ:

$$\alpha^3 V^2 / (kT)^2 > \gamma. \tag{21}$$

For $T < \Theta$, when $F_0''' \neq 0$, the condition of positiveness of the fluctuations is satisfied automatically. However, there is another circumstance here which does not allow use to be made of the expansion (16) as close to the transition point as is desired. The fact is that for $T < \Theta$, Eq. (16) is the nonequilibrium thermodynamic potential of a system with two equilibrium positions η_0 and $-\eta_0$, where

$$\eta_{0}^2 = (-\beta + \sqrt{\beta^2 - 2\alpha\gamma}) / \gamma. \tag{22}$$

To speak of equilibrium positions makes sense, naturally, only when

$$\overline{(\Delta\eta_i)^2} < \eta_{i0}^2, \tag{23}$$

where $\Delta\eta$ is the fluctuation about one of the equilibrium positions. In the opposite case, one cannot generally speak of equilibrium, and the possibility of determining the thermodynamic potential is lost, not to speak of the fact that that the usual method of calculation of fluctuations loses its meaning when one considers that the fluctuations take place about a mean position.

Setting $\beta^2 \gg 2\alpha\gamma$, which is satisfied in particular for transitions that are far from the critical Curie point, and taking (17) and (10) into account, we get from (23)

$$4\alpha^2 V / kT > \beta. \tag{24}$$

Thus we can consider that the condition (20) should be satisfied above and below the transition points.

We further note that in (20) and (24) the sign $\gg$ should actually appear, and not $>$. For (24), this does not require any explanation. For (20), we see from (10) and (12) that $(\overline{\Delta\eta})^2$ initially increases with increasing $(\overline{\Delta\eta})^4$ (with decreasing F_0''), and then decreases. It is natural to assume that an increase in $(\overline{\Delta\eta})^4$ corresponds in reality only to an increase in $(\overline{\Delta\eta})^2$, which is satisfied for the stronger inequality.

Conditions (20) and (24) refer to the spatially homogeneous case, and do not take correlations into account. If by V we understand the total volume of the body, then these conditions are satisfied everywhere with the exception of an extremely narrow region in the vicinity of the transition point. But in consideration of fluctuations in small volumens, we must consider correlations, that is we must use not (20) and (24), but conditions obtained by means of successive consideration of spatial inhomogeneity and correlations. In this case, we must take the fluctuations of the Fourier components of η into account and consider the gradient term in (16). Conditions (20) and (24) remain here also, as do conditions on the fluctuations of the zero Fourier components, while V denotes the total volume of the body. However, in this case, there are additional positive definite quantities, for example the intensity of the scattered light I, the condition of positiveness of which represents certain conditions on $F(\eta)$, in particular on the quantity δ. We shall give further details on this matter below after obtaining exact formulas for I.

3. We now set about to obtain exact expressions for I. We denote the intensity of scattering associated with the first term of the right hand side of (5) by I_2, that associated with the second and third terms by I_3, and that associated with the fourth term by I_4. As has already been shown, the value of I_2 computed with the aid of Boltzmann's principle coincides with the exact value; therefore it is necessary to compute only I_3 and I_4. Making use of (4) and (16), we obtain

$$\langle F_{1,2} \rangle = V(F_0'' + 2\delta\mathbf{q}_1^2)\,\delta_{\mathbf{q}_1, -\mathbf{q}_2}; \tag{28}$$

$$\langle F_{1,2,3} \rangle = VF_0'''\delta_{\mathbf{q}_3, -\mathbf{q}_1-\mathbf{q}_2}; \tag{29}$$

$$\langle F_{1,2,3,4} \rangle = VF_0''''\delta_{\mathbf{q}_4, -\mathbf{q}_1-\mathbf{q}_2-\mathbf{q}_3}. \tag{30}$$

Here $F_{i,\ldots,n}$ denotes the derivative of F with respect to $A_{\mathbf{q}_1} \ldots A_{\mathbf{q}_n}$, $\delta_{\mathbf{q}_1,\mathbf{q}_2}$ is the Kronecker symbol. To express the right hand side of (14) and (15) in terms of (28) – (30), we renumber the variables $A_{\mathbf{q}}$, that is, we renumber the vector $\mathbf{q}$. We carry out the numbering on both sides of zero in such a fashion that if $\mathbf{q}_1$ and $\mathbf{q}_2$ have the corresponding numbers n_1 and n_2, and $\mathbf{q}_1 = -\mathbf{q}_2$, then $n_1 = -n_2$, and conversely. If we denote by n the total number of vectors with integral coordinates, smaller

in modulus than a certain k_{max}, then the indices of the matrix F_{ik} will take on the values from $-(n-1)/2$ to $(n-1)/2$. We can arrive at a matrix with such indices from the ordinary matrix by means of a transformation of the indices $i' = i - (n+1)/2$, $k' = k - (n+1)/2$. This transformation is possible since $n+1$ is an integer.

It is seen from (28) that the elements in the matrix $\langle F_{ik}\rangle$ that are different from zero lie only on the diagonal which is orthogonal to the principle diagonal. It then follows that

$$D(\langle F\rangle) = \prod_{a=-(n-1)/2}^{(n-1)/2} \langle F_{a,-a}\rangle, \qquad (31)$$

$D(\langle F\rangle)$ is the determinant of the matrix $\langle F_{ik}\rangle$. As is well known, we have for an element of the inverse matrix

$$F_{ik}^{-1} = F_{ki}^{adj} / D(F), \qquad (32)$$

where F_{ki}^{adj} is the adjoint of the matrix F_{ik} relative to the element F_{ki}. Furthermore,

$$\langle F_{ki}^{adj}\rangle = \delta_{i,-k} \prod_{b=-(n-1)/2}^{(n-1)/2}{}^{i} \langle F_{b,-b}\rangle. \qquad (33)$$

Here Π^{i} denotes that $\langle F_{b,-b}\rangle$ as a factor runs over all b except $b = i$. We have from (31) – (33)

$$\langle F_{ik}^{-1}\rangle = \delta_{i,-k}/\langle F_{i,-i}\rangle. \qquad (34)$$

Let us first calculate I_3. In what follows we shall write η_p in place of A_q, where p is the number of the vector q. We now calculate $\langle \partial F_{ik}^{-1}/\partial\eta_p\rangle$. Taking (32) into account,

$$\frac{\partial F_{ik}^{-1}}{\partial\eta_p} = \frac{1}{D(F)}\frac{\partial F_{ki}^{adj}}{\partial\eta_p} - \frac{F_{ki}^{adj}}{D^2(F)}\frac{\partial D(F)}{\partial\eta_p}. \qquad (35)$$

Further,

$$F_{ki}^{adj} = (-1)^{i+k}\sum(-1)^{[r_1\dots p_{k-1}\,p_{k+1}\dots p_n]} \times F_{-(n-1)/2,\,p_1}\dots F_{(n-1)/2,\,p_n} \qquad (36)$$

$[p_1\dots p_{k-1}p_{k+1}\dots p_n]$ denotes the number of disorders in the permutation of $p_1\dots p_{k-1}p_{k+1}\dots p_n$ from the numbers $-(n+1)/2\dots i-1,\ i+1,\dots (n-1)/2$. Summation is carried out over all permutations. We differentiate (36) with respect to η_p. On the right hand side there are $n-1$ sums over the permutations. We consider one of such sums:

$$(-1)^{i+k}\sum(-1)^{[p_1\dots p_{k-1}p_{k+1}\dots p_n]} \times F_{-(n-1)/2,\,p_1}\dots \frac{\partial F_{a,\,p_a}}{\partial\eta_p}\dots F_{(n-1)/2,\,p_n}. \qquad (37)$$

We now set $\eta_p = 0$, that is, we consider the equilibrium values for the derivatives. We shall show that for $a \neq -i$, the expression (37) at equilibriums values of η_p differs from zero only for $i = -k$. In fact, if $i \neq -k$, for equilibrium values of its derivatives, the product (37) contains a term of the form $\langle F_{-i},\, p_{-i}\rangle$ which differs from zero only for $p_{-i} = i$, but this equality is not possible. It is easy to see that in such a case $p_a = -a$. It follows from (29) that in this case $p = 0$. If $a = -i$ (this is possible only for $i \neq -k$) then, by an argument similar to the foregoing, it is easy to show that $p_a = -k$. By virtue of (29) $q_i + q_k = q_p$, where q_l is the vector corresponding to the number l.

For $a \neq -i$ in the sum (37), considered at equilibrium, only one component is different from zero with $p_1 = -(n-1)/2, \dots p_a = -a, \dots p_n = (n-1)/2$. We shall determine its sign. The required number of rearrangements in it is maximum, that is, it is equal to

$$\sum_{i=1}^{n-2} i = (n-1)(n-2)/2.$$

Since $n-1$ is divisible by 8, the number of required rearrangements is even. Taking into account, moreover, that $i = -k$, we conclude that this component is positive. For $a = -i$, calculation of the required rearrangements is somewhat lengthier. In this case we obtain a negative value. Thus we obtain

$$\langle \partial F_{ki}^{adj}/\partial\eta_{i_p}\rangle = VF_0'''\delta_{p,\,0}\delta_{i,-k} \times \sum_{a=-\frac{n-1}{2}}^{\frac{n-1}{2}} D(\langle F\rangle)/\langle F_{a,-a}\rangle\langle F_{i,-i}\rangle - VF_0'''\delta_{q_p,\,q_i+q_k} D(\langle F\rangle)/\langle F_{i,-i}\rangle\langle F_{k,-k}\rangle \qquad (38)$$

$(i \neq -k)$

Carrying out similar considerations for

$$D(F) = \sum(-1)^{[p_1\dots p_n]} F_{-(n-1)/2,\,p_1}\dots F_{(n-1)/2,\,p_n}, \qquad (39)$$

we obtain

$$\langle \partial D(F)/\partial\eta_p\rangle = VF_0'''\delta_{p,\,0}\sum_{a=-(n-1)/2}^{(n-1)/2} D(\langle F\rangle)/\langle F_{a,-a}\rangle. \qquad (40)$$

From (35) and from (38) – (40) we obtain

$$\langle \partial F_{ik}^{-1}/\partial\eta_p\rangle = -VF_0'''\delta_{q_p,\,q_i+q_k}/\langle F_{i,-i}\rangle\langle F_{k,-k}\rangle. \qquad (41)$$

For I_3 we have

$$I_3 = C2a^2\tau_0\left\{\sum_{\mathbf{k}}\overline{A_{\mathbf{q}}A_{-\mathbf{q}-\mathbf{k}}A_{\mathbf{k}}} + \sum_{\mathbf{k}}\overline{A_{-\mathbf{q}}A_{\mathbf{q}-\mathbf{k}}A_{\mathbf{k}}}\right\}, \qquad (42)$$

where

$$C = (V/A\pi)^2(2\pi/\lambda_0)^4\sin^2\varphi.$$

We now substitute (41) in (14) and (42) and obtain

$$I_3 = -C\,4\,a^2\gamma_0 V F_0''' \sum_{\mathbf{k}} (kT)^2 \langle F_{\mathbf{q},-\mathbf{q}}\rangle\langle F_{\mathbf{k},-\mathbf{k}}\rangle\langle F_{\mathbf{q}-\mathbf{k},\mathbf{k}-\mathbf{q}}\rangle$$

$$= -\frac{Ca^2 24\beta\gamma_0^2}{V^2(-2\alpha+\delta q^2)} \sum_{\mathbf{k}} (kT)^2/[F_0^* + 2\delta\mathbf{k}^2]$$

$$\times[F_0^* + 2\delta(\mathbf{k}-\mathbf{q})^2]. \qquad (43)$$

Here we assume $\gamma = 0$, i.e., we consider a transition that is far from the critical Curie point. Changing now from summation to integration, we have

$$I_3 = -\frac{V}{(4\pi)^3}\left(\frac{2\pi}{\lambda_0}\right)^4 a^2 (kT)^2 \frac{12\beta\gamma_0^2}{-2\alpha+\delta q^2} S\sin^2\varphi; \qquad (44)$$

$$S = \frac{1}{8\pi\delta^2 q}\operatorname{arc\,tg}(q/2\sqrt{F_0^*/2\delta}). \qquad (45)$$

I_4 is computed in a fashion similar to I_3. This computation is rather lengthy; we therefore give only the result:

$$I_4 = Ca^2 \sum_{\mathbf{k},\mathbf{k}'} \overline{A_{\mathbf{k}}A_{\mathbf{q}-\mathbf{k}}A_{\mathbf{k}'}A_{-\mathbf{q}-\mathbf{k}'}}$$

$$= Ca^2\Big\{-VF_0'''' \sum_{\mathbf{k},\mathbf{k}'} (kT)^3/\langle F_{\mathbf{k},-\mathbf{k}}\rangle$$

$$\times\langle F_{\mathbf{q}-\mathbf{k},\mathbf{k}-\mathbf{q}}\rangle\langle F_{\mathbf{k}',-\mathbf{k}'}\rangle\langle F_{-\mathbf{q}-\mathbf{k}',\mathbf{k}'+\mathbf{q}}\rangle$$

$$+ V^2(F_0''')^2 \sum_{\mathbf{k},\mathbf{k}'} (kT)^3/\langle F_{\mathbf{k},-\mathbf{k}}\rangle$$

$$\times\langle F_{\mathbf{q}-\mathbf{k},\mathbf{k}-\mathbf{q}}\rangle\langle F_{\mathbf{k}',-\mathbf{k}'}\rangle\langle F_{-\mathbf{q}-\mathbf{k}',\mathbf{k}'+\mathbf{q}}\rangle\langle F_{\mathbf{q},-\mathbf{q}}\rangle$$

$$+ 2\sum_{\mathbf{k}} (kT)^2/\langle F_{\mathbf{k},-\mathbf{k}}\rangle\langle F_{\mathbf{k}-\mathbf{q},\mathbf{q}-\mathbf{k}}\rangle\Big\}. \qquad (46)$$

On the right hand side of (46) we omit terms that vanish upon subsequent integration over $\mathbf{k}$.

We denote the scattering connected with the first term on the right hand side of (46) by I_{44}, with the second, by I_{43}. The scattering connected with the latter term is I_4, computed with the aid of Boltzmann's principle. We denote it by I_4^0. It was obtained in reference 1, whence

$$I_4^0 = \frac{V}{(4\pi)^2}\left(\frac{2\pi}{\lambda_0}\right)^4 a^2 (kT)^2 S\sin^2\varphi. \qquad (47)$$

In reference 1, I_4^0 was written as I_2. Transforming in (46) from summation to integration over $\mathbf{k}$, we obtain for I_{44} and I_{43}:

$$I_{44} = -\frac{V}{(4\pi)^2}\left(\frac{2\pi}{\lambda_0}\right)^4 a^2 3\beta (kT)^3 S^2\sin^2\varphi; \qquad (48)$$

$$I_{43} = \frac{V}{(4\pi)^2}\left(\frac{2\pi}{\lambda_0}\right)^4 a^2 \frac{18\beta^2\gamma_0^2}{-2\alpha+\delta q^2} (kT)^3 S^2\sin^2\varphi. \qquad (49)$$

We also cite an expression for I_2 obtained in reference 1:

$$I_2 = \frac{V}{(4\pi)^2}\left(\frac{2\pi}{\lambda_0}\right)^4 a^2 \frac{2\gamma_0^2}{-2\alpha+\delta q^2} kT\sin^2\varphi. \qquad (50)$$

Here and throughout we consider only regions far from the critical Curie point.

We now compare the exact expression for the total intensity of scattered light

$$I = I_2 + I_4^0 + I_3 + I_{43} + I_{44}$$

with the intensity $I^0 = I_2 + I_4^0$, computed by Boltzmann's principle. For $T > \Theta$, we obtain

$$I_2 = I_3 = I_{43} = 0, \quad I/I^0$$

$$= 1 + I_{44}/I_4^0 = 1 - 3\beta kTS. \qquad (51)$$

The condition for the validity of the calculation carried out in reference 1, as also the condition for the validity of the expansion (16), takes the form

$$3\beta kTS \ll 1. \qquad (52)$$

For each given substance, S is a function of T and q. For fixed T, the inequality (52) must be satisfied for any q, since we are discussing the positiveness of I or, irrespective of the physical meaning of I, the positiveness of some positive definite combination of Fourier components of $\Delta\eta$. Thus, fixing T, we must prove whether (52) is satisfied for a q which brings about a maximum for S. It is easy to see that for fixed T, S is maximum for q = 0. In this case

$$S = 1/16\pi\delta^{3/2}\sqrt{F_0^*/2}. \qquad (53)$$

Further, taking it into account that $\delta \sim \alpha'_\Theta \Theta d^2$ (the discontinuity in the heat capacity at the transition $\Delta c = \alpha'_\Theta \Theta/\beta$ and $F_\Theta = 2\alpha'_\Theta(T-\Theta)$ for $T > \Theta$), we write (52) in the form

$$T - \Theta \gg (3/16\pi)^2 \Theta (k/\Delta c d^3)^2. \qquad (54)$$

For the $\alpha - \beta$ transition in quartz we have $\Delta c = 4\times 10^7$ erg/deg-cm^3 (reference 8), $\Theta \sim 10^3$. Setting $d \sim 10^{-7}$, we obtain from (54)

$$T - \Theta \gg 10^{-4} \div 10^{-3}. \qquad (55)$$

In this region of temperatures above the transition point the expansion (16) does not lead to a contradiction and the exact expressions are insignificantly different from the expressions obtained with the help of Boltzmann's principle.

For the λ-transition in liquid helium, $\Delta c \sim 10^7$ erg/deg-cm^3, $d \sim 2\times 10^{-8}$ (see references 9, 1), $\Theta \sim 1$. Substituting these values in (54) we obtain

$$T - \Theta \gg 10^{-2}. \qquad (56)$$

For $T < \Theta$ such estimates do not present any fundamental difficulty, although there are rather tedious. As can be shown, the condition (54) holds with accuracy up to an insignificant numerical factor.

We see in total that the conditions for applica-

bility of the calculations reduce to the inequality (52). If it is not satisfied, use of the expansion (16) is not valid. If the inequality (54) is satisfied, then the results obtained in reference 1 remain valid both for scattering on fluctuations of second order and also for scattering of fluctuations of fourth order.

In conclusion the author expresses his sincerest gratitude to Professor V. L. Ginzburg for suggesting the theme and for valuable discussions connected with the present work.

[1] V. L. Ginzburg and A. P. Levanyuk, Сб. статей посвященных памяти акад. Г. С. Ландсберга (Collected papers in honor of the memory of Acad. G. S. Landsberg) Acad. Science Press, Moscow-Leningrad, (in press); in brief form in J. Phys. Chem. Solids **6**, 51 (1958).

[2] M. A. Leontovich, Статистическая физика (Statistical Physics), Sec. 31 (Gostekhizdat, 1944).

[3] A. Einstein, Ann. Physik **33**, 1275 (1910).

[4] V. V. Vladimirskiĭ, J. Exptl. Theoret. Phys. (U.S.S.R.) **9**, 1226 (1939).

[5] V. L. Ginzburg, Dokl. Akad. Nauk SSSR **105**, 240 (1955).

[6] L. D. Landau and E. M. Lifshitz, Статистическая физика (Statistical Physics) (English translation, Addison Wesley, 1958).

[7] I. P. Terletskij, Nuovo cimento **7**, 308 (1958).

[8] N. N. Sinel'nikov, Dokl. Akad. Nauk SSSR **92**, 369 (1953).

[9] V. L. Ginzburg and L. P. Pitaevskii, J. Exptl. Theoret. Phys. (U.S.S.R.) **34**, 1240 (1958); Soviet Phys. JETP **7**, 858 (1958).

Translated by R. T. Beyer
146

SOVIET PHYSICS JETP VOLUME 36 (9), NUMBER 3 SEPTEMBER, 1959

INDIRECT COUPLING OF d ELECTRONS IN TRANSITION METALS

I. FERROMAGNETISM

A. A. BERDYSHEV and B. V. KARPENKO

Ural' State University

Submitted to JETP editor August 3, 1958; resubmitted January 14, 1959

J. Exptl. Theoret. Phys. (U.S.S.R.) **36**, 819-822 (March, 1959)

The second-order perturbation for the s-d exchange model of transition metals yields an indirect interaction between d electrons via the conduction electrons. Consequently ferromagnetism may arise when direct d-d coupling is entirely absent or even when the d-d exchange integral is negative.

FERROMAGNETISM and antiferromagnetism in transition metals are usually accounted for by an exchange interaction between core d-electrons. A positive exchange integral between nearest neighbors makes a metal ferromagnetic, while a negative integral results in antiferromagnetism. A number of difficulties arise,[1] of which we shall mention only three: (1) Many experimental results cannot be accounted for by using the Bethe-Slater curve for the exchange integral of transition metals.[1] (2) Most theoretical evaluations of the exchange integral lead to a negative value.[2] (3) Both ferromagnetic and antiferromagnetic forms are found in dilute alloys of manganese in precious metals;[3] in these alloys transition metal atoms are separated by such large distances that any direct exchange interaction between them is entirely excluded. Similarly, ferromagnetism and antiferromagnetism in rare earths cannot be attributed to the extremely weak direct coupling between the magnetic 4f electrons.

Other possible exchange mechanisms have therefore been sought, one of which is the indirect exchange interaction suggested by Zener,[1] which he discussed from a phenomenological point of view. The present paper considers the relation of the indirect interaction to ferromagnetism.

The calculation will be based on the s-d exchange model of transition metals.[4] The energy operator of the system of s and d electrons is

$$H = H_0 + H_1 + H_2,$$

where

$$H_0 = \sum_k E_k [a_k^+ a_k + a_k^+(-) a_k(-)] + \sum_g \varepsilon_g b_g^+ b_g, \qquad H_1 = -N^{-1/2} \sum_{k,g} I(\mathbf{k}, \mathbf{k}-\mathbf{g}) b_g a_k^+ a_{k-g}(-) + \text{compl. conj.},$$

$$H_2 = -\sum_k I(\mathbf{k}, \mathbf{k}) a_k^+(-) a_k(-) + N^{-1} \sum_{\mathbf{k}_2 - \mathbf{k}_1 + \mathbf{g}_1 - \mathbf{g}_2 = 0} I(\mathbf{k}_1, \mathbf{k}_2) b_{g_2}^+ b_{g_1} [a_{k_1}^+(-) a_{k_2}(-) - a_{k_1}^+ a_{k_2}],$$

where $E_k = Ak^2$ is the translational energy of a conduction electron in one-electron theory, A is the transport integral, $\epsilon_g = Jg^2$ is the energy of a spin wave with wave number $\mathbf{g}$, J is the d-d exchange integral, $I(\mathbf{k}_1, \mathbf{k}_2)$ is the s-d exchange integral, a_k and $a_k(-)$ are Fermi operators for conduction electrons with wave number $\mathbf{k}$ and spins $+\frac{1}{2}$ and $-\frac{1}{2}$ respectively, b_g is the Bose operator and N is the number of lattice sites.

Previous papers on the s-d exchange model of ferromagnets and antiferromagnets[4] have considered only the energy terms H_0 and H_2; this amounted to a first-order perturbation. The "ternary" terms in H_1 comprise a second-order energy correction, which can be obtained either by perturbation theory[5] or through a canonical transformation.[6] The energy then becomes

$$W = \sum_g (\varepsilon_g + g_0 \mu H) n_g + \sum_k (E_k^+ - \mu H) N_k^+ + \sum_k (E_k^- + \mu H) N_k^- - N g_0 \mu H,$$

$$E_k^+ = E_k + \frac{1}{N} \sum_g E_{kg}^+ n_g + \varepsilon_{sd}^0,$$

$$E_k^- = E_k - I(\mathbf{k}, \mathbf{k}) + \frac{1}{N} \sum_g E_{kg}^- n_g,$$

$$E_{kg}^+ = -I(\mathbf{k}, \mathbf{k}) + |I(\mathbf{k}, \mathbf{k}-\mathbf{g})|^2 / (E_k - E_{k-g} - \varepsilon_g),$$

$$E_{kg}^- = I(\mathbf{k}, \mathbf{k}) - |I(\mathbf{k}, \mathbf{k}+\mathbf{g})|^2 / (E_{k+g} - E_k - \varepsilon_g)$$

$$\varepsilon_{sd}^0 = \frac{1}{N} \sum_{kg} |I(\mathbf{k}, \mathbf{k}-\mathbf{g})|^2 / (E_k - E_{k-g} - \varepsilon_g),$$

where g_0 is the Landé factor, μ is the Bohr magneton, n_g and N_k^+ are the occupation numbers of

ferromagnons and conduction electrons. We assume for simplicity that $I(\mathbf{k}_1, \mathbf{k}_2) = I_0 = \text{const}$. The state sum and the free energy are calculated by the method of steepest descent;[7] the free energy of the system is given by

$$F = F_s + F_{sd} + F_d,$$

$$F_s = \zeta N - kT \sum_k \left[\ln\left\{1 + \exp\left(-\frac{E_k - \zeta - \mu H}{kT}\right)\right\} + \ln\left\{1 + \exp\left(-\frac{E_k - I_0 - \zeta + \mu H}{kT}\right)\right\}\right],$$

$$F_{sd} = \frac{I_0^2}{N} \sum_{k,g} f(E_k - \mu H)/(E_k - E_{k-g} - \varepsilon_g),$$

$$F_d = -Ng_0\mu H + kT \sum_g \ln(1 + \exp) - \mathscr{E}_g/kT)),$$

$$\mathscr{E}_g = \varepsilon_g + g_0\mu H + \Delta_1 + \Delta_2,$$

$$\Delta_1 = \frac{I_0}{N} \sum_k [f(E_k - I_0 + \mu H) - f(E_k - \mu H)],$$

$$\Delta_2 = \frac{I_0^2}{N} \sum_k \left[\frac{f(E_k - \mu H)}{2Ak g \cos\vartheta - (A+J)g^2} - \frac{f(E_k - I_0 + \mu H)}{2Ak g \cos\vartheta + (A-J)g^2}\right],$$

where $f(E)$ is the Fermi distribution function; the chemical potential ζ of conduction electrons (the Fermi energy) is given by

$$\sum_k [f(E_k - \mu H) + f(E_k - I_0 + \mu H)] = N - \frac{1}{N_k T} \sum_{k,g} N(\mathscr{E}_g) \times \left[E^+_{kg} \frac{\partial f(E_k - \mu H)}{\partial \zeta} + E^-_{kg} \frac{\partial f(E_k - I_0 + \mu H)}{\partial \zeta}\right] - \frac{I_0^2}{N} \sum_{k,g} \frac{\partial f(E_k - \mu H)/\partial \zeta}{E_k - E_{k-g} - \varepsilon_g}.$$

The magnetic moment of the electron system is determined by

$M = -\partial F/\partial H$ and is equal to $M = M_s + M_{sd} + M_d$, where

$$M_d = Ng_0\mu \left\{1 - \frac{1}{N}\left[1 + \frac{1}{g_0}(\Delta_1^1 + \Delta_2^1)\right] \sum_g N(\mathscr{E}_g)\right\},$$

$N(\mathscr{E}_g)$ being the Bose distribution function. For $g \ll 1$ we obtain approximately

$$\Delta_1 = \Delta_0 + \Delta_1^1 \mu H,$$

$$\Delta_0 = \frac{I_0^2}{4\pi^2 A} \sqrt{\frac{\zeta}{A}} \left[1 - \frac{\pi^2}{24}\left(\frac{kT}{\zeta}\right)^2\right], \quad \Delta_1^1 = \frac{I_0}{2\pi^2 A} \sqrt{\frac{\zeta}{A}},$$

$$\Delta_2 = \Delta_2^0 + \Delta_2^1 \mu H,$$

$$\Delta_2^0 = -\Delta_0 + \frac{I_0^2(A^2 + 3J^2)}{48\pi^2 A^2 \sqrt{\zeta A}} \left[1 - \frac{\pi^2}{16}\left(\frac{kT}{\zeta}\right)^2\right], \quad \Delta_2^1 = 0.$$

Then $\mathscr{E}_g = J_{\text{eff}} g^2 + g_0\mu H$,

$$J_{\text{eff}} = J + J^{(s)} = J + \frac{I_0^2(A^2 + 3J^2)}{48\pi^2 A^2 \sqrt{\zeta A}} \left[1 - \frac{\pi^2}{16}\left(\frac{kT}{\zeta}\right)^2\right].$$

Integration over $\mathbf{g}$ (neglecting the correction $\Delta_1^1 \ll 1$) gives

$$M_d = Ng_0\mu \left\{1 - \gamma \left(\frac{T}{\Theta_c}\right)^{3/2}\right\}, \quad \gamma = 0.1174, \quad 2k\Theta = J_{\text{eff}}$$

which is the familiar $T^{3/2}$ law for low-temperature magnetization. It thus results from the second-order correction that the free energy and magnetic moment contain, instead of the direct coupling $J \equiv J_{dd}$, the effective exchange integral J_{eff} consisting of a direct d-d exchange integral and an "integral" $J^{(s)}$ of indirect interaction. The latter is always positive, so that the existence of ferromagnetism does not require that J_{dd} be necessarily positive. Ferromagnetism also may exist when $J_{dd} = 0$ (in rare earths and dilute alloys of manganese) and even with a negative d-d exchange integral. The more general criterion for ferromagnetism is now $J_{\text{eff}} = J + J^{(s)} > 0$.

In addition, the second-order correction completely nullifies the first-order magnetization correction. It has previously been shown[8] that the existence of a "zero-point" energy Δ_0 of a spin wave leads either to the exponential dependence of M_d on T when Δ_0 is large, or to a small departure from the $T^{3/2}$ law when Δ_0 is small. In the second approximation the correction Δ_0 drops out of $\mathscr{E}_g$ completely, so that there is no departure from the $T^{3/2}$ law.

The still unconsidered last two components of the total magnetic moment of the s and d electron system are easily calculated, giving

$$M_s + M_{sd} = \left[\frac{N\mu I_0}{4\pi^2 A} \sqrt{\frac{\zeta}{A}} + \mu^2 N \frac{H}{\pi^2 A} \sqrt{\frac{\zeta}{A}}\right] + \frac{3N\mu}{64\pi^2} \frac{I_0^2}{\zeta A} \sqrt{\frac{\zeta}{A}}.$$

The first and third terms of this sum describe the "magnetization" of conduction electrons by the "field" of core electrons and the spontaneous magnetic moment of conduction electrons. This moment depends on the magnitude and sign of the s-d exchange integral I_0. The second term describes the usual Pauli paramagnetic susceptibility of conduction electrons.

We note in conclusion that the effective exchange integral J_{eff} is slightly reduced as the temperature rises. However, this dependence is too weak to account for the transition from ferromagnetism to antiferromagnetism at a high temperature, which is observed in some alloys and rare earths.[3,5] Also, the entire calculation is based on the approximating assumption that the magnetization of the system is close to its maximum value, so that we cannot draw conclusions that will be valid for high temperatures. The different methods required at high temperatures will be discussed in another paper.

We have also considered the case of a negative effective exchange integral. The indirect interaction "integral" $J^{(s)}$ now differs somewhat because of the different dispersion laws for spin waves in ferromagnets and antiferromagnets. This case will be discussed in the next paper.

The authors are grateful to S. V. Vonsovskiĭ and E. A. Turov for discussions and a number of valuable comments.

[1] C. Zener and R.R. Heikes, Revs. Modern Phys. **25**, 191 (1953); [cf. also C. Zener, Пробл. совр. физ. (Problems of Contemporary Physics) No. 5, (1952)].

[2] H. Kaplan, Phys. Rev. **85**, 1038 (1952); E. P. Wohlfarth, Nature **163**, 57 (1949).

[3] J. Owen and M. E. Browne, Phys. Chem. Solids **2**, 85 (1957); F. A. Otter, J. Franklin Inst. **260**, 75 (1955).

[4] S. V. Vonsovskiĭ and E. A. Turov, J. Exptl. Theoret. Phys. (U.S.S.R.) **24**, 419 (1953); S. V. Vonsovskiĭ and A. A. Berdyshev, Izv. Akad. Nauk SSSR, Ser. Fiz. **18**, 328 (1954).

[5] T. Kasuya, Progr. Theoret. Phys. **16**, 45 (1956); K. Yosida, Phys. Rev. **106**, 893 (1957), **107**, 396 (1957).

[6] Y. Kitano and H. Nakano, Progr. Theoret. Phys. **9**, 370 (1953).

[7] M. A. Leontovich, Статистическая физика (Statistical Physics), Gostekhizdat, 1944, Ch. 5.

[8] A. A. Berdyshev and Yu. A. Izyumov, Физика металлов и металловедение (Physics of Metals and Metal Research) **5**, 552 (1957); E. A. Turov, J. Exptl. Theoret. Phys. (U.S.S.R.) **25**, 352 (1953).

Translated by I. Emin
147

THE ROLE OF GROUP VELOCITY OF LIGHT EMITTED IN A REFRACTIVE MEDIUM

I. M. FRANK

P. N. Lebedev Physics Institute, Academy of Sciences, U.S.S.R.

Submitted to JETP editor August 16, 1958

J. Exptl. Theoret. Phys. (U.S.S.R.) **36**, 823-831 (March, 1959)

The emission of light by a system of particles possessing an arbitrary natural frequency is considered for the case when the system moves uniformly in a refractive medium that is transparent to the emitted light. The role of the group velocity of the light emitted by such a source is investigated.

1. INTRODUCTION

THE Vavilov-Cerenkov effect has been extensively used recently in research in nuclear physics, particularly the physics of high-energy particles. At the present time one observes in the experiments either radiation from individual charged particles that move in a refractive medium or the total incoherent radiation produced by many charges that move independently of each other. However, this immediately raises the question of radiation by a moving system of particles.* A system of particles may have a natural frequency of oscillation. Therefore, an examination of the behavior of a radiator of arbitrary natural frequency moving in a medium may be not merely of fundamental but also of practical interest.

The purpose of this article is to clarify the role of the group velocity of light in radiation from such a source, moving uniformly in a refractive isotropic medium that is transparent to the radiated light.

It is known that the radiation from a moving source of light depends substantially on the ratio of the radiator velocity to the phase velocity of light at the radiated frequency. Thus, a particle producing a time-invariant electromagnetic field (electric charge, fixed magnetic dipole, etc.) i.e., a particle with a zero natural frequency, is subject to the Vavilov-Cerenkov effect if its velocity of motion reaches or exceeds the phase velocity of the light. Here the connection between the direction of the emission of light and the radiated frequency ω_θ is determined by the ratio of the velocity of motion v to the phase velocity of the light $u = c/n(\omega_\theta)$ for this frequency, namely

$$v\cos\theta/(c/n(\omega_\theta)) = 1, \quad n(\omega_\theta) = c/v\cos\theta. \quad (1.1)$$

If a particle (or a system of particles) produces a time-varying field of frequency ω_0' while moving in a medium (ω_0' is measured in the reference frame of the radiator), the radiated frequencies are subject to the Doppler effect. As in the case of the Vavilov-Cerenkov effect, the Doppler frequency is a function of the ratio $v/[c/n(\omega_\theta)] = \beta n(\omega_\theta)$. Actually, the radiated Doppler frequencies satisfy one of the following relations

$$\omega_\theta = \omega_0/(1-\beta n(\omega_\theta)\cos\theta), \quad \beta n(\omega_\theta)\cos\theta < 1; \quad (1.2)$$

$$\omega_\theta = \omega_0/(\beta n(\omega_\theta)\cos\theta - 1), \quad \beta n(\omega_\theta)\cos\theta > 1. \quad (1.3)$$

Here $\omega_0 = \omega_0'\sqrt{1-\beta^2}$ is the natural frequency measured in the coordinate system in which the medium is at rest.

The first equation corresponds to the case when the projection of the radiator velocity on the direction of the beam, v cos θ, is less than the phase velocity of light $u = c/n(\omega_\theta)$ for the Doppler frequency (Doppler frequencies of the usual type). The second formula corresponds to the "faster than light" Doppler effect, i.e.,

$$v\cos\theta > c/n(\omega_\theta).$$

The group velocity of light does not enter the foregoing expressions explicitly. It is known, however, that it is precisely the group velocity of light that determines the rate of propagation of the radiated energy in the medium. It is therefore natural to raise the question of whether any singularities will arise in the radiation if the velocity of motion exceeds the group velocity, i.e., if the radiator overtakes the light energy it radiates. It will be shown later on that this is indeed so: Equality of the velocity of radiator motion to the group velocity of light is a necessary (although not sufficient) condition for the appearance of new radiation components.

*This statement of the problem arises, in particular, in connection with the so called coherent method of charged-particle acceleration, proposed by V. I. Veksler.

This result is elementary in the case of the Vavilov-Cerenkov effect. In fact, the least velocity at which Vavilov-Cerenkov radiation occurs at at angle θ is, according to (1.1)

$$v_{\min} \cos \theta = c / n_{\max}, \tag{1.4}$$

where n_{max} is the maximum value that the index of refraction can assume in the given medium (we denote the corresponding limiting frequency by ω_{lim}). Since the group velocity w is determined by the relation

$$\frac{1}{w} = \frac{1}{c} \frac{d}{d\omega} (\omega n) = \frac{1}{c} \left(n + \omega \frac{dn}{d\omega} \right) \tag{1.5}$$

and $[dn/d\omega]_{\omega=\omega_{lim}} = 0$ for the maximum index of refraction, we get

$$w(\omega_{lim}) = c / n_{max}. \tag{1.6}$$

Comparing with (1.4) we obtain

$$v \cos \theta / w(\omega_{lim}) = 1. \tag{1.7}$$

Thus, the condition of the threshold is that v cos θ be equal to the group velocity of the light for the frequency that first appears in the spectrum of the Vavilov-Cerenkov radiation. In other words, the threshold is determined by the fulfillment of conditions (1.1) and (1.7) for a frequency that is the same in both cases, $\omega_\theta = \omega_{lim}$.

Equation (1.7) has remained unnoticed apparently because the problem is usually formulated in a different manner when the radiation threshold is determined. Usually the radiation frequency is assumed specified, say in the optical region of the spectrum, and the threshold velocity is determined from the known index of refraction for this frequency.

A condition like (1.7) is significant also for other types of radiation in a medium. To explain this we must turn to an examination of the question of the splitting of the radiated frequencies, to the so called "complex" radiation effects.[1]

It is seen from (1.1) – (1.3) that in the case a dispersing medium these equations are not linear in ω_θ, since the index of refraction $n(\omega_\theta)$ may depend on the frequency in a complicated manner. As a result, for specified ω_0, v, and θ there are several possible frequencies ω_θ satisfying the Doppler condition[1] (complex Doppler effect). Mandel'shtam was the first to indicate in his lectures that the occurrence of the complex Doppler effect is related to the value of the group velocity of light.[2*] Actually, it was found that the previously-derived condition for the occurrence of the complex Doppler effect[1] is tantamount to stating that the ratio of v cos θ to the group velocity of light exceeds unity for one of the Doppler frequencies.[3]

It can be shown that Eq. (1.7) is a condition for the threshold of the complex radiation effect, meaning also the threshold for the appearance of new components of the spectrum, under all circumstances.

An examination of this group of phenomena leads also to other conclusions. Thus, it can be stated that, in any refractive medium, a high-speed radiator of arbitrary natural frequency cannot overtake fully the light it radiates, no matter what its velocity of motion.

2. CONDITIONS FOR THE OCCURRENCE OF RADIATION OF COMPLEX COMPOSITION

For a more detailed examination of the problem of the spectrum of radiated frequencies, we used a graphical method, somewhat modified from the one used previously for this same purpose.[1]

We write Eqs. (1.1) – (1.3) in such a form that the left side contains the quantity $\omega_0 n(\omega_\theta)/c$ (in the case of Eq. (1.1) we multiply the left and right halves by ω_θ):

$$\frac{1}{c} \omega_0 n(\omega_0) = \frac{\omega_0 - \omega_\theta}{v \cos \theta}, \quad n(\omega_0) \beta \cos \theta < 1; \tag{2.1}$$

$$\frac{1}{c} \omega_0 n(\omega_0) = \frac{\omega_\theta + \omega_0}{v \cos \theta}, \quad n(\omega_0) \beta \cos \theta > 1; \tag{2.2}$$

$$\frac{1}{c} \omega_0 n(\omega_0) = \frac{\omega_0}{v \cos \theta}, \quad n(\omega_0) \beta \cos \theta = 1. \tag{2.3}$$

These equations have a simple physical meaning: they result from the law of conservation of momentum in the emission of a photon. This becomes obvious immediately if the right and left sides of all equations are multiplied by $\hbar \cos \theta$. We then obtain on the left sides of all equations $(n\hbar\omega_\theta/c) \cos \theta$, i.e., the projection of the momentum of the emitted photon on the direction of motion of the radiator. As to the quantity on the right side of the equation, it is easy to verify that it equals the momentum given up by the moving system to radiation. Actually, in all cases this is the quantity ΔE, consumed in radiation from the kinetic energy of motion, divided by the velocity v. For example, in (2.1) we have on the right side $(\hbar\omega_\theta - \hbar\omega_0)/v$, i.e., 1/v times the difference between the energy of the radiated photon and the energy of transition to the excited state. Obviously, this difference comes from the kinetic energy. As to Eq. (2.2) the distinguishing feature of the faster-than-light Doppler effect is that the emission of the photon is accompanied by the excitation of the

*The published text of the Mandel'shtam lectures[2] covers this briefly and not clearly enough. See also reference 3.

system.[3] This is why the kinetic energy loses an amount equal to $\hbar\omega_\theta + \hbar\omega_0$. The right half of Eq. (2.3) is obvious and requires no explanation.

The change in momentum accompanying a small change in kinetic energy, as is well known, satisfies the relation

$$\Delta p = \Delta E / v. \tag{2.4}$$

Thus, Eqs. (2.1) – (2.3) really follow from the law of conservation of energy and momentum, while (1.1) – (1.3) can be considered as their consequences.

Let us note also that Eq. (2.3) is a particular case of Eqs. (2.1) and (2.2). It corresponds, as expected, to the case of a radiator field that is stationary with time, i.e., $\omega_0 = 0$. It is obvious that (2.1) and (2.2) can be satisfied for $\omega_0 = 0$ only if the inequality sign on the right side is replaced by an equal sign. The difference between (2.1) and (2.2) is also not of fundamental nature: one equation is derivable from the other by reversing the sign of ω_0 or ω_θ, which, from the wave point of view, means merely reversal of the phase of the oscillation. Thus, Eqs. (2.1) – (2.3) can be considered as different cases of the same relation.

The field of any radiator moving uniformly in the medium can be expanded into a spectrum of natural frequencies $\omega_0' = \omega_0/\sqrt{1-\beta^2}$. Therefore, the corrolaries of Eqs. (2.1) – (2.3), which remain valid for arbitrary ω_0', are also correct for any spectrum of frequencies ω_0', i.e., they include the general case of radiation during uniform motion in a medium.*

Figure 1 shows graphically the magnitude of the wave vector

$$k(\omega) = \omega n(\omega)/c \tag{2.5}$$

as a function of ω. The curve k (ω) divides (provided n (ω) > 0) the portion of the plane bounded by the positive coordinate axis, into two regions: region I below the curve k (ω), and region II above it.

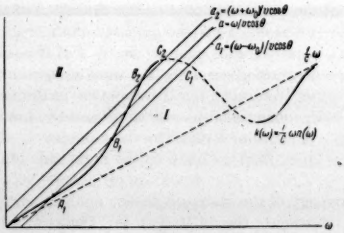

FIG. 1

The same diagram shows the straight lines that satisfy the following equations

$$a_1 = (\omega - \omega_0)/v\cos\theta, \tag{2.6}$$

$$a_2 = (\omega + \omega_0)/v\cos\theta, \tag{2.7}$$

$$a = \omega/v\cos\theta. \tag{2.8}$$

The intersections of these lines with the curve k (ω) obviously yield values of ω_θ satisfying (2.1), (2.2), and (2.3) respectively, i.e., yielding the Doppler frequencies in the medium under consideration for given κ_0, v, and θ, and yielding the frequency of the Vavilov-Cerenkov radiation for given v and θ.

For convenience in the analysis, the same values of v and θ are used in all three cases of Fig. 1. Therefore all three straight lines are parallel and inclined to the ω axis at an angle $\alpha = \tan\varphi = 1/v\cos\theta$ (Fig. 1 shows the case $0 \le \theta \le \pi/2$, i.e., $\cos\theta > 0$).

The character of the intersection of the lines a with the curve k (ω) may vary. If one moves along a straight line in the direction of increasing ω, the line may go at the point of intersection from region I into region II, provided the slope of the tangent to the curve k (ω) i.e., dk/dω is less than $\alpha = 1/v\cos\theta$. To the contrary, if $dk/d\omega > 1/v\cos\theta$, a transition from II into I occurs at the intersection point. Finally, $dk/d\omega = 1/v\cos\theta$ corresponds, obviously, to tangency (from the inner or outer side).

The slope of the tangent to the curve k (ω) is, as is obvious from (2.5), the reciprocal of the group velocity of light for the frequency ω:

$$\frac{d}{d\omega}k(\omega) = \frac{1}{c}\frac{d}{d\omega}\omega n(\omega) = \frac{1}{w(\omega)}. \tag{2.9}$$

Thus, we have three cases:

$v\cos\theta / w(\omega_0) < 1$	transition from I to II	(2.10)
$v\cos\theta / w(\omega_0) > 1$	transition from II to I	(2.11)
$v\cos\theta / w(\omega_0) = 1$	tangency	(2.12)

A transition from I to II or from II into I can occur also at the point of tangency (tangency at a point of inflection). In principle, therefore, the equal sign is also possible in Eqs. (2.10) and (2.11). Actually, however, the angle θ is always specified with accuracy to certain very small but finite $\Delta\theta$, which defines a certain frequency interval $\Delta\omega$, for which the quantity w is indeed determined. If the tangency occurs at a point of inflection, then at neighboring points, on the right or on the left, the quantity w satisfies the particular inequality sign

*In particular, the path along which the radiation occurs may be bounded. This corresponds to a frequency spectrum at which the field vanishes outside a specified time interval.

that characterizes the corresponding intersection. Thus, when averaged over the angular interval $\Delta\theta$, the inequality assumes a definite sign and the equal sign can be discarded.

For the same reason, Eq. (2.12) implies that the tangency occurs without intersection. In this case when going through the point of tangency the inequality reverses its sign, and consequently, averaged over a small $\Delta\theta$, we can consider the equal sign to hold.

Part of the curve $k(\omega)$ is shown dotted in Fig. 1 (and in the analogous Fig. 2). In this frequency region it is incorrect to identify the derivative to the curve $k(\omega)$ with the reciprocal of the group velocity. This region, which includes also the region of negative w (if it exists), corresponds to the frequency interval at which the absorption of light cannot be neglected. In this case, as is known, the quantity defined by (1.5) cannot be given the meaning of a group velocity of light.

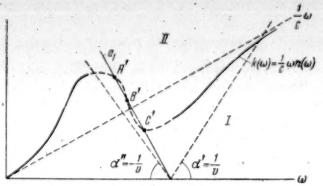

FIG. 2

The foregoing pertains only to the physical meaning of the derivative of $k(\omega)$. As to the curve itself, it retains its meaning in the entire region of variation of ω, provided n is taken to mean its real part and its intersections with the straight lines, a, give the values of the radiated frequencies. We shall not exclude from consideration the region of negative w, since in principle such values are possible, although in an isotropic refractive medium this case is not realizable outside the strong-absorption region.

Let us discuss the consequences that result from an examination of Fig. 1 and Eqs. (2.10) — (2.12). At sufficiently large ω, $n(\omega)$ approaches unity and, consequently, the slope of the curve $k(\omega) = \omega n(\omega)/c$ is equal to $[1/w]_{\omega\to\infty} = 1/c < 1/v \cos\theta$ for $\theta \le \pi/2$. Consequently, at sufficiently large values of ω, all the three straight lines a lie in region II. The line a_1, the intersection of which with $k(\omega)$ determines the frequencies of the ordinary Doppler effect [Eqs. (1.2) or (2.1)], intercepts the abscissa axis at $\omega = \omega_0$, and consequently lies in region I. Therefore the line a_1 must have at least one intersection accompanied by a transition from region I to region II (for example A_1 or C_1 in Fig. 1). This is true not only for $\cos\theta \ge 0$, i.e., $\theta \le \pi/2$, shown in Fig. 1, but for all $0 \le \theta \le \pi$. When θ increases from 0 to π, the slope of the line a_1 ranges from $\alpha' = +1/v$ to $\alpha'' = -1/v$ (see dotted lines, Fig. 2). It is seen from Fig. 2 that when $\cos\theta < 0$ the line a_1 must intersect the curve $k(\omega)$.

Thus, for any velocity v, for any angle θ, and for any natural frequency ω_0 there must be at least one Doppler frequency satisfying (1.2) and satisfying, in addition, (2.10).

The Doppler effect may be complex, since this frequency may be accompanied by several other frequencies (crossings B_1 and C_1, Fig. 1 or B′ and C′, Fig. 2). The number of such additional frequencies must be even, since they should be due to an equal number of crossings from regions I into II and from II into I (in the limiting case of tangency, they may become equal to each other). Thus, the complex Doppler effect is known to occur if there is at least one crossing from II into I or a tangency of the line a_1 to the curve $k(\omega)$ from the outside or from the inside. From this we get that the condition for the occurence of the complex Doppler effect is the presence of a Doppler frequency for which, according to (2.11) or (2.12)

$$v\cos\theta / w(\omega_0) \ge 1. \qquad (2.13)$$

From an examination of Fig. 2 we can conclude that all the above pertains to the case of obtuse angles θ. For the complex Doppler effect to occur in this case, Eq. (2.13) must be satisfied. Since $\cos\theta < 0$ when $\theta > \pi/2$, this is possible only for a group velocity that has a negative absolute magnitude, less than $|v\cos\theta|$. In this case, if the frequency splits up, the larger frequency satisfies inequality (2.10).

A complex Doppler effect may also result from the appearance of faster-than-light Doppler components. The line a_2 which determines these frequencies at small values of ω, as well as at large ω, lies in region II and therefore cannot in general cross the curve $k(\omega)$. This is understandable, since unlike ordinary frequencies, which occur always, faster-than-light Doppler frequencies are supplementary and occur only under certain conditions, and naturally, only for acute angles θ. However, if a_2 does cross $k(\omega)$, it does so in at least two points (in general as even number), since every time the line a_2 passes from II into I, it crosses back from I into II at large frequencies. The former transitions are satisfied by (2.11) while

the transition corresponding to the higher frequency obeys (2.10). In the limiting cases the intersection is replaced by tangency, i.e., a pair of such frequencies becomes one. Thus, the threshold for the occurence of the faster-than-light Doppler effect is (1.7). For each given θ, the faster-than-light Doppler effect is always complex, and contains a component that satisfies (2.13).

It follows, therefore, that satisfaction of condition (2.13) for any Doppler frequency is a necessary and sufficient condition for the complex Doppler effect to occur. This indeed is the previously derived condition for the occurence of the complex Doppler effect,[1] expressed in a somewhat more general form.

The foregoing can be readily generalized to include Vavilov-Cerenkov radiation. For large ω, as indicated, the line a lies in region II. At small ω (excluding from consideration the point $\omega = 0$), the line may lie either above or below the curve $k(\omega)$. In the former case there must be an intersection with a crossing from I to II, i.e., light is radiated in the direction θ with a frequency for which condition (2.10) holds. In addition to this frequency, there can exist an even number of supplementary frequencies, determined by the equal number of crossings from I to II and from II to I.

In the second case there may be no crossing, i.e., the condition for the occurence of the Vavilov-Cerenkov effect for a given θ is not satisfied for any of the frequencies. If crossings do occur, there are at least two (in general an even number), and after each crossing from II into I there occurs, at large θ, a crossing from I into II.

The threshold of the Vavilov-Cerenkov effect or of new additional radiation components remains, obviously, the tangency of the line a to the curve $k(\omega)$, i.e., (2.12) or, what is the same, (1.7). The complex effect is certain to occur if a component exists for which condition (2.11) is satisfied. In the limiting case, when the inequality goes into the equality (2.12), these components merge into a dual frequency.

We note that it is precisely the complex Vavilov-Cerenkov effect that is observed in the experiments. Actually, the Vavilov-Cerenkov effect is practically always observed in the visible or near-ultraviolet region of the spectrum. This is a region of normal dispersion, in which $w < c/n$. Since, according to (1.1), we have in the case of the Vavilov-Cerenkov radiation $c/n = v \cos\theta$, consequently, for the radiated frequency, $w(\omega) < v \cos\theta$. The frequencies paired with the observed one lie in the ultraviolet portion of the spectrum, in the region of anomalous dispersion, and are not observed because of the strong absorption.

Thus, the foregoing relations between the value of the group velocity and the velocity of motion are common for all radiators moving uniformly in space. One must not forget here that these relations are meaningful only when the group velocity satisfies the corresponding Doppler condition (1.2) – (1.3) or condition (1.1) for the Vavilov-Cerenkov effect. These conditions may be expressed in terms of the magnitude of the group velocity if they are represented in the form of an integral equation. Actually, Eqs. (2.1) – (2.3) can obviously be written

$$\int_0^{\omega_0} \left(\frac{1}{w(\omega)} - \frac{1}{v\cos\theta}\right) d\omega = \pm\frac{\omega_0}{v\cos\theta}. \qquad (2.14)$$

Here $w(\omega)$ means a value of $d\omega/dk$ equal to the group velocity in the absence of absorption. The minus sign corresponds to the ordinary Doppler effect, the plus sign to the faster-than-light effect, and $\omega_0 = 0$ corresponds to the Vavilov-Cerenkov effect.

If the Doppler effect is complex, then for any pair of Doppler frequencies ω'_θ and ω''_θ of the same type, i.e., ordinary or faster-than-light frequencies, we obtain directly from (2.14)

$$\int_{\omega'_\theta}^{\omega''_\theta} \left(\frac{v\cos\theta}{w(\omega)} - 1\right) d\omega = 0, \qquad (2.15)$$

or

$$\left(\frac{1}{w}\right) = \frac{1}{\omega''_\theta - \omega'_\theta}\int_{\omega'_\theta}^{\omega''_\theta} \frac{1}{w(\omega)}\, d\omega = \frac{1}{v\cos\theta}. \qquad (2.16)$$

Thus, the mean value $1/w$ over the interval of ω, contained between the Doppler frequencies ω'_θ and ω''_θ, is always equal to $1/v \cos\theta$.

We note that Eqs. (2.15) and (2.16) do not contain ω_0 and, consequently, are valid both for the Doppler effect and for the Vavilov-Cerenkov radiation.

If one of the radiated frequencies is known, for example ω'_θ, then, considering ω''_θ as the variable in (2.16) or (2.17) it is possible to determine in principle all the remaining frequencies of a given type.

3. CONNECTION BETWEEN THE VELOCITY OF THE RADIATOR AND THE GROUP VELOCITY OF LIGHT

Based on the foregoing, it still remains quite unclear why the resultant relations refer specifically to the projection of the velocity of the radiator and the direction of the beam. This can be ex-

plained as follows. It is obvious that the spectrum of the frequencies radiated in the direction θ is given by the quantity ω_0 and by the product $v \cos \theta$. We obtain the same frequency spectrum at a velocity $v' = v \cos \theta$ and the same value of ω_0. (The natural frequency of the system should be changed in this case, since $\omega_0 = \omega_0' \sqrt{1-\beta^2}$). It corresponds to forward radiation if $v' > 0$, i.e., $\cos \theta > 0$, or to backward radiation if $v' < 0$, i.e., $\cos \theta$ is negative. If we disregard the case when the angle θ has the threshold value for the production of radiation, we find, from the fact that a component satisfying (2.10) always exists, that the radiation spectrum should contain a frequency for which

$$v' / w(\omega') < 1. \qquad (3.1)$$

Let v' be positive. This means that the light emitted forward should have a frequency such that the group velocity is greater than the velocity of motion. Thus, in the case of forward radiation the radiated energy must outpace the motion of the source.

Let us assume that v' is negative. Condition (3.1) it is satisfied in this case for all $w > 0$. Thus, no limitations are imposed on the group velocity of the light radiated backwards.

The consequences of inequality (3.1) can be extended to include also the case of negative group velocity. This case deserves a special analysis and we shall treat it here only briefly,* At negative group velocities the directions of the phase and group velocities are opposite. If radiation does take place, i.e., energy is carried away, the group velocity should be directed along the ray drawn from the radiator and consequently the phase velocity should be directed towards the radiator. Fig. 3a shows the picture obtained when $w < 0$ for an acute angle θ (as before, θ is the angle between the direction of the phase velocity u and the velocity of the radiator v). It is seen from Fig. 3a that the radiated energy makes in this case an acute angle $(\pi - \theta)$ to the direction of the velocity. Figure 3b shows the case $\theta = \theta_1 > \pi/2$. In this case the energy is obviously carried away at an acute angle $(\pi - \theta_1)$ to the direction of motion.

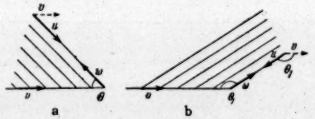

FIG. 3

Let us turn now to the consequences of inequality (3.1) at negative w. The angle $\theta < \pi/2$ corresponds to positive v'. Inequality (3.1) will be fulfilled in this case for any negative w. In this case the energy is carried away, as we have seen, backward and no conditions whatever, as before, are imposed on its removal.

The quantity w can be negative also when $v' < 0$, corresponding to $\theta_1 > \pi/2$. In this case condition (3.1) is satisfied only if the absolute value of w is greater than that of v'. Since the energy is carried away forward in this case, this means that here too we have a case when the velocity of energy propagation outpaces the velocity of the radiator.

In our analysis we went from radiation at an angle θ to the direction of the velocity to forward radiation at the same frequency, i.e., to $\theta = 0$. Obviously, we can proceed in an opposite sequence Were the radiation in a forward direction to contain no components that outpace the radiator, then for the same ω_0 and $v \cos \theta = v'$, we would find that there exists no component satisfying (2.10), which, as we have seen, is impossible.

Complex radiation effects are accompanied by the appearance of components or a component satisfying (2.11). Such an anomalous component must be accompanied by a normal one, satisfying (2.10) and having a higher frequency at that. Thus, the normal component that outpaces the radiator carries more energy per unit frequency interval than the anomalous one.

The relations between the quantity $v \cos \theta$ and the group velocity are a direct consequence of the fact that the radiator cannot overtake fully the light signal that it radiates in the direction of its own motion.

Condition (2.12), corresponding to a threshold of appearance or vanishing of the frequencies, means for $\theta' = 0$ that the group of waves moves at the same velocity as the radiator. Obviously, in this case there is no radiation, merely the motion of the field with the radiator. That this is a threshold case at $\theta' = 0$ is almost obvious.

No conditions whatever were imposed in this analysis on the value of ω_0 and on the corresponding initial phase of the oscillations. Thus the spectrum of ω_0 is arbitrary and, consequently, everything said here concerning the role of the group

*Certain features connected with negative group velocity for the Vavilov-Cerenkov effect in crystals are discussed by V. E. Pafomov.[4]

velocity applies also for any source of light uniformly moving in a refractive medium.

[1] I. M. Frank, Izv. Akad. Nauk SSSR, Ser. Fiz. **6**, 3 (1942).

[2] L. I. Mandel'shtam, Collected Works, U.S.S.R. Acad. Sci. Press, vol 5, p 456.

[3] V. L. Ginzburg and I. M. Frank, Dokl. Akad. Nauk SSSR **56**, 583 (1947).

[4] V. E. Pafomov, J. Exptl. Theoret. Phys. (U.S.S.R.) **32**, 366 (1957), Soviet Phys. JETP **5**, 307 (1957).

Translated by J. G. Adashko
148

NON-UNIQUENESS OF THE PHASE SHIFT ANALYSIS OF PROTON-PROTON COLLISIONS

V. S. BARASHENKOV and HUANG NEN-NING

Joint Institute for Nuclear Research

Submitted to JETP editor September 1, 1958

J. Exptl. Theoret. Phys. (U.S.S.R.) **36**, 832-834 (March, 1959)

A method based on the optical model is proposed for the phase shift analysis of p-p collisions at energies $E \lesssim 10$ Bev. The refractive and absorption coefficients for energies $E \sim 1$ Bev are found to be of the same order of magnitude. The calculated differential cross sections for elastic scattering, the total cross section, and the cross section for inelastic processes agree with experiment.

THE analysis of nucleon-nucleon scattering experiments at high energies on the basis of the phenomenological optical model has been the subject of many papers.[1-4] In references 1,* 2, and 4 it is assumed that the real part of the complex phase η_l can be neglected in comparison to the imaginary part

$$\operatorname{Re}\eta_{il} \ll \operatorname{Im}\eta_{il}. \qquad (1)$$

Without assumption (1) the phase shift analysis of the experimental angular distributions becomes exceedingly complicated. No results of such calculations have so far been published.

Since the validity of assumption (1) becomes better as the energy increases owing to the fast increase in the number of possible channels for inelastic processes,[5] we can, for sufficiently high energy $E = E^*$, compute $\eta_l(E^*) \approx i \operatorname{Im}\eta_l(E^*)$ and the corresponding spatial distribution of the absorption coefficient $K = K(E^*; r)$ by the method described in reference 6. The refractive coefficient is then

$$N(E^*; r) = 1 + N_0(E^*; r) \approx 1.$$

Applying the optical model to the interaction of nucleons with nuclei, we can write the coefficients $K(E; r)$ and $N_0(E; r)$ in the form

$$K(E; r) = k(E)\rho(r), \quad N_0(E; r) = n(E)\rho(r), \qquad (2)$$

where $\rho(r)$ is the nuclear matter density. For nucleon-nucleon interactions relation (2) is not satisfied in general, since the refraction and absorption coefficients in different regions of the nucleon describe an interaction between different kinds of particles. For example, the energy dependence of $K(E; r)$ may be notably different for central collisions and for grazing collisions, where only the pion clouds interact with each other. However, it can be assumed that for energies < 10 Bev, where the wave length λ is still large, it is admissible within the present-day experimental errors to write the experimental coefficients $K(E; r)$ and $N_0(E; r)$, averaged over the internal structure of the nucleon, in the form (2).

Let us now consider the relative coefficients of absorption, k, and refraction, n:

$$K(E; r) = k(E)K(E^*; r);$$
$$N(E; r) = n(E)K(E^*; r), \qquad (3)$$

where $K(E^*; r) \equiv K^*(r)$ is the average coefficient computed by Grishin;[4] $E^* = 6.15$ Bev. The imaginary and real parts of the phase shift $\eta_l(E)$ can then be determined from the equations

$$\sigma_{in} = \pi\lambda^2 \sum_{l=0}^{\infty} (2l+1)[1 - \exp(-4k\eta_{il}^*)],$$
$$\sigma_t = 2\pi\lambda^2 \sum_{l=0}^{\infty} (2l+1)[1 - \exp(-2k\eta_{il}^*)\cos(2n\eta_{il}^*)], \qquad (4)$$

where

$$\eta_{il}^* = \int_0^{\infty} K^*\left(\sqrt{\lambda^2 l(l+1) + s^2}\right) ds, \qquad (5)$$

and σ_t and σ_{in} are the experimental values of the total cross section and the cross section for all inelastic processes in p-p collisions at the energy E.

The results of the calculation are listed in Table I. In accordance with the results obtained at Dubna,[7] we set $\sigma_t = 30 \times 10^{-27}$ cm^2 and $\sigma_{in} =$

TABLE I

E, Bev	1.5	2.24	2.75	4.40	6.15	10.0
$k \cdot 10^{13}$ cm	1.28	1.16	1.16	1.02	1.00	0.94
$n \cdot 10^{13}$ cm	1.48	1.36	1.10	0.52	0.0	0.050

*We thank the authors of reference 1 for sending us the manuscript before publication.

23.0×10^{-27} cm^2 at the energy E = 10 Bev; the cross sections for the other energies are the same as in the paper by Grishin, Saitov, and Chuvilo.[3]

It follows from Table I that condition (1) is not valid for our kind of phase shift analysis in the region of energies of the order of a few Bev. However, we do have the relation Re F < Im F in this energy region. This can be seen from Table II, where we list the computed values of the ratio $\nu(\theta) = \text{Re } F(\theta)/\text{Im } F(\theta)$ for $\theta = 0°$ and $\theta = 10°$. The values of σ_t [see formula (4)] are therefore less sensitive to the choice of n than to the choice of k. At E = 10 Bev the computed value of n is ≈ 0. This confirms our assumption that $n(E^*) = 0$.

TABLE II

E, Bev	1.5	2.24	2.75	4.40	6.15	10.0
ν (0)	0.47	0.45	0.44	0.31	0.00	0.036
ν (10)	0.47	0.46	0.42	0.29	0.00	0.031

Using the values of the coefficients k and n of Table I and the values of K*(r) from the paper by Grishin,[4] we calculated the angular distribution $d\sigma/d\Omega$ of the elastically scattered protons. The results of this calculation are shown in the figure.

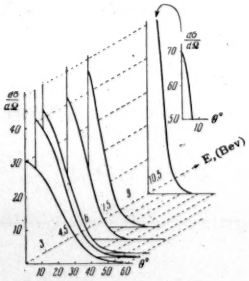

Differential cross sections for the elastic scattering of protons in the center of mass system in mbn/sterad.

The theoretical and experimental values are in satisfactory agreement within the experimental limits of error (for the bibliography see references 3 and 4).*

*There is a small discrepancy between the computed and experimental distributions in the small angle region at E = 2.24 Bev. This comes from the fact that we used the average experimental value of σ_t for the calculation of n(E). The angular distribution agrees better with experiment, if one chooses for σ_t a value which is closer to the lowest experimental value $\sigma_t = (44.1 \pm 4) \times 10^{-27}$ cm^2.

All the presently available experimental results can in this way be adequately described on the basis of quite different assumptions about the magnitude of the phase shifts. However, in our opinion the phase shifts calculated by formulas (3) to (5) are preferable to those calculated on the basis of assumption (1). Our assumptions include condition (1) as a special case and define the limits of its applicability. Even in this case the results depend, of course, on the values of σ_t and σ_{in} used (within the experimental errors).

For a definite conclusion one needs more exact measurements of the angular distributions at energies of ~ 1 to 3 Bev.

We thank D. I. Blokhintsev for a discussion of various questions on the optical model and for comments on the results, and also I. V. Chuvilo for a discussion of the results and valuable critical comments.

[1] Ito, Minami, and Tanaka, Nuovo cimento **8**, 135 (1958).

[2] V. G. Grishin and I. S. Saito, J. Exptl. Theoret. Phys. (U.S.S.R.) **33**, 1051 (1957); Soviet Phys. JETP **6**, 809 (1958).

[3] Grishin, Saitov, and Chuvilo, J. Exptl. Theoret. Phys. (U.S.S.R.) **34**, 1221 (1958); Soviet Phys. JETP **7**, 844 (1958).

[4] V. G. Grishin, J. Exptl. Theoret. Phys. (U.S.S.R.) **35**, 501 (1958); Soviet Phys. JETP **8**, 345 (1959).

[5] Barashenkov, Barbashev, Bubelov, and Maksimenko, Nucl. Phys. **5**, 17 (1957); Nuovo cimento **8**, Suppl. 1; V. S. Barashenkov and V. M. Maltsev, Acta Phys. Polon. **17**, 177 (1958).

[6] Blokhintsev, Barashenkov, and Grishin, Nuovo cimento **9**, 249 (1958). J. Exptl. Theoret. Phys. (U.S.S.R.) **325**, 311 (1958); Soviet Phys. JETP **8**, 215 (1959).

[7] V. Banník et al., Communication at the Conference on High Energy Physics at Geneva, June 1958.

Translated by R. Lipperheide
149

RADIATION FROM A CURRENT-CARRYING RING MOVING UNIFORMLY IN A PLASMA SITUATED IN A MAGNETIC FIELD

L. S. BOGDANKEVICH

P. N. Lebedev Physics Institute, Academy of Sciences, U.S.S.R.

Submitted to JETP editor September 2, 1958; resubmitted December 22, 1958

J. Exptl. Theoret. Phys. (U.S.S.R.) **36**, 835-838 (March, 1959)

Energy losses due to Vavilov-Cerenkov radiation are computed for a current-carrying ring moving uniformly in a plasma perpendicular to its plane and parallel to the external magnetic field.

It is known that the Vavilov-Cerenkov effect is possible in a plasma placed in a magnetic field. The problem of the radiation from a charge moving uniformly in a magnetized plasma has been discussed in detail by Kolomenskii.[1,2] In connection with the coherent method of acceleration of charged particles proposed by V. I. Veksler[3] it is of interest to investigate the radiation from a current filament in an active an isotropic medium. Morozov[4] has obtained the radiation from an infinite current in a plasma in a magnetic field. In this paper we investigate the radiation from a ring current.

We consider a perfectly conducting ring of radius a and carrying a current I_0 moving in a plasma placed in a magnetic field. The velocity of the motion of the ring is perpendicular to the plane of the ring and is parallel to the externally applied magnetic field (which we later choose for the direction of the z axis).

If the external magnetic field is considerably greater than the field produced by the ring itself, then the electron plasma behaves as a gyrotropic crystal whose properties are described by the dielectric constant tensor

$$\tilde{\varepsilon} = \begin{pmatrix} \varepsilon & -i\gamma_i & 0 \\ i\gamma_i & \varepsilon & 0 \\ 0 & 0 & \varepsilon_z \end{pmatrix},$$

$$\varepsilon = (\omega^2 - \omega_0^2 - \omega_H^2)/(\omega^2 - \omega_H^2);$$

$$\varepsilon_z = 1 - (\omega_0/\omega)^2; \quad \gamma_i = \omega_0^2\omega_H/\omega(\omega^2 - \omega_H^2);$$

$$\omega_0^2 = 4\pi e^2 N/m, \quad \omega_H = eH/mc. \tag{1}$$

To obtain the field of the moving ring it is necessary to solve the following system of equations for the potentials

$$\Delta\mathbf{A} - \frac{1}{c^2}\frac{\partial^2}{\partial t^2}(\tilde{\varepsilon}\mathbf{A}) - \operatorname{grad}\operatorname{div}\mathbf{A} = -\frac{4\pi}{c}\mathbf{j} + \frac{\tilde{\varepsilon}}{c}\operatorname{grad}\frac{\partial\varphi}{\partial t},$$

$$(\nabla\tilde{\varepsilon}\nabla)\varphi = -4\pi\rho$$

subject to the subsidiary condition

$$\operatorname{div}(\tilde{\varepsilon}\mathbf{A}) = 0.$$

Since the current-carrying ring is moving perpendicularly to its own plane, then $\rho = 0$ and we may set $\varphi = 0$. Consequently it is necessary to find the solution of the equation

$$\Delta\mathbf{A} - \frac{1}{c^2}\frac{\partial^2}{\partial t^2}(\tilde{\varepsilon}\mathbf{A}) - \operatorname{grad}\operatorname{div}\mathbf{A} = -\frac{4\pi}{c}\mathbf{j}.$$

The solution of this equation in general form may be written as follows:[5]

$$\mathbf{A} = -\frac{4\pi}{c}\int\Lambda^{-1}\left(\mathbf{j}_\mathbf{k} - \mathbf{k}\frac{(\mathbf{k}\tilde{\varepsilon}\Lambda^{-1}\mathbf{j}_\mathbf{k})}{(\mathbf{k}\tilde{\varepsilon}\Lambda^{-1}\mathbf{k})}\right)e^{i\mathbf{k}\cdot(\mathbf{x}-\mathbf{v}t)}d\mathbf{k}, \tag{2}$$

where

$$\mathbf{j} = \int\mathbf{j}_\mathbf{k}e^{i\mathbf{k}\cdot(\mathbf{x}-\mathbf{v}t)}d\mathbf{k},$$

while the matrices Λ^{-1} and $\tilde{\varepsilon}\Lambda^{-1}$ are of the form:

$$\Lambda^{-1} = \begin{pmatrix} \lambda & -i\lambda_1 & 0 \\ i\lambda_1 & \lambda & 0 \\ 0 & 0 & \lambda_2 \end{pmatrix}, \qquad \tilde{\varepsilon}\Lambda^{-1} = \begin{pmatrix} p & -ip_1 & 0 \\ ip_1 & p & 0 \\ 0 & 0 & p_2 \end{pmatrix},$$

$$\lambda = (k^2 - \varkappa^2\varepsilon)/L_1; \quad i_1 = \varkappa^2\gamma_i/L_1;$$

$$\lambda_2 = 1/L_2, \quad p = [\varkappa^2(\gamma_i^2 - \varepsilon^2) + \varepsilon k^2]/L_1$$

$$p_1 = k^2\gamma_i/L_1, \quad p_2 = \varepsilon_z/L_2, \quad L_1 = \gamma_i^2\varkappa^4 - (\varkappa^2\varepsilon - k^2)^2;$$

$$L_2 = \varkappa^2\varepsilon_z - k^2; \qquad \varkappa = \mathbf{k}\cdot\mathbf{v}/c.$$

We shall solve the problem in the cylindrical system of coordinates with the z axis directed along the direction of motion of the ring. Therefore it is convenient to write $\mathbf{j}$ in the form

$$\mathbf{j} = I_0\delta(z - vt)\operatorname{curl}\mathbf{B}_z, \quad \mathbf{B}_z = \mathbf{z}\begin{cases} 1 & r < a, \\ 0 & r > a. \end{cases}$$

Then

$$\mathbf{j} = \frac{iI_0 a}{(2\pi)^3} \int \frac{[\mathbf{k}\times\mathbf{z}]}{k_r} J_1(k_r a)\, e^{ik\,(\mathbf{x}-\mathbf{v}t)} d\mathbf{k}, \qquad (3)$$

$$\mathbf{k} = \mathbf{k}_r + \mathbf{z}\,(\mathbf{k}\cdot\mathbf{v})/v.$$

Vavilov-Cerenkov waves will be radiated when the following condition is fulfilled

$$\mathbf{k}\tilde{\varepsilon}\mathbf{k} = 0.$$

This condition leads to two values n_1 and n_2 for the indices of refraction in the directions of maximum radiation determined by the condition for the Cerenkov radiation:

$$\cos^2\vartheta_{1,2} = 1/\beta^2 n_{1,2}^2;$$

$$n_{1,2}^2 = \frac{1}{2\varepsilon}\Big\{\varepsilon\varepsilon_z + \frac{\varepsilon-\varepsilon_z}{\beta^2} + \varepsilon^2 - \gamma_i^2 \pm \Big[\Big(\varepsilon\varepsilon_z + \frac{\varepsilon-\varepsilon_z}{\beta^2} + \varepsilon^2 - \gamma_i^2\Big)^2 + 4\varepsilon\Big[\frac{\varepsilon\varepsilon_z}{\beta^2} + (\gamma_i^2 - \varepsilon^2)\Big(\varepsilon_z + \frac{1}{\beta^2}\Big)\Big]^{1/2}\Big]\Big\}. \qquad (4)$$

On substituting (3) into (2) and on integrating over φ and k_r, we can obtain expressions for the components of the vector potential **A** which we do not give here. We simply note that the optical activity of the medium leads to the appearance of the components A_r and A_z, which are absent when the current-carrying ring is moving in an inactive medium.[4]

The power losses in the form of Vavilov-Cerenkov radiation are given by

$$P = 2\pi a I_0 E_\varphi|_{r=a,\ z=vt}.$$

As a result of some calculation we obtain

$$P = \frac{4\pi^2 a^2 I_0^2}{c^2}\frac{1}{v}\,\mathrm{Re}\times\Big\{\int\limits_{n_1^2\beta^2>1} \frac{n_1^2-n_0^2}{n_1^2-n_2^2} H_1^{(2)}\Big(\frac{|\omega|}{v}a\sqrt{n_1^2\beta^2-1}\Big) J_1\Big(\frac{|\omega|}{v}a\sqrt{n_1^2\beta^2-1}\Big)\omega d\omega - \int\limits_{n_2^2\beta^2>1} \frac{n_2^2-n_0^2}{n_1^2-n_2^2} H_1^{(2)}\Big(\frac{|\omega|}{v}a\sqrt{n_2^2\beta^2-1}\Big) \times J_1\Big(\frac{|\omega|}{v}a\sqrt{n_2^2\beta^2-1}\Big)\omega d\omega\Big\},$$

$$n_0^2 = \varepsilon_z + \beta^{-2} - \varepsilon_r/\varepsilon_r\beta^2. \qquad (5)$$

The integration extends over the range of frequencies for which $n_{1,2}^2(\omega)\beta^2 \gg 1$.

From (5) we can obtain the energy losses due to radiation from a magnetic dipole with a moment directed parallel to the direction of motion. To do this we set $a \to 0$ and by considering that the magnetic moment is given by $M = \pi a^2 I_0/c$ we obtain

$$P = \frac{M^2}{v^3}\Big[\int\limits_{n_1^2\beta^2>1} \frac{n_1^2-n_0^2}{n_1^2-n_2^2}(n_1^2\beta^2-1)\,\omega^3 d\omega - \int\limits_{n_2^2\beta^2>1} \frac{n_2^2-n_0^2}{n_1^2-n_2^2}(n_2^2\beta^2-1)\,\omega^3 d\omega\Big]. \qquad (6)$$

The magnitude of the indices of refraction $n_{1,2}$ in a plasma placed in a magnetic field is a complicated function of ω, ω_0, ω_H, β. $n_{1,2}$ may be determined by substituting into (4) the specific dependence on ω of $\epsilon(\omega)$, $\epsilon_z(\omega)$, $\eta(\omega)$. It is of interest to note that when a magnetic field is applied to the plasma there exists no frequency for which all the components of the dielectric constant tensor would vanish simultaneously. Therefore in a plasma placed in a magnetic field polarization losses are not possible. Cerenkov losses occur in their place, so that the integral of the losses given by (5) determines the total losses of the ring current due to so-called distant collisions. The conditions $n_{1,2}^2(\omega)\beta^2 \gg 1$ define the range of frequencies radiated. When $\beta \to 1$ waves are radiated whose frequencies lie within the limits

$$\omega_0 < \omega < \sqrt{\omega_H^2 + \omega_0^2}. \qquad (7)$$

When $\beta < 1$ waves of frequency $\omega < \omega_0$ can also be radiated.

Let us now consider the losses accompanying the relativistic motion of the ring. This case is of the greatest interest for the coherent method of accelerating the rings, since it corresponds to the initial instant of acceleration (the inverse of the Vavilov-Cerenkov effect). Taking into account the fact that as $\beta \to 1$ $n_1^2\beta^2 > 1$, $n_2^2\beta^2 < 1$ we are able to obtain in a general form the integral of the losses given by (5), viz.:

$$P = \frac{2\pi^2 a^2 I_0^2 \omega_H^2}{c^3}\Big\{\frac{\omega_0 a}{c}\Big[I_1'\Big(\frac{\omega_0 a}{c}\Big)K_1\Big(\frac{\omega_0 a}{c}\Big) + I_1\Big(\frac{\omega_0 a}{c}\Big)K_1'\Big(\frac{\omega_0 a}{c}\Big)\Big] + \Big(\frac{\omega_0 a}{c}\Big)^2\Big[I_1'\Big(\frac{\omega_0 a}{c}\Big)K_1\Big(\frac{\omega_0 a}{c}\Big) + 2I_1'\Big(\frac{\omega_0 a}{c}\Big)K_1'\Big(\frac{\omega_0 a}{c}\Big) + I_1\Big(\frac{\omega_0 a}{c}\Big)K_1'\Big(\frac{\omega_0 a}{c}\Big)\Big]\Big\}. \qquad (8)$$

From (8) it is easy to obtain the losses for a rarefied plasma and for small rings by utilizing expansions of $I_1(\omega_0 a/c)$, $K_1(\omega_0 a/c)$ in the case $\omega_0 a/c \ll 1$

$$P = 2\pi^2 a^4 I_0^2 c^{-3}\omega_H^2\omega_0^2 \ln(2c/\omega_0 a). \qquad (9)$$

In the case of a magnetic dipole this integral diverges logarithmically as $a \to 0$. This divergence is associated with the fact that the upper limiting frequency $\omega_{\lim} = \sqrt{\omega_H^2 + \omega_0^2}$ for a point dipole

corresponds to zero wave length. Therefore at the upper limit we cannot utilize the results of macroscopic electrodynamics. The integral (6) for a magnetic dipole should be cut off at a certain maximum frequency ω_m. If close collisions are taken into account the total losses will not depend on the indefinite choice of the cutoff parameter ω_m.

For a dense plasma and for rings of large radius, i.e., $\omega_0 a/c \gg 1$ the losses will be given by the following expression:

$$P = \pi^2 a^3 I_0^2 \omega_H^2 \omega_0 / c^4. \qquad (10)$$

One of the characteristic features of the medium under investigation is the possibility of Cerenkov radiation for $\beta \ll 1$. It may be shown that losses due to Cerenkov radiation at nonrelativistic velocities are proportional to β^2

$$P = \frac{\pi^2 I_0^2}{c^2} \left(\frac{a\omega_0}{v}\right)^4 \beta^2 \frac{v\omega_0^2}{\omega_H^2},$$

with $\omega_0 \ll v/a$, $\omega_H > \omega_m > \omega_0$.

In conclusion the author expresses his deep gratitude to Academician V. I. Veksler for suggesting the topic and to B. M. Bolotovskiĭ for valuable advice and suggestions.

[1] A. A. Kolomenskiĭ, Dokl. Akad. Nauk. S.S.S.R. **106**, 982 (1956), Soviet Phys. "Doklady" **1**, 133 (1956).

[2] A. A. Kolomenskiĭ, Report of the Physics Institute, Academy of Sciences, U.S.S.R., 1951.

[3] V. I. Veksler, Атомная энергия (Atomic Energy) **2**, 427 (1957); CERN Symposium on High Energy Accelerators and Pion Physics, Proceedings **1**, Geneva, 1956.

[4] A. I. Morozov, Thesis, Moscow State University, 1957.

[5] B. M. Bolotovskiĭ, Usp. Fiz. Nauk. **62**, 201 (1957).

Translated by G. Volkoff
150

OSCILLATIONS OF A COMPLETELY IONIZED PLASMA IN A CYLINDRICAL CAVITY

L. M. KOVRIZHNYKH

P. N. Lebedev Physics Institute, Academy of Sciences, U.S.S.R.

Submitted to JETP editor September 2, 1958

J. Exptl. Theoret. Phys. (U.S.S.R.) **36**, 839-841 (March, 1959)

Within the framework of magnetohydrodynamics, under the assumption of ideal conductivity, a study has been made of oscillations of a cylindral cavity in a completely ionized plasma located in a magnetic field. It is shown that such a system is stable and that under certain conditions no waves can propagate along the cavity.

THE stability of an ideal conducting gas in a cylinder with respect to small perturbations has been studied by Kruskal and Schwarzschild[1] and by Shafranov.[2]

In the present paper an analogous method will be applied to solve the problem of plasma oscillations in an infinite cylindrical cavity of radius a, containing the conducting medium in a coaxial cylinder of radius a_0, in which a current I_0 is flowing. In the equilibrium state the pressure of the plasma on the cavity boundary is balanced by the magnetic pressure resulting from the surface currents flowing at the plasma-vacuum interface.

The starting point is the system of equations consisting of the magnetohydrodynamic equations for an ideal fluid conductor

$$\rho\, d\mathbf{v}/dt = [\mathbf{j}\times\mathbf{H}]/c - \nabla p;$$

$$\partial\rho/\partial t + \nabla\rho\mathbf{v} = 0, \quad p = \text{const}\cdot\rho^{\gamma}; \tag{1}$$

$$\partial\mathbf{H}/\partial t = \operatorname{curl}[\mathbf{v}\times\mathbf{H}]; \quad \operatorname{curl}\mathbf{H} = 4\pi\,\mathbf{j}/c \tag{2}$$

for the region within the plasma; the equations

$$\mathbf{H} = \nabla\varphi, \quad \Delta\varphi = 0 \tag{3}$$

for the vacuum; and the boundary conditions at the interface,

$$\overline{\mathbf{H}}\{\mathbf{H}\} = -4\pi\{p\}; \quad \mathbf{n}\{\mathbf{H}\} = 0. \tag{4}$$

Here $\overline{\mathbf{H}}$ denotes the mean value of the field at the boundary, and the letters in brackets denote the magnitudes of the discontinuities in the corresponding quantities at the interface, and $\mathbf{n}$ is the unit vector normal to the plasma surface, directed into the plasma. Since this surface moves with the plasma, the relationship

$$dn/dt = [\mathbf{n}\times[\mathbf{n}\times\nabla u]], \quad u = \mathbf{n}\,\mathbf{v}. \tag{5}$$

must be satisfied.

In the equilibrium state $\mathbf{v} = 0$, and the plasma is uniform in the z and φ directions, and the non-zero components of the magnetic field are H_z^0 and H_φ^0. It will be assumed that within the plasma $H_\varphi^0 = 0$ and H_z^0 is uniform, i.e.,

$$H_{\varphi 1}^0 = 2I/cr, \quad H_{\varphi 2}^0 = 0, \quad H_{z1}^0 = \text{const}, \quad H_{z2}^0 = \text{const}, \tag{6}$$

where the indices 1 and 2 denote that the corresponding value of the quantity refers to the cavity and the plasma, respectively. Then according to Eq. (4) we must have

$$H_{z1}'^2 - H_{z2}'^2 + H_{\varphi 1}'^2 = 8\pi p_0. \tag{7}$$

Solving the system (1) and (2) by the method of small oscillations, subject to the boundary conditions (4) and (5), we obtain the desired dispersion relation*

$$\Omega^2 = f_m(\Omega^2, k) = \frac{2}{\gamma'}(k^2 - \Omega^2)\left[h_z^2 - \frac{1}{\zeta}\frac{K_m'(\zeta)}{K_m(\zeta)}\,\alpha_m(k)\right] \tag{8}$$

under the conditions $-\pi/2 < \arg\zeta \le \pi/2$, where

$$\Omega^2 = \frac{\omega^2 a^2}{v_T^2}, \quad v_T^2 = \gamma\frac{p_0}{\rho_0}, \quad \zeta^2 = \frac{(\Omega^2 - k^2)(\Omega^2 - q^2 k^2)}{q^2 k^2 - (1+q^2)\Omega^2},$$

$$q^2 = 2h_z^2/\gamma', \quad \gamma' = \gamma[h_1^2 - h_z^2 + 1],$$

$$h_i = H_{zi}^0/H_\varphi^0, \quad x_0 = a_0/a,$$

$$\alpha_m(k) = \left\{1 + \frac{I_m(k)K_m'(kx_0) - I_m'(kx_0)K_m(k)}{I_m'(k)K_m'(kx_0) - I_m'(kx_0)K_m'(k)}\,\frac{(m+kh_1)^2}{k}\right\}, \tag{9}$$

I_m and K_m being the modified Bessel functions of order m.

It follows from the self-adjoint nature of the operator which occurs in the linearized equation of motion that the expression (8) has no roots in the complex region. Hence in studying this expression it is sufficient to limit ourselves to real values of Ω^2.

*Here we assume, as usual, that all quantities are proportional to $\exp i(kz + m\phi + \omega t)$.

First of all, we observe that, although as Ω^2 varies from zero to $-\infty$ the function $f_m(\Omega^2, k)$ increases monotonically and

$$f_m(0, k) = \frac{2}{\gamma'} k^2 \left[h_2^2 - \frac{1}{k} \frac{K'_m(k)}{K_m(k)} \varkappa_m(k) \right] > 0,$$

yet the dispersion equation has no solution for $\Omega^2 < 0$. Thus Ω is always real, and the system is stable with respect to small perturbations for which $k \neq 0$. However, if $k = 0$, the dispersion equation has the solution $\Omega^2 = 0$ for any arbitrary value of m when $H_\varphi^0 = 0$, but only for $m = 0$ when $H_\varphi^0 \neq 0$; i.e., in this case we have a state of neutral equilibrium.

Let us now consider equation (8) in more detail for the case $\Omega^2 > 0$.

1. $q^2 < 1$, i.e., $v_T^2 > v_H^2 = H_{z2}^{02}/4\pi\rho_0$.

(a) $m = 0$. As the frequency varies from zero to $q^2k^2/(1+q^2)$, the function $f_m(\Omega^2, k)$ decreases, and for $\Omega^2 \to q^2k^2/(1+q^2)$ it tends to the value $q^2k^2/(1+q^2)$; at the same time ζ tends toward infinity. With further increase in the frequency, f_m becomes complex, and then when $\Omega^2 = q^2k^2$ it returns to the real domain again, varying from $+\infty$ for $\Omega^2 = q^2k^2$ to zero when $\Omega^2 = k^2$. In the region $\Omega^2 > k^2$ the function f_m is always complex, i.e., there is no solution. There is therefore only a single branch, coinciding with the acoustic branch at small values of k and q^2.

(b) $m \neq 0$. Just as in the case $m = 0$, the dispersion equation has no roots $\Omega^2 < q^2k^2$. For $\Omega^2 > q^2k^2$ the function f_m is positive, and varies from $+\infty$ at $\Omega^2 = q^2k^2$ to the value

$$f_m(k^2, k) = \frac{2m}{\gamma'} \frac{\alpha_m(k)}{1-q^2} \tag{10}$$

at $\Omega^2 = k^2$, and then becomes complex. Consequently, solutions exist only for those cases where

$$k^2 > f_m(k^2, k), \tag{11}$$

i.e., the only waves which can propagate in the system are those with a wavelength greater than some critical wavelength $\lambda_{cr}^{(m)} = 2\pi/k_{cr}^{(m)}$, where $k_{cr}^{(m)}$ is the smallest root of the equation $k^2 = f_m(k^2, k)$.

In both of the above cases the frequency Ω^2 lies in the interval from q^2k^2 to k^2.

2. $q^2 > 1$. In this case f_m is positive only when $\Omega^2 < q^2k^2/(1+q^2)$. For values of Ω^2 greater than $q^2k^2/(1+q^2)$ the function f_m is either complex or negative; that is, the dispersion equation has no solutions at all.

Thus we have seen that the dispersion equation (8) has no solutions corresponding to acoustic or Alfven waves in a gas. There is only a single mode that vanishes as $q \to 1$. For $q^2 > 1$ no solutions are possible at all; i.e., no wave-like motion is possible.

[1] M. Kruskal and M. Schwarzschild, Proc. Roy. Soc. **A223**, 348 (1954).

[2] V. D. Shafranov, Атомная энергия (Atomic Energy) **5**, 38 (1956).

Translated by D. C. West
151

THEORY OF THE NONLINEAR FIELD $(\Box - \lambda\varphi^2)\varphi = 0$

D. F. KURDGELAIDZE

Moscow State University

Submitted to JETP editor June 9, 1958; resubmitted November 5, 1958

J. Exptl. Theoret. Phys. (U.S.S.R.) **36**, 842-849 (March, 1959)

The nonlinear field described by the equation $(\Box - \lambda\varphi^2)\varphi = 0$ is considered. Starting from the exact wave-type solution of the field equation, the spectral analysis of the energy of the nonlinear field is obtained. The mass spectrum derived has the form $M_0^{(n)} = (2n + 1) M_0^{(0)}$, $n = 0, 1, 2, \ldots$. The exact radially symmetric solution of the field equation is found. A general method of integrating the nonlinear field of Dirac is given, and it is shown that in some cases it is possible to go over to a two-component spinor equation of the second order.

1. THEORY OF THE NONLINEAR FIELD $(\Box - \lambda\varphi^2)\varphi = 0$

We considered the nonlinear field $(\Box - \lambda\varphi^2)\varphi = 0$ in previous papers,[1,2] where a wave solution of the field equation was found and it was shown that a nonlinear state could appear as a superposition of linear states with the integral frequencies $(2n + 1)$, $n = 0, 1, 2, \ldots$. Recently Heisenberg has obtained by different means the mass spectrum of particles, and in particular that of mesons, in a nonlinear theory.[3,4] This spectrum obeys only approximately the $(2n + 1)$ rule; but, as Heisenberg shows, it has the property that the ratio $M_0^{(n)}/M_0^{(0)}$ is almost independent of the nonlinearity parameter, as in the case of the $(2n+1)$ rule. In connection with this, the present paper gives a more detailed derivation of the $(2n+1)$ rule for mass spectra by means of the spectral analysis of the energy of the nonlinear field.

(a) Spectral Decomposition of the Energy of the Nonlinear Field

The Lagrangian of our nonlinear field has the form

$$L = -\frac{1}{2}\left\{\varphi_\mu{}^2 + k_0{}^2\varphi^2 + \frac{1}{2}\lambda\varphi^4\right\},$$

$$\mu = 1, 2, 3, 4. \quad x_4(x_n, x_4 = it), \qquad c = \hbar = 1, \tag{1.1}$$

where, for the sake of generality, the term $k_0^2\varphi^2$ is included.

From Eq. (1.1) we find by the usual methods expressions for the energy and momentum and also obtain the field equation

$$H = \frac{1}{2V}\int\left\{\varphi_n{}^2 - \varphi_4{}^2 + k_0{}^2\varphi^2 + \frac{1}{2}\lambda\varphi^4\right\}(dx), \tag{1.2}$$

$$\mathbf{G} = -\frac{i}{V}\int\varphi_4(\nabla\varphi)\,(dx), \tag{1.3}$$

$$-\varphi_{\mu\mu} + k_0{}^2\varphi + \lambda\varphi^3 = 0. \tag{1.4}$$

In reference 2, the time-averaged energy and momentum densities of the field were calculated, starting from an exact wave-type solution

$$\varphi = \varphi_0\,\mathrm{cn}\,(\sigma + C), \quad \sigma = k_\mu x_\mu, \quad k_\mu(k_n, k_4 = i\omega),$$

$$-k_\mu{}^2 = -k^2 + \omega^2 = k_0{}^2 + \lambda\varphi_0{}^2,$$

$$k_1{}^2 = \lambda\varphi_0{}^2/2\,(k_0{}^2 + \lambda\varphi_0{}^2); \tag{1.5}$$

where φ_0 and C are arbitrary constants and k_1 is the modulus of an elliptic function.

The final results of the calculations are

$$H = a\,(k^2 + K_0{}^2)/\omega, \quad \mathbf{G} = a\mathbf{k}, \quad a = \varphi_0{}^2\omega l/2,$$

$$K_0{}^2 = \frac{1}{l}\left(k_0{}^2 + \frac{1}{2}\lambda\varphi_0{}^2\right),$$

$$l = \frac{2}{3}\left\{2 - (1 - k_1{}^2)\,\frac{1}{k_1{}^2}\left(1 - \frac{E(k_1)}{K(k_1)}\right)\right\}. \tag{1.6}$$

From this, in particular, it follows when $\mathbf{k} = 0$ that

$$H = \frac{1}{2}\varphi_0{}^2\left(k_0{}^2 + \frac{1}{2}\lambda\varphi_0{}^2\right), \tag{1.7}$$

and, as we see, in the case where $k_0 = 0$ the quantity

$$\bar{k}_0{}^2 = \lambda\varphi_0{}^2/2. \tag{1.8}$$

corresponds to the square of the mass in the ordinary case. Now, setting the energy of the field in (1.7) equal to the meson mass $\bar{k}_0$, with $k_0 = 0$, we get

$$\varphi_0{}^2 = 2/\bar{k}_0, \quad \lambda = \bar{k}_0{}^3. \tag{1.9}$$

We then examine the energy spectrum of the nonlinear field. To do this, we write the solution (1.5) in the form $(C = 0)$

$$\varphi_\tau/\varphi_0 = \sum_{n=0}^{\infty} a_n \cos \sigma_n, \quad \sigma_n = (2n+1)\, B(\lambda)\, \sigma = k_\mu^{(n)} x_\mu,$$

$$B(\lambda) = \pi/2K(k_1), \quad a_n = \pi/k_1 K(k_1) \operatorname{ch} \rho_n,$$

$$\rho_n = (2n+1)\rho_0, \quad \rho_0 = \pi K'(k_1)/2K(k_1), \qquad (1.10)$$

where k_1 is the modulus of the elliptic function and $K(k_1)$ is the elliptical integral of the first kind. $K'(k_1) = K(k_1')$, $k_1^2 + k_1'^2 = 1$.

From (1.4) and (1.10) we find

$$\lambda\varphi_\tau^3/\varphi_0 = \sum_{n=0}^{\infty} b_n \cos \sigma_n, \qquad (1.11)$$

where

$$b_n = -(k_0^2 + k_\mu^{(n)2})$$

$$= -\{k_0^2 - (k_0^2 + \lambda\varphi_0^2)(B(\lambda)(2n+1))^2\} a_n. \qquad (1.12)$$

Putting (1.10) – (1.12) into (1.2) and (1.3), we get

$$H = \varphi_0^2 \sum_{n=0}^{\infty} H_n, \quad \mathbf{G} = \varphi_0^2 \sum_{n=0}^{\infty} \mathbf{G}_n, \qquad (1.13)$$

where

$$H_n = \tfrac{1}{2} a_n^2 \omega^{(n)2} \{1 + (k_0^2 + k_\mu^{(n)2})/4\omega^{(n)2}\},$$

$$\mathbf{G}_n = \tfrac{1}{2} a_n^2 \omega^{(n)} \mathbf{k}^{(n)}. \qquad (1.14)$$

We introduce the new amplitude N_n, defined by the formula

$$N_n = a_n^2 \omega^{(n)}/2. \qquad (1.15)$$

Then we have

$$H_n = N_n \omega^{(n)} \{1 + (k_0^2 + k_\mu^{(n)2})/4\omega^{(n)2}\},$$

$$\mathbf{G}_n = N_n \mathbf{k}^{(n)}. \qquad (1.16)$$

From this, for the case $\mathbf{k} = 0$, $k_0 = 0$, we find

$$H_n = \tfrac{3}{4} N_n \omega^{(n)}, \quad \mathbf{G}_n = 0. \qquad (1.17)$$

Further, according to (1.5) and (1.10), we have

$$k_1^2 = \tfrac{1}{2}, \quad K'(k_1) = K(k_1) = 1.85,$$

$$B(\lambda) = \pi/2 \cdot 1.85 = 0.84,$$

$$\rho_0 = \frac{\pi}{2}, \quad a_n = \frac{\pi\sqrt{2}}{1.85} \frac{1}{\operatorname{ch}[\pi(2n+1)/2]} = \frac{2.396}{\operatorname{ch}[\pi(2n+1)/2]},$$

$$(2\sqrt{2}\, a_0)^2 = 7.29, \quad (\sqrt{3}\, B(\lambda)/4)^2 = 0.355. \qquad (1.18)$$

Then we get on rearranging

$$\omega^{(n)} = \sqrt{2}\, B(\lambda)(2n+1)\bar{k}_0 = \sqrt{32/3}\, M_0^{(n)},$$

$$N_n = \tfrac{1}{2} a_n^2 \omega^{(n)} = \frac{1}{16}(2\sqrt{2}\, a_0)^2 \left(\frac{a_n}{a_0}\right)^2 \omega^{(n)}$$

$$= \frac{1}{4}\sqrt{\frac{2}{3}} \left(\frac{K_0}{\bar{k}_0}\right) \left(\frac{a_n}{a_0}\right)^2 M_0^{(n)},$$

$$H_n = \frac{3}{4} N_n \omega^{(n)} = \tfrac{1}{2}(K_0/\bar{k}_0)(a_n/a_0)^2 M_0^{(n)}, \qquad (1.19)$$

where

$$M_0^{(n)} = (2n+1)\, M_0^{(0)}, \quad K_0 = (2\sqrt{2}\, a_0)^2 \bar{k}_0 = 7.29\, \bar{k}_0,$$

$$M_0^{(0)} = (\sqrt{3}\, B(\lambda)/4)^2 \bar{k}_0 = 0.3554\, \bar{k}_0. \qquad (1.20)$$

The total energy of the field then has the form

$$H = \varphi_0^2 (K_0/\bar{k}_0) \sum_{n=0}^{\infty} \tfrac{1}{2} (a_n/a_0)^2 M_0^{(n)2} \qquad (1.21)$$

Calculating (1.9), we find

$$H = \bar{k}_0 \left\{ (K_0/\bar{k}_0) \sum_{n=0}^{\infty} (a_n/a_0)^2 \, (M_0^{(n)}/\bar{k}_0)^2 \right\}. \qquad (1.22)$$

Equating (1.22) and (1.7) for $k_0 = 0$, we get

$$(K_0/\bar{k}_0) \sum_{n=0}^{\infty} (a_n/a_0)^2 \, (M_0^{(n)}/\bar{k}_0)^2 = \frac{3}{2} B^2(\lambda) \sum_{n=0}^{\infty} [(2n+1)a_n]^2$$

$$= \frac{3}{8} \left(\frac{\pi}{\sqrt{k_1 K(k_1)}} \right)_{k_1^2 = 1/2}^4 \sum_{n=0}^{\infty} \left(\frac{2n+1}{\operatorname{ch}(\pi(2n+1)/2)} \right)^2 = 1. \qquad (1.23)$$

The reader can easily convince himself of the validity of (1.23).

The mesonic mass spectrum we have derived

$$M_0^{(n)}/\bar{k}_0 \approx (2n+1) \cdot 0.36 \qquad (1.24)$$

is listed below. For comparison, Heisenberg's results are also shown

n	0	1	2	3	4	5
From (1.24)	0.36	1.08	1.80	2.52	3.24	3.96
Heisenberg	0.33	0.94	1.74	—	3.32	—

(b) The Radially Symmetric Solution of the Wave Equation

If, for $k_0 = 0$, we examine the solution of (1.4) in the form

$$\psi = \psi(s), \quad s = \sqrt{x_\mu^2}, \quad \mu = 1, 2, 3, 4, \qquad (1.25)$$

the field equation becomes

$$\frac{d^2\psi}{ds^2} + \frac{3}{s}\frac{d\psi}{ds} + \lambda\psi^3 = 0, \qquad (1.26)$$

the solution of which is

$$\psi = \sqrt{\frac{2k_1^2}{\lambda s_0^2 (2k_1^2 - 1)}} \frac{1}{(s/s_0)} \operatorname{cn}\left[\frac{1}{\sqrt{2k_1^2 - 1}} \ln (s/s_0) \right], \qquad (1.27)$$

where s_0 is an arbitrary constant and k_1 is the modulus of an elliptic function. For $k_1^2 = 1$, we get

$$\psi = 2\sqrt{\frac{2}{\lambda s_0^2}} \left/ \left(1 + \left(\frac{s}{s_0}\right)^2\right)\right..$$

2. INTEGRATION OF THE NONLINEAR DIRAC EQUATION

In the linear theory, one can go over from the Dirac equation for a free field to the Klein-Gordon

equation and vice versa. Furthermore, there exists a connection between the solutions of the Dirac equation and those of the corresponding Klein-Gordon equation: if a solution of the Klein-Gordon equation is known, it is then possible to construct a solution of the Dirac equation.

It is shown below that in some sense an analogous situation occurs even in the nonlinear theory. However, as a rule, this dependence has a more complicated nature.

The nonlinear Dirac equation has the following general form:

$$\{\gamma_\mu(\partial/\partial x_\mu + B_\mu(\bar\psi,\psi)) + A(\bar\psi,\psi)\}\psi = 0, \quad (2.1)$$

where

$$x_\mu(x_n, x_4 = it), \quad \gamma_\mu{}^T = \gamma_\mu,$$

$$\gamma_5 = \gamma_1\gamma_2\gamma_3\gamma_4, \quad \gamma_\mu\gamma_\nu + \gamma_\nu\gamma_\mu = 2\delta_{\mu\nu}. \quad (2.2)$$

The functions $A(\bar\psi,\psi)$ and $\gamma_\mu B_\mu(\bar\psi,\psi)$ are scalars constructed from $\bar\psi$, ψ, and the γ_μ matrices in line with invariance requirements. As a rule, they have the form

$$f(\Gamma_\mu(\bar\psi\Gamma_\mu\psi)), \quad \Gamma_\mu = 1,\ \gamma_5,\ \gamma_\mu,\ \gamma_\mu\gamma_5. \quad (2.3)$$

The equation adjoint to (2.1) is

$$\bar\psi\{(\partial/\partial x_\mu + \overline{B}_\mu(\bar\psi,\psi))\gamma_\mu - \overline{A}(\bar\psi,\psi)\} = 0, \quad (2.4)$$

where

$$\bar\psi = \psi^*\gamma_4, \quad \overline{A}(\bar\psi,\psi) = \gamma_4 A^T(\bar\psi,\psi)\gamma_4, \quad \bar\psi\partial/\partial x_\mu \equiv \partial\bar\psi/\partial x_\mu$$

$$\overline{B}_n(\bar\psi,\psi) = \gamma_4 B_n{}^T(\bar\psi,\psi)\gamma_4,$$

$$\overline{B}_4(\bar\psi,\psi) = -\gamma_4 B_4{}^T(\bar\psi,\psi)\gamma_4. \quad (2.5)$$

We introduce the operators

$$\hat p = \gamma_\mu(\partial/\partial x_\mu + B_\mu(\bar\psi,\psi)),$$

$$\hat{\bar p} = (\partial/\partial x_\mu + \overline{B}_\mu(\bar\psi,\psi))\gamma_\mu, \quad (2.6)$$

$$\hat D = -(m\widetilde A/A\widetilde A)\hat p, \quad \hat{\bar D} = -\hat{\bar p}(m\widetilde A/\widetilde A\widetilde A), \quad (2.7)$$

where $A\widetilde A$ is a quantity not dependent on the matrices. For example, for $A = \lambda_1(\bar\psi\psi) + \lambda_2\gamma_5(\bar\psi\gamma_5\psi)$ we would have

$$\widetilde A = \lambda_1(\bar\psi\psi) - \lambda_2\gamma_5(\bar\psi\gamma_5\psi), \quad A\widetilde A = (\lambda_1(\bar\psi\psi))^2 - (\lambda_2\gamma_5(\bar\psi\gamma_5\psi))^2.$$

Then Eqs. (2.1) and (2.4) can be written in the form

$$(\hat D - m)\psi = 0, \quad \bar\psi(\hat{\bar D} + m) = 0. \quad (2.8)$$

We introduce the new functions

$$\psi = \frac{1}{m}(\hat D + m)\varphi, \quad \bar\psi = \bar\varphi(-\hat{\bar D} + m)\frac{1}{m}. \quad (2.9)$$

Then, substituting (2.9) into (2.8), we find

$$(\hat D\hat{\bar D} - m^2)\varphi = 0, \quad \bar\varphi(\hat{\bar D}\hat D - m^2) = 0. \quad (2.10)$$

As we see, (2.8) and (2.10) have exactly the same form with respect to the operator $\hat D$ as in the linear case.

For the transition from the Dirac equation to the Klein-Gordon equation to be complete, the functions $\bar\psi$ and ψ entering into the nonlinear operators $\hat D$ and $\hat{\bar D}$ must be expressed in terms of $\bar\varphi$ and φ. Since it is difficult to carry through the indicated procedure in the general case, we examine a few individual cases

$$1. \quad B_\mu(\bar\psi,\psi) = 0, \quad A(\bar\psi,\psi) = \lambda(\bar\psi\psi). \quad (2.11)$$

We then get

$$\hat D = -\frac{m}{\lambda(\bar\psi\psi)}\gamma_\mu\frac{\partial}{\partial x_\mu}, \quad \hat{\bar D} = -\frac{\partial}{\partial x_\mu}\gamma_\mu\frac{1}{\lambda(\bar\psi\psi)} \quad (2.12)$$

and, correspondingly,

$$\psi = \varphi - \gamma_\mu\frac{\partial\varphi}{\partial x_\mu}\frac{1}{\lambda(\bar\psi\psi)}, \quad \bar\psi = \bar\varphi + \frac{\partial\bar\varphi}{\partial x_\mu}\gamma_\mu\frac{1}{\lambda(\bar\psi\psi)}, \quad (2.13)$$

From this we find

$$(\bar\psi\psi) = \bar\varphi\varphi + \frac{1}{\lambda(\bar\psi\psi)}(\bar\varphi_\mu\gamma_\mu\varphi - \bar\varphi\gamma_\mu\varphi_\mu)$$

$$-(\bar\varphi_\mu\gamma_\mu\gamma_\nu\varphi_\nu)\frac{1}{(\lambda(\bar\psi\psi))^2}, \quad (2.14)$$

that is

$$Y^3 - \lambda(\bar\varphi\varphi)Y^2 - \lambda(\bar\varphi_\mu\gamma_\mu\varphi - \bar\varphi\gamma_\mu\varphi_\mu)Y + \lambda(\bar\varphi_\mu\gamma_\mu\gamma_\nu\varphi_\nu) = 0,$$

$$Y \equiv \lambda(\bar\psi\psi), \quad (2.15)$$

whose solution gives

$$Y = f(\bar\varphi\theta\varphi), \quad (2.16)$$

where θ is some operator. The corresponding Klein-Gordon equation is

$$\left\{\frac{\partial^2}{\partial x_\mu{}^2} - Y^2\left[1 - \frac{1}{2}\left(\frac{\partial}{\partial x_\mu}\frac{1}{Y^2}\right)\gamma_\mu\gamma_\nu\frac{\partial}{\partial x_\nu}\right]\right\}\varphi = 0. \quad (2.17)$$

In particular, if we look at only wave-type solutions, as we did in Sec. 1, we arrive at the results of references 2 and 6. There, for this special case, the reverse problem is also solved and it is shown that the equation $(\Box - \lambda\varphi^2)\varphi = 0$ can be "linearized" to yield the equations

$$\gamma_\mu\frac{\partial\psi}{\partial x_\mu} + \left[c_1 + \frac{\lambda}{2}(\bar\psi\psi)^2\right]^{1/2}\chi(s) = 0, \quad (2.18)$$

where

$$\psi = \chi(s)\varphi(\sigma), \quad \bar\psi = \varphi(\sigma)\overline{\chi}(\sigma), \quad \overline{\chi}\chi = 1,$$

$\chi(s)$ being a constant spinor; s, the spin coordinate; and c_1, an arbitrary constant.

If c_1 is given in terms of φ_0, the amplitude of (1.5), by $c_1 = -\kappa^2\varphi_0^2/2$ where $\kappa^2 = \lambda\varphi_0^2$, we get for the solution of (2.18) $\psi = \chi(s)\varphi(\sigma)$, where $\varphi(\sigma)$ is given by (1.5) and $\chi(s)$ is a solution of the equation $(\gamma_\mu k_\mu - i\kappa)\chi(s) = 0$. Consequently,

the nonlinear field ψ can be represented as a particular combination of the linear states (1.10) with the integral frequencies $(2n+1)$.

It is easy to see that in the given case both (2.1) and (2.17) are invariant with respect to the transformations

$$\varphi \to \gamma_5\varphi, \quad \bar{\varphi} \to -\bar{\varphi}\gamma_5, \tag{2.19}$$

$$\psi \to \gamma_5\psi, \quad \bar{\psi} \to -\bar{\psi}\gamma_5, \tag{2.20}$$

respectively. According to (2.13), the transformation (2.19) induces (2.20) and inversely. Taking this circumstance into account we can, following Feynman, choose the solutions $\psi \equiv \psi_I$, $\varphi \equiv \varphi_I$, satisfying the conditions

$$(1-\gamma_5)\varphi_I = 0, \quad {}^1/_2(1+\gamma_5)\varphi_I = \varphi_I, \quad \bar{\varphi}_I(1+\gamma_5) = 0,$$
$$ {}^1/_2\bar{\varphi}_I(1-\gamma_5) = \bar{\varphi}_I \tag{2.21}$$

$$(1-\gamma_5)\psi_I = 0, \quad {}^1/_2(1+\gamma_5)\psi_I = \psi_I,$$
$$\bar{\psi}_I(1+\gamma_5) = 0, \quad {}^1/_2\bar{\psi}_I(1-\gamma_5) = \bar{\psi}_I. \tag{2.22}$$

Then from (2.13) we have $\varphi_I = \psi_I$, $\bar{\varphi}_I = \bar{\psi}_I$. However, since $(1-\gamma_5)(1+\gamma_5) = 0$, we find

$$(\bar{\psi}\psi) = (\bar{\psi}_I\psi_I) = (\bar{\varphi}\varphi) = (\bar{\varphi}_I\varphi_I) = (\bar{\varphi}_I(1-\gamma_5)\,{}^1/_4(1+\gamma_5)\varphi) = 0.$$

Thus a two-component nonlinear equation is not possible in this case.*

2. Now let us consider the case[5]

$$A(\bar{\psi},\ \psi) = m = \text{const},$$
$$B_\mu(\bar{\psi},\ \psi) = \beta(\bar{\psi}\gamma_\mu\psi),\ \beta = \text{const}. \tag{2.23}$$

Then we have

$$\hat{D} = -\gamma_\mu\left(\frac{\partial}{\partial x_\mu} + \beta(\bar{\psi}\gamma_\mu\psi)\right)\frac{1}{m},$$

$$\hat{\bar{D}} = -\frac{1}{m}\left(\frac{\partial}{\partial x_\mu} - \beta(\bar{\psi}\gamma_\mu\psi)\right)\gamma_\mu \tag{2.24}$$

and, correspondingly

$$\psi = \varphi - \gamma_\mu\left(\frac{\partial}{\partial x_\mu} + \beta(\bar{\varphi}\gamma_\mu\psi)\right)\varphi\,\frac{1}{m},$$

$$\bar{\psi} = \bar{\varphi} + \frac{1}{m}\bar{\varphi}\left(\frac{\partial}{\partial x_\mu} - \beta(\bar{\psi}\gamma_\mu\psi)\right)\gamma_\mu. \tag{2.25}$$

From this we find the equation for $(\bar{\psi}\gamma\mu\psi)$

$$\frac{1}{\beta}Y_\nu + a_{\nu\rho}Y_\rho + b_{\mu\nu\rho}Y_\mu Y_\rho = g_\nu, \tag{2.26}$$

where

$$Y_\nu = \beta(\bar{\psi}\gamma_\nu\psi),$$

$$a_{\nu\rho} = \frac{2}{m}(\bar{\varphi}\partial_{\nu\rho}\varphi) + \frac{1}{m^2}(\bar{\varphi}_\mu\gamma_\mu\gamma_\nu\gamma_\rho\varphi - \bar{\varphi}\gamma_\rho\gamma_\nu\gamma_\mu\varphi_\mu),$$

$$b_{\mu\nu\rho} = -\frac{\beta}{m^2}(\bar{\varphi}\gamma_\mu\gamma_\nu\gamma_\rho\varphi),$$

$$g_\nu = (\bar{\varphi}\gamma_\nu\varphi) + \frac{1}{m}(\bar{\varphi}_\mu\gamma_\mu\gamma_\nu\varphi - \bar{\varphi}\gamma_\nu\gamma_\mu\varphi_\mu)$$
$$-\frac{1}{m^2}(\bar{\varphi}_\mu\gamma_\mu\gamma_\nu\gamma_\rho\varphi_\rho), \tag{2.27}$$

and the Klein-Gordon equation takes the form

$$\left\{\left(\frac{\partial}{\partial x_\mu} + B_\mu\right)\left(\frac{\partial}{\partial x_\mu} + B_\mu\right) - \sigma_{\mu\nu}H_{\mu\nu} - m^2\right\}\varphi = 0, \tag{2.28}$$

where

$$\sigma_{\mu\nu} = {}^1/_2(\gamma_\mu\gamma_\nu - \gamma_\nu\gamma_\mu),\ H_{\mu\nu} = \partial B_\nu/\partial x_\mu - \partial B_\mu/\partial x_\nu, \tag{2.29}$$

$B_\mu = \beta(\bar{\psi}\gamma\mu\psi) \equiv Y_\mu$, the solution of (2.26). It is easy to verify that although the operator of (2.28) does commute with γ_5, nevertheless $\gamma_5\varphi$ is not a solution of (2.28). Equation (2.26) is not invariant under the transformations (2.19), which implies the noninvariance of (2.28) under these transformations.

The transformation (2.19) leads to that of (2.20) [in virtue of (2.13)], only provided that $m \to -m$, just as the invariance of (2.1) relative to (2.20) requires the change $m \to -m$. Therefore, if ψ and φ are solutions of (2.1) and (2.28) for $+m$, $\gamma_5\psi$ and $\gamma_5\varphi$ are solutions for $-m$. We therefore cannot get the relations (2.21) and (2.22), and it is impossible to go over to the two-component spinor equation.*

The problem is greatly simplified when $m = 0$. Then instead of (2.3) and (2.25) one must take

$$\psi = \hat{D}\varphi = -\gamma_\mu\left(\frac{\partial}{\partial x_\mu} + \beta(\bar{\varphi}\gamma_\mu\varphi)\right)\varphi,$$

$$\bar{\psi} = -\bar{\varphi}\hat{\bar{D}} = \bar{\varphi}\left(\frac{\partial}{\partial x_\mu} - \beta(\bar{\varphi}\gamma_\mu\varphi)\right)\gamma_\mu \tag{2.30}$$

and we find

$$V_\nu/\beta = (\bar{\varphi}\gamma_\mu\gamma_\nu\gamma_\rho\varphi)Y_\mu Y_\rho - (\bar{\varphi}_\mu\gamma_\mu\gamma_\nu\gamma_\rho\varphi - \bar{\varphi}\gamma_\rho\gamma_\nu\gamma_\mu\varphi_\mu)$$
$$\times Y_\rho - (\bar{\varphi}_\mu\gamma_\mu\gamma_\nu\gamma_\rho\varphi_\rho), \tag{2.31}$$

where

$$Y_\nu \equiv \beta(\bar{\psi}\gamma_\nu\psi). \tag{2.32}$$

The quadratic equation coincides with (2.28) and

*It should be noticed that the indicated special solutions φ_I and ψ_I are obtained in a natural manner from (2.13). Indeed, if we write the solution of (2.13) in the form $\varphi = c\psi$, we find that $\psi = (c + \bar{c})\psi$, where $c\gamma_\mu = \gamma_\mu\bar{c}$; that is, $c + \bar{c} = 1$, $c = {}^1/_2(1 + l\gamma_5)$, $\bar{c} = {}^1/_2(1 - l\gamma_5)$; where l is number. Now, if we require that $cc = c$, we get $l = 1$.

*If we introduce the new functions $\varphi = {}^1/_2(1+\gamma_5)\varphi'$ and $\varphi' = \bar{\varphi}'\,{}^1/_2(1-\gamma_5)$, Eq. (2.28) for φ' remains unchanged, and in (2.26) the term $\sim 1/m$ drops out. This last circumstance makes (2.28) invariant under the transformation $\varphi' \to \gamma_5\varphi'$, $\bar{\varphi}' \to -\bar{\varphi}'\gamma_5$. However, from the point of view of φ this last transformation is the identity transformation.

(2.29) for m = 0, but now $Y_\nu = \beta(\bar{\psi}\gamma_\nu\psi)$ is a solution of (2.31). It is easily seen from (2.30) that the transformation (2.19) leads to (2.20) and that (2.28) is invariant under these transformations. In addition, (2.1) is invariant under (2.20); consequently, the solutions $\psi = \psi_I$ and $\varphi = \varphi_I$ can be chosen with the aid of (2.21) and (2.22).

Following Feynman, we use the relations

$$\varphi_I = \frac{1}{2}(1+\gamma_5)\psi = \begin{pmatrix} \Phi \\ -\Phi \end{pmatrix},$$

$$\psi = \begin{pmatrix} a \\ b \end{pmatrix}, \quad \Phi = \frac{1}{2}(a-b), \tag{2.33}$$

where a and b are two-component spinors. We then get to the two-component nonlinear spinor equations (now $\bar{\psi}\gamma_\mu\psi = \bar{\psi}_I\gamma_\mu\psi_I \neq 0$) of the first and second orders, respectively.*

We can consider analogously the cases

$$A = \lambda_1(\bar{\psi}\psi) + \lambda_2\gamma_5(\bar{\psi}\gamma_5\psi), \quad B_\mu = 0 \tag{2.34}$$

or

$$A = m, \quad B_\mu = \beta_1(\bar{\psi}\gamma_\mu\psi) + \beta_2\gamma_5(\bar{\psi}\gamma_\mu\gamma_5\psi). \tag{2.35}$$

Several topics touched upon in this article were discussed with Professor D. D. Ivanenko.

*Note (added November 5, 1958). After the present work had gone to press we learned about an article by Ascoli, in which the author considers a first-order two-component nonlinear spinor equation, but under more stringent conditions. The two-component equation contains all the solutions of the fundamental equation; at the same time, as in our case, it contains only a part of the solutions we picked out of the fundamental four-component equation.

[1] D. D. Ivanenko and D. F. Kurdgelaidze, Dokl. Akad. Nauk SSSR **88**, 39 (1954). D. F. Kurdgelaidze, Вестн. МГУ, (Bull. Moscow State University) **8**, 81 (1954), and dissertation, Moscow State University, 1954.

[2] D. F. Kurdgelaidze, J. Exptl. Theoret. Phys. (U.S.S.R.) **32**, 1156 (1957), Soviet Phys. JETP **5**, 941 (1957).

[3] W. Heisenberg, Revs. Modern Phys. **29**, 269 (1957).

[4] W. Heisenberg, Z. Naturforsch. **9a**, 292 (1954).

[5] D. D. Ivanenko and A. M. Brodskiĭ, Dokl. Akad. Nauk SSSR **84**, 683 (1952) and J. Exptl. Theoret. Phys. (U.S.S.R.) **24**, 383 (1953).

[6] D. F. Kurdgelaidze, J. Exptl. Theoret. Phys. **34**, 1587 (1958), Soviet Phys. JETP **7**, 1093 (1958).

[7] R. Ascoli, Nuovo cimento **8**, 501 (1958).

Translated by W. Ramsay
152

ON THE ROLE PLAYED BY EXCHANGE EFFECTS IN STRIPPING REACTIONS

V. G. NEUDACHIN, I. B. TEPLOV, and O. P. SHEVCHENKO

Institute of Nuclear Physics, Moscow State University

Submitted to JETP editor September 10, 1958

J. Exptl. Theoret. Phys. (U.S.S.R.) 36, 850-853 (March, 1959)

A general expression has been obtained for the cross-section for "heavy particle stripping" as one of the exchange effects in stripping theory. Results of numerical computations of exchange effects in stripping reactions are presented for some of the simplest cases.

TAKING exchange effects into account in stripping reactions[1-3] leads to the result that in addition to the "ordinary" mechanism of stripping it is also necessary to consider two other processes: (a) the ejection (we are considering the (p, d) reaction) by a proton of a deuteron from the nucleus accompanied by proton capture into a bound state ("knock-out") in a manner similar to what may occur in the (p, n) reaction; (b) "heavy particle stripping."[2-4] In reference 3 a general discussion is given of the problem of determining the cross section for the stripping reaction with an antisymmetric wave function for the system. In this paper we present and compare with experiment results of specific calculations of exchange effects in stripping reactions for the simplest cases.

We designate the amplitude for the "ordinary" stripping reaction by I_1, the amplitude for the process (a) by I_2, and for the process (b) by I_3'. Then the amplitude for the reaction is given by

$$I = I_1 + (n-1)I_2 + (n-1)I_3', \qquad (1)$$

where n is the number of nucleons outside a closed shell in the initial nucleus.

The expressions for I_1^2 and I_2^2 are given in reference 3. For the calculation of $I_3'^2$ we have used the method of calculation presented in reference 3 after replacing the interaction V_{pn} by the interaction $V_{p\xi}$, where ξ represents the nuclear "core." This enabled us to obtain a more complete expression for the amplitude of the process (b):

$$I_3'^2 = (4\pi)^2 \; (T_1 M_{T_1} \tau m_\tau | T_2 M_{T_2})^2 \sum \langle j^n \alpha_1 | j^{n-2} \alpha_3; \; j^2 \alpha_d \rangle$$
$$\times \langle j^n \alpha_1 | j^{n-2} \alpha_3^*; \; j^2 \alpha_d^* \rangle \langle j^{n-1} \alpha_2 | j^{n-2} \alpha_3 \rangle \langle j^{n-1} \alpha_2 | j^{n-2} \alpha_3^* \rangle$$
$$\times \langle lsj, \; lsj, \; J_d | llL_d, \; ssS_d, \; J_d \rangle \langle lsj, \; lsj, \; J_d^* | llL_d^*, ssS_d, J_d^* \rangle$$
$$\times [J_1][J_2][j][l][L_d]^{1/2}[L_d^*]^{1/2}[J_d]^{1/2}[J_d^*]^{1/2}(-1)^R C_{000}^{llL} C_{000}^{L_d L_d^*}$$
$$\times W(lj\,lj;\; s\Lambda)\, W(jJ_3 J_3^*;\; J_2\Lambda)\, W(J_3 J_d J_3^* J_d^*;\; J_1\Lambda)$$
$$\times W(J_d L_d J_d^* L_d^*;\; S_d\Lambda)\, A_q(l^2,\; L_d)$$
$$\times A_q^*(l^2,\; L_d^*)\, B_k(l)\, B_k^*(l)\, P_\Lambda(\cos\beta). \qquad (2)$$

Here $j^n\alpha_1$ is the state of the initial nucleus [α_1 is the set of quantum numbers required to specify it uniquely, $\alpha_1 = (J_1, T_1, T_{1z}$, seniority etc.)]; $j^{n-1}\alpha_2$ is the state of the final nucleus, $\alpha_2 = (J_2, T_2, T_{2z}$ etc.); $j^{n-2}\alpha_3$ is the state of the nuclear "core," $\alpha_3 = (J_3, T_3, T_{3z}$ etc.); $j^2\alpha_d$ is the state of the deuteron, $\alpha_d = (L_d, S_d = 1; J_d; T_d = 0)$; s, l, j are the spin, orbital and total angular momentum of the nucleon in the nucleus; $\langle lsj, \; lsj \,|\, llL_d, \; ssS_d, \; J_d\rangle$ is the matrix element of the unitary transformation of the two-nucleon wavefunction from jj- to LS-coupling,[5] expressed by means of the 9j-symbol;[5,6] $\langle j^n\alpha_1 \,|\, j^{n-2}\alpha_3; \; j^2\alpha_d\rangle$ is the fractional parentage coefficient; $[x] \equiv 2x+1$; $R = s - J_1 + J_2 + 2J_3 + 2J_3^*$; C are the Clebsh-Gordan coefficients; W are the Racah coefficients;

$$4\pi Y_{L_d M_d}(q)\, A_q(l^2,\; L_d) = \langle \mathbf{k}_d(1,\; 2)\, | l^2 L_d M_d(1,\; 2)\rangle;$$

$$4\pi Y_{lm_l}^*(k)\, B_k(l) = \langle lm_l(0) \,|\, V_{0\xi} \,|\, \mathbf{k}_p(0)\rangle;$$

$$\mathbf{q} = \mathbf{k}_d + (M_d/M_f)\,\mathbf{k}_p; \quad \mathbf{k} = \mathbf{k}_p + (M_p/M_i)\,\mathbf{k}_d;$$

$\mathbf{k}_d$, $\mathbf{k}_p$ are the propagation vectors for the deuteron and for the proton in the center of mass system; M_d, M_p, M_i, M_f are the masses of the deuteron, the proton, the initial and the final nuclei (for an infinitely heavy nucleus $\mathbf{q} = \mathbf{k}_d$ and $\mathbf{k} = \mathbf{k}_p$); β is the angle between $\mathbf{k}$ and $\mathbf{q}$. The summation is carried out over α_3, α_3^*, α_d, α_d^*, Λ.

An explicit expression for $B_k(l)$ in terms of the spherical Bessel functions is obtained in a manner similar to the way this is done in the case of "ordinary" stripping. In the same way, by regarding the deuteron as a whole and by utilizing the deuteron reduced width, one may evaluate the integral $A_q(l^2, L_d)$. An expression for this integral may also be obtained by utilizing oscillator wave functions.[7] Both methods of calculation lead to closely similar results.

A numerical calculation was carried out of the differential cross-section for neutron production

in the reaction (d, n). The expressions for I_1^2, I_2^2 and $I_3'^2$ obtained for the reaction (p, d) are also valid for the reaction (d, p) and, consequently, for the reaction (d, n), if the Coulomb interaction is not taken into account. For the calculation we have chosen the simplest case when n = 2, i.e., when in the target nucleus there is only one nucleon outside a closed shell. In this case the spin of the nuclear "core" (J_3) is equal to zero and the formulas are considerably simplified.

The following cases have been considered:

(a) $l = 1$, $j = 1/2$, $J_1 = 1$, $T_1 = 0$ (jj-coupling),

(b) $l = 1$, $L_1 = 0$, $S_1 = 1$, $T_1 = 0$ (LS-coupling),

(c) $l = 0$, $J_1 = 1$, $T_1 = 0$.

Specific reaction parameters for cases a and b have been taken corresponding to the case C^{13} (d, n) N^{14}, in particular, Q = 5.19 Mev, R = 4.5×10^{-13} cm; for case c the reaction parameters were taken corresponding to Si^{29} (d, n) P^{30} (ground state), i.e., Q = 3.27 Mev, R = 5.5×10^{-13} cm. The deuteron energy in all these cases was taken to be equal to 8 Mev. For both reactions the differential cross sections $\sigma_1(\vartheta)$ and $\sigma_2(\vartheta)$ were calculated corresponding to the amplitudes I_1 and I_2; in the case C^{13} (d, n) N^{14} we have also calculated $\sigma_3(\vartheta)$ which corresponds to the amplitude I_3'.

The results of the calculations are shown in Figs. 1 and 2 from which it may be seen that the shapes of the angular distributions of σ_1 and σ_2 are similar to each other, particularly in the case of LS coupling. With reference to the angular distribution of σ_3 we see that it practically coincides with the angular distribution calculated on the assumption of LS-coupling by a simpler method which was used in the papers of Owen and Madansky.[2,4]

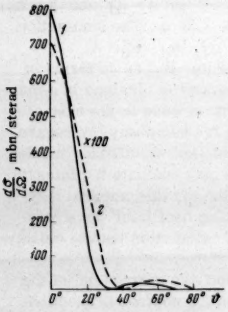

FIG. 1. Differential cross sections for the reaction Si^{29} (d, n) P^{30}: 1 – "ordinary" stripping and 2 – "knockout."

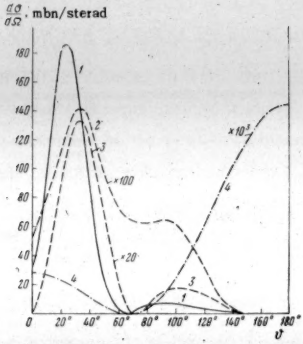

FIG. 2. Differential cross sections for the reaction C^{13} (d, n) N^{14}: 1 – "ordinary" stripping, 2 – "knockout" (jj-coupling), 3 – "knockout" (LS coupling), 4 – "heavy particle stripping."

The absolute cross section was calculated on the assumption that the reduced widths for a single nucleon are equal to the Wigner limit. The results have shown (Figs. 1 and 2) that the cross section σ_2 is lower by approximately one-two orders of magnitude compared to the cross section of "ordinary stripping. This is not accidental, since the relative smallness of σ_2 is explained by the fact that the integrals E_l, which appear in the expression for I_2^2 are practically always smaller than the integrals D_l, upon which I_1^2 depends.

Because of the difference in the way angular momenta combine the cross section σ_3 calculated according to formula (2) turns out to be smaller by a factor of two or three compared to the cross section calculated by a formula similar to (2) but derived on the assumption of LS coupling. In this last case the results are close to the results of calculation using formulas from the papers of Owen and Madansky if we assume that the reduced nucleon widths are equal to the Wigner limit. (We note that in references 2 and 4 there are certain inaccuracies in the formulas.) The reason for the smallness of the magnitude of σ_3 compared to σ_1 (the ratio of the cross sections at their maxima is approximately 10^{-3}) may be easily understood if we examine the formulas of Owen and Madansky. According to these formulas the cross section is approximately proportional to $j_{L_d}^2(qR) \times j_l^2(kR)$. Since in our case $M_d \ll M_f$, q varies slowly as the angle ϑ between $\mathbf{k}_d$ and $\mathbf{k}_p$ is varied, and is approximately equal to k_d. Therefore, for not too low energies of the deuteron the quantities qR are not small (for the reaction with C^{13} $qR \approx 3.5$) and, consequently, they correspond to comparatively small values of $j_{L_d}(qR)$.

At their maxima the cross sections σ_1 and σ_3 are comparable in magnitude if we assume that $L_d = 0$ and that the reaction parameters are such that at large angles qR is small while kR is near the value of the argument corresponding to the first maximum of the function j_l. In particular, this in many cases should occur at low deuteron energies, since as the energy is reduced $qR \to 0$, while $kR \to \sim 2$, if $Q \approx 5$ Mev and $R \approx 4 \times 10^{-13}$ cm. For some specific reactions the cross sections σ_1 and σ_3 are of the same order of magnitude at not very low energies; for example, in the case $B^{11}(d, n)C^{12}$ this occurs up to deuteron energy of 4 or 5 Mev. However, for deuteron energies exceeding 7 or 8 Mev the cross section σ_3 is considerably smaller than σ_1 for all the reactions. Consequently, at these energies the angular distribution of particles in stripping reactions should be very well described by the formulas of "ordinary" stripping.

The effect of the Coulomb interaction must be approximately the same for "ordinary" stripping and for "heavy particle stripping." Therefore, one can hope that if σ_1 and σ_3 are of the same order of magnitude, then by measuring the relative values of the maxima of the differential cross section at small and at large angles one could obtain the ratio of the deuteron and the proton (in the case of the (d, n) reaction) reduced widths. This is possible due to the fact that in formula (2) there is essentially contained the expression for the reduced deuteron widths in the shell model (jj coupling).

It must be noted that there is one circumstance which is difficult to understand on the basis of the concepts adopted by us above. In a number of cases "heavy particle stripping" practically does not show up even at low energies, for example, in the reactions (d, p) in Li^6, B^{10}, and N^{14}.[8-10] In specific reactions there may be reasons for this. For example, in those cases when the isotopic spin of the nuclear "core" is $T_3 = 0$, while the isotopic spin of the final nucleus is $T = 1$, "heavy particle stripping" is forbidden, since $T_\alpha = 0$ and, consequently, the equality $T_1 = T_3$ must hold. Example: the reaction $O^{17}(d, n)F^{18*}$, $T^* = 1$. However, for the reactions enumerated above in Li^6, B^{10}, and N^{14} it is difficult to formulate any reason for the reaction being forbidden. Perhaps in these cases the explanation lies in the smallness of the fractional parentage coefficients.

[1] A. P. French, Phys. Rev. **107**, 1655 (1957).

[2] G. E. Owen and L. Madansky, Phys. Rev. **105**, 1766 (1957).

[3] V. G. Neudachin, J. Exptl. Theoret. Phys. (U.S.S.R.) **35**, 1165 (1958), Soviet Phys. JETP **8**, 815 (1959).

[4] G. E. Owen and L. Madansky, Phys. Rev. **99**, 1608 (1955).

[5] Arima, Horie, and Tanabe, Prog. Theoret. Phys. **11**, 143 (1954).

[6] I. B. Levinson and V. V. Vanagas, Оптика и спектроскопия, (Optics and Spectroscopy) **2**, 10 (1957).

[7] I. Talmi, Helv. Phys. Acta **25**, 185 (1952).

[8] W. E. Nickell, Phys. Rev. **95**, 426 (1954).

[9] W. C. Redman, Phys. Rev. **79**, 6 (1950).

[10] L. D. Wyly, Phys. Rev. **76**, 104 (1949).

Translated by G. Volkoff
153

ON A CERTAIN VERSION OF NONLOCAL ELECTROMAGNETIC FIELD THEORY

A. A. KOMAR and M. A. MARKOV

P. N. Lebedev Physical Institute, Academy of Sciences, U.S.S.R.

Submitted to JETP editor September 10, 1958

J. Exptl. Theoret. Phys. (U.S.S.R.) **36**, 854-858 (March, 1959)

A nonlocal theory is considered which corresponds to a modification of the Lienard-Wiechert potential (2). It is shown that if, in this version of the theory, the potential is assumed to satisfy the usual type of equation (3), the consistent relativistic treatment (many-time formalism) leads to self-contradictions already within the framework of the classical theory.

At various times a number of authors[1-3] investigated one of the versions of nonlocal electromagnetic field theory from different points of view. This version is based on a modification of the form of the Lienard-Wiechert potentials. Instead of the usual way of writing,

$$A_\mu = -e\,(u_\mu(r')/R_\nu u_\nu(r'))_{R_\nu^2=0} \qquad (1)$$

(where u_μ is the four-velocity of the charge, $R_\nu = r_\nu - r'_\nu$ is the difference of the coordinates of the point of observation and the charge), one starts from the following expression:

$$A_\mu = -e\,(u_\mu(r')/R_\nu u_\nu(r'))_{R_\nu^2+a^2=0}. \qquad (2)$$

Here a is a new constant with the dimension of a length. It is further assumed that the potential satisfies the usual equation

$$\Box A_\mu = -\frac{4\pi}{c} j_\mu, \qquad (3)$$

which essentially defines the current. In the static case $u_\nu = (p, 0, 0, i)$, and (3) leads to the charge density

$$\rho(\mathbf{r}-\mathbf{r}') = (e/4\pi)\,3a^2/(R^2+a^2)^{7/2}, \qquad (4)$$

i.e., the point charge is spread out. Analogously, the current is spread out in a more complicated way. In this theory the field at the location of the charge is finite, and so is the self energy.

The aim of the present paper is to show that this approach is unsatisfactory, and that self-contradictions arise from the adoption of the usual type of equation for the potential leading to a spreading out of the charge: the classical system of equations for charged particles is internally inconsistent. For the proof we make use of the many-time formulation of the classical electrodynamics of a system of charged particles.[4] We assume that each particle, and the field, has its own time, different from that of the others. The interaction for such a system may be written in the form

$$S = \sum_{n=1}^{N}\left\{\int_0^{t_n^0}[-m_n c^2 + u_\nu(\mathbf{r}_n,\ t_n) \times \int \rho_n(\mathbf{r}-\mathbf{r}_n)\,A_\nu(\mathbf{r},\ t_n)\,d\mathbf{r}]\sqrt{1-\beta_n^2}\,dt_n\right\} + \int_0^{t^0} dt \int\left[-\frac{1}{8\pi}\left(\frac{\partial A_\nu}{\partial x_\mu}\right)^2\right] d^3x. \qquad (5)$$

The Hamiltonian of the particles is

$$H_n = \int \rho_n(\mathbf{r}-\mathbf{r}_n)\,\varphi(\mathbf{r},\ t_n)\,d\mathbf{r} + c\left[m_n^2 c^2 + \left(\mathbf{p}_n - \frac{1}{c}\int \rho_n(\mathbf{r}-\mathbf{r}_n)\,\mathbf{A}(\mathbf{r},\ t_n)\,d\mathbf{r}\right)^2\right]^{1/2}, \qquad (6)$$

the Hamiltonian of the field is

$$H = \frac{1}{8\pi}\int\left(\sum_{i=1}^{3}\left(\frac{\partial A_\nu}{\partial x_i}\frac{\partial A_\nu}{\partial x_i}\right) + (4\pi)^2 c^2 \Pi_\nu^2\right) d^3x, \qquad (7)$$

where

$$\Pi_\nu = (1/4\pi c^2)\,\partial A_\nu/\partial t.$$

We note that, in the many-time formalism, the electromagnetic field is described by the free Hamiltonian and the corresponding free field equation $\Box A_\mu = 0$. A current at the right hand side of the field equation appears only if the transition to a single time is made.

For the following it is convenient to go over to different canonical field variables. Let

$$A_\nu(\mathbf{r},\ t) = V^{-1/2}\sum_k\left[\frac{P_k^\nu}{k}\cos(\mathbf{k}\cdot\mathbf{r}-kct) + cQ_k^\nu \sin(\mathbf{k}\cdot\mathbf{r}-kct)\right],$$

$$4\pi\Pi_\nu(\mathbf{r},\ t) = (V^{-1/2}\sum_k\left[\frac{1}{c}P_k^\nu \sin(\mathbf{k}\cdot\mathbf{r}-kct) - Q_k^\nu k\cos(\mathbf{k}\cdot\mathbf{r}-kct)\right]. \qquad (8)$$

P_k^ν and Q_k^ν are the new canonical variables:

$$[P_k^\nu,\ Q_{k'}^\mu] = 4\pi\delta_{\mu\nu}\delta_{kk'},\ [P_k^\nu,\ P_{k'}^\mu] = 0,\ [Q_k^\nu,\ Q_{k'}^\mu] = 0. \quad (9)$$

Expressions (8) explicitly give the time dependence of P_k^ν and Q_k^ν.

The field Hamiltonian in the new canonical variables has the form

$$H = \frac{1}{8\pi}\sum_k [(P_k^\nu)^2 + c^2k^2\,(Q_k^\nu)^2]. \quad (10)$$

The terms in the Hamiltonian for the particles which depend on the field are conveniently rewritten in the following way:

$$\int \rho_n(\mathbf{r}-\mathbf{r}_n)\,A_\nu(\mathbf{r},\ t_n)\,d\mathbf{r}$$

$$= \int \rho_n(\mathbf{r}-\mathbf{r}_n)\Big[V^{-1/2}\sum_k\Big(\frac{P_k^\nu}{k}\cos(\mathbf{k}\cdot\mathbf{r}-kct_n)$$

$$+ cQ_k^\nu \sin(\mathbf{k}\cdot\mathbf{r}-kct_n)\Big)\Big]\,d\mathbf{r}$$

$$= \int \rho_n(\mathbf{R})\Big[V^{-1/2}\sum_k\Big(\frac{P_k^\nu}{k}\cos(\mathbf{k}\cdot\mathbf{R}+\mathbf{k}\cdot\mathbf{r}_n-kct_n)$$

$$+ cQ_k^\nu \sin(\mathbf{k}\cdot\mathbf{R}+\mathbf{k}\cdot\mathbf{r}_n-kct_n)\Big)\Big]\,d\mathbf{R}.$$

Since $\rho_n(\mathbf{R})$ depends only on R^2, this expression becomes

$$V^{-1/2}\sum_k\Big[\Big(\int \rho_n(R)\cos\mathbf{k}\cdot\mathbf{R}\,d\mathbf{R}\Big)\Big(\frac{P_k^\nu}{k}\cos(\mathbf{k}\cdot\mathbf{r}_n-kct_n)$$

$$+ cQ_k^\nu \sin(\mathbf{k}\cdot\mathbf{r}_n-kct_n)\Big)\Big]$$

$$= V^{-1/2}e_n\sum_k f(k)$$

$$\times\Big(\frac{P_k^\nu}{k}\cos(\mathbf{k}\cdot\mathbf{r}_n-kct_n)+cQ_k^\nu\sin(\mathbf{k}\cdot\mathbf{r}_n-kct_n)\Big), \quad (11)$$

where

$$f(k) = \frac{1}{e_n}\int \rho_n(R)\cos\mathbf{k}\cdot\mathbf{R}\,d\mathbf{R}.$$

The Hamilton-Jacobi equations for our system of charged particles are written in the following form:

$$\partial S(t_1\ldots t_N)/\partial t_n = -H_n(\mathbf{r}_n, t_n,\ \partial S/\partial\mathbf{r}_n,\ Q_k^\nu,\ \partial S/\partial Q_k^\nu),$$

$$(n = 1\ldots N). \quad (13)$$

The condition of consistency for such a system of equations is (see, e.g., reference 5)

$$(\partial^2/\partial t_{n'}\,\partial t_n - \partial^2/\partial t_n\partial t_{n'})\,S(t_1\ldots t_N) = 0. \quad (14)$$

According to (13) this leads to

$$\partial H_n\Big(\mathbf{r}_n, t_n, \frac{\partial S}{\partial\mathbf{r}_n},\ Q_k^\nu,\ \frac{\partial S}{\partial Q_k^\nu}\Big)\Big/\partial t_{n'}$$

$$-\partial H_{n'}\Big(\mathbf{r}_{n'},\ t_{n'},\ \frac{\partial S}{\partial\mathbf{r}_{n'}}, Q_k^\mu,\ \frac{\partial S}{\partial Q_k^\mu}\Big)\Big/\partial t_n = 0$$

or

$$\frac{\partial H_n}{\partial(\partial S/\partial\mathbf{r}_n)}\frac{\partial^2 S}{\partial t_{n'}\partial\mathbf{r}_n} + \frac{\partial H_n}{\partial(\partial S/\partial Q_k^\nu)}\frac{\partial^2 S}{\partial t_{n'}\partial Q_k^\nu}$$

$$-\frac{\partial H_{n'}}{\partial(\partial S/\partial\mathbf{r}_{n'})}\frac{\partial^2 S}{\partial t_n\partial\mathbf{r}_{n'}} - \frac{\partial H_{n'}}{\partial(\partial S/\partial Q_k^\mu)}\frac{\partial^2 S}{\partial t_n\partial Q_k^\mu} = 0.$$

We note that $\partial S/\partial\mathbf{r}_n$ and $\partial S/\partial Q_k^\nu$ correspond to the canonical momenta of the particles and the field and that the order of differentiation with respect to the time and to the coordinates (of the particles and the field) can be interchanged if the condition of consistency is satisfied. The last expression can then be rewritten in form

$$\frac{\partial H_n}{\partial\mathbf{p}_n}\frac{\partial H_{n'}}{\partial\mathbf{r}_n} + \frac{\partial H_n}{\partial P_k^\nu}\frac{\partial H_{n'}}{\partial Q_k^\nu} - \frac{\partial H_{n'}}{\partial\mathbf{p}_{n'}}\frac{\partial H_n}{\partial\mathbf{r}_{n'}} - \frac{\partial H_{n'}}{\partial P_k^\mu}\frac{\partial H_n}{\partial Q_k^\mu} = 0.$$

Since always $\partial\mathbf{H_n}/\partial\mathbf{p_{n'}} = \partial\mathbf{H_n}/\partial\mathbf{r_{n'}} = 0$ $(\mathbf{n}\neq\mathbf{n'})$, we finally get instead of (14)

$$[H_n,\ H_{n'}] = 0. \quad (15)$$

Here $[\mathbf{H_n}, \mathbf{H_{n'}}]$ is the classical Poisson bracket. It is clear from the foregoing that in our case the Poisson bracket is calculated from the canonical field variables only.

From (6) and (11) we have

$$[H_n,\ H_{n'}] = \frac{e_n e_{n'}\,c}{V}\sum_k\Big\{\frac{f^2(k)}{k}\,[\cos(\mathbf{k}\cdot\mathbf{r}_n - kct_n)$$

$$\times\sin(\mathbf{k}\cdot\mathbf{r}_{n'} - kct_{n'}) - \sin(\mathbf{k}\cdot\mathbf{r}_n - kct_n)\cos(\mathbf{k}\cdot\mathbf{r}_{n'} - kct_{n'})]$$

$$\times\Big(\frac{\delta_{\nu 4}}{i} - \sum_{\alpha=1}^{3}\beta_\alpha^n\delta_{\nu\alpha}\Big)\Big(\frac{\delta_{\nu 4}}{i} - \sum_{\gamma=1}^{3}\beta_\gamma^{n'}\delta_{\nu\gamma}\Big)\Big\} = \frac{e_n e_{n'}\,c}{V}(1-\beta_n\beta_{n'})$$

$$\sum_k\Big\{\frac{f^2(k)}{k}\sin[\mathbf{k}\cdot(\mathbf{r}_n-\mathbf{r}_{n'}) - kc\,(t_n-t_{n'})]\Big\}$$

$$= \frac{1}{(2\pi)^3}e_n e_{n'}\,c\,(1-\beta_n\beta_{n'})$$

$$\times\int\frac{f^2(k)}{k}\sin[\mathbf{k}\cdot(\mathbf{r}_n-\mathbf{r}_{n'}) - kc\,(t_n-t_{n'})]\,d^3k.$$

Finally,

$$[H_n,\ H_{n'}] = \frac{e_n e_{n'}\,c}{(2\pi)^3}\,(1-\beta_n\beta_{n'})$$

$$\times\int\frac{f^2(k)}{k}\sin[\mathbf{k}\cdot(\mathbf{r}_n-\mathbf{r}_{n'}) - kc\,(t_n-t_{n'})]\,d^3k. \quad (16)$$

In the case of a point charge, $f(k) = 1$, and the expression

$$-(2\pi)^{-3}\int\sin[\mathbf{k}\cdot(\mathbf{r}_n-\mathbf{r}_{n'}) - kc\,(t_n-t_{n'})]\,\frac{d^3k}{kc}$$

$$= (2\pi)^{-3}\int\cos\mathbf{k}\cdot(\mathbf{r}_n-\mathbf{r}_{n'})\sin kc\,(t_n-t_{n'})\,\frac{d^3k}{kc} = D(x_n - x_{n'})$$

agrees with the well-known commutator function. For point particles the conditions of consistency are therefore satisfied everywhere outside the light cone and hence, what is especially important, in the space-like region.

In our case $f(k)$ is equal to unity, and

$$\hat{f}(k) = \frac{3a^2}{4\pi}\int \frac{\cos \mathbf{k}\cdot\mathbf{R}\, d\mathbf{R}}{(R^2+a^2)^{5/2}} = 3a^2\int_0^\infty \frac{\sin kR}{k(R^2+a^2)^{5/2}} R dR$$

$$= a^2\int_0^\infty \frac{\cos kR}{(R^2+a^2)^{3/2}} dR = kaK_1(ka). \qquad (17)$$

Here K_1 is the Hankel function with imaginary argument. Since $f(k)$ depends only on the absolute value of k, the integral expression in (16) becomes

$$-\frac{4\pi}{|\mathbf{r}_n-\mathbf{r}_{n'}|}\int_0^\infty \hat{f}^2(k)\sin k|\mathbf{r}_n-\mathbf{r}_{n'}|\sin kc(t_n-t_{n'})\,dk$$

$$= \frac{2\pi a^2}{|\mathbf{r}_n-\mathbf{r}_{n'}|}\int_0^\infty k^2K_1^2(ka)\{\cos[k(|\mathbf{r}_n-\mathbf{r}_{n'}|+c(t_n-t_{n'}))]$$

$$-\cos[k(|\mathbf{r}_n-\mathbf{r}_{n'}|-c(t_n-t_{n'}))]\}\,dk$$

and therefore

$$[H_n,\ H_{n'}] = \frac{e_ne_{n'}c}{4\pi^2|\mathbf{r}_n-\mathbf{r}_{n'}|}(1-\beta_n\beta_{n'})\,a^2$$

$$\times\int_0^\infty k^2K_1^2(ka)\{\cos[k(|\mathbf{r}_n-\mathbf{r}_{n'}|$$

$$+c(t_n-t_{n'}))]-\cos[k(|\mathbf{r}_n-\mathbf{r}_{n'}|-c(t_n-t_{n'}))]\}\,dk. \qquad (18)$$

The integration cannot be performed analytically. The integral can, however, be evaluated approximately near the light cone. For this purpose we make use of the integral representation

$$kK_1(ka) = a\int_0^\infty \frac{\cos kR}{(R^2+a^2)^{3/2}}\,dR$$

and change the order of integration in the integral (18). Using the notation

$$|\mathbf{r}_n-\mathbf{r}_{n'}|+c(t_n-t_{n'}) = \Delta_1,\ |\mathbf{r}_n-\mathbf{r}_{n'}|-c(t_n-t_{n'}) = \Delta_2;$$

we have

$$\int_0^\infty k^2K_1^2(ka)\left[\cos k\Delta_1-\cos k\Delta_2\right]dk$$

$$= \frac{a^2\pi}{4}\int_0^\infty \frac{dR}{(R^2+a^2)^{3/2}}\{[(\Delta_1+R)^2+a^2]^{-1/2}-[(\Delta_1-R)^2+a^2]^{-1/2}$$

$$+[(\Delta_2-R)^2+a^2]^{-1/2}-[(\Delta_2+R)^2+a^2]^{-1/2}\}. \qquad (19)$$

We note that Δ_1/a may be quite large for $\Delta_2/a \ll 1$ and vice versa, for $|\mathbf{r}_n-\mathbf{r}_{n'}|$ and $c(t_n-t_{n'})$ may be taken as large as one pleases. Let us assume that $\Delta_2/a \ll 1$, and let us neglect the terms with Δ_1 in view of what has just been said. Making a series expansion, we then obtain from (19)

$$-(3\pi^2/32a^3)(1-15\Delta_2^2/32a^2).$$

With $\Delta_2/a \ll 1$, $\Delta_1/a \gg 1$ we then have

$$[H_n,\ H_{n'}] \approx -\frac{3e_ne_{n'}c}{128a|\mathbf{r}_n-\mathbf{r}_{n'}|}(1-\beta_n\beta_{n'})\left(1-\frac{15\Delta_2^2}{32a^2}\right)$$

$$= -0{,}023\,\frac{e_ne_{n'}c}{a|\mathbf{r}_n-\mathbf{r}_{n'}|}(1-\beta_n\beta_{n'})\left(1-\frac{15\Delta_2^2}{32a^2}\right),$$

i.e., this expression is different from zero on the cone and near the cone in the space-like region.

An analogous calculation can be carried out for the case $\Delta_1/a \ll 1$, $\Delta_2/a \gg 1$. Furthermore, we calculated the integral numerically for the value $\Delta_2/a = 10$, i.e., in a region which is comparatively far from the cone (Δ_1/a was assumed to be sufficiently large, so that the terms with Δ_1 could be omitted). The result is

$$[H_n,\ H_{n'}] \approx -0.0006\,\frac{e_ne_{n'}c}{a|\mathbf{r}_n-\mathbf{r}_{n'}|}(1-\beta_n\beta_{n'}).$$

Hence $[H_n, H_{n'}]$ is different from zero on the light cone and everywhere in the space-like region, and, although it decreases fast with the distance from the cone, it nowhere reduces to zero, except at infinity ($\Delta_1/a = \infty$, $\Delta_2/a = \infty$).*

In other words, the conditions of consistency of the system (13) are not fulfilled in this version of the theory.

In the process of quantization the classical Poisson bracket goes over into the commutator of the corresponding quantities:

$$[H_n,\ H_{n'}]_{c1} \to \frac{i}{\hbar}[\hat{H}_n,\ \hat{H}_{n'}]_{qu} = \frac{i}{\hbar}[\hat{H}_n\hat{H}_{n'}-\hat{H}_{n'}\hat{H}_n].$$

In the case of point particles this leads to (with $\beta_n \to \alpha_n$, $\beta_{n'} \to \alpha_{n'}$, where α_n, $\alpha_{n'}$ are the Dirac matrices)

$$[\hat{H}_n,\ \hat{H}_{n'}]_{c1} = -ihc^2e_ne_{n'}(\boldsymbol{\alpha}_n\boldsymbol{\alpha}_{n'}-1)D(x_n-x_{n'}),$$

the well-known expression for the Bloch condition.[6] The failure of $[H_n, H_{n'}]_{cl}$ to reduce to zero in the space-like region in this nonlocal version of the theory must lead to similar difficulties in the quantum region.

[1] H. I. Groenewold, Physica **6**, 115 (1939).

[2] A. Landé, Phys. Rev. **56**, 482 (1939) and **76**, 1176 (1949).

[3] R. Ingraham, Phys. Rev. **101**, 1411 (1956).

[4] M. A. Markov, Doctoral Dissertation, Inst. of Physics, Acad. Sci. U.S.S.R., 1941.

[5] D. A. Grave, Об интегрировании частных дифференциальных уравнений первого порядка (On the Integration of Partial Differential Equations of First Order), Dissertation, St. Petersburg Academy of Sciences, 1889.

[6] F. Bloch, Phys. Z. d. Sowjetunion **5**, 301 (1934). Translated by R. Lipperheide 154

*This may also be seen qualitatively from expression (18), for as Δ_1/a and Δ_2/a increase, the cosine begins to oscillate rapidly, thus making the value of the integral smaller.

SOVIET PHYSICS JETP VOLUME 36 (9), NUMBER 3 SEPTEMBER, 1959

INTERACTION BETWEEN CONDUCTION ELECTRONS IN FERROMAGNETS

A. I. AKHIEZER and I. Ya. POMERANCHUK

Physico-Technical Institute, Academy of Sciences, Ukrainian S.S.R.

Submitted to JETP editor September 12, 1958

J. Exptl. Theoret. Phys. (U.S.S.R.) 36, 859-862 (March, 1959)

It is shown that in ferromagnets there is an additional attraction between conduction electrons, because of spin-wave exchange.

1. If the interaction of electrons in a metal leads to an effective mutual attraction between them in the vicinity of the Fermi surface, then a pair of electrons can have, as is known,[1] a bound state with a negative energy of binding. This phenomenon forms the basis of a recently developed theory of superconductivity.[2,3]

In ordinary metals, the effective mutual attraction between electrons originates from virtual exchange of phonons. In the interaction energy, the matrix element dependent on this exchange approaches a finite limit as the phonon momentum approaches zero. This behavior of the matrix element is connected with the fact that it contains in its denominator the energy of a phonon, whereas the matrix elements of phonon absorption and emission are proportional to the square root of the phonon energy.

We should like to call attention to the fact that in ferromagnets there occurs an additional mutual attraction between conduction electrons, connected with the virtual emission and absorption of spin waves. Since the energy of a spin wave is proportional to the square of its momentum, and since the matrix elements of spin-wave emission and absorption contain no additional factors proportional to the square root of the spin-wave energy, therefore the matrix element of the effective energy of interaction between electrons resulting from spin-wave exchange is inversely proportional to the square of the spin-wave momentum, i.e., to the square of the momentum transferred.

The momentum transferred must, however, exceed a certain minimum value, since the energy of a conduction electron in a ferromagnet depends on the orientation of its spin,[4] and therefore to the two spin orientations there correspond Fermi spheres of different radii. This circumstance leads to a diminution of the effective interaction between electrons.

In this note we determine the nature of the effective interaction between electrons caused by spin-wave exchange.

2. We use a simplified model of a ferromagnet; we start from the concept of two groups of electrons — the conduction electrons (s electrons) and the ferromagnetic electrons (d electrons).

The operator $V(\mathbf{r})$ of interaction energy between s and d electrons must obviously contain linearly both the spin $\mathbf{s}$ of the s electron and the magnetic moment $\mathbf{M}(\mathbf{r})$ of unit volume of the ferromagnet, due to the d electrons. Therefore $V(\mathbf{r})$ may be represented in the form

$$V(\mathbf{r}) = \hat{C}\mathbf{s}\cdot\mathbf{M}(\mathbf{r}),$$

where $\hat{C}$ is a certain linear integral operator. Since the exchange forces fall off rapidly with distance, the size of $\hat{C}$ may be considered approximately constant. We write it in the form $C = \Delta a^3/\mu_0$, where μ_0 is the Bohr magneton, a is the lattice constant, and Δ is a certain energy connected with the Curie temperature Θ by the relation $\Delta \sim \sqrt{\Theta A}$. Here A has the order of magnitude of the atomic energy. Such an estimate of the magnitude of Δ corresponds to the idea that the exchange energy between d-electrons is caused by s-electrons and leads, apparently, to an increased value of Δ (cf. reference 5).

Thus the energy of interaction between s and d electrons has the form[5]

$$V(\mathbf{r}) = (\Delta a^3/\mu_0)\,\mathbf{s}\cdot\mathbf{M}(\mathbf{r}). \qquad (1)$$

From this formula it follows that the energy of a conduction electron in a ferromagnet has the form

$$\varepsilon(\mathbf{p}, \sigma) = \varepsilon^0(\mathbf{p}) + 2\sigma\Delta,$$

where $\mathbf{p}$ is the momentum of the electron, $\sigma = \pm\frac{1}{2}$ is the projection of the electron spin on the z axis, and $\epsilon^0(\mathbf{p})$ is a quantity independent of σ; in the further calculations we consider for simplicity that $\epsilon^0(\mathbf{p}) = p^2/2m$.

The emission and absorption of spin waves is connected with the projection of the vector $\mathbf{M}(\mathbf{r})$ perpendicular to the axis of easiest magnetization (the z axis). This projection is determined by the formulas[6]

$$M_x = \sqrt{\mu_0 M_0 / 2\Omega} \sum_{\mathbf{k}} (a_{\mathbf{k}} + a^*_{-\mathbf{k}}) e^{i\mathbf{k}\cdot\mathbf{r}},$$

$$M_y = i\sqrt{\mu_0 M_0 / 2\Omega} \sum_{\mathbf{k}} (a^*_{-\mathbf{k}} - a_{\mathbf{k}}) e^{i\mathbf{k}\cdot\mathbf{r}}, \qquad (2)$$

where M_0 is the saturation magnetic moment, Ω is a normalizing volume, and $a_{\mathbf{k}}$ and $a^*_{\mathbf{k}}$ are the creation and annihilation operators for spin waves of momentum $\mathbf{k}$; they satisfy the relations

$$[a_{\mathbf{k}}, a^*_{\mathbf{k}'}] = \delta_{\mathbf{k}\mathbf{k}'}.$$

We now determine the matrix element of the energy of effective interaction between two s electrons, connected with spin-wave exchange. We denote the initial momenta and spins of the electrons by $\mathbf{p}_1$, $\mathbf{p}_2$, σ_1, σ_2 and the final by $\mathbf{p}'_1$, $\mathbf{p}'_2$, σ'_1, σ'_2. The interaction of interest to us, like the known Møller interaction, is an outcome of the second approximation of perturbation theory. Since the matrix elements of the operators $s_x \pm is_y$ differ from zero only if $\sigma + \sigma' = 0$, the electrons interact only in the case in which their spins have opposite directions.

On taking account of the two types of intermediate state, corresponding to emission of a spin wave by the first and by the second electron, we get the following expression for the desired matrix element:

$$U_{if} = \frac{a^3}{i\Omega} \Delta^2 \left\{ \frac{\delta_{\sigma_1, \sigma'_1} \delta_{\sigma_2, -\sigma'_2}}{\varepsilon(\mathbf{p}_1, \sigma_1) - \varepsilon(\mathbf{p}_1 - \mathbf{k}, \sigma'_1) - \theta(ak)^2} + \frac{\delta_{\sigma_2, \sigma'_1} \delta_{\sigma_1, -\sigma'_2}}{\varepsilon(\mathbf{p}_2, \sigma_2) - \varepsilon(\mathbf{p}_2 + \mathbf{k}, \sigma'_2) - \theta(ak)^2} \right\}, \qquad (3)$$

where $\theta(ak)^2$ is the energy of the spin wave.

Attraction between the electrons occurs in a triplet state with resultant projection of the spin equal to zero. From this it follows that the spatial part of the wave function of the electrons is antisymmetric. (In the simplest case it represents a p state.)

We introduce the radii p_+ and p_- of the Fermi spheres of electrons with different spin orientations. On assuming that $\epsilon^0(p) = p^2/2m$, we get

$$p_+ = \sqrt{2m(\mu - \Delta)}, \quad p_- = \sqrt{2m(\mu + \Delta)},$$

where μ is the chemical potential.

It is clear that if $p_1 \sim p_+$, then $p'_1 \sim p_-$. From this it is easily deduced that the minimum value of the spin-wave momentum will be

$$k_{\min} = p_0 (\sqrt{1 + \Delta/\mu} - \sqrt{1 - \Delta/\mu}),$$

where $p_0 = \sqrt{2m\mu}$. If we consider that $\Delta \ll \mu$, we get from this $k_{\min} \sim p_0 \Delta/\mu$. Therefore the maximum value of a matrix element is equal to

$$(U_{if})_{\max} \equiv -a^3 U/\Omega, \quad U = \mu^2/\Theta. \qquad (4)$$

To this value of the interaction energy corresponds, obviously, a resultant momentum of the electron pair equal to

$$P_0 = \sqrt{p_-^2 - p_+^2} = p_0 \sqrt{2\Delta/\mu}$$

(cf. the figure, in which the Fermi spheres of radii p_+ and p_- are shown displaced by $\mathbf{P}$. The greatest interaction will occur in the case when the circle of intersection is a great circle of the smaller sphere. The shaded areas in the figure are those in which the electron momenta are distributed before and after scattering.)

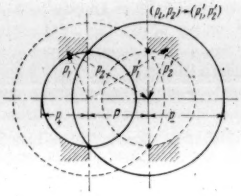

Comparison of the matrix element (4) with the matrix elements of interaction due to phonon exchange shows that the latter is smaller than the matrix element (4) by a factor of order of magnitude μ/Θ. The stronger interaction due to spin-wave exchange is compensated, however, by a diminution of statistical weight, connected with the fact that the resultant momentum of the interacting electrons is different from zero. Furthermore, the antisymmetry of the wave function contributes to a decrease of the effective attraction of the electrons. Consequently the problem of bound states of electrons resulting from spin-wave exchange requires a special study. As a general principle, however, the presence of an additional attraction between conduction electrons in ferromagnets can under suitable conditions contribute to the appearance of superconductivity. It is possible that such conditions may be realized in thin films, in which the critical magnetic field is increased.[7]

Note in proof (Feb. 12, 1959). In a recent paper [Matthias, Suhl, and Corenzwit, Phys. Rev. Let. **1**, 449 (1958)], the presence of superconductivity in the ferromagnetic alloys (Ce, Pr)Ru_2 and (Ce, Gd)Ru_2 has been established experimentally.

[1] L. Cooper, Phys. Rev. **104**, 1189 (1956).

[2] Bardeen, Cooper, and Schrieffer, Phys. Rev. **108**, 1175 (1957).

[3] N. N. Bogolyubov, J. Exptl. Theoret. Phys. (U.S.S.R.) **34**, 58 and 73 (1958), Soviet Phys. JETP **7**, 41 and 51 (1958).

[4] A. A. Abrikosov and I. E. Dzyaloshinskiĭ, J. Exptl. Theoret. Phys. (U.S.S.R.) **35**, 771 (1958), Soviet Phys. JETP **8**, 535 (1959).

[5] C. Kittel and A. Mitchell, Phys. Rev. **101**, 1611 (1956).

[6] C. Kittel and E. Abrahams, Revs. Modern Phys. **25**, 233 (1953).

[7] V. L. Ginzburg, J. Exptl. Theoret. Phys. (U.S.S.R.) **31**, 202 (1956), Soviet Phys. JETP **4**, 153 (1957).

Translated by W. F. Brown, Jr.
155

A MODEL OF A FIELD THEORY WITH NONVANISHING RENORMALIZED CHARGE

A. A. ANSEL' M

Physico-Technical Institute, Academy of Sciences, U.S.S.R.

Submitted to JETP editor September 13, 1958

J. Exptl. Theoret. Phys. (U.S.S.R.) **36**, 863-868 (March, 1959)

Two fermion fields are considered in a space of one dimension (and in time), with interaction of each field with itself and of the two with each other. The first term in the expansion of the vertex part in an asymptotic series of well known form is obtained. It is shown that within certain limits the renormalized charge can have an arbitrary (nonvanishing) value.

IN a number of papers[1-3] attempts have been made to deal with a relativistically invariant model of a field theory — the one-dimensional four-fermion interaction.

It was expected that the relation between the renormalized and bare charges in this theory would be such that the renormalized charge would not vanish when one goes to the limit of a point interaction.[2] A more detailed examination showed, however, that on account of a certain special cancellation of terms in the perturbation-theory series the theory contains no divergences at all, so that there is no charge renormalization and the question of the vanishing of the charge simply does not arise. In the present paper we consider two spinor fields in a one-dimensional space, with interaction of the four-fermion type between the two fields and of each field with itself. There is then a logarithmic divergence in the vertex part, and consequently an infinite charge renormalization. Unlike the various three-dimensional types of field theory, however, in which up to now it has not been possible to avoid the vanishing of the renormalized charge in the point-interaction theory, in the present model it is possible to construct a renormalized solution (or, more precisely, its asymptotic form for large momenta) with an arbitrary value of the renormalized charge.

1. THE EQUATIONS FOR THE VERTEX PART

Let us consider two fermion fields ψ and χ that depend on a single space coordinate x and the time x_0.

In our case the Hamiltonian can be chosen in the form:

$$H=\sum_{\mu}[(g_1/4)(\bar{\psi}\sigma_\mu\psi)(\bar{\psi}\sigma_\mu\psi)+(g_2/4)(\bar{\chi}\sigma_\mu\chi)(\bar{\chi}\sigma_\mu\chi)+(g_3/2)(\bar{\psi}\sigma_\mu\psi)(\chi\sigma_\mu\chi)],\quad \sum_{\mu}\sigma_\mu\times\sigma_\mu=\sigma\times\sigma-1\times 1. \quad (1)$$

The product $\sum_{\mu}\sigma_\mu\times\sigma_\mu$ is a mixture of interaction types $-S+P+V$, which in the one-dimensional case is the only completely antisymmetric type of interaction.[2] For the first two terms in Eq. (1) this spinor form is necessary; in the third term $\sigma_\mu\times\sigma_\mu$ can in principle be replaced by an arbitrary invariant operator $O_j\times O_j$, so that $\sigma_\mu\times\sigma_\mu$ has been kept here just for simplicity. Thus we are dealing with the one-dimensional analogue of the "universal interaction" of the type proposed by Feynman and Gell-Mann.

The introduction of terms of the type $(\bar{\psi}\sigma_\mu\chi)\times(\bar{\psi}\sigma_\mu\chi)$ into the Hamiltonian makes the problem much more complicated, and this case is not considered here. We now introduce a field $\Phi_\alpha=\begin{pmatrix}\psi\\ \chi\end{pmatrix}$ with the components ψ and χ. Then Eq. (1) can be rewritten in the form

$$H=\sum_{\mu}[(g_1/4)(\bar{\Phi}\sigma_\mu\tau_1\Phi)(\bar{\Phi}\sigma_\mu\tau_1\Phi)+(g_2/4)(\bar{\Phi}\sigma_\mu\tau_2\Phi)(\bar{\Phi}\sigma_\mu\tau_2\Phi)+(g_3/2)(\bar{\Phi}\sigma_\mu\tau_1\Phi)(\bar{\Phi}\sigma_\mu\tau_2\Phi)],$$

$$\tau_1=\begin{pmatrix}1&0\\0&0\end{pmatrix},\quad \tau_2=\begin{pmatrix}0&0\\0&1\end{pmatrix}. \quad (2)$$

The matrices τ_i act on the "isotopic" index of the function Φ_α.

The most general form of the vertex part is

$$\Gamma=\sum_{i,k}\alpha_{ik}(\tau_i\times\tau_k)\sum_{\mu}(\sigma_\mu\times\sigma_\mu)$$

where α_{ik} is a set of scalar functions, and τ_i and τ_k are all possible two-rowed matrices. It can be shown, however, that the equations for Γ are satisfied by the following spinor form:*

*This is a consequence of the law of conservation of the number of particles ψ and χ, which follows from the Hamiltonian (1).

$$\Gamma = [\alpha_1(\tau_1 \times \tau_2) + \alpha_2(\tau_2 \times \tau_3) + 2\alpha_3(\tau_1 \times \tau_2)] \sum_\mu \tau_\mu \times \sigma_\mu. \quad (3)$$

A method for obtaining an integral equation for Γ in the asymptotic region $p^2 \gg m^2$ has been developed by Dyatlov, Sudakov, and Ter-Matirosyan.[4] In the present case we have to do with a situation entirely analogous to that considered in reference 2. Carrying out some simple algebraic manipulations, we get the following system for the "lying" and "standing bricks" (the definition of these functions and some explations about the equations are given in reference 2):

$$f_1(\xi) = -\frac{1}{2\pi}\int_\xi^L \alpha_1^2(z)\,dz,$$

$$f_2(\xi) = -\frac{1}{2\pi}\int_\xi^L \alpha_2^2(z)\,dz, \quad f_3(\xi) = -\frac{1}{2\pi}\int_\xi^L \alpha_3^2(z)\,dz,$$

$$\tau_1(\xi) = \frac{1}{2\pi}\int_\xi^L [\alpha_1^2(z) + \alpha_3^2(z)]\,dz,$$

$$\tau_2(\xi) = \frac{1}{2\pi}\int_\xi^L [\alpha_2^2(z) + \alpha_3^2(z)]\,dz,$$

$$\tau_3(\xi) = \frac{1}{2\pi}\int_\xi^L [\alpha_1(z) + \alpha_2(z)]\,\alpha_3(z)\,dz,$$

$$\alpha_i = g_i + f_i + \tau_i, \quad \xi = \ln(p^2/m^2), \quad L = \ln(\Lambda^2/m^2), \quad (4)$$

Λ is the maximum momentum, and all the momenta entering and leaving the vertex part are of the order of p. In Eq. (4) the Green's function is taken equal to its zeroth approximation, since it is in general free from divergences.[2] From Eq. (4) it at once follows that

$$\alpha_1(\xi) = g_1 + \frac{1}{2\pi}\int_\xi^L \alpha_3^2(z)\,dz, \quad \alpha_2(\xi) = g_2 + \frac{1}{2\pi}\int_\xi^L \alpha_3^2(z)\,dz,$$

$$\alpha_3(\xi) = g_3 + \frac{1}{2\pi}\int_\xi^L [\alpha_1(z) + \alpha_2(z) - \alpha_3(z)]\,\alpha_3(z)\,dz. \quad (5)$$

2. SOLUTION OF THE INTEGRAL EQUATIONS

Combining the first and second equations of the system (5), we get the following system, which includes the third equation:

$$f(\xi) = \lambda + \frac{1}{\pi}\int_\xi^L \varphi^2(z)\,dz,$$

$$\varphi(\xi) = \nu + \frac{1}{2\pi}\int_\xi^L [f(z) - \varphi(z)]\,\varphi(z)\,dz. \quad (6)$$

Here we have introduced the notations

$$f = \alpha_1 + \alpha_2, \quad \varphi = \alpha_3, \quad \lambda = g_1 + g_2, \quad \nu = g_3. \quad (7)$$

Since the independent variable does not appear explicitly in Eq. (6), it is convenient first to try to find f as a function of φ. The first equation of the system (6) then has the form:

$$f = \lambda + \frac{1}{\pi}\int_\varphi^\nu \varphi^2\left(\frac{d\xi}{d\varphi}\right)d\varphi. \quad (8)$$

From the second equation it follows that

$$d\varphi/d\xi = -(f-\varphi)\varphi/2\pi, \quad (9)$$

that is,

$$f(\varphi) = \lambda - 2\int_\varphi^\nu \frac{\varphi'\,d\varphi'}{f(\varphi') - \varphi'}, \quad (10)$$

or

$$df/d\varphi = 2\varphi/(f-\varphi). \quad (11)$$

Equation (11) is a homogeneous equation; integrating it in the usual way, we easily get

$$(f-2\varphi)(f+\varphi)^2 = (\lambda - 2\nu)(\lambda+\nu)^2 \equiv G^3. \quad (12)$$

Let us consider the important case G = 0. Here we have either: (a) $\lambda = 2\nu$, $g_1 + g_2 = 2g_3$, $f = 2\varphi$, or else (b) $\lambda = -\nu$, $g_1 + g_2 = -g_3$, $f = -\varphi$. In each case we can substitute φ, expressed in terms of f, in the first equation of (6); we thus easily get the following expressions for the vertex parts:

$$\text{(a)}\quad f(\xi) = \frac{2\nu}{1-(\nu/2\pi)(L-\xi)}, \quad \varphi(\xi) = \frac{\nu}{1-(\nu/2\pi)(L-\xi)},$$

$$\alpha_1(\xi) = \frac{g_1-g_2}{2} + \frac{\nu}{1-(\nu/2\pi)(L-\xi)},$$

$$\alpha_2(\xi) = -\frac{g_1-g_2}{2} + \frac{\nu}{1-(\nu/2\pi)(L-\xi)},$$

$$\text{(b)}\quad f(\xi) = \frac{-\nu}{1+(\nu/\pi)(L-\xi)}, \quad \varphi(\xi) = \frac{\nu}{1+(\nu/\pi)(L-\xi)},$$

$$\alpha_1(\xi) = \frac{g_1-g_2}{2} - \frac{\nu/2}{1+(\nu/\pi)(L-\xi)},$$

$$\alpha_2(\xi) = -\frac{g_1-g_2}{2} - \frac{\nu/2}{1+(\nu/\pi)(L-\xi)}. \quad (13)$$

When $\nu = 0$ we have for both sets of relations between the constants the results $\alpha_1 = g_1$, $\alpha_2 = g_2$, $\alpha_3 = 0$, in agreement with the results obtained in reference 2. If $g_1 + g_2 < 0$, then for the usual reasons the renormalized charge goes to zero, but if $g_1 + g_2 > 0$ the zero charge does not appear. Furthermore, the connection between the renormalized and bare charges is given by the following relation (for example, in case a) or:

$$\nu_c = \frac{\nu}{1-\nu L/2\pi}, \quad g_{1c} = \frac{g_1-g_2}{2} + \frac{\nu}{1-\nu L/2\pi},$$

$$g_{2c} = -\frac{g_1-g_2}{2} + \frac{\nu}{1-\nu L/2\pi}, \quad (14)$$

and the expressions for the renormalized vertex parts have no nonphysical pole:

$$\varphi_c(\xi)=\frac{\nu_c}{1+\nu_c\xi/2\pi},\quad \alpha_{1c}(\xi)=\frac{g_{1c}-g_{2c}}{2}+\frac{\nu_c}{1+\nu_c\xi/2\pi},$$

$$\alpha_{2c}(\xi)=-\frac{g_{1c}-g_{2c}}{2}+\frac{\nu_c}{1+\nu_c\xi/2\pi}. \qquad (15)$$

Let us now go back to the determination of the functions f and φ in the general case $G=(\lambda-2\nu)^{1/3}(\lambda+\nu)^{2/3}\neq 0$. Equation (12) in principle makes it possible to express the function φ in terms of f, after which the first of the equations (6) reduces to a quadrature. We shall, however, proceed in a different way, which allows us to get the solution in a more compact form. We define $F(\xi)$ by the relation

$$f+\varphi=(\lambda+\nu)/F, \qquad (16a)$$

and then from Eq. (12) we get

$$f-2\varphi=(\lambda-2\nu)F^2, \qquad (16b)$$

from which we have

$$f=\frac{2(\lambda+\nu)}{3}\frac{1}{F}+\frac{\lambda-2\nu}{3}F^2,$$

$$\varphi=\frac{\lambda+\nu}{3}\frac{1}{F}-\frac{\lambda-2\nu}{3}F^2. \qquad (17)$$

Substituting these expressions in the first equation of (6) and differentiating it with respect to ξ, we find a differential equation for F. Separating the variables and integrating, we find

$$3\alpha^2\int_1^F\frac{dx}{x^3-\alpha^3}=\frac{G}{2\pi}(L-\xi),$$

$$\alpha=\left(\frac{\lambda+\nu}{\lambda-2\nu}\right)^{1/3},\quad G=(\lambda-2\nu)^{1/3}(\lambda+\nu)^{2/3},$$

$$3\alpha^2\int_1^F\frac{dx}{x^3-\alpha^3}=\frac{1}{2}\ln\frac{(F-\alpha)^2(1+\alpha+\alpha^2)}{(F^2+\alpha F+\alpha^2)(1-\alpha)^2}$$

$$-\sqrt{3}\arctan\frac{2F+\alpha}{\alpha\sqrt{3}}+\sqrt{3}\arctan\frac{2+\alpha}{\alpha\sqrt{3}}. \qquad (18)$$

Together with the (17), Eq. (18), which implicitly determines F, gives the solution of our stated problem. We shall now show that the solution we have obtained has the property of normalizability, and shall carry out the renormalization program explicitly. We introduce the renormalized charges λ_c and ν_c as the values of the vertex parts f and φ when the incoming and outgoing momenta are real ($p^2=-m^2$, $\xi=0$):

$$\lambda_c=\frac{2(\lambda+\nu)}{3}\frac{1}{F_0}+\frac{\lambda-2\nu}{3}F_0^2,$$

$$\nu_c=\frac{\lambda+\nu}{3}\frac{1}{F_0}-\frac{\lambda-2\nu}{3}F_0^2,$$

$$3\alpha^2\int_1^{F_0}\frac{dx}{x^3-\alpha^3}=\frac{G}{2\pi}L. \qquad (19)$$

From this we have

$$\lambda+\nu=(\lambda_c+\nu_c)F_0,\quad \lambda-2\nu=(\lambda_c-2\nu_c)F_0^{-2} \qquad (20)$$

and

$$G=G_c,\quad \alpha=\alpha_cF_0. \qquad (21)$$

These formulas enable us to eliminate from Eqs. (17) and (18) the renormalized charges and the logarithm of the cut-off L:

$$3\alpha_c^2F_0^2\int_{F_0}^{F}\frac{dx}{x^3-\alpha_c^3F_0^3}=-\frac{G_c}{2\pi}\xi,$$

$$f=\frac{2(\lambda_c+\nu_c)}{3}\frac{F_0}{F}+\frac{\lambda_c-2\nu_c}{3}\frac{F^2}{F_0^2},$$

$$\varphi=\frac{\lambda_c+\nu_c}{3}\frac{F_0}{F}-\frac{\lambda_c-2\nu_c}{3}\frac{F^2}{F_0^2}. \qquad (22)$$

Introducing the quantity $F_c(\xi)=F(\xi)/F_0$, we can verify that the renormalization invariants $f_c=f$, $\varphi_c=\varphi$ can be expressed in terms of the renormalized quantities only:

$$f_c(\xi)=\frac{2(\lambda_c+\nu_c)}{3}\frac{1}{F_c}+\frac{\lambda_c-2\nu_c}{3}F_c^2,$$

$$\varphi_c(\xi)=\frac{\lambda_c+\nu_c}{3}\frac{1}{F_c}-\frac{\lambda_c-2\nu_c}{3}F_c^2,$$

$$3\alpha_c^2\int_1^{F_c}\frac{dx}{x^3-\alpha_c^3}=-\frac{G_c}{2\pi}\xi. \qquad (23)$$

We have still to examine the problem of the zero charge in the general case. For this purpose we rewrite Eq. (19), which defines the function F_0, in the following form:

$$\frac{1}{2}\ln\frac{(1-\alpha_c)^2(1+\alpha_cF_0+\alpha_c^2F_0^2)}{(1+\alpha_c+\alpha_c^2)(1-\alpha_cF_0)^2}$$

$$-\sqrt{3}\arctan\frac{2+\alpha_c}{\alpha_c\sqrt{3}}+\sqrt{3}\arctan\frac{2+\alpha_cF_0}{\alpha_cF_0\sqrt{3}}=\frac{G_c}{2\pi}L. \qquad (24)$$

For $L\to\infty$ the right member of this equation goes to $+\infty$ for $G_c>0$ and to $-\infty$ for $G_c<0$. The left member can go to $+\infty$ if $1-\alpha_cF_0\to 0$.* Thus for $G>0$, $\lambda>2\nu$ the zero-charge situation does not arise, and the bare charges approach the following limiting values [cf. Ea. (20)]:

$$\lambda+\nu\to(\lambda_c+\nu_c)\alpha_c^{-1}=G_c,\quad \lambda-2\nu\to(\lambda_c-2\nu_c)\alpha_c^2=G_c,$$

that is,

$$\lambda\to G_c,\quad \nu\to 0. \qquad (25)$$

This limiting behavior can be understood in a qualitative way. All the divergence in the theory is due to the presence of the third term in the

*If $\alpha_c^2F_0^2+\alpha_cF_0+1\to 0$, then F_0 is complex and the theory is non-Hermitian.

Hamiltonian (1) (cf. reference 2). When this term is absent ($\nu = 0$, $\nu_c = 0$), λ requires no renormalization, $\lambda = \lambda_c$. In the general case the renormalization of λ still turns out to be a finite one.

3. CONCLUSION

Various attempts to construct a consistent physically useful field theory with nonvanishing renormalized charge have so far been unsuccessful.[5] Therefore the idea has been put forward recently that it is impossible in principle for there to be a relativistically invariant Hermitian theory with a point interaction. We have analyzed here an example of such a theory, though of course it is of no use for the description of physical phenomena. It seems to us that the very fact of the existence of such a scheme shows how complicated the problem is of proving rigorously the zero-charge result

[1] W. Thirring, Annals of Physics **3**, 91 (1958).

[2] A. A. Ansel'm, J. Exptl. Theoret. Phys. (U.S.S.R.) **35**, 1522 (1958), Soviet Phys. JETP **8**, 1065 (1959).

[3] M. E. Maĭer and D. V. Shirkov, Joint Institute of Nuclear Studies Preprint, 1958.

[4] Dyatlov, Sudakov, and Ter-Martirosyan, J. Exptl. Theoret. Phys. (U.S.S.R.) **32**, 767 (1957), Soviet Phys. JETP **5**, 631 (1957).

[5] Pomeranchuk, Sudakov, and Ter-Martirosyan, Phys. Rev. **103**, 784 (1956); Abrikosov, Galanin, Gorkov, Landau, Pomeranchuk, and Ter-Martirosyan, Phys. Rev. **111**, 321 (1958).

Translated by W. H. Furry
156

SOVIET PHYSICS JETP VOLUME 36 (9), NUMBER 3 SEPTEMBER, 1959

ON THE THEORY OF NUCLEAR MAGNETIC MOMENTS

D. F. ZARETSKIĬ

Submitted to JETP editor September 16, 1958

J. Exptl. Theoret. Phys. (U.S.S.R.) **36**, 869-873 (March, 1959)

The strong spin-orbit coupling gives rise to an additional interaction between the nucleons in the nucleus and the electromagnetic field. The effect of this additional interaction on the nuclear magnetic moments is considered for spherical and nonspherical nuclei. It is shown, in particular, that about half of the anomalous deviation of the magnetic moment of Bi^{209} from the Schmidt line may be due to this effect.

1. INTRODUCTION

IN the shell theory of the nucleus the spin-orbit coupling plays an important role. The corresponding operator can be written in the form

$$\mathcal{H}_{ls}' = -(\lambda\hbar/m^2c^2)\,\mathbf{s}\,[\nabla U\times\mathbf{p}], \qquad (1)$$

where λ is the phenomenological spin-orbit coupling constant, $\mathbf{s}$ is the spin operator for the nucleon, $U(\mathbf{r})$ is the self-consistent nuclear potential, and $\mathbf{p}$ is the momentum operator for the nucleon.

If the nucleus is located in an electromagnetic field, general principles prescribe that the momentum of the nucleon, $\mathbf{p}$, be replaced in the Hamiltonian by the generalized momentum, $\mathbf{p}-e\mathbf{a}/c$. In addition to the usual terms, the Hamiltonian will then contain another term connected with the interaction (1):

$$\mathcal{H}' = (\lambda e\hbar/m^2c^3)\,\mathbf{s}\,[\nabla U\times\mathbf{a}], \qquad (2)$$

where $\mathbf{a}$ is the vector potential of the electromagnetic field.

It should be noted that the interaction (2) may play an essential role in the case of a proton. For a neutron, the effective charge due to the separation of the motion of the center of charge is equal to Ze/A for electric dipole transitions. In general, the effective charge is equal to Ze/A^l for electric multipoles, and to Ze/A^{l+1} for magnetic multipoles, where l is the order of the multipole. In the case of a neutron the interaction (2), therefore, does not give a significant contribution to the magnetic moment and the magnetic dipole transitions, if only the effective charge of the abovementioned origin is considered.

Mayer and Jensen[1] first pointed out the necessity of including the spin-orbit effect in the discussion of the electromagnetic properties of nuclei. However, they did not use expression (2), and their estimates are very crude. Grechukhin[2] investigated the effect of the spin-orbit coupling on the forbidden (in the shell model) magnetic transitions of the type $d_{3/2}\rightarrow s_{1/2}$.

In the present paper we consider the effect of the interaction (2) on the magnetic moments of spherical and nonspherical nuclei with an odd number of protons. The interaction (2) is, of course, not the only reason for the deviation of the observed magnetic moments from the Schmidt lines. Nevertheless, an estimate of the magnitude of the interaction (2) is undoubtedly of interest, since it allows to isolate the role of the other effects. Furthermore, this interaction may in some cases give the main contribution to deviation of the magnetic moments from the Schmidt lines, and to the probability of the forbidden M1 transitions in nuclei with an extra proton. In the case of nuclei with an extra neutron it becoms meaningful to include the interaction (2), if there exists an effective charge owing to the interaction of the neutron with the nuclear core. The possible existence of such a charge was recently considered in the Brueckner model.[3]

For the calculation of the magnetic moments it is necessary to make use of the following relation for a constant uniform magnetic field:

$$\mathbf{a} = {}^1/_2\,[\mathbf{H}\times\mathbf{r}].$$

Hence

$$\hat{\mathcal{H}}' = \frac{\lambda e\hbar}{2m^2c^3}\,\mathbf{s}\nabla U\times[\mathbf{H}\times\mathbf{r}]$$

$$= \frac{\lambda e\hbar}{2m^2c^3}\,\mathbf{s}\,[\mathbf{H}(\nabla U\cdot\mathbf{r}) - \mathbf{r}(\nabla U\cdot\mathbf{H})]. \qquad (3)$$

Let $H_Z = H$, $H_{X,Y} = 0$. We then obtain the following expression for the operator of the magnetic moment connected with this interaction:

$$\hat{\mu}_z = (\lambda e\hbar/2m^2c^3)\,[(\mathbf{s}\cdot\mathbf{r})\nabla_z U - s_z(\nabla U\cdot\mathbf{r})]. \qquad (4)$$

To calculate the radiative transition probabili-

ties we must know the expression for the current operator corresponding to the interaction (2). This operator obviously has the form

$$\hat{\mathbf{j}} = -c\delta\hat{\mathcal{H}}'/\delta\mathbf{a} = -(\lambda e\hbar/m^2c^2)[\mathbf{s}\times\nabla U]. \qquad (5)$$

With the help of this operator we can calculate the radiative transition probabilities by well-known formulas.[4]

2. MAGNETIC MOMENTS OF SPHERICAL NUCLEI

The magnetic moment of a spherical nucleus can be written in the form of the following matrix elements:*

$$\mu = \langle J, J|\hat{\mu}_z|J, J\rangle. \qquad (6)$$

It follows that

$$\mu = \frac{\lambda e\hbar}{2m^2c^2}\left\langle J\left|r\frac{\partial U}{\partial r}\right|J\right\rangle\langle J, J|(\mathbf{s}\cdot\mathbf{n})n_z - s_z|J, J\rangle, \qquad (7)$$

where $\mathbf{n}$ is a unit vector in the direction of $\mathbf{r}$.

First of all we calculate the angular matrix element in formula (7):

$$(\mathbf{s}\cdot\mathbf{n})n_z = (\mathbf{J}\cdot\mathbf{n})n_z = [J_zn_z + {}^1/_2(J_x - iJ_y)(n_x + in_y) + {}^1/_2(J_x + iJ_y)(n_x - in_y)]n_z,$$

$$\langle J, J|J_zn_z^2|J, J\rangle = \sqrt{4\pi/9}\,J[(2/\sqrt{5})\langle Y_{2,0}\rangle + \langle Y_{0,0}\rangle] = J/2(J+1). \qquad (8)$$

Obviously,

$$\langle J, J|(J_x - iJ_y)(n_x + in_y)n_z|J, J\rangle = 0.$$

The matrix element of the last term in formula (8) is also computed without difficulty. We obtain

$$\langle J, J|(J_x + iJ_y)(n_x - in_y)n_z|J, J\rangle = \langle J, J|(J_x + iJ_y)|J, J-1\rangle\langle J, J-1|(n_x - in_y)n_z|J, J\rangle = (8\pi/3)\sqrt{3/20\pi}\sqrt{J}\langle J, J-1|Y_{2,-1}|J, J\rangle = -(2J-1)/2(J+1).$$

As a result we obtain the following expression for the additional magnetic moment connected with the interaction (2):

$$\mu = \mp\frac{J+{}^1/_2}{2(J+1)}\frac{e\hbar}{2mc}\frac{\lambda}{mc^2}\left\langle J\left|r\frac{\partial U}{\partial r}\right|J\right\rangle, \qquad (9)$$

where the minus sign refers to $J = l + \frac{1}{2}$, and the plus sign to $J = l - \frac{1}{2}$. The sign of this additional moment corresponds to the sign of the deviation of the nuclear magnetic moments from the Schmidt lines.

Let us now estimate the magnitude of the additional magnetic moment (9). Observing that $\partial U/\partial r$ is different from zero only near the nuclear surface, we obtain

$$\frac{\lambda}{mc^2}\left\langle J\left|\frac{1}{r}\frac{\partial U}{\partial r}r^2\right|J\right\rangle \approx \frac{\lambda}{mc^2}R_0^2\left\langle J\left|\frac{1}{r}\frac{\partial U}{\partial r}\right|J\right\rangle,$$

where R_0 is the effective radius of the nucleus. This matrix element enters into the expression for the energy of the spin-orbit coupling

$$E_{sl} = -\frac{\lambda\hbar^2}{m^2c^2}\left\langle J\left|\frac{1}{r}\frac{\partial U}{\partial r}\right|J\right\rangle(\mathbf{s}\cdot\mathbf{l})$$

and can be obtained from the energy of the spin-orbit splitting

$$\frac{\lambda}{m^2c^2}\left\langle J\left|\frac{1}{r}\frac{\partial U}{\partial r}\right|J\right\rangle = \frac{2\Delta E_{sl}}{\hbar^2(2l+1)}. \qquad (10)$$

The diffuseness of the nuclear boundary is supposedly the same for all nuclei. The function $f(r) = \partial U/\partial r$ will then also be practically the same for all spherical nuclei. This conclusion is confirmed by the experiments on the scattering of fast electrons from nuclei, as well as by the calculations in the framework of the optical model with diffuse boundary.[5,6] The region in which this function is noticeably different from zero is of order 1.5 to 2×10^{-13} cm. The wave functions of the states without radial nodes and with $l \neq 0$ differ significantly from zero in the neighborhood of the nuclear surface in approximately the same region where $f(r)$ is different from zero. It should therefore be expected that for these states

$$\frac{\lambda\hbar^2}{m^2c^2}\left\langle J\left|\frac{1}{r}\frac{\partial U}{\partial r}\right|J\right\rangle \approx CA^{-1/3}, \qquad (11)$$

where C is an empirical constant, which can be determined, for example, from the splitting of the levels $d_{5/2} - d_{3/2}$ in O^{17} (reference 7). In the case of one-nucleon states corresponding to wave functions with radial nodes, one should expect that the abovementioned matrix element depends more strongly on A than as $A^{-1/3}$.

These qualitative considerations are confirmed in a wide range of atomic weights by shell-model calculations with a potential with diffuse boundary. Such calculations were recently carried out by Nemirovskiĭ.[6]

It should also be noted that Nilsson[8] assumed in his calculations that the matrix element depends on the atomic weight as in formula (11). Using (11) with the constant C determined in the indicated fashion, and taking $R_0 = 1.23 \times 10^{-13}A^{1/3}$ (reference 6) as the value of the effective radius of the charge, we obtain the following estimate:

$$\mu \approx \mp A^{1/3}0.11\,\frac{2J+1}{2(J+1)}\frac{e\hbar}{2mc}. \qquad (12)$$

*In formulas (6) and (7), as in the following, the second index in the matrix elements denotes the projection of the moment J.

In the case of Bi^{209}, for example, this estimate gives the value $\mu \approx +0.6\, e\hbar/2mc$. This is slightly less than half the anomalous magnetic moment of this nucleus.

3. MAGNETIC MOMENTS OF NONSPHERICAL NUCLEI

In the strong coupling approximation the wave function of the nonspherical nucleus can be written as a product of the wave function for the motion of the nucleon relative to the nuclear axis and the wave function for the collective motion:[9]

$$\psi^{J}_{\Omega, K} = \chi_{\Omega} D^{J}_{M, K}. \tag{13}$$

In this case the magnetic moment is conveniently calculated with the help of the relation

$$\mu = \langle \hat{\boldsymbol{\mu}} \mathbf{J} \rangle / (J+1), \tag{14}$$

where

$$\hat{\boldsymbol{\mu}} = \frac{\lambda}{mc^2}\frac{e\hbar}{2mc}[(\mathbf{s}\cdot\mathbf{r})\nabla U(r) - \mathbf{s}(\nabla U \cdot \mathbf{r})].$$

If the deformation of the nucleus is small ($\Delta R/R \ll 1$), formula (14) may be written in the form

$$\mu = \frac{\lambda}{mc^2}\frac{e\hbar}{2mc}\,\frac{\langle r\,(\partial U/\partial r)\,[(\mathbf{s}\cdot\mathbf{n})(\mathbf{n}\cdot\mathbf{J}) - (\mathbf{s}\cdot\mathbf{J})]\rangle}{J+1}, \tag{15}$$

For the matrix element we have

$$\begin{aligned}\langle \Omega, K | (\mathbf{s}\cdot\mathbf{n})(\mathbf{n}\cdot\mathbf{J}) | \Omega, K\rangle &= \langle \Omega, K | (\mathbf{j}\cdot\mathbf{n})(\mathbf{n}\cdot\mathbf{J}) | \Omega, K\rangle \\ &= \langle \Omega, K | (\mathbf{j}\cdot\mathbf{n}) | \Omega' K'\rangle \langle \Omega' K' | (\mathbf{n}\cdot\mathbf{J}) | \Omega K\rangle \\ &= K \langle \Omega | (\mathbf{j}\cdot\mathbf{n}) n_{z'} | \Omega\rangle,\end{aligned} \tag{16}$$

Ω, K, $n_{z'}$ are the projections of j, J, n on the z′ axis of the nucleus, respectively.

With the help of (16) we obtain the additional magnetic moment of nuclei with spin other than $\frac{1}{2}$ in the form

$$\mu = K\mu_{\text{int}}/(J+1),$$

where

$$\mu_{\text{int}} = \left\langle \Omega \left| r\frac{\partial U}{\partial r}[(\mathbf{j}\cdot\mathbf{n})n_{z'} - s_{z'}] \right| \Omega \right\rangle \frac{\lambda}{mc^2}\frac{e\hbar}{2mc} \tag{17}$$

is the additional magnetic moment of the nucleon in the coordinate system defined by the nuclear axes. The order of magnitude of μ_{int} is, of course, the same as for spherical nuclei.

The formula of Bohr and Mottelson[10] for the magnetic moments,

$$\mu = g_{\Omega} J^2/(J+1) + g_R/(J+1), \tag{18}$$

therefore remains valid for nuclei with $J = K = \Omega \geq \frac{3}{2}$; g_{Ω} and g_R are the gyromagnetic ratios for the one-nucleon and collective motions. However, besides the usual terms, g_{Ω} must also contain the gyromagnetic ratio arising from the additional magnetic moment (17).

Let us now consider the magnetic moments of nuclei with spin $\frac{1}{2}$. We shall assume that the case of coupling b according to Hund[11] applies to these nuclei. The one-nucleon states in these nuclei can then be classified as Σ^{+}_{g} and Σ^{+}_{u}.

The symbol Σ^{+}_{g} refers to one-nucleon states with positive parity ($\frac{1}{2}^{+}$), and Σ^{+}_{u} refers to states with negative parity ($\frac{1}{2}^{-}$).

In this classification we have the following constants of the motion (besides the trivial ones): the nucleon spin s, the total rotational moment $\kappa = l + R$ (R is the vector of the moment of the collective rotation), the projection of the vector of the orbital angular momentum of the nucleon l on the nuclear axis $\Lambda = 0$, and the projection of κ on the nuclear axis $\kappa_{z'} = 0$.

Using the above-mentioned symmetry properties of the wave function, we can in this case easily compute the matrix element (14). We obtain the result

$$\begin{aligned}\frac{\lambda}{mc^2}\left\langle r\frac{\partial U}{\partial r}[(\mathbf{s}\cdot\mathbf{n})(\mathbf{n}\cdot\mathbf{J}) - (\mathbf{s}\cdot\mathbf{J})]\right\rangle &= \left[\frac{1}{4}\left\langle r\frac{\partial U}{\partial r}(n^2_{z'} - n^2_{x'})\right\rangle\right. \\ &\left. + \langle(\mathbf{s}\cdot\mathbf{J})\rangle\left\langle r\frac{\partial U}{\partial r}n^2_{x'}\right\rangle - \left\langle(\mathbf{s}\cdot\mathbf{J})\, r\frac{\partial U}{\partial r}\right\rangle\right]\frac{\lambda}{mc^2}.\end{aligned} \tag{19}$$

It follows from the theory of the rotational spectra of nuclei with spin $\frac{1}{2}$, developed by us earlier,[11] that the energies of the rotational levels of these nuclei can be obtained from the Hamiltonian

$$\mathcal{H}_{\text{coll}} = \hbar^2\kappa^2/2I + \gamma\boldsymbol{\kappa}\cdot\mathbf{s}, \tag{20}$$

where I is the moment of inertia, β the deformation parameter, and

$$\gamma = \frac{3}{2}\sqrt{\frac{5}{4\pi}}\beta\frac{\hbar^2}{I}\frac{\lambda}{mc^2}\left\langle r\frac{\partial U}{\partial r}(n^2_{z'} - n^2_{x'})\right\rangle.$$

Finally, we obtain the following expression for the additional magnetic moment of nuclei with spin $\frac{1}{2}$:

$$\begin{aligned}\mu = \frac{e\hbar}{2mc(J+1)}\left\{\frac{\gamma}{(^3/_2)\sqrt{5/4\pi}\beta\hbar^2/I}[^1/_4 - {}^1/_3\langle(\mathbf{s}\cdot\mathbf{J})\rangle]\right. \\ \left. - {}^2/_3\langle(\mathbf{s}\cdot\mathbf{J})\rangle\left\langle r\frac{\partial U}{\partial r}\right\rangle\frac{\lambda}{mc^2}\right\}.\end{aligned} \tag{21}$$

Let us apply formula (21) to the calculation of the magnetic moment of Tm^{169}. The rotational spectrum corresponds in this case[12] to the Σ^{+}_{u} state, for which $\kappa = 1, 3, 5, \ldots$. For this nucleus $\beta = 0.3$ (reference 13) and $\gamma/(\hbar^2/I) = 0.24$. If we further assume that $\langle r\partial U/\partial r\rangle$ is in this case of the same order of magnitude as for spherical nuclei, and that $g_R = 0.41$, we obtain $\mu_{\text{tot}} = -0.35$ nuclear magnetons for the total magnetic moment of this nucleus. The experimental value for this

magnetic moment is $\mu_{exp} = -0.20 \pm 0.05$. The comparison of these two values shows that the magnetic moment of Tm^{169} does not contradict the adopted classification of the ground state of this nucleus.

It is seen from these calculations that the interaction (2) can make a significant contribution to the magnetic moments of spherical and nonspherical nuclei, which must not be neglected.

In conclusion I should like to express my gratitude to P.E. Nemirovskiĭ for very helpful comments.

[1] M. Goeppert-Mayer and J. H. D. Jensen, Phys. Rev. **85**, 1041 (1952).

[2] D. P. Grechukhin, J. Exptl. Theoret. Phys. (U.S.S.R.) **31**, 513 (1956); Soviet Phys. JETP **4**, 448 (1957).

[3] J. S. Bell, Nucl. Phys. **4**, 295 (1957).

[4] J. Blatt and V. Weisskopf, Theoretical Nuclear Physics, J. Wiley, N.Y., 1952.

[5] P. É. Nemirovskiĭ, J. Exptl. Theoret. Phys. (U.S.S.R.) **32**, 1143 (1957); Soviet Phys. JETP **5**, 932 (1957).

[6] P. É. Nemirovskiĭ, J. Exptl. Theoret. Phys. (U.S.S.R.) **33**, 746 (1957); Soviet Phys. JETP **6**, 573 (1958).

[7] I. I. Levintov, J. Exptl. Theoret. Phys. (U.S.S.R.) **30**, 987 (1956); Soviet Phys. JETP **3**, 796 (1956).

[8] S. Nilsson, Kgl. Danske Videnskab. Selskab, Mat.-fys. Medd. **29**, No. 16 (1955).

[9] A. Bohr, Kgl. Danske Videnskab. Selskab, Mat.-fys. Medd. **26**, No. 14 (1952).

[10] A. Bohr and B. Mottelson, Kgl. Danske Videnskab. Selskab, Mat.fys. Medd. **27**, No. 16 (1953).

[11] D. F. Zaretskiĭ and A. V. Shutko, J. Exptl. Theoret. Phys. (U.S.S.R.) **32**, 370 (1957); Soviet Phys. JETP **5**, 323 (1957).

[12] Hatch, Boehm, Marmier, and Du Mond, Phys. Rev. **104**, 745 (1956). Baranov, Polevoĭ, Radionov, and Shishkin, Атомная энергия (Atomic Energy) **3**, 256 (1957).

[13] B. Mottelson and S. Nilsson, Z. Physik **141**, 217 (1955).

Translated by R. Lipperheide
157

ON THE ELECTROMAGNETIC RADII OF THE LIGHTEST NUCLEI IN THE GROUND AND LOWEST EXCITED STATES

A. K. KAMINSKIĬ and Yu. M. SHIROKOV

Moscow State University

Submitted to JETP editor September 16, 1959

J. Exptl. Theoret. Phys. (U.S.S.R.) **36**, 874-878 (March, 1959)

The radii of nuclei of mass numbers 5 to 8 are calculated for the ground and excited states from experimental data on isotopic multiplets and on the scattering of high energy electrons by nuclei. It is shown that for all the nuclei with the exception of the doublet He^5-Li^5 the radii increase monotonically with energy. One of the levels of Be^8 is identified with greater precision.

1. INTRODUCTION

AT the present time nuclear radii have been measured only very roughly. The formula $R = r_0 A^{1/3}$ is based on the model of a uniformly charged sphere and is very inaccurate, particularly in the region of the light nuclei.

Recently a number of sufficiently accurate experimental data has been accumulated which enable us to determine the mean square radius for the charge distribution in the lightest nuclei and to draw certain conclusions with respect to the dependence of the electromagnetic radii on the energy of excitation of the nuclei. For this purpose the present paper makes use of data on charge multiplets. The energy of isotopically similar levels must differ only by the Coulomb interaction. The nuclear forces are assumed to have isotopic invariance. The energy levels of the lightest nuclei have been measured with a sufficient degree of accuracy, many of them have been identified with respect to their angular momentum, parity and isotopic spin. We also make use of data on the scattering of fast electrons by nuclei which enable us to determine in a different way the mean square radii of the charge distribution for the ground states of certain light nuclei.

There exists also a third independent type of experiments: the energy levels of mesic atoms, but these experiments are not yet accurate and allow us only to conclude that the electromagnetic radii of the nuclei are considerably smaller than the values obtained from experiments on the scattering of nucleons by nuclei.

2. CALCULATIONS

The wave function for the nucleus is constructed in accordance with the shell model using jj coupling from oscillator single nucleon wavefunctions taking the Pauli exclusion principle into account and incorporating the total angular momentum J and its component M along the z axis, the isotopic spin T (as an approximate quantum number) and its component T_ζ, determined by the nuclear charge Z.

Such a function may be constructed explicitly if the symmetrization is carried out by means of Young's tableau and utilizing vector addition rules, but this is very complicated. This may be avoided if one uses the technique of fractional parentage coefficients. This enables us to reduce the calculation of the matrix elements of the Coulomb energy (and of any arbitrary pair operator) with respect to the nuclear wavefunctions to the calculation of matrix elements with respect to wavefunctions of a pair of particles. The latter may be easily computed since both the functions and the operators are known. The corresponding formulas have been derived by utilizing methods of second quantization as proposed by Balashov, Tumanov, and Shirokov.[1]

Making use of these formulas we have calculated the matrix elements of the Coulomb energy for all of the nuclear states up to Be^8.

The experimentally obtained binding energies have been taken from the review by Wapstra,[2] while the energies of the excited states of nuclei have been taken from the review article of Ajzenberg and Lauritsen.[3]

Theoretically the difference in Coulomb energies turns out to be equal to $ke^2/\sqrt{2\pi r_0}$, where k is a certain numerical factor, while r_0 is the parameter which determines the single nucleon wavefunctions, which are equal to

$$P_n(r/r_0)\exp(-r^2/2r_0^2),$$

where $P_n(r/r_0)$ are the generalized Laguerre

polynomials; $r_0 = \sqrt{\hbar/m\omega}$, where m is the nucleon mass, while ω is the characteristic oscillator frequency; r_0 is proportional to the mean square radius a of the charge distribution in the nucleus. Similar calculations for the ground states of nuclei have been carried out under certain simplifying assumptions by Carlson and Talmi.[4] They assumed that there are no neutrons in the unfilled shell while the protons are in the state with the lowest "seniority," i.e., they have been paired as far as possible into pairs with zero angular momentum.

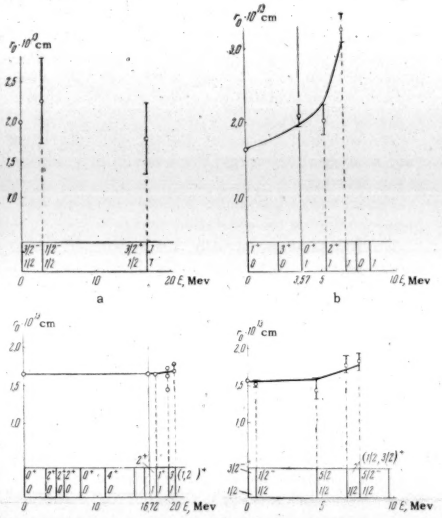

a – $He^5 - Li^5$; b – $He^6 - Li^6 - Be^6$, E – excitation energy in Li^6; c – $Li^8 - Be^8 - B^8$, E – excitation energy in Be^8; d – $Li^7 - Be^7$.

The dependence of r_0 (and therefore also of the mean square radius of the charge distribution in the nucleus) on the excitation energy of the nucleus is shown by means of graphs. The magnitude of the error in this is determined by two factors: the accuracy with which the energies of the corresponding levels have been measured, and the contribution which may be introduced by an admixture of other configurations within the limits of the p-shell (intermediate coupling).

In this way we can determine the values of r_0 for all the levels of the isotopic doublets (He^5-Li^5, Li^7-Be^7) and for the levels with T = 1 of isotopic triplets. However, it is not possible by this method to determine r_0 for the levels of Li^6 and Be^8 with T = 0 since there simply are no corresponding levels in neighboring nuclei.

To extrapolate the curves showing the energy dependence of r_0 to states with T = 0 we have used data on the scattering of fast electrons by nuclei given in the paper of Hofstadter.[5] Hofstadter discusses the relation between the various models of charge distribution in the nucleus and the scattering cross section for fast electrons by nuclei. For light nuclei the first Born approximation is applicable, according to which the effective cross section for elastic scattering of electrons by nuclei is equal to

$$\sigma_s(\theta) = \left(\frac{Ze^2}{2E}\right)^2 \frac{\cos^2(\theta/2)}{\sin^2(\theta/2)} \left[\int_0^\infty \rho(r)\, \frac{\sin p_0 r}{p_0 r}\, 4\pi r^2 dr\right]^2,$$

i.e., $\sigma_s(\theta)$ represents the effective cross section for elastic scattering of electrons by a point charge multiplied by the square of the structure factor

$$F = \frac{4\pi}{p_0} \int_0^\infty \rho(r) \sin p_0 r \cdot r dr.$$

Here $\hbar p_0$ is the change in momentum on scattering:

$$p_0 = \frac{2E}{\hbar c} \sin\frac{\theta}{2} = \frac{2}{\lambda} \sin\frac{\theta}{2},$$

where E is the electron energy, $\lambda = \hbar/p$. The calculation is carried out in the center of mass system, i.e., the recoil of the nucleus is not taken into account.

Hofstadter[5] gives mean square radii a and the form factors F corresponding to different assumptions on the distribution of charge in the nucleus. For H and He the distribution assumed by us coincides with the Gauss distribution. In this case

$$a^2 = \frac{3}{2} r_0^2, \quad \rho(r) = \frac{Ze}{\pi^{3/2} r_0^3} \exp\left(-\frac{r^2}{r_0^2}\right),$$

$$F = \exp\left(-\frac{r_0^2 p_0^2}{4}\right) = \exp\left(-\frac{p_0^2 a^2}{6}\right).$$

For nuclei in which the p shell is being filled

$$a^2 = \frac{r_0^2(5Z-4)}{2Z},$$

$$\rho(r) = \frac{2e}{\pi^{3/2} r_0^3} \exp\left(-\frac{r^2}{r_0^2}\right) + \frac{2(Z-2)}{3\pi^{3/2} r_0^5} r^2 \exp\left(-\frac{r^2}{r_0^2}\right),$$

$$F = \left\{\frac{2}{Z} + \frac{Z-2}{Z}\left(1 - \frac{r_0^2 p_0^2}{6}\right)\right\} \exp\left(-\frac{p_0^2 r_0^2}{4}\right).$$

A direct evaluation of r_0 from Hofstadter's data gives an overestimate of r_0 compared to the value obtained from the difference in Coulomb energies by about 25%. We make use of the fact that the mean square radius a is proportional to r_0.

By utilizing the value of r_0 for the ground level of Li^7, obtained from the difference in Coulomb energies, and the value of a for the ground states of Li^6, Li^7, and Be^9 given by Hofstadter,[5] we can roughly determine r_0 for the ground states of the nuclei Li^6 and Be^8, and extrapolate the curves giving the dependence on the excitation energy to the state with T = 0.

If the experiments on the scattering of fast electrons by nuclei are accurate, then the difference in the magnitude of the radii determined on the basis of the data of these experiments and on the basis of the Coulomb differences indicates the amount by which the true charge distribution in the nucleus differs from the distributions assumed by us.

The theoretically calculated Coulomb energy and electromagnetic radius of the nucleus depends on the choice of wave functions which, in particular, determines the distribution $\rho(r)$ of the electric charge in the nucleus. For levels with very great widths, for example, for the nuclei He^5-Li^5, the oscillator function is a very rough approximation and allows us to investigate the nature of the increase in radius with energy only qualitatively.

The agreement between experimental data on the scattering of fast electrons by nuclei and the values of nuclear radii obtained from differences in Coulomb energy may be improved if we assume that r_0 has different values for s and p shells (r_s and r_p). This may be done, since levels with even and odd values of l are orthogonal. Then for nuclei in which the p-shell is being filled $\rho(r)$ is of the form:

$$\rho(r) = \frac{Ze}{\pi^{3/2} r_s^3} \exp\left(-\frac{r^2}{r_s^2}\right) + \frac{2(Z-2)}{3\pi^{3/2} r_p^5} r^2 \exp\left(-\frac{r^2}{r_p^2}\right).$$

We have determined r_s and r_p from the difference in the Coulomb energies of the ground state of Li^7 and from the mean squared radius of the charge distribution Li^7 which is equal to 2.71 $\times 10^{-13}$ cm. They turned out to be equal to:

$$r_s = 2.42 \cdot 10^{-13} \text{ cm}, \qquad r_p = 1.32 \cdot 10^{-13} \text{ cm}.$$

The differences in Coulomb energies calculated with these values of r_s and r_p for all the nuclei with $A \leq 8$ differ from the experimental ones by not more than 10%.

Hofstadter notes[6] that such a $\rho(r)$ with $r_s = 2.65 \times 10^{-13}$ cm, $r_p = 1.07 \times 10^{-13}$ cm gives satisfactory agreement between experiment and the theoretical angular dependence of the scattering cross section for fast electrons by the Li^6 nucleus.

3. ANALYSIS OF THE CURVES

For the nuclear pair H^3-He^3 we obtain $r_0 = 1.48 \times 10^{-13}$ cm.

In contrast to all other nuclei the radius of the nuclei He^5 and Li^5 does not increase monotonically with energy. The radius of the nucleus in the second excited level with E = 16.69 Mev is lower than in the first excited state and even than in the ground state. This level has positive parity (the two first ones have negative parity) and is distinguished by relatively great stability. Apparently it corresponds to the breaking up of the s shell. If a neutron goes over from the s shell into the p shell then $r_0 = 1.79 \times 10^{-13}$ cm, but if a proton is excited (which, apparently, is more probable since we then obtain the triton + deuteron system, which explains the great stability), then $r_0 = 1.73 \times 10^{-13}$ cm.

The radius of the nuclei He^6-Li^6-Be^6 increases very sharply with energy; these nuclei are similar to the deuteron.

The radius of the nuclei Li^7-Be^7 does not depend strongly on the excitation energy.

The radius of nuclei with A = 8 depends very weakly on excitation energy. The level of Li^8 with E = 3.3 Mev and the level corresponding to it in Be^8 of 19.9 Mev have not been accurately identified, the following values are given $J = (1^+, 2^+)$. The graph shows both points, the upper one corresponding to $J = 2^+$, the lower one corresponding to $J = 1^+$.

The level of Li^8 with E = 2.28 Mev in the paper by Ajzenberg and Lauritsen[3] is compared with the level in Be^8 of 19.2 Mev. The corresponding point does not appear on the graph. Apparently the analogue to this Li^8 level in the case of Be^8 is not the 19.2-Mev level, but the 19.0 or the 18.9-Mev level. The graph shows all three points: the top one corresponds to E = 18.9 Mev, the middle one to 19.0, and the lowest one to 19.2 Mev.

4. CONCLUSIONS

On the basis of the simple method described above one can draw conclusions with respect to nuclear size and its increase, the "swelling" of nuclei in going to excited levels. It turns out that the electromagnetic nuclear radii increase monotonically with increasing excitation energy with the exception of one level of He^5-Li^5 which is distinguished by changed parity and by great stability. Moreover, the strong dependence of the radius on energy is observed only in the case of nuclei with A = 6 which are analogous to the deuteron.

Apparently it is possible by this method to make more precise the classification of levels of certain nuclei, since the Coulomb energy depends on the spatial correlation of nucleons in the nucleus. The possibility of obtaining more precise values for the radii of light nuclei in their different states is also of importance for theoretical calculations referring to levels of light nuclei utilizing the two nucleon interaction Hamiltonian by methods of the type used in references 7 and 8.

[1] Balashov, Tumanov, and Shirokov, Труды конференции по ядерным реакциям при малых и средних энергиях (Proceedings of the Conference on Nuclear Reactions at Low and Medium Energies, Moscow State University and Physics Institute Academy of Sciences, U.S.S.R.) 1957.

[2] A. H. Wapstra, Physica **21**, 367 (1955).

[3] F. Ajzenberg and T. Lauritsen, Revs. Modern Phys. **27**, 77 (1955).

[4] B. C. Carlson and I. Talmi, Phys. Rev. **96**, 436 (1954).

[5] R. Hofstadter, Revs Modern Phys. **28**, 214 (1956).

[6] R. Hofstadter, Report at the Paris Conference on Nuclear Reactions, 1958 (preprint).

[7] Balashov, Dorofeev, Kalitkin, Kaminskii, Smirnov, Tumanov, and Shirokov, Труды конференции по ядерным реакциям при малых и средних энергиях (Proceedings of the Conference on Nuclear Reactions at Low and Medium Energies, Moscow State University and Physics Institute Academy of Sciences, U.S.S.R.) 1957.

[8] Balashov, Tumanov, and Shirokov, J. Exptl. Theoret, Phys. (U.S.S.R.) **32**, 167 (1957), Soviet Phys. JETP **5**, 136 (1957).

Translated by G. Volkoff
158

SOVIET PHYSICS JETP VOLUME 36 (9), NUMBER 3 SEPTEMBER, 1959

A GROUP-THEORETICAL CONSIDERATION OF THE BASIS OF RELATIVISTIC QUANTUM MECHANICS V.

The Irreducible Representations of the Inhomogeneous Lorentz Group, Including Space Inversion and Time Reversal*

Yu. M. SHIROKOV

Moscow State University

Submitted to JETP editor September 16, 1958

J. Exptl. Theoret. Phys. (U.S.S.R.) **36**, 879-888 (March, 1959)

A complete classification is obtained of all the irreducible representations of the inhomogeneous Lorentz group, including space inversion and time reversal. It is shown that the concept of time parity cannot be introduced for particles with nonvanishing rest mass; for particles with zero rest mass and given spin there are two nonequivalent representations that differ in their space-time parity properties. On the basis of the concept of a universal covering group it is shown that for particles with half-integral spins the number of possible representations with different reflection laws is larger than has previously been supposed.

1. STATEMENT OF THE PROBLEM

THE problem of the invariance of a quantum theory with respect to time reversal is a comparatively complicated one, and despite the large number of papers on the subject (cf., e.g., the review articles, references 5 and 6) it cannot be regarded as having been exhaustively studied up to the present.

Papers in recent years have mainly dealt with the law of time reversal for particles with spin $\frac{1}{2}$, with the Dirac equation taken as fundamental.

In order to eliminate the negative energies, however; one has to subtract out in the quantized Dirac equation the infinite energy of the negative-energy sea, i.e., to carry out a certain nonidentical operation which, as it turns out, changes the transformation properties with respect to time reversal. Moreover, in studies based on concrete equations of motion there is always the danger of getting a result relating only to particles that obey the equation in question, and not to arbitrary particles of the given spin. These limitations are not present in group-theoretical methods based only on the geometrical properties of space and on the linearity of the equations of quantum mechanics. Furthermore the work must be based on the inhomogeneous Lorentz group containing four-dimensional rotations and displacements, since the irreducible representations of precisely this group describe the free motions of relativistic particles.

Usually the group-theoretical formulation of invariance under certain transformations consists of the assumption that the wave function transforms according to one of the representations of the group in question. In treatments of time reversal, however, it is more customary to use a different formulation, due to Wigner,[7] in which a change to the complex conjugate of the wave function is associated with time reversal.

The purpose of the present paper is a consistent study of the law of time reversal in the framework of the ordinary theory of the representations of the inhomogeneous Lorentz group, without the use of a concrete form of the equations of motion. A separate paper will be devoted to the Wigner formulation of the law of time reversal. The present paper is also not concerned with problems connected with the CPT theorem, which requires the introduction of a charge operator.

The inhomogeneous Lorentz group, including all possible space-time reflections (we denote this group by G_{st}) is obtained from the group G_s, which contains only the space reflections, by adjoining the operation I_{st} of the reflection of all four coordinates to the operations contained in G_s. According to Eqs. (I.36) and (IV.43) the operator I_{st} satisfies the commutation relations

*Notations introduced without explanation are the same as in references 1–4. Equation numbers such as (I.36), (IV.1) refer to formulas in references 1–4.

$$[I_{st},\ P_\mu]_+ = 0, \quad [I_{st},\ M_{\mu\nu}]_- = 0, \quad [I_{st},\ \Gamma_\lambda]_+ = 0. \quad (1)$$

2. THE IMPROPER GROUPS $G_1 - G_8$ OF TRANSFORMATIONS OF THE COORDINATES

In order completely to define the group G_{st} we must prescribe the commutation relations (I.31) between the components of the operators $M_{\mu\nu}$, P_λ, the relations (IV.1) between the inversion I_s and the operators $M_{\mu\nu}$, P_λ, the relations (1) for the operator I_{st}, and also all possible products of the operators I_s and I_{st} by themselves and each other. In this connection, as was already pointed out in reference 4, in order not to have to deal with two-valued representations, one must consider instead of the proper inhomogeneous Lorentz group its universal covering group.

It is important to note that the universal covering group is uniquely defined by the topological properties of the corresponding continuous group and is locally isomorphic to the latter. The transition to the universal covering group $\widetilde{G}$ is accomplished by adjoining to the generators of the group G the element $I_{2\pi}$ of a rotation through the angle 2π, which commutes with all the elements of the group and satisfies the relations

$$I_{2\pi}^2 = I, \qquad \lim_{\varphi \to 2\pi} I_\varphi = I_{2\pi} \quad (2)$$

for one of the space rotations.

As in reference 4, when we go to the improper group $\widetilde{G}_{st}$ that includes in itself the space and time reflections we must prescribe the values of the squares of the operators I_s, I_{st}, and of the operator I_t defined by the relation

$$I_{st} = I_s I_t. \quad (3)$$

The application of any reflection operator twice over returns the system to its original position. But there are two operations that leave the directions of all the axes unchanged: the identity I and the rotation $I_{2\pi}$ through the angle 2π. Since the reflections I_s, I_t, I_{st} are not reducible to each other, the square of any one of them, independent of the others, can be equal to either I or $I_{2\pi}$. Accordingly we find that there are eight different improper groups of space-time transformations $\widetilde{G}_1 - \widetilde{G}_8$, for which the squares of the reflections have the values

Group	$\widetilde{G}_1$	$\widetilde{G}_2$	$\widetilde{G}_3$	$\widetilde{G}_4$	$\widetilde{G}_5$	$\widetilde{G}_6$	$\widetilde{G}_7$	$\widetilde{G}_8$
I_s^2	I	I	$I_{2\pi}$	$I_{2\pi}$	$I_{2\pi}$	$I_{2\pi}$	I	I
I_t^2	I	$I_{2\pi}$	I	$I_{2\pi}$	$I_{2\pi}$	I	$I_{2\pi}$	I
I_{st}^2	I	$I_{2\pi}$	$I_{2\pi}$	I	$I_{2\pi}$	I	I	$I_{2\pi}$

(4)

Besides the groups $\widetilde{G}_1 - \widetilde{G}_8$ there also exist eight groups $\widetilde{G}'_1 - \widetilde{G}'_8$ for which instead of Eq. (3) we have the relation

$$I_{st} = I_{2\pi} I_s I_t. \quad (3a)$$

But substituting in Eq. (3a)

$$I_s I_{2\pi} = I'_s, \qquad I'_s I_{2\pi} = I_s,$$

we find that because of the lack of real distinction between the operators I_s and I'_s the primed groups are indistinguishable from the corresponding unprimed groups. The relations (3), (4) completely define the improper elements of each of the groups $\widetilde{G}_1 - \widetilde{G}_8$, in the sense that they suffice for the calculation of the product of any two of the improper elements (with use of Eq. (2) and of the fact that all the operators commute with $I_{2\pi}$). Multiplying Eq. (3) on the left by I_s, and also on the right by I_t, we get for all eight groups the respective relations

$$I_s^2 I_t = I_s I_{st}, \quad (5)$$

$$I_t^2 I_s = I_{st} I_t. \quad (6)$$

Multiplying Eq. (6) by I_{st}, we get

$$I_t^2 I_{st} I_s = I_{st}^2 I_t. \quad (7)$$

From Eqs. (5) and (7) it follows that

$$I_{st} I_s = \left(I_s^2 I_t^2 I_{st}^2\right) I_s I_{st}. \quad (8)$$

In the derivation of Eq. (8) we have made use of the fact that for all the groups the squares of the reflections commute with all the elements of the group, and their fourth powers are equal to the identity. In analogous fashion one can obtain the relations

$$I_{st} I_t = \left(I_s^2 I_t^2 I_{st}^2\right) I_t I_{st}, \qquad I_s I_t = \left(I_s^2 I_t^2 I_{st}^2\right) I_t I_s. \quad (9)$$

For the groups $\widetilde{G}_1 - \widetilde{G}_4$

$$I_s^2 I_t^2 I_{st}^2 = I, \quad (10)$$

and the operators I_s, I_t, I_{st} commute with each other in all representations. For the groups $\widetilde{G}_5 - \widetilde{G}_8$

$$I_s^2 I_t^2 I_{st}^2 = I_{2\pi}, \quad (11)$$

so that the operators I_s, I_t, I_{st} commute in the

single-valued representations and anticommute in the double-valued representations. (We shall continue to use the usual terms "single-valued" and "double-valued" representations although, strictly speaking, with respect to the groups $\tilde{G}_1 - \tilde{G}_8$ all the representations are single-valued, and the representations with integral and half-integral spins differ in the eigenvalues of the invariant $I_{2\pi}$, which are one and minus one, respectively.)

3. THE IRREDUCIBLE REPRESENTATIONS OF THE GROUPS $\tilde{G}_1 - \tilde{G}_8$

The construction of the irreducible representations of one of the groups $\tilde{G}_1 - \tilde{G}_8$ reduces to the finding of an irreducible manifold of operators $M_{\mu\nu}$, p_λ, I_S, I_t, I_{St} that satisfy the commutation relations (I.31) that define the proper Lorentz group and also the relations (IV.1), (1), and the corresponding column of the table (4).

For the construction of the complete system of irreducible representations one can proceed as in Sec. 3 of reference 4, using the properties of the invariants of the representations of the proper group G that contains no reflections.

Repeating for the operators I_S, I_{St} (by Eq. (3) the operator I_t is not independent) the arguments given in Sec. 1 of reference 4 for the operator I_S, we get the result that irreducible representations of the group that includes the space and time reflections can either coincide with representations of the proper group or be direct sums of two or four representations. Therefore the operators I_S, I_t, I_{St} can be written in the form

$$I_s = I_{s0}\lambda_s g_s, \tag{12}$$

$$I_t = I_{t0}\lambda_t g_t, \tag{13}$$

$$I_{st} = I_{st0}\lambda_{st}\, g_{st}, \tag{14}$$

where I_{S0}, I_{t0}, I_{St0} are operators that act only on the variables of the representations of the proper group. λ_S, λ_t, λ_{St} are factors that do not act on the variables of the representations of the proper group (but that may, for example, cause an interchange of representations of the proper group). g_S, g_t, g_{St} are numerical coefficients equal to unity for all single-valued representations and for the double-valued representations of the groups $\tilde{G}_1$ and $\tilde{G}_5$.

For the double-valued representations of the other groups the table (4) requires that the factors g_S, g_t, g_{St} have the values

Coefficient	Group			
	$\tilde{G}_1, \tilde{G}_5$	$\tilde{G}_2, \tilde{G}_6$	$\tilde{G}_3, \tilde{G}_7$	$\tilde{G}_4, \tilde{G}_8$
g_s	1	1	i	i
g_t	1	i	1	$-i$
g_{st}	1	i	i	1

(15)

It is obvious that the operators I_{S0}, I_{t0}, I_{St0} commute with λ_S, λ_t, and λ_{St}, and that the numerical factors they contain can be chosen so that

$$I_{s0} I_{t0} = I_{st0}, \tag{16}$$

$$\lambda_s\lambda_t = \lambda_{st}. \tag{17}$$

Let us consider first irreducible representations that do not contain noncommuting reflection operators, i.e., the single-valued representations of all the groups and the double-valued representations of groups $\tilde{G}_1 - \tilde{G}_4$. According to Sec. 3 of reference 4, in the construction of the representations of groups including reflections an important part is played by the transformation properties under the reflections of the invariants of the corresponding representations of the proper group.

The basic invariants p_μ^2 and Γ_σ^2 of the proper group commute with all the reflection operators. Therefore in the classes P_π^S, P_π^a, P_π^b, P_π^α (cf. reference 2), in which there are no additional invariants, each representation of the proper group G will at the same time be also a representation of the improper group $\tilde{G}_i$ (we must remember that we are not as yet considering the double-valued representations of the groups $\tilde{G}_5 - \tilde{G}_8$). For these representations the operators I_{S0}, I_{t0}, I_{St0} are given by

$$I_{s0} = A(\mathbf{p}),\ I_{t0} = A(p_0),\ I_{st0} = A(\mathbf{p})\,A(p_0), \tag{18}$$

where A denotes an operator that changes the sign of the indicated quantity in the wave function. For example

$$A(\mathbf{p})\,\psi(\mathbf{p}) = \psi(-\mathbf{p}). \tag{19}$$

If, in accordance with Eq. (II.62), we write a wave function of a representation of the class P_π in four-dimensional polar coordinates

$$p_1 = \Pi \operatorname{ch}\chi \sin\vartheta\cos\varphi, \quad p_2 = \Pi \operatorname{ch}\chi \sin\vartheta\sin\varphi, \tag{20}$$

$$p_3 = \Pi \operatorname{ch}\chi\cos\vartheta, \quad p_0 = \Pi \operatorname{sh}\chi,$$

the action of the operator is just to replace χ by $-\chi$.

A similar situation exists for representations of class O_0 with the invariant W equal to zero (cf. reference 3)

$$W = \mathbf{M}\cdot\mathbf{N} = 0.$$

In this case also, since the remaining additional invariant F,

$$F = \mathbf{M}^2 - \mathbf{N}^2,$$

is a scalar with respect to space and time reflections, a representation of the proper group is at the same time a representation of the group $\tilde{G}_i$. In this case the operator I_{s0} is identical with that defined in Eq. (IV.14), the operator I_{t0}, is equal to I_{s0}, and the operator I_{st0} is equal to the identity. The quantities belonging to representations of this type include, in particular, four-dimensional vectors and tensors.

In this present case of representations of the classes $P^{s,a,b,\alpha}_{\pm}$, and O_0 with $W = 0$, the operators λ_s, λ_t, λ_{st} are numbers. The square of each of them is unity. Moreover, they satisfy Eq. (17). Therefore the factors λ_s, λ_t can independently take the values

$$\lambda_s = \pm 1, \tag{21}$$

$$\lambda_t = \pm 1. \tag{22}$$

Thus to each irreducible representation of the group G of any of the classes enumerated above there correspond four nonequivalent representations of the group $\tilde{G}_i$, having the same number of dimensions and differing in space and time parities. The existence of time parity for the vector and tensor representations of the homogeneous Lorentz group was first pointed out by Watanabe[8] and Shapiro.[9]

In all the other classes of irreducible representations of the proper group there are additional invariants that change sign on one or more of the reflections. Therefore in these cases an irreducible representation of a group $\tilde{G}_i$ cannot be an irreducible representation with respect to the proper group G, and will be the direct sum of representations corresponding to different signs of the additional invariant in question.

In the representations of greatest importance for physics, of the class $P^s_{\pm m}$ (cf. reference 2), and also in representations of the classes $P^c_{\pm 0}$, $P^{-c}_{\pm 0}$, $P^{\alpha}_{\pm 0}$ (cf. reference 3), the only additional invariant is the sign of the energy, S_H (cf. reference 2, Sec. 3). The operator S_H commutes with I_s and anticommutes with I_t, I_{st}

$$[S_H, I_s]_- = 0, \quad [S_H, I_t]_+ = 0, \quad [S_H, I_{st}]_+ = 0. \tag{23}$$

Since by definition the operators I_{s0}, I_{t0}, I_{st0} act only on the variables of the proper group, they must commute with the invariant S_H of the proper group. Therefore it follows from Eqs. (12) – (14) and (23) that

$$[\lambda_s, S_H]_- = 0, \ [\lambda_t, S_H]_+ = 0, \ [\lambda_{st}, S_H]_+ = 0. \tag{24}$$

Since according to Eq. (23) the operators I_t, I_{st} acting on a wave function change the sign of the energy, in a representation irreducible with respect to $\tilde{G}_i$ there must appear representations of G with both signs of the energy. Therefore the representations irreducible with respect to $\tilde{G}_i$ will be direct sums

$$P^s_{+m} + P^s_{-m} \tag{25}$$

and similarly for the classes $P^{c,-c}_{\pm 0}$. A wave function of the representation (25) will depend on the variables of the proper group, i.e., on the three-dimensional momentum $\mathbf{p}$ and the spin component, and also will be a two-rowed matrix, with indices referring to the representations P_{+m}, P_{-m} (P_{+0}, P_{-0}). In accordance with Eqs. (I.11), (I.12), (IV.1), (IV.11), (1), (12) – (14), (19), and (24), the operators $\mathbf{M}$, $\mathbf{N}$, $\mathbf{p}$, p_0, I_{s0}, I_{t0}, I_{st0} have for the representation (25) the forms, to within a unitary transformation,

$$\mathbf{M} = -i[\mathbf{p}\partial/\partial\mathbf{p}] + \mathbf{S}, \quad \mathbf{N} = iE_p\partial/\partial\mathbf{p} - [\mathbf{Sp}]/(E_p + m),$$
$$\mathbf{p} = \mathbf{p}, \ p_0 = \rho_3 E_p, \ I_{s0} = A(\mathbf{p}), \ I_{t0} = I, \ I_{st0} = A(\mathbf{p}),$$
$$\lambda_s = \pm I, \ \lambda_t = \rho_1, \ \lambda_{st} = \lambda_s\lambda_t, \tag{26}$$

Here and in our other formulas the matrices ρ_1, ρ_2, ρ_3 have the forms of the Pauli matrices

$$\rho_1 = \begin{pmatrix} 0 & 1 \\ 1 & 0 \end{pmatrix}, \quad \rho_2 = \begin{pmatrix} 0 & -i \\ i & 0 \end{pmatrix}, \quad \rho_3 = \begin{pmatrix} 1 & 0 \\ 0 & -1 \end{pmatrix} \tag{27}$$

and act on the wave function of the representation (25), namely

$$\Omega = \begin{pmatrix} \Omega_{+m} \\ \Omega_{-m} \end{pmatrix}. \tag{28}$$

The double sign on the λ_s in Eq. (26) means that for given spin and absolute value of the mass there exist two nonequivalent representations that differ only in the spatial parity. It might seem that, independently of λ_s, one could also assign both signs to the operator λ_t and thus introduce two more representations, differing in the time parity. But the representations with $\lambda_t = -\rho_1$ reduce to those in Eq. (26) by the transformation

$$\Omega = \rho_3\Omega' \tag{29}$$

Since representations of the class P^s_m describe free particles (with non-zero rest mass) we can say, contrary to the statement in references 5 and 6, that from the point of view of the theory of the representations of the inhomogeneous Lorentz group the concept of time parity cannot be introduced for physical particles. We note further that here, as in Sec. 5 of reference 4, for the double-

valued representations there exists only the relative parity of a pair of particles, but not absolute parity of each individual particle. The irreducible representations of the classes $P_{\pm 0}^{c_1-c_2,\alpha}$ have the same structure

$$P_{+0}^{c_1-c_2,\alpha} \dotplus P_{-0}^{c_1-c_2,\alpha} \tag{30}$$

and are constructed in analogous ways. With the exception of the operators **M** and **N**, which must be chosen in accordance with Sec. 1 of reference 3, all of the operators have the forms shown in Eq. (26).

Let us now examine the representations of class O_0 with the invariant W not equal to zero,

$$W = \mathbf{M} \cdot \mathbf{N} \neq 0. \tag{31}$$

According to Eqs. (IV.1) and (1) the operator W commutes with I_{st} and anticommutes with I_s and I_t

$$[I_s, W]_+ = 0, \; [I_t, W]_+ = 0, \; [I_{st}, W]_- = 0. \tag{32}$$

Therefore the direct sum

$$P_W \dotplus P_{-W}, \tag{33}$$

is a representation that is irreducible with respect to $\widetilde{G}_i$, and the operators λ_s, λ_t, λ_{st} will have the forms

$$\lambda_s = \pm\rho_1, \; \lambda_t = \rho_1, \; \lambda_{st} = \lambda_s\lambda_t. \tag{34}$$

The operator I_{s0}, which we denote by B for this case, is determined in accordance with Eq. (IV.14), and the operator I_{st0} is equal to the identity, so that we can write

$$I_{s0} = I_{t0} = B, \quad I_{st0} = I. \tag{35}$$

Thus for representations of the type (33) (in particular for the Dirac bispinor) it would also seem that there is a distinction between representations for the space parity and that the concept of time parity does not exist. Such a conclusion, however, is not entirely correct, since on applying to the representation

$$\lambda_s = -\rho_1, \; \lambda_t = \rho_1, \; \lambda_{st} = -1$$

the equivalence transformation

$$\Omega = \rho_3\Omega',$$

we find that for representations of this type the time parity exists and space parity does not. Obviously both of these conclusions lack invariance under equivalence transformations. The difference from the preceding case is that here λ_{st} is a multiple of the unit matrix, instead of λ_s. Strictly speaking, therefore, for this type of representation only space-time parity exists.

The representations $P_{\pi}^{\pm I}$ have as an additional invariant the sign of the fourth component of the pseudovector Γ_σ, denoted in reference 4 by the symbol S_Γ. According to Eqs. (IV.1) and (1) the operator S_Γ commutes with I_t and anticommutes with I_s, I_{st}

$$[I_s, S_\Gamma]_+ = 0, \quad [I_t, S_\Gamma]_- = 0, \; [I_{st}, S_\Gamma]_+ = 0. \tag{36}$$

The direct sum

$$P_{\Pi}^{+I} \dotplus P_{\Pi}^{-I}, \tag{37}$$

is a representation irreducible with respect to $\widetilde{G}_i$, and the operators λ_s, λ_t, λ_{st} have the forms

$$\lambda_s = \rho_1, \quad \lambda_t = \pm 1, \; \lambda_{st} = \lambda_s\lambda_t. \tag{38}$$

The operators I_{s0}, I_{t0}, I_{st0} have the values (18). In this case the time parity exists, but there is no space parity.

Finally, in the representations of the class $P_{\pm 0}^{\pm\Sigma}$, which is important for physics (the wave functions of particles of zero rest mass transform according to representations of this type), there exist the two additional invariants S_H and S_Γ, which do not commute with the reflections [cf. Eqs. (23) and (26)]. Therefore here a representation irreducible with respect to $\widetilde{G}_i$ will be the direct sum of four representations corresponding to the four possible choices of the signs of the invariants S_H, S_Γ

$$P_{+0}^{+\Sigma} \dotplus P_{+0}^{-\Sigma} \dotplus P_{-0}^{+\Sigma} \dotplus P_{-0}^{-\Sigma}.$$

Here the operators I_{s0}, I_{t0}, I_{st0} are the same as in Eq. (26). For the operators λ_s, λ_t, λ_{st} there are two possible inequivalent systems of four-rowed matrices

$$\lambda_s = \rho_1, \; \lambda_t = \rho_1', \; \lambda_{st} = \rho_1\rho_1', \tag{39}$$

and

$$\lambda_s = \rho_1\rho_3, \; \lambda_t = \rho_2\rho_1', \; \lambda_{st} = \rho_2\rho_2'. \tag{40}$$

A wave function has the form

$$\Omega = \begin{pmatrix} \Omega_{+0} \\ \Omega_{-0} \end{pmatrix}, \quad \Omega_{+0} = \begin{pmatrix} \Omega_{+0}^{+\Sigma} \\ \Omega_{+0}^{-\Sigma} \end{pmatrix}, \quad \Omega_{-0} = \begin{pmatrix} \Omega_{-0}^{+\Sigma} \\ \Omega_{-0}^{-\Sigma} \end{pmatrix}. \tag{41}$$

The primed matrices ρ' act on the first of the functions (41), i.e., on the variable sign of the energy; the unprimed matrices act on the variable sign S_Γ.

Thus to each value of $|\Sigma|$ there correspond two nonequivalent irreducible representations of the group $\widetilde{G}_i$.

Let us now consider the double-valued representations of the groups $\widetilde{G}_5 - \widetilde{G}_8$, in which the operators I_s, I_t, I_{st} anticommute with each other. The

operators I_{S0}, I_{t0}, I_{St0} are not changed in this case. The operators λ_S, λ_t, λ_{St} are changed in two respects. Firstly, they must now anticommute with each other; secondly, in accordance with the table (15) the square of each of them must be equal to minus one. In the foregoing discussion, in representations of the classes P^S_π, P^a_π, P^b_π, P^α_π, and O_0 with $W = 0$, the operators λ were all numbers. Therefore, in order to make these operators anticommuting quantities, one has to double the dimensionality of the representation. Thus for the classes listed above the double-valued representations of the groups $\tilde{G}_5 - \tilde{G}_8$ have doubled dimensionalities as compared with the analogous representations of the groups $\tilde{G}_1 - \tilde{G}_4$. In all the other classes the operators λ are matrices that can be taken to be anticommuting without changing the dimensionality of the representation. On going over to the double-valued representations of the groups $\tilde{G}_5 - \tilde{G}_8$ the number of nonequivalent representations, differing as to parity, remains unchanged in all classes. The final results as to the factors λ can be summarized as follows:

		$P^{S,a,b,\alpha}_{\Pi}$ O_0 for $W=0$	$P^{S}_{\pm m}$ $P^{c,-c,\alpha}_{\pm 0}$	O_0 for $W \neq 0$	$P^{\pm l}_{\Pi}$	$P^{\pm\Sigma}_{\pm 0}$	
$\tilde{G}_1 - \tilde{G}_4$	λ_s	$\pm I$	$\pm I$	$\pm \rho_1$	ρ_1	ρ_1	$\rho_1\rho_2'$
	λ_t	$\pm I$	ρ_1	ρ_1	$\pm I$	ρ_1'	$\rho_2\rho_1'$
$\tilde{G}_5 - \tilde{G}_8$	λ_s	$\pm i\rho_3$	$\pm i\rho_3$	$\pm i\rho_1$	$i\rho_2$	$i\rho_2$	$i\rho_1\rho_2'$
	λ_t	$\pm i\rho_2$	$i\rho_2$	$i\rho_2$	$\pm i\rho_3$	$i\rho_2\rho_1'$	$i\rho_2'$

(42)

If we compare the representations of the group $\tilde{G}_S$ (G'_S) containing only the space reflections with the representations of the group $\tilde{G}_i$ (other than the double-valued representations of groups $\tilde{G}_5 - \tilde{G}_8$), it turns out that when the time reflection is included the dimensionalities of the irreducible representations are doubled in the classes $P_{\pm m}$, $P_{\pm 0}$, and are unchanged in the other cases. We note also for completeness that besides the representations enumerated above the groups $\tilde{G}_1 - \tilde{G}_8$ also have three single-valued one-dimensional irreducible representations J_S, J_t, J_{St}, for which

$$M_{\mu\nu} \equiv 0, \quad p_\lambda \equiv 0, \tag{43}$$

and the operators I_S, I_t, I_{St} are shown in the table:

Representation	Coefficient		
	I_s	I_t	I_{st}
J_s	−1	1	−1
J_t	1	−1	−1
J_{st}	−1	−1	1

(44)

4. DISCUSSION OF RESULTS

In the preceding section we have found all the irreducible representations of the inhomogeneous Lorentz group that contains the space and time reflections, and now we can discuss the problem of what physical results can be obtained from a discussion of time reversal carried out in the framework of the usual representation theory (without the Wigner change to the complex conjugate of the wave function.

The discussion here is more general than those in previous papers on this problem in the following three ways. First, no use has been made of concrete equations of motion, so that the results depend only on the geometrical properties of space-time. Second, the treatment has been based on the inhomogeneous Lorentz group, including not only four-dimensional rotations, but also four-dimensional displacements. Third, use has been made of the concept of the universal covering group, which has made possible a more precise examination of the problem of the factors ± 1, $\pm i$ in the reflection operators. These differences in the statement of the problem have led to a number of differences in the final results.

Ordinarily the study of the transformation properties under reflections has been made not with free-particle wave functions, transforming according to the infinite-dimensional (in the momentum coordinates) representations of the inhomogeneous Lorentz group, P^S_m, $P^\Sigma_{\pm 0}$, but with the spin parts of the wave functions as defined for concrete equations of motion. These spin parts of the wave functions transform according to representations of the class O_0; for integral spins $W = 0$, and for half-integral spins $W \neq 0$. This artificial and actually incorrect separation of the coordinate (momentum) part of the wave function has led to a number of results that do not follow from the rigorous statement of the problem.

The differences that thus arise are easily traced out in the table (42). We see that the representations of the class O_0 with W = 0 (scalars, vectors, and so on) have independent space and time parities.[8,9] For real particles with nonvanishing rest mass, however, (class P_m) the time parity is absent. On the other hand, for particles with zero rest mass (class P_0), according to reference 4, the intrinsic space parity is absent, but still, according to the table (42), there exist two systems of representations that differ in their parity properties with respect to space and time reflections. Another difference between our treatment and previous ones lies in the establishing of the eight groups $\tilde{G}_1 - \tilde{G}_8$, with different double-valued representations. Inclusion of the fact that the squares of the reflections can be either positive or negative for the double-valued representations, together with the stipulation that there cannot exist at the same time particles with different signs for the squares of the reflections,[6] is equivalent to the introduction of the universal covering group. In reference 6, however, only reflections that anticommute with each other were considered, i.e., only the groups $\tilde{G}_5 - \tilde{G}_8$. The representations of the groups $\tilde{G}_1 - \tilde{G}_4$ were rejected in reference 6 on the grounds that in this case the Dirac equation leads to an incorrect relation between energy and momentum. The present treatment shows that wave functions can also transform according to representations of the groups $\tilde{G}_1 - \tilde{G}_4$ with commuting reflection operators in the double-valued representations.

We note also that according to our treatment the existence of antiparticles does not follow from the transformation properties under reflections but, according to reference 4, is a direct consequence of the pseudoscalar nature of the charge for charged particles.

All of the results obtained here can be applied to arbitrary kinds of particles, including those that obey the Dirac equation, both in the quantized and also in the unquantized form; a complete analysis of the relations will be given in a separate paper.

5. ON THE INVARIANCE OF THE EQUATIONS OF QUANTUM THEORY

The equations of a quantum theory must be covariant in the sense that the physical results must not depend on the sense of the time axis.[6] From the covariance of an equation, however, it by no means follows that it must be invariant. Moreover, a correct equation for the wave function (state vector), containing no infinities of any kind, cannot be invariant with respect to time reversal. In fact, the condition for the invariance of the equation

$$L\Omega = 0, \tag{45}$$

where L is a linear operator, has the form

$$[L,\ I_t]_- = 0. \tag{46}$$

Therefore, if Ω is a solution of Eq. (45), in virtue of Eq. (46) the function $I_{st}\Omega$ will also be a solution. According to the first of the relations (1) the functions Ω and $I_{st}\Omega$ describe physical systems with different signs of the energy and mass. But masses of different signs not only are never observed in nature, but also are not permissible, since a system of two particles with masses of different signs can have a space-like energy-momentum vector, which leads to signals faster than light and the loss of causality. Thus when we use representations of the usual type the equations of motion must be noninvariant with respect to time reversal and have solutions corresponding to only one sign of the mass. On time reversal the signs of all masses and energies are changed. The formal invariance of a number of equations in general use exists either because they have solutions with both signs of the mass (the unquantized Dirac equation) or because of an infinite vacuum background (the quantized scalar and Dirac equations).

[1] Yu. M. Shirokov, J. Exptl. Theoret. Phys. (U.S.S.R.) **33**, 861 (1957), Soviet Phys. JETP **6**, 664 (1958).

[2] Yu. M. Shirokov, J. Exptl. Theoret. Phys. (U.S.S.R.) **33**, 1196 (1957), Soviet Phys. JETP **6**, 919 (1958).

[3] Yu. M. Shirokov, J. Exptl. Theoret. Phys. (U.S.S.R.) **33**, 1208 (1957), Soviet Phys. JETP **6**, 929 (1958).

[4] Yu. M. Shirokov, J. Exptl. Theoret. Phys. (U.S.S.R.) **34**, 717 (1957), Soviet Phys. JETP **7**, 493 (1958).

[5] S. Watanabe, Revs. Modern Phys. **27**, 40 (1955).

[6] I. S. Shapiro, Usp. Fiz. Nauk **53**, 7 (1954).

[7] E. P. Wigner, Nachr. Akad. Wiss. Göttingen, Math. Phys., p. 546 (1932).

[8] S. Watanabe, Phys. Rev. **84**, 1008 (1951).

[9] I. S. Shapiro, J. Exptl. Theoret. Phys. (U.S.S.R.) **22**, 524 (1952).

Translated by W. H. Furry
159

ON THE STABILITY OF NUCLEI

P. É. NEMIROVSKIĬ

Submitted to JETP editor September 20, 1958

J. Exptl. Theoret. Phys. (U.S.S.R.) **36**, 889-895 (March, 1959)

The dependence of the interaction between a nucleon and the nucleus on N/Z was investigated. An estimate of the maximal A/Z is given; this ratio is found to vary between 3 and 3.8. It is shown that when N equals the number of neutrons in a closed shell, the minimal Z changes discontinuously by several units. It is suggested that these jumps in the values of Z_{min} on closing the neutron shell may be responsible for the exceptionally great abundance of certain isotopes, provided that the synthesis of atomic nuclei occurred in brief neutron bursts.

IN a previous paper[1] we considered the single-particle levels of light nuclei obtained with the help of the optical model potential. The ordering and the energy of the levels can also be determined for the heavier nuclei. In comparing the obtained results with experiment it is necessary to make certain additional assumptions about the dependence of the nuclear radius and the well depth on A and Z. The comparison of theory and experiment with regard to the total cross sections, the angular distributions, and the polarization shows that the scattering from all nuclei can be described by a potential with one and the same depth, assuming that $R = (1.16A^{1/3} + 0.33) \times 10^{-13}$, where R is the distance at which the potential has fallen off to half its maximum value.

The agreement remains very good if we make the contrary assumption that the nuclear radius obeys the $A^{1/3}$ law, but the potential becomes smaller as the ratio N/Z increases. The well depth will then be less for heavy nuclei than for light ones. However, this effect should show up also in the different isotopes of the same element. It is therefore a natural step to add to the optical potential a term which takes account of the isotopic effect.*

Such a potential can be used for the calculation of the levels of nuclei with a closed shell plus one extra particle. In the framework of this model we regard the proton and neutron shells as independent, which is correct for heavy nuclei. We can then find the binding energies of closed-neutron-shell nuclei that differ from each other in the number of protons.

In studying these binding energies we can also determine the isotopic effect. It appears to be in agreement with the optical model data. The isotopic effect thus obtained may be extrapolated to the limits of nuclear stability in order to find the limiting value of N/A as a function of A. The answer to this problem permits certain conclusions about the creation of the elements.

*The author is grateful to L. A. Sliv for a conversation which stimulated the development of these ideas.

1. CHOICE OF THE POTENTIAL

We now take up the problem of the correct way of including the isotopic effect in the optical potential.

We chose the simplest model,

$$V = \frac{Z}{A} V_{np} + \frac{N}{A} V_{nn} \qquad (1)$$

where V_{np} and V_{nn} are the potentials for the interaction of the neutron with the proton and neutron matter, respectively. This means that we assume the additivity of the two interactions, both in the ordinary and in the spin-orbit potential. Furthermore, since the potential does not change very strongly, we retained the assumption $\alpha = k_0 = \sqrt{2mV_0}/\hbar$, where α is the diffuseness parameter. This condition implies that α varies at most by 10%. This has no significant effect on the overall picture. We can therefore use the results obtained with a well of the same depth for all nuclei (i.e., which is independent of N/Z).

In the calculations we made use of the following potential:[2,3]

$$V = -\frac{V_0}{1+e^{\alpha(r-R)}} - \frac{\varkappa}{r}\frac{d}{dr}\left[\frac{V_0}{1+e^{\alpha(r-R)}}\right](\mathbf{l}\cdot\boldsigma),$$

where $V_0 = \frac{Z}{A} V_{np}^0 + \frac{N}{A} V_{nn}^0$, with $2mV_0\varkappa/\hbar^2 = 0.66$. The nuclear radius was taken to be equal to $R = 1.25 \times 10^{-13}$.

We assumed that $V_0 = 49$ Mev for nuclei with Z/N = 0.80. This assumption gives good agree-

TABLE I

$E_b = 0$				$E_b = 0.16\ V_0 \approx 8$ Mev			
$X = k_0R$	l	j	Level	$X = k_0R$	l	j	Level
0.67	0	1/2	$1s$	2.19	0	1/2	$1s$
2.77	1	3/2	$1p_{3/2}$	3.80	1	3/2	$1p_{3/2}$
3.35	1	1/2	$1p_{1/2}$	4.34	1	1/2	$1p_{1/2}$
3.98	1	1/2	$2s$	5.30	2	5/2	$1d_{5/2}$
4.35	2	5/2	$1d_{5/2}$	5.66	0	1/2	$2s$
5.04	2	3/2	$1d_{3/2}$	6.00	2	3/2	$1d_{3/2}$
5.75	3	7/2	$1f_{7/2}$	6.74	3	7/2	$1f_{7/2}$
5.755	1	3/2	$2p_{3/2}$	7.24	1	3/2	$2p_{3/2}$
6.078	1	1/2	$2p_{1/2}$	7.46	3	5/2	$1f_{5/2}$
6.54	3	5/2	$1f_{5/2}$	7.52	1	1/2	$2p_{1/2}$
7.068	4	9/2	$1g_{7/2}$	8.13	4	9/2	$1g_{7/2}$
7.12	0	1/2	$3s$	8.78	2	5/2	$2d_{5/2}$
7.34	2	5/2	$2d_{5/2}$	8.89	4	7/2	$1g_{7/2}$
7.76	2	3/2	$2d_{3/2}$	9.08	0	1/2	$3s$
7.70	4	9/2	$1g_{7/2}$	9.16	2	3/2	$2d_{3/2}$
8.33	5	11/2	$1h_{11/2}$	9.474	5	11/2	$1h_{11/2}$
8.80	3	7/2	$2f_{7/2}$	10.278	3	7/2	$2f_{7/2}$
8.81	1	3/2	$3p_{3/2}$	10.29	5	9/2	$1h_{9/2}$
9.02	1	1/2	$3p_{1/2}$	10.73	1	3/2	$3p_{3/2}$
9.20	5	9/2	$1h_{9/2}$	10.74	3	5/2	$2f_{5/2}$
9.30	3	5/2	$2f_{5/2}$	10.91	1	1/2	$3p_{1/2}$

ment with the experimental interaction cross sections. It follows from the polarization data, which are very sensitive to k_0R, that the above-mentioned relations lead to the correct sign and magnitude of the polarization for Zr, Nb, and Mo. The data on the interaction cross sections for bismuth and lead show that, with $R = \eta_0 A^{1/3}$, V_0 for $A = 200$ must be 2.5 to 3 Mev less than for $A = 90$.

We chose $V_{np} = 3V_{nn}$. We then obtain $V_{np}^0 = 78$ Mev and $V_{nn}^0 = 26$ Mev. The potential V_0 is equal to 46.6 Mev for Pb^{208} and to 52 Mev for Ca^{40} and O^{16}. On the basis of these assumptions, which lead to good agreement with the experimental cross sections, we found the energies of the single-particle levels.

The order in which the levels are filled is given in Table I for $E_b = 0$ and $E_b = 0.16\,V_0$ (E_b is the binding energy). This table was used to find the ground states of a number of nuclei with a closed neutron shell plus one extra particle. The results are listed in Table II.

It is seen from Table II that the computed spin and parity* of the states are in agreement with experiment in all reliable cases. With regard to the binding energy there is a discrepancy of order 2 Mev for the shells $1p_{3/2}$, $1p_{1/2}$, $1d_{5/2}$, $1d_{3/2}$, and $2s$; but even in these cases the isotopic effect (the difference in the binding energies) comes out correctly.

The computed binding energy for the heavier nuclei agrees with experiment within the limits of 0.5 Mev (and much better in many cases). This shows that the potential as a whole as well as the isotopic effect have been treated correctly.

It was not possible to regard the state with 64 neutrons as a closed shell in view of the closeness of the neighboring states.

2. THE LIMITS OF STABILITY OF NUCLEI

We only considered neutral single-particle states, and left the calculation of the proton single-particle states for the future. Hence we can only study the neutron stability of the nuclei.

Experimental data on nuclei with neutron binding energies close to zero are available only for the beginning of the periodic system. This applies, in particular, to He^6 and Li^9. We see that $(N/A)_{max} = 2/3$ in the beginning of the periodic system (for H^3, He^6, and Li^9). The highest known value of N/A in the region of large A is $N/A = 0.62$ to 0.63 (0.618 for U^{240}).

We now ask, how does $(N/A)_{max}$ depend on A? We can attempt the answer on the basis of the data on the nuclear shells.

We have made the following assumptions: (1) the potential (1) holds for all nuclei, and (2) the diffuseness of the boundary and the spin-orbit interaction do not change with N/Z.

With these assumptions one can determine the number of protons for which the binding energy of the $(N+1)$ th neutron is equal to zero, where N is the number of neutrons in the closed shell. One

*The parity of the single-particle states is determined by the orbital angular momentum.

TABLE II.* Ground states of nuclei with a closed neutron shell plus 1 neutron

Nucleus	N − 1	Experimental state	Theoretical state	Experimental binding energy	Theoretical binding energy
O^{17}	8	$1d_{5/2}$	$1d_{5/2}$	4.14	5.4
Mg^{27}	14	$2s$	$2s$	6.43	8.7
Si^{29}	14	$2s$	$2s$	8.46	10.8
Si^{31}	16	$1d_{3/2}$	$1d_{3/2}$	1.6	8.6
S^{33}	16	$1d_{3/2}$	$1d_{3/2}$	8.64	10.6
Ca^{41}	20	$1f_{7/2}$	$1f_{7/2}$	8.37	8.53
S^{37}	20	$1f_{7/2}$	$1f_{7/2}$	5.01	4.90
A^{39}	20	$1f_{7/2}$	$1f_{7/2}$	6.64	6.84
Ca^{49}	28	$2p_{3/2}$	$2p_{3/2}$	5.15	5.55
Ti^{51}	28	$2p_{3/2}$	$2p_{3/2}$	6.43	6.76
Cr^{53}	28	$2p_{3/2}$	$2p_{3/2}$	7.93	8.04
Fe^{55}	28	$2p_{3/2}$	$2p_{3/2}$	9.29	9.41
Ni^{57}	28	$2p_{3/2}$	$2p_{3/2}$		
Zn^{71}	40	$1g_{9/2}$	$1g_{9/2}$	6.12	6.04
Ge^{73}	40	$1g_{9/2}$	$1g_{9/2}$	6.64	7.05
Se^{75}	40	$5/2^*$	$1g_{9/2}$	7.96	8.14
Kr^{87}	50	$2d_{5/2}$	$2d_{5/2}$	5.51	5.43
Sr^{89}	50	$2d_{5/2}$	$2d_{5/2}$	6.52	6.24
Zr^{91}	50	$2d_{5/2}$	$2d_{5/2}$	7.16	7.02
Mo^{93}	50	$2d_{5/2}$	$2d_{5/2}$	7.88	7.85
Sn^{115}	64	$3s$	$3s$	7.91	9.05
Xe^{137}	82	$2f_{7/2}$	$2f_{7/2}$	4.45	4.32
Ba^{139}	82	$2f_{7/2}$	$2f_{7/2}$	4.66	4.86
Ce^{141}	82	$2f_{7/2}$	$2f_{7/2}$	5.40	5.36
Nd^{143}	82	$2f_{7/2}$	$2f_{7/2}$	6.02	5.88
Pb^{209}	126	$2g_{9/2}$	$2g_{9/2}$	3.87	4.45
Po^{211}	126	$2g_{9/2}$	$2g_{9/2}$	4.55	4.80

*The data on the binding energy for the nuclei Xe^{137} to Nd^{143} are taken from Johnson and Nier;[5] the other data are from Wapstra.[4]

only has to find the nucleus for which k_0R at a given N is smaller than the value given in column 1 of Table I. We carried through this calculation using the empirical values of $V_{np} = 3V_{nn}$. The results obtained are shown in the figure (only the even Z are given).

It is seen that Z_{min} changes by from 26 to 37.5% as a function of A. These data may, of course, be incorrect in the region of light nuclei, as here there is no good agreement with the experimental values for the binding energies. But in the region of intermediate and heavy nuclei, where one has to extrapolate to 38 to 30% of the protons, our results should come rather close to the truth.

Here we assume, however, that the instability is due to transitions to the next shell, and that inside a given shell the binding energy of the third, fifth, ... nucleon is positive if that of the first nucleon is positive.

In Table III we give the values A for which Z_{min} changes.

TABLE III

Z	A_{max}	N_{max}	Z	A_{max}	N_{max}
8	28	20	14	48	34
10	30	20	16	56	40
12	46	34	18	58	40
20	72	52	52	178	126
22	80	58	54	180	126
24	82	58	56	182	126
26	88	62	58	184	126
28	98	70	60	198	138
30	100	70	62	200	138
32	114	82	64	220	156
34	116	82	66	222	156
36	118	82	68	252	184
38	132	94	70	254	184
40	136	96	72	256	184
42	138	96	74	258	184
44	156	112	76	260	184
46	158	112	78	262	184
48	174	126	80	264	184
50	176	126	82	266	184
			84	282	198

We see from Table III that $Z/A_{max} \approx 0.3$, varying between 0.261 and 0.33. Of special interest is the behavior of Z_{min} as a function of N. For N = 82, Z_{min} increases from 32 to 38, for

TABLE IV. Neutron binding energies for the isotopes of Ca with odd A in filling one shell

A	Shell	E_n	A	Shell	E_n
41	$(1f_{7/2})_1$	8.37	61	$(1f_{7/2})_3(2p_{3/2})_3$	7.77
43	$(1f_{7/2})_3$	7.94	63	$(1f_{7/2})_4(2p_{3/2})_3$	6.84
45	$(1f_{7/2})_5$	7.41	65	$(1f_{7/2})_5$	6.13
63	$(1f_{7/2})_3(2p_{3/2})_3$	9.25	91	$(2d_{5/2})_1$	7.16
65	$(1f_{7/2})_4(2p_{3/2})_3$	7.98	93	$(2d_{5/2})_3$	6.610
67	$(1f_{7/2})_5$	7.03	95	$(2d_{5/2})_5$	6.42

N = 126, it changes from 48 to 60, and for N = 184, from 68 to 82.

One may ask, how sensitive are these results to the initial assumptions?

In the region of light nuclei the potential may be different from (1), and the assumption of j-j coupling may break down. Therefore our picture is certainly not correct for nuclei with $A < 30$.

In the region of heavier nuclei one can vary the potential parameters somewhat without changing the results of Table III appreciably. For example, changing the width of the surface region by 25% has only a slight effect on the results for Z/A_{max}. The dependence on the isotopic effect is more significant. However, big changes in the value of V_{np}/V_{nn} destroy the agreement with the experimental binding energies, while changing V_{np}/V_{nn} by from 10 to 15% does not make any appreciable difference. The width of the surface region for nuclei with large N/Z can be somewhat greater than for β-stable nuclei, since the binding energy of the neutrons is small and the wave function drops slowly outside the nucleus. It is difficult to estimate this effect, but one should expect that it slightly lowers A_{max} for a given Z. Finally, the assumption that the binding energy of all the neutrons in the shell is positive if that of the first neutron is positive, presumably is correct in the majority of cases. Indeed, the binding energy within the shell changes slowly and without jumps, as can be seen from the example of the isotopes of Ca (Table IV) and of certain other elements. The scheme given in Table III can therefore be regarded as a preliminary estimate of the limits of stability of nuclei with the maximum number of neutrons.

It should be noted that estimates of this kind cannot possibly be made on the basis of the Weizsaecker formula. For the semi-empirical formula includes only the first term of the expansion in terms of (N-Z). But together with the quadratic term, all the even power terms in the expansion should be present and should make a contribution as one gets away from the region of β stable nuclei. The binding energy of Ca^{48} computed by the semi-empirical formula is wrong by 6 Mev (if the errors for Ca^{40}, Ca^{42}, and Ti^{48} are discounted). The inaccuracy is the same for Sn^{124} and Xe^{136}. This shows that even close to the limits of stability the Weizsaecker formula is completely inadequate. It always underestimates the binding energy. Furthermore, since the shell structure is of decisive significance in the study of the stability, it is altogether impossible to use statistical formulas.

3. A FEW REMARKS ON THE ORIGINS OF THE ELEMENTS

The capture of neutrons plays an important role in the existing theories of the creation of the elements. The theory of Alpher and Herman[7] explains the creation of all nuclei by successive neutron capture.

We assume today that the neutron capture plays a role in the synthesis of the nuclei heavier than oxygen or neon.[8] It seems plausible that the mechanism of neutron capture may not have anything to do with the initial stage of the evolution of the universe. For example, if the creation of the elements is continuous, the most suitable "cauldrons" are the red giants and the supernovae. There may exist shortlived energetic neutron currents in the supernovae. If these currents act at the moment of the explosion of the star and last for about a second or a fraction of a second, the formation of the nuclei should go through a minimal number of β decays, i.e., through a minimal Z for a given A or through a Z which is close to the minimal value.

It should be noted that the synthesis of uranium and thorium from lighter nuclei in quantities comparable to those of the other elements is possible only in shortlived neutron bursts. The most probable synthesis is via nuclei with a Z which is lower than in the region of β stability. In this case the synthesis should take no longer than the periods of the β decay of the nuclei Bi^{215}, Bi^{216}, and Bi^{217}, which are estimated to be of order 1 min.

We also call attention to reference 9, where it is assumed that the luminosity curve of the supernovae of the first type* can be interpreted with the help of the decay of Cf^{254}.

Then those nuclei which have an atomic weight A for which the minimal Z increases abruptly, will have a particularly strong tendency to accumulate. Indeed, for these values of A, β decay must occur before the capture of the next neutron is possible. These nuclei will thus accumulate in much greater than average quantities. As a rule, the nucleus remaining after β decay can capture another neutron; however, during the time of the β decay the neutron current may have gone down appreciably, which means that there will be an accumulation of nuclei with the given A. After the capture of one neutron we again obtain a closed shell, further neutron capture may be impossible, and at the mass number A+1, β decay occurs again and leads to the accumulation of nuclei with the mass number A+1, etc. The mass distribution curve of the nuclei will then have peaks followed by deep dips. In general, this is what actually happens. The position of the peaks will now be determined by the closed neutron shells. Here we must not take the closed neutron shells for β-stable nuclei, but those for nuclei with the minimal Z.

The list of mass numbers in Table III should then give an approximate idea of the position of the peaks in the distribution of the elements. The peaks should appear at the beginning of the sharp increases, i.e., for A = 28, 46, 56, 72, 80, 98, and 114. In the region of higher A one should, obviously, consider only N = 126 and N = 184, since in the intervals N = 82 to 126 and N = 126 to 184 the nuclei are nonspherical, and have no separate closed shells. The mass numbers A = 174 and 252 therefore play a special role in our model. However, this picture is only very approximate, and it is entirely possible that the value of A deviates by several units. Of special interest among the values of A considered are A = 28 and especially A = 56. The first of these values corresponds to the basic isotope of Si, which is one of the most abundant elements in the world.

Even more significant is the fact that our model predicts the great abundance of Fe^{56}. It is well known that this nucleus has the highest abundance of all nuclei with A > 28 in nature. All previous hypotheses were not able to explain the great abundance of this nucleus. It is true that the maximum at A = 46 is unwarranted, but a slight change in the parameters may change the position of this peak to A = 40, in accordance with observation.

From the nuclear point of view, these considerations presuppose the fulfilment of the following conditions: (1) the basic maxima are unaffected by changes in the parameters, (2) the chain of captures does not break up until the shell is filled, and (3) arguments can be found to explain away the spurious maxima.

From the cosmological point of view, everything depends on the intensity and the duration of the neutron bursts. There is no upper limit to the intensity of the burst if it is impossible to add not only one, but even two neutrons to the closed shell. If the pairing energy is such that capture of a neutron pair is possible, and if the probability for three-body collisions is high, the breaks in the chain of captures will not be important any more. For example, assume that two neutrons can be added to a nucleus with Z = 16, A = 56; this makes the nucleus Z = 16, A = 58 possible; after β decay we obtain Z = 17, A = 58, which is unstable and emits a neutron, giving Z = 17, A = 57. This nucleus then undergoes β decay. The privileged role of A = 56 disappears. The currents, therefore, must be sufficiently weak to make three-body collisions improbable. The lowest estimate for the currents is determined from the relative abundance of burnt out and intact nuclei for different A.

The duration of the neutron burst is determined by the period of the β decay of the nuclei with minimal Z. The latter can be estimated roughly. It is natural to assume that the transitions in nuclei with minimal Z are allowed, because there are sufficiently many possibilities for β decay to excited levels. The lowest estimate for ft in the region of intermediate and heavy nuclei is approximately $ft = 10^4$. However, β decay can occur not only in the ground state, but also in excited states. In actual fact the period may therefore be several times smaller than that determined from the ft value. The energies of the decays should be of order 10 to 15 Mev. As is well-known, f is proportional to E_0^5, so that an error of 20% in E_0 does not change the order of magnitude of the decay period. The half-life will be within the limits 10^{-3} sec < T < 10^{-1} sec.

In many cases the decay goes mainly into excited states, so that the emission of a neutron may follow the β decay. As a rule, the excitation energies are not high and will be essentially removed by the emission of the first neutron. This implies a spreading of the peak, which will then include the

*The supernovae of the first type have exponentially decaying luminosity curves with a half-life of 55 days. Explosions of this kind are observed in our galaxy about once in 300 years.

mass numbers preceding the break in the basic chain.

The author plans a more detailed study of the separate neutron chains for the near future.

[1] P. É. Nemirovskiĭ, J. Exptl. Theoret. Phys. (U.S.S.R.) **33**, 746 (1957); Soviet Phys. JETP **6**, 573 (1958).

[2] R. Woods and D. Saxon, Phys. Rev. **95**, 577 (1954).

[3] Ross, Mark, and Lawson, Phys. Rev. **102**, 1613 (1956).

[4] A. H. Wapstra, Physica **21**, 367 (1955).

[5] W. H. Johnson and A. O. Nier, Phys. Rev. **105**, 1014 (1954).

[6] J. S. Smart, Phys. Rev. **75**, 1379 (1949).

[7] R. A. Alpher and R. C. Herman, Revs. Modern Phys. **22**, 153 (1950).

[8] Fowler, Burbridge, and Burbridge, Astrophys. J. **122**, 271 (1955).

[9] Burbridge, Hoyle, Burbridge, Christy, and Fowler, Phys. Rev. **103**, 1145 (1956).

[9a] Burgridge, Hoyle, Burbridge, and Fowler, Revs. Modern Phys. **29**, 547 (1957).

Translated by R. Lipperheide
160

FOCK EXPANSION FOR THE WAVE FUNCTIONS OF A SYSTEM OF CHARGED PARTICLES

Yu. N. DEMKOV and A. M. ERMOLAEV

Leningrad State University

Submitted to JETP editor September 22, 1958

J. Exptl. Theoret. Phys. (U.S.S.R.) 36, 896-899 (March, 1959)

The method with which Fock[1] investigated the wave function of the ^1S state of helium is generalized to an arbitrary system of charged particles and to states of any symmetry.

1. In 1954, Fock[1] established the fact that the wave function of the ^1S state of helium and helium-like ions could be expanded in a double series of integral powers of $r = \sqrt{r_1^2 + r_2^2}$ and $\ln r$, where r_1 and r_2 are the distances of the first and second electrons from the nucleus. In this case, the proof was made by a method of successive determination of the expansion coefficients, which were homogeneous functions of zeroth order in the cartesian coordinates of the electrons (if the origin of the coordinates is fixed in the nucleus). We shall show that an expansion of this type, which we shall call a Fock expansion, has a very general character and is valid for any system composed of an arbitrary number of charged particles; there is also no need of placing any restrictions on the symmetry of the wave function.

As an example, we consider an N-electron atom (generalization of the results to more complicated systems presents no difficulties and is discussed below). The Schrödinger equation for the wave function of a stationary state (in atomic units) then has the form

$$H\psi = \left[-\frac{1}{2}\Delta_{3N} + U(x_1, x_2, \ldots, x_{3N})\right]\psi = E\psi. \quad (1)$$

Here $x_1, \ldots, x_{3N}$ are the cartesian coordinates of the electrons, Δ_{3N} is the Laplace operator in the configuration space of 3N variables, while the potential energy U contains the Coulomb interaction of the electrons with the nucleus and between themselves, and is a homogeneous function of the coordinates of order -1. We introduce spherical coordinates in the configuration space. Then Eq. (1) takes the form

$$\left[\frac{1}{r^{3N-1}}\frac{\partial}{\partial r}\left(r^{3N-1}\frac{\partial}{\partial r}\right) + \frac{1}{r^2}\Delta_{3N}^*\right]\psi + \frac{2V}{r}\psi = 2E\psi, \quad (2)$$

where $r = (x_1^2 + \ldots + x_{3N}^2)^{1/2}$, Δ_{3N}^* is the Laplace operator on a sphere in a space of 3N dimensions, and V is a vector function of $3N-1$ spherical angles.

We shall now seek a solution of this equation in the form of a series

$$\psi = \sum_n \sum_p a_{np} r^n (\ln r)^p, \quad (3)$$

where a_{np} are certain functions of the spherical angles which must be determined, and the subscripts n and p can take on integer values only. Substituting this expansion in Eq. (2), we obtain a system of equations for a_{np}:

$$\Delta_{3N}^* a_{np} + n(n+3N-2)a_{np} = -(p+1)(2n+3N-2)a_{n,p+1} - (p+1)(p+2)a_{n,p+2} + 2Va_{n-1,p} - 2Ea_{n-2,p}. \quad (4)$$

We shall carry out further investigation of this system by a method which was assumed by Fock for the helium atom, and we shall not therefore give the details of all the analysis.

First, we note that the factor $n(n+3N-2)$ on the left-hand side is precisely the eigenvalue of the operator Δ_{3N}^*. If we set the right-hand side of Eq. (4) equal to zero, then its solution will be a linear combination of the generalized spherical functions Φ_n of order n on the sphere in the 3N-dimensional space (we shall call them, here and below, spherical harmonics). With accuracy up to the same linear combination, both the solutions of Eq. (4) are determined; however the solution exists in this or that case only when the right-hand side of the equation is orthogonal to all spherical harmonics of order n.*

Another important property of the system (4) is that the coefficients a appear on the right hand side of the equation for the coefficient a_{np} for which either the first index is smaller than n, or the second index is larger than p. It then follows

*The function V on the right-hand side of Eq. (4) contains singularities; however, these singularities are weak and do not affect the finiteness and continuity of the coefficients a_{np}.

that if the coefficients a_{np} are known for sufficiently small n and sufficiently large p, then, as a consequence of the "triangularity" of the system, we can determine the a_{np} successively for any n and p. To satisfy these conditions we can, in the first place, require that all the terms of the series (3) be finite at r = 0. For this, it is necessary to set all the a_{np} equal to zero for $n < 0$, and all the a_{0p} equal to zero for $p > 0$. In the second place, we must require that, for any fixed n, but for sufficiently large p, the coefficients a_{np} must vanish. This condition is necessary in order that the expansion be single-valued.

We can then solve the system (4) successively for n = 0, 1, 2, ..., and for each fixed n, beginning with the largest p for which the coefficient a_{np} is different from zero. Setting n = p = 0, we obtain a_{00} = const. Further, let $a_{1,p+1}$, $a_{1,p+2}$, ... be equal to zero. Then, successively solving the equations for $a_{1,p}$, $a_{1,p-1}$, ..., a_{10}, and satisfying the conditions of orthogonality, we obtain $a_{1,p} = a_{1,p-1} = \ldots = a_{10} = 0$; the coefficient a_{11} is uniquely determined, and a_{10} — with accuracy up to a linear combination of spherical harmonics of first order. Then, solving Eq. (4) for n = 2, 3, ..., we obtain the expansion

$$\psi = \sum_{n=0}^{\infty} \sum_{p=0}^{n} a_{np} r^n (\ln r)^p, \qquad (5)$$

where the coefficients a_{n0} are determined with accuracy up to a linear combination of spherical harmonics of order n, and all the remaining coefficients are established uniquely. All the a_{np} for $p < 0$ vanish, due to the presence of the factors p+1 and (p+1)(p+2) on the right side of equation (4) for the coefficients $a_{n,p+1}$ and $a_{n,p+2}$, respectively. The Fock expansion for the wave function has such a form if we do not set any considerations of symmetry on the potential energy U.

We can further take into account the fact that the energy operator is invariant relative to inversion (i.e., change of sign of all coordinates), and, consequently, the solutions of Eq. (1) must be either even or odd. Then, in a number of cases, the parity of the right side of Eq. (4) and of the spherical harmonic of order n will be different; the orthogonality condition will be satisfied automatically, and certain coefficients a_{np} vanish. Furthermore, let us consider that some of the first terms of the expansion with n = 0, 1, ..., k − 1, can be equal to zero. For this reason, the coefficients a_{np} again vanish and we obtain the expansion

$$\psi = \sum_{n=0}^{\infty} \sum_{p=0}^{[n/2]} a_{n+k,\,p}\, r^{n+k} (\ln r)^p, \qquad (6)$$

in which only the coefficients $a_{k,0}$, $a_{k+2,0}$, ... are determined non-uniquely, with accuracy up to linear combinations of spherical harmonics of k, k+2, ..., respectively. The parity of the function (6) coincides with the parity of the number k, which can take on the values 0, 1, 2, ... If $k > 0$, then the wave function ψ vanishes for r = 0. The expansion is of just this type for the two electron system and for k = 0 was obtained in reference 1. Comparing the exact functions considered here with the approximate functions, obtained by the method of separation of variables, it is easy to become convinced that the number k is equal to the sum of the azimuthal quantum numbers of all the electrons.

The solution of the Eq. (1) in the form (4) is obtained nonuniquely. For each fixed n, there remain arbitrary coefficients for the terms $r^n \Phi_{n\ldots}$, where $\Phi_{n\ldots}$ is the set of spherical harmonics of order n. Such a lack of uniqueness is obtained also in the solution of the Laplace equation in 3N dimensional space — its character is determined only by the differential part of the operator and is not connected in explicit fashion with the potential energy U. In our case, as also for the Laplace equation, this non-uniqueness is removed by the imposition of boundary conditions, i.e., by giving the asymptotic form of ψ for $r \to \infty$.

In our consideration, the spherical symmetry of the problem (in ordinary three dimensional space) has not been taken into account. Thanks to this symmetry, we can look for a general eigenfunction of the energy operator H and the operator of the square of the total angular momentum $\mathbf{m}^2$. Then the dependence of the coefficients a_{np} on those angles which characterize the simultaneous rotation of all the N electrons around the nucleus can be investigated independently of the explicit form of the operator H for each of the eigenvalues of the operator $\mathbf{m}^2$. For example, the function ψ does not generally depend (for the S state) on these angles, and thus the number of arguments in a_{np} is decreased by three. For the case N = 2, which was investigated by Fock, a_{np} depends only on two parameters: the angle θ between the radius vectors of the two electrons, and the ratio of the lengths of these vectors r_1/r_2. It is easy to become convinced that if we change to the variables $R = r^2$, θ, $\alpha = 2 \arctan (r_1/r_2)$ in Eqs. (2) and (3), then we get the Fock equation (3.10) of reference 1.*

If the potential energy of the interaction between

*A correction must be made in Eqs. (3.09) and (3.10) of reference 1: in the second term of the right hand side of Eq. (3.09) we must add the factor k, and in the first term of the right side of Eq. (3.10), we must add the factor k + 1.

the electrons is neglected in the energy operator H, then the variables are separated and the problem can be solved exactly; the wave functions can be expanded in integral powers of r and thus the logarithmic terms in the expansion (3) should be absent. Actually, it is not difficult to show that in this special case the expression $2Va_{n-1,0} - 2Ea_{n-2,0}$ is orthogonal to all the spherical harmonics of order n, whence it follows that all the coefficients a_{np} with $p > 0$ vanish.

So far, we have assumed that the potential energy $U = U_{-1}$ is a homogeneous function of order -1. However, if it happens that the function U can be represented in the form of a series

$$U = U_{-1} + U_0 + U_1 + \ldots$$
$$= r^{-1} V_{-1} + V_0 + rV_1 + \ldots, \qquad (7)$$

where U_i are homogeneous functions of order i, while the functions V_i depend only on the spherical angles, then on the right side of Eq. (4), the term $2Va_{n-1,p}$ must be replaced by the expression

$$2(V_{-1}\, a_{n-1,\,p} + V_0\, a_{n-2,\,p} + V_1\, a_{n-3,\,p} + \ldots), \qquad (8)$$

in this case all the characteristics of the set (4) are preserved, and the solution can be obtained in the same way in the form (5). It is then evident that the expansion (5) remains valid for the potential energy of very general form, in particular, for the presence of an external electric field or for the placing of the origin of the coordinates of the nucleus at an arbitrary point of space.

It is also evident that similar considerations are applicable to an equation of the type (1), if a differential operator with constant coefficients, which can be transformed into a Laplace operator by a linear transformation of coordinates, replaces the Laplace operator.

This, for example, takes place for a quantum system of charged particles with different masses. In this case the role of the parameter r is played by the quantity

$$(m_1 r_1^2 + m_2 r_2^2 + \ldots + m_N r_N^2)^{1/2}. \qquad (9)$$

As is well known, this very same quantity is widely used in the classical consideration of the many body problem.

Thus the Fock expansion is valid for a very wide class of equations in partial derivatives. It is a generalization of the well known expansion of the solution of ordinary differential equations in the vicinity of a regular singular point which contains a logarithm only in the first degree.

Consideration of the Fock expansion for a wave function of a many-electron system is evidently necessary in the case when the functions are computed with a high degree of accuracy, for example, for two electron systems by the Ritz method in high approximation. The attempt at multiple calculations[2,3] shows that if the test functions do not take into account the behavior of the wave function close to the nucleus, then it is extremely difficult to obtain the accuracy required for a comparison of the relativistic and radiative corrections with experiment.

In some cases, the matrix elements are strongly dependent on the behavior of the wave function close to the nucleus; the calculation of the Fock expansion is then especially necessary. Thus, for example, this is the case in the calculation of the matrix elements of the operator H^2, and for just this reason the estimate below for the energy of the ground state of helium in references 3 and 4 is much worse than the corresponding estimate above by the Ritz method. It is also evident that the behavior of the wave function close to the nucleus is important in the calculations of the interaction of the electronic shell with the nucleus.

It must therefore be expected that the Fock expansion, which takes into consideration the behavior of the wave function in this important region, finds application in a wide variety of atomic calculations.

A detailed investigation of the solution of the set (4), the connection of the Fock expansion with other types of expansions of wave functions of helium, the possible generalization of this expansion, and also certain other problems will be set forth in a paper by A. M. Ermolaev, which will appear in the "Herald" (Vestnik) of Leningrad University.

In conclusion, we thank Academician V. A. Fock for his valuable advice.

[1] V. A. Fock, Izv. Akad. Nauk SSSR, Ser. Fiz. **18**, 161 (1954).

[2] Chandrasekhar, Elbert, and Herzberg, Phys. Rev. **91**, 1172 (1953); S. Chandrasekhar and G. Herzberg, Phys. Rev. **98**, 1050 (1955); J. F. Hart and G. Herzberg, Phys. Rev. **106**, 79 (1957).

[3] T. Kinoshita, Phys. Rev. **105**, 1490 (1956); Demkov, Neigauz, and Seiyukov, Оптика и спектроскопия (Optics and Spectroscopy) **4**, 709 (1958).

[4] L. Wilets and I. J. Cherry, Phys. Rev. **103**, 113 (1956).

Translated by R. T. Beyer
161

ON THE APPLICATION OF QUANTUM-FIELD-THEORY METHODS TO PROBLEMS OF QUANTUM STATISTICS AT FINITE TEMPERATURES

A. A. ABRIKOSOV, L. P. GOR'KOV, and I. E. DZYALOSHINSKIĬ

Institute of Physical Problems, Academy of Sciences, U.S.S.R.

Submitted to JETP editor December 4, 1958

J. Exptl. Theoret. Phys. (U.S.S.R.) **36**, 900-908 (March, 1959)

A formulation of thermodynamic perturbation theory is proposed which makes it possible to make full use of quantum-field-theory methods in quantum statistics at finite temperatures. The method is a generalization of the Matsubara technique and is based on the expansion of the Green's functions in Fourier series in the "imaginary time" variable. The technique so obtained differs from the usual diagram technique for $T = 0$ by the replacement of integration over the frequencies by summation over discrete values of the imaginary frequency. The analytic properties of the Fourier components of the Green's functions are examined. It is shown that owing to the possibility of analytic continuation a knowledge of the corresponding equilibrium Green's functions is sufficient for the solution of various kinetic and nonstationary processes.

1. INTRODUCTION

THE methods of quantum field theory have recently been successfully applied to problems of statistics.[1-4] The application is based on the fact that the apparatus of quantum field theory is developed through the wide use of the "diagram technique," which provides a very intuitive representation of the structure and character of any approximation. Earlier methods of quantum statistics, which started from ideal-gas approximations, could scarcely take the interaction between the particles into account beyond one or two approximations because of the complexity of the older quantum perturbation theory. This is utterly inadequate for the actual many-body problem; to obtain any approximation of physical significance it is necessary to sum over an infinite set of different terms of the perturbation-theory series. The diagram technique is extraordinarily useful in such problems, since it formulates simple rules by which any term of the perturbation theory can be written down.

The basis of the quantum-field-theory methods is the calculation of the so-called Green's function of a particle, which for the case of temperatures different from zero is defined as

$$G(1,2) = -iSp\{\exp[(\Omega + \mu N - \hat{H})/T] \cdot T(\tilde{\psi}(x_1)\tilde{\psi}^+(x_2))\}, \quad (1)$$

where $\tilde{\psi}$, $\tilde{\psi}^+$ are second-quantization operators in the Heisenberg representation. Knowledge of the Green's function makes it possible easily to calculate all the thermodynamic quantities of the system. For example, the particle number density as a function of the chemical potential μ and the temperature is connected with G by the relation

$$N(\mu, T) = \mp iG(x, x)|_{t=t+0}$$

(the minus sign is for Fermi statistics, the plus for Bose statistics).

At the absolute zero of temperature the Green's function is calculated by going over to the so-called "interaction representation." In this representation $G(1, 2)$ has the form

$$G(1,2) = -i\langle T(\psi_1\psi_2^+ S)\rangle / \langle S\rangle, \quad (1a)$$

where $\langle \ldots \rangle$ means the average over the ground state of the system, and S is the well known S matrix of the quantum field theory. Expanding S in powers of the interaction constant, we obtain the usual Feynman diagram technique.

For temperatures other than zero it is already impossible to represent G in a form like Eq. (1a), and consequently it is impossible to calculate G by means of the diagram technique.

Several years ago Matsubara[4] proposed a new formulation of the thermodynamic perturbation theory which is almost completely analogous to the diagram technique of field theory. The present paper is devoted to the description of a technique which is a further development of the Matsubara method. This technique makes it possible to calculate the thermodynamic quantities at finite tem-

peratures with almost the same simplicity with which this is done for $T = 0$. It will further be shown that by establishing the connection of the quantities that figure in this technique with the corresponding quantities in the usual technique one can determine all the kinetic characteristics of the system.*

2. THE MATSUBARA METHOD

The basic idea of the Matsubara method is the passage from the time t to a certain imaginary "time" τ. We note that the ordinary Green's function $G(1, 2)$ can be represented in the form

$$G(1,2)=\begin{cases} -i\mathrm{Sp}\left\{\exp\left[\frac{\Omega+\mu N-\hat{H}}{T}\right]\right. \\ \times\exp\left[\frac{i(\hat{H}-\mu N)}{\hbar}(t_1-t_2)\right]\hat{\psi}(\mathbf{r}_1) \\ \left.\times\exp\left[-\frac{i(\hat{H}-\mu N)}{\hbar}(t_1-t_2)\right]\hat{\psi}^+(\mathbf{r}_2)\right\}, & t_1>t_2, \\ \pm i\mathrm{Sp}\left\{\exp\left[\frac{\Omega+\mu N-\hat{H}}{T}\right]\right. \\ \times\exp\left[-\frac{i(\hat{H}-\mu N)}{\hbar}(t_1-t_2)\right]\hat{\psi}^+(\mathbf{r}_2) \\ \left.\times\exp\left[\frac{i(\hat{H}-\mu N)}{\hbar}(t_1-t_2)\right]\hat{\psi}(\mathbf{r}_1)\right\}, & t_1<t_2. \end{cases} \tag{2}$$

where ψ, ψ^+ are the second-quantization operators in the Schrödinger representation.

In the Matsubara method one introduces a temperature-dependent Green's function $\mathcal{G}$, which is obtained from G by the replacement $t \to -i\tau\hbar$:

$$\mathcal{G}(1,2)=\begin{cases} -\mathrm{Sp}\left\{\exp\left[\frac{\Omega+\mu N-\hat{H}}{T}\right]\right. \\ \times\exp\left[(\hat{H}-\mu N)(\tau_1-\tau_2)\right]\hat{\psi}(\mathbf{r}_1) \\ \left.\times\exp\left[-(\hat{H}-\mu N)(\tau_1-\tau_2)\right]\hat{\psi}^+(\mathbf{r}_2)\right\}, & \tau_1>\tau_2, \\ \pm\mathrm{Sp}\left\{\exp\left[\frac{\Omega+\mu N-\hat{H}}{T}\right]\right. \\ \times\exp\left[-(\hat{H}-\mu N)(\tau_1-\tau_2)\right]\hat{\psi}^+(\mathbf{r}_2) \\ \left.\times\exp\left[(\hat{H}-\mu N)(\tau_1-\tau_2)\right]\hat{\psi}(\mathbf{r}_1)\right\}, & \tau_1<\tau_2. \end{cases} \tag{3}$$

Matsubara showed that in the formula (3) one can go over to a sort of "interaction representation". Namely, let us represent the statistical matrix $\hat{\rho} = \exp\{(\mu N - \hat{H})/T\}$ in the form

$$\exp\left[\frac{\mu N-\hat{H}}{T}\right]=\exp\left[\frac{\mu N-\hat{H}_0}{T}\right]\hat{S}(1/T) \tag{4}$$

and introduce the new operators $\bar{\psi}(\mathbf{r}, \tau)$, $\psi(\mathbf{r}, \tau)$ in the "interaction representation" by the formulas

$$\psi(\mathbf{r}, \tau)=\exp\left[\tau(\hat{H}_0-\mu N)\right]\psi(\mathbf{r})\exp\left[-\tau(\hat{H}_0-\mu N)\right],$$
$$\bar{\psi}(\mathbf{r}, \tau)=\exp\left[\tau(\hat{H}_0-\mu N)\right]\psi^+(\mathbf{r})\exp\left[-\tau(\hat{H}_0-\mu N)\right]. \tag{5}$$

Then, using the formal resemblance of the equation satisfied by the matrix $\hat{S}(1/T)$, $-\partial\hat{S}(\tau)/\partial\tau = H(\tau)\hat{S}(\tau)$, with the Schrödinger equation, we write $\hat{S}(1/T)$, in complete analogy with the usual S matrix, in the form

$$\hat{S}(1/T)=T_\tau\exp\left\{-\int_0^{1/T}\hat{H}_{\mathrm{int}}(\tau)\,d\tau\right\},$$

where T_τ is the time-ordering operator with respect to the imaginary "time" τ. The interaction Hamiltonian $H_{\mathrm{int}}(\tau)$ now depends on the operators $\psi(\mathbf{r}, \tau)$ and $\bar{\psi}(\mathbf{r}, \tau)$ in the same way that it formerly depended on $\psi(\mathbf{r})$ and $\psi^+(\mathbf{r})$.

Now, using the possibility of cyclic permutation of the operators under the sign Sp in Eq. (2), we can show that $\mathcal{G}$ can be written in a form analogous to that used in the field theory:

$$\mathcal{G}(1,\ 2)=-\frac{\mathrm{Sp}\{\exp[(\mu N-\hat{H}_0)/T]T_\tau[\psi_1\bar{\psi}_2\hat{S}(1/T)]\}}{\mathrm{Sp}\{\exp[(\mu N-\hat{H}_0)/T]\hat{S}(1/T)\}}. \tag{6}$$

It is not hard to see that for the potential Ω we can write the following formula:

$$\Omega=\Omega_0-T\ln\left[\frac{\mathrm{Sp}\left\{\exp\left[\frac{\mu N-\hat{H}_0}{T}\right]\hat{S}(1/T)\right\}}{\mathrm{Sp}\left\{\exp\left[\frac{\mu N-\hat{H}_0}{T}\right]\right\}}\right]. \tag{6a}$$

The expressions (6) and (6a) have the forms of the corresponding formulas of field theory:

$$\mathcal{G}(1,2)=-\langle T(\psi_1\bar{\psi}_2 S)\rangle/\langle S\rangle,\quad \Omega=\Omega_0-T\ln\langle S\rangle, \tag{7}$$

if we understand the averaging symbol $\langle \ldots \rangle$ to mean the operation

$$\mathrm{Sp}\left\{\exp\left[\frac{\mu N-\hat{H}_0}{T}\right]\ldots\right\}\Big/\mathrm{Sp}\left\{\exp\left[\frac{\mu N-\hat{H}_0}{T}\right]\right\}.$$

Matsubara showed that for such averages of T-products of several ψ-operators there exists a "Wick's theorem," according to which the average in question breaks up into a sum of products of averages by pairs of operators:

*We have learned that similar results have been obtained by E. S. Fradkin (J. Exptl. Theoret. Phys. (U.S.S.R.), in press).

$$\mathcal{G}_0(1,2) = -\langle T_\tau(\psi_1\bar{\psi}_2)\rangle.$$

Of course this does not apply to Bose systems below the point of the Bose condensation. Similarly, the Wick's theorem is not applicable to Fermi systems in which superconductivity exists. For the construction of a thermodynamic perturbation theory in this range of temperatures one must use in the first case an obvious generalization of some work of Belyaev,[5] and in the second case, work of Gor'kov.[6]

Expanding the expression for $S(1/T)$ appearing in Eq. (7) in a series of powers of the interaction Hamiltonian and using Wick's theorem, we get the usual diagram technique, in which each line corresponds to a zeroth-order Green's function $\mathcal{G}_0(1, 2)$. For example, in the case of the four-fermion interaction with

$$\hat{H}_{\text{int}} = \frac{g}{2}\Lambda_{\alpha\beta;\,\gamma\delta}\bar{\psi}_\alpha(x)\bar{\psi}_\beta(x)\psi_\gamma(x)\psi_\delta(x),$$

where $\mathbf{x} = \{\mathbf{r}, \tau\}$ and $\Lambda_{\alpha\beta;\gamma\delta}$ is some function of the spin indices antisymmetric in $\alpha\beta$ and $\gamma\delta$,

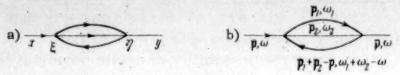

FIG. 1

we find for the second-approximation correction to the Green's function, corresponding to the diagram of Fig. 1a

$$2g^2\Lambda_{\lambda\mu\nu\tau}\Lambda_{\rho\pi\varkappa\omega}\int_0^{1/T}d\tau_\xi\int_0^{1/T}d\tau_\eta\int d\boldsymbol{\xi}\int d\boldsymbol{\eta}\,\mathcal{G}^0_{\varkappa\lambda}(x-\xi)$$
$$\times\,\mathcal{G}^0_{\nu\rho}(\xi-\eta_i)\,\mathcal{G}^0_{\tau\pi}(\xi-\eta_i)\mathcal{G}^0_{\varkappa\mu}(\eta_i-\xi)\,\mathcal{G}^0_{\omega\beta}(\eta_i-y). \quad (8)$$

In the case of the electron-phonon interaction[1,4]

$$\hat{H}_{\text{int}} = g\bar{\psi}\psi\varphi,$$

the first correction to the electron Green's function, corresponding to the diagram of Fig. 2a, has

FIG. 2

the form (the dotted line indicates the phonon Green's function $\mathcal{D}_0 = -\langle T_\tau(\varphi_1\varphi_2)\rangle$, which is the analogue of the ordinary D function of the phonon):

$$-g^2\int_0^{1/T}d\tau_\xi\int_0^{1/T}d\tau_\eta\int d\boldsymbol{\xi}\int d\boldsymbol{\eta}\,\mathcal{G}^0$$
$$\times(x-\xi)\,\mathcal{G}^0(\xi-\eta_i)\,\mathcal{D}^0(\xi-\eta_i)\,\mathcal{G}^0(\eta_i-y). \quad (9)$$

The actual calculation of expressions of types (8), (9) and of the more complicated expressions in the higher approximations is, however, very laborious in the Matsubara technique. The point is that the success of field-theory methods in statistics for $T = 0$ is due to the highly automatic nature of the calculations, which is achieved by the use of Fourier expansions of all the quantities with respect to all four coordinates. It is obvious that in the Matsubara method the automatic feature is lacking because of the finiteness of the range of τ, from zero to $1/T$. Indeed in the coordinate representations (as regards τ) $\mathcal{G}^0$ (and $\mathcal{G}$) is a discontinuous function of the variable τ; therefore in fact all the integrals over τ break up into integrals over a very large number of regions. The number of such regions obviously increases rapidly with increase of the order of the approximation.

3. THE EXPANSION IN FOURIER SERIES

The Matsubara technique can be decidedly improved by the exploitation of certain general properties of the thermodynamic Green's functions.

As we have shown, by Eq. (3) the Green's function $\mathcal{G}(1, 2)$ is a function of the difference $\tau_1 - \tau_2$, specified in the interval from $-1/T$ to $1/T$. It is therefore expedient to continue it periodically and expand it in Fourier series in the variable τ:*

$$\mathcal{G}(\tau) = T\sum_n e^{-i\omega_n\tau}\mathcal{G}(\omega_n),\ \omega_n = \pi Tn,$$

$$\mathcal{G}(\omega_n) = \frac{1}{2}\int_{-1/T}^{1/T}e^{i\omega_n\tau}\mathcal{G}(\tau)\,d\tau. \quad (10)$$

One major property of the function $\mathcal{G}$ is essential for the transformation of the perturbation-theory series. It follows from Eq. (3) that the function $\mathcal{G}$ for negative values of τ is simply related to the $\mathcal{G}$ for $\tau > 0$, namely we have the relation

$$\mathcal{G}(\tau) = \mp\mathcal{G}(\tau + 1/T),\ \tau < 0, \quad (11)$$

where the minus sign is for Fermi statistics and the plus for Bose statistics. The formula (11) is easily derived if we use the fact that one may cyclically permute the operators under the sign of the trace. The relation (11) is of course also valid for the free Green's functions. For the functions as periodically continued this relation is valid for any value of τ.

*Recently I. M. Khalatnikov called our attention to the fact that the idea of expanding the temperature-dependent Green's functions of Matsubara in Fourier series is also contained in a paper by Ezawa, Tomozawa, and Umezawa.[9] These writers, however, being interested only in the application of the Matsurbara method to the problem of multiple production, confined themselves to the case of zero chemical potention. Meanwhile the construction of the technique is nontrivial just in the case $\mu \neq 0$.

If we note further that at each vertex of a Feynman diagram an even number of fermion lines come together, it is easy to see that all the integrals $\int_0^{1/T} \ldots d\tau$ in formulas of the type of Eqs. (8) and (9) can be replaced by $\frac{1}{2}\int_{-1/T}^{1/T} \ldots d\tau$. When this is done the Fourier transformation (10) is easily carried out in all terms of the perturbation-theory series.

The relation (11) also has the consequence that in the Fourier expansion of a fermion Green's function only the components with $\omega_n = \pi T(2n+1)$ are different from zero, and the expansion of a boson Green's function has only components with $\omega_n = \pi T \cdot 2n$. We shall present the expressions for the zeroth-order Green's functions $\mathcal{G}_0(\omega_n, \mathbf{p})$ (here the Fourier integral transformation for the space coordinates has also been carried out).

Fermions:

$$\mathcal{G}_0(\omega_n, \mathbf{p}) = [i\omega_n + \mu - \varepsilon(\mathbf{p})]^{-1}, \quad \omega_n = (2n+1)\pi T$$

(here $\epsilon(\mathbf{p}) = p^2/2m$, and μ is the chemical potential); bosons above the Bose condensation point:

$$\mathcal{G}_0(\omega_n, \mathbf{p}) = [i\omega_n + \mu - \varepsilon(\mathbf{p})]^{-1}, \quad \omega_n = 2n\pi T;$$

phonons:

$$\mathcal{D}_0(\omega_n, \mathbf{k}) = -\omega^2(\mathbf{k})/[\omega^2(\mathbf{k}) + \omega_n^2], \quad \omega_n = 2n\pi T$$

($\omega(\mathbf{k})$ is the energy of a phonon).

Carrying out the Fourier transformation in all the terms of the expansion of the Green's function in the perturbation-theory series, we can verify that the technique so obtained is entirely equivalent to the diagram technique in the momentum space at absolute zero. To each line of a diagram there corresponds a zeroth-order Green's function $\mathcal{G}_0(\omega_n, \mathbf{p})$, and to each vertex a δ function expressing the conservation laws $\Sigma p = 0$, $\Sigma\omega_n = 0$. The only difference is that in our case we have instead of an integration over frequency a summation over discrete imaginary "frequencies" $i\omega_n$. For example, the formula (8) for the correction to the electron Green's function from the four-fermion interaction is transformed into the form

$$\Lambda_{\alpha\mu\nu\tau}\Lambda_{\nu\tau\mu\beta}\frac{2g^2T^2}{(2\pi)^6}\sum_{\omega_1\omega_2}\int d^3\mathbf{p}_1 d^3\mathbf{p}_2 [i\omega_1 + \mu - \varepsilon(\mathbf{p}_1)]^{-1}$$

$$\times [i\omega_2 + \mu - \varepsilon(\mathbf{p}_2)]^{-1}[i(\omega_1 + \omega_2 - \omega) + \mu - \varepsilon(\mathbf{p}_1 + \mathbf{p}_2 - \mathbf{p})]^{-1}$$

$$\times [i\omega + \mu - \varepsilon(\mathbf{p})]^{-2},$$

corresponding to the diagram of Fig. 1b.

The expression (9) takes the form

$$\delta\mathcal{G}(\omega, \mathbf{p}) = \frac{g^2T}{(2\pi)^3}\left\{\sum_{\omega'}\int d^3\mathbf{p}' [i\omega' + \mu - \varepsilon(\mathbf{p}')]^{-1}\omega^2(\mathbf{p} - \mathbf{p}')\right.$$

$$\left.\times [\omega^2(\mathbf{p} - \mathbf{p}') + (\omega - \omega')^2]^{-1}\right\}[i\omega + \mu - \varepsilon(\mathbf{p})]^{-2},$$

which corresponds to the diagram of Fig. 2b.

On passage to the absolute zero of temperature, large values of n play the main part in the sums. Therefore in the perturbation-theory formulas we must make the replacement

$$T\sum_{\omega_n} \to \frac{1}{2\pi}\int_{-\infty}^{\infty} \ldots d\omega.$$

Furthermore, it is obvious that when one replaces all frequencies by imaginary values, $\omega \to -i\omega'$, integrals with respect to $d\omega$ from $-\infty$ to $+\infty$ of products of several factors of the form

$$(i\omega + \mu - \varepsilon(\mathbf{p}))^{-1}$$

go over into integrals of products of factors

$$(\omega' + \mu - \varepsilon(\mathbf{p}))^{-1}, \tag{12}$$

which corresponds to a rotation of the path of integration to real ω. In the case of Fermi Green's functions $\epsilon(p) - \mu$ can be either positive or negative. Therefore after the indicated transformation of the contour of integration the path around the poles is chosen as shown in Fig. 3a. For Bose particles the chemical potential μ of an ideal gas

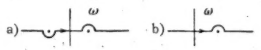

FIG. 3

is always negative; therefore the poles in Eq. (11) lie in the lower half-plane of ω' (Fig. 3b). Conversely, it can be seen from this how from the well known rules of the diagram technique for $T = 0$ one can write down the corresponding term of the perturbation theory for $T \neq 0$. To do this we first make the replacement $\omega' \to i\omega_n$ ($n = (2m+1)$ for Fermi particles and $n = 2m$ for Bose systems) in the corresponding expressions for $T = 0$, and must then go from integration over the frequencies to summation:

$$\int_{-\infty}^{+\infty} d\omega \to -2\pi T i\sum_{\omega_n}.$$

Everything said up to now has referred to calculations by perturbation theory. In quite a number of problems, however, calculations by perturbation theory have been found to be inadequate. For these purposes it is essential to know certain exact equations connecting the quantities with each other. One such relation is the Dyson equation. As is well

known, in field theory one can write an equation connecting the Green's function with the so-called vertex part (the Dyson equation). The analogue of this equation can of course be obtained in the technique proposed here. For the case of the four-fermion interaction it is shown schematically, in the language of the diagrams, in Fig. 4. Here heavy

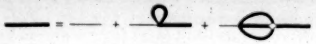

FIG. 4

lines mean the complete Green's function $\mathfrak{G}$, and the rhomb means the complete vertex part, i.e., the sum of all connected diagrams having four external fermion lines. In the momentum representation the Dyson equation corresponding to this diagram has the form:

$$\mathfrak{G}^{-1}_{\alpha\beta}(\omega, \mathbf{p}) = \mathfrak{G}^{0-1}_{\alpha\beta}(\omega, \mathbf{p}) - \frac{2gT}{(2\pi)^3}\sum_{\omega'}\int d^3\mathbf{p}\,\mathfrak{G}_{\gamma\mu}(\omega', \mathbf{p}')\,\Lambda_{\alpha\mu;\nu\beta}$$
$$- \frac{2gT^2}{(2\pi)^6}\,\Lambda_{\alpha\lambda,\mu\nu}\sum_{\omega_1\omega_2}\int d^3\mathbf{p}_1 d^3\mathbf{p}_2\,\mathfrak{G}_{\mu\tau}(\omega_1, \mathbf{p}_1)\,\mathfrak{G}_{\nu\rho}(\omega_2, \mathbf{p}_2)$$
$$\times\mathfrak{G}_{\kappa\lambda}(\omega_1+\omega_2-\omega;\ \mathbf{p}_1+\mathbf{p}_2-\mathbf{p})$$
$$\times\mathfrak{T}_{\tau\rho,\kappa\beta}(\omega_1, \mathbf{p};\ \omega_2, \mathbf{p}_2;\ \omega_1+\omega_2-\omega,\ \mathbf{p}_1+\mathbf{p}_2-\mathbf{p};\omega, \mathbf{p}).$$

Here $\mathfrak{T}$ is the complete vertex part already mentioned. It is connected with the Fourier components of the two-particle Green's function

$$\mathfrak{G}_{\alpha\beta,\gamma\delta}(x_1, x_2; x_3, x_4) = \langle T(\hat{\psi}_\alpha(x_1)\hat{\psi}_\beta(x_2)\bar{\hat{\psi}}_\gamma(x_3)\bar{\hat{\psi}}_\delta(x_4)\hat{S})\rangle / \langle\hat{S}\rangle$$

by the relation

$$\mathfrak{G}_{\alpha\beta,\gamma\delta}(\omega_1, \mathbf{p}_1, \omega_2, \mathbf{p}_2; \omega_3, \mathbf{p}_3, \omega_4, \mathbf{p}_4)$$
$$= \frac{(2\pi)^3}{T}\left\{\frac{(2\pi)^3}{T}\Big[\mathfrak{G}_{\alpha\delta}(\omega_1, \mathbf{p}_1)\mathfrak{G}_{\beta\gamma}(\omega_2, \mathbf{p}_2)\right.$$
$$\times\delta_{\omega_1\omega_4}\,\delta(\mathbf{p}_1-\mathbf{p}_4) - \mathfrak{G}_{\alpha\gamma}(\omega_1, \mathbf{p}_1)\,\mathfrak{G}_{\beta\delta}(\omega_2, \mathbf{p}_2)\,\delta_{\omega_1\omega_3}\,\delta(\mathbf{p}_1-\mathbf{p}_3)\Big]$$
$$-\frac{1}{2}\,\mathfrak{G}_{\alpha\lambda}(\omega_1, \mathbf{p}_1)\,\mathfrak{G}_{\beta\mu}(\omega_2, \mathbf{p}_2)\,\mathfrak{T}_{\lambda\mu,\nu\tau}(\omega_1, \mathbf{p}_1;\ \omega_2, \mathbf{p}_2;\ \omega_3, \mathbf{p}_3;\ \omega_4, \mathbf{p}_4)$$
$$\left.\times\,\mathfrak{G}_{\nu\gamma}(\omega_3, \mathbf{p}_3)\mathfrak{G}_{\tau\delta}(\mathbf{p}_4, \omega_4)\right\}\delta_{\omega_1+\omega_2,\omega_3+\omega_4}\,\delta(\mathbf{p}_1+\mathbf{p}_2-\mathbf{p}_3-\mathbf{p}_4).$$

We shall not write out the analogous Dyson equation for the case of the electron-phonon interaction.

Knowing the thermodynamic Green's function $\mathfrak{G}$ one can find thermodynamic functions of the system. For this purpose one can use, for example, the following simple relation

$$\frac{\partial\Omega}{\partial g} = T\frac{n}{g}\sum_{\omega}\int\frac{d^3\mathbf{p}}{(2\pi)^3}[\mathfrak{G}^{0-1}_{\alpha\beta}(\mathfrak{G}_{\beta\alpha} - \mathfrak{G}_{\beta\alpha}{}^0)].$$

Here n is a coefficient depending on the form of the interaction. For the interaction with phonons $n = 1$; for the four-fermion interaction $n = \frac{1}{2}$.

4. THE ANALYTICAL PROPERTIES OF THE GREEN'S FUNCTIONS AND THE TRANSITION TO TIME-DEPENDENT QUANTITIES

As has already been mentioned, a knowledge of the Green's function is sufficient for the determination of the thermodynamic characteristics of a system. But for the study of various kinetic phenomena, such as scattering or absorption of light or sound, diffusion, and so on, one must know the ordinary time-dependent functions. We shall show how, knowing the thermodynamic one-particle function $\mathfrak{G}(\omega_n, \mathbf{p})$, one can find the time-dependent $G(\omega, \mathbf{p})$.

Beginning with the coordinate space, and comparing Eqs. (2) and (3), we see that in the range of τ from $-1/T$ to $1/T$ the transition from $\mathfrak{G}$ to G is accomplished by replacing τ by it. It is much more interesting, however, to find the connection between the Fourier components $G(\omega, \mathbf{p})$ and $\mathfrak{G}(\omega_n, \mathbf{p})$.

As has been shown by Landau,[7] when the function $G(\omega, \mathbf{p})$ is expanded as a Fourier integral, its Fourier transform is a nonanalytic function of ω. Its real and imaginary parts are connected by the relation

$$G'(\omega, \mathbf{p}) = \frac{1}{\pi}\int_{-\infty}^{+\infty}\coth\frac{x}{2T}\,\frac{G''(x, \mathbf{p})}{x-\omega}\,dx$$

for the Fermi statistics, and the relation

$$G'(\omega, \mathbf{p}) = \frac{1}{\pi}\int_{-\infty}^{+\infty}\tanh\frac{x}{2T}\,\frac{G''(x, \mathbf{p})}{x-\omega}\,dx$$

for Bose statistics.

It can be shown that the Fourier transform of the so-called retarded Green's function $G^R(\mathbf{r}_1-\mathbf{r}_2, t_1-t_2)$,

$$G^R(1,2) = \begin{cases} -i\,\mathrm{Sp}\left\{\exp\left[\frac{\Omega+\mu N-\hat{H}}{T}\right]\right. \\ \left.\times[\tilde{\hat{\psi}}(x_1)\tilde{\hat{\psi}}^*(x_2) \pm \tilde{\hat{\psi}}^*(x_2)\tilde{\hat{\psi}}(x_1)]\right\}, & t_1 > t_2, \\ 0, & t_1 < t_2. \end{cases}$$

is analytic in the upper half-plane. Here the plus sign is for Fermi statistics, the minus for Bose statistics. It turns out that the Fourier transform $G^R(\omega, \mathbf{p})$ of this function is simply related to $G(\omega, \mathbf{p})$. Namely, their real parts are identical, and

$$G''^R(\omega, \mathbf{p}) = \coth(\omega/2T)\,G''(\omega, \mathbf{p})$$

for the Fermi statistics, and

$$G''^R(\omega, \mathbf{p}) = \tanh(\omega/2T)\,G''(\omega, \mathbf{p})$$

for the Bose statistics. For $G^R(\omega, \mathbf{p})$ we can write an expansion of the type used by Lehmann[8]

$$G^R(\omega, \mathbf{p}) = \int_{-\infty}^{+\infty} \frac{\rho(x, \mathbf{p})}{x - \omega - i\delta}\, dx, \tag{13}$$

where

$$\rho(\omega, \mathbf{p}) = -(2\pi)^3 \sum_{n,m} \exp\left[\frac{\Omega + \mu N_n - E_n}{T}\right] \times |\psi_{mn}(0)|^2 \left(1 \pm \exp\left[-\frac{\omega_{mn}}{T}\right]\right) \times \delta(\mathbf{p} - \mathbf{p}_{mn})\, \delta(\omega - \omega_{mn}). \tag{14}$$

Here $\omega_{mn} = E_m - E_n - \mu$, $\mathbf{p}_{mn} = \mathbf{p}_m - \mathbf{p}_n$; E_n, $\mathbf{p}_n$ are the energy and momentum in the n-th state of the system. It can be seen from Eq. (14) that $\rho(\omega, \mathbf{p})$ is a real function, for which the integral $\int_{-\infty}^{+\infty} \rho(\omega, \mathbf{p})\, d\omega$ is finite.

Let us write the analogous Lehmann expansion for $G(\omega_n, \mathbf{p})$. By the use of Eq. (6) it is easy to show, by a method analogous to that of reference 7, that

$$\mathfrak{G}(\omega_n, \mathbf{p}) = \int_{-\infty}^{\infty} \frac{\rho(x)\, dx}{x - i\omega_n}. \tag{15}$$

Comparing Eqs. (13) and (15), we see that

$$\mathfrak{G}(\omega_n) = G^R(i\omega_n), \quad \omega_n > 0. \tag{16}$$

On the other hand, let us use the integral (15), regarded formally as a function of the complex variable $i\omega_n$, to determine a function $\mathfrak{G}(\omega)$ analytic in the upper half-plane. In virtue of Eq. (16) and the well known theorem of the theory of functions of a complex variable regarding the analytic continuation of a function given at an infinite set of discrete points possessing a point of concentration, we find from the above that G^R is, apart from a constant factor, the analytic continuation of the function $\mathfrak{G}(-i\omega_n)$ into the upper half-plane. Namely, we have

$$G^R(\omega) = \mathfrak{G}(-i\omega). \tag{17}$$

The converse problem of finding $\mathfrak{G}(\omega_n)$ from a given $G^R(\omega)$ is solved by Eq. (16) and the relation

$$\mathfrak{G}(\omega_n < 0) = \mathfrak{G}^*(|\omega_n|), \tag{16a}$$

which follows from Eq. (15).

Relations of the types (16) and (17) can in principle be obtained also for the vertex parts Γ and $\mathfrak{T}$. The general relations will, however, be more complicated. For physical applications one ordinarily needs not Γ and $\mathfrak{T}$ themselves, but the correlation functions, i.e., certain integrals of these quantities, and the practical procedure is to establish the connections between them separately for each concrete case.

In conclusion we express our gratitude to Academician L. D. Landau and L. P. Pitaevskiĭ for helpful discussions of the results of this work.

[1] A. Salam, Prog. Theor. Phys. **9**, 550, 1953.
[2] A. B. Migdal, J. Exptl. Theoret. Phys. (U.S.S.R.) **34**, 1438 (1958), Soviet Phys. JETP **7**, 996 (1958).
[3] V. M. Galitskiĭ and A. B. Migdal, J. Exptl. Theoret. Phys. (U.S.S.R.) **34**, 139 (1958), Soviet Phys. JETP **7**, 96 (1958).
[4] T. Matsubara, Prog. Theor. Phys. **14**, 351 (1955).
[5] C. T. Belyaev, J. Exptl. Theoret. Phys. (U.S.S.R.) **34**, 517 (1958), Soviet Phys. JETP **7**, 289 (1958).
[6] L. P. Gor'kov, J. Exptl. Theoret. Phys. (U.S.S.R.) **34**, 735 (1958), Soviet Phys. JETP **7**, 505 (1958).
[7] L. D. Landau, J. Exptl. Theoret. Phys. (U.S.S.R.) **34**, 262 (1958), Soviet Phys. JETP **7**, 182 (1958).
[8] H. Lehmann, Nuovo cimento **11**, 342 (1954).
[9] Ezawa, Tomozawa, and Umezawa, Nuovo cimento **5**, 810 (1957).

Translated by W. H. Furry
162

REACTIONS INVOLVING POLARIZED PARTICLES OF ZERO REST MASS

CHOU KUANG-CHAO

Joint Institute of Nuclear Studies

Submitted to JETP editor May 31, 1958

J. Exptl. Theoret. Phys. (U.S.S.R.) **36**, 909-918 (March, 1959)

In this paper the group-theoretical point of view is used for the description of the spin states of particles of zero rest mass. Complete sets of operators and of their eigenfunctions for a system of two particles are found in the representation of the momenta and spins. The statistical tensors for the particles produced in a reaction of the type $a + b \to c + d$ or $a \to c + d$ are obtained in the case in which one of these particles has no rest mass. The most general selection rules are derived for the reaction $a + b \to c + d$ in the form of relations between the statistical tensors, under the condition that the space and time parities are conserved. The wave functions are calculated for a system of two identical particles of zero rest mass.

1. INTRODUCTION

In reference 1 a study was made of the relativistic theory of reactions involving polarized particles with non-zero rest masses. This theory is not applicable to reactions involving photons and neutrinos. In what follows we shall call a particle (a photon, neutrino, or graviton) with zero rest mass a γ-particle. The purpose of the present paper is to study the theory of reactions involving γ-particles.

The general theory of reactions involving photons has already been extensively developed in papers of Simon[2] and of Morita and others;[3] these authors describe the spin states of photons by a vector potential, using the Lorentz supplementary condition to exclude the longitudinal and scalar components. Such a procedure is complicated, and it is difficult to extend it to cases of higher spins.

The group-theoretical description of the spin states of γ-particles has been given by Wigner and by Yu. M. Shirokov.[4] Starting from the theory of the irreducible representations of the inhomogeneous Lorentz group, they showed that the spin states of free γ-particles are completely determined by the operator

$$\hat{\Sigma} = (\mathbf{j} \cdot \mathbf{n}), \qquad (1)$$

where $\mathbf{j}$ is the total angular momentum of the γ-particle; $\mathbf{n}$ is the unit vector parallel to the momentum of the γ-particle. $\hat{\Sigma}$ is a Lorentz-invariant operator with integral and half-integral values of i. Since the total angular momentum $\mathbf{j}$ is an axial vector and $\mathbf{n}$ is a polar vector, the operator $\hat{\Sigma}$ transforms as a pseudoscalar under space reflections. Thus if a γ-particle has a definite parity, then for each momentum there exist two spin states with eigenvalues $\pm i$ of the operator $\hat{\Sigma}$. If, on the other hand, it does not have a definite parity, then it can have only one spin state (of longitudinal polarization).

In the present paper we use the operator $\hat{\Sigma}$ for the description of the spin states of γ-particles. As can be seen from Eq. (1), the operator $\hat{\Sigma}$ is closely connected with the direction of the momentum. Therefore we shall work directly in the momentum representation. We emphasize that a spin vector does not exist for a γ-particle, and the total angular momentum $\mathbf{j}$ cannot be represented in the form of the sum of an orbital angular momentum and a spin. Because of this the complete sets of operators for the description of the states of a system containing γ-particles, given in Sec. 2 of the present paper, differ from the sets generally used for a system without γ-particles. In Sec. 2 we shall find the complete sets of operators and of their eigenfunctions for systems of two particles. To obtain the formulas for the statistical tensors (s-tensors for short) of reaction products, and to obtain the selection rules under the condition that space and time parities are conserved, we use a method developed by M. I. Shirokov.[5,6]

Landau and Yang have established the existence of specific selection rules for the decay of a particle into two photons.[7] Generalized selection rules of this type have been obtained by Shapiro.[8] Because of the peculiarities of a system of two identical γ-particles it is of interest to calculate the explicit form of the wave functions of this sys-

tem for a definite total angular momentum, angular momentum component, and parity; these functions can be used to obtain angular distributions and polarizations for the decay of particles into pairs of identical γ-particles. It is shown that certain selection rules remain valid when parity is not conserved in a decay.

2. COMPLETE SETS OF OPERATORS AND OF THEIR EIGENFUNCTIONS

We denote state vectors of γ-particles characterized by the momentum $\mathbf{p}$ and the spin operator $\hat{\Sigma}$ by symbols $|\mathbf{p}, \mu\rangle$, where $\mu = \pm 1$ is the eigenvalue of the operator $\hat{\Sigma}$. Since $\hat{\Sigma}$ is invariant under the proper Lorentz group, μ remains unchanged by a Lorentz transformation. Therefore state vectors in different coordinate systems differ only by a phase factor

$$|\mathbf{p}, \mu\rangle \xrightarrow{L} |\mathbf{p}, \mu\rangle' = \eta_{\mu\mu}(L, \mathbf{p})\,|L^{-1}\mathbf{p}, \mu\rangle, \qquad (2)$$

where L is a Lorentz transformation; $\eta_\mu(L, \mathbf{p})$ satisfies the group relation

$$\eta_{\mu\mu}(L_1, \mathbf{p})\,\eta_{\mu\mu}(L_2, L_1^{-1}\mathbf{p}) = \eta_{\mu\mu}(L_2 L_1, \mathbf{p}).$$

The explicit form of the factor η_μ depends on the choice of the coordinate system in which the total angular momentum is quantized. If we choose the axis of quantization of the total angular momentum in such a way that the z axis is parallel to $\mathbf{p}$ and the x axis to $[\mathbf{v}\times\mathbf{p}]$, where $\mathbf{v}$ is the velocity of the new coordinate system relative to the old for the Lorentz transformation L, then by means of the formalism developed in reference 9 it can easily be shown that in this case $\eta_\mu = 1$.*

From Eq. (2) we easily find the transformation function between the state vectors of a γ-particle in two different coordinate systems 1 and 2:

$$\langle \mathbf{p}_1, \mu_1 | \mathbf{p}_2, \mu_2 \rangle$$

$$= \sqrt{p_1/p_2}\,\delta^3\left(p_{1i} - \sum_{j=1}^{3} a_{ij}\,p_{2j}\right)\delta_{\mu_1\mu_2}, \quad i = 1, 2, 3, \qquad (3)$$

where a_{ij} is the matrix of the Lorentz transformation, and the factor $(p_1/p_2)^{1/2}$ is the square root of the Jacobian of the transformation,

$$[\partial(p_{1x}, p_{1y}, p_{1z})/\partial(p_{2x}, p_{2y}, p_{2z})]^{1/2}.$$

We note that if the rest mass of the particle is not equal to zero but its speed approaches that of light, then the angle of rotation of the spin in a Lorentz transformation (cf. reference 1) goes to zero,[10] so that the corresponding transformation function approaches the form (3).

Let us consider the state of a system of two free particles 1 and 2. The rest mass of the system of two free particles is in general not zero.* As is shown in reference 1, for such a system of particles there exists a reference system in which the total momentum is zero and the total angular momentum equals the angular momentum relative to the center of mass of the system of particles. In what follows all results are given in the center-of-mass system. They can be expressed in another coordinate system, if need be, by means of the transformation function (3).

Let us denote the total angular momentum of the system by $\mathbf{J}$, and the total angular momentum of particle α by $\mathbf{j}_\alpha$. We suppose at first that the rest mass of particle 2 is not zero. In this case $\mathbf{j}_2$ can be represented as a sum of an orbital angular momentum $\boldsymbol{l}_2$ and a spin $\mathbf{s}_2$.[1] We introduce a new vector $\mathbf{j}$ in the following way:

$$\mathbf{J} = \mathbf{j}_1 + \mathbf{j}_2 = \mathbf{j} + \mathbf{s}_2, \quad \mathbf{j} = \mathbf{j}_1 + \boldsymbol{l}_2. \qquad (4)$$

The spin operator of particle 2 commutes with the operator $\mathbf{j}$, by definition. Since $\mathbf{J}$ and $\mathbf{s}_2$ satisfy the usual commutation relations for angular momenta, $\mathbf{j}$ also satisfies these relations.

In the center-of-mass system a complete set of operators for the two-particle system consists of the following operators:

$$\mathbf{J}^2,\ J_z,\ \mathbf{j}^2,\ \hat{\Sigma}_1,\ \mathbf{p}. \qquad (5)$$

If particles 1 and 2 have definite parities and parity is conserved in the reaction under consideration, then it is better to replace the operator $\hat{\Sigma}_1$ in the set (5) by the space-inversion operator I.

To express observable quantities in terms of diagonal elements of the R matrix ($R = S - 1$, where S is the scattering matrix), we must find the eigenfunctions of the complete set of operators (5) in the representation of the momenta and spins of the free particles. We write these eigenfunctions in the center-of-mass system in the form

$$\langle \mathbf{n}, \mu_1, \mu_2, p\,|\,J,\ M,\ j,\ \mu_1', p'\rangle, \qquad (6)$$

where μ_α is the eigenvalue of the operator $(\mathbf{j}_\alpha\mathbf{n})$, M is the eigenvalue of the operator J_z, and $\mathbf{n}$ is the unit vector parallel to the direction of the relative momentum $\mathbf{p}$.

*If the coordinate system is chosen as in reference 9, then $\eta_\mu(L, \mathbf{p}) = \exp[i\mu\varphi(L, \mathbf{p})]$, where $\varphi(L, \mathbf{p})$ is given by Eq. (1.91) of reference 9.

*The rest mass M of the system is given by

$$M^2 = (\sqrt{\mathbf{p}_1^2 + M_1^2} + \sqrt{\mathbf{p}_2^2 + M_2^2})^2 - (\mathbf{p}_1 + \mathbf{p}_2)^2,$$

and is zero only when the rest masses M_1 and M_2 of the two particles are zero and their momenta are parallel ($\mathbf{p}_1 \parallel \mathbf{p}_2$).

The functions (6) are determined by the following conditions.

1. If we choose the z axis in the direction $\mathbf{n}$, then

$$\langle \mathbf{k}, \mu_1, \mu_2, p | J, M, j, \mu_1', p' \rangle = C \delta_{\mu_1 \mu_1'} \delta_{\mu_1+\mu_2, M} \delta_{pp'}, \quad (7)$$

where $\mathbf{k}$ is the unit vector in the direction of the z axis, and C is a constant which depends on $\mathbf{J}$, $\mathbf{j}$, and μ_α. The relation (7) follows from the equation $J_z = \hat{\Sigma}_1 + \hat{\Sigma}_2$, if the z axis is parallel to $\mathbf{n}$.

2. Under a three-dimensional rotation the functions (6) transform in the following way (like spherical functions):

$$\langle \mathbf{n}, \mu_1, \mu_2, p | J, M, j, \mu_1', p' \rangle = \sum_{M'} \langle \mathbf{n}', \mu_1, \mu_2, p | J, M', j, \mu_1', p' \rangle D^J_{M'M}(g), \quad (8)$$

if the transformation of the unit vector $\mathbf{n}$ under the rotation is written $\mathbf{n}' = g\mathbf{n}$ (cf. Note 4 in reference 5). In what follows we shall use the Euler angles $\{\varphi_1, \vartheta, \varphi_2\}$ and the functions $D^J_{M'M}$ introduced in reference 5. We emphasize that the angle ϑ is defined here as a rotation around the y axis.

3. The total angular momentum $\mathbf{J}$ is the vector sum of the operators $\mathbf{j}$ and $\mathbf{s}_2$ (Eq. (4)).

4. The functions (6) form a complete set of orthogonal and normalized eigenfunctions. The normalization is based on a volume V with the radius R.

5. The time-reversal operator T is represented by the product of a unitary operator K and the operation of complex conjugation. The phase factor of the function (6) is determined by the condition[11]

$$\begin{aligned} &K\langle \mathbf{n}, \mu_1, \mu_2, p | J, M, j, \mu_1', p' \rangle^* \\ &= \eta_T \langle -\mathbf{n}, \mu_1, \mu_2, p | J, M, j, \mu_1', p' \rangle^* \\ &= (-1)^{J+M} \langle \mathbf{n}, \mu_1, \mu_2, p | J, -M, j, \mu_1', p' \rangle. \end{aligned} \quad (9)$$

Taking $\mathbf{n}' = \mathbf{k}$ in Eq. (8) and substituting Eq. (7) in the right member of Eq. (8), we get

$$\langle \mathbf{n}, \mu_1, \mu_2, p | J, M, j, \mu_1', p' \rangle = C \delta_{\mu_1 \mu_1'} \delta_{pp'} D^J_{\mu_1+\mu_2, M}(g_{\mathbf{n}}), \quad (10)$$

where $g_{\mathbf{n}}$ is the rotation of the coordinate system zyx into the system $z_1y_1x_1$ (z_1 axis parallel to $\mathbf{n}$). If we choose the y_1 axis in the direction of $[\mathbf{k}\times\mathbf{n}]$, the Euler angles for the rotation $g_{\mathbf{n}}$ are $\{-\pi, \vartheta, \pi-\varphi\}$ where ϑ and φ are the spherical angles of the unit vector $\mathbf{n}$ in the zyx coordinate system.

The constant C is determined by conditions 3, 4, and 5. Choosing the phase factor of the state vector $|\mathbf{n}, \mu_1, \mu_2, \mathbf{p}\rangle$ so that $\eta_T = (-1)^{\mu_1+\mu_2}$, and using the relation

$$D^{J*}_{\mu_1+\mu_2, M}(g_{-\mathbf{n}}) = (-1)^{J+M-\mu_1-\mu_2} D^J_{\mu_1+\mu_2, -M}(g_{\mathbf{n}}),$$

we find the phase factor C from Eq. (9). We thus get

$$C = \frac{2\pi\hbar\sqrt{R}}{p\sqrt{V}} \left(\frac{2j+1}{4\pi}\right)^{1/2} C^{J\mu_1+\mu_2}_{j\mu_1 s_2 \mu_2}. \quad (11)$$

Under the reflection I the function (10) with the constant C from Eq. (11) transforms in the following way:

$$\begin{aligned} &I\langle \mathbf{n}, \mu_1, \mu_2, p | J, M, j, \mu_1', p' \rangle \\ &= I_0' \eta_{If} \langle -\mathbf{n}, -\mu_1, -\mu_2, p | J, M, j, \mu_1', p' \rangle \\ &= I_0' \eta_{If} (-1)^{j-s_2} \langle \mathbf{n}, \mu_1, \mu_2, p | J, M, j, -\mu_1', p' \rangle, \end{aligned} \quad (12)$$

where I_0' is the product of the intrinsic parities of the two particles.

We assume that $I^2 = 1$ in Eq. (12). This condition determines the factor η_I apart from its sign: $\eta_I = \pm(-1)^{S_2+i}$, or

$$\begin{aligned} &I\langle \mathbf{n}, \mu_1, \mu_2, p | J, M, j, \mu_1', p' \rangle \\ &= \pm(-1)^{j-i_1} I_0' \langle \mathbf{n}, \mu_1, \mu_2, p | J, M, j, -\mu_1', p' \rangle, \end{aligned} \quad (13)$$

where $i_1 = |\mu_1|$. The eigenfunctions with definite parity I' have the form

$$\begin{aligned} &\langle \mathbf{n}, \mu_1, \mu_2, p | J, M, j, I', p' \rangle \\ &= 2^{-1/2}(1 + I'I) \langle \mathbf{n}, \mu_1, \mu_2, p | J, M, j, i_1, p' \rangle, \end{aligned} \quad (14)$$

where I' is an eigenvalue of the operator I.

We introduce new variables t:

$$I' = \pm(-1)^{j-i_1+t}.$$

Here $t = 0$ or $t = 1$. In reactions with photons one value corresponds to electric radiation, and the other to magnetic radiation (cf. reference 3). The lack of uniqueness in the sign affects only the value of t, but cannot affect the final observable results for the density matrix. Therefore in what follows we can consider the expression (13) with the plus sign only.

Substituting Eqs. (10), (11), and (13) in Eq. (14), we get the eigenfunctions of the complete set of operators $\mathbf{J}^2$, J_z, $\mathbf{j}^2$, I, and $\mathbf{p}$ in the representation of the momenta and spins:

$$\begin{aligned} &\langle \mathbf{n}, \mu_1, \mu_2, p | J, M, j, I', p' \rangle \\ &= \frac{2\pi\hbar\sqrt{R}}{p\sqrt{V}} \left(\frac{2j+1}{4\pi}\right)^{1/2} C^{J\mu_1+\mu_2}_{j\mu_1 s_2 \mu_2} D^J_{\mu_1+\mu_2, M}(g_{\mathbf{n}}) \delta_{pp'} \sigma^t, \end{aligned} \quad (16)$$

where

$$\mu_1 = i_1\sigma, \quad \sigma = \pm 1.$$

If the rest masses of both particles are zero, we cannot introduce the operator $\mathbf{j}$. In this case we use the following complete set of operators:

$$\mathbf{J}^2, J_z, \hat{\Sigma}_1, \hat{\Sigma}_2, p. \quad (17)$$

The eigenfunctions of the operators (17) are found in a similar way, and have the form

$$\langle \mathbf{n}, \mu_1, \mu_2, p \,|\, J, M, \mu_1', \mu_2', p' \rangle = \frac{2\pi\hbar}{p}\frac{\sqrt{R}}{\sqrt{V}}\left(\frac{2J+1}{4\pi}\right)^{1/2} D^J_{\mu_1+\mu_2, M}(g_{\mathbf{n}})\,\delta_{\mu_1\mu_1'}\delta_{\mu_2\mu_2'}\delta_{pp'}. \quad (18)$$

The complete sets (5) and (18) can also be used for a system of two particles with nonvanishing rest masses, which is usually described by the set $\mathbf{J}^2$, J_Z, $\mathbf{l}^2$, $\mathbf{S}^2$, $\mathbf{p}$, where $\mathbf{l}$ is the orbital angular momentum of the relative motion, and $\mathbf{S} = \mathbf{i}_1 + \mathbf{i}_2$ is the sum of the spins of the two particles. Between the eigenfunctions of these sets of operators there exist unitary transformations (transformation functions)

$$\langle J, M, j, \mu \,|\, J', M', l, S, p' \rangle = \delta_{JJ'}\delta_{MM'}\delta_{pp'}(2l+1)^{1/2}(2S+1)^{1/2} C^{j\mu}_{l0S\mu} W(lSji_2, Ji_1)$$

and

$$\langle J, M, \mu_1, \mu_2, p \,|\, J', M', l, S, p' \rangle = \delta_{JJ'}\delta_{MM'}\delta_{pp'}\{(2l+1)/(2J+1)\}^{1/2} C^{S\mu_1+\mu_2}_{l\mu_1 i_1\mu_2 i_2} C^{J\mu_1+\mu_2}_{l0S\mu_1+\mu_2},$$

where W(abcd, ef) is the Racah coefficient.

3. GENERAL FORMULAS FOR THE ANGULAR DISTRIBUTIONS AND THE POLARIZATION VECTORS AND TENSORS FOR THE REACTIONS a + b → c + d AND a → c + d

Let us first consider the density matrix of the γ-particles, $\langle \mu_\gamma \,|\, \rho \,|\, \mu_\gamma' \rangle$. Since μ_γ takes only the two values $\pm i$, we cannot construct the s-tensors from $\langle \mu_\gamma \,|\, \rho \,|\, \mu_\gamma' \rangle$ in the ordinary way. Fano[12] has shown that for photons it is convenient to use the Stokes parmeters. This idea is easily generalized and is adopted in the present work. The Stokes parameters are related to the density matrix of the γ-particles in the following way:

$$\rho(q_\gamma \chi_\gamma) = 2^{1/2}\sum_{\sigma_\gamma, \sigma_\gamma'} (-1)^{1/2 - 1/2\sigma_\gamma'} C^{q_\gamma \chi_\gamma}_{1/2, 1/2\sigma_\gamma, 1/2, -1/2\sigma_\gamma'} \langle \mu_\gamma \,|\, \rho \,|\, \mu_\gamma' \rangle, \quad (20)$$

where $\rho(q_\gamma, \chi_\gamma)$ are the Stokes parameters, $\mu_\gamma = i_\gamma \sigma_\gamma$, and $\mu_\gamma' = i_\gamma \sigma_\gamma'$.

We emphasize that $\rho(1, \chi_\gamma)$ defined by Eq. (20), do not transform like a vector under rotations. The physical interpretation of the Stokes parameters given in Fano's paper for photons is also correct for any γ-particles. We shall not repeat it. In this paper the Stokes parameters will for convenience also be called s-tensors.

The calculations of the s-tensors of the reaction-product particles is made by the method of M. I. Shirokov.[5] We use the notations introduced in reference 5. If the masses of particles 1 and 2 in the initial and final states of the reaction are not zero, we use the complete set of operators $\mathbf{J}^2$, J_Z, $\mathbf{l}^2$, $\mathbf{S}^2$, $\mathbf{p}$, where $\mathbf{l}$ is the orbital angular momentum and $\mathbf{S}$ is the total spin of the two particles. We get the following results:

1. $\gamma + b \rightarrow c + d$.

$$\rho'(q_c \chi_c q_d \chi_d;\ \mathbf{n}_c) = [N_1/(4\pi)^2]\,[(2i_c+1)(2i_d+1)2^{-1}(2i_b+1)^{-1}]^{1/2} \times \sum Y^*_{q_c\chi_c q_d\chi_d}(J_1 l_1' S_1',\ Jq'\chi',\ J_2 l_2' S_2') \langle S_1' l_1' \alpha \,|\, R^{J_1} \,|\, j_1 l_1 \alpha_1 \rangle \times \langle S_2' l_2' \alpha' \,|\, R^{J_2} \,|\, j_2 l_2 \alpha_2 \rangle^* \ Y_{q_\gamma \chi_\gamma q_b \chi_b}(J_1 l_1 t_1,\ Jq\chi,\ J_2 l_2 t_2) \times D'_{\chi'\chi}(g_c g_\gamma^{-1})\,\rho(q_\gamma \chi_\gamma q_b \chi_b,\ \mathbf{n}_\gamma), \quad (21)$$

where

$$Y_{q_c\chi_c q_d\chi_d}(J_1 l_1' S_1',\ Jq'\chi',\ J_2 l_2' S_2') = [(2q_c+1)(2q_d+1)]^{1/2} C^{q'\chi'}_{q_c\chi_c q_d\chi_d} \times (-1)^{q'+\chi'} i^{l_1'-l_2'} X(i_c q_c i_c, S_1' q' S_2',\ i_d q_d i_d) \times G_{\chi'}(J_1 l_1' S_1',\ Jq,\ J_2 l_2' S_2'); \quad (22)$$

$$Y_{q_\gamma\chi_\gamma q_b\chi_b}(J_1 j_1 t_1,\ Jq\chi,\ J_2 j_2 t_2) = \sum [(2J_1+1)(2J_2+1) \times (2j_1+1)(2j_2+1)(2J+1)(2q+1)]^{1/2} \times C^{h\chi_\gamma - \chi_b}_{J\chi q_b - \chi_b}(-1)^{J_1+l_\gamma\chi_\gamma+q_b+\chi_b} \times X(J_1 J J_2,\ j_1 h j_2,\ i_b q_b i_b)\, F_h(j_1 t_1,\ j_2 t_2 q_\chi \chi_\gamma); \quad (23)$$

$$F_h(j_1 t_1,\ j_2 t_2,\ q_\gamma 0) = (-1)^{-i_{t_1}}[1 + I_{t_1} I_{t_2}(-1)^{h+q_\gamma}]\, C^{q_\gamma 0}_{1/2\,1/2,\,1/2,-1/2} C^{h0}_{j_1 t_1 j_2 t_2 - i_{t_2}}, \quad (24)$$

$$F_h(j_1 t_1, j_2 t_2, 11) = (-1)^{j_1+i_{t_1}+h+t_1+1} C^{h-2i_{t_2}}_{j_1-i_{t_1} j_2 i_{t_2}},$$

$$F_h(j_1 t_1, j_2 t_2, 1-1) = (-1)^{j_1+j_2+t_1+t_2} C^{h2i_{t_2}}_{j_1 i_{t_1} j_2 i_{t_2}};$$

$$I_{t_\alpha} = (-1)^{j_\alpha - i_{t_\alpha} + t_\alpha},\ N_1 = (2\pi\hbar)^4 R^2 [V^2 p_b^2 p_d^2]^{-1}(p_b; p_d)^2.$$

The sum is taken over q', χ', J', l_1', S_1', J_2, l_2', S_2', j_1, t_1, j_2, t_2, J, q, χ, q_γ, χ_γ, q_b, χ_b.

2. $a + b \rightarrow \gamma + d$.

$$\rho'(q_\gamma \chi_\gamma q_d \chi_d;\ \mathbf{n}_\gamma) = [N_1/(4\pi)^2]\,[2(2i_d+1)(2i_a+1)^{-1}(2i_b+1)^{-1}]^{1/2} \times \sum Y^*_{q_\gamma\chi_\gamma q_d\chi_d}(J_1 j_1' t_1',\ Jq'\chi',\ J_2 j_2' t_2') \times \langle j_1' t_1' \alpha \,|\, R^{J_1} \,|\, S_1 l_1 \alpha_1 \rangle \langle j_2' t_2' \alpha' \,|\, R^{J_2} \,|\, S_2 l_2 \alpha_2 \rangle \times Y_{q_a\chi_a q_b\chi_b}(J_1 l_1 S_1,\ Jq\chi,\ J_2 l_2 S_2) \times D^J_{\chi'\chi}(g_\gamma g_a^{-1})\,\rho(q_a\chi_a q_b\chi_b;\ \mathbf{n}_a). \quad (25)$$

3. $\gamma + b \rightarrow \gamma' + d$.

$$\rho'(q_\gamma\chi_\gamma, q_d\chi_d; \mathbf{n}_\gamma) = [N_1/(4\pi)^2]\,[(2i_d+1)(2i_b+1)^{-1}]^{1/2} \times \sum Y^*_{q_\gamma\chi_\gamma q_d\chi_d}(J_1 j_1' t_1', Jq'\chi', J_2 j_2' t_2') \times \langle j_1' t_1' \alpha \,|\, R^{J_1} \,|\, j_1 t_1 \alpha_1 \rangle \langle j_2' t_2' \alpha' \,|\, R^{J_2} \,|\, j_2 t_2 \alpha_2 \rangle \times Y_{q_\gamma\chi_\gamma q_b\chi_b}(J_1 j_1 t_1, Jq\chi, J_2 j_2 t_2) \times D^J_{\chi'\chi}(g_\gamma g_\gamma^{-1})\,\rho(q_\gamma\chi_\gamma q_b\chi_b; \mathbf{n}_\gamma). \quad (26)$$

4. a → γ + d.

$$\rho'(q_\gamma\chi_\gamma q_d\chi_d, \mathbf{n}_\gamma) = (N_2/4\pi)\,[2(2i_d+1)(2i_a+1)^{-1}]^{1/2} \times \sum Y^*_{q_\gamma\chi_\gamma q_d\chi_d}(i_a j_1' t_1', q_a q'\chi', i_a j_2' t_2') \langle j_1' t_1' \alpha \,|\, R^{i_a} \,|\, \alpha_1 \rangle \times \langle j_2' t_2' \alpha' \,|\, R^{i_a} \,|\, \alpha_2 \rangle^* D^{q_a}_{\chi'\chi_a}(g_\gamma)\,\rho(q_a, \chi_a), \quad (27)$$

where $N_2 = (2\pi\hbar)^3\, R\,(Vp^2)^{-1}\,(E_\gamma \,|\, E_a)$. The sum is taken over j_1', t_1', j_2', t_2', q_a, χ_a, q', χ'.

In particular for $q_\gamma = q_b = q_c = q_d = 0$ the formula (21) gives the angular distribution of the products of the reaction $\gamma + b \to c + d$ for unpolarized incident beam and unpolarized target. In this case our formula agrees with the result obtained by Morita et al., if we eliminate certain phase factors by means of a redefinition of the elements of the R matrix. Our results confirm the conclusion that Simon's formulas are erroneous.

4. SELECTION RULES

If parity is conserved selection rules exist in the form of relations between the s-tensors. These selection rules have been obtained in references 2, 5, 6, 13 for the case in which all the particles have nonvanishing rest masses. The results are easily extended to reactions involving γ-particles. As an example we shall consider a reaction of the type $\gamma + b \to c + d$.

The conservation of spatial parity gives the following equation:

$$I_{t_1} I_{t_2} = (-1)^{i_1'+i_2'}. \quad (28)$$

From the properties of the D-function and Eqs. (22) – (24) it follows that:

$$D^J_{\chi'\chi}(g_c g_\gamma^{-1}) = D^J_{\chi'\chi}(-\pi, \vartheta_c, \pi - \varphi_c) = (-1)^{\chi'-\chi} D^J_{-\chi'-\chi}(-\pi, \vartheta_c, \pi + \varphi_c), \quad (29)$$

$$Y_{q_c\chi_c q_d\chi_d}(J_1 l_1' S_1', Jq'\chi', J_2 l_2' S_2) = (-1)^{l_1'+l_2'+J+q_c+q_d} \times Y_{q_c,-\chi_c,\, q_d,-\chi_d}(J_1 l_1' S_1', Jq'-\chi', J_2 l_2' S_2'), \quad (30)$$

$$Y_{q_\gamma\chi_\gamma q_b\chi_b}(J_1 j_1 t_1, Jq\chi, J_2 j_2 t_2) = (-1)^{J+q_\gamma+q_b} \times I_{t_1} I_{t_2} Y_{q_\gamma-\chi_\gamma q_b-\chi_b}(J_1 j_1 t_1, Jq-\chi, J_2 j_2 t_2'). \quad (31)$$

Equation (31) is obtained by the use of the equations $(-1)^{\gamma q} = (-1)^{\chi\gamma}$ for $\chi\gamma = \pm 1$ and $(-1)^h = I_{t_1} I_{t_2} (-1)^{q\gamma}$ for $\chi\gamma = 0$. Substituting Eqs. (29), (30), and (31) in Eq. (21), we get the most general selection rules holding when parity is conserved; these rules are expressed as follows: if we replace the s-tensors $\rho(q_\gamma\chi_\gamma q_b\chi_b, \mathbf{n}\gamma)$ of the initial state by

$$\rho_I = (-1)^{q_\gamma+q_{I_\gamma}\chi_\gamma+q_b+\chi_b}\,\rho(q_\gamma, -\chi_\gamma, q_b, -\chi_b; \mathbf{n}_\gamma),$$

then we get in the final state the s-tensors

$$\rho_I' = (-1)^{q_c+\chi_c+q_d+\chi_d}\,\rho'(q_c - \chi_c q_d - \chi_d; \vartheta, -\varphi).$$

The results obtained here for the reaction involving γ-particles and the writer's results[13] for the reaction without γ-particles are consistent with each other. We emphasize that the spin states of the γ-particles are described not by s-tensors, but by Stokes parameters. We shall not consider here the special cases dealt with in reference 13, for which the results have just the same form.

The conservation of time parity gives a relation between the s-tensors of the direct $(\gamma + b \to c + d)$ and inverse $(c + d \to \gamma + b)$ reactions. Such relations have been obtained by M. I. Shirokov[6] for the reaction without γ-particles. His formulas require only a slight change for the reactions involving γ-particles. In what follows we suppose that spatial parity is also conserved.

Repeating the calculations of reference 6 step by step and using the same notations, we get the relation for the reaction with γ-particles that corresponds to Eq. (8) of reference 6:

$$\langle q_\gamma, \chi_\gamma, q_b, \chi_b \,|\, W_I(\varphi_1, \vartheta, -\varphi_2) \,|\, q_c, \chi_c, q_d, \chi_d \rangle = (-1)^{q_\gamma+q_{I_\gamma}\chi_\gamma+q_b+\chi_b+q_c+\chi_c+q_d+\chi_d} \langle q_c, -\chi_c, q_d, -\chi_d, \times |\, W_D(-\pi+\varphi_2, \vartheta, \pi-\varphi_1) \,|\, q_\gamma, -\chi_\gamma, q_b, -\chi_b \rangle, \quad (32)$$

where the Euler angles $\{-\pi + \varphi_2,\ \vartheta,\ \pi - \varphi_1\}$ are those for the rotation $g_c g_\gamma^{-1}$ in the direct reaction, and $\{\varphi_1,\ \vartheta,\ -\varphi_2\}$ are those for the rotation $g_\gamma g_c^{-1}$ in the inverse reaction. We emphasize that in the direct reaction the y_c axis is not parallel to the vector $[\mathbf{n}_\gamma, \mathbf{n}_c]$, but is obtained by clockwise rotation of this vector through the angle φ_2 around the z_c axis. The angles ϑ and φ_1 are equal to the spherical angles of the vector $\mathbf{n}_c$ in the coordinate system $z_\gamma y_\gamma x_\gamma$. In the inverse reaction ϑ and $\pi + \varphi_2$ are equal to the spherical angles of the vector $\mathbf{n}_\gamma$ in the system $z_c y_c x_c$, and the y_γ axis makes the angle $\pi + \varphi_1$ with the direction of $[\mathbf{n}_c \times \mathbf{n}_\gamma]$.*

Replacing the factor F in Eq. (9) of reference 6 by

*We note that Eq. (8) of reference 6 is valid only in the specially chosen systems $z_c y_c x_c$ and $z_a y_a x_a$ in which $\varphi_1 = \varphi_2$.

$$F = [(2i_c + 1)(2i_d + 1)]^{1/2} [2(2i_b + 1)]^{-1/2} \quad (33)$$

and $(-1)^{q_a+\chi_a}$ by $(-1)^{q_\gamma+2i_\gamma\chi_\gamma}$, we get relations corresponding to Eqs. (9) and (10) in reference 6.

Let us go on to the consideration of the special cases studied in reference 6. The relation of detailed balancing between the differential cross-sections of the direct and inverse reactions for unpolarized initial state has the well known form

$$p_\gamma^2 (2i_b + 1)\, \sigma_D(\vartheta) = p_c^2 (2i_c + 1)(2i_d + 1)\, \sigma_I(\vartheta). \quad (34)$$

The difference $\sigma'_D(\vartheta, \varphi_1) - \sigma_D(\vartheta, \varphi_1)$ between the cross-sections with a polarized beam of γ-particles and with an unpolarized beam in the direct reaction can be expressed in the form

$$\sigma'_D(\vartheta, \varphi_1) - \sigma_D(\vartheta, \varphi_1) = -F^2 p_c^2 p_\gamma^{-2} [(-1)^{2i_\gamma} \rho'_{1} \rho_{-1} + \rho'_0 \rho_0 + \rho'_{-1} \rho_1 (-1)^{2i_\gamma}] = -F^2 p_c^2 p_\gamma^{-2} (\rho'(\varphi_1, \vartheta, -\varphi_1)\rho), \quad (35)$$

where ρ_{-1}, ρ_0, and ρ_1 are the Stokes parameters characterizing the spin state of the incident γ-particles in the direct reactions; ρ'_{-1}, ρ'_0, and ρ'_1 are the Stokes parameters for the spin state of the γ-particles produced in the inverse reaction with unpolarized initial state.

5. SYSTEM WITH TWO IDENTICAL γ-PARTICLES

Let us construct symmetric or antisymmetric wave functions with definite parity, total angular momentum, z-component of angular momentum, and energy, for a system of two identical γ-particles. The state vector $|J, M, \mu'_1, \mu'_2, p\rangle$ transforms under reflection in the following way:

$$I\,|J, M, \mu'_1, \mu'_2, p\rangle = I'_0 \eta'_I\, |J, M, -\mu'_1, -\mu'_2, p\rangle,$$

where I'_0 is the product of the intrinsic parities of the two identical particles, which is always equal to unity; η'_I is a phase factor.

Since the state vector $|J, M, \mu'_1, \mu'_2, p\rangle$ transforms under rotations according to an irreducible representation of the rotation group with the weight J, a rotation through the angle φ around the direction $\mathbf{n}$ of the relative momentum of the particles gives a factor $\exp[i(\mu'_1 + \mu'_2)\varphi]$. Accordingly, in the rotated coordinate system the factor η'_I is replaced by $\eta''_I = \eta'_I \exp[2i(\mu'_1 + \mu'_2)\varphi]$. Therefore the value of the phase factor η'_I depends on the direction of the x (or y) axis in the coordinate system with the z axis parallel to $\mathbf{n}$. In view of the fact that the system of two γ-particles occurs only in the final state of some reaction, we choose the coordinate system with axes $z \parallel \mathbf{n}$, $y \parallel \boldsymbol{\zeta} - (\boldsymbol{\zeta}\cdot\mathbf{n})\mathbf{n}$, $x \parallel [\boldsymbol{\zeta}\times\mathbf{n}]$, where $\boldsymbol{\zeta}$ is the polarization vector of the particles in the initial state of the reaction. After reflection the z and x axes change their directions, but the y axis remains unchanged. The "reflected" coordinate system differs from the original system only by a rotation through the angle π around the y axis. Therefore from the relation $D^J_{\mu'\mu}(0, \pi, 0) = (-1)^{J-\mu}\delta_{\mu',-\mu}$ we get

$$I\,|J, M, \mu'_1, \mu'_2, p\rangle = I'_1 \sum_{\mu''_1\mu''_2} |J, M, \mu''_1, \mu''_2; p\rangle\, D^J_{\mu''_1+\mu''_2,\mu'_1+\mu'_2}(0, \pi, 0)$$

$$= I'_1 (-1)^{J-\mu'_1-\mu'_2} |J, M, -\mu_1, -\mu_2, p\rangle. \quad (36)$$

Let us now consider the operator S that replaces the first particle by the second and vice versa. In the chosen coordinate system the operator S can be expressed as the product of the operator I, which changes the direction of the relative momentum, and the operator that interchanges the spin indices μ'_1 and μ'_2. Thus

$$S\,|J, M, \mu'_1, \mu'_2, p'\rangle = (-1)^{J-\mu'_1-\mu'_2} |J, M, -\mu'_2, -\mu'_1, p\rangle. \quad (37)$$

From Eqs. (36) and (37) we get the symmetric or antisymmetric wave vectors with definite parity I', total angular momentum, z-component of angular momentum, and energy

$$|J, M, \mu, I', p\rangle = A[1 + I'I + S'S + I'S'IS]\,|J, M, \mu'_1, \mu'_2, p\rangle\, \delta_{|\mu'_1+\mu'_2|,\mu}, \quad (38)$$

where $\mu = 2i$ or 0 is the eigenvalue of the operator $|\hat{\Sigma}_1 + \hat{\Sigma}_2|$, A is a normalization constant, and $S' = +1$ for particles obeying Bose statistics and $S' = -1$ for Fermi statistics. Multiplying Eq. (38) from the left by $\langle \mathbf{n}, \mu_1, \mu_2, p|$ and using Eqs. (19), (36), and (37), we get the wave functions for this system in the momentum-spins representation.

1. $\mu = 2i$, $\mu_1 = \mu_2 = \pm i$.

$$\langle n, \mu_1, \mu_2, p\,|\,J, M, 2i, I', p'\rangle = (1/2\sqrt{2})(1 + S'I')(2\pi\hbar\sqrt{R}/p\sqrt{V})\left(\frac{2J+1}{4\pi}\right)^{1/2}\delta_{pp'} \times [D^J_{2i,M}(g_{\mathbf{n}})\,\delta_{\mu_1+\mu_2,2i} + I'(-1)^{J+2i} D^J_{-2i,M}(g_{\mathbf{n}})\,\delta_{\mu_1+\mu_2,-2i}]. \quad (39)$$

2. $\mu = 0$, $\mu_1 = -\mu_2 = \pm i$.

$$\langle \mathbf{n}, \mu_1, \mu_2, p\,|\,J, M, 0, I', p\rangle = (1/2\sqrt{2})(1 + S'(-1)^J)(2\pi\hbar\sqrt{R}/p\sqrt{V})[(2J+1)/4\pi]^{1/2}\delta_{pp'} \times D^J_{0M}(g_{\mathbf{n}})\,(\delta_{\mu_1 i}\delta_{\mu_2,-i} + I'(-1)^J\,\delta_{\mu_1,-i}\,\delta_{\mu_2 i}). \quad (40)$$

As can be seen from Eqs. (39) and (40), the wave functions are nonvanishing only when $S'I' = 1$ for $\mu = 2i$, and $S'(-1)^J = 1$ for $\mu = 0$. These are just the specific selection rules obtained by Landau

and by Yang for photons and by Shapiro in the general case. We note that when parity is not conserved the selection rule $S'(-1)^J = 1$ for $\mu = 0$ remains valid, but the factor $\delta_{\mu_1 i}\delta_{\mu_2 -i} + I'(-1)^J \times \delta_{\mu_1 -i}\delta_{\mu_2 i}$, which characterizes the polarization of the system, is changed. Therefore in the decay of a particle with spin $J < 2i$ into two identical γ-particles a measurement of the correlation of the polarizations of the γ-particles not only will give the parity of this particle when parity is conserved (cf. Yang, reference 7), but also will give information about the nonconservation of parity in the decay.

The wave functions (39) and (40) can be written together in a single formula:

$$\langle \mathbf{n}, \mu_1, \mu_2, p \mid J, M, \mu, I', p' \rangle = \frac{1}{2\sqrt{2}} F_\mu \frac{2\pi\hbar\sqrt{R}}{p\sqrt{V}} \times \left(\frac{2J+1}{4\pi}\right)^{1/2} D^J_{\mu_1+\mu_2, M}(g_R)\, \sigma^{I'}\delta_{|\mu_1+\mu_2|,\mu}, \qquad (41)$$

where $\sigma i = \mu_1$, $I' = (-1)^{J-2i+t}$,

$$F_\mu = (1 + S'I') \text{ for } \mu = 2i,$$
$$F_\mu = (1 + S'(-1)^J) \text{ for } \mu = 0.$$

By means of Eq. (41) one can easily calculate the angular distributions and the polarizations for the decay of a particle into two identical γ-particles. We shall not do this here.

In conclusion I express my gratitude to Professor M. A. Markov, M. I. Shirokov, and L. G. Zastavenko for interest shown in this work and a discussion of the results.

[1] Chou Kuang-Chao and M. I. Shirokov, J. Exptl. Theoret. Phys. (U.S.S.R.) **34**, 1230 (1958), Soviet Phys. JETP **7**, 851 (1958).

[2] A. Simon, Phys. Rev. **92**, 1050 (1953).

[3] Morita, Sugie, and Yoshida, Prog. Theor. Phys. **12**, 713 (1954).

[4] E. P. Wigner, Ann. of Math. **40**, 1490 (1939). Yu. M. Shirokov, J. Exptl. Theoret. Phys. (U.S.S.R.) **33**, 1208 (1957), Soviet Phys. JETP **6**, 929 (1958).

[5] M. I. Shirokov, J. Exptl. Theoret. Phys. (U.S.S.R.) **32**, 1022 (1957), Soviet Phys. JETP **5**, 835 (1957).

[6] M. I. Shirokov, J. Exptl. Theoret. Phys. (U.S.S.R.) **33**, 975 (1957), Soviet Phys. JETP **6**, 748 (1957).

[7] L. D. Landau, Dokl. Akad. Nauk SSSR **60**, 207 (1948). C. N. Yang, Phys. Rev. **77**, 242 (1950).

[8] I. S. Shapiro, J. Exptl. Theoret. Phys. (U.S.S.R.) **27**, 393 (1954).

[9] Chou Kuang-Chao and L. G. Zastavenko, J. Exptl. Theoret. Phys. (U.S.S.R.) **35**, 1417 (1958), Soviet Phys. JETP **8**, 990 (1959).

[10] E. P. Wigner, Revs, Modern Phys. **29**, 255 (1957).

[11] L. C. Biedenharn and M. E. Rose, Revs. Modern Phys. **25**, 729 (1953). R. Huby, Proc. Phys. Soc. **A67**, 1103 (1954).

[12] U. Fano, Phys. Rev. **93**, 121 (1954).

[13] Chou Kuang-Chao, J. Exptl. Theoret. Phys. (U.S.S.R.) **35**, 783 (1958), Soviet Phys. JETP **8**, 543 (1959).

Translated by W. H. Furry
163

Letters to the Editor

A PARAMAGNETIC AMPLIFIER AND GENERATOR, USING Fe^{3+} IONS IN CORUNDUM

L. S. KORNIENKO and A. M. PROKHOROV

Moscow State University

Submitted to JETP editor November 27, 1958

J. Exptl. Theoret. Phys. (U.S.S.R.) **36**, 919-920 (March, 1959)

IN published reports on the construction of quantum-mechanical amplifiers and generators, Gd^{3+} (reference 1) and Cr^{3+} (references 2-8) have been used as the paramagnetic ions. There is also a report of an attempt, as yet unsuccessful, to utilize the ion Ni^{2+} (reference 2) for this purpose.

We have carried out a study of the possibility of constructing a paramagnetic amplifier and generator using the ion Fe^{3+} in corundum. The spectrum of the electronic paramagnetic resonance of the ions Fe^{3+} in the lattice Al_2O_3 has been studied earlier by the authors.[9] The Fe^{3+} ion is in an S state, and has electronic spin $S = 5/2$. In corundum the Fe^{3+} ions form two nonequivalent systems, differing from one another in the direction of the cubic axes of the crystalline electric field. The axes of trigonal symmetry of both systems are parallel. If the trigonal axis of the crystalline electric field is parallel or perpendicular to an externally applied constant magnetic field, then the energy levels of both systems coincide for any magnitude of the magnetic field and arbitrary orientation of the cubic axes. If, however, the trigonal axis of the crystal makes an angle with the direction of the external magnetic field, then the energy levels of both systems coincide only for some definite orientations of the cubic axes of the non-equivalent systems of ions; these orientations can be found by turning the crystal around the trigonal axis until the spectra of the electronic paramagnetic resonances of both systems coincide. In the absence of an external magnetic field the six spin levels of each system are split by the electric field of the crystal into three doublets, the distances between which are 0.39 and 0.62 cm^{-1}. From a comparison of the relative intensities of the spectral lines at 290 and 4.2°K., it was established that the lowest spin doublet is the one which in strong magnetic fields is split into levels characterized by magnetic quantum numbers $M = \pm 1/2$, i.e., the constant, D, in the spin Hamiltonian is positive. For the paramagnetic amplifier levels were used which, if the influence of the cubic components of the crystalline field is neglected, are characterized in the parallel orientation by the quantum numbers $M = -5/2, -3/2, -1/2$. The presence in the crystalline field of a cubic component mixes the states, even in the parallel orientation, as a result of which transitions are allowed between any of the chosen levels. For amplification the levels with $M = -3/2$ and $-1/2$ are used, and the auxiliary radiation induces transitions between the levels with $M = -5/2, -1/2$. The trigonal axis of the crystal made a small angle with the direction of the constant magnetic field. The cubic axes were oriented so that the energy levels of both non-equivalent systems of ions coincided.

Amplification and generation were observed at a temperature of 1.8°K. for a wave-length ~ 3.2 cm. with auxiliary radiation of wave-length ~ 1.2 cm. The magnitude of the constant magnetic field was ~ 1200 Oe.

[1] Scovil, Feher, and Seidel, Phys. Rev. **105**, 762 (1957).

[2] A. L. McWhorter and J. W. Meyer, Phys. Rev. **109**, 312, (1958).

[3] Artman, Bloembergen, and Shapiro, Phys. Rev. **109**, 1392 (1958).

[4] Makhov, Kikuchi, Lambe, and Terhune, Phys. Rev. **109**, 1399 (1958).

[5] Strandberg, Davis, Faughnan, Kyhl, and Wolga, Phys. Rev. **109**, 1988 (1958).

[6] S. H. Autler and N. McAvoy, Phys. Rev. **110**, 280 (1958).

[7] R. H. Kingston, Proc. IRE **46**, 916 (1958).

[8] Zverev, Kornienko, Manenkov, and Prokhorov, J. Exptl. Theoret. Phys. (U.S.S.R.) **34**, 1660 (1958), Soviet Phys. JETP **7**, 1141 (1958).

[9] L. S. Kornienko and A. M. Prokhorov, J. Exptl. Theoret. Phys. (U.S.S.R.) **33**, 805 (1957), Soviet Physics JETP **6**, 620 (1958).

Translated by K. F. Hulme
164

ANGULAR ANISOTROPY OF SCATTERING OF FRAGMENTS IN FISSION OF Am^{241} *BY 14.7-Mev NEUTRONS*

A. N. PROTOPOPOV, I. A. BARANOV, and V. P. ÉĬSMONT

Submitted to JETP editor December 6, 1958

J. Exptl. Theoret. Phys. (U.S.S.R.) **36**, 920-921 (March, 1959)

To explain the influence of nuclear structure on the angular anisotropy of fission it is necessary to study the angular distribution of the fission products of as many nuclei as possible. To extend the investigations[1-3] to include the heavier elements, we studied in the present work the angular distribution of the fragments of Am^{241} fission induced by 14.7-Mev neutrons.

The method previously described[2] was used to determine the relative amount of fragments in directions parallel and perpendicular to the direction of the incident neutrons. Taking into account the effect of the motion of the center of mass, the finite nature of the angular resolution, and the background of scattered neutrons, we found that the degree of angular anisotropy of Am^{241} is 1.08 ± 0.06.

The small anisotropy of Am^{241}, which has a spin $5/2$ and which forms an odd-odd nucleus upon capture of a neutron, is not in contradiction with the ideas of O. Bohr.[4] However, within the framework of these ideas, it is difficult to understand why the anisotropy is weaker in Am^{241} than in Np^{237} (for which the degree of anisotropy is 1.16 ± 0.02, see reference 1), although both nuclei have equal spins and parities.

The value obtained for the degree of anisotropy of Am^{241} confirms the previously noted[1-3] tendency towards reduced anisotropy with increasing value of Z^2/A of the fissioned nucleus. Yet, comparing the anisotropies in the fission of Np^{237}, Tu^{239}, and Am^{241}, with values of 1.16 ± 0.02 (reference 1), 1.15 ± 0.05 (reference 2), and 1.08 ± 0.06 respectively, it is noted that the degree of anisotropy varies relatively slowly in the region of transuranic elements.*

It is possible that the observed reduction in the anisotropy with increasing Z^2/A can be understood within the framework of Strutinskiĭ's statistical theory.[5]

In conclusion, the authors express their gratitude to G. I. Khlebnikov for precipitating the americium on an aluminum foil.

*It appears that the small difference in the value of the energies of the neutrons causing the fission (14.3, 14.8 and 14.7 Mev respectively for the fission of Mp^{237}, Tu^{239} and Am^{241}) is not very significant in this case.

[1] R. L. Henkel and J. E. Brolley Jr., Phys. Rev. **103**, 1292 (1956).

[2] A. N. Protopopov and V. P. Éĭsmont, J. Exptl. Theoret. Phys. (U.S.S.R.) **34**, 250 (1958), Soviet Phys. JETP **7**, 173 (1958).

[3] J. Halpern, Paper delivered at All-Union Conference on Nuclear Reactions at Low and Medium Energies, Moscow, 1957.

[4] O. Bohr, Paper delivered at International Conference on Peaceful Uses of Atomic Energy, Geneva, 1955.

[5] V. M. Strutinskiĭ, Атомная энергия (Atomic Energy) **6**, 508 (1957).

Translated by J. G. Adashko
165

MEASUREMENT OF THE MASS OF COSMIC-RAY PARTICLES UNDERGROUND

M. I. DAĬON and L. I. POTAPOV

P. N. Lebedev Physics Institute, Academy of Sciences, U.S.S.R.

Submitted to JETP editor July 30, 1958

J. Exptl. Theoret. Phys. (U.S.S.R.) **36**, 921-922 (March, 1959)

THE present note describes the results of experiments to measure the mass of cosmic-ray particles underground by means of a magnetic spectrometer, which was simultaneously used for the measurement of the momentum spectrum and the positive excess of μ mesons at a depth of ~ 40 m. water equivalent.

The diagrams showing the apparatus, and a short description of it, are given in reference 1. A block of lead 6 cm thick was placed above the instrument to screen it from electrons. A system of lead absorbers separated by trays of hodoscope counters was placed under the telescope. For particles stopping in the absorbers, it was possible to determine the value of the mass from their momentum and range. The purpose of the experiment was not to conduct precision measurements of the particle mass and therefore thick absorbers were used. The absorbers, (V, VI, VII in Fig. 1[1]) were each of 4 cm thickness.

The uncertainty in the determination of a particle mass is due to errors in the measurement of the momentum of the particle and in the determination of its range. The method of accounting for these errors is described in a number of articles. In our case, for μ mesons stopping in the absorbers V, VI, and VII, the expected mean square errors in the determination of the masses are approximately equal to 30, 17, and 12% respectively.

A histogram of the obtained experimental data is shown in Fig. 1. The x axis shows the values of the particle mass, and the y axis the corresponding number of cases. 370 trajectories are included in the given spectrum.

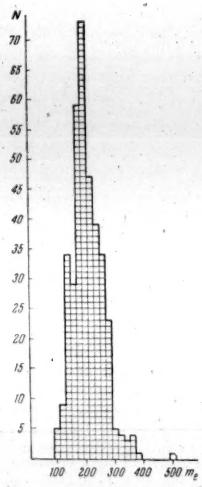

All recorded positive and negative particles having a range 4 cm < R ≤ 16 cm, can be identified as μ mesons. (π and μ mesons were not separated by the instrument). It can be seen that the given data do not indicate the presence, at different observation depths, of particles different from μ mesons (and π mesons). It is, of course, necessary to remember that this method has a limited possibility as far as the detection of short-lived particles is concerned (with lifetime of the order of $\tau \lesssim 10^{-8}$ sec), and that it is impossible to detect neutral particles. Besides, particles having a long-range decay product (for instance K_μ) can, in certain cases avoid detection (being regarded as the penetrating component), and even if they do not, the apparent value of their mass might be lower (in view of an apparent lengthening of the range). However, the amount of such particles detected in our instrument cannot exceed 50% of their number. A more exact identification of such particles can be made using a mass spectrometer in conjunction with a cloud chamber.[2,3]

It should be noticed that, in the mass spectrum, only one particle was observed in which the measured value of mass is much larger than the mass of a μ meson ($\sim 500\ m_e$). This particle stopped in the 5th absorber, where the accuracy of mass determination is smallest. The possibility cannot be excluded that random experimental errors might in that case have lead to the increase of the mass of a μ meson, for instance as a result of the particle skipping through the row of counters VI below.

From our data, one can obtain the upper limit for the possible number of protons in the flux. The chosen range interval 4 cm Pb < R < 16 cm Pb corresponds to a momentum interval of protons 6×10^8 ev/c < P < 10^9 ev/c. In this momentum range, about 1500 particles were detected which passed through all absorbers V, VI, VII, and not a single particle stopped in the absorbers. Hence, we obtain the value of 0.06% for the possible number of protons in the flux in the momentum range $6 \times 10^8 < P < 10^9$ ev/c, and this represents the upper limit.

The authors wish to express a deep gratitude to A. I. Alikhanyan for his great help in carrying out the work, for his helpful advice and discussion of the data, and to V. Kh. Volinskiĭ and V. V. Krugovykh for their great help in carrying out the experimental part of the work.

[1] M. I. Daĭon, and L. N. Potapov, J. Exptl. Theoret. Phys. (U.S.S.R.) **36**, 697 (1959), Soviet Phys. JETP, this issue, p. 000.

[2] Alikhanyan, Kirillov-Ugriumov, Shostakovich, and Fedorov, Dokl. Akad. Nauk SSSR **92**, 255 (1953),

[3] Daĭon, Fedorov, Merzon, and Shostakovich, Приборы и техника эксперимента (Instruments and Meas. Engg.) **1**, 3 (1957).

Translated by H. Kasha
166

NUCLEAR EXCITATION BY HIGH ENERGY PARTICLES

M. Z. MAKSIMOV

Submitted to JETP editor September 2, 1958

J. Exptl. Theoret. Phys. (U.S.S.R.) **36**, 922-924 (March, 1959)

THE quantities which, in the main, characterize the first stage of interaction of fast particles with nuclei are the mean number of nucleons $\overline{N}$ knocked out and the mean excitation energy $\overline{U}$ of the remaining nucleus.[1] Knowledge of these quantities is also important in the description of the evaporation stage. Experimental determination of them is very difficult;[2,3] therefore, the well-known Monte-Carlo method[2] is used to provide estimates. Use of it also involves a lot of work. Thus, it would be of interest to have another method of calculation, which would make it possible to obtain $\overline{N}$ and $\overline{U}$ analytically as functions of the energy E_0 and mass number A.

We consider a case, averaged over neutrons and protons ($A \approx 2Z$), and will assume that all cascade nucleons travel mainly in the forward direction.[2,3] Then, the weak dependence of the effective cross section for collision with the nucleons inside the nucleus makes it possible to use results of the theory of slowing down of neutrons in hydrogen. (The mean effective cross section is $\sigma_{eff} \approx \frac{1}{2}(\sigma_{pp}+\sigma_{pn})(1-7E_f/5E_c)$; $\sigma_{pp} \approx \sigma_{nn}$, $\sigma_{pn} = \sigma_{np}$ are the total cross sections for elastic collisions of free nucleons; E_f = 22 to 25 Mev is the Fermi energy; $E_c = E_0 + V_0$ is the kinetic energy of the nucleons in the nucleus, and V_0 is the depth of the potential well.) In this case, the number of cascade nucleons at distance 2Rx (x is dimensionless) and with energy in the interval dE is equal to

$$dN = \left\{\delta(E_c - E)e^{-\beta x} + \sum_{n=1}^{\infty} 2^n W_n\right\} dE, \qquad (1)$$

where the summation is carried out over all the collisions and W_n is of the form[4]

$$W_n = \frac{(\beta x)^n}{n!}\, e^{-\beta x}\, \frac{\ln^{n-1}(E_c/E)}{E_c(n-1)!}. \qquad (2)$$

The excitation energy of the remaining nucleus, averaged over the geometrical cross section, is equal to

$$\overline{U}(E_0, \beta) = E_0 + |\varepsilon| - (V_0 + B/2)\overline{F} + (V_0 - |\varepsilon|)\overline{N}, \qquad (3)$$

where the following quantities have been introduced

$$\overline{N} = 2\beta^{-2}\int_0^{\beta} ye^{-y}\Psi(\alpha, 2y)\,dy; \quad \overline{F} = 2\beta^{-2}e^{\alpha}\int_0^{\beta} ye^{-y}\Psi(2\alpha, y)\,dy,$$

$$\Psi(x,z) = 1 + \int_0^{\sqrt{4xz}} \exp\left\{-\frac{t^2}{4z}\right\} I_1(t)\,dt;$$

$$\alpha = \ln\frac{E_0 + V_0}{V_0 + B/2}; \quad \beta = \frac{3A\bar{\sigma}_{2\Phi}}{2\pi R^2}; \qquad (4)$$

$I_1(t)$ is the Bessel function of imaginary argument, ϵ is the mean binding energy of nucleons in the nucleus and B is the Coulomb barrier for protons.

On the figure we show values of $\overline{U}$ calculated from these formulae with the initial data: $V_0 \approx$ 31 Mev, $R = 1.41 \cdot 10^{-13} A^{1/3}$ cm (σ_{pp} and σ_{pn} are taken from reference 5, with mean error ±10%, corresponding to the two curves on the figure, the upper for +10% and the lower for −10%), as well as several experimental data and results of Monte Carlo calculations. Although most of these data are only claimed to be estimates,[2,6] the agreement is quite satisfactory.

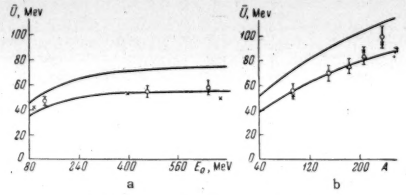

Dependence of the mean excitation energy: a – on proton energy for AgBr nuclei; b – on the mass number, for E_0 = 460 kev. ○, □ and Δ are experimental data from references 3 and 6, × – are Monte Carlo calculations; [2,7] the solid curves are from the present work.

The main feature of the proposed method is its simplicity. Using it, it is possible to evaluate cross sections for the reactions (p, xn); (p, pxn) etc. at high energies, and to show simply the influence of errors in the initial data, e.g., in the nuclear radius, or in the cross sections σ_{pp}, σ_{pn}. For the latter purpose, it is useful to employ approximate expressions for $\overline{F}$ and $\overline{N}$

$$\overline{F} \approx \tfrac{1}{2}e^{\alpha}\{1 + \Phi(\sqrt{2\alpha} - \sqrt{y_0})\};$$

$$\overline{N} \approx \tfrac{1}{2}e^{y_0}\{1 + \Phi(\sqrt{\alpha} - \sqrt{2y_0})\}, \qquad (5)$$

where $y_0 = A\sigma_{eff}/\pi R^2$; $\Phi(z)$ is the error function.

Bombardment of nuclei by fast particles of mass a and energy E_a is equivalent to bombardment of them by a nucleons, each of mean

energy E_a/a. Therefore, we have the following expressions for $\overline{U}_a$:

$$\overline{U}_a(E_a, \beta) \approx |\varepsilon_a| - |\varepsilon| + a\,\overline{U}(E_a/a, \beta). \quad (6)$$

Here ϵ_a is the binding energy of particles of the same type as the incident ones in the nucleus and $\overline{U}(E_a/a, \beta)$ can be obtained from Eqs. (3) and (4). From this formula and the preceding ones it follows that bombardment of a nucleus by complex particles is advantageous with respect to obtaining high excitation energies of the remaining nucleus. From analysis of the graph in the figure, we conclude that there is little chance of a cascade for $E_a/a \lesssim 30$ to 50 Mev and that nuclear reactions here go through formation of the compound nucleus.

In conclusion, I would like to thank M. M. Agrest and I. M. Rozman for advice and discussion, and N. V. Khaikhyan for calculational help.

[1] R. Serber, Phys. Rev. **72**, 1114 (1947); M. L. Goldberger, Phys. Rev. **74**, 1269 (1948).

[2] Bernardini, Booth, and Lindenbaum, Phys. Rev. **85**, 826 (1952); **88**, 1017 (1952); Anthology, Nuclear Reactions at High Energies (Russ. Transl.) Chapt. II, 19-126 (1954).

[3] V. I. Ostroumov, Dokl. Akad. Nauk SSSR **103**, 409 (1955); J. Exptl. Theoret. Phys. **32**, 3 (1957), Soviet Phys. JETP **5**, 12 (1957).

[4] G. C. Wick, Phys. Rev. **75**, 738 (1949).

[5] Dzhelepov, Kazarinov, Golovin, Flyagin and Satarov, Izv. Akad. Nauk SSSR, Ser. Fiz. **19**, 573 (1955), Columbia Tech. Transl. p. 513.

[6] McManus, Sharp, and Gell-Mann, Phys. Rev. **93**, 924 A (1954); B. Rossi, in Anthology, High Energy Particles (Russ. Transl.), GITTL, M. 1955, p. 433.

Translated by G. E. Brown
167

A METHOD OF EVALUATING ELECTRICAL CONDUCTIVITY

V. L. BONCH-BRUEVICH

Moscow State University

Submitted to JETP editor September 15, 1958

J. Exptl. Theoret. Phys. (U.S.S.R.) **36**, 924-926 (March, 1959)

IT is well known that in the electron theory of solids the standard transport equation method meets with a number of difficulties (see, e.g., references 1 – 3). A number of authors have in this connection in recent years made attempts to construct an accurate theory of the transport coefficients using relaxation functions.[4-7] In the present note we give a new method to evaluate the reaction of a system of particles to an external field, using quantum-mechanical Green functions. To be specific, we shall deal with the electrical conductivity, but it will be clear from the results that the method could be equally well used to evaluate any parameter characterizing the reaction of the system. We note also that to apply the general results to the Bose case one needs only change the sign in some of the intermediate equations. It is obvious that if one wants to evaluate the average current produced in the system by the action of an external electrical field it is sufficient to find the change in the "one-particle" density matrix $R_1(\mathbf{x}, \mathbf{y}; t)$. It was shown in reference 8 that this matrix is connected with the one-fermion Green function through the equation

$$R_2(\mathbf{x}, \mathbf{y}; t) = i \lim G(x, y) \quad \text{as} \quad x_0 \to y_0 = t, \quad x_0 < y_0 \quad (1)$$

(x, y, are points in four-dimensional space, the spin indices are omitted for the sake of simplicity). Let the field be characterized by the four-potential A_i ($i = 0, 1, 2, 3$, $A_0 = -\varphi$, φ is the scalar potential). If we are interested only in effects which are linear in the field we have for the change in the Green function

$$\Delta G(x, y) = (e/\hbar) \int dz dz' dz'' G_0(x_1 z') \times \Gamma_i(z', z''; z)\, G_0(z'', y)\, A_i(z), \quad (2)$$

where $\Gamma_i = -\hbar G^{-1}(\mathbf{z}', \mathbf{z}'')/\delta e A_i(\mathbf{z})$ is the "electromagnetic" vertex part and G_0 the Green function for $A_i = 0$.

For a number of problems it is sufficient to restrict the discussion to the case of spatial uniformity, when ($\hbar = 1$)

$$G_0(x, y) = \int dp G_0(p)\, e^{-i(p_0 x_0 - \mathbf{p}\cdot\mathbf{x} - p_0 y_0 + \mathbf{p}\cdot\mathbf{y})},$$
$$\Gamma_i(x, y; z) = (-2\pi)^{-8} \int dq' dq'' \Gamma_i(q', q'')\, e^{-i(q'x - z) + i(q'' y - z)} \quad (3)$$

($px = p_0 x_0 - \mathbf{p}\cdot\mathbf{x}$). We shall also assume $A_i = A_{mi} e^{-ikz - s|z_0|}$ (s is a small positive number; if damping is present, e.g., when the electrical conductivity is finite, we can at once put $s = 0$). Equation (2) then gives

$$\Delta G(x, y)\Big|_{s=0} = eA_i(y)(2\pi)^4 \times \int dp G_0(p)\, G_0(p - k)\, \Gamma_i(p, p - k)\, e^{-i(p, x - y)}. \quad (4)$$

The electrical conductivity can be evaluated from this in a trivial manner.

As an illustration we shall consider the case of a constant field ($A_\alpha = 0$, $\alpha = 1, 2, 3$) in the approximation $\Gamma_1(q', q'') = 1$. We shall assume (compare reference 8; the equation has a meaning also for the determination of the Green function as an ensemble average)

$$G_0(p) = -\frac{1}{(2\pi)^4}\left\{\frac{n_p}{p_0 - \omega_p - i\gamma'_p} - \frac{1-n_p}{p_0 - \omega_p + i\gamma''_p}\right\}$$

$$(\omega, \gamma', \gamma'' - \text{real};\ \gamma', \gamma'' > 0). \qquad (5)$$

We must note that Eq. (5) is by no means general (in particular, this assumption means that we restrict ourselves to one — perhaps spin-degenerate-band). A number of interesting cases, however, are included here. One can easily evaluate $\Delta G(x, y)$ under the given conditions. Taking (1) into account we get for the change in the occupation numbers in momentum space:

(a) if $\gamma' = \gamma'' = \eta \to 0$:

$$\Delta n_p = -\frac{eE_\alpha}{s + ik_0}\frac{\partial n_p}{\partial p_\alpha}; \qquad (6)$$

(b) if γ', γ'' are finite and $k_0 = 0$ (the calculation is also simple for $k_0 \neq 0$, but leads to a more unwieldy result):

$$\Delta n_p = -eE_\alpha \frac{\partial}{\partial p_\alpha}\frac{n_p(1-n_p)}{\gamma_p}. \qquad (7)$$

Here $\mathbf{E}$ is the field strength (with potential φ), $\gamma_p = \gamma'_p + \gamma''_p$. The right hand side of (6) agrees, as was to be expected, exactly with the "accelerating" term of the transport equation, if we understand by s^{-1} the time of action of the field. The static electrical conductivity tensor has from (7) the form (in the usual units, m is the true electron mass)

$$\sigma_{\alpha\beta} = -\frac{e^2}{m}\frac{2}{(2\pi\hbar)^3}\int dp\, p_\alpha \frac{\partial}{\partial p_\beta}\frac{n_p(1-n_p)}{\gamma_p}. \qquad (8)$$

In the particular case of Boltzmann statistics and and isotropic model ($n_p \sim \exp(-\hbar\omega_p/kT)$, $\omega_p = \omega(|p|)$, $\gamma_p = \gamma(|p|)$) Eq. (7) agrees formally with the result of applying the transport equation, if we take for the "relaxation time" the quantity

$$\tau_p = \frac{1}{\gamma_p}\left[1 + kT\frac{\partial \ln \gamma_p}{\partial \hbar\omega_p}\right]. \qquad (9)$$

We emphasize, however, that Eq. (8) is valid over a far wider range than the transport equation.

[1] L. E. Gurevich, Основы физической кинетики (Fundamentals of Physical Kinetics) Gostekhizdat, 1940.

[2] S. I. Pekar, Usp. Fiz. Nauk **60**, 191 (1956).

[3] A. G. Samoĭlovich and L. L. Korenblit, Usp. Fiz. Nauk **49**, 337 (1953).

[4] R. Kubo and K. Tumita, J. Phys. Soc. Japan **9**, 888 (1954); R. Kubo, Can. J. Phys. **34**, 1274 (1956); J. Phys. Soc. Japan **12**, 570 (1957).

[5] H. Nakano, Progr. Theoret. Phys. **15**, 77 (1956); **17**, 145 (1957).

[6] R. Zigenlaub, Dokl. Akad. Nauk SSSR **117**, 395 (1957); Soviet Phys. Doklady **2**, 505 (1957).

[7] M. I. Klinger, J. Tech. Phys. (U.S.S.R.) **27**, 2780 (1957), Soviet Phys. JTP **2**, 2578 (1957).

[8] V. L. Bonch-Bruevich, J. Exptl. Theoret. Phys. (U.S.S.R.) **30**, 342 (1956); Soviet Phys. JETP **3**, 278 (1956).

Translated by D. ter Haar
168

THERMODYNAMIC THEORY OF FERROMAGNETIC ABSORPTION

V. L. BESHIDZE

Sukhumi Pedagogical Institute

Received by JETP editor December 19, 1957; resubmitted September 29, 1958

J. Exptl. Theoret. Phys. (U.S.S.R.) **36**, 926-928 (March, 1959)

If a ferromagnet is in an alternating magnetic field, its macroscopic state changes; this means that the specimen is absorbing energy from the field (ferromagnetic absorption). The basic causes of ferromagnetic absorption are, as is known, the following: the nonvanishing time for establishment of equilibrium within the spin system (intraspin relaxation), and the nonvanishing time for establishment of equilibrium between the spin system and the lattice (spin-lattice relaxation). In this article it is shown that for an isotropic ferromagnetic medium near the Curie temperature, it is possible to determine the law of ferromagnetic resonance if the specific form of the thermodynamic potential is known.

A nonequilibrium state of the system can be described by a thermodynamic potential that depends on nonequilibrium thermodynamic parameters. We suppose that a ferromagnet without hysteresis is in an external magnetic field, and that the amplitudes of the constant and alternating fields are pointed in mutually perpendicular planes (the case of perpendicular fields). In the second case $\mathbf{H}_0$ and $\mathbf{h}$ are pointed along the z axis

(the case of parallel fields). The nonequilibrium thermodynamic potential in the stated problem has the form

$$\Phi = \Phi_0 + \alpha M^2 + {}^1/_2 \beta M^4 - MH', \qquad (1)$$

where Φ_0, α, and β are functions of temperature and pressure, M is the magnetization, and H′ is the effective magnetic field.[1] In the case of weak fields the magnetization M coincides with the spontaneous magnetization M_S.

A nonequilibrium state of the system may be described[1-3] by nonequilibrium thermodynamic parameters, which are given by the relations

$$\mathbf{h} = \mathbf{H}' - \mathbf{H}_0 = \mathbf{h}_0 e^{i\omega t},$$

$$\mathbf{m} = \mathbf{M} - \mathbf{M}_0 = \mathbf{m}_0 e^{i\omega t}, \quad \vartheta = T - T_0. \qquad (2)$$

Here the quantities with index 0 correspond to an equilibrium state of the system; T is the temperature of the spin system, T_0 is the temperature of the lattice, ω is the frequency of the alternating field. The equation of motion for the alternating part of the magnetization is expressed by the formula

$$\dot{\mathbf{m}} = -\varphi(H', T)\nabla\Phi + g[\mathbf{H}'\cdot\mathbf{M}], \qquad (3)$$

where $\varphi(H', T)$ is some function, which remains undetermined within the framework of thermodynamic theory; g is the gyromagnetic ratio. On limiting ourselves to terms linear in h and m, we shall have for the perpendicular field

$$\tau\dot{m}_x + A_x m_x - \tau\omega_{0x} m_y = \chi_f h_x,$$

$$\tau\dot{m}_y + A_y m_y + \tau\omega_{0y} m_x = \chi_f \omega_{0x} h_x,$$

$$\tau\dot{m}_z + A_z m_z + (\chi_f H'/T)\vartheta = 0,$$

$$\omega_0 \equiv (\omega_{0x}\omega_{0y})^{1/2}$$

$$= g\{H_0 + (N_x - N_y)M_0\}^{1/2}\{H_0 + (N_y - N_z)M_0\}^{1/2},$$

$$A_{(x,y,z)} \equiv 1 + \alpha^{-1}[\beta M_s^2 + N_{(x,y,z)}], \qquad (4)$$

where $\tau \equiv \chi_f/\varphi$ is the spin-spin relaxation time for h perpendicular to $\mathbf{H}_0$, χ_f is the magnetic susceptibility, which depends on α (reference 4), ω_0 is the resonance frequency, and N is a demagnetizing factor.

For complete solution of the problem it is necessary to introduce another equilibrium equation in m and θ; it will correspond to spin-lattice interaction. According to the first law of thermodynamics, with (1) and (2) taken into account, we find:

$$(A'T/\chi_f H')\delta\tau'\dot{m} - (1-\delta)\tau'\dot{\vartheta} - \vartheta = 0, \qquad (5)$$

where $\tau' = \alpha_1 T^2/(\alpha + CH')$ is the spin-lattice relaxation time, $A' = 1 + 3\beta M_S^2/\alpha$, $\delta = CH'^2/(\alpha + CH'^2)$, and α_1, α, and C are constant coefficients.

For parallel fields the last equation in (4) gives

$$\tau\dot{m} + A'm + A''(\chi_f H'/T)\vartheta = \chi_f h, \qquad (6)$$

where $A'' = 1 + kM_S^2$, and where K is a constant. On eliminating θ from (5) and (6), we get an equation relating to the magnetization m, namely

$$(1-\delta)\ddot{m} + (\gamma/\tau + 1/\tau')\dot{m} + A'm/(\tau'\tau) = [(1-\delta)\dot{h} + h/\tau']\chi_f/\tau, \qquad (7)$$

where τ represents the "transverse" relaxation time and τ' the "longitudinal" relaxation time according to Bloch, and $\gamma = A'[1 - \delta(A'' - 1)]$.

If we bear in mind that m and h are the periodic functions (2), solution of equation (4) in the case of perpendicular fields gives

$$\frac{\chi'}{\chi_f} = \frac{[A_x A_y + \tau^2(\omega_0^2 - \omega^2)](A_y + \tau^2\omega^2) + \tau^2\omega^2(A_x + A_y)}{[A_x A_y + (\omega_0^2 - \omega^2)\tau^2]^2 + (A_x + A_y)^2\tau^2\omega^2},$$

$$\frac{\chi''}{\chi_f} = \frac{\{[A_y + \tau^2\omega_0^2(A_x + A_y)] - [A_x A_y + \tau^2(\omega_0^2 - \omega^2)]\}\tau\omega}{[A_x A_y + (\omega_0^2 - \omega^2)\tau^2]^2 + (A_x + A_y)^2\tau^2\omega^2}. \qquad (8)$$

In the case of parallel fields, we find from (7):

$$\frac{\chi'}{\chi_f} = \frac{\{(\tau + \gamma\tau') - (1-\delta)[A'\tau' - \tau\tau'(1-\delta)\omega^2]\tau'\}\omega}{[A' - (1-\delta)\tau\tau'\omega^2]^2 + (\tau + \gamma\tau')^2\omega^2},$$

$$\frac{\chi''}{\chi_f} = -\frac{\{\tau + [\gamma - (1-\delta)A']\tau'\}\omega + (1-\delta)^2\tau\tau'^2\omega^3}{[A' - (1-\delta)\tau\tau'\omega^2]^2 + (\tau + \gamma\tau')^2\omega^2}. \qquad (9)$$

The mean absorption energy of the spin system per unit time, by virtue of (2) and (8), has the form:

$$\varepsilon = \frac{1}{2}\chi_f h_0^2 \frac{\{(A_y + \tau^2\omega_x^2)(A_x + A_y) - [A_x A_y + \tau^2(\omega_x^2 - \omega^2)]\}\tau\omega^2}{[A_x A_y + (\omega_x^2 - \omega^2)\tau^2]^2 + (A_x + A_y)^2\tau^2\omega^2}.$$

Above the Curie point, $M_S = 0$, $A = A' = A'' = \gamma = 1$, and $\omega_0 = gH_0$; i.e., results are obtained that agree with the results of references 2 and 5.

[1] N. Bloembergen, Phys. Rev. **78**, 572 (1950).
[2] I. G. Shaposhnikov, J. Exptl. Theoret. Phys. (U.S.S.R.) **18**, 533 (1948).
[3] G. R. Khutsishvili, J. Exptl. Theoret. Phys. (U.S.S.R.) **29**, 329 (1955), Soviet Phys. JETP **2**, 187 (1956).
[4] V. L. Ginzburg, J. Exptl. Theoret. Phys. (U.S.S.R.) **17**, 833 (1947).
[5] G. V. Skrotskiĭ and L. V. Kurbatov, Izv. Akad. Nauk SSSR, Ser. Fiz., **21**, 833 (1957) [Columbia Tech. Transl. p. 833].

Translated by W. F. Brown, Jr.
169

ALPHA DECAY OF Th^{227} *IN THE COLLECTIVE MODEL AND THE SPIN OF* Ra^{223} *IN ITS LOWEST STATE*

S. G. RYZHANOV

Submitted to JETP editor October 22, 1958

J. Exptl. Theoret. Phys. (U.S.S.R.) **36**, 928-930 (March, 1959)

FRILLEY et al.[1] have shown that the relative intensities of the α-groups of Th^{227}, which arise during its decay from the ground state to the single-particle levels of Ra^{223} (0.59, 286 kev), are approximately the same and amount to 17 – 21%. Such levels must therefore be considered as the ground states for the three rotational series, one of which was considered by the author elsewhere.[2]

In this communication we establish the spin of the lower level of Ra^{223} with the aid of the Ter-Martirosyan formula[3] for the probability of the α decay of a parent nucleus of spin I_0.

$$W_{I'} = C \sum_{l=I-I'}^{I+I'} \left| C^{I'I_0}_{I'lm} \right|^2 (2l+1) \exp\{-\alpha E_r - \beta l(l+1)\}. \quad (1)$$

In our calculations the projection m of the orbital moment of the α particle l on the symmetry axis of the nucleus is assumed to differ from zero. Here $m = I_0 - I'$, where I' is an analogous projection of the spin I of the corresponding level of the daughter nucleus. The semi-empiral coefficients α and β are taken from reference 2 and the values of the excitation energy E_r are taken from the level scheme given in reference 1. It was also established in reference 1 that $59 - 29 - 0$ kev level transitions are electric quadrupole, and consequently the following assumptions can be made concerning the spin of the lowest level: (a) $I = I' = I_0 - 2$; (b) $I = I' = I_0 - 1$; (c) $I = I' = I_0$. The 29-kev level, in view of the relatively low intensity of the α particles, (5%) should logically be considered the first rotational sublevel of the lower level. In the case (c) we could not obtain an empirical relation for the intensities of the α groups for the 29 and 0 kev levels, leaving therefore only cases (a) and (b). Upon calculating the Clebsch-Gordan coefficients that enter into (1), and considering that by the parity rule l can be only even, we obtain for case (a) the following ratios for the intensities of the groups for the 29 and 0 kev levels

$$\frac{J_{29}}{J_0} = \frac{2}{I_0 + 1} e^{-14.2 \cdot 0.029} \quad (2)$$

(Here $l = 2$ and $m = 2$, and the terms with $l > 2$ in the sum of Eq. (1) can be neglected). Relation (2) assumes the empirically-established value of 5% : 19%, either when the spin of the ground state of the daughter nucleus (Th^{227}) is $I_0 = 7/2$, or when $I_0 = 9/2$. We therefore conclude that the spin of the lower level of Ra^{223} is either $3/2$ or $5/2$. Calculations made for case (b) lead to $I_0 = 3/2$, which, however, from considerations given in reference 2, is excluded.

The same method of calculations can also be applied to the calculation of the spin of the 286-kev ground state of the third rotational series. The 307-kev level must, for the same reason, be taken as the first sublevel of this series. Since a magnetic dipole 286 – 0 kev transition and an electric dipole 286 – 238 kev transition were empirically established in reference 1, the only assumption that can be made is $I = I' = I_0 - 1$, for the 286-kev level and $I = I_0$ and $I' = I_0 - 1$ for the first sublevel (307 kev). In both cases we have $l = 2$ and $m = 1$. The calculated ratio of the intensities of the α groups for the 307 and 286 kev levels is

$$\frac{J_{307}}{J_{286}} = \frac{3(2I_0 - 1)}{8(I_0 - 1)(2I_0 + 3)} e^{-14.2 \cdot 0.02} \quad (3)$$

and when $I_0 = 7/2$ and $9/2$ it is close to the empirical ratio, 1% : 17%. The best agreement occurs in this case for the second value, corresponding to a spin of $5/2$ for the lower level. The calculated ratio of the intensities for the α groups of the 59-kev and 0 levels is ≈ 1.3; the empirical value is 0.9.

Sliv and Peker[4] computed the effect of the nonsphericity of the nucleus on the transparency coefficient of the nuclear barrier for an α particle with velocity $\beta = v/c$. This effect is introduced into the probability of the α decay by the factor

$$P = \exp\left\{-\frac{8Z}{137\beta} \frac{4}{5} \sqrt{x(1-x)}\, \zeta\right\}, \quad (4)$$

where $x = E_p/V_0$, with E_p being the decay energy and V_0 the maximum height of the potential barrier; ζ is the relative deformation of the nucleus. The calculated ratio of the foregoing intensities agrees with the empirical values at a difference of 0.1 in the relative deformations (elongations) at the 59-kev and 0 level. For the 238-kev and 0 levels, the difference becomes 0.15. Both values are fully acceptible and readily explain the empirically established fact that the rotation constants B for the first and third rotational series (4.5 and 4 kev) coincide approximately with the rotation constant (5 kev) of the second rotational band, considered in reference 2.

[1] Frilley, Rosenblum, Waladares, and Boussier, J. Phys. et radium **16**, 378 (1955).

[2] S. G. Ryzhanov, Атомная энергия (Atomic Energy) **4**, 80 (1958).

[3] K. I. Ter-Martirosyan, Izv. Akad. Nauk SSSR, Ser. Fiz. **20**, 868 (1956), Columbia Tech. Transl. p. 789. Gol'din, Adel'son-Vel'skii, Birzgal, Piliya, and Ter-Martirosyan, J. Exptl. Theoret. Phys. (U.S.S.R.) **35**, 184 (1958), Soviet Phys. JETP **8**, 127 (1959).

[4] L. A. Sliv and L. K. Peker, Dokl. Akad. Nauk SSSR **99**, 727 (1954).

Translated by J. G. Adashko
170

ON THE PROBLEM OF THE COVARIANT DEFINITION OF THE SPIN PSEUDOVECTOR

A. A. SOKOLOV, I. M. TERNOV, and Yu. M. LOSKUTOV

Moscow State University

Submitted to JETP editor October 27, 1958

J. Exptl. Theoret. Phys. (U.S.S.R.) **36**, 930-932 (March, 1958)

As is well known, the spin operator is defined by an antisymmetric tensor of the third rank, i.e., it is a pseudovector: $\sigma_\mu = (\boldsymbol{\sigma}, i\rho_1)$. In previous papers it has been shown[1,2] (cf. also Sections 17-20 in reference 3) that the longitudinal polarization of free Dirac particles can be characterized by the operator $(\boldsymbol{\sigma}\cdot\mathbf{k})/k$. This operator is an integral of the motion with eigenvalue s. We shall try to relate to the quantity s not only the longitudinal polarization, but also the transverse and time components of the spin vector.

The wave function for positive energy and with inclusion of the spin states has the form (cf. references 1-3)

$$\psi = L^{-3/2}\sum_s C_s b_s e^{-i\varepsilon Kt + i\mathbf{k}\cdot\mathbf{r}}. \tag{1}$$

Here

$$b_s = \frac{1}{\sqrt{2}}\begin{vmatrix} sf(K)\cos\theta_s \\ sf(K)\sin\theta_s e^{i\varphi} \\ f(-K)\cos\theta_s \\ f(-K)\sin\theta_s e^{i\varphi} \end{vmatrix}$$

$$f(K) = \sqrt{1 + k_0/K},\quad \theta_s = \theta/2 - (\pi/4)(1 - s),$$
$$K = \sqrt{k^2 + k_0^2},\quad \beta_1 = k/K. \tag{2}$$

The amplitude C_S describes the state with longitudinal spin component $s = \pm 1$, and θ and φ are the spherical angles of the vector $\mathbf{k}$.

The transverse and time components are not integrals of the motion, and therefore they can be characterized only by the average values

$$\zeta_\mu = K\int \psi^+\sigma_\mu\psi d^3x, \tag{3}$$

where the factor $K = k_0(1-\beta_1^2)^{-1/2}$ is introduced in order to preserve for the average values ζ_μ the same relativistic covariance as possessed by the expression $\psi^+\sigma_\mu\psi$.

Let us introduce an auxiliary coordinate system in which the z axis is directed along the momentum $\mathbf{k}$. Then, using the fact that for this system $\theta = \varphi = 0$, we find

$$\zeta_3 = K(C_1^+C_1 - C_{-1}^+C_{-1}) = Ks$$

(longitudinal component); for $C_1 \neq 0$ and $C_{-1} \neq 0$ the quantity $|s|$ will be smaller than unity:

$$\zeta_1 = k_0(C_1^+C_{-1} + C_{-1}^+C_1) = k_0\sqrt{1-s^2}\cos\delta,$$

$$\zeta_2 = ik_0(C_{-1}^+C_1 - C_1^+C_{-1}) = k_0\sqrt{1-s^2}\sin\delta$$

(transverse components); δ is the phase difference between the complex amplitudes C_1 and C_{-1}. Finally, $\zeta_4 = ik(C_1^+C_1 - C_{-1}^+C_{-1}) = iks$ is the time component.*

For an unpolarized beam of electrons $s = 0$ and the phase δ is a rapidly changing quantity, so that on the average $\cos\delta$ and $\sin\delta$ go to zero.

Partial polarization is also possible: for example, $0 < |s| < 1$, and the angle δ is again a rapidly changing quantity. For complete polarization the quantities s and δ are fixed constants. In this case one can make one of the transverse components zero by a rotation around the axis $\mathbf{k}$, and then we shall have $\zeta_3 = Ks$, $\zeta_1 = k_0(1-s^2)^{1/2}$, $\zeta_2 = 0$, and $\zeta_4 = iks$, i.e., the quantity s will determine all the components of the spin vector.

Let us assume that in some coordinate system the momentum vector $k_\mu(\mathbf{k}, iK)$ is parallel to the spin vector, $s = 1$, $\zeta_\mu(Kk/k, ik)$, i.e., the two vectors make the same angle $\theta_k = \theta_S = \theta$ with the z axis. Then in a new coordinate system moving relative to the first with the velocity $c\beta$ directed along the z axis these angles are already different:†

$$\cos\theta'_k = (\beta_1\cos\theta - \beta)/\sqrt{(1-\beta\beta_1\cos\theta)^2 - (1-\beta^2)(1-\beta_1^2)},$$

$$\cos\theta'_s = (\cos\theta - \beta\beta_1)/\sqrt{(\beta_1 - \beta\cos\theta)^2 + (1-\beta^2)(1-\beta_1^2)} \neq \cos\theta'_k,$$

owing to which the quantity s′ is smaller and is given by

$$s' = (\beta_1 - \beta\cos\theta)/\sqrt{(1-\beta\beta_1\cos\theta)^2 - (1-\beta^2)(1-\beta_1^2)} < 1.$$

Here $c\beta_1 = ck/K$ is the speed of the motion of the particle in the original coordinate system.

As is well known, in the decay of a stationary π meson into a μ meson and a neutrino the spin of the μ meson must be directed exactly along the momentum of the μ meson ($s = 1$). But in the laboratory system, relative to which the π meson may be in motion, we have $s' < 1$, and therefore there must be a transverse component of the spin of the μ meson, lying in the plane of the momenta of the π and μ mesons.

We note that for particles with zero rest mass ($k_0 = 0$) the speed is always given by $\beta_1 = 1$. In this case $\theta'_s = \theta'_k$, and therefore the quantity s' is unchanged ($s' = s = 1$). This fact was used by one of us, following the ideas of Lee and Yang, in constructing a theory of the neutrino with oriented spin,[6,7] in which neutrino and antineutrino are characterized by different values of s ($s = 1$ and $s = -1$).

*Analogous expressions for the average value of the spin vector with only positive energies taken into account can be obtained from the work of Tolhoek,[4] and also from that of Alikhanov et al.[5] But the expression for $\sigma_\mu^{\wedge}$ introduced in reference 5 (see note on page 789),

$$\sigma^{\wedge} = (K\rho_3\sigma + \rho_2[\mathbf{k}\times\sigma])\,k_0 = \sigma + i\,\rho_2\mathbf{k}/k_0,$$

$$\sigma_4^{\wedge} = i\rho_2(\sigma\cdot\mathbf{k})\,k_0 = \sigma_4 - \rho_2 K\,k_0$$

will satisfy neither the law of conservation of total angular momentum nor the law of conservation of the longitudinal component of the spin. For $K > 0$ the results agree, since the average value of ρ_1 is zero.

†This is due to the fact that the momentum four-vector is timelike: $k_\mu k_\mu = -k_0^2$, and the spin is spacelike: $\zeta_\mu\zeta_\mu = k_0^2$, with the two vectors orthogonal to each other: $\zeta_\mu k_\mu = 0$.

[1] A. Sokolow, J. Phys. (U.S.S.R.) **9**, 363 (1945).

[2] A. Sokolov and B. Kerimov, Nuovo cimento **5**, 921 (1957).

[3] A. A. Sokolov, Введение в квантовую электродинамику (Introduction to Quantum Electrodynamics), Fizmatgiz, Moscow-Leningrad 1958.

[4] H. A. Tolhoek, Revs. Modern Phys. **28**, 277 (1956).

[5] Alikhanov, Eliseev, Lyubimov, and Érshler, J. Exptl. Theoret. Phys. (U.S.S.R.) **34**, 785 (1958), Soviet Phys. JETP **7**, 541 (1958).

[6] A. A. Sokolov, J. Exptl. Theoret. Phys. (U.S.S.R.) **33**, 794 (1957), Soviet Phys. JETP **6**, 611 (1958).

[7] A. Sokolov and B. Kerimov, Ann. Physik **2**, 46 (1958).

Translated by W. H. Furry
171

RANDOM FREE PRECESSION OF MAGNETIC MOMENTS OF ATOMIC NUCLEI

G. V. SKROTSKIĬ and A. A. KOKIN

Ural' Polytechnical Institute

Submitted to JETP editor October 28, 1958

J. Exptl. Theoret. Phys. (U.S.S.R.) **36**, 932-933 (March, 1959)

THE free precession of magnetic moments of atomic nuclei in an external magnetic field H_0 is usually observed by measuring the voltage and the frequency $\omega_0 = \gamma H_0$ at the terminals of a receiving coil which contains a sample initially magnetized perpendicularly to H_0. In a sufficiently homogeneous field H_0 the phenomenon is observed as long as the signal which decays with the time constant $T_{||}$ exceeds the noise in the system.

After the signal has decayed the voltage at the terminals of the receiver coil is of a fluctuating nature and is determined on the one hand by the thermal noise in the receiver circuit, and on the other hand by the fluctuations in the magnetization of the sample.

The spectral density of the mean square of the voltage across the load resistor R_0 of the receiver circuit due to thermal noise in the receiver system is given by Nyquist's formula, which in the case under consideration is of the form:[1]

$$(V_T^2)_\omega = \frac{\hbar\omega}{2\pi}\coth\frac{\hbar\omega}{2kT}\frac{RR_0^2}{|Z(\omega)|^2}, \qquad (1)$$

where $Z(\omega)$ is the impedance, while R is the effective resistance of the whole receiver circuit. The presence in the receiver coil of a sample containing atomic nuclei with a magnetic moment different from zero and situated in an external field H_0, leads to the appearance of an additional voltage due to the fluctuations of the component of the magnetization of the sample in the direction perpendicular to H_0. The spectral density of the mean square of the component of the magnetization in this direction is given by the expression

$$(M^2)_\omega = (h\chi''/2\pi)\coth(\hbar\omega/2kT), \qquad (2)$$

where

$$\chi'' = \frac{1}{2}\chi_0\left(\frac{\omega T_\perp}{1+(\gamma H_0+\omega)^2T_\perp^2} + \frac{\omega T_\perp}{1+(\gamma H_0-\omega)^2T_\perp^2}\right) \qquad (3)$$

is the imaginary part of the complex nucleus susceptibility, while $T_\perp$ is the transverse relaxation time.

The spectral density of the mean square of the

fluctuations in the corresponding voltage is of the form:

$$(V_M^2)_\omega = 16\pi^2 S^2 N^2 c^{-2}\omega^2 R_0^2 |Z(\omega)|^{-2} (M^2)_\omega, \quad (4)$$

where N is the number of turns, S is the cross section of the coil placed perpendicular to the field H_0.

By utilizing (2) we obtain:

$$(V_M^2)_\omega = 8\pi\chi'' S^2 N^2 \omega^2 c^{-2} \hbar R_0^2 |Z(\omega)|^{-2} \coth(\hbar\omega/2kT). \quad (5)$$

As may be seen from (5) the voltage fluctuations have a resonance character, and as a result of the large value of the relaxation time $T_\perp$ attain a sharp maximum in the field $H_0 = \pm\omega/\gamma$.

If one takes for water $\gamma = 2.8 \times 10^4$ gauss-sec, $\chi_0 = 3.3 \times 10^{-10}$ and $T_\perp = 3$ sec, then the ratio of the spectral densities (5) and (1) for $H_0 = \omega/\gamma$ has the form:

$$\eta = (V_M^2)_{\gamma H_0}/(V_T^2)_{\gamma H_0} = 6.3 \cdot 10^{-8} S^2 N^2 H_0^2/R, \quad (6)$$

where R is the effective resistance of the receiver circuit in ohms. In the case $N = 10^3$ turns, $S = 100$ cm^2 in the earth's magnetic field $H_0 = 0.6$ gauss, $\eta = 220/R$.

Thus, in this case under appropriate conditions one may separate from the spectrum of thermal noise the signal due to the random free precession of magnetic moments of atomic nuclei. The ratio η in the case of resonance is proportional to $(\gamma H_0)^2$. This last consideration may be used as the basis of the theory of self excitation of a spin generator.[2]

[1] L. D. Landau and E. M. Lifshitz, Электродинамика сплошных сред (Electrodynamics of Continuous Media), Gostekhizdat, 1957.

[2] S. S. Kurochkin, Радиотехн. и электрон. (Radio Engineering and Electronics) **2**, 198 (1958).

Translated by G. Volkoff
172

PRODUCTION OF STRANGE PARTICLES IN 3-Bev p-p COLLISIONS

V. S. BARASHENKOV and V. M. MAL' TSEV

Joint Institute for Nuclear Research

Submitted to JETP editor October 27, 1958

J. Exptl. Theoret. Phys. (U.S.S.R.) **36**, 933-934 (March, 1959)

In references 1 — 3, the statistical theory of multiple production of strange particles was considered. In the case of π-N collisions, this theory describes the experiments satisfactorily, if the energy of the colliding particles is sufficiently high.[4,5] Comparison between theoretical calculations and experiments can now also be carried out for p-p collisions.

If we assume that the effective inelastic cross section for 3-Bev p-p collisions is equal to 26 mbn,[6] then the cross section for production of K^+-particles in p-p collisions calculated according to references 1 — 3 is $\sigma^+ = 1.0$ mbn for the variant $V = V_2$ (the K mesons being produced in a volume of radius $r_K = \hbar/m_K c = 0.4 \times 10^{-13}$ cm; all other particles in a volume of radius $r_\pi = \hbar/m_\pi c = 1.4 \times 10^{-13}$ cm), and $\sigma^+ = 0.05$ mbn for the variant $V = V_3$ (all strange particles produced in a volume of radius r_K; all other particles, in a volume of radius r_π). The calculated cross section for production of all strange particles $\sigma_{st} = 1.5$ mbn for $V = V_2$ and $\sigma_{st} = 0.07$ mbn for $V = V_3$.

Baumel et al.[7] obtained the value $\sigma_{exp} = (4.5 \pm 0.9) \times 10^{-32}$ cm^2/sterad-Mev for the cross section for the production of K^+ particles of momentum $1.9\,m_\pi$ ($m_\pi = 140$ Mev) at $\theta = 180°$ (center-of-mass-system) in 3 Bev p-p collisions. In order to integrate the cross section over all momenta, we calculated the momentum distribution of the K mesons produced. Assuming an isotropic angular distribution in the c.m.s., for $V = V_2$, $\sigma^+ = 0.33$ mbn.* An analogous calculation for the variant $V = V_3$ gives nearly the same value. However, this quantity is an order different from the cross section calculated for $V = V_3$ from only the statistical weights without use of σ_{exp} and the momentum distribution. Thus, as in the case of π-N collisions, the variant $V = V_3$ leads to contradictions. For the variant $V = V_2$, the value of σ^+ calculated taking into account the momentum distribution is three times smaller than that calculated only on the basis of statistical weights without employing σ_{exp} and the momentum distribution. This difference can be explained by the fact that at low energies $E \leq 3$ Bev, the energy of the strange particles produced in N-N collisions is near to threshold, and the number of them is not appreciable. Hence, statistical methods can give only

order-of-magnitude values. This consideration is especially important in the calculations of spectra which are very sensitive to assumptions about the form of the matrix element. Thus, one can expect the value $\sigma^+ = 1.0$ mbn following from calculations from statistical weights to be, apparently, closer to experiment than the value $\sigma^+ = 0.33$ mbn obtained by integration of the calculated spectrum.†

In our opinion there are, at present, no reasons to assert that the cross section for production of strange particles in p-p collisions is significantly less than the cross section for production of strange particles in π-N collisions at equivalent energies in the c.m.s. (see references 7 – 9). The very small value of the cross section observed in the work of Cool et al.[9] would appear to result from inadequate statistics.

*In reference 7, $\sigma^+ = 0.2$ mbn was obtained. The difference comes from the fact that we took into account a series of additional factors: the resonance interaction of pions and nucleons in states with angular momentum and isotopic spin $P = T = 3/2$, the difference in statistical weights of the reactions.

†An annalogous situation occurs in π-N collisions for energies equal in the c.m.s. ($E_{lab} \leq 2$ Bev).

[1] Barashenkov, Barbashev, Bubelev, and Maksimenko, Nuclear Phys. **5**, 17 (1957).

[2] Barashenkov, Barbashev, and Bubelev, Nuovo cimento, Suppl. **1**, 7, 177 (1958).

[3] V. S. Barashenkov and V. M. Mal'tsev, Acta Phys. Polon. **17**, 177 (1958).

[4] V. S. Barashenkov, J. Exptl. Theoret. Phys. (U.S.S.R.) **34**, 1016 (1958), Soviet Phys. JETP **7**, 701 (1958).

[5] E. K. Mikhul, J. Exptl. Theoret. Phys. (U.S.S.R.) **35**, 298 (1958), Soviet Phys. JETP **8**, 205 (1959).

[6] Block et al., Phys. Rev. **103**, 1484 (1956); Fowler et al., Phys. Rev. **103**, 1489 (1956).

[7] Baumel, Harris, Orear, and Taylor, Phys. Rev. **108**, 1322 (1957).

[8] Proc. Seventh Rochester Conf. and Proc. Padua-Venice Conf., 1957.

[9] Cool, Morris, Ran, Thorndike, and Whittermore, Preprint (1958).

Translated by G. E. Brown
173

INTERPRETATION OF THE MAXIMUM IN THE TOTAL CROSS SECTION FOR PROTON-PROTON SCATTERING IN THE 1 Bev REGION

V. I. RUS' KIN

Institute of Nuclear Physics, Academy of Sciences, Kazakh S.S.R.

Submitted to JETP editor November 1, 1958

J. Exptl. Theoret. Phys. (U.S.S.R.) **36**, 935 (March, 1959)

In the last few years, several articles[1-4] have employed the resonance interaction between the π meson and nucleon ("isobar") in the 200 Mev region; this follows from the presence of the maximum in the total cross section for scattering of π^+ and π mesons on protons in this energy range.[5]

We shall show that the maximum in proton-proton scattering near 1 Bev can be explained as coming from the excitation of one of the nucleons to an "isobaric" level. For this, we use methods proposed by Takeda.[7] Assuming charge independence for the total proton-proton and proton-neutron cross sections, we have

$$\sigma(pp) = P\left\{\frac{2}{3}\sigma_{1/2} + \frac{1}{3}\sigma_{3/2}\right\},$$
$$\sigma(pn) = P\left\{\frac{5}{6}\sigma_{1/2} + \frac{1}{6}\sigma_{3/2}\right\}, \qquad (1)$$

where $\sigma_{1/2}$ and $\sigma_{3/2}$ are the cross sections for the meson-nucleon resonance systems with isotopic spin $T = 1/2$ and $T = 3/2$; P is the probability of the one-meson state of the π-meson cloud surrounding the nucleon core. According to experiment, in the 1 Bev region, $\sigma(p, p) > \sigma(p, n)$. This inequality can be satisfied if $\sigma_{3/2} > \sigma_{1/2}$. Consequently, the resonance in the meson-nucleon system occurs in the $T = 3/2$ state.

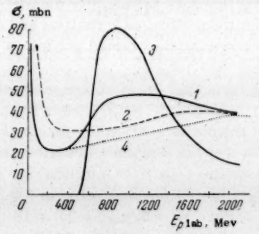

1 – total p – p scattering cross section. 2 – total p – n scattering cross section, according to the experimental data of Chen and Shapiro.[6] 3 – resonance value of $P\sigma_{3/2}$, obtained from Eq. (1). 4 – approximate non-resonance part of $P\sigma_{3/2}$.

From Eq. (1), we can find the experimental value of $P\sigma_{3/2}$. Using Eq. (1) and the Breit-Wigner resonance formula for the meson-nucleon system in the $T = 3/2$ state:

$$P\sigma_{3/2} = 2\pi P\lambda^2 (2J+1) \frac{(\Gamma/2)^2}{(\varepsilon-\varepsilon_0)^2 + (\Gamma/2)^2}, \qquad (2)$$

(where $\lambda = 2.4 \times 10^{-13}$ is the wave length of the π meson in the center-of-mass system, J is the total angular momentum), we obtain $J = 3/2$, $P = 0.1$, $\Gamma = 82$ Mev, $\epsilon_0 = 110$ Mev, in satisfactory agreement with the parameters of the isobar.[5*]

*Some of the difference of ε_0 from the corresponding resonance energy in reference 5 may arise from the fact that we did not consider the velocity of the virtual π mesons in the meson clouds surrounding the nucleon cores.

[1] F. Belinfante, Phys. Rev. **92**, 145 (1953).
[2] D. Peaslee, Phys. Rev. **94**, 1085 (1954).
[3] S. Z. Belen'kiĭ and A. I. Nikishov, J. Exptl. Theoret. Phys. (U.S.S.R.) **28**, 744 (1955), Soviet Phys. JETP **1**, 593 (1955).
[4] S. Lindenbaum and R. Sternheimer, Phys. Rev. **105**, 1874 (1957).
[5] Tamm, Gol'fand and Fainberg, J. Exptl. Theoret. Phys. (U.S.S.R.) **26**, 649 (1954).
[6] Chen, Shapiro and Leavitt, Phys. Rev. **103**, 212 (1956).
[7] G. Takeda, Phys. Rev. **100**, 440 (1955).

Translated by G. E. Brown
174

RANGE-ENERGY DEPENDENCE OF C_{12}, C_{14}, AND O_{16} IONS IN ALUMINUM, COPPER, AND GOLD IN THE ENERGY INTERVAL FROM 50 TO 110 Mev.

Yu. Ts. OGANESYAN

Submitted to JETP editor, November 17, 1958

J. Exptl. Theoret. Phys. (U.S.S.R.) **36**, 936-937 (March, 1959)

FOR detailed study of nuclear reactions caused by multiply-charged ions, data must be obtained on the range-energy dependence of the heavy ions in various substances. For ions with $Z > 3$ it is difficult to obtain the range-energy curves by calculation, since the multiple charge exchange of such ions during the slowing down process introduces a substantial indeterminacy into the quantities that enter into the equations.[1]

We have consequently set up experiments on the direct experimental determination of these relationships for ions of carbon, nitrogen, and oxygen in aluminum, copper, and gold.

The ions C_{12}^{+4}, N_{14}^{+5}, O_{16}^{+5}, and O_{16}^{+6} were accelerated in a 150-cm cyclotron with an exit system having a focusing magnet, intended for the production of a narrow beam of deuterons in a specially shielded cabin 12 meters away from the center of the cyclotron. Experience has shown that it is possible, without substantial changes, to use the same exit system to obtain in the cabin a sufficiently intense beam of ions of carbon, nitrogen, and oxygen. This is apparently due to the fact that part of the ion beam passes, as a result of scattering, through the exit channel in the field of the focusing magnet, which focuses the ions on the entrance diaphragm of the receiver of the recording apparatus. This mechanism for obtaining a working beam has insured an intensity on the order of $10^5 - 10^6$ ions/cm^2-sec at the receiver, with the current at the terminal radius of the cyclotron being on the order of 0.1 microamperes.

The ions were registered by a photomultiplier with a ZnS crystal, deposited in the form of a thin layer on glass, so as to insure a sufficient sensitivity of measurements in an ion beam on the order of $10^2 - 10^6$ ions/cm^2-sec. With the beam thus extracted from the cyclotron, the ions entering the field of focusing magnet had an energy spectrum (50 – 110 Mev). Narrow beams of practically-monoenergetic ions were gathered from this spectrum by a suitable choice of the intensity of the focusing magnetic field. A focusing magnet could be used as an analyzer because the experimentally-obtained relationship between the magnetizing current and the induction of the magnetic field in the gap was linear over the entire range of the field employed. The analyzer was calibrated with a beam of accelerated deuterons, whose energy was determined from the known range-energy curve in aluminum.[2]

The ions accelerated in the cyclotron passed through a specially installed two-micron aluminum foil on their path to the focusing magnet, and acquired in this foil an equilibrium charge corresponding to their velocity. The ions were then deflected in the magnetic field, entered the recorder in front of which foils of various thickness of aluminum, copper, and gold were mounted on a rotating disk. Thus, the ion energy was determined from the current in the windings in the magnetic analyzer, while the ranges of ions at a given energy in the selected substance were determined from the decrease in intensity with in-

creasing absorber thickness. Since it is much easier to vary smoothly the ion energy than the thickness of the absorber, the actual measurements were performed as follows: the energy of the ions, whose intensity was decreased to one half the initial value by passage through a given absorber, was determined for each foil by varying the magnetic field of the analyzer. Each such operation yielded one point on the range-energy curve. To exclude errors due to uncontrollable variations in the intensity of the initial beam, a proportional counter, placed in tandem with the entrance diaphragm, was used as a monitor.

It is obvious that with the measurement method described, the sensitivity threshold of the registrator can introduce a substantial error in the range. This method was therefore used, in special experiments, to measure the range in nickel of doubly-charged oxygen ions with energies 9.7 Mev, for which data obtained by other registration methods are available. The agreement between our data and those found in the literature,[3-6] indicates that the sensitivity threshold of the system comprising the ZnS and the photomultiplier is so low, that it can increase substantially the error in the determination of the range-energy curve, an error due to the finite resolving power of the analyzer magnet, to inaccuracy of the determination of the thickness of the absorber, etc. By our estimate, the total error in the determination of the values of the range does not exceed 2%.

The results of the measurements of the mean ranges of the ions of carbon, nitrogen, and oxygen in aluminum are shown in the figure. Data on ranges in copper and gold are given in the table.

Our data are in good agreement with the semi-empirical calculation curves made by Papineau (private communication), and lie somewhat lower than the experimental curves for the ranges of nitrogen and oxygen ions in photoemulsions in the energy interval from 0 to 130 Mev, obtained in our laboratory.[7] This discrepancy was apparently due to inaccurate calibration of the magnetic analyzer in the investigation of reference 7.

The author is grateful to Professor G. N. Flerov for valuable remarks and to D. M. Parfanovich for daily help in the performance of the experiment and in the analysis of the results of this work.

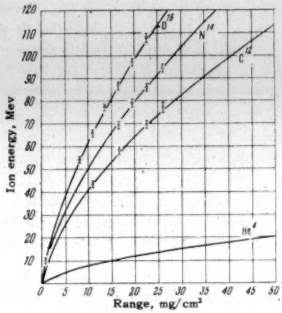

Range vs. energy for C^{12}, N^{14}, and O^{16} in aluminum. Solid line – Papineau's calculations. Points – data of present work.

Substance	Ion	Range, mg/cm²	Energy, Mev
Copper	C^{12}	18.9	52.0
		27.1	66.0
		32.0	69.5
	O^{16}	18.8	75.2
		27.1	96.5
Gold	C^{12}	22.3	36.0
		30.0	50.5
		37.6	56.0
		47.2	66.5
	O^{16}	30.0	73.0
		37.6	85.0
		40.2	90.3

[1] Brunings, Knipp, and Teller, Phys. Rev. **60**, 675 (1941).

[2] Bichsel, Morley, and Aron, Phys. Rev. **105**, 1788 (1957).

[3] Reynolds, Scott, and Zucker, Phys. Rev. **95**, 671 (1954).

[4] Teplova, Nikolaev, Dmitriev, and Fateeva, J. Exptl. Theoret. Phys. (U.S.S.R.) **34**, 559 (1958), Soviet Phys. JETP **7**, 387 (1958).

[5] W. H. Barkas, Phys. Rev. **89**, 1019 (1953).

[6] Teplova, Nikolaev, Dmitriev, and Fateeva, J. Exptl. Theoret. Phys. (U.S.S.R.) **32**, 974 (1957), Soviet Phys. JETP **5**, 797 (1957).

[7] Parfanovich, Semchinova, and Flerov, J. Exptl. Theoret. Phys. (U.S.S.R.) **33**, 343 (1957), Soviet Phys. JETP **6**, 266 (1958).

Translated by J. G. Adashko
175

SOME SYMMETRY PROPERTIES IN PROCESSES OF ANTIHYPERON PRODUCTION WITH ANNIHILATION OF ANTINUCLEONS

CHOU KUANG-CHAO

Joint Institute for Nuclear Studies

Submitted to JETP editor November 20, 1958

J. Exptl. Theoret. Phys. (U.S.S.R.) **36**, 938-939 (March, 1959)

LET us consider the reaction

$$\tilde{p} + p \to \tilde{\Sigma}^- + \Sigma^+. \qquad (1)$$

We denote the amplitude for it by $f(\mathbf{p_i}, \mathbf{p_f}, \sigma_p, \sigma_a)$, where $\mathbf{p_i}$ and $\mathbf{p_f}$ are the relative momenta in the initial and final states, and σ_p and σ_a are the Pauli matrices of the particles and antiparticles. From invariance with respect to charge conjugation it follows that

$$f(\mathbf{p}_i, \mathbf{p}_f, \sigma_p, \sigma_a) = f(-\mathbf{p}_i, -\mathbf{p}_f, \sigma_a, \sigma_p). \qquad (2)$$

If the initial state is unpolarized, then it is not hard to prove by Eq. (2) that the polarization vectors of the hyperon (P_Σ) and of the antihyperon ($P_{\tilde{\Sigma}}$) in the final states are given by

$$\mathbf{P}_\Sigma = \mathbf{P}_{\tilde{\Sigma}} = A[\mathbf{p}_i\mathbf{p}_f]/|[\mathbf{p}_i\mathbf{p}_f]|, \qquad (3)$$

where A is a function of the scalar $(\mathbf{p_i} \cdot \mathbf{p_f})$.

Measurement of the angular asymmetries in the decay of the Σ^- and $\tilde{\Sigma}^-$ produced in the reaction (1) gives the ratio

$$\mathbf{P}_\Sigma \alpha_\Sigma / \mathbf{P}_{\tilde{\Sigma}} \alpha_{\tilde{\Sigma}} = \alpha_\Sigma / \alpha_{\tilde{\Sigma}}, \qquad (4)$$

where α_Σ and $\alpha_{\tilde{\Sigma}}$ are the antisymmetry coefficients of the decays. As has been shown in reference 1, measurement of the ratio $\alpha_\Sigma / \alpha_{\tilde{\Sigma}}$ is of great significance for testing the conservation laws associated with time reversal T and charge conjugation C; this ratio differs from unity only if T and C are not conserved in the decay.

Let us go on to the consideration of the two cases

$$\tilde{p} + p\,(\tilde{n} + n) \to Y_1 + \tilde{Y}_2 + m\pi^+ + n\pi^- + l\pi^0 \qquad (5)$$

$$\to \tilde{Y}_1 + Y_2 + n\pi^+ + m\pi^- + l\pi^0. \qquad (6)$$

The amplitudes for the reactions (5) and (6) are expressed in the form

$$f_1(\mathbf{p}_i, \mathbf{p}_f, \mathbf{p}_\alpha^+, \mathbf{p}_\beta^-, \mathbf{p}_\gamma^0, \sigma_p, \sigma_a), \quad \alpha = 1, 2, \ldots m, \quad \beta = 1, \ldots n,$$

$$f_2(\mathbf{p}_i, \mathbf{p}_f, \mathbf{p}_\beta^+, \mathbf{p}_\alpha^-, \mathbf{p}_\gamma^0, \sigma_p, \sigma_a), \quad \gamma = 1, \ldots l, \qquad (7)$$

where $\mathbf{p}^{\pm,0}$ are the momenta of $\pi^{\pm,0}$ mesons. From invariance with respect to C it follows that

$$f_2(\mathbf{p}_i, \mathbf{p}_f, \mathbf{p}_\beta^+, \mathbf{p}_\alpha^-, \mathbf{p}_\gamma^0, \sigma_p, \sigma_a) = f_1(-\mathbf{p}_i, -\mathbf{p}_f, \mathbf{p}_\alpha^-, \mathbf{p}_\beta^+, \mathbf{p}_\gamma^0, \sigma_a, \sigma_p). \qquad (8)$$

Using the relation (8), we get not only equality of the total cross-sections and the angular distributions of these two processes (σ_1 and σ_2), but also equality of the polarization vectors of the hyperons and antihyperons in the final state (P_Y and $P_{\tilde{Y}}$). When the initial state is unpolarized we have

$$\sigma_1(\mathbf{p}_i, \mathbf{p}_f, \mathbf{p}_\alpha^+, \mathbf{p}_\beta^-, \mathbf{p}_\gamma^0) = \sigma_2(-\mathbf{p}_i, -\mathbf{p}_f, \mathbf{p}_\beta^-, \mathbf{p}_\alpha^+, \mathbf{p}_\gamma^0),$$

$$\mathbf{P}_{Y_1}(\mathbf{p}_i, \mathbf{p}_f, \mathbf{p}_\alpha^+, \mathbf{p}_\beta^-, \mathbf{p}_\gamma^0) = \mathbf{P}_{\tilde{Y}_1}(-\mathbf{p}_i, -\mathbf{p}_f, \mathbf{p}_\beta^-, \mathbf{p}_\alpha^+, \mathbf{p}_\gamma^0),$$

$$\mathbf{P}_{\tilde{Y}_2}(\mathbf{p}_i, \mathbf{p}_f, \mathbf{p}_\alpha^+, \mathbf{p}_\beta^-, \mathbf{p}_\gamma^0) = \mathbf{P}_{Y_2}(-\mathbf{p}_i, -\mathbf{p}_f, \mathbf{p}_\beta^-, \mathbf{p}_\alpha^+, \mathbf{p}_\gamma^0). \qquad (9)$$

Analogous relations exist also for reactions in which K mesons and nucleons are produced.

There are also a number of selection rules for reactions of the types

$$\tilde{n} + p\,(\tilde{p} + n) \to Y_1 + \tilde{Y}_2 + m\pi^+ + n\pi^- + l\pi^0$$

$$\to \tilde{Y}_1' + Y_2' + m\pi^+ + n\pi^- + l\pi^0, \qquad (10)$$

where $\tilde{Y}_1'$ and Y_2' are obtained from Y_1 and $\tilde{Y}_2$ by means of the operator G, which is the product of the charge-conjugation operator and a rotation through the angle π around the x axis of the isobaric space.[2] For example

$$\tilde{\Sigma}^- = G\Sigma^+, \quad \tilde{\Sigma}^0 = G\Sigma^0, \quad \tilde{\Sigma}^+ = G\Sigma^-,$$

$$\tilde{\Lambda}^0 = G\Lambda^0, \quad \tilde{n} = Gp, \quad \pi^{\pm,0} = G\pi^{\pm,0}$$

and so on. We denote the respective amplitudes of the reactions (10) by

$f_1(\mathbf{p}_i, \mathbf{p}_f, \mathbf{p}_\alpha^+, \mathbf{p}_\beta^-, \mathbf{p}_\gamma^0, \sigma_p, \sigma_a)$ and $f_2(\mathbf{p}_i, \mathbf{p}_f, \mathbf{p}_\alpha^+, \mathbf{p}_\beta^-, \mathbf{p}_\gamma^0, \sigma_p, \sigma_a)$.

From invariance with respect to G it follows that

$$f_1(\mathbf{p}_i, \mathbf{p}_f, \mathbf{p}_\alpha^+, \mathbf{p}_\beta^-, \mathbf{p}_\gamma^0, \sigma_p, \sigma_a) = \eta f_2(-\mathbf{p}_i, -\mathbf{p}_f, \mathbf{p}_\alpha^+, \mathbf{p}_\beta^-, \mathbf{p}_\gamma^0, \sigma_a, \sigma_p), \qquad (11)$$

where $\eta = \pm 1$ is a phase factor.

It is easy to show from Eq. (11) that for an unpolarized initial state

$$\sigma_1(\mathbf{p}_i, \mathbf{p}_f, \mathbf{p}_\alpha^+, \mathbf{p}_\beta^-, \mathbf{p}_\gamma^0) = \sigma_2(-\mathbf{p}_i, -\mathbf{p}_f, \mathbf{p}_\alpha^+, \mathbf{p}_\beta^-, \mathbf{p}_\gamma^0),$$

$$\mathbf{P}_{Y_1}(\mathbf{p}_i, \mathbf{p}_f, \mathbf{p}_\alpha^+, \mathbf{p}_\beta^-, \mathbf{p}_\gamma^0) = \mathbf{P}_{\tilde{Y}_1'}(-\mathbf{p}_i, -\mathbf{p}_f, \mathbf{p}_\alpha^+, \mathbf{p}_\beta^-, \mathbf{p}_\gamma^0),$$

$$\mathbf{P}_{\tilde{Y}_2}(\mathbf{p}_i, \mathbf{p}_f, \mathbf{p}_\alpha^+, \mathbf{p}_\beta^-, \mathbf{p}_\gamma^0) = \mathbf{P}_{Y_2'}(-\mathbf{p}_i, -\mathbf{p}_f, \mathbf{p}_\alpha^+, \mathbf{p}_\beta^-, \mathbf{p}_\gamma^0). \qquad (12)$$

[1] Chou Kuang-Chao, Nuclear Phys. (in press).

[2] T. D. Lee and C. N. Yang, Nuovo cimento **3**, 749 (1956).

Translated by W. H. Furry
176

THE GAMMA RAYS OF As^{74}

Yu. E. LOGINOV and K. I. YAKOVLEV

Radium Institute, Academy of Sciences, U.S.S.R.

Submitted to JETP editor November 21, 1958

J. Exptl. Theoret. Phys. (U.S.S.R.) **36**, 940 (March, 1959)

WE have studied the γ-ray spectrum of As^{74} by means of a single-channel scintillation γ-ray spectrometer, using a NaI(Ta) crystal with a type FEU-S photomultiplier. The efficiency curve of the γ-ray spectrometer was obtained by taking measurements with it on standards giving known numbers of disintegrations.

The energies and relative intensities of the lines observed in the γ-ray spectrum are given below,

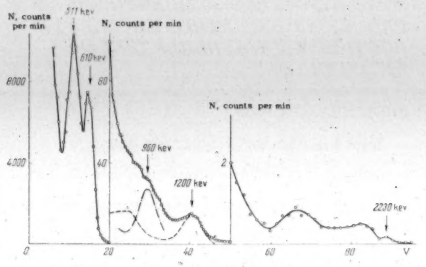

Gamma-ray spectrum of As^{74}, taken with a scintillation γ-ray spectrometer. The dashed curves show the resolution of a section of the spectrum into components.

together with the results of the latest two papers on this spectrum:

Present work		Grigor'ev et al.[1]		Horen and Wells[2]
$h\nu$, kev	Relative intensity	$h\nu$, kev	Relative intensity	$h\nu$, kev
610±30	1	635	1	—
960±50	0.015±0.008	—	—	—
1200±30	0.023±0.008	1190	0.018±0.005	1190±10
—	—	—	—	1600±40
2230±70	$\sim 10^{-4}$	>1190	<0.004	2220±20

The work of Grigor'ev et al.[1] was done earlier than ours; we received the brief communication of Horen and Wells after the completion of our measurements.

The existence of γ-ray lines of energies of 1190 and 2220 kev can evidently be regarded as established; the other two lines, at 960 and 1600 kev, still need further investigation.

[1] Grigor'ev, Dzhelepov, Zolotavin, Mishin, Prikhodtseva, Khol'nov, and Shchukin, Izv. AN SSSR, Ser. Fiz. 22, 831 (1958), Columbia Tech. Transl. in press.

[2] D. J. Horen and D. O. Wells, Bull. Am. Phys. Soc., Ser. II, **3**, 315 (1958).

Translated by W. H. Furry
177

ULTRASONIC ATTENUATION IN METALS

G. L. KOTKIN

Moscow State University

Submitted to JETP editor November 22, 1958

J. Exptl. Theoret. Phys. (U.S.S.R.) **36**, 941-942 (March, 1959)

THE attenuation of ultrasonic waves in metals at low temperatures is determined by the electron-phonon interaction. The absorption coefficient, γ, has been calculated by Pippard,[1] and Steinberg[2] has examined the corresponding change in the velocity of sound. Bömmel[3] measured the attenuation in the presence of an external magnetic field and found that γ did not vary monotonically with H. This effect was explained by Pippard[4] as a type of cyclotron resonance. Steinberg[5] carried out the calculation for transverse waves in a longitudinal magnetic field and concluded that resonance absorption does not occur in this case. Here we examine the attenuation of transverse waves in metals in a transverse magnetic field.

We regard the motion of the atoms of the lattice as given and consider the electrons to be free. We are interested in the case when $l \gtrsim \lambda$, $R \sim \lambda$. Here λ is the wavelength of the sound waves and l is their mean free path. $R = mvc/eH$, is the

radius of the electron orbits. It turns out that the equilibrium electron distribution is the same as the distribution, f_0, in the absence of the sound waves. The electron distribution $f = f_0 - \chi(\partial f_0/\partial\epsilon)$ and the electric field **E** are determined by the kinetic equations

$$(1/\tau + i\omega - ikv\sin\theta\sin\varphi)\chi - (v/R)\partial\chi/\partial\varphi - \overline{\chi}/\tau - ev(E_x\sin\theta\cos\varphi + E_y\sin\theta\sin\varphi + E_z\cos\theta) = 0 \quad (1)$$

and the electromagnetic field equations

$$E_x = (4\pi is^2/\omega c^2)j_x,$$

$$E_z = (4\pi is^2/\omega c^2)j_z, \quad E_y = (4\pi is/\omega)\rho. \quad (2)$$

where

$$\rho = (3Ne/mv^2)\overline{\chi}, \quad \overline{\chi} = \int \chi d\Omega/4\pi, \quad (3)$$

$$j_x = (3Ne/4\pi mv)\int \chi\sin\theta\cos\varphi d\Omega - Neu_x, \quad (4)$$

$$j_z = (3Ne/4\pi mv)\int \chi\sin\theta\sin\varphi d\Omega - Neu_z, \quad (5)$$

s is the velocity of sound, **u** the velocity of the atoms in the lattice, N the number of atoms (and electrons) per cm^3. The field **H** is directed along the z axis and the wave vector **k** is along the y axis. A solution of Eq. (1) is

$$\chi = -\frac{eR\exp(2\pi R/l')}{\exp(2\pi R/l')-1}\exp(ikR\sin\theta\cos\varphi) \times\int_0^{2\pi} d\psi\,[E_x\sin\theta\cos(\varphi+\psi) + E_y\sin\theta\sin(\varphi+\psi) + E_z\cos\theta + \overline{\chi}/el] \times\exp[-R\psi/l' - ikR\sin\theta\cos(\varphi+\psi)], \quad (6)$$

where $l' = v\tau/(1+i\omega\tau)$. Making use of (2) and (3) we find $\overline{\chi}/el \ll E_y$. The discussion below will be confined to the case when $l \gg R$.

We consider waves polarized parallel to the field H ($u_x = 0$). From (5) and (6) we obtain

$$j_z = A\sigma E_z - Neu, \quad (7)$$

where

$$\sigma = Ne^2\tau/m,$$

$$A(z) = 6z^{-1}\left[(1+z^{-2})\int_0^z J_0(t)\,dt - J_1(z) - z^{-1}J_0(z)\right],$$

$$z = 2kR. \quad (8)$$

Substituting in (2) we obtain

$$E_z = mu/e\tau(A+iB), \quad (9)$$

where $B = \omega c^2/4\pi s^2\sigma$. Calculation shows that $B \ll A$ for $\omega < 10^8\ sec^{-1}$.

In one second the lattice loses an amount of energy

$$\dot{Q} = {}^1/_2\,\mathrm{Re}(Neu\,E_z), \quad (10)$$

and the absorption coefficient is

$$\gamma = 2\dot{Q}/NMu^2s = m/Ms\tau A, \quad (11)$$

where M is the atomic mass.

If the sound waves are polarized perpendicular to the field ($u_z = 0$), then in this expression A_1 must be substituted for A, where

$$A_1(z) = {}^3/_2 z^{-1}\left[(1+3z^{-2})\int_0^z J_0(t)\,dt - 3J_1(z) - 3z^{-1}J_0(z)\right]. \quad (12)$$

From Eqs. (8), (11), and (12) it follows that $\gamma(H)$ has a succession of maxima. Their position is not, however, determined by the simple conditions indicated by Pippard[4] and Steinberg.[5]

In conclusion I would like to thank V. P. Silin, under whose direction this work was carried out.

[1] A. B. Pippard, Phil. Mag. **46**, 1104 (1955).
[2] M. S. Steinberg, Phys. Rev. **111**, 425 (1958).
[3] H. E. Bömmel, Phys. Rev. **100**, 758 (1955).
[4] A. B. Pippard, Phil. Mag. **2**, 1147 (1957).
[5] M. S. Steinberg, Phys. Rev. **110**, 772 (1958).
[6] M. S. Steinberg, Phys. Rev. 110, 1467 (1958).

Translated by R. Berman
178

FREE ENERGY OF STRONG ELECTROLYTES

A. A. VEDENOV

Moscow State University

Submitted to JETP editor November 25, 1958

J. Exptl. Theoret. Phys. (U.S.S.R.) **36**, 942-943 (March, 1959)

THE diagram technique, developed by the author[1] to calculate the paired correlation function in classical statistical physics, was used to determine the free energy of a strong electrolyte, i.e., of a system of charged particles which is neutral as a whole, in which the interaction potential of the particles $V(x)$ behaves arbitrarily at small distances (and corresponds to a repulsion of particles) and goes at large distances into the pure Coulomb potential $Z_1Z_2e'^2/r$ (where $e' = e/\sqrt{\epsilon}$) for particles with charges Z_1 and Z_2 in a medium with dielectric constant ϵ.

The calculation is carried out under the assumption that the radius of the short-distance repulsion forces r_0 and the averaged scattering amplitude e'^2/T in the Coulomb field e'^2/r are considerably smaller than the average distance between particles $\bar{r} = \nu^{-1/3}$. These conditions signify that the system is close to ideal, i.e., the correction to the free energy, due to the interaction, are small compared with the free energy of the ideal gas. It was also assumed that the probability of molecule formation is small and the contribution of molecules to the free energy of the system can be neglected. The electrolyte was assumed to consist of two types of particles with charges Z_1 and Z_2.

The expression used for the paired correlation function was that given in reference 1 (correct for distances $|\mathbf{x}| \gg e^2T$), and was "joined," at distances much smaller than the Debye radius, with the expression $\exp\{-\beta V(\mathbf{x})\}$ for the correlation function at small distances.

With all the foregoing conditions satisfied, the free energy of a strong electrolyte is an expansion in the particle density ν, given, with accuracy to terms up to the second power in ν inclusive, by the following formula (for the free energy per unit volume):

$$F = F_0 - \frac{T\varkappa^3}{12\pi}$$
$$+ \lim_{R\to\infty}\left\{-2\pi T\int_0^R r^2 dr \sum_{\alpha\beta}\nu_\alpha\nu_\beta\left(e^{-\beta V_{\alpha\beta}(r)}-1\right) + \frac{T\varkappa^4}{16\pi}R\right.$$
$$\left. - \frac{\pi}{3}\beta^2 e'^6\left(\sum\nu Z^3\right)^2\ln\varkappa R\right\} + \pi\beta^2 e'^6\left[\left(\sum\nu Z^3\right)^2\frac{1}{3}\left(C-\ln 3\right)\right.$$
$$\left. - \sum\nu Z^2\sum\nu Z^4\right], \quad \varkappa = \sqrt{4\pi\beta e'^2\sum_\alpha\nu_\alpha Z_\alpha^2}. \qquad (1)$$

Here F_0 is the free energy of an ideal gas, κ is the reciprocal of the Debye radius, ν_α and Z_α are the density and charge of particles of type α, $\beta = 1/T$ is the reciprocal of the temperature, and C is Euler's constant. The summation in (1) is by particle type.

We note that the expression obtained in reference 2 for the free energy F for the case of charged ideally-hard spheres is incorrect, since the expression used there for the paired correlation function is inaccurate, and, furthermore, the limit for the case of ideally hard spheres was approached incorrectly, and as a result the contribution of the non-electric (i.e., repulsive short-range) forces to the free energy was lost.

I thank Academician L. D. Landau for valuable comments, made during an examination of the results.

[1] A. A. Vedenov, Dokl. Akad. Nauk SSSR, in press.

[2] V. V. Tolmachev and S. V. Tyablikov, Dokl. Akad. Naul SSSR **119**, 314 (1958). Научные доклады высшей школы (Scientific Reports of the Higher Schools) **1**, 101 (1958).

Translated by J. G. Adashko
179

ON THE POSSIBLE MULTIPLE PRODUCTION OF MUONS

I. L. ROZENTAL'

P. N. Lebedev Physics Institute, Academy of Sciences, U. S.S.R.

Submitted to JETP editor November 26, 1958

J. Exptl. Theoret. Phys. (U.S.S.R.) **36**, 943-945 (March, 1959)

In a study of the curve of the spreading of shower μ mesons of very high energy ($\sim 10^{12}$ ev) Barrett and others[1] observed a remarkable break in the curve at small distances ($\sim 1-2$ m) between the counter systems used for the measurements. This break was at once interpreted as an indication of two different processes. In the opinion of the authors of the paper in question multiple production of μ mesons from the decay of π mesons is responsible for the coincidences at large distances ($> 1-2$ m), whereas the sharp rise in the number of coincidences at small distances is due to local showers in the earth (the thickness of earth in these experiments was 1600 m water equivalent). The latter conclusion was based on the following chain of argument: the production of μ mesons in the air should occur at distances of about a nuclear range from the boundary of the atmosphere, which means a height of about 10 km. Consequently, the angle of divergence of the particles responsible for the rise of the spreading curve is $\sim 10^{-4}$ rad. If we assume that when a primary particle makes a collision the secondaries are distributed isotropically in the center-of-mass system, such values of the angle correspond to primary particle energies of the order of 10^{17} ev, which considerably exceeds the observed value of the energy of the showers accompanying the μ mesons ($\sim 3\times 10^{15}$ ev). Therefore the authors of reference 1 reject the "air hypothesis" of the origin of the break. In the light of the latest data such an argument does not seem convincing, since it has now been established (see, e.g., reference 2) that the angular distribution in the center-of-mass system is aniso-

tropic, and the angle of 10^{-4} rad corresponds to an energy $\sim 10^{14} - 10^{15}$ ev. Therefore additional analysis is needed to settle the question of the origin of the break in the curve.

Possible causes of local showers at great depths are: (1) pairs of μ mesons produced by photons; (2) μ mesons arising from the decay of π mesons produced by nuclear interactions in the ground; (3) secondary particles accompanying high-energy π mesons. The first process is of negligible importance because of the fact that the probability for the production of an electron pair is much larger (by a factor of about 40,000) than that for the production of a pair of μ mesons. The second process must be rejected, since for a π meson of energy $\sim 10^{12}$ ev the probability of interaction is larger than that of disintegration by a factor 10^5.

Let us examine the third process in more detail. μ mesons can produce: (a) δ showers or radiative showers, (b) electron-nuclear showers, (c) μ-meson pairs. The phenomena involving electrons can be of no importance, since the apparatus used in the work[1] was screened by about 10 cm of lead. To estimate the second effect we assume that the cross-section for production of electron-nuclear showers by μ mesons is $\sim 10^{-29}$ cm^2 per nucleon.[3] Assuming that the range of nuclear-active particles in the ground is ~ 1 m, we easily find that only one out of 1000 μ mesons will be accompanied by a shower. This ratio is already smaller than the experimental value by about an order of magnitude; actually, because of the narrow angular distribution of the secondary particles[3] the effective value must be still smaller.

Although an estimate of the direct production of μ-meson pairs by μ mesons gives a value of the ratio in agreement with experiment (one shower per hundred particles), nevertheless there is a difficulty in explaining the increase of the coincidences at small distances by means of this process. In fact, in passing through earth to a depth of 1600 m water equivalent μ mesons are scattered in transverse directions to distances of about 1 m.[4] Two particles fell on a detector of area ~ 0.5 m^2.* Assuming for our estimate that the μ mesons are uniformly distributed over a circle of radius 2 m, we readily see that the total number of μ mesons falling on this circle is ~ 10. Such a large number cannot be explained by the direct production of μ-meson pairs.

Assuming that the increase at small distances is caused by "air" μ mesons, we can estimate the possibility of their production in the decay of π mesons. We adopt a plausible model,[5] according to which in an individual nuclear interaction one-third of the energy of the interacting particles goes into π mesons, and assume that the μ mesons are uniformly distributed over a circle of radius 10 m (the experimental data[1] indicate this). Then the calculated number of μ mesons in a circle of radius ~ 2 m is smaller than that observed by a factor 50.

Attention has been called to the discrepancy between the calculated and observed values of the density of μ mesons in the columns of broad showers by Hayakawa[6] in connection with experiments by Japanese physicists.[7] To explain it he suggested that the high-energy primary component consists of heavy nuclei, which cause a high multiplicity of π mesons from collisions (the multiplicity increasing in proportion to the atomic weight A). But a comparison made by Zhdanov of the multiplicities of showers produced by α particles and nucleons in photographic emulsions led to the conclusion that the multiplicity increases much more slowly (approximately as $A^{1/5}$). Therefore it is hard to believe that Hayakawa's hypothesis could be correct. Accordingly we must suppose that there is an additional source of μ mesons, and in particular that direct multiple production of μ mesons can occur.†

It must be noted that this conclusion is only of a preliminary nature, since the estimates made here are based on not very precise data (in particular on the energy distributions). For a final decision we need more exact studies of high-energy μ-meson showers and the accompanying electrons.

The writer expresses his gratitude to N. A. Dobrotin for a number of valuable comments.

*A comparison of the frequency of passage of pairs of particles through the apparatus used in reference 1 with the expected frequency of passage of the axes of broad showers of energy $\sim 3 \times 10^{15}$ ev shows that the probability is close to unity that such pairs of particles accompany the showers.

†Some justification of such an assumption can be found in arguments based on extrapolation of the theory of weak interactions to very small distances.[8,9]

[1] Barrett, Bollinger, Cocconi, Eisenberg, and Greisen, Revs. Modern Phys. **24**, 133 (1952).

[2] I. L. Rozental' and D. S. Chernavskiĭ, Usp. Fiz. Nauk **52**, 185 (1954).

[3] D. Kessler and R. Maze, Nuovo cimento **5**, 1540 (1957).

[4] S. Z. Belen'kiĭ, Лавинные процессы в космических лучах (Cascade Processes in Cosmic Rays), p. 187, Gostekhizdat, 1948.

[5] Vernov, Grigorov, Zatsepin, and Chudakov, Izv. Akad. Nauk SSSR, Ser. Fiz. **19**, 493 (1955), Columbia Tech. Transl. p. 445.

[6] S. Hayakawa, Nuovo cimento **5**, 608 (1957).
[7] Higashi, Oshio, Shibata, Watanabe, and Watase, Nuovo cimento **5**, 597 (1957).
[8] W. Heisenberg, Z. Physik **101**, 533 (1956).
[9] D. I. Blokhintsev, Usp. Fiz. Nauk **62**, 381 (1957).

Translated by W. H. Furry
180

ON THE MAGNITUDE OF THE RATIO σ^-/σ^+ NEAR THE THRESHOLD OF MESON PHOTOPRODUCTION

S. P. KHARLAMOV, M. I. ADAMOVICH, and V. G. LARIONOVA

P. N. Lebedev Physics Institute, Academy of Sciences, U.S.S.R.

Submitted to JETP editor November 26, 1958

J. Exptl. Theoret. Phys. (U.S.S.R.) **36**, 945-947 (March, 1959)

THE magnitude of the ratio of the yields of positive to negative photo mesons from deuterium $\eta = N_d^-/N_d^+$ can differ appreciably from the ratio σ^-/σ^+ for the photoproduction of π mesons from free nucleons. As we have shown earlier[1] this can be due to a difference in the final state interaction of the particles after photoproduction of a π^- or a π^+ meson on deuterium. Furthermore one has to keep in mind that the difference of the thresholds for π^- and π^+ production on deuterium can have a strong influence on the quantity η if one measures it utilizing photons close to the high energy limit of the bremsstrahlung spectrum.

In the present note the ratio σ^-/σ^+ is deduced from experimental values of η taking into account the above mentioned effects. The experimental results are given in the Table. The ratio of the π^- to π^+ yields on deuterium were measured at an angle of 73° with respect to the photon beam with bremsstrahlung of maximum energy $\nu_m = 300$ Mev[2] and at angle of 60° with bremsstrahlung of $\nu_m = 165$ Mev[3] (first row). In the second row the deduced values for the ratio σ^-/σ^+ are given. They were obtained from the experimental data by applying corrections for the Coulomb interaction of the π^- meson with the protons and of the protons with themselves, and by applying corrections to take into account that π^- and π^+ mesons of the same energy have been produced by photons of different energy.

The Coulomb corrections have been computed on the basis of Baldin's calculations[4] concerning our earlier experiments[1] on the distribution of the relative momenta, p, of the protons, and of the recoil momenta, q, in the reaction $\gamma + d \to \pi^- + p + p$ for the photon energies given in the table.

We now shall discuss in greater detail the corrections which have to be applied to account for the difference in the threshold energies for π^- and π^+ photoproduction considering the strong energy dependence of the bremsstrahlung spectrum near the upper energy tip. We will do so for the case $\nu_m = 165$ Mev.* Figure 1 shows the experimental momentum distribution of the π^- mesons from

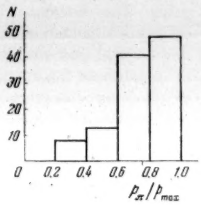

FIG. 1

the reaction $\gamma + d \to \pi^- + p + p$ for photon energies 155 — 165 Mev. It has been obtained by our method described in reference 1. On the abscissa we have plotted the ratio of the meson momentum p_π to the maximum possible meson momentum p_{max} (given by the meson emission angle θ and the photon energy). The curves in Fig. 2 show the yields $N_d^\mp(\nu)$ of π^- and π^+ mesons of energies between 6.7 and 11.7 Mev emitted at an angle of 60° with respect to the photon direction as a function of the photon energy (when $\nu_m = 165$ Mev). For the π^- mesons the momentum distribution of Fig. 1 and the cross sections for the $\gamma + d \to \pi^- + p + p$ reaction from reference 1 was utilized. For the π^+ mesons the same momentum distribution was taken and it was assumed that the cross sections are given by

ν_m	165 Mev	310 Mev			
ν	159	170	180	190	200
N_d^-/N_d^+	2.10±0.17	1.50±0.15	1.41±0.10	1.41±0.09	1.28±0.09
σ^-/σ^+	1.30±0.11	1.39±0.14	1.33±0.09	1.35±0.09	1.25±0.09

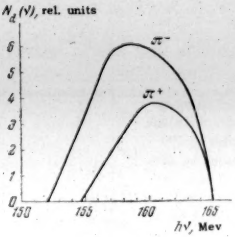

FIG. 2

$\sigma_d^-(\nu + \Delta\nu, E_\pi)/(\sigma^-/\sigma^+)$,

where $\Delta\nu$ is the difference between the threshold energies for π^- and π^+ production on deuterium. The curves of Fig. 2 were normalized such that the ratio of the yields $N_d^\pm = \int_{\nu_m}^{} N_d^\pm(\nu)\,d\nu$ equals the experimental value $N_d^-/N_d^+ = 2.10 \pm 0.17$.[3] Taking further into account the Coulomb correction (at a photon energy of ~160 Mev this amounts to 1.065) we find from the normalization the value $\sigma^-/\sigma^+ = 1.30 \pm 0.11$. Only the statistical error has been indicated. The use of the same momentum distribution for the π^+ mesons as for the π^- mesons can introduce a further error of a few percent. However, a much larger error can be present due to the uncertainty in the determination of the high energy limit of the bremsstrahlung spectrum. Thus, for example, if in the work of Carlson-Lee[3] the high energy limit were 167 instead of 165 Mev, our value of N_d^-/N_d^+ would correspond to $\sigma^-/\sigma^+ = 1.42 \pm 0.12$. The data of Carlson-Lee as reported in the abstract do not allow a more accurate determination of the quantity σ^-/σ^+ for the photon energy $\nu \approx 159$ Mev.

As can be seen from the table the ratio σ^-/σ^+ is approximately constant in the photon energy interval 159 to 200 Mev. Its value agrees well with the results of reference 1 and with the theoretical value.[5]

It should be mentioned that the influence of the sharp drop off of the bremsstrahlung spectrum near the tip has a still larger effect if one compares the π^- and π^+ yields from reactions with large difference in the thresholds. A particularly extreme example is the case of meson photoproduction on beryllium. Since π^- mesons can be created in the reaction $\gamma + Be^9 \rightarrow \pi^- + p + Be^8$ the threshold for production is roughly 17.9 Mev lower than for π^+ production. This way can be explained the anomalous behavior of the value N^-/N^+ with decreasing bremsstrahlung energy or with increasing meson energy or emission angle. This was earlier interpreted as being due to the nuclear structure or due to the special position of the weakly bound neutron. The above described effect has to be taken into account also in the study of the ratio N^-/N^+ in other complex nuclei.

*These corrections amount to around 1.5% on the values N_d^-/N_d^+ given in the table for the case with $\nu_m = 300$ Mev.

[1] Adamovich, Kuz'micheva, Larionova, and Kharlamov, J. Exptl. Theoret. Phys. (U.S.S.R.) **35**, 27 (1958); Soviet Phys. JETP **8**, 21 (1959).

[2] Benventano, Stoppini, Tau, and Beruardini, Proc. CERN Symp., Geneva, **2**, 259 (1956).

[3] D. Carlson-Lee, Bull. Am. Phys. Soc. **3**, 334 (1958).

[4] A. M. Baldin, Nuovo cimento **8**, 569 (1958).

[5] Chew, Goldberger, Low, and Nambu, Phys. Rev. **106**, 1345 (1957).

Translated by M. Danos
181

ON THE SCATTERING OF PIONS BY DEUTERONS

G. M. VAGRADOV and I. B. SOKOLOV

P. N. Lebedev Physics Institute, Academy of Sciences, U.S.S.R.

Submitted to JETP editor November 26, 1958

J. Exptl. Theoret. Phys. (U.S.S.R.) **36**, 948-949 (March, 1959)

SEVERAL authors[1-5] have compared the results of theoretical calculations with experimental data on the elastic scattering of π mesons by deuterons.[2,6,7] Green[1] and Rockmore[3] have used the impulse approximation[8] and note the disagreement between calculated and experimental cross-sections at small angles.[2,7] Differential cross sections calculated by Bruekner's method[4] give better agreement with experiment. This is attributed to taking multiple scattering into account.[9] Bransden and Moorhouse[5] calculated π-d scattering using a variational method. They also obtained agreement with experiment, but in this method of calculation the contributions from multiple scattering are small.

We note in the following, however, that the calculation of the differential cross-section in the impulse approximation is based on different assumptions than those used either in Brueckner's method or the variational method: the impulse approxima-

tion partially takes into consideration the recoil of the nucleons in the deuteron, while in references 4, 5, and 9 the nucleons are considered to be infinitely heavy. It is possible to show that if the nucleon mass is considered infinite in the impulse approximation, then the differential cross-section calculated under such an assumption is not very different from the calculations of Bransden and Moorhouse[5] and Brueckner.[9]

Actually, in the impulse approximation, the differential cross section for the elastic scattering of π mesons by deuterons has the form[3,4]

$$(d\sigma(\theta)/d\Omega)_{lab} = C(q_0, \theta_{lab})\{(d\sigma(\theta)_p/d\Omega)_{cm} + (d\sigma(\theta)_n/d\Omega)_{cm} + \text{i.t.}\}, \quad (1)$$

where q_0 is the momentum of the impinging meson, $(d\sigma(\theta)_p/d\Omega)_{cm}$ and $(d\sigma(\theta)_n/d\Omega)_{cm}$ are the differential cross sections for π mesons scattered by protons and neutrons, respectively, in the center of mass frame, and i.t. are the interference terms. The expression inside the braces in Eq. (1) is independent of the nucleon mass. For small angles:

$$C \approx 1 + 2\omega_0/M, \quad (2)$$

where w_0 is the total energy of the meson in the laboratory frame, while M is the nucleon mass.

From an analysis of the experimental data[2,6,7] one deduces that, for small angles, the experimental cross section is less than that calculated by Eq. (1) approximately by the amount:

$$(2\omega_0/M)\{(d\sigma(\theta)_p/d\Omega)_{cm} + (d\sigma(\theta)_n/d\Omega)_{cm} + \text{i.t.}\}.$$

At low energies this correction is small and the impulse approximation is in agreement with experiment.[3,6] For meson energies of 140 and 300 Mev, $2w_0/M \approx 0.6$ and ≈ 0.9, respectively, hence the disagreement.[1,2] If M is set equal to infinity in Eq. (1), then C = 1 for small angles and the usual impulse approximation is in agreement with experiment. In reference 9, M is also set equal to infinity, i.e., C = 1 for small angles in the impulse approximation, and consequently, the correction due to multiple scattering decreases the matrix elements in Brueckner's method insignificantly compared with the matrix elements in the impulse approximation for C = 1.

The above explanation can be illustrated by calculating elastic π-d scattering for 300-Mev mesons. The calculations are made in three ways: (a) in the impulse approximation using Eq. (1), see curve "a" in the diagram; (b) using Eq. (1), with C = 1, see curve "b," and (c) taking into account double scattering at angles $\leq 90°$ for S and P

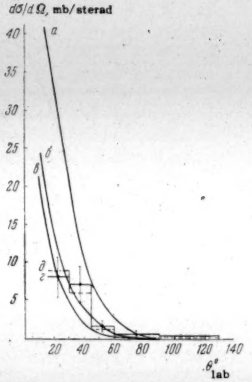

Differential cross-sections for the elastic scattering of 300 Mev π mesons by deuterons. a, b and c – calculated curves; d – experimental data for π^+ mesons; e – experimental data for π^- mesons.[3]

waves in the scattering of π mesons on nucleons, see curve "c." Here C is again set equal to one. The π^--nucleon phase shifts obtained by Dul'kova et al.[2] were used in the calculation. The difference between curves "b" and "c," 15% for $\theta \leq 10°$, lies beyond the limit of experimental precision.

Thus, if we always make the assumption that $M \to \infty$, then the different theoretical methods give the same result, which does not disagree with experiment. Clearly, the assumption that $M \to \infty$ is not justified at higher energies. On the other hand, the disagreement of the impulse approximation ($C \neq 1$) with experiment at small angles is evidence of the incorrectness of the initial assumptions. For example, to derive Eq. (1) it is assumed that the matrix element for the scattering of π mesons by nucleons is independent of the internal motion of the nucleons in the deuteron. Taking this motion into account, a factor of $\frac{1}{2}$ is introduced into Eq. (1) at small angles.

In conclusion, the authors express their thanks to V. Ya. Fel'berg for useful discussions.

[1] T. A. Green, Phys. Rev. **90**, 161 (1953).

[2] Dul'kova, Sokolova, and Shafranova, J. Exptl. Theoret. Phys. (U.S.S.R.) **35**, 313, (1958), Soviet Phys. JETP **8**, 217 (1959).

[3] R. M. Rockmore, Phys. Rev. **105**, 256, (1957).

[4] K. A. Brueckner, Phys. Rev. **89**, 834 (1953); **90**, 715, (1953).

[5] B. H. Bransden and R. G. Moorehouse, Nucl. Phys. **6**, 310 (1958).

[6] K. C. Rogers and L. M. Lederman, Phys. Rev. **105**, 247 (1957).

[7] Arase, Goldhaber, and Goldhaber, Phys. Rev. **90**, 160 (1953).

[8] Fernbach, Green, and Watson, Phys. Rev. **84**, 1084 (1951).

[9] K. A. Brueckner, Phys. Rev. **90**, 715 (1953).

Translated by Kenneth Smith
182

NEW SHORT-LIVED ISOMERS As^{75m} *AND* Ga^{70m} *EXCITED BY FAST PROTONS*

A. M. MOROZOV and P. A. YAMPOL'SKIĬ

Institute of Chemical Physics, Academy of Sciences, U.S.S.R.

Submitted to JETP editor November 27, 1958

J. Exptl. Theoret. Phys. (U.S.S.R.) **36**, 951-952 (March, 1959)

In earlier work we observed short-lived isomeric activity in germanium bombarded with fast protons ($E_\gamma = 0.31$ Mev, $T_{1/2} = 17.5 \pm 2.0$ msec).[1] Through comparison with the results obtained by other investigators[2,3] this was identified as belonging to As^{75m} from the reaction $Ge^{76}(p, 2n)As^{75m}$. This identification has been confirmed by Vegors and Axel[4] and by Schardt.[5] In this connection it is of interest to look for short-lived proton-induced isomeric activity in arsenic.

The 19.6-Mev linear accelerator of the Ukrainian Academy of Sciences Physico-Technical Institute with a repetition rate of 2 pulses per second served as the proton source. The measuring technique was described earlier in references 1 and 6. Gamma-ray energy and half-life was measured by means of a gray-wedge pulse-height analyzer[7] and multichannel time-delay analyzer,[8] respectively. We used an external proton beam extracted through a 40 μ aluminum window, which was monitored by a liminescent thin willemite screen placed in front of the target.

The observed radiation was compared with the result obtained by bombarding a blank carbon target, which revealed no activity.

In the present work we obtained more accurate values for the properties of As^{75m} than those obtained previously through fast-proton bombardment of germanium: $E_\gamma = 0.30 \pm 0.01$ Mev, $T_{1/2} = 16 \pm 1$ millisec. Through Ge^{76} enrichment from 7.67 to 70% it was also established that Ge^{76} is the isotope involved in the reaction that produces the short-lived isomer.

A metallic arsenic target irradiated by fast protons revealed very intense short-lived emission with $E_\gamma = 0.29 \pm 0.01$ Mev and $T_{1/2} = 16 \pm 1$ millisec, and with the reaction threshold ≈ 13 Mev for a thick target. These results are in good agreement with the improved values for As^{75m} ($E_\gamma = 0.305$ Mev, $T_{1/2} = 17$ millisec) given by Schardt in reference 5, where As^{75m} is produced by an E2 transition from the 402-kev level which arises from electron capture in Se^{75}. Thus fast-proton bombardment of arsenic also produces As^{75m} through the reaction $As^{75}(p, p')As^{75m}$.

In our earlier work[1] we also detected short-lived isomeric gamma rays (of a few milliseconds) from gallium reacting with fast protons. The present work established $E_\gamma = 0.19 \pm 0.01$ Mev and $T_{1/2} = 19 \pm 1$ millisec for this radiation.

A short-lived isomer with $E_\gamma = 0.17 \pm 0.01$ Mev and $T_{1/2} = 16 \pm 1$ millisec was discovered in our laboratory during 1957[9] through neutron bombardment of germanium. The good agreement of these values with those obtained in the present work suggests that the same isomeric level is involved in both instances.

There are two stable gallium isotopes (69, 71) and five stable germanium isotopes (70, 72, 73, 74, 76). An analysis of the possible reactions between protons and gallium nuclei and between neutrons and germanium nuclei which would result in the same isomeric level shows that the excited nuclei of Ga^{70}, Ge^{69}, Ge^{70}, or Ge^{71} could be the final reaction products. Ge^{70}: which is an even-even nucleus, is excluded. Thus only the following proton-gallium reactions can produce these excited nuclei: $Ga^{71}(p, pn)Ga^{70}$, $Ga^{69}(p, n)Ge^{69}$ and $Ga^{71}(p, n)Ge^{71}$. The experimental thresholds for the production of these nuclei in their ground states are 9, 4.1, and 1.0 Mev, respectively.[10]

By using enriched gallium isotopes (with Ga^{69} enriched from 60.2 to 97.6% in one instance and depleted to 1.3% in another instance) we determined that Ga^{71} is involved in a reaction where a short-lived level is formed. The experimental threshold of this reaction for a thick target is about 9 Mev. We can thus infer that the aforementioned level $E_\gamma = 0.19$ Mev belongs to Ga^{70m} produced in the reaction $Ga^{71}(p, pn)Ga^{70m}$. Glagolev et al.[9] obtained this level through the reaction $Ge^{70}(n, p)Ga^{70m}$. The half-life for an E3 transition is estimated to be of the order 10^{-2} sec, which agrees with experimental results.

The ground-state spin of Ga^{70} is 1^+.[11] If the spin of the excited Ga^{70} state is assumed to be 4^-, which is likely for a number of reasons, the observed short-lived isomeric transition is of the E3 type.

The authors are deeply grateful to O. I. Leipunskiĭ for his continued interest and assistance, to Yu. V. Makarov for a discussion of the results and to N. M. Meleshin and O. B. Likin for experimental assistance. They also wish to thank K. D. Sinel'nikov, A. K. Val'ter, A. P. Klyucharev, and A. M. Smirnov for their assistance.

[1] Leipunskiĭ, Morozov, Makarov, and Yampol'skiĭ, J. Exptl. Theoret. Phys. (U.S.S.R.) **32**, 393 (1957), Soviet Phys. JETP **5**, 305 (1957).

[2] A. W. Schardt, Bull. Am. Phys. Soc. Ser. II, **1**, 85 (1956).

[3] S. H. Vegors and P. Axel, Bull. Am. Phys. Soc. **30**, No. 7, 11 (1955).

[4] S. H. Vegors and P. Axel, Phys. Rev. **101**, 1067 (1956).

[5] A. W. Schardt, Phys. Rev. **108**, 398 (1957).

[6] Leipunskiĭ, Miller, Morozov, and Yampol'skiĭ, Dokl. Akad. Nauk SSSR **109**, 935 (1956), Soviet Phys. "Doklady" **1**, 505 (1956).

[7] O. B. Likin, Приборы и техника эксперимента (Instruments and Measurement Engg.) **2**, 000 (1958).

[8] Yu. V. Makarov, Report, Inst. of Chem. Phys., Acad. Sci. U.S.S.R., 1957.

[9] Glagolev, Kovrizhnykh, Makarov and Yampol'skiĭ, J. Exptl. Theoret. Phys. (U.S.S.R.) **36**, 1046 (1959), Soviet Phys. JETP **9**, in press.

[10] B. L. Cohen and E. Newman, Phys. Rev. **99**, 718 (1955).

[11] B. G. Dzhelepov and L. K. Peker, Схемы распада радиоактивных изотопов (Decay Schemes of Radioactive Isotopes), Acad. Sci. Press (1957).

Translated by I. Emin
183

ON A RELATION IN QUANTUM STATISTICS

E. S. FRADKIN

P. N. Lebedev Physics Institute, Academy of Sciences, U.S.S.R.

Submitted to JETP editor November 29, 1958

J. Exptl. Theoret. Phys. (U.S.S.R.) **36**, 952-953 (March, 1959)

As is well known, the density matrix ρ of a canonical ensemble has the form

$$\rho = e^{-\beta H}, \quad H = H_0 + H_1 = \int [H_0(x) + H_1(x)]\, d^3x, \quad (1)$$

where $\beta = 1/kT$; H is the Hamiltonian of the system; H_0 is the "free" Hamiltonian (in general it may also partially take into account the interaction between the particles, for example in the Hartree-Fock approximation); H_1 is the interaction Hamiltonian.

Let us take instead of H the Hamiltonian $H_\lambda = H_0 + \lambda H_1$. Then

$$-\partial\rho/\partial\beta = (H_0 + \lambda H_1)\rho. \quad (2)$$

Following the general methods of the S matrix (cf. e.g., reference 1), we write down the formal operator solution of Eq. (2):*

$$\hat{\rho} = e^{-\beta H_0}\, T\left\{\exp\left[-\lambda\int H_1(xt)\, dt d^3x\right]\right\}, \quad (3)$$

where T calls for arrangement of the operators from right to left in the order of increasing t, and any operator $f(x, t)$ is connected with $f(x)$ by the relation

$$f(xt) = e^{tH_0} f(x)\, e^{-tH_0}. \quad (4)$$

To determine all the thermodynamic quantities it is sufficient to know the function

$$Z = \ln \mathrm{Sp}\, e^{\alpha N - \beta H}, \quad (5)$$

where the averaging (Sp) is taken over a complete orthogonal system of eigenfunctions of the Hamiltonian H or of H_0; N is the operator for the total number of particles and commutes with the total Hamiltonian; $\alpha = \beta\mu$, where μ is the chemical potential. Using Eqs. (5) and (3), one can easily verify that

$$\frac{\partial Z}{\partial\lambda} = -\mathrm{Sp}\left[\exp(\alpha N - \beta H_\lambda) \times \int \tilde{H}_1(xt)\, d^3x dt\right] \Big/ \mathrm{Sp}\,[\exp(\alpha N - \beta H_\lambda)], \quad (6)$$

where $\tilde{H}_1(xt) = e^{H\lambda t} H_1(x) e^{-H\lambda t}$ (i.e., the operator in the Heisenberg representation).

From Eq. (6) it follows that

$$Z = Z_{\lambda=1} = Z_0 - \int_0^1 \frac{\mathrm{Sp}\left[\exp(\alpha N - \beta H_\alpha)\int \tilde{H}_1(xt)\, d^3x dt\right]}{\mathrm{Sp}\,[\exp(\alpha N - \beta H_\lambda)]}\, d\lambda, \quad (7)$$

where Z_0 is the known expression for Z when $H = H_0$. It can be shown that the expression in the integrand of Eq. (7) is

$$\frac{1}{\lambda}\int (M(xt, x't')\, G(x't', xt)\, d^3x dt d^3x' dt',$$

where M is the mass operator for the "one-particle" Green's function[1] $G(xt, x't')$ (integration with respect to t, t' from 0 to β).

In the case in which H_0 does not contain the charge g, we can take the charge g as the parameter λ, and Z takes the form

$$Z = Z_0 - \int_0^g \frac{dg'}{g}\int M(xt, x't')\, G(x't', xt)\, d^3x dt dt' d^3x'. \quad (8)$$

Thus all the statistical characteristics of the system are determined by the mass operator of the "one-particle" Green's function. This fact makes the application of field-theory methods to statistics very fruitful. It is not hard to show from Eq. (8) that for the case $\beta = \infty$ ($T = 0$) one gets the following well known relation for the energy of the ground state

$$\overline{E} = E(g=0) + \int_0^1 \frac{dg'}{g'} \int M(x^3, x't') G(x't', x^3) d^3x d^3x' dt'. \quad (9)$$

One can verify this by choosing as the complete orthogonal set of functions for the summation the eigenfunctions of the total Hamiltonian and noting that for $\beta = \infty$ the ground-state term is the only one contributing to the sum.

*The integration with respect to t is everywhere taken from 0 to β.

[1] T. Matsubara, Prog. Theor. Phys. **14**, 351 (1955).

Translated by W. H. Furry
184

POLARIZATION OF THE NUCLEUS BY CAPTURE OF POLARIZED NEGATIVE MUONS INTO THE MESONIC K SHELL

I. M. SHMUSHKEVICH

Leningrad Physico-Technical Institute, Academy of Sciences, U.S.S.R.

Submitted to JETP editor December 7, 1958

J. Exptl. Theoret. Phys. (U.S.S.R.) **36**, 953-954 (March, 1959)

THE formation of μ-mesonic atoms with transition of μ^- mesons to the K shell is accompanied by considerable depolarization of the originally polarized μ mesons.[1-3] If the nucleus has a spin I a polarization of the nucleus is also produced, owing to the magnetic interaction of the spins.

The hyperfine splitting in the ground state of the mesonic atom is much larger than $\hbar/\tau$, where τ is the lifetime of the μ^- meson. Therefore the states with $F = I + \frac{1}{2}$ and $F = I - \frac{1}{2}$ form an incoherent mixture.[4] Accordingly the spin state of the mesonic atom is best described by the corresponding density matrix ρ. Since the nucleus is supposed unpolarized before the capture, the only direction singled out if that of the original polarization of the μ^- mesons. Let $\mathbf{j}$ be the unit vector in that direction. For a given F, from the requirements of invariance and the Hermitian character of ρ and its being linear in $\mathbf{j}$, we have

$$\rho_F = \frac{1}{2F+1}\left(1 + \frac{3\lambda_F}{F+1}\mathbf{jF}\right) P_F, \quad (1)$$

P_F is the projection operator onto states with the given value of F. From the condition $\overline{\mathbf{jF}} = \mathrm{Sp}(\rho_F \mathbf{jF}) \leq F$ it follow that $|\lambda_F| \leq 1$.

For $F = I + 1/2$ $\quad P_F = \frac{I + 1 + 2\mathbf{Is}}{2I+1}$;

for $F = I - 1/2$ $\quad P_F = \frac{I - 2\mathbf{Is}}{2I+1}$,

$\mathbf{s}$ and $\mathbf{I}$ are the spin operators of the μ^- meson and the nucleus. Substituting Eq. (2) in Eq. (1), we get:

for $F = I + \frac{1}{2}$:

$$\rho_+ = \frac{1}{2(2I+1)}\left\{1 + \frac{2\mathbf{Is}}{I+1} + \lambda_+ \mathbf{j}\left(\frac{3\mathbf{I}}{I+1} + 2\mathbf{s}\right) + \frac{3\lambda_+}{(I+1)(I+3/2)}\left[(\mathbf{jI})(\mathbf{sI}) + (\mathbf{sI})(\mathbf{jI}) - \frac{2I(I+1)}{3}\mathbf{js}\right]\right\}, \quad (3)$$

from which we have

$$\frac{\overline{\mathbf{s}}}{s} = \frac{1}{s}\mathrm{Sp}(\rho_+ \mathbf{s}) = \lambda_+ \mathbf{j}, \quad \frac{\overline{\mathbf{I}}}{I} = \frac{1}{I}\mathrm{Sp}(\rho_+ \mathbf{I}) = \lambda_+ \mathbf{j}; \quad (4)$$

for $F = I - \frac{1}{2}$:

$$\rho_- = \frac{1}{2(2I+1)}\left\{1 - \frac{2\mathbf{Is}}{I} + \lambda_- \frac{I - 1/2}{I + 1/2}\mathbf{j}\left(\frac{3\mathbf{I}}{I} - 2\mathbf{s}\right) - \frac{3\lambda_-}{I(I+1/2)}\left[(\mathbf{jI})(\mathbf{sI}) + (\mathbf{sI})(\mathbf{jI}) - \frac{2I(I+1)}{3}\mathbf{js}\right]\right\}; \quad (5)$$

$$\frac{\overline{\mathbf{s}}}{s} = \frac{1}{s}\mathrm{Sp}(\rho_- \mathbf{s}) = -\lambda_- \frac{I - 1/2}{I + 1/2}\mathbf{j},$$

$$\frac{\overline{\mathbf{I}}}{I} = \frac{1}{I}\mathrm{Sp}(\rho_- \mathbf{I}) = \frac{(I - 1/2)(I+1)}{(I+1/2)I}\lambda_- \mathbf{j}. \quad (6)$$

For nuclei with $I = \frac{1}{2}$, for example for μ-mesonic hydrogen,

$$\rho_+ = 1/4\,[1 + \lambda_+ \mathbf{j}(\sigma_p + \sigma_\mu) + 1/2\,\sigma_p \sigma_\mu],$$

$$\rho_- = 1/4\,(1 - \sigma_p \sigma_\mu). \quad (7)$$

One must take this effect (polarization of the nucleus) into account in the analysis of experiments relating to the capture of μ^- mesons by nuclei, in particular in the determination of the angular distribution of the neutrons produced. Formulas for the asymmetry parameter of the angular distribution of the neutrons produced in the reaction $\mu^- + p \rightarrow n + \nu$ have been obtained in references 5 — 7. In these papers it was assumed that before the capture the proton is unpolarized, despite the fact that the μ^- meson located in the K shell is polarized. It thus appears that the results in question are unreliable.

[1] Garwin, Lederman, and Weinrich, Phys. Rev. **105**, 1415 (1957).

[2] Ignatenko, Egorov, Khalupa, and Chultém, J. Exptl. Theoret. Phys. (U.S.S.R.) **35**, 1131 (1958), Soviet Phys. JETP **8**, 792 (1959).

[3] I. M. Shmushkevich, J. Exptl. Theoret. Phys. (U.S.S.R.) **36**, 645 (1959), Soviet Phys. JETP **9**, 000 (1959); Nucl. Phys. (in press).

[4] Bernstein, Lee, Yang, and Primakoff, Phys. Rev. **111**, 313 (1958).

[5] Shapiro, Dolinskiĭ, and Blokhintsev, Dokl. Akad. Nauk SSSR **116**, 946 (1957), Soviet Phys. "Doklady" **2**, 475 (1957).

[6] Huang, Yang, and Lee, Phys. Rev. **108**, 1340 (1957).

[7] B. L. Ioffe, J. Exptl. Theoret. Phys. (U.S.S.R.) **33**, 308 (1957), Soviet Phys. JETP **6**, 239 (1958).

Translated by W. H. Furry
185

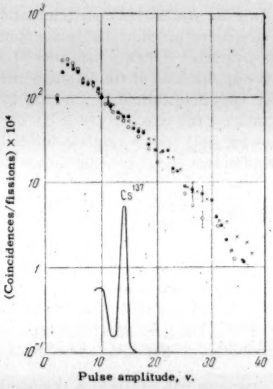

FIG. 1. Distribution of γ-quanta pulses by amplitudes. ● – fission of U^{235} by thermal neutrons. ○ – fission of U^{238} by 2.8-Mev neutrons. × – fission of U^{238} by 14.7-Mev neutrons.

GAMMA RAYS ACCOMPANYING THE FISSION OF U^{238} BY 2.8 AND 14.7 Mev NEUTRONS

A. N. PROTOPOPOV and B. M. SHIRYAEV

Radium Institute, Academy of Sciences, U.S.S.R.

Submitted to JETP editor December 6, 1958

J. Exptl. Theoret. Phys. (U.S.S.R.) **36**, 954-955 (March, 1959)

MOST recent investigations of the prompt fission gammas pertain either to fission of U^{235}, by neutrons or to spontaneous fission of Cf^{252}. The latest determinations of the average total energy of the gamma-quanta emitted in one fission yield approximately 7.5 Mev for fission of U^{235} by thermal neutrons[1] and 8.2 Mev for spontaneous fission of Cf^{252} (reference 2). It was found experimentally that when U^{235} is fissioned by thermal neutrons and by neutrons of energies 2.8 and 14.7 Mev, the total energy of the gamma quanta is the same in all cases, within a range of ±15% (reference 3).

The purpose of this work was to obtain data on the energy liberated in the form of gamma rays during fission of U^{238} by fast neutrons. Using a procedure and apparatus previously employed,[3] we compared the gamma-ray spectra obtained in the fission of U^{238} by fast neutrons, with the gamma-ray spectrum obtained in fission of U^{235} by thermal neutrons. The gamma quanta were registered with a scintillation counter with a NaI(Tl) crystal, connected for coincidence with a single-layer fission chamber that registered the fissions. Placed in the chamber were targets of equal diameter made of U^{235} and U^{238} with an average density of 1.8 and 2.2 mg/cm² respectively. The relative placement of the crystal and of the layers of the fissioning substance was the same for thermal and fast neutrons. The spectra of the pulses obtained from the scintillation counter, after eliminating the random coincidences, are shown in the diagram. To estimate the values of the energy, the abscissa of the diagram shows the amplitude distribution of the momenta for gamma rays of 661 kev energy (Cs^{137}). The ratio of the number of coincidences between gamma quanta and fragments obtained by fission of U^{238} by 2.8 and 14.7 Mev neutrons to the number of coincidences for fission of U^{235} by thermal neutrons, are respectively 1.03 ± 0.03 and 1.00 ± 0.02. For the measured range of amplitudes, as can be seen from the diagram, the spectra have the same appearance for all cases. Taking account, however, of the fact that the indeterminacy in the final results is greater, owing to the possible divergence of the spectra at large energies, one can conclude that in the fission of U^{238} by 2.8 and 14.7 Mev neutrons the average total energies of the gamma rays are the same, within 15%, as in the case of fission of U^{235} by thermal neutrons.

In comparing the data obtained with the results of other investigations we see firstly, that the average total gamma-quanta energies per fission are nearly equal for all the investigated nuclei (U^{235},

U^{238}, and Cf^{252}). Secondly, the gamma quanta energies depends little on the excitation energy of the compound nucleus prior to fission.

The authors express their gratitude to Yu. I. Belyanin for insuring operation of the accelerated tube in the performance of this experiment.

[1] R. B. Leachman, Phys. Rev. **101**, 1005 (1956). Artem'ev, Protopopov, and Shiryaev, Труды РИАН (Trans. Radium Inst. Acad. Sci.) **9**, in press.

[2] Smith, Fields, and Friedman, Phys. Rev. **104**, 699 (1956).

[3] A. N. Protopopov and B. M. Shiryaev, J. Exptl. Theoret. Phys. (U.S.S.R.) **34**, 331 (1958), Soviet Phys. JETP **7**, 231 (1958).

Translated by J. G. Adashko
186

ZEMPLEN'S THEOREM IN RELATIVISTIC HYDRODYNAMICS

R. V. POLOVIN

Physico-Technical Institute, Academy of Sciences, Ukrainian S.S.R.

Submitted to JETP editor December 12, 1958

J. Exptl. Theoret. Phys. (U.S.S.R.) **36**, 956 (March, 1959)

KHALATNIKOV[1] has shown that for a relativistic shock wave of low intensity the theorem of Zemplen and the conditions of mechanical stability, $v_1 > c_1$, $v_2 < c_2$, are applicable provided only that the following inequality holds;

$$\left(\frac{\partial^2 (w/n)}{\partial p^2}\right)_s > 0 \qquad (1)$$

(where w is the heat function per particle, s the entropy per particle, n the density of particles measured in the rest system of the particles, and p the pressure.)

These results are also applicable for relativistic shock waves of any intensity. The proof can be done in a similar way to Landau and Lifshitz, (reference 2, paragraph 84,) for the case when the shock adiabate lies in the plane (p, w/n.) In this case, formula (84,6) will correspond to

$$w_2 T_2 ds_2 = {}^1/_2 (w_1/n_1 - w_2/n_2)^2 \, d(j^2),$$

and the expression

$$1 - \frac{v_2^2}{c_2^2} = (V_1 - V_2)\left[1 - \frac{j^2 (V_1 - V_2)}{2T_2}\left(\frac{\partial V_2}{\partial s_2}\right)_{p_2}\right]\frac{d(j^2)}{dp_2}$$

is replaced by

$$1 - \frac{u_2^2}{a_2^2}$$

$$= \left(\frac{w_1}{n_1} - \frac{w_2}{n_2}\right)\left[1 - \frac{j^2 (w_1/n_1 - w_2/n_2)}{2w_2 T_2}\left(\frac{\partial (w_2/n_2)}{\partial s_2}\right)_{p_2}\right]\frac{d(j^2)}{dp_2},$$

$$j = nu, \quad u = v/\sqrt{1 - v^2}, \quad a = c/\sqrt{1 - c^2},$$

(where c is the velocity of sound, and the velocity of light is taken as unity.) It follows from this that the quantity n/w, as well as the pressure and the density, are increased on the shock wave.

The inequality (1), for the nonrelativistic case, reduces to the well known conditions, $(\partial^2(1/n)\partial p^2)_S > 0$. For a relativistic ideal gas we have

$$\left(\frac{\partial^2 (w/n)}{\partial p^2}\right)_s = \frac{2(2-\gamma)}{\gamma(\gamma-1)}\frac{1}{pn^2}.$$

The last expression is always positive, since the quantity γ is within the interval[3] $1 < \gamma \leq {}^5/_3$.

It should be noted that for an ultra-relativistic ideal gas,[2] $\gamma = {}^4/_3$.

The author wishes to thank A. I. Akhiezer and G. Ya. Lyubarski for valuable discussions.

[1] I. M. Khalatnikov, J. Exptl. Theoret. Phys. (U.S.S.R.) **27**, 529 (1954).

[2] L. D. Landau and E. M. Lifshitz, Механика сплошных сред (Mechanics of Continuous Media), GITTL, M. 1954.

[3] A. H. Taub, Phys. Rev. **74**, 328 (1948).

Translated by S. Kotz
187

ON ELECTROMAGNETIC SHOCK WAVES IN FERRITES

A. V. GAPONOV and G. I. FREĬDMAN

Radiophysics Institute, Gorkiĭ State University

Submitted to JETP editor December 18, 1958

J. Exptl. Theoret. Phys. (U.S.S.R.) **36**, 957-958 (March, 1959)

WE investigate the propagation of a uniform plane electromagnetic wave in a medium with nonlinear dependence of the induction **B** on the magnetic field **H**.* We assume to begin with that the

medium is isotropic, i.e., that a relation exists between the magnitudes of the fields ($B = B(H)$; $\mu(H) = \partial B/\partial H$). It is easy to show that Maxwell's equations for this case have solutions given by the relations

$$H_y = f\left(z \mp ct/\sqrt{\varepsilon\mu(H_y)}\right),$$
$$\sqrt{\varepsilon}\,E_x = \pm \int_0^{H_y} \sqrt{\mu(H)}\,dH, \qquad (1)$$

where $f(\xi)$ is an arbitrary smooth function and ϵ the dielectric constant.

The solutions (1) describe simple waves in a nonlinear medium (waves of this type in gas dynamics are described, e.g., in references 1 and 2). The deformation of a simple wave can be most easily investigated by looking at the propagation of a single pulse. It can be easily seen that if $\mu(H)$ is a monotonically decreasing function then in the course of time the leading edge will become steeper and the trailing edge more sloping.† Beginning from a particular moment t^* there will appear in the function $H_y(t^*, z)$ an infinite derivative. This points to the appearance of an electromagnetic shock wave.

The boundary conditions which connect the fields on both sides of the discontinuity with its velocity of propagation, v, can be obtained by integrating Maxwell's equations over an infinitesimal interval Δz, containing the discontinuity. Thus we obtain

$$\{H_y\} = \frac{v}{c}\varepsilon\{E_x\}, \quad \{E_x\} = \frac{v}{c}\{B_y\},$$
$$\text{hence } v^2/c^2 = \{H_y\}/\varepsilon\{B_y\}, \qquad (2)$$

where the brackets $\{\ \}$ denote the jump in the values of the respective quantities across the discontinuity.

Immediately after the appearance the shock wave is weak ($\{\mu\} \ll \mu$) and the structure of the field is in this approximation the same as in a simple wave. Equation (2) together with (1) thus allow the description of the development of simple waves and of weak shock waves.

To investigate the structure of the shock front one needs further information on the characteristics of the medium. We shall investigate here the simplest example, of plane uniform waves in a ferrite saturated by a dc field parallel to the direction of propagation of the wave by means of a uniform field H_0. The connection between the magnetization $\mathbf{M}$ ($\mathbf{B} = \mathbf{H} + 4\pi\mathbf{M}$; $M = \text{const}$) and the field $\mathbf{H}(z, t)$ in this case is given by the following equation[3]‡

$$\partial\mathbf{M}/\partial t = \gamma\mathbf{M}\times(\mathbf{H} + \mathbf{H}_0) - \gamma M^{-2}\mathbf{M}\times[\mathbf{M}\times(\mathbf{H} + \mathbf{H}_0)], \qquad (3)$$

where γ is the gyromagnetic ratio for the electron spin and $1/\lambda = \tau_0$ is the relaxation time.

In particular, it follows from (3) that for sufficiently slow processes (with a characteristic time $T \gg \tau_0$) $\mathbf{M} \parallel \mathbf{H} + \mathbf{H}_0$. The connection between $H_\perp = H_y$ and $M_\perp = M_y$ is then given by

$$H_y = M_y(H_0/\sqrt{M^2 - M_y^2} - 4\pi). \qquad (4)$$

By means of (4) it is easy to find the functions $B_y(H_y)$ and $\mu = 1 + 4\pi dM_y/dH_y = \mu(H_y)$ which enter Eqs. (1) and (2), for the case of simple and shock waves.

It turns out that it is not possible to obtain a general solution of Maxwell's equations taking into account the relation (3). We therefore limit ourselves to the case of a stationary plane shock wave.** The equations can in that case be easily integrated. It turns out[4] that in a stationary wave the vector $\mathbf{M}$ rotates around the direction of propagation of the wave, z (precession angle, φ), while the angle between M and the z-axis, θ, changes according to

$$\ln\frac{(\cos\theta - \cos\theta')^2}{(1+\cos\theta)^{1-\cos\theta'}(1-\cos\theta)^{1+\cos\theta'}} = \left(\frac{z}{v} - t\right)\frac{2\lambda}{M}(H'_y + 4\pi M\sin\theta')\sin\theta', \qquad (5)$$

The precession frequency $\omega = \partial\varphi/\partial t$ is given by

$$\omega = \gamma\{H'_y\cos\theta/\sin\theta' - (H_0 - 4\pi M\cos\theta)\}, \qquad (6)$$

Here θ' and H'_y are the values of the respective magnitudes for $z \to -\infty$ (far behind the wave front); the wave velocity v depends on the amplitude of the transverse part of the magnetic field***

$$v^2/c^2 = H_y/(H_y + 4\pi M\sin\theta)$$
$$= H'_y/(H'_y + 4\pi M\sin\theta') = \text{const}, \qquad (7)$$

while the angle θ' is connected with the field amplitude of the shock wave H'_y by the equation $H'_y\cot\theta' = H_0 - 4\pi M\cos\theta'$.

It follows from (5) that the time width of the wave front, τ, is given by

$$\tau = M/2\lambda(H'_y + 4\pi M\sin\theta')\sin\theta' \qquad (8)$$

and it depends on the relaxation time of the ferrite, $\tau_0 = 1/\lambda$ and on the amplitude H'_y. In a very strong wave ($H'_y \gg H_0$, M) obtains

$$v \approx c, \ \tau \approx \tau_0 M/2H'_y, \ \omega_{max} \approx \gamma H'_y. \qquad (9)$$

In a weak shock wave ($H'_y \ll H_0 - 4\pi M$) the passage time of the front is considerably longer and the maximum frequency component is less.

$$\omega_{max} \approx {}^1/_2\gamma H_0[H'_y/(H_0 - 4\pi M)]^2, \ \tau\omega_{max} \approx {}^1/_4\gamma M\tau_0. \qquad (10)$$

Thus for sufficiently large $\tau\omega_{max}$ the wave front of an electromagnetic shock wave consists of a circularly polarized oscillation with a variable frequency.

*The case of a nonlinear relation between the electric displacement D and field E can be treated similarly, as well as the case of nonlinearity with respect to both the electric and the magnetic fields.

†This circumstance (for electromagnetic waves) was first pointed out and utilized by I. G. Kataev.

‡The anisotropy field will not be considered. In the following it will be assumed that $H_{z0} = H_0 - 4\pi M > 0$ since only this leads to stability in the initial conditions in the medium.

**In a stationary wave the field components (which, in general, are not transverse) have the form $f(z - vt)$ where the velocity v = const.

***We note that the value for the velocity of the shock wave determined from (2) and (4) coincides with that from (7).

[1] L. Landau and E. M. Lifshitz, Механика сплошных сред (Mechanics of Continuous Media) Moscow, Gostekhizdat, 1954.

[2] R. Courant and K. O. Friedrichs, Supersonic Flow and Shock Waves, Interscience, New York, 1948, (Russ. transl. IIL, Moscow, 1950).

[3] L. Landau and E. Lifshitz, Phys. Z. d. Sowjetunion **8**, 153 (1935).

[4] A. V. Gaponov and G. J. Freidman, Изв. ВУЗ, Радиофизика (News of the Universities, Radiophysics), in press.

Translated by M. Danos
188

ON THE HEAT CONDUCTIVITY AND ATTENUATION OF SOUND IN SUPERCONDUCTORS

B. T. GEĬLIKMAN and V. Z. KRESIN

Moscow State Pedagogical Institute

Submitted to JETP editor December 18, 1958

J. Exptl. Theoret. Phys. (U.S.S.R.) **36**, 959-960 (March, 1959)

WE have previously calculated the electronic heat conductivity[1] κ_e, of superconductors and the phonon conductivity,[2] κ_p, determined by the scattering of phonons by electrons. It will be shown here that from the theoretical temperature dependence of κ_e and κ_p found, we can explain, to a considerable extent, all the relationships in the existing experimental data on the heat conductivity of superconductors.

According to our earlier paper[2] κ_p can be expressed as:*

$$\varkappa_p^s = \varkappa_p^n F(T)/F(T_k),$$

$$F(T) = -8(b^4 + b^3)(e^b - 1)^{-1} + 6\zeta(3)(e^b + 1) - 3(e^b + 1)\sum_s s^{-3}\exp(-2bs) \times (4b^2s^2 + 4bs + 2) + 6\zeta(4)(e^b - 1) - (e^b - 1)\sum_s s^{-4}\exp(-2bs)(8b^3s^3 + 12b^2s^2 + 12bs + 6) + 32b^3(e^{2b} - 1)^{-1} - a^4\sum_s\{s\exp(-2bs)\,\mathrm{Ei}[-s(2b-a)]\} + 6\sum_s s^{-3}\exp(-2bs),$$

$$a = 2b - 0{,}16,\quad \zeta(s) = \sum_{n=1}^{\infty} n^{-s}. \qquad (1)$$

In the normal state $\kappa_p^n = \mathrm{const}\cdot T^2$; $b = \Delta(T)/kT$, where $\Delta(T)$ is the energy gap, and κ_s/κ_n depends only on T and T/T_k. For comparison with experiment one must use a specimen with sufficient impurity concentration for κ_e to be small. In Fig. 1 the theoretical curve is drawn according to Eq. (1) and the experimental points are for an In-Tl alloy measured by Sladek.[3]

If $(T_k - T)/T_k$ is not very small, κ_e is not appreciably affected by the electron-phonon interaction.

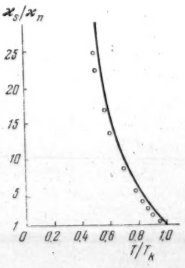

FIG. 1. Points – experimental data[3] for Tl concentration 38%. Solid curve – theoretical

As can be seen from Fig. 1, the conductivity κ_p increases exponentially as $T \to 0$, owing to the increase in phonon mean free path with decreasing scattering by electrons. At sufficiently low temperatures the lattice thermal resistance due to electron scattering, $1/\kappa_{pe}$, becomes less than the resistance due to scattering by lattice defects and crystal boundaries, $1/\kappa_{pd}$ (κ_{pd} is the same as κ_{pd} in a normal metal). Since the resulting lattice conductivity is $\kappa_p = \kappa_{pe}\kappa_{pd}/(\kappa_{pe} + \kappa_{pd})$, we get $\kappa_p \approx \kappa_{pd}$ at still lower temperatures. κ_{pd} usually decreases according to a power law[4] ($\sim T^3$) at low temperatures. For temperatures

such that $\kappa_{pd} \sim \kappa_{pe}$, the lattice conductivity should then have a maximum (see curve 1 of Fig. 2). Such a maximum was found in experiments on Pb + 10% Bi.[5]

The electronic heat conductivity varies in quite a different way, because of the reduction in the number of electronic excitations, as was shown by Gel'likman.[1] κ_e first decreases slowly and then exponentially with decreasing temperature (see curve 2 of Fig. 2).

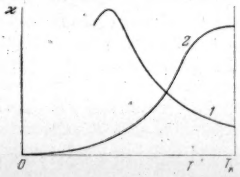

FIG. 2

The total heat conductivity κ is the sum of κ_e and κ_p. In pure specimens $\kappa_p \ll \kappa_e$ at almost all temperatures, and $\kappa \approx \kappa_e$. This is confirmed by measurements on Al and Zn,[6] Sn,[7,9] In,[7] and Pb.[8]

Only at very low temperatures do we have $\kappa_e < \kappa_p$ and $\kappa \approx \kappa_{pd}$. In very impure specimens $\kappa_p \gg \kappa_e$ and $\kappa \simeq \kappa_p$ at all temperatures.[3,5] For intermediate cases of not very pure superconductors, κ_e is the main component near T_k, so that κ falls with decreasing temperature. At sufficiently low temperatures κ_p becomes larger than κ_e, and κ is then determined by curve 1 of Fig. 2. Such a temperature dependence was found in experiments on Sn, Hg and Pb,[9-11] while de Haas and Rademakers[11] and Mendelssohn and Olsen[5] found a maximum in κ, related to the maximum in κ_p (the collected experimental data are contained in Shoenberg's book[12]).

Let us now examine the coefficient γ of absorption of sound in superconductors, due to electronic excitations, when the frequency is $\omega \gg 1/\tau$, where τ is the relaxation time. The absorption due to phonons is, under these conditions, the same as in a normal metal.

From a consideration of the probabilities of absorption of a sound quantum and of the reverse process, we obtain for the ratio

$$\frac{\gamma_s}{\gamma_n} = \frac{x - \ln[(e^{b+x}+1)(e^b+1)^{-1}] + D(x)(2b - x + 2\ln[(e^{x-b}+1)(e^b-1)^{-1}])}{\ln[(e^x+1)/2]}$$

$$x = \hbar\omega/kT;\quad D(x) = \begin{cases} 1, & x \geqslant 2b \\ 0 & x < 2b \end{cases}$$

For $x \ll 1$ this gives $\gamma_s/\gamma_n = 2/(e^b + 1)$, which agrees with the expression previously obtained by Bardeen, Cooper, and Schrieffer.[13]

We thank Academician L. D. Landau for valuable advice.

*There is a misprint in the final formula of reference 2.

[1] B. T. Gel'likman, J. Exptl. Theoret. Phys. (U.S.S.R.) **34**, 1042 (1958), Soviet Phys. JETP **7**, 721 (1958).

[2] B. T. Gel'likman and V. Z. Kresin, Dokl. Akad. Nauk SSSR **123**, 259 (1958).

[3] R. J. Sladek, Phys. Rev. **97**, 902 (1955).

[4] R. Peierls, Quantum Theory of Solids, Russian translation, IIL page 69 (1956). [Clarendon Press, Oxford, 1955].

[5] K. Mendelssohn and J. L. Olsen, Proc. Phys. Soc. **63A**, 2 (1950).

[6] N. V. Zavaritskiĭ, J. Exptl. Theoret. Phys. (U.S.S.R.) **34**, 1116 (1958), Soviet Phys. JETP **7**, 773 (1958).

[7] K. Mendelssohn and C. A. Renton, Phil. Mag. **44**, 776 (1953).

[8] J. L. Olsen and C. A. Renton, Phil. Mag. **43**, 946 (1952).

[9] S. J. Laredo, Proc. Roy. Soc. **229A**, 473 (1955).

[10] J. K. Hulm, Proc. Roy. Soc. **204A**, 98 (1950).

[11] W. J. de Haas and A. Rademakers, Physica **7**, 992 (1940), Leiden Comm. 261e (1940).

[12] D. Shoenberg, Superconductivity, Russian translation IIL page 80 (1955) [Cambridge, 1952].

[13] Bardeen, Cooper, and Schrieffer, Phys. Rev. **108**, 1175 (1957).

Translated by R. Berman
189

ANISOTROPIC FISSION OF ROTATING NUCLEI

G. A. PIK-PICHAK

Submitted to JETP editor November 18, 1958

J. Exptl. Theoret. Phys. (U.S.S.R.) **36**, 961-962 (March, 1959)

WHEN the probability of fission depends on nuclear angular momentum,[1] in order to determine the dependence of the anisotropy on $x = (Z^2/A)/(Z^2/A)_{cr}$, where Z and A are the charge and mass of the fissioning nucleus, we must take other competing processes into account (specifically here, neutron evaporation). The fission probability of a nucleus with angular momentum j and its projection K on the symmetry axis of the nucleus, for the direction $d\omega = \sin\vartheta\, d\vartheta$, where ϑ is the angle between the incident beam direction and the direction in which a fragment come off, is given by

$$dw_f(j, K, \vartheta) = \frac{\gamma_f(j, K, \vartheta)\, d\omega}{\Gamma_n + \Gamma_f(j)}, \quad \Gamma_f(j) = \int_0^j dK \int_0^\pi \gamma_f \sin\vartheta d\vartheta, \quad (1)$$

where Γ_n is the neutron width and Γ_f is the fission width for the given angular momentum. When $j_{cr} \gg j \gg 1$ (where j_{cr} is the angular momentum for which the nucleus is not stable against fission[1]) for γ_f we can use a statistical formula such as[2]

$$\gamma_f(j, K, \vartheta) = \frac{\Gamma_f(0)}{j\pi}\left(\sin^2\vartheta - \frac{K^2}{j^2}\right)^{-1/2} \exp\left\{\frac{\hbar^2 j^2}{2\tau}\left(\frac{1}{I_0} - \frac{1}{I_A}\right) - \frac{\hbar^2 K^2}{2\tau}\left(\frac{1}{I_C} - \frac{1}{I_A}\right)\right\}, \quad (2)$$

where $\Gamma_f(0)$ is the fission width for zero angular momentum, $\tau = \sqrt{10U/A}$ is the temperature, U is the nuclear excitation energy, I_0 is the moment of inertia of a spherical nucleus, I_A is the moment of inertia about an axis perpendicular to the symmetry axis and I_C is the moment of inertia about the symmetry axis of the nucleus. I_A and I_C are taken for a deformation corresponding to the top of the fission barrier. For a moment of inertia equal to that of a rigid body we have

$$\frac{1}{I_0} - \frac{1}{I_A} = \frac{1}{I_0}(1.2z + 5.6z^2) = \frac{\beta^2 2\tau}{\hbar^2};$$

$$\frac{1}{I_C} - \frac{1}{I_A} = \frac{1}{I_0}(3.5z + 8.8z^2) = \frac{\alpha^2 4\tau}{\hbar^2},$$

where $z = 1 - x$. Inserting (2) into (1), summing over all K and averaging over j, we obtain the angular distribution

$$w_f(\vartheta)\, d\omega = d\omega \frac{\Gamma_f(0)}{j_{max}^2} 2 \times \int_0^{j_{max}} \frac{I_0(\alpha^2 j^2 \sin^2\vartheta) \exp(j^2\beta^2 - \alpha^2 j^2 \sin^2\vartheta)}{\Gamma_n + \Gamma_f(0)\,\Phi(j\alpha)\exp(j^2\beta^2)} j dj = \int_0^{j_{max}} j dj \cdot \varphi(j), \quad (3)$$

where

$$\Phi(j\alpha) = (j\alpha)^{-1} \int_0^{j\alpha} dt \cdot e^{-t^2},$$

$$\hbar^2 j_{max}^2 = 2m(E - B)(R + R_1)^2 = 2mE\sigma/\pi;$$

I_0 is a Bessel function with imaginary argument; m, E, B, R are the mass, energy, Coulomb barrier and radius of the incident particle; R_1 is the radius of the target nucleus; σ is the cross section for the formation of a compound nucleus.

Equation (3) gives the angular distribution for one stage of the cascade process of neutron evaporation. For $\Gamma_f \gg \Gamma_n$ fission occurs without neutron evaporation and $w_f(0)/w_f(\pi/2)$ determines the anisotropy. In this case (3) agrees with Strutinskiĭ's formula.[2] For $\Gamma_f \ll \Gamma_n$ the entire neutron evaporation cascade must be taken into account. Therefore the anisotropy is given by

$$\sigma_f(0) / \sigma_f(\pi/2) = \sum_{i=0}^{N} w_{fi}(0) \Big/ \sum_{i=0}^{N} w_{fi}(\pi/2),$$

$$w_{fi} = \int_0^{j_{max}} j dj \varphi_i(j) \prod_{s=0}^{i} \Gamma_{ns} \Big/ (\Gamma_{ns} + \Gamma_{fs}(j)),$$

where i is the number of the cascade stage. In w_{fi} exp $(j^2\beta^2)$ remains in the numerator; this represents the increased weight of states with high angular momentum and, consequently, increased anisotropy. The essential point is that when $\Gamma_f \gg \Gamma_n$ fission is equally probably for different values of the angular momentum, while when $\Gamma_f \ll \Gamma_n$ mainly nuclei with high angular momentum will fission.

If it is assumed that the dependence of the nuclear moment of inertia about the symmetry axis (I_C) on z is determined just as for a rigid body, where $\xi < 1$, then for nuclei with $\Gamma_f \gg \Gamma_n$ we can obtain ξ; then assuming that ξ is identical for all nuclei and is independent of temperature, we obtain the anisotropy for nuclei with $\Gamma_f \ll \Gamma_n$. Using experimental data[3] on fission induced by α particles, we obtain $\xi = 0.46$ for Pu^{239}, Np^{237}, and U^{235}. If for Ra^{226} $\Gamma_f \ll \Gamma_n$ the anisotropy is 1.87 (compared with the experimental value 2.03 ± 0.05).

We note that the theory can be tested for both $\Gamma_f \gg \Gamma_n$ and $\Gamma_f \ll \Gamma_n$ by studying $\sigma_f(\vartheta)\ \sigma_f(\pi/2)$. For $\vartheta \neq 0$ this ratio approaches a constant limit as $\alpha^2 j_{max}^2$ increases. Thus $\sigma_f(\pi/4)/\sigma_f(\pi/2) \to \sqrt{2}$ as $\alpha^2 j_{max}^2 \to \infty$ and is independent of the nuclear parameters.

In conclusion I wish to thank D. P. Grechukhin for a discussion and I. Halpern for his kindness in making experimental data available.

[1] G. A. Pik-Pichak, J. Exptl. Theoret. Phys. (U.S.S.R.) **34**, 341 (1958), Soviet Phys. JETP **7**, 238 (1958).

[2] V. M. Strutinskiĭ, Атомная энергия (Atomic Energy) **2**, 508 (1957). (Translation, Consultants Bureau, Inc., p. 621).

[3] C. T. Coffin and I. Halpern, Phys. Rev. **112**, 536 (1958).

Note added in proof (January 27, 1959). $\sigma(0°)/\sigma(90°)$ was also calculated for Ra, assuming $\xi = 1$ but with a more exact value of the angular momentum of the compound nucleus (See I. Halpern and V. M. Strutinskiĭ, Report P/1315 at the Second Geneva Conference on the Peaceful Uses of Atomic Energy, 1958). It was assumed that $\tau = \sqrt{a\,(U - E_f)}$, where E_f is the fission threshold and the constant a was determined from the anisotropy for Pu. The initial temperature of the nucleus Pu + α particle at the saddle point is 1.3 to 1.5 Mev. The anisotropy for Ra is calculated to be 2.0. For Bi, taking into account the dependence of fissionability on excitation energy, we obtain $\sigma(0°)/\sigma(90°) = 1.9\,(\sigma(0°)/\sigma(90°)_{exp} = 2.02$; $\Gamma_f^{(0)}/\Gamma_n \sim \exp[(E_n - E_f)/\tau]$, where $E_f - E_n \approx 8$ Mev and $E_f \approx 15$ Mev. Agreement of the calculated and experimental anisotropy for Ra shows that we have no reason to assume the absence of correspondence between the nuclear moment of inertia and that of a rigid body, including the cases of excitations below 10 or 12 Mev, as was suggested by Halpern and Strutinskiĭ on the basis of neutron experiments.

The results given here were obtained in collaboration with V. M. Strutinskiĭ.

Translated by I. Emin
190

ON THE THERMODYNAMICS OF HELIUM

M. P. MOKHNATKIN

Submitted to JETP editor October 21, 1958

J. Exptl. Theoret. Phys. (U.S.S.R.) **36**, 963 (March, 1959)

In the paper by Esel'son, Kaganov, and Lifshitz[1] it is shown that the lambda transition in a solution of helium isotopes is a phase transition of the second order. Using the condition for equilibrium between phases and the equations for the chemical potentials of the components in the gaseous phase, the authors obtain the equation

$$kT \ln P_3 + \chi(T) = \varphi + (1 - x_{liq})\,\partial\varphi/\partial x_{liq},$$
$$kT \ln P_4 + \chi(T) = \varphi - x_{liq}\,\partial\varphi/\partial x_{liq} \qquad (2)$$

(the equation numbers are those of reference 1). If we take the total derivative of both sides of Eq. (2), we get, according to the authors, the expression

$$-S_3 + kT\left(\frac{d}{dT}\ln P_3\right) = \frac{\partial\varphi}{\partial T} + (1 - x_{liq})\frac{\partial^2\varphi}{\partial x_{liq}\partial T} \qquad (3)$$

and so on. It is further asserted that at the temperature T_λ one obtains

$$kT_\lambda\Delta\left(\frac{d}{dT}\ln P_3\right) = (1 - x_{liq})\,\Delta\left(\frac{\partial^2\varphi}{\partial T\partial x_{liq}}\right) \qquad (4)$$

and so on, since the first derivative with respect to the thermodynamic potential has a break and the second derivative a jump at a phase transition of the second order. Substituting, according to Eqs. (6) and (9), for the quantities which occur here the authors obtain the following equation for the total pressure

$$kT_\lambda\Delta\left(\frac{d}{dT}\ln P\right) = (x_{vap} - x_{liq})\frac{\Delta C_p}{T_\lambda}\frac{\partial T_\lambda}{\partial x_{liq}}. \qquad (10)$$

Since, as is shown in reference 1, $\partial T_\lambda/\partial x_{liq} < 0$, $\Delta C_p > 0$, $x_{vap} > x_{liq}$, we have $\Delta\{d \ln p/dT\} < 0$ which is in accordance with experimental data.[2]

The authors conclude from this that the lambda transition is a phase transition of the second order.

We must draw attention to an error which has crept in in the process of this proof. If we take into account that along the equilibrium curve the total derivative with respect to the temperature is given by the expression $d\mu/dT = \partial\mu/\partial T + (\partial\mu/\partial P)\,dP/dT$ one must write the basic equations (3) and (4) in the form

$$\frac{d}{dT}[kT \ln P_3 + \chi(T)] = \frac{\partial\varphi}{\partial T} + (1 - x_{liq})\frac{\partial^2\varphi}{\partial T\partial x_{liq}}$$
$$+\left[(1 - x_{liq})\frac{\partial^2\varphi}{\partial P\partial x_{liq}} + \frac{\partial\varphi}{\partial P}\right]\frac{dP}{dT}, \qquad (3')$$

$$kT_\lambda \Delta\left(\frac{d}{dT}\ln P_s\right) = (1 - x_{liq})\,\Delta\frac{\partial^2\varphi}{\partial T\,\partial x_{liq}}$$

$$+\left\{\frac{\partial\varphi}{\partial P}\,\Delta\left(\frac{dP}{dT}\right) + (1 - x_{liq})\left[\Delta\frac{\partial^2\varphi}{\partial P\,\partial x_{liq}}\frac{dP}{dT}\right]\right\} \qquad (4')$$

and so on. The authors of reference 1 have incorrectly discarded the additional terms within the curly brackets in Eq. (4′) and thus obtained some agreement of the theory with experiment. However, an analysis of the complete Eq. (4′) for phase transitions does not confirm those conclusions which were made by the authors on the basis of the incorrect Eqs. (3) and (4). In that case any assertions about the character of the lambda transition in solutions of helium isotopes remain unproved assumptions.

[1] Esel'son, Kaganov, and Lifshitz, J. Exptl. Theoret. Phys. (U.S.S.R.) **33**, 936 (1957), Soviet Phys. JETP **6**, 719 (1958).

[2] Esel'son, Bereznyak, and Kaganov, Dokl. Akad. Nauk SSSR **111**, 568 (1956), Soviet Phys. "Doklady" **1**, 683 (1956).

Translated by D. ter Haar
191

REPLY TO THE LETTER BY M. P. MOKHNATKIN

B. N. ESEL'SON, M. I. KAGANOV, and I. M. LIFSHITZ

Submitted to JETP editor November 25, 1958

J. Exptl. Theoret. Phys. (U.S.S.R.) **36**, 964 (March, 1959)

As was shown at the beginning of our paper, the character of the lambda transition in solutions of helium isotopes follows from a large number of experimental data, in particular from the fact that the elasticity of the vapor over the solution depends essentially on the lighter isotope concentration over a large range of temperatures (absence of a plateau in the P-x diagram).

The proof of the fact that the lambda transition is of the second order was therefore not the object of our paper. The object of the paper was the analysis of different thermodynamic consequences from the fact that a lambda transition (a transition of the second order) existed in solutions and a comparison of these consequences with experimental data. In particular the character of the singularity in the P-T curve at the lambda point was elucidated in the paper. The conclusions of that consideration were in accordance with experiment and corroborated the conclusion about the second order transition.

M. P. Mokhnatkin asserts that this conclusion is illegitimate. An error was discovered in the fact that we neglected in a number of formulae derivatives of the pressure with respect to the chemical potential of the condensed phase. This neglect was, to be sure, made deliberately and was justified by the smallness of the specific volume of the liquid (v_{liq}) as compared with the specific volume of the vapor (v_{vap}). We remark that in those cases where this was necessary we took the derivative of the pressure with respect to the chemical potential of the liquid into account [see Eq. (19) and following].

Even if we retain the terms which M. P. Mokhnatkin writes down [see his Eqs. (3′) and (4′)] which, of course, leads to needlessly complicated equations, the conclusions obtained on the basis of Eq. (10) remain completely the same. Indeed, when the derivatives of the pressure with respect to the chemical potential of the liquid are taken into account, the equation analogous to Eq. (10) has the form

$$\frac{kT_\lambda}{P}\left\{1 - \frac{v_{liq} + (x_{liq} - x_{vap})(\partial v_{liq}/\partial x_{liq})_\lambda}{v_{vap}}\right\}\Delta\frac{dP}{dT},$$

$$= (x_{vap} - x_{liq})\frac{\Delta C_p}{T_\lambda}\frac{\partial T_\lambda}{\partial x_{liq}}\left\{1 - \left(\frac{\partial P}{\partial T}\right)_\lambda\left(\frac{\partial T_\lambda}{\partial P}\right)\right\}.$$

We have used here the notation of our paper and the index λ at the derivatives indicates that one must take half of the sum of the values for the two phases at $T = T_\lambda$. The expressions within curly brackets differ quite insignificantly from unity: on the left hand side the difference is about 10^{-2} and on the right hand side about 10^{-3}, which also confirms the legitimacy of the omissions made.

Translated by D. ter Haar
192

PARITY NONCONSERVATION IN THE FIRST ORDER IN THE WEAK-INTERACTION CONSTANT IN ELECTRON SCATTERING AND OTHER EFFECTS

Ya. B. ZEL' DOVICH

Submitted to JETP editor December 25, 1958

J. Exptl. Theoret. Phys. (U.S.S.R.) **36**, 964-966 (March, 1959)

We assume that besides the weak interaction that causes beta decay,

$$g(\bar{P}ON)(\bar{e}^{-}O\nu) + \text{Herm. conj.}, \qquad (1)$$

there exists an interaction

$$g(\bar{P}OP)(\bar{e}^{-}Oe^{-}) \qquad (2)$$

with $g \approx 10^{-49}$ and the operator $O = \gamma_\mu(1+i\gamma_5)$ characteristic[1] of processes in which parity is not conserved.*

Then in the scattering of electrons by protons the interaction (2) will interfere with the Coulomb scattering, and the nonconservation of parity will appear in terms of the first order in the small quantity g. Owing to this it becomes possible to test the hypothesis used here experimentally and to determine the sign of g.

The matrix element of the Coulomb scattering is of the order of magnitude e^2/k^2, where k is the momentum transferred ($\hbar = c = 1$). Consequently, the ratio of the interference term to the Coulomb term is of the order of gk^2/e^2. Substituting $g = 10^{-5}/M^2$, where M is the mass of the nucleon, we find that for $k \sim M$ the parity nonconservation effects can be of the order of 0.1 to 0.01 percent.

In the scattering of fast ($\sim 10^9$ ev) longitudinally polarized electrons through large angles by unpolarized target nuclei it can be expected that the cross-sections for right-hand and left-hand electrons (i.e., for electrons with $\sigma \cdot p > 0$ and $\sigma \cdot p < 0$) can differ by 0.1 to 0.01 percent. Such an effect is a specific test for an interaction not conserving parity.

A magnetized iron plate can served as a source of polarized electrons.[6] When electrons are ejected from it by ion or electron impacts (dynatron effect), photoelectric effect,[6] or as delta electrons, one can expect a polarization even larger than that corresponding to the ratio of the number of magnetization electrons to the total number of of electrons in the iron, since the inner electrons do not take much part in these processes. From thermoelectric emission or field emission one cannot expect an appreciable polarization of the emerging electrons, since the chemical potential of the electrons with spins parallel and antiparallel to the magnetization is evidently the same.

The interaction (2) leads to a displacement of the electron levels of different parities in the free atom.

In the hydrogen atom the probability of the metastable transition $2S_{1/2} \to 1S_{1/2}$, which appears on account of the admixture of $2P_{1/2}$ to the $2S_{1/2}$, still turns out to be even smaller that the transition probability on account of the magnetic moment of the electron, and is less than the probability of the two-quantum transition $2S \to 1S$ by a factor of more than 10^7. Finally, the interaction (2) leads to a rotation of the plane of polarization of visible light by any substance not containing molecules optically active in the ordinary sense of the words. The rotation of the plane of polarization also occurs because the weak interaction mixes atomic electronic states of different parity. A calculation of the effect gives an expression of the form

$$|n_{\text{right}} - n_{\text{left}}| \sim N_0(a^4/\lambda)\, g\, |\psi_S(0)|\, |\psi_P(0)|\, /(E_P - E_S), \qquad (3)$$

where n is the index of refraction for circularly polarized light; $N_0 \sim a^{-3}$ is the number density of the atoms; a is the linear dimension of an atom; λ is the wavelength of the light; $|\psi_S(0)| \sim 1/a^{3/2}$; in $|\psi_P(0)|$ there are nonvanishing "small components" χ, given by $\chi \sim (\hbar/2mc)\sigma \operatorname{grad} \varphi$, where φ are the "large components"; $|\psi_P(0)| \sim (\hbar/mc)a^{-5/2}$, so that

$$|n_{\text{right}} - n_{\text{left}}| \sim (g/a^3 \Delta E_{SP})(\lambda/mc\lambda) \sim 10^{-20}. \qquad (4)$$

Rotation of the plane of polarization by 1 radian occurs in a length of the order $\lambda/10^{-20} = 10^{15}$ cm, so that even in the first order in g the effect obviously cannot be observed.

How plausible is the assumption that the interaction (2) exists? Let us regard νe^- as a doublet in isotopic space and denote by l_1 the two-component quantity ν, e^-. We denote by B (baryons) the two-component quantity P, N. The interaction that causes β decay is written

$$g(\bar{B}\tau_- OB)(\bar{l}_1\tau_- Ol_1) + g(\bar{B}\tau_- OB)(\bar{l}_1\tau_- Ol_1)$$
$$\equiv 2g(\bar{B}\tau_x OB)(\bar{l}_1\tau_x Ol_1) + 2g(\bar{B}\tau_y OB)(\bar{l}_1\tau_y Ol_1). \qquad (5)$$

It is natural to add to this formulation a term that complements the expression (5) to make the scalar product $\tau_B \tau_{l_1}$:

$$2g\,(\bar{B}\tau_z OB)\,(\bar{l}_1\tau_z Ol_1)$$

$$= 2g\,[(\bar{P}OP) - (\bar{N}ON)]\,[(\bar{\nu}O\nu) - (\bar{e}^-Oe^-)], \qquad (6)$$

and this term contains the interaction in which we are interested here. In addition the formalism leads to the conclusion that the sign of the interaction will be different for the proton and the neutron. For the μ-meson interactions one will have to introduce another two-component quantity l_2, consisting of ν, μ^-. Then in the scalar product $(\bar{l}_1\tau l_1)\,(\bar{l}_2\tau l_2)$ there are no terms that would give the decay $\mu^- \to 2e^- + e^+$, and the objection of Gell-Mann and Feynman[1] falls to the ground.

Assumptions have been put forward about a direct interaction $g\,(\bar{e}^-O\nu)\,(\bar{\nu}Oe^-)$, which would lead to a scattering of neutrinos by electrons,[1] and also about a weak interaction of four nucleons,[2] which leads to parity nonconservation in first order in g in nuclear reactions and the stationary states of nuclei. The four-nucleon interaction has as a consequence that odd nuclei (spin $\neq 0$) will have an "anapole" moment[3] proportional to g. The electromagnetic interaction of the electron with the anapole moment leads to parity nonconservation in the order ge^2. Thus in the absence of a direct weak interaction of electrons with nucleons the effects considered above, caused by mixtures of atomic electron levels of different parities, do not vanish, but are weakened by a factor of about 100.

I take this occasion to express my unchanging gratitude to G. M. Gandel'man, A. S. Kompaneets, L. D. Landau, L. B. Okun', I. Ya. Pomeranchuk, and Ya. A. Smorodinskiĭ for valuable comments and discussions.

*Such an interaction has been repeatedly discussed in the past in connection with the problem of the isotope shift of electron levels (I. E. Tamm). On an analogous interaction between the neutron and the electron, see references 4 and 5. New experimental possibilities arise in connection with the nonconservation of parity in the interaction (2).

[1] M. Gell-Mann and R. P. Feynman, Phys. Rev. **109**, 193 (1958).

[2] Roberts, Survey Report at the Geneva Conference on High Energies, 1958.

[3] Ya. B. Zel'dovich, J. Exptl. Theoret. Phys. (U.S.S.R.) **33**, 1531 (1957), Soviet Phys. JETP **6**, 1184 (1958).

[4] L. L. Foldy, Phys. Rev. **87**, 693 (1952).

[5] J. L. Lopes, Nucl. Phys. **8**, 234 (1958).

[6] H. A. Tolhoek, Revs. Modern Phys. **28**, 277 (1956).

Translated by W. H. Furry
193

SOVIET PHYSICS JOURNALS

Published in English by the American Institute of Physics

Soviet Physics – JETP

A translation, beginning with 1955 issues of "Journal of Experimental and Theoretical Physics" of the USSR Academy of Sciences. Leading physics journal of Soviet Union. Similar to "The Physical Review" in quality and range of topics. Outstanding new work is most likely to appear in this journal.

Twelve issues, approximately 3,500 pages. $75 domestic, $79 foreign. Libraries $35 domestic, $39 foreign. Single copies, $8.*

Soviet Physics – SOLID STATE

A translation, beginning with 1959 issues of "Fizika Tverdogo Tela" of the USSR Academy of Sciences. Offering results of theoretical and experimental investigations in the physics of semiconductors, dielectrics, and on applied physics associated with these problems. Also publishes papers on electronic processes taking place in the interior and on the surface of solids.

Twelve issues, approximately 2,000 pages. $55 domestic, $59 foreign. Libraries $25 domestic, $29 foreign. Single copies, $8.*

Soviet Physics – TECHNICAL PHYSICS

A translation, beginning with the 1956 issues of the "Journal of Technical Physics" of the USSR Academy of Sciences. Contains work on plasma physics and magnetohydrodynamics, aerodynamics, ion and electron optics and radio physics. Also publishes articles in mathematical physics, the physics of accelerators and molecular physics.

Twelve issues, approximately 2,000 pages, $55 domestic, $59 foreign. Libraries $25 domestic, $29 foreign. Single copies, $8.*

Soviet Physics– ACOUSTICS

A translation, beginning with 1955 issues of "Journal of Acoustics" of USSR Academy of Sciences. Devoted principally to physical acoustics but includes electro, bio, and psycho acoustics. Mathematical and experimental work with emphasis on pure research.

Four issues, approximately 400 pages. $12 domestic, $14 foreign. (No library discounts) Single copies, $4.

Soviet Physics – DOKLADY

A translation, beginning with 1956 issues of "Physics Sections" of Proceedings of USSR Academy of Sciences. All-science journal offering four-page reports of recent research in physics and borderline subjects.

Six issues, approximately 1,500 pages. $35 domestic, $38 foreign. Libraries $15 domestic, $18 foreign. Single copies Vols. 1 and 2, $5; Vol. 3 and later issues, $7.*

Soviet Physics – CRYSTALLOGRAPHY

A translation, beginning with 1957 issues of the journal "Crystallography" of USSR Academy of Sciences. Experimental and theoretical papers on crystal structure, lattice theory, diffraction studies, and other topics of interest to crystallographers, mineralogists, and metallurgists.

Six issues, approximately 1,000 pages. $25 domestic, $27 foreign. Libraries $10 domestic, $12 foreign. Single copies, $5.*

SOVIET ASTRONOMY – AJ

A translation, beginning with 1957 issues of "Astronomical Journal" of USSR Academy of Sciences. Covers various problems of interest to astronomers and astrophysicists including solar activity, stellar studies, spectroscopic investigations of radio astronomy.

Six issues, approximately 1,100 pages. $25 domestic, $27 foreign. Libraries $10 domestic, $12 foreign. Single copies, $5.*

Soviet Physics – USPEKHI

A translation, beginning with September, 1958 issue of "Uspekhi Fizicheskikh Nauk" of USSR Academy of Sciences. Offers reviews of recent developments comparable in scope and treatment to those carried in "Reviews of Modern Physics." Also contains reports on scientific meetings within the Soviet Union, book reviews, and personalia.

Six issues, approximately 1,700 pages. (Contents limited to material from Soviet sources.) $45 domestic, $48 foreign. Libraries $20 domestic, $23 foreign. Single copies, $9.*

*For libraries of non-profit degree-granting academic institutions.

Subscription prices subject to annual variation depending on size of Russian originals.

Please send orders and inquiries to

American Institute of Physics

335 East 45 Street, New York 17, N. Y.

CONTENTS—continued

	Page	Russian Reference
A Group-Theoretical Consideration of the Basis of Relativistic Quantum Mechanics V. Yu. M. Shirokov	620	36, 879
On the Stability of Nuclei P. É. Nemirovskiĭ	627	36, 889
Fock Expansion for the Wave Functions of a System of Charged Particles Yu. N. Demkov and A. M. Ermolaev	633	36, 896
On the Application of Quantum-Field-Theory Methods to Problems of Quantum Statistics at Finite Temperatures A. A. Abrikosov, L. P. Gor'kov, and I. E. Dzyaloshinskiĭ	636	36, 900
Reactions Involving Polarized Particles of Zero Rest Mass Chou Kuang-Chao	642	36, 909

LETTERS TO THE EDITOR

A Paramagnetic Amplifier and Generator, Using Fe^{3+} Ions in Corundum L. S. Kornienko and A. M. Prokhorov	649	36, 919
Angular Anisotropy of Scattering of Fragments in Fission of Am^{241} by 14.7-Mev Neutrons A. N. Protopopov, I. A. Baranov, and V. P. Él'smont	650	36, 920
Measurement of the Mass of Cosmic-Ray Particles Underground M. I. Dalon and L. I. Potapov	650	36, 921
Nuclear Excitation by High Energy Particles M. Z. Maksimov	652	36, 922
A Method of Evaluating Electrical Conductivity V. L. Bonch-Bruevich	653	36, 924
Thermodynamic Theory of Ferromagnetic Absorption V. L. Beshidze	654	36, 926
Alpha Decay of Th^{227} in the Collective Model and the Spin of Ra^{223} in Its Lowest State S. G. Ryzhanov	656	36, 928
On the Problem of the Covarient Definition of the Spin Pseudovector A. A. Sokolov, I. M. Ternov, and Yu. M. Loskutov	657	36, 930
Random Free Precession of Magnetic Moments of Atomic Nuclei G. V. Skrotskiĭ and A. A. Kokin	658	36, 932
Production of Strange Particles in 3-Bev p-p Collisions V. S. Barashenkov and V. M. Mal'tsev	659	36, 933
Interpretation of the Maximum in the Total Cross Section for Proton-Proton Scattering in the 1 Bev Region V. I. Rus'kin	660	36, 935
Range-Energy Dependence of C_{12}, C_{14}, and O_{18} Ions in Aluminum, Copper, and Gold in the Energy Interval from 50 to 110 Mev Yu. Ts. Oganesyan	661	36, 936
Some Symmetry Properties in Process of Antihyperon Production with Annihilation of Antinucleons Chou Kuang-Chao	663	36, 938
The Gamma Rays of As^{74} Yu. E. Loginov and K. I. Yakovlev	664	36, 940
Ultrasonic Attenuation in Metals G. L. Kotkin	664	36, 941
Free Energy of Strong Electrolytes A. A. Vedenov	665	36, 942
On the Possible Multiple Production of Muons I. L. Rozental'	666	36, 943
On the Magnitude of the Ratio σ^-/σ^+ Near the Threshold of Meson Production S. P. Kharlamov, M. I. Adamovich, and V. G. Larionova	668	36, 945
On the Scattering of Pions by Deuterons G. M. Vagradov and I. B. Sokolov	669	36, 948
New Short-Lived Isomers As^{73m} and Ga^{70m} Excited by Fast Protons A. M. Morozov and P. A. Yampol'skiĭ	671	36, 950
On a Relation in Quantum Statistics E. S. Fradkin	672	36, 951
Polarization of the Nucleus by Capture of Polarized Negative Muons into the Mesonic K Shell. I. M. Shmushkevich	673	36, 953
Gamma Rays Accompanying the Fission of U^{238} by 2.8 and 14.7 Mev Neutrons A. N. Protopopov and B. M. Shiryaev	674	36, 954
Zemplen's Theorem in Relativistic Hydrodynamics R. V. Polovin	675	36, 956
On Electromagnetic Shock Waves in Ferrites A. V. Gaponov and G. I. Freĭdman	675	36, 957
On the Heat Conductivity and Attenuation of Sound in Superconductors B. T. Geĭlikman and V. Z. Kresin	677	36, 959
Anisotropic Fission of Rotating Nuclei G. A. Pik-Pichak	679	36, 961
On the Thermodynamics of Helium M. P. Mokhnatkin	680	36, 963
Reply to the Letter by M. P. Mokhnatkin B. N. Esel'son, M. I. Kaganov, and I. M. Lifshitz	681	36, 964
Parity Nonconservation in the First Order in the Weak-Interaction Constant in Electron Scattering and Other Effects Ya. B. Zel'dovich	682	36, 964

CONTENTS

	Page	Russian Reference
Academician Lev Andreyevich Artsimovich	453	36, 649
Bi Fission at Very High Excitation Energies — V. F. Darovskikh and N. A. Perfilov	456	36, 652
Range-Energy Relation for 660-Mev Protons — V. P. Zrelov and G. D. Stoletov	461	36, 658
Investigation of the Core of Extensive Air Showers — S. N. Vernov, N. N. Goryunov, G. T. Zatsepin, G. V. Kulinkov, Yu. A. Nechin, Z. S. Strugalskiĭ, and G. B. Khristiansen	468	36, 669
Some Features of Multiplet Ferromagnetic Resonance in Ferrites — V. N. Lazukin	477	36, 682
Generation of Neutral Pions in the Interaction between 9 Bev Protons and Photographic Emulsion Nuclei — G. L. Bayatyan, I. M. Gramenitskiĭ, A. A. Nomofilov, M. I. Podgoretskiĭ, and E. S. Skrzypczak	483	36, 690
Exact Measurement of the Ratios of Internal-Conversion Coefficients of 411.7-kev Gamma Quanta in Hg^{198} — V. M. Kel'man and R. Ya. Metskhvarishvili	486	36, 694
Underground Muon Spectrum at ~40 Meter Water Equivalent — M. I. Dalon and L. I. Potapov	488	36, 697
Ionization along the Tracks of High-Energy Electron-Positron Pairs — A. A. Varfolomeev, R. I. Gerasimova, L. A. Makarina, A. S. Romantseva, and S. A. Chueva	495	36, 707
Investigation of High Current Pulse Discharges in Conical Chambers — N. A. Borzunov, D. V. Orlinskiĭ, and S. M. Osovets	502	36, 717
High-Energy Neutrons in Cosmic Rays — G. N. Flerov, V. I. Kalashnikova, A. V. Podgurskaya, E. D. Vorob'ev, and G. A. Stolyarov	511	36, 727
Scattering of 590 Mev Neutrons by Protons in the Small Angle Region — B. M. Golovin, V. P. Dzhelepov, Yu. V. Katyshev, A. D. Konin, and S. V. Medved'	516	36, 735
Ratio of the Deuteron and Proton Yields in the Photodisintegration of Au^{197} — E. D. Makhnoyskiĭ	519	36, 739
Fission Induced in Heavy Elements by Carbon, Nitrogen, and Oxygen Nuclei — S. M. Polikanov and V. A. Druin	522	36, 744
Two-Neutron Capture Reaction in the Interaction between N^{14} and Nuclei of Some Elements — V. A. Karnaukhov, G. M. Ter-Akop'yan, and V. I. Khalizev	525	36, 748
High-Energy Nuclear-Active Component of Extensive Air Showers at Sea Level. A. T. Abrosimov, V. A. Dmitriev, G. V. Kulikov, E. I. Massal'skiĭ, K. I. Solov'ev, and G. B. Khristiansen	528	36, 751
Cross-Sections for the Production of Californium Isotopes by the Bombardment of U^{238} by Accelerated Carbon Ions — V. V. Volkov, L. I. Guseva, A. S. Pasyuk, N. I. Tarantin, and K. V. Filippova	536	36, 762
Investigation of Weak Ferromagnetism in the $MnCO_3$ Single Crystal — A. S. Borovik-Romanov	539	36, 766
Converging Cylindrical Detonation Wave — Ya. B. Zel'dovich	550	36, 782
Fission of Nonspherical Nuclei — A. G. Sitenko	555	36, 793
On the Theory of the Coherent Spontaneous Emission — V. M. Faĭn	562	36, 798
Quadrupole Oscillations of Deformed Nuclei — B. L. Birbrair, L. K. Peker, and L. A. Sliv	566	36, 803
Contribution to the Theory of Light Scattering near the Second-Order Phase-Transition Points — A. P. Levanyuk	571	36, 810
Indirect Coupling of d Electrons in Transition Metals. I. Ferromagnetism — A. A. Berdyshev and B. V. Karpenko	577	36, 819
The Role of Group Velocity of Light Emitted in a Refractive Medium — I. M. Frank	580	36, 823
Non-Uniqueness of the Phase Shift Analysis of Proton-Proton Collisions — V. S. Barashenkov and Huang Nen-Ning	587	36, 832
Radiation from a Current-Carrying Ring Moving Uniformly in a Plasma Situated in a Magnetic Field — L. S. Bogdankevich	589	36, 835
Oscillations of a Completely Ionized Plasma in a Cylindrical Cavity — L. M. Kovrizhnykh	592	36, 839
Theory of the Nonlinear Field $(\Box - \lambda\varphi^2)\varphi = 0$ — D. F. Kurdgelaidze	594	36, 842
On the Role Played by Exchange Effects in Stripping Reactions — V. G. Neudachin, I. B. Teplov, and O. P. Shevchenko	599	36, 850
On a Certain Version of Nonlocal Electromagnetic Field Theory — A. A. Komar and M. A. Markov	602	36, 854
Interaction between Conduction Electrons in Ferromagnets — A. I. Akhiezer and I. Ya. Pomeranchuk	605	36, 859
A Model of a Field Theory with Nonvanishing Renormalized Charge — A. A. Ansel'm	608	36, 863
On the Theory of Nuclear Magnetic Moments — D. F. Zaretskiĭ	612	36, 869
On the Electromagnetic Radii of the Lightest Nuclei in the Ground and Lowest Excited States — A. K. Kamińskiĭ and Yu. M. Shirokov	616	36, 874

(Contents continued on inside back cover)